



Keele
University

This work is protected by copyright and other intellectual property rights and duplication or sale of all or part is not permitted, except that material may be duplicated by you for research, private study, criticism/review or educational purposes. Electronic or print copies are for your own personal, non-commercial use and shall not be passed to any other individual. No quotation may be published without proper acknowledgement. For any other use, or to quote extensively from the work, permission must be obtained from the copyright holder/s.

Biosilicification in *Oryza sativa* and other plants

Ian Stokes

Doctorate of Chemistry (Ph.D)

July 2016

Keele University

SUBMISSION OF THESIS FOR A RESEARCH DEGREE**Part I. DECLARATION by the candidate for a research degree. To be bound in the thesis**

Degree for which thesis being submitted

Title of thesis

This thesis contains confidential information and is subject to the protocol set down for the submission and examination of such a thesis.**YES/NO [please delete as appropriate; if YES the box in Part II should be completed]**

Date of submission

(Date of submission must comply with Regulation 2D)

Original registration date

Name of candidate

Research Institute

Name of Lead Supervisor

I certify that:

- (a) The thesis being submitted for examination is my own account of my own research
- (b) My research has been conducted ethically. Where relevant a letter from the approving body confirming that ethical approval has been given has been bound in the thesis as an Annex
- (c) The data and results presented are the genuine data and results actually obtained by me during the conduct of the research
- (d) Where I have drawn on the work, ideas and results of others this has been appropriately acknowledged in the thesis
- (e) Where any collaboration has taken place with one or more other researchers, I have included within an 'Acknowledgments' section in the thesis a clear statement of their contributions, in line with the relevant statement in the Code of Practice (see Note overleaf).
- (f) The greater portion of the work described in the thesis has been undertaken subsequent to my registration for the higher degree for which I am submitting for examination
- (g) Where part of the work described in the thesis has previously been incorporated in another thesis submitted by me for a higher degree (if any), this has been identified and acknowledged in the thesis
- (h) The thesis submitted is within the required word limit as specified in the Regulations

Total words in submitted thesis (including text and footnotes, but excluding references and appendices)

Signature of candidate Date

Note

Extract from Code of Practice: If the research degree is set within a broader programme of work involving a group of investigators – particularly if this programme of work predates the candidate's registration – the candidate should provide an explicit statement (in an 'Acknowledgments' section) of the respective roles of the candidate and these other individuals in relevant aspects of the work reported in the thesis. For example, it should make clear, where relevant, the candidate's role in designing the study, developing data collection instruments, collecting primary data, analysing such data, and formulating conclusions from the analysis. Others involved in these aspects of the research should be named, and their contributions relative to that of the candidate should be specified (*this does not apply to the ordinary supervision, only if the supervisor or supervisory team has had greater than usual involvement*).

Abstract

Rice (*Oryza sativa*) is well known as a biosilicifier though the mechanisms which underlie the silica deposition in them are still relatively unknown. Silica deposits in rice were imaged through various complementary techniques including PDMPO staining and fluorescence microscopy, scanning electron microscopy, micro-particle induced X-ray emission and low-energy X-ray fluorescence. These techniques showed silica deposition throughout all expected sites of silica deposition, as well as revealing novel areas of silica deposition in the xylem, a region not usually considered to be a zone of silicification despite its known role in transporting silicic acid.

Silicon was found to be co-localised with aluminium at the silica cells through the use of low-energy X-ray fluorescence. This is, to the best of our knowledge, the first evidence of silicon/aluminium co-localisation in rice leaves.

The link between the hemicellulose callose and silicification was investigated, with aniline blue and immunofluorescence staining revealing numerous sites of callose deposition in rice leaf tissue, all of which matched with known areas of silica deposition.

It was demonstrated that silicic acid uptake in rice does occur at a rate which would require active transport through the use of a simple experiment where the silicic acid content of solutions with rice plants growing in them were measured over time.

Silicification was studied in developing rice seedlings using PDMPO staining and fluorescence microscopy to image structures from different developmental stages of seedlings. Silicification was found to occur at all stages of development, with evidence of silicification of precursor leaf tissue inside ungerminated seeds.

The implications of these findings were discussed and the possibility that silicon may be maintained in a form other than solid silica in certain areas of rice plants was put forward.

Acknowledgements

Professional Acknowledgements

I would like to thank my supervisor Professor Christopher Exley for his assistance and guidance throughout the course of my Ph. D. I would also like to thank my secondary supervisor Dr Chrystelle Egger for her assistance throughout my Ph. D.

For their assistance with callose staining, I thank our friends in Greece Professor Panagiotis Apostolakos and Dr Pantelis Livanos. For their assistance with Micro-PIXE and LEXRF imaging, I thank Dr Paula Pongrac and Dr Katerina Vogel-Mikus. For his assistance with the hydroponic growth and PDMPO staining of developing rice seedlings, I thank William Mackveley. I am also grateful to Karen Walker for all her training and assistance with tissue fixation, microtome and SEM operation. For his assistance with TGA and FTIR, as well as his support throughout my time at Keele, I would also like to thank Dr Vladimir Zholobenko.

Personal Acknowledgements

I express my undying gratitude to my loving girlfriend Christina Hughes, who has supported me throughout my Ph.D. Thank you to my family for their support, I wouldn't have made it this far without their help. I would also like to thank everyone within the Aluminium and Silicon research group for their support and friendship. Good luck to you all with your own projects. And there is one more person I'd like to thank...and his name is John Cena.

Table of Contents

1. Introduction	1
1.1 Silicon Essentiality in Plants	1
1.2 Biosilicification	3
1.3 Silicon Uptake in Plants	3
1.4 Silicon Transporters	5
1.5 Sites of Silica Deposition	7
1.6 How is Silicification Initiated?	9
1.7 When Does Silicification Occur?	11
1.8 Benefits of Silicification	12
1.9 Aims and Objectives	14
2. Materials and Methods	16
2.1 Hydroponic Growth of Plants	16
2.1.1 Growth Trays	17
2.1.2 Growth Medium	18
2.1.3 Lighting	18
2.1.4 Nutrient Solution	18
2.1.5 Seed Germination	20
2.2. Microwave Acid Digestion & Filtration	20
2.2.1 Sample Preparation	21
2.2.2 Acid Digestion Procedure	21
2.2.3 Filtration	22
2.2.4 PDMPO Staining	23
2.3 Light & Fluorescence Microscopy	23
2.4 Graphite Furnace Atomic Absorption Spectrometry	24
2.5 Molybdenum Blue Assay	24
3. Micro-PIXE and LEXRF Imaging of Silicon and Aluminium in Rice Tissue	26
3.1 Introduction	26
3.2 Method	29
3.2.1 Hydroponic Growth	29

3.2.2 Cryofixation and Sectioning	30
3.2.2.1 Laboratory Materials	30
3.2.2.2 Cryofixation	31
3.2.2.3 Cryosectioning	33
3.2.2.4 Freeze-Drying	33
3.2.2.5 Sample Mounting	33
3.2.3 Micro-Particle-Induced X-Ray Emission	34
3.2.4 Low-Energy X-Ray Fluorescence	35
3.3.1 Micro-PIXE Imaging	37
3.3.1.1 Micro-PIXE Images of Rice Leaf Tissue – Control Group	37
3.3.1.2 Micro-PIXE Images of Rice Leaf Tissue – Silicon +	41
3.3.1.3 Micro-PIXE Images of Rice Leaf Tissue – Aluminium +	45
3.3.1.4 Micro-PIXE Images of Rice Leaf Tissue – Aluminium and Silicon +	49
3.3.1.5 Micro-PIXE Images of Rice Root Tissue – Control Group	53
3.3.1.6 Micro-PIXE Images of Rice Root Tissue – Silicon +	57
3.3.1.7 Micro-PIXE Images of Rice Root Tissue – Aluminium +	61
3.3.1.8 Micro-PIXE Images of Rice Root Tissue – Aluminium and Silicon +	65
3.3.2 Micro-PIXE Quantitative Data	70
3.3.2.1 Total Leaf Silicon Content	70
3.3.2.2 Total Leaf Aluminium Content	71
3.3.2.3 Leaf Silicon and Aluminium Comparison	72
3.3.2.4 Rice Root Silicon Content	73
3.3.2.5 Rice Root Aluminium Content	74
3.3.2.6 Root Silicon/Aluminium Comparison	75
3.3.3 LEXRF Imaging	76
3.3.3.1 Silicon + Leaf Tissue	76
3.3.3.2 Silicon/Aluminium + Group Leaf Tissue	81
3.4 Discussion	88
3.4.1. Micro-PIXE Image Analysis	88

3.4.1.1 Control Leaf: Grown in the Absence of Added Silicon or Aluminium	88
3.4.1.2 Silicon + Leaf: Grown in the Presence of Added Silicon	89
3.4.1.3 Aluminium + Leaf: Grown in the Presence of Added Aluminium	90
3.4.1.4 Aluminium/Silicon + Leaf: Grown in the Presence of Added Aluminium and Silicon	90
3.4.1.5 Control Root: Grown in the Absence of Added Aluminium or Silicon	92
3.4.1.6 Silicon + Root: Grown in the Presence of Added Silicon	92
3.4.1.7 Aluminium + Root: Grown in the Presence of Added Aluminium	93
3.4.1.8 Silicon/Aluminium + Root: Grown in the Presence of Added Aluminium and Silicon	94
3.4.2 Micro-PIXE Quantitative Analysis	95
3.4.3 LEXRF Image Analysis	97
3.4.4 General Discussion	98
4. Callose Detection in Rice Using Fluorescence Microscopy	102
4.1 Introduction	102
4.2 Method	105
4.2.1 Rice Plant Hydroponic Growth	105
4.2.2 Aniline Blue Staining Protocol	105
4.2.3 Immunofluorescence Protocol	106
4.2.4 Fluorescence Microscopy	110
4.3 Results	110
4.3.1 Aniline Blue Imaging	110
4.3.1.1 Autofluorescence of Rice Leaf Samples	110
4.3.1.2 Aniline Blue Stained Rice Leaf	113
4.3.2 Immunofluorescence Imaging Results	121
4.3.2.1 Autofluorescence of Rice leaf Tissue	122
4.3.2.2 Immunofluorescence Stained Rice Leaf Tissue	125
4.4 Discussion	140
4.4.1 Aniline Blue Autofluorescence	140

4.4.2 Immunofluorescence Autofluorescence	140
4.4.3 Callose Seen at Silica Cells in Both Aniline Blue and Immunofluorescence	141
4.4.4 Callose Seen at Papilla in Both Aniline Blue and Immunofluorescence	142
4.4.5 Callose Seen at Trichomes in Both Aniline Blue and Immunofluorescence	142
4.4.6 Callose Seen at Stomata in Both, Though Only in Young Tissue for Immunofluorescence	143
4.4.7 Callose Seen at Epidermal Cell Walls in Immunofluorescence	146
4.4.8 These Callose Locations are All Known Sites of Silica Deposition in Rice	147
5. Investigation into the Effects of Sample Preparation Procedure on Silica Morphology through SEM Imaging	148
5.1 Introduction	148
5.2 Method	151
5.2.1 Hydroponic Growth of Rice Samples	151
5.2.2 Wet Digest vs Dry Digest Preparation	151
5.2.3 Scanning Electron Microscopy	152
5.2.3.1 Sample Preparation	152
5.2.3.2 TM-3000 Tabletop SEM	152
5.2.3.3 S-45000 SEM	153
5.2.4 Thermogravimetric Analysis	153
5.2.5 Fourier Transform InfraRed (FTIR)	154
5.3 Results	154
5.3.1 TM3000 Tabletop Microscope	154
5.3.1.1 Wet-Digested Rice Leaf	154
5.3.1.2 Wet-Digested Rice Stem	160
5.3.1.3 Dry-Digested Rice Leaf	165
5.3.1.4 Dry-Digested Rice Stem	174
5.3.2 Hitachi S-4500 Scanning Electron Microscope	178
5.3.2.1 Wet-Digested Rice Leaf	179
5.3.2.2 Dry-Digested Leaf Tissue	188
5.3.3 Thermogravimetric Analysis	197
5.3.4 Fourier-Transformed Infrared Spectroscopy	198
5.4 Discussion	199

5.4.1 Comparison between TM3000 SEM and S-4500 SEM Images	199
5.4.2 TGA & FTIR	200
5.4.4 Differences between Silica Samples Obtained from Wet and Dry Digestion of Rice Tissue	201
6. Investigation into Silicic Acid Uptake in Rice	206
6.1 Introduction	206
6.2 Materials and Method	208
6.2.1 Oil Suitability Tests: Evaporation Prevention and Silicon Leaching	208
6.2.2 Transpiration Experiment	210
6.3 Results	212
6.3.1 Oil Suitability Tests: Evaporation Prevention	212
6.3.2 Oil Suitability Tests: Silicon Leaching	213
6.3.3 Oil Properties and Selection	213
6.3.4 Transpiration Experiment	214
6.4 Discussion	216
7. PDMPO Staining of Mature Rice Silica	220
7.1 Introduction	220
7.2 Method	222
7.2.1 Hydroponic Growth of Rice Plants	222
7.2.2 Acid Digestion and Filtration	222
7.2.3 PDMPO Staining	222
7.2.4 Fluorescence Microscopy	223
7.3 Results	223
7.3.1 Silicon Replete Rice	223
7.3.1.1 Epidermal Cells	223
7.3.1.2 Silica Cells	236
7.3.1.3 Bulliform Cells	241
7.3.1.4 Trichomes	243
7.3.1.5 Xylem	246
7.3.1.6 Silica Aggregation	249
7.3.2 Silicon Deplete Rice	250

7.3.3 Silicon and Aluminium Replete Rice	251
7.4 Discussion	258
7.4.1 Epidermal Cells and Stomata	258
7.4.2 Trichomes	259
7.4.3 Silica Cells	261
7.4.5 Bulliform Cells	261
7.4.6 Xylem	263
7.4.7 Conclusions	265
8. PDMPO Staining of Silica Structures in Rice through Development from Seed to Seedling	267
8.1 Introduction	267
8.2 Method	268
8.2.1 Plants Grown Hydroponically	268
8.2.2 Acid Digestion and Filtration	269
8.2.3 PDMPO Staining and Fluorescence Microscopy	269
8.3 Results	269
8.3.1 Un-germinated Rice Seeds	270
8.3.1.1 Summary	272
8.3.2 Germinated Rice Seeds with Radical	273
8.3.2.1 Summary	276
8.3.3 Germinated Seed with Radical and Shoot Apical Meristem	277
8.3.3.1 Summary	281
8.3.4 Rice Seedling – Second Leaf Stage	282
8.3.4.1 Summary	286
8.3.5 Rice Seedling – Third Leaf Stage	287
8.3.5.1 Summary	291
8.3.6 Rice Seedling – Fourth Leaf Stage	292
8.3.6.1 Summary	305
8.4 Discussion	306
9. Conclusions	314
9.1 Silicon and Aluminium Interactions	314
9.2 Silicification of Xylem	315

9.3 The Role of Callose in Silicification	317
9.4 Active or Passive Transport	320
9.5 Silicification of Developing and Motile Tissue	321
9.6 Final Word	324
10. Reference List	325

1. Introduction

1.1 Silicon Essentiality in Plants

Silicon is the second most abundant element in the Earth's crust, after oxygen, and is present in all soils in some quantity (Exley, 1998). When in solid form, silicon is almost always found as silica or a silicate in nature due to its high affinity for oxygen; silicon and oxygen, the two components of which silicates are comprised, account for 75% of the mass of the Earth's crust between them (Knight & Kinrade, 2001). Silicon is also found in the soil solution as monomeric silicic acid (H_4SiO_4) at varying concentrations, usually between 100 – 500 μM , and it is silicic acid which acts as silicon's main biologically available form (Sommer et al., 2006). The saturation point of silicic acid in water at a temperature of 25°C is 2 mM, with the polymerisation of silicic acid into amorphous hydrated silica occurring at concentrations which exceed this saturation point (Ma et al., 2002).

Despite the abundance of silicon in nature, especially the biologically available form of silicic acid, silicon is not considered to be an essential element for plant growth, though what the definition of essential should mean has led to contention in this area. The development of hydroponic culture in the 19th century led plant physiologists to discover that they could grow perfectly healthy plants without adding silicon into the growth medium (Epstein, 2009). This led to the rather logical conclusion that silicon is not a requirement for healthy plant growth and therefore silicon is not an essential element. The area of contention comes from the fact that whilst plants can be grown without silicon in artificial conditions, in their natural environments plants would not survive the barrage of abiotic and biotic stresses which assail them without the presence of silicon in their growth solution. The argument can most accurately be compared to the immune system in animals: under controlled conditions where viruses, bacteria and other pathogens could be prevented from contacting the vulnerable animal, it could survive perfectly healthily. However, in any real-world situation an animal without an immune system will very quickly fall ill and die.

However, the classical definition of a plant essential element states that an element is essential if: a deficiency of said element makes it impossible for the plant to complete its life cycle, and if that effect is not due to the amelioration of unfavourable chemical or microbiological conditions by the element, but rather that element must be involved in the direct nutrition of the plant (Arnon & Stout, 1939). This rather rigid definition of essentiality provides a clear point on where to draw the line between essential and non-essential elements, however, difficulties arise in practical application of this theory. Silicon is considered to be a universal contaminant, present in dust, nutrient salts which are used to make up hydroponic growth solutions and water (even distilled) and therefore despite the best efforts of researchers to remove it from growth solutions, a nutrient solution can only ever be said to be absent of added silicon, not absent of silicon altogether (Epstein, 1994). Monomeric silicic acid is a small, neutral molecule which acts as an analogue of water in its behaviour and as such it is nigh impossible to remove silicic acid completely from any system which also contains water (Exley, 2009b). As a result, it is equally difficult to state with certainty that silicon is not essential for a plant, when in reality that plant cannot be grown in the true absence of silicon.

Rather than argue over the semantics of the definition of the word essential, it was suggested that silicon be termed a 'quasi-essential element' to some plants, given that it fits the criteria for essentiality in some but not all plants (Epstein, 1999). However, even Epstein's definition of silicon as a quasi-essential element can be argued with, given that the plants thought to require silicon to live, even in hydroponic conditions, have been shown to survive without its presence in the growth medium (Law & Exley, 2011).

Horsetail (*Equisetum arvense*) is one of the best known silicifiers in the plant kingdom and it was considered for some time to be one of the few plants which actually required silicon for healthy growth (Currie & Perry, 2007). In support of this supposition, it was shown that when grown hydroponically in the absence of silicon, horsetail suffered various symptoms of silicon deficiency,

including necrosis, wilting and drooping of the branches (Chen & Lewin, 1969). However, a more recent study found that whilst horsetail grown in the absence of silicon did indeed show those symptoms, they found that these symptoms occurred exclusively in areas of the plant which also showed evidence of powdery mildew infection, suggesting these were symptoms of the infection and not silicon deficiency (Law & Exley, 2011). It was also noted that there was no sign of fungal infection in horsetail grown in the presence of silicic acid under the same conditions.

Despite its definition as a non-essential element in plant growth, silicon is found in almost all plants, with concentrations varying from a fraction of 1% up to 10% of a plant's dry weight. Even at the low end of this scale, 0.1% silicon dry weight, silicon is in line with the concentrations of other essential macronutrients such as P, S, Ca and Mg, whilst at the highest concentrations of 10% dry weight silicon exceeds the levels of K and N (Epstein, 1994).

1.2 Biosilicification

All plants which grow in soil contain significant amounts of silicon in one form or another, regardless of whether they are considered silicon accumulators or not (Ma & Takahashi, 2002). Those plants which do accumulate silica are known as biosilicifiers. Biosilicification was recently described as *'the movement of silicic acid from environments in which its concentration does not exceed its solubility (< 2 mM) to intracellular or systemic compartments in which it is accumulated for subsequent deposition as amorphous hydrated silica'* (Exley, 2009b). In essence, this means that for a plant to be classified as a biosilicifier, it must be capable of creating a saturated solution of silicic acid internally from an under-saturated external solution.

1.3 Silicon Uptake in Plants

Whilst the mechanisms and concentrations of silicon that various plant species take up may be different, what is known is that all plants take up silicon in the form of silicic acid from the soil into their roots. Once inside the plant, silicic acid is transported to the xylem, where it follows the

transpiration stream up to the stem and leaves, where it is then deposited as amorphous biogenic silica (Yoshida, 1965).

It was proposed that there are three different silicic acid uptake methods which plants can employ – active, passive or rejective – and that which of these uptake methods it uses determines whether a plant is classified as a silicon accumulator or not (Takahashi et al., 1990). Active uptake of silicic acid is the movement of silicic acid through metabolic, energy-dependent processes against the concentration gradient; an active uptaker of silicic acid would fit Exley's definition of a biosilicifier in that it can accumulate silicic acid from an under-saturated external solution. Passive uptake is the diffusion of silicic acid across the lipid component of cell membranes from an area of high concentration on one side of the membrane to an area of low concentration on the opposite side (Raven, 2001). Conventional wisdom states that passive uptake of silicic acid would not usually allow for the accumulation of a sufficiently concentrated silicic acid solution within the plant to allow for polymerisation into silica; once the internal and external solutions reached equilibrium then silicon uptake would cease. This would rule out passive uptakers as biosilicifiers, however, as will be discussed later, this is not necessarily the case. The final uptake method, rejective, requires that the plant limits the uptake of silicic acid, resulting in a lower concentration of silicic acid inside the plant when compared with the external solution.

In my opinion, the case for rejective uptake seems to be built upon a weak foundation. Tomato plants were grown in the presence of silicic acid for 37 hours, with xylem sap collections occurring at multiple intervals during this period, including at the experiment start (Okuda & Takahashi, 1962). At the beginning of the experiment, the silicon concentration in the tomato xylem sap was found to be lower than the initial concentration of the growth solution, but as time progressed the xylem sap's silicic acid concentration rose to around the same level as the external solution. Given that the silicon concentration within the xylem eventually reached that of the external medium, it would seem that rejective uptake is simply slower passive uptake, likely caused by the

difference in permeability of membranes in tomato and barley roots (the passive transporter discovered in the same study) to silicic acid.

Active transport of silicic acid is considered to be the most likely method by which plants accumulate silicic acid, however, the active transport of silicic acid would require the presence of silicon transport molecules. One research group in particular, led by Jian Feng Ma, has driven the search for silicon transporters in rice and discovered several potential candidates.

1.4 Silicon Transporters

Within the roots there are two processes which must occur either by active or passive transport: the transport of silicon from the soil solution through the meristem and into the cortex of the roots and secondly the transport of silicon from the cortex into the xylem (Mitani et al., 2005). A potentially silicon-deficient rice mutant strain dubbed GR1 was identified using germanium screening (Ma et al., 2002). Germanium is a cognate element of silicon with similar properties to silicon, however, germanium is toxic to rice and therefore any seed found to be resistant to germanium could potentially also exclude silicon. The mutant was then compared to the wild-type in a silicon uptake experiment where it was found that the mutant did indeed possess a significantly reduced capacity to uptake silicic acid.

Using gene mapping and sequencing to compare the silicon deficient mutant with the wild-type, researchers were able to identify the mutation; a single amino acid change from alanine in the wild-type to threonine in the mutant (Ma et al., 2006). By analysing this gene in the wild-type, it was determined that the gene, named low silicon 1 (Lsi1), belongs to the aquaporin family of transport proteins. Aquaporins are a family of membrane proteins that play a central role in water balance and transport between cells (Nyugen et al., 2013). Lsi1 was found to be primarily expressed in the roots, more specifically at the plasma membrane of the distal side of both the exodermis and endodermis cells, where the casparian strip is located (Ma et al., 2006).

Interestingly, Lsi1 was expressed only in the main and lateral roots, but not in the root hairs –

these findings are in keeping with earlier research, which shows that the lateral roots contribute to silicon uptake, but the root hairs do not (Ma et al., 2001b). Finally, it was shown that Lsi1 suppression in the wild-type using RNA interference led to a reduction in silicic acid uptake whilst not affecting water transport, which suggests that Lsi1 is a transporter specific to silicic acid (Ma et al., 2006). Unfortunately, the data on water transport was not shown and given that silicic acid is a behavioural analogue of water and can be transported through almost any membrane that water can, it seems strange that the same would not be true in reverse; that water would be unable to pass through a silicic acid transport channel (Exley, 1998). Aquaporins have been found that are only slightly permeable to water, whilst allowing other substances such as anions or urea through them, but these substances do not share the level of similarity that water and silicic acid do (Lui et al., 2005).

Lsi1 was an influx transporter of silicic acid, purportedly bringing silicic acid into the roots from the external solutions and it was the first silicon transporter identified in any plant. Soon after, a second silicic transporter was identified in rice, this time an efflux transporter (Ma et al., 2007). The newly identified gene, named low silicon 2 (Lsi2), was found to be a putative anion transporter with no similarities to Lsi1. Despite this, Lsi2 was also found to be localised in the roots, only this time at the plasma membrane of the proximal side of both the exodermis and endodermis cells, rather than the distal side. It was suggested that Lsi1 and Lsi2 work together to form a unique mechanism of nutrient transport in plants, with an influx transporter at one side of a cell and an efflux transporter on the other side, pulling silicic acid in at its distal side and expelling it at its proximal side. A gene similar to Lsi2 was identified in *Escherichia coli* which codes for an efflux transporter of arsenic and antimony (Meng et al., 2004). The role of both Lsi1 and Lsi2 in arsenite uptake were later investigated, where it was discovered that both transport proteins were also capable of transporting arsenite, showing that neither of them was a specific transporter for silicic acid (Ma et al., 2008).

Using Lsi1 as a starting point, a search of similar genes led to the discovery of a close homologue of Lsi1 called Lsi6 (Yamaji et al., 2008). Unlike Lsi1 and Lsi2 which were expressed in the roots, Lsi6 was found to be expressed in the shoot. Lsi6 was once again a gene which coded for a transport protein in the aquaporin family. Localisation of Lsi6 revealed that it was primarily expressed in the xylem parenchyma cells of the leaf sheath and blade, with a polar localisation towards the side of the cells facing the xylem vessel itself. The removal of the Lsi6 gene via T-DNA knockdown had no effect on the uptake of silicon from the growth medium, but it did cause significant changes in the pattern of silica deposition seen in the shoots, with much more silicon being exuded in the guttation fluid when compared with the wild-type. These results suggested that Lsi6 transports silicic acid from within the xylem outwards towards sites of silica deposition in the leaf and stem. Following up this research on Lsi6, it was revealed that Lsi6 is also responsible for the intervascular transport of silicon, transporting it from the large vascular bundles into the diffuse vascular bundles which connect with the panicles (Yamaji et al., 2009).

It is my opinion that there is significant work to be done in this area before it can be declared that silicic acid transport is an active process in rice, though the work performed by Jian Feng Ma and his research group does offer exciting results in this field. There is a lack of evidence for the specificity of these transport proteins with regards to silicon, specifically with regards to water; aquaporins are primarily transporters of water and silicic acid is a known analogue of water which renders it much more likely that these silicon transporters are, in fact, just water channels that also allow certain uncharged molecules like silicic acid through.

1.5 Sites of Silica Deposition

Leaving the matter of how silicon is transported behind, the sites of silica deposition are of equal importance when considering the process of biosilicification. Different plant species have different patterns and structures formed by the process of silica deposition, but the locations of silicification are fairly consistent.

The primary site of silica deposition in rice, and indeed almost all silicifiers, is at the leaves, beneath the cuticle but above the epidermal cells where silica forms a roughly 2.5 µm thick layer over the surface of the leaf (Yoshida, 1965). This epidermal layer of silica makes up the vast majority of the silica found in plant tissues, however, there are other notable areas of deposition. Silica has also been shown to accumulate in the cell walls of guard cells at rice stomata, with silica deposition found at every wall except the anticlinal walls adjacent to the subsidiary cells (Ueno & Agarie, 2005).

Other sites of heavy silicification are at the silica cells and bulliform cells, both of which are completely silicified, unlike the epidermis which is just covered by a surface layer of silica (Ma, 1990). Silica cells are heavily silicified, hence their name, and are found in an alternating formation with cork cells to form ladder-like structures which cover the veins of rice leaves above the vascular bundles. Research has shown that these structures provide the leaf with structural support, preventing twisting torsions of the leaf (Yamanaka et al., 2009). Trichomes, the spine-like structures which occupy the epidermal regions of many grass leaves, including rice, are also known areas of silicification (Kaufman et al., 1985). These hair-like protrusions have been ascribed many potential functions, including temperature regulation and defence against herbivory. It was even suggested that silicified trichomes might play a role in enhancing the photosynthetic abilities of a plant by acting as windows, allowing light to pass through them to the photosynthetic cells, though this theory has since been disproven (Agarie et al., 1996).

Similar patterns of silica deposition have been found in another well-known biosilicifier, the living fossil horsetail. The genus *Equisetum* is the only surviving genus from the entire *Equisetopsida* class. Scanning and transmission electron microscopy have been used to show the morphology and ultrastructure of silica deposits in the cell walls of *Equisetum arvense* (Perry & Fraser, 1991). Papilla, small nodules of silica, were located on the surface of silica from all areas. With the exception of these papilla, which do not appear to represent any structural body on the plant

tissue, it was concluded that the silica acted as an *in vivo* stain, replicating the organic matrix at both macro and microscopic scales.

Recent work from within our own research group has shown a new method of observing these silica structures in horsetail (Law & Exley, 2011). The plant tissue was acid-digested in a microwave and the silica remains were then stained using a specific silica stain called 2-(4-pyridyl)-5-((4-(2-dimethylaminoethylaminocarbonyl)methoxy)phenyl)oxazole (PDMPO), allowing them to be viewed under a fluorescent microscope. Silica was found to be present in all regions of the plant and many specific structures were shown to be silicified, including cell walls, cell plates, papilla, plasmodesmata and stomata.

1.6 How is Silicification Initiated?

Whilst the areas in which silicification occurs are well studied, how that process actually occurs at these sites remains a mystery. The commonly held assumption is that silicic acid accumulates in these regions until it reaches a 2 mM concentration, the level of saturation required for the auto-condensation of silicic acid into silica. Silicic acid is transported along with water through the transpiration stream and when it reaches its terminus at the surface of the leaves, water will evaporate away, increasing the concentration past the point of saturation at which point silica forms. Whilst this is a logical assumption to make, it does not explain why certain cells are silicified more heavily than others, such as the silica and bulliform cells which are completely silicified, unlike the epidermal cells which merely have a layer of silica covering their outer surface (Ma, 1990).

It has been shown that silica does not merely deposit at the surface of cellular structures, but is actually incorporated into the cell walls of some silicified cells, both at the leaf epidermis in horsetail and at the stomatal guard cells in rice (Perry & Fraser, 1991; Ueno & Agarie, 2005). It is entirely possible that organic compounds involved in cell wall formation are capable of templating silica deposition in developing cells.

In a recent study into horsetails, it was suggested that a hemicellulose called mixed-linkage (1→3, 1→4)-β-D-glucan (MLG) could act as a template for silica deposition in multiple *Equisetum* species (Fry et al., 2009). Hemicelluloses are polysaccharides found in plant cell walls that serve multiple roles, the most important of which is considered to be the strengthening of cell walls via binding with cellulose and lignin. Hemicelluloses come in several variations including xyloglucans, xylans, mannans and glucomannans, and β-(1→3, 1→4)-glucans (Scheller & Ulvskov, 2010). Interestingly, β-(1→3, 1→4)-glucans were until recently believed to be isolated to a limited section of the plant kingdom; the Poales, an order of plants which includes grasses. However, Fry has shown that this variation of hemicelluloses is also present in horsetail, an evolutionarily isolated genus of plants. The vast majority of known biosilicifiers and certainly the most extensive biosilicifiers by dry weight (horsetail and rice) fall into these two categories.

The link between β-(1→3, 1→4)-glucans and silica deposition was investigated further in horsetails, where it was found that in *Equisetum arvense* silica deposition at the stomata exactly mirrored known locations of callose deposition (Figure 1.1). Horsetail samples were acid digested, stained with a silica specific fluorophore called PDMPO and observed using fluorescence microscopy.

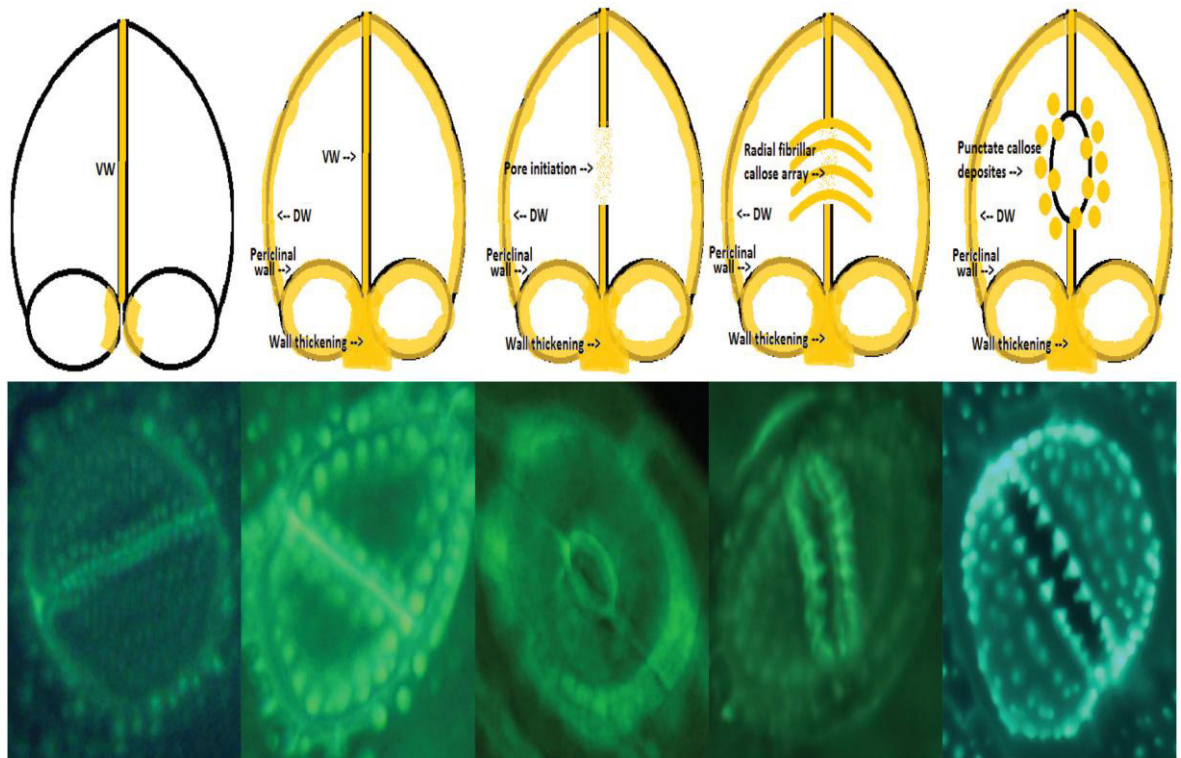


Figure 1.1 Comparison between known regions of callose deposition in horsetail (*Equisetum arvense*) stomata (Top) and PDMPO stained silica deposits obtained from the acid digestion of horsetail tissue samples (Bottom) (Law & Exley, 2011).

Callose is a hemicellulose in the form of β -1,3-glucan with some β -1,6-branches which is found in numerous areas throughout many plant tissues, including the cell walls and plasmodesmata (Chen & Kim, 2009). The co-localisation of callose and silica in horsetail has provided a solid foundation upon which further research into the links between hemicelluloses and silica deposition can be built (Law & Exley, 2011).

1.7 When Does Silicification Occur?

Whilst there is a significant knowledge base on the sites of silicification in plants, much less is known about when the process of silicification occurs in developing plants. Several studies have analysed the silica structures found in the early stages of seedling growth in other species of grass including wheat (*Triticum aestivum*) and crab grass (*Digitaria anguinalis*), but silicification in developing rice seedlings remains a neglected area of study (Blackman, 1969; Sangster, 1977). These studies came to the same general conclusion, that silicification does not occur until at least the second week of seedling growth.

Whilst studying the silicification of rice under varying concentrations of silicic acid, it was found that silica cells were silicified in rice plants with silica concentrations below 5% weight, whilst bulliform cells were only silicified above 5% weight (Ma et al., 2001b). From this observation, it was proposed that silicification occurs at the silica cells at an earlier stage of rice development, before progressing from the silica cells to the bulliform cells.

Further study into the early silicification of rice tissue could yield new insight into the biosilicification process, especially when the possible links between callose deposition and silica localisation are considered. As stated previously, callose is a transient molecule that binds with cellulose during cell wall formation. As a result of this, callose is most commonly found in younger, developing tissues where significant growth is still taking place; almost all studies into callose localisation take place in young seedlings for this reason (Yim & Bradford, 1998; Apostolakos et al., 2009).

1.8 Benefits of Silicification

Despite its relegation to the leagues of a non-essential element in plant nutrition, the benefits of silicon for numerous plant species include stimulation of photosynthesis, structural support, defence against pathogens and herbivory, drought resistance and amelioration of metal toxicity (Ma & Takahashi, 2002).

The silica layer at the epidermis has been shown to reduce the mechanical breakdown of leaf tissue in grasses by herbivorous locusts (Hunt et al., 2008). Many silicifying plants also incorporate the substance into their array of defensive structures such as spines, thorns, trichomes and raphides, all of which can be constructed partially or completely out of silicon (Epstein, 2009). In addition to the mechanical benefits, silicon can also enhance some plant chemical defences against biological stresses. For example, work has shown that whilst silicon fails to accumulate at fungal infection sites, its presence still increases cucumber's resistance to infection (Cherif et al., 1992). Further research into these findings suggested that silicon enhanced the cucumber's

defence mechanisms, which in turn increased the activity of chitinases, peroxidases and polyphenoloxydases (Cherif et al., 1994). Additional evidence for the enhancement of chemical defences of plants against fungal attacks has been shown in cucumber (Fawe et al., 1998), wheat (Bélanger et al., 2003) and rice (Rodrigues et al., 2003).

In addition to the benefits afforded to silicified plants against biotic stress, many abiotic factors can be alleviated by silicon's presence in the growth medium and/or the plant itself. Using scanning electron microscopy (SEM), ladder-like silica structures were identified in the epidermal region of rice leaves, the purpose of which were found to be mechanical and structural support (Yamanaka et al., 2009). Their findings suggested that the ladder-like structures prevented the leaf from undergoing twisting torsions due to wind or gravity, maximising the leaf's exposure to sunlight for photosynthesis.

Given the background and expertise of our research group with regards to aluminium, the relationship between aluminium and silicon is of great interest. Aluminium toxicity is a major problem in acidic soils, as it is under these conditions that it is solubilised into $Al(H_2O)_6^{3+}$ which is toxic to plants (Matsumoto, 2000). Aluminium exposure has been shown to inhibit root elongation and cause radial swelling of the roots in barley (Zelinová et al., 2011). Aluminium toxicity has a range of other symptoms which include disruption of calcium transport (Huang et al., 1992), decreased stomata and root hair frequency (Singh et al., 2011), a reduction in photosynthetic rate and decreased protein synthesis (Roy et al., 1988).

Despite the toxic effects of aluminium on plant development, the presence of silicon in growth solutions has been shown to ameliorate this toxicity. Addition of silicon to the growth solution of rice was shown to reduce aluminium-induced root growth inhibition (Rahman et al., 1998).

The relationship between silicon and aluminium was investigated in the leaves and stem of *Faramaea marginat*, where it was suggested that the formation of inert, silicon-aluminium complexes in the shoot and leaves were responsible for the alleviation of aluminium toxicity

(Britez et al., 2002). Silicon can also help to ameliorate aluminium toxicity outside the plant. A study into the toxic effects of aluminium in soybeans found that the presence of silicon caused the precipitation of hydroxyaluminosilicates, which in turn led to a reduction in available phytotoxic aluminium in the growth solution (Baylis et al., 1994).

An interesting note into aluminium toxicity: aluminium has been shown to induce callose formation in the root apices of several plants including soybean (Wissemeier et al., 1987), tobacco (Chang et al., 1999) and maize (Eticha et al., 2004). Callose itself has been shown to induce silica formation in undersaturated silicic acid solutions (Law & Exley, 2011) and the formation of silicon-aluminium complexes has been implicated as a method by which plants alleviate aluminium toxicity (Baylis et al., 1994). The possible links between callose, silicon and aluminium are an area of study which requires further investigation.

1.9 Aims and Objectives

The aims of this research project were to further knowledge in the field of biosilification in plants, with rice (*Oryza sativa*) serving as the model plant. More specifically, several areas where a gap in the knowledge base was noted were identified and a series of objectives were devised:

- To map silica deposition in mature rice plants using complementary imaging methods to provide a comprehensive understanding of where silica is deposited.
- To map the deposition of callose in rice tissue and compare this data with known locations of silica deposition to determine if there is co-localisation between these two substances.
- To study the silicification process in developing rice seedlings to better understand how and when the process occurs.
- To determine if silicic acid uptake in rice could be the result of a passive transport process, or if the level of silicification observed would require active uptake.

- To determine if the amelioration of aluminium toxicity in rice is part achieved by the co-deposition of silicon and aluminium in silica structures, such as hydroxyaluminosilicates.

2. Materials and Methods

This sections lists general methodologies which were used on multiple occasions throughout this doctoral research project. For specifics relating to individual experiments, see the relevant chapter's method section.

2.1 Hydroponic Growth of Plants

A simple hydroponic setup was used to grow plants inside the laboratory (Fig 1.1 & Fig 1.2). A plastic tray containing nutrient solution and a sheet of plastic netting which acts as an anchor point for plant roots were used. Above this a fluorescent light was suspended by a metal frame.

Germinated rice seeds were placed upon the plastic netting which floated on top of the surface of the nutrient solution. As the plants grew, their roots would grow down through the netting into the solution, providing them an anchor point and preventing the plant from falling over. The nutrient solution was changed at regular intervals to refresh nutrients and oxygen supply to the roots.

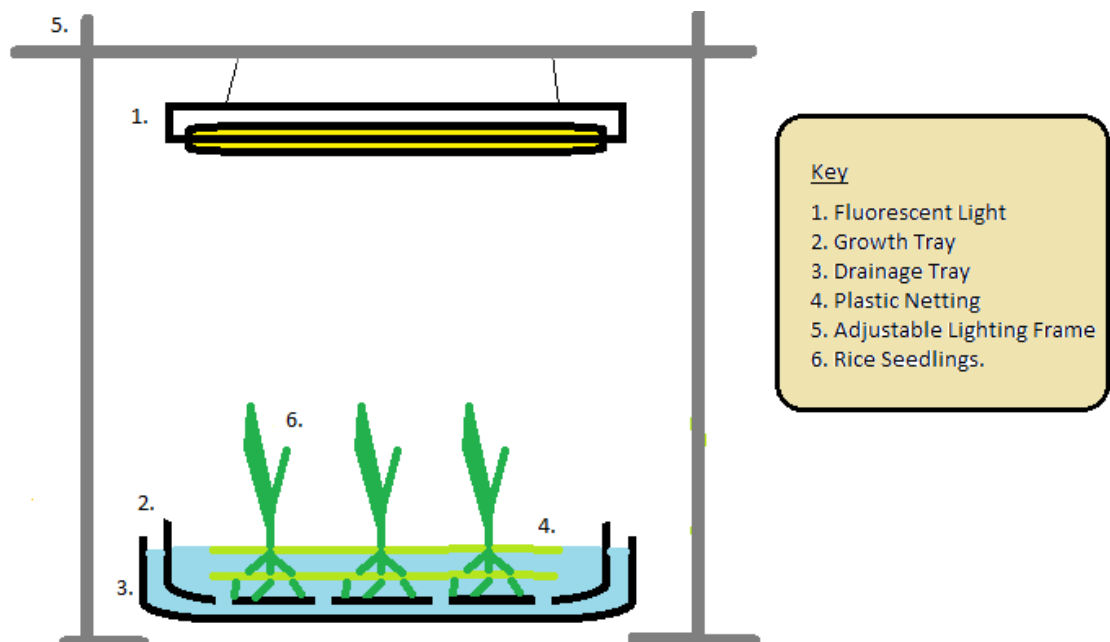


Figure 1.1 Diagram displaying the hydroponic growth setup used for culture of rice.



Figure 1.2 Photograph displaying rice growing in a hydroponic growth tank..

This section provides an overview of the materials and methods used in hydroponic culture, for specifics on experimental procedures, see the relevant experimental chapters.

2.1.1 Growth Trays

Black plastic trays were used as growth trays; several sizes of plastic tray were used depending on the scale of the experiment. The larger trays were 38 cm long, 24 cm wide and 6.5 cm deep. The smaller trays were 22 cm long, 16 cm wide and 5.5 cm deep.

Trays were stored in large plastic bins filled with 5% HCl when not in use. Before use, trays were sterilised with a 4% sodium hypochlorite solution. Trays were then rinsed thoroughly three times with ultrapure water before use.

2.1.2 Growth Medium

To give the plants an anchor point within the trays, a sheet of plastic netting was placed within each growth tray. The netting had 3 mm x 1.5 mm holes which allowed roots to grow through without letting seeds fall through. The netting was supplied in large rolls from which sections were cut. For large trays, a section of 37 cm x 23 cm was used. For the small trays, a section of 21 cm x 15 cm was used.

2.1.3 Lighting:

A Maxibright T5 2' 4-way grow light was used as a light source for growing plants. The grow light measures 59 cm long by 37 cm wide and houses four 24 W fluorescent lighting tubes. The bulbs used were the standard 6500 K blue fluorescent tubes supplied with the lamp, each delivering 4,450 lumens of light.

The grow light was held in place by a support frame built using clamp stands. The frame was constructed using four support pillars and a central beam which held the light. The central beam could be raised and lowered to adjust the distance between the light and the plants as required.

2.1.4 Nutrient Solution:

The nutrient solution used for plant growth is Murashige and Skoog basal salt mixture (Sigma Aldrich M5524). Murashige and Skoog is supplied as a powder which is dissolved into ultrapure water to make up the growth solution. The nutrient contents of the Murashige and Skoog mixture are listed in Table 1.

Component	Amount (mg/L)	Amount in 1/5th Strength Solution
Ammonium nitrate	1650	330
Boric acid	6.2	1.24
Calcium chloride anhydrous	332.2	66.44
Cobalt chloride • 6H ₂ O	0.025	0.005
Cupric sulfate • 5H ₂ O	0.025	0.005
Na ₂ -EDTA	37.26	7.452
Ferrous sulfate • 7H ₂ O	27.8	5.56
Magnesium sulphate	180.7	36.14
Manganese sulfate • H ₂ O	16.9	3.38
Molybdic acid (sodium salt) • 2H ₂ O	0.25	0.05
Potassium iodide	0.83	0.166
Potassium nitrate	1900	380
Potassium phosphate monobasic	170	34
Zinc sulfate • 7H ₂ O	8.6	1.72

Table 1: Table showing contents of Murashige & Skoog nutrient solution.

Murashige and Skoog Basal salt mixture is formulated to contain 4.3 g of mixture per litre of water, which provides a full strength solution. As shown in previous work, a full strength solution is not required for healthy plant growth (Law & Exley, 2011). Unless otherwise stated, a 1/5th strength solution was used for hydroponic plant growth, which contains 0.86 g of Murashige and Skoog salt mixture per litre of ultrapure water.

Two variants of nutrient solution were used, a silicon plus solution and silicon minus. Silicon was added to the silicon plus solution in the form of sodium orthosilicate (Alfa Aesar) which would form silicic acid once dissolved into solution. To create a 1 mM silicic acid solution, 0.184 g of sodium orthosilicate was added to 1 litre of Murashige and Skoog solution.

In order to balance the levels of sodium between the silicon plus and minus solutions, 0.16 g sodium hydroxide was added to silicon minus solutions. The pH of the solutions was adjusted to pH 6 through the addition of analytical reagent grade nitric acid (Fisher Scientific).

To replenish available nutrients and maintain a healthy oxygen supply to the plants' roots, nutrient solutions were replaced every four days. The plants and plastic netting were carefully lifted out of the tray and rinsed with ultrapure water. The old solution was poured away and the tray was rinsed thoroughly three times with ultrapure water. The plants and plastic netting were then placed back in the tray and the new solution was poured in.

2.1.5 Seed Germination:

Rice seeds (*Oryza Sativa Koshihikari*) were germinated in 90 mm diameter petri dishes. Each Petri dish was lined with a VWR 90mm diameter filter paper, which was trimmed down in size with scissors to fit inside the dish. Into each dish, 5 mL of ultrapure water was added to dampen the filter papers. Approximately 30 seeds were then placed into each Petri dish and a second damp VWR 90 mm diameter filter paper was placed over the top of the seeds. The dishes were covered with lids and placed in the dark at room temperature for one week, or until the seeds showed signs of germination via root formation.

2.2. Microwave Acid Digestion & Filtration

In order to view silica deposits from within a plant, free from interference from the plant tissue itself, it was necessary to remove the living tissue whilst leaving the silica deposits intact. This was achieved through microwave acid digestion.

During acid digestion, the sample was exposed to a cocktail of highly corrosive mineral acids within a sealed container. These containers were then subjected to a microwave digestion program which breaks down the sample matrix leaving behind its component elements in solution. It has been previously demonstrated that although this procedure successfully digests all organic plant tissue, the inorganic silica structures from within the plant are left intact (Law & Exley, 2011).

2.2.1 Sample Preparation

Prior to the acid digest procedure, plants were cleaned with ultrapure water to remove any impurities from their growth environment, such as nutrient solution remaining on the roots. Plants were then placed into weighing boats and weighed using weighing scales, to record their wet weight. At this point samples were cut into roughly 1 cm sections and, if applicable separated into groupings (leaf, stem and root for example).

Once weighed and cut, plant samples were then dried in an incubator at 37°C until they reached a steady dry weight. This process usually took several days, but the length of time varied between samples depending on their mass and water content. Once the tissue samples had reached a constant weight, they were weighed once again to record their dry weight. Tissue samples were now ready for acid digestion

2.2.2 Acid Digestion Procedure

To ensure a complete digestion of the plant material, up to, but no more than 0.5 g of plant tissue was placed into each 20 mL PFA Teflon© digest vessel. Using a Gilson PIPETMAN Classic P1000 pipette, 1 mL HNO₃ (70%) and 1ml H₂SO₄ (95%) were added to each digest vessel. Each digest vessel was then covered with a pressure cap and the lids were screwed on tightly by hand. The digest tubes were then sealed and placed within an insulating carousel capable of holding up to 40 digest tubes at one time. The carousel was then placed inside the microwave.

The microwave used was a Microwave Accelerated Reaction System, Model MARS, which is designed for digesting, dissolving, hydrolysing, extracting or drying materials. Its primary purpose is the digestion of materials in preparation for analysis by atomic absorption. The MARS uses microwave energy to heat samples. Samples are placed within sealed vessels with a polar liquid, usually an acid, and placed within the MARS where they are subjected to rapid heating and pressure increase, which results in the digestion of the sample within a short period of time (MARS operating manual, 2006). The samples were then run through the Basic – Xpress program. Samples tubes inside the microwave are heated to 180°C over the course of 15 minutes and then maintained at 180°C for a further 30 minutes. The sample tubes were then left for one hour before handling as they retain a significant level of heat and pressure after this process.

2.2.3 Filtration

Sample tubes were opened slowly, to gently release the pressure built up within them. Each tube was diluted with 8 mL of ultrapure water and filtered through a 0.45 µM Whatman filter paper using a pressurised filtration system. Each digest tube was given several further rinses of ultrapure water, all of which were flushed through the filtration system to ensure that all of the sample was removed from the digest tube and to dilute the acid within the filtration system.

2.2.4 PDMPO Staining

Wet filter papers covered with the harvested silica residue were placed inside plastic Petri dishes and stored in an incubator at 37°C until dried. Once dried the filter papers were soaked with 3 mL of 20 mM PIPES buffer solution at pH 7 for approximately 5 seconds. The solution of PIPES and suspended silica was then transferred into a 5 mL plastic Bijoux tube. 0.125 µM PDMPO was added to the buffer solution containing the silica residue. The Bijoux tubes containing the samples were then stored at room temperature for 24 hours in the dark to allow the binding reaction between PDMPO and silica to occur. Samples were then ready for analysis under fluorescence microscope.

2.3 Light & Fluorescence Microscopy

Unless otherwise stated, all light and fluorescence microscope images were taken using Olympus BX50 microscope. Fluorescence imaging was achieved using a BX-FLA reflected light fluorescence attachment, equipped with a mercury burner and a vertical illuminator. The microscope was fitted with 4x, 10x, 20x and 40x objectives, along with a 100x Oil Immersion objective. Images from the microscope were taken with an SIS Colorview III camera and captured using the CELL D imaging software.

The filter cubes attached to the microscope for fluorescence microscopy included a U-MNIB3 filter cube (Excitation Filter: 470-490 nm; Dichroic Mirror 505 nm; Barrier Filter: 515IF--), a U-MWBV filter cube (Excitation Filter: 400-440 nm; Dichroic Mirror: 455 nm; Barrier Filter: 475--), and a U-MWU filter cube (Excitation Filter: 330-385 nm; Dichroic Mirror: 400 nm; Barrier Filter: 420--). For PDMPO fluorescence imaging the U-MWU filter cube was used.

Aqueous samples were mounted onto cavity slides (76 mm x 26 mm, 15 mm cavity). Solid samples were mounted onto Thermo Scientific Superfrost glass slides (76 mm x 26 mm). In both cases, thin glass cover slips (18 mm x 18 mm) were used to cover the samples. Glass slides and cover slips were cleaned with lint-free tissues before use, and slides were disposed of after use.

2.4 Graphite Furnace Atomic Absorption Spectrometry

Graphite furnace atomic absorption spectrometry (GFAAS) is a method of measuring the concentration of elements, such as silicon, within a solution. GFAAS was performed at using an atomic absorption spectrometer (AAS) with a transversely heated graphite atomizer (THGA) and longitudinal Zeeman-effect background corrector. The THGA AAS was also equipped with an AS-800 auto-sampler. THGA AAS was operated using the WinLab32 operating software.

A 300 µg/L silicon standard solution was carefully prepared in 1% nitric acid (HNO₃) inside a 25 mL volumetric flask. 2 mL of the silicon standard solution was added to a 2.5 mL sample pot and

inserted into the THGA AAS, using the auto-sampler tray. The THGA AAS used this standard to prepare the further 200 µg/L, 100 µg/L and 50 µg/L standards to form a calibration curve.

With the standard curve prepared, samples could be analysed. Aqueous samples were acidified to 1% using nitric acid to bring them in line with the standards. A 1% HNO₃ blank was used as the background for readings. If samples were expected to have a silicon concentration above the highest standard of 300 µg/L, they would require dilution with 1% HNO₃ to bring them down below the threshold. Samples were then placed into sample pots and loaded into the auto-loader, whereupon a pre-set program for silicon detection was run.

2.5 Molybdenum Blue Assay

The molybdenum blue assay is a method of determining the silicic acid concentration of a solution. It comprises of several chemical reactions which result in colour changes within a solution, which can be analysed by UV-VIS spectroscopy. A sample containing silicic acid is combined with ammonium molybdate, to produce a yellow complex (SiMo₁₂O₄₀³⁻).

The yellow complex is then reduced by ascorbic acid to form the blue coloured complex (SiMo₁₂O₄₀⁷⁻). The amount of this blue coloured complex produced can be used to determine the amount of silicic acid present. The absorption can be measured using a UV-VIS Spectrometer, reading at 700 nm, to determine the concentration of silicic acid. By comparing the reading against prepared stock solutions with known concentrations of silicic acid, the concentration of the samples can be determined.

Molybdenum Blue Assay Procedure:

- Add 2.5 mL of each sample to be measured to a 7 mL Bijoux.
- Add 0.5 mL hydrochloric acid (HCl) (1M) to each tube.
- Add 0.25 mL ammonium molybdate (10% solution in ultrapure water) to each tube.
- Stand the sample tubes in the dark for 12 minutes.

- Add 1 mL sulphuric acid (H_2SO_4) (25% solution in ultrapure water) to each tube.
- Add 100 μL of freshly-made Ascorbic Acid (10% solution in ultrapure water) to each tube.
- Stand the sample tubes in the dark for one hour.
- Add 0.65 μL ultrapure water to each sample tube.
- Measure the absorption using UV-VIS reading at 700 nm.

3. Micro-PIXE and LEXRF Imaging of Silicon and Aluminium in Rice Tissue

3.1 Introduction

Silicon is the second most abundant element in the Earth's crust, not only in terms of pure weight but also in the number of atoms present (Ma & Takahashi, 2002). Despite this ubiquity in our environment, silicon is not considered to be an essential element in plant growth despite the known benefits it yields to crop production, such as alleviating abiotic and biotic stresses on plants (Datnoff et al., 2001). Part of this view of non-essentiality comes from the fact that not all plants are silicon accumulators, with the majority of known silicon accumulators falling into the *Cyperaceae*, *Gramineae* (aka *Poaceae*) and *Equisetaceae* families (Ma & Takahashi, 2002).

Whilst silicon may be viewed as non-essential, its benefits to plant health and crop yield cannot be argued. Silicon's presence in the growth solution has been shown to alleviate drought stresses by reducing the transpiration rate, and therefore water loss, in silicon rich plants when compared with silicon deficient plants (Matoh et al., 1991). Silicon can also inhibit various other abiotic and biotic stresses, of which numerous summaries can be found (Datnoff et al., 2001; Ma & Takahashi, 2002; Ma, 2004).

Aluminium toxicity is a major factor on crops grown in acidic soils, such as rice. Aluminium has been shown to inhibit root growth and limit nutrient uptake in plants exposed to its presence. However, the addition of silicic acid to the growth solution was shown to drastically reduce the aluminium-induced inhibition of root growth (Ma et al., 1997). It was suggested by these results that the alleviative qualities of silicic acid were probably the result of interactions between silicon and aluminium in the solution rather than in the plants.

However, there are other methods by which silicon could alleviate aluminium toxicity in plants. In *Faramea marginata* a strong co-localisation was found between silicon and aluminium in the shoots suggesting that the sequestration of aluminium into a silicon-aluminium complex is a

method used by aluminium-accumulating plants to alleviate the metal's toxic effects (Britez et al., 2002). In order to determine if a similar process could be occurring in rice, an imaging method which could identify the presence of both silicon and aluminium would be required.

Various methods have been employed in the detection and visualisation of silica in plant tissues, with early investigations using a mixture of tissue ashing, toluidine blue staining and mounting using a medium of differing refractive index, which resulted in silica being visible under light microscope (Blackman, 1968). Methods for silica staining were advanced through the use of methyl red, crystal violet lactone and silver amine chromate which reacted with silanol groups on the surface of the silica bodies (Kaufman et al., 1985). These stains were not specific to silica, with certain compounds such as calcium carbonate interfering with the staining process and requiring removal through the use of acid treatment. However, despite the non-specificity of these stains they did allow for the in-situ staining of silica, unlike the previous tissue ashing techniques.

A novel and specific fluorescent tracer for silica was discovered in the form of 2-(4-pyridyl)-5-((4-(2-dimethylaminoethylaminocarbonyl)methoxy)phenyl)oxazole (PDMPO) which was found to bind with silica and give off a bright green fluorescence (Shimizu et al., 2001). This was demonstrated beautifully by exposing diatoms, who form their outer shell called a frustule from silica, to PDMPO. The PDMPO was incorporated into the silica frustule and allowed for the visualisation of the silicified diatom under fluorescence microscopy.

More recently PDMPO was used in the staining of biogenic silica extracted from horsetail (*Equisetum arvense*) through the use of acid digestion (Law & Exley, 2011). This staining method provided detailed fluorescent images of numerous silica structures from within horsetail, including the epidermal cells, papilla and stomata. Whilst this staining method is certainly an advance on previous, less specific methods of visualising plant silica, it is, like the tissue ashing methods discussed earlier, destructive to the plant tissue. With only the silica visible, researchers

must determine where the silica came from within the plant tissue, with varying degrees of success.

Micro-PIXE is a variant of the standard particle-induced x-ray emission (PIXE) technique which uses a micro-focused ion beam for elemental analysis in a wide range of sample types. PIXE functions through the detection of characteristic X-rays emitted by the elements within the sample when excited with an ion beam (Ortega et al., 2009). The energy of the X-rays emitted by each element is unique and by cross-referencing the readings with the known energy emissions of each element, the make-up of the sample can be determined.

Micro-PIXE allows for the quantitative analysis of elemental distribution in samples with a lateral resolution of the order of 1 μm for elements above Na in atomic weight (Mesjasz-Przybylowicz & Przybylowicz, 2002). Micro-PIXE has been used extensively to map elemental distribution in plant tissues. In *Thlaspi praecox*, a known cadmium and zinc accumulator, a recent study produced elemental maps of the leaf to reveal the distribution of essential and non-essential elements: striking images show the localisation of zinc at the leaf epidermis, whilst cadmium was centred at the mesophyll (Vogel-Mikus et al., 2008). Micro-PIXE has also been used to map iron distribution in the roots of barley (*Hordeum vulgare*), where it was found that iron accumulated at the outermost cell layers of the root (Schneider et al., 2002). These studies show the versatility of Micro-PIXE and the detailed images it can provide with regards to mapping elements in plant tissue.

Low Energy X-ray Fluorescence (LEXRF) is a variant of the standard X-ray Fluorescence (XRF) imaging method. LEXRF is more useful in biological research as it can detect the elemental distribution of low-atomic weight elements such as carbon, nitrogen, oxygen, fluorine, iron, zinc, magnesium and other elements, all of which have fundamental importance in biological systems (Kaulich et al., 2009). Both LEXRF and Micro-PIXE are capable of detecting silicon and aluminium with ease, though of the two methods LEXRF is the more demanding and expensive technique.

Like Micro-PIXE, LEXRF has been used for the localisation of specific elements within plant tissues. A recent study used LEXRF to help elucidate the aluminium tolerance mechanism of tea (*Camellia sinensis*) by determining which areas of the leaf were used to deposit aluminium (Tolra et al., 2011).

3.2 Method

3.2.1 Hydroponic Growth

Approximately 120 rice seeds were germinated in four petri dishes, roughly 30 seeds per petri dish. Each petri dish was lined with damp filter paper, along with a layer of damp filter paper covering the top of the seeds. The lids to the petri dishes were then placed over, slightly askew to allow for air circulation whilst reducing evaporation from the filter paper. The petri dishes were left at room temperature in the dark until the root radical had formed, at which point the seeds were transferred into growth trays.

The germinated seedlings were split into two groups and placed into either the silicon + group tray or the silicon – group tray. The silicon + group tray contained 500 mL 1/5th strength Murashige and Skoog solution with 1 mM silicic acid. The silicon – group tray contained just 500 mL 1/5th strength Murashige and Skoog solution. The seedlings were placed onto plastic netting that provided an anchor point for the roots to attach to, which floated just under the surface of the growth solution. The seedlings were grown for six weeks in the growth trays, with the growth solution being changed twice per week. For further details on the growth set-up, see section 2.1 Hydroponic Growth Section.

After the six week growth period, the rice plants were removed from the growth trays and split into two further groups of roughly 30 seedlings each. Four new growth tray treatments were set-up: two of the trays contained 500 μM CaCl_2 and the other two trays contained 500 μM CaCl_2 with 100 μM Al. Both the CaCl_2 solution and the CaCl_2 with 100 μM Al solutions were pH balanced to

pH 5.5 using nitric acid. Rice plants were grown under these conditions for a further two weeks, with the growth solutions being changed twice per week. This set-up resulted in the formation of four rice plant groupings:

- Control group (Control) – Grown in the absence of both silicon and aluminium.
- Silicon + group (Si+) – Grown in the presence of silicon, but the absence of aluminium.
- Aluminium + group (Al+) – Grown in the absence of silicon, but the presence of aluminium.
- Silicon/Aluminium + group (Si/Al+) – Grown in the presence of both silicon and aluminium.

3.2.2 Cryofixation and Sectioning

The sample preparation, cryofixation and sectioning protocol was taken from pre-established methods (Vogel-Mikuš et al., 2009).

3.2.2.1 Laboratory Materials

- Scalpels and forceps.
- Needles with polished tips.
- Aluminium foil for making tissue-freezing medium beds.
- Beakers.
- Tissue-freezing medium.
- Liquid nitrogen.
- Propane.
- Pioloform in chloroform.
- Microscope object-glass.
- Aluminium sample holders.
- Glue (two-component Araldite).

- Leica CM3050 cryotome.

3.2.2.2 Cryofixation

All rice plant tissue was thoroughly washed with distilled water to ensure the removal of contaminants before the tissue processing began. Fresh leaf and root samples of around 0.5 cm in length were carefully cut using a scalpel from living rice plants. The 0.5 cm root samples were inserted into stainless steel needles with polished tips, with care taken to choose a needle with the appropriate diameter to best suit the sample to ensure a tight hold on the sample during the sectioning process. The 0.5 cm leaf samples were transferred into aluminium foil beds (0.5 cm x 0.5 cm x 0.5 cm) that were filled with tissue-freezing medium.

After the samples were cut and secured into their appropriate mounting beds, they were dipped into propane cooled with liquid nitrogen, which is superior to liquid nitrogen due to its higher cooling rate. A specially designed heat-block was used for this process: a central container of liquid propane was surrounded by a larger container of liquid nitrogen (Fig 3.1). The entire set-up was itself surrounded by a polystyrene bed to avoid the rapid evaporation of the liquid nitrogen. Due to the dangerous nature of both propane and liquid nitrogen the freezing procedure must be carried out in a well-ventilated room.

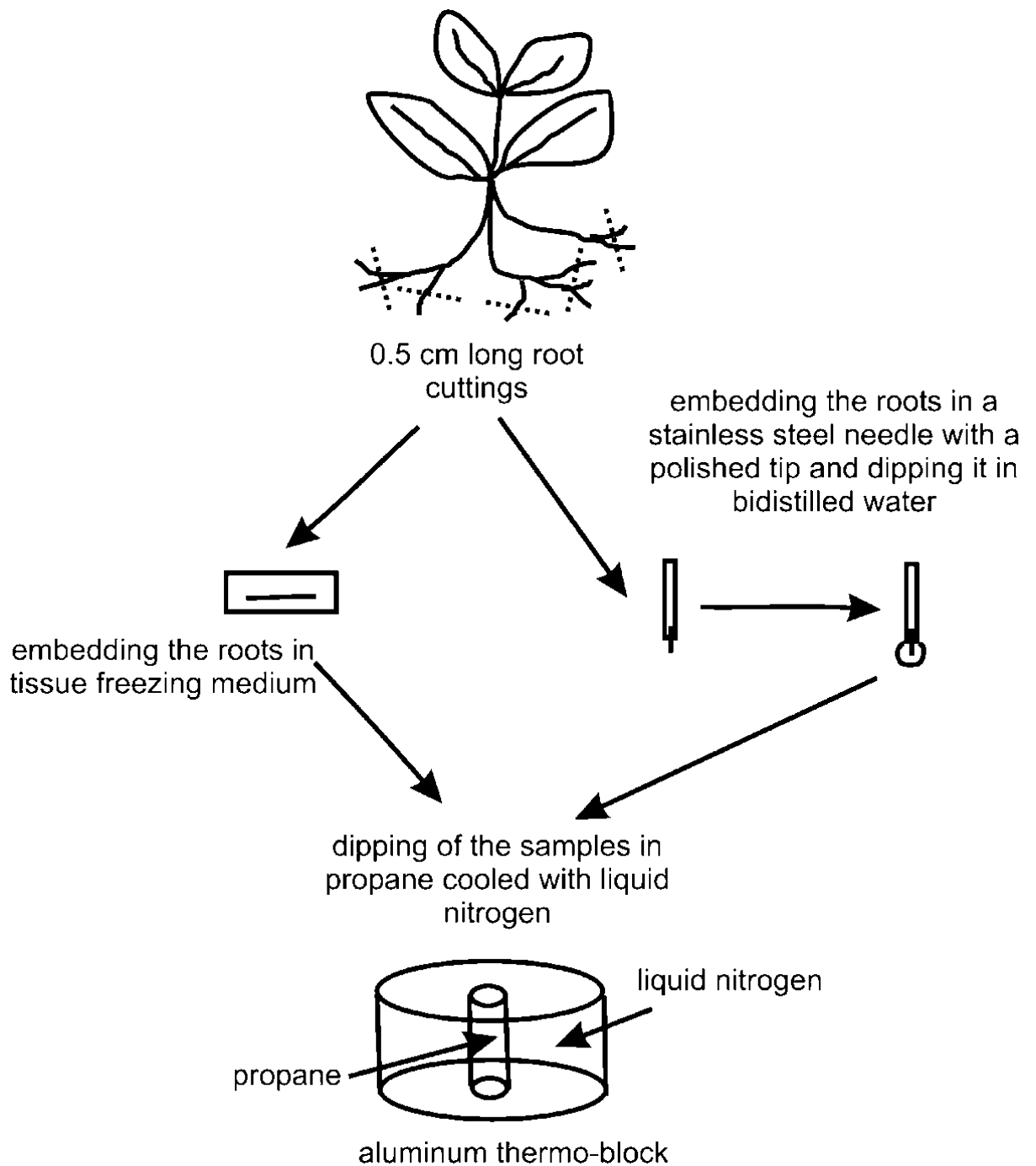


Figure 3.1 Diagram of the thermo-block used in freezing the rice leaf and root tissue samples (Vogel-Mikuš et al., 2009).

The freezing process should be carried out as swiftly as possible to reduce the growth of ice crystals within the tissue samples, which would damage the structure of the tissue sample. After the first freezing stage, the samples were rapidly transferred from the propane into the liquid

nitrogen in the outer section of the thermo-block. From this outer block, the samples were then transferred into the cryo-microtome chamber to avoid the thawing of the samples.

3.2.2.3 Cryosectioning

Sections were cut using a Leica CM3050 cryotome at a thickness of 30 μm . For root samples, a specially designed adaptor was used to fit the needles to the head of the cryotome – this was not necessary for the leaf samples. All sections were cut using disposable stainless steel blades.

Once sections were cut they were placed onto pre-cooled filter papers into specially designed, pre-cooled aluminium beakers with a cover and kept immersed in liquid nitrogen until freeze-drying.

3.2.2.4 Freeze-Drying

Freeze-drying is required in order to prevent the samples from wilting and shrinking due to the high concentrations of water within the plant tissues. The samples, contained within the aluminium beakers, were transferred into an Alpha 2-4 Christ Freeze Dryer via a cryo-transfer assembly cooled by liquid nitrogen. They were then freeze-dried at $-50\text{ }^{\circ}\text{C}$ and a pressure of 0.04 mbar for three days. In order to ensure that the samples remained flat they were placed between two pieces of pre-cooled filter paper and then covered with a pre-cooled piece of microscope object glass.

3.2.2.5 Sample Mounting

Freeze-dried samples were then mounted into aluminium holders and covered with a thin foil of Pioloform (around 300 μm thick). The Pioloform foil is prepared by adding 1 g of Pioloform to 75 mL of chloroform to form a dissolved solution. To create the thin foil of Pioloform, a clean glass microscope slide is dipped into the Pioloform solution for two seconds, then removed and allowed to dry for three minutes. Once the foil has dried, another clean glass slide is used to peel away the edge of the foil and detach it from the first glass slide. The foil is then floated onto the

surface of distilled water by dipping the slide into a beaker of water, allowing the foil to float away. The foil is then floated onto the aluminium holder. From there, the sample is transferred onto the aluminium holder covered with Pioloform and then covered with a second aluminium holder also covered with a Pioloform foil to sandwich the sample between two Pioloform layers. At this point samples are ready for either Micro-PIXE or LEXRF analysis

3.2.3 Micro-Particle-Induced X-Ray Emission

Micro-Particle-Induced X-Ray Emission (Micro-PIXE) allows for quantitative analysis of element distributions in a variety of samples, with lateral resolution of the order of 1 μm for elements from sodium to uranium. Micro-PIXE analysis was performed at the Jožef Stefan Institute, situated just outside Ljubljana, Slovenia.

Analysis of biological samples is achieved by the sequential application of high and low current modes to a region of the sample. In high-current mode, a proton beam is generated with an energy of 3 MeV and a variable diameter of between 1 and 3 μm , with ion currents ranging from 60 to 500 pA depending on the required lateral resolution (Vogel-Mikuš et al., 2009). In low-energy mode, object slits located at the beam entry point are closed, bringing the beam flux down to approximately 500 protons per second.

The detection of X-ray energies from between 1 - 25 keV is provided by a pair of X-ray detectors: a high-energy, high-purity germanium X-ray detector and a low-energy Si(Li) X-Ray detector. The high-purity germanium detector has an active area of 95 mm^2 , a 25 mm thick beryllium window and a 100 mm thick polyimide absorber which is positioned at an angle of 135° in respect to the proton beam direction. The low-energy Si(Li) detector has an active area of 10 mm^2 and an 8 mm thick beryllium window which is positioned at an angle of 125° in respect to the proton beam direction. The low-energy detector is used to detect low-energy X-rays within the energy range of 0.8 to 4 keV. During measurement, samples were sprayed with low-energy electrons from a hot tungsten filament to prevent sample charging. An in-beam chopping device is positioned towards

the end of the beam line, after the last collimation of the beam before it hits the sample to ensure an accurate proton dose determination, or the number of protons hitting the sample.

Areas of interest in the sample are determined by short PIXE mapping in high-current mode and once the sample positioning and scan area size have been selected the object slits are closed and in scanning transmission ion microscopy (STIM) measurements are made. A planar silicon detector is positioned directly in the beam, to obtain the best contrast in STIM, which is used to determine the thickness of the sample (Vogel-Mikuš et al., 2009). Once STIM measurements have been made, the samples are analysed in high-current mode during which time the PIXE element maps are measured. The measurement period varies depending on the concentration of and atomic number of the elements being measured for, varying from around one hour to 30 hours. At the end of the sample measurement another STIM measurement is made to check for sample consistency and possible damage such as thinning or shrinking.

3.2.4 Low-Energy X-Ray Fluorescence

The Low-Energy X-Ray Fluorescence (LEXRF) imaging protocol was taken from pre-established methods (Tolra et al., 2010). The LEXRF measurements were performed using the TwinMic X-ray fluorescence spectro-microscope at the Elettra Synchrotron Radiation Facility in Trieste.

The lateral resolution that can be achieved by the TwinMic beamline is vastly superior to that of Micro-PIXE, between 0.03 and 1 μm depending on the imaging mode used. LEXRF is performed in the 280–2,200 eV photon energy range, allowing for the detection of lower atomic weight elements such as carbon, nitrogen and oxygen which are of biological importance, in addition to silicon and aluminium which are of importance in the current study.

The transmission signal was acquired using a fast-readout, electron-multiplying, CCD camera (Andor Ixon). The camera was coupled to a phosphor-screen-based visible light converting system, which allowed simultaneous detection of bright-field or absorption, differential absorption and

differential phase contrast signals (Tolra et al., 2010). Morphological analysis of the samples at the cellular and sub-cellular levels was complemented by a set-up consisting of four large-area, Si-drift detectors in an annular back-scattering configuration surrounding the sample.

During LEXRF measurement, the selected regions of the sample were scanned first with 1.7 keV excitation energy to reach the Al–K absorption edge, with 10 second dwell time per pixel. The same regions were then scanned again with 2.2 keV excitation energy to reach the P–K absorption edge, with 11 second dwell time per pixel. The x-ray fluorescence (XRF) spectra obtained were fitted using the PyMCAXRF data analysis software with the application of the MCA Hypermath algorithm and a constant baseline correction.

3.3.1 Micro-PIXE Imaging

Micro-PIXE image grids were taken for a number of elements, but only a select few were chosen for display. Aluminium (Al) and silicon (Si) are displayed as images A and B respectively to show their localisation within each sample grid. Image C shows the distribution of sulphur (S); sulphur is of little interest in this experiment, but the sulphur map helps to highlight the sample tissue within the grid. Sulphur is detected in almost all areas of the plant tissue, so the sulphur map can be used to determine the sample edges and structure, giving the other element maps context.

The colour scale on the right side of each image shows the percentage weight detection of each element in that region of the sample. It is important to note that the scale varies between images. Within each image's colour scale, the darker colours of blue and purple represent the lower end of the scale, moving up through the lighter greens and yellow, with red representing the highest levels of element detection within the sample.

3.3.1.1 Micro-PIXE Images of Rice Leaf Tissue – Control Group

This first sample group is comprised of cross-sectioned leaf tissue from the control sample group; plants exposed to neither added silicon nor aluminium in their growth solution. Two representative samples were chosen for a detailed analysis here, the other samples from this group are displayed below them in more compact images.

Plant 37 – Rice Leaf – Sample 1a (706023):

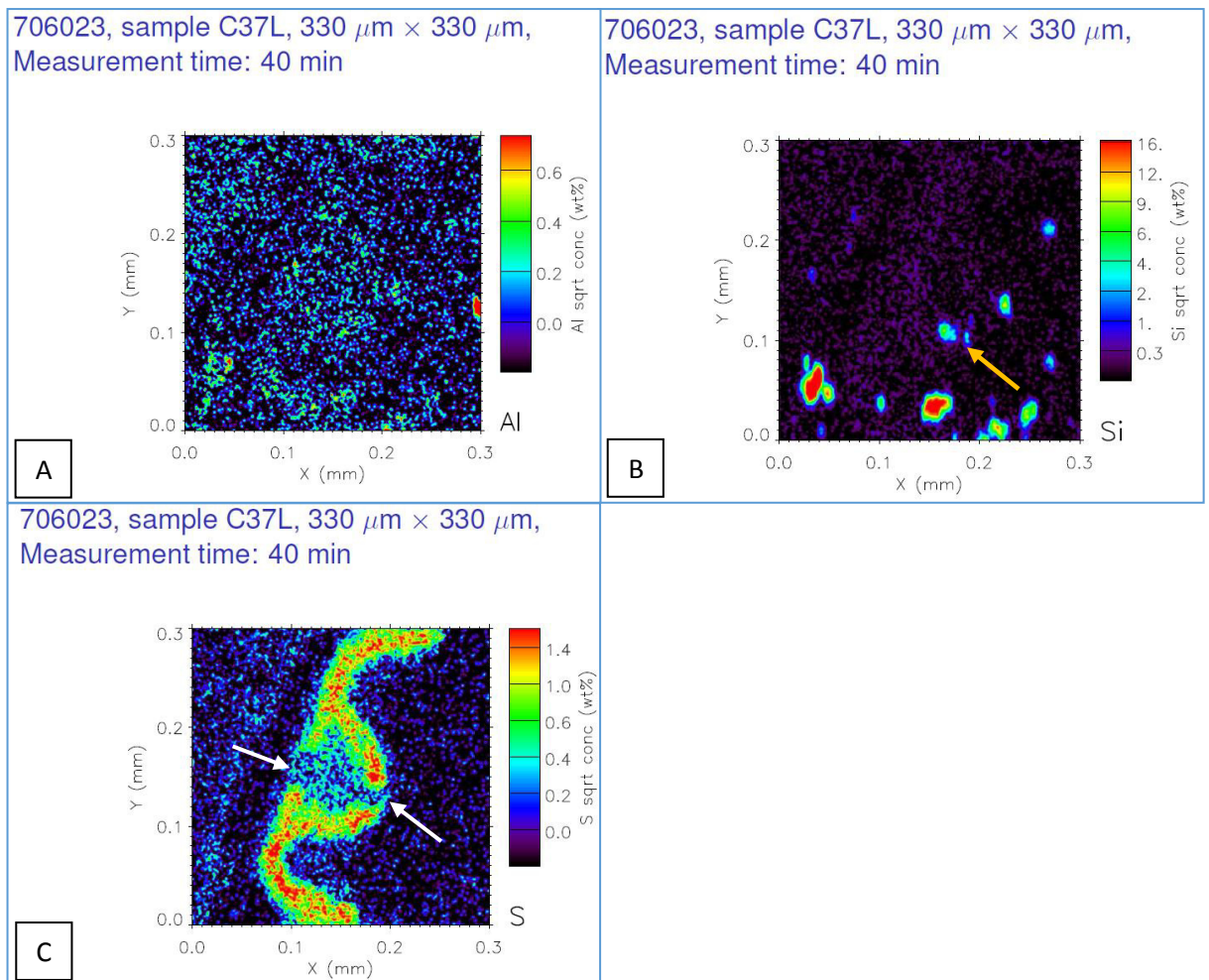


Figure 3.2 Micro-PIXE images showing aluminium (A), silicon (B) and sulphur (C) detection in rice leaf tissue from control group plant 37 sample a. Arrows label areas of note, discussed in text.

Aluminium was not detected in any significant amount within the tissue (Fig 3.2A). Only one significant peak for Si was detected (Fig 3.2B) the signal peaking at about 6% by weight (see gold arrow). This Si is located within the mesophyll region of the leaf, bordering the vascular bundle. A gap is observed in the sulphur signal above the vascular bundle (Fig 3.2C), indicating the region where silica cells would be found (see white arrows).

Plant 38 – Rice Leaf – Sample 4 (707003):

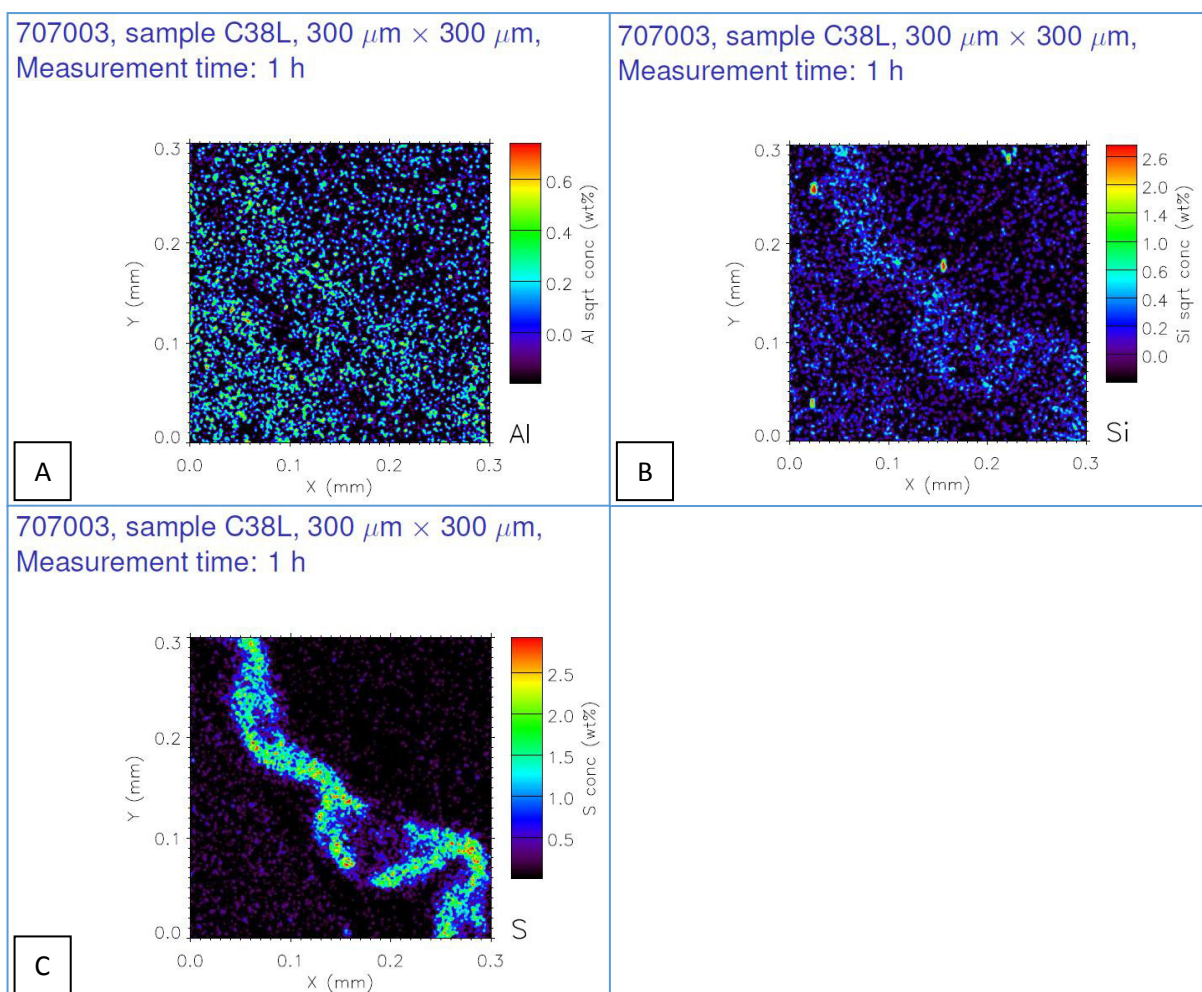


Figure 3.3 Micro-PIXE images showing aluminium (A), silicon (B) and sulphur (C) detection in rice leaf tissue from control group plant 38.

Neither silicon or aluminium were detected in any detectable quantity in this sample. There are signs of a small, diffuse silicon detection throughout the plant tissue (Fig 3.3B) noted by a slightly lighter blue signal mirroring the shape of the plant tissue shown in the sulphur map (Fig 3.3C). This signal strength is too low to be quantified, but it's presence can be observed.

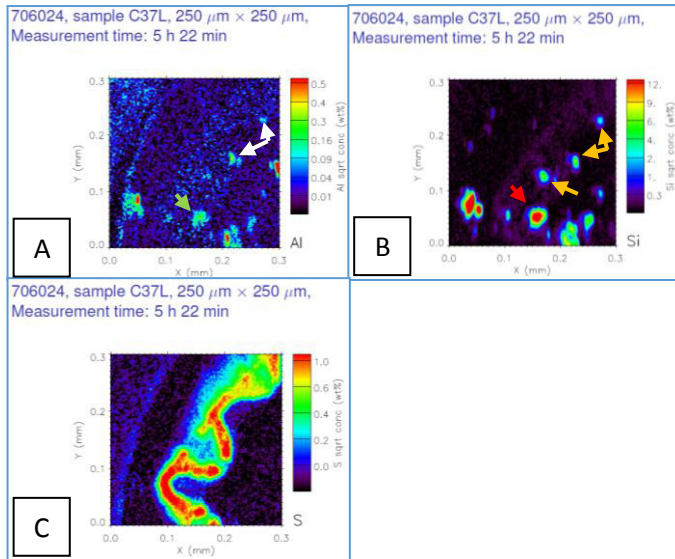


Figure 3.4 Micro-PIXE images showing aluminium (A), silicon (B) and sulphur (C) detection in rice leaf tissue from control group plant 37 sample b. Arrows label areas of note, discussed in text.

There are multiple readings for aluminium (Fig 3.4A) (see white arrows) and silicon (Fig 3.4B) (see gold arrows) which are shown to be within or bordering the sample when cross-referenced with the sulphur map (Fig 3.4C). One large aluminium (Fig 3.4A) (see green arrow) and silicon signal is external to the sample tissue (Fig 3.4B) (see red arrow).

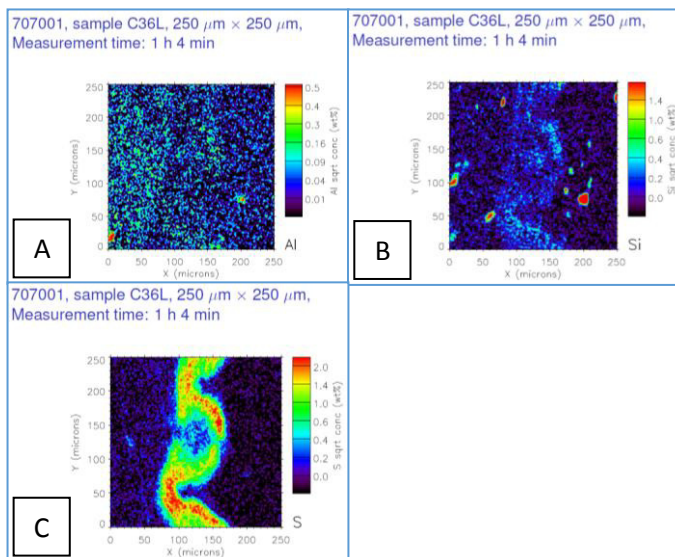


Figure 3.5 Micro-PIXE images showing aluminium (A), silicon (B) and sulphur (C) detection in rice leaf tissue from control group plant 36.

Aluminium was not detected in any significant amount within the tissue (Fig 3.5A). Silicon was not detected within the sample tissue in any quantifiable amount, though a small silicon signal is present throughout the sample (Fig 3.5B).

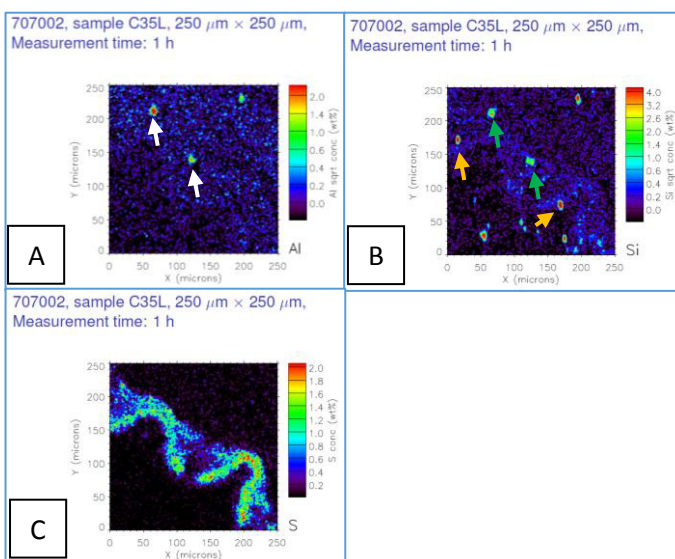


Figure 3.6 Micro-PIXE images showing aluminium (A), silicon (B) and sulphur (C) detection in rice leaf tissue from control group plant 35. Arrows label areas of note, discussed in text.

There are two signals for aluminium at 2% weight (Fig 3.6A) (see white arrows). Four signals within the sample for silicon peaking at 4% weight (Fig 3.6B) (see green and gold arrows), two of which are co-localised with aluminium (see green arrows).

Summary

Of the five control group samples, two showed evidence of aluminium detection in isolated readings (Fig 3.4A & Fig 3.6A). These readings were co-localised with silicon signals in all instances (Fig 3.4B & Fig 3.6B). Aluminium readings in the control group were low, with readings peaking at 0.5% weight (Fig 3.4A) and 2% weight (Fig 3.6A).

Three control group samples showed silicon detection (Fig 3.2B, Fig 3.4B & Fig 3.6B). Silicon was found in small, isolated areas of both the epidermis and mesophyll tissue. Silicon readings peaked at around 9% weight in two samples (Fig 3.2B & Fig 3.4B) and 4% weight in the final sample (Fig 3.6B).

Silicon hotspots were detected outside the sample tissue in all samples, though in varying amounts and sizes. These readings are not within the sample tissue and therefore must come from an external source, such as dust contamination of the sample. Aluminium hotspots were less common but still present in four of the five samples (Fig 3.2A, Fig 3.4A, Fig 3.5A & Fig 3.6A).

3.3.1.2 Micro-PIXE Images of Rice Leaf Tissue – Silicon +

This sample group is comprised of cross-sectioned leaf tissue from the silicon + sample group; plants grown in the presence of added silicon, but not aluminium in their growth solution. Of the four samples, two representative samples were chosen for a detailed analysis here, the other two samples from this group are displayed below them in more compact images.

Plant 40 – Rice Leaf – Sample 20 (708010):

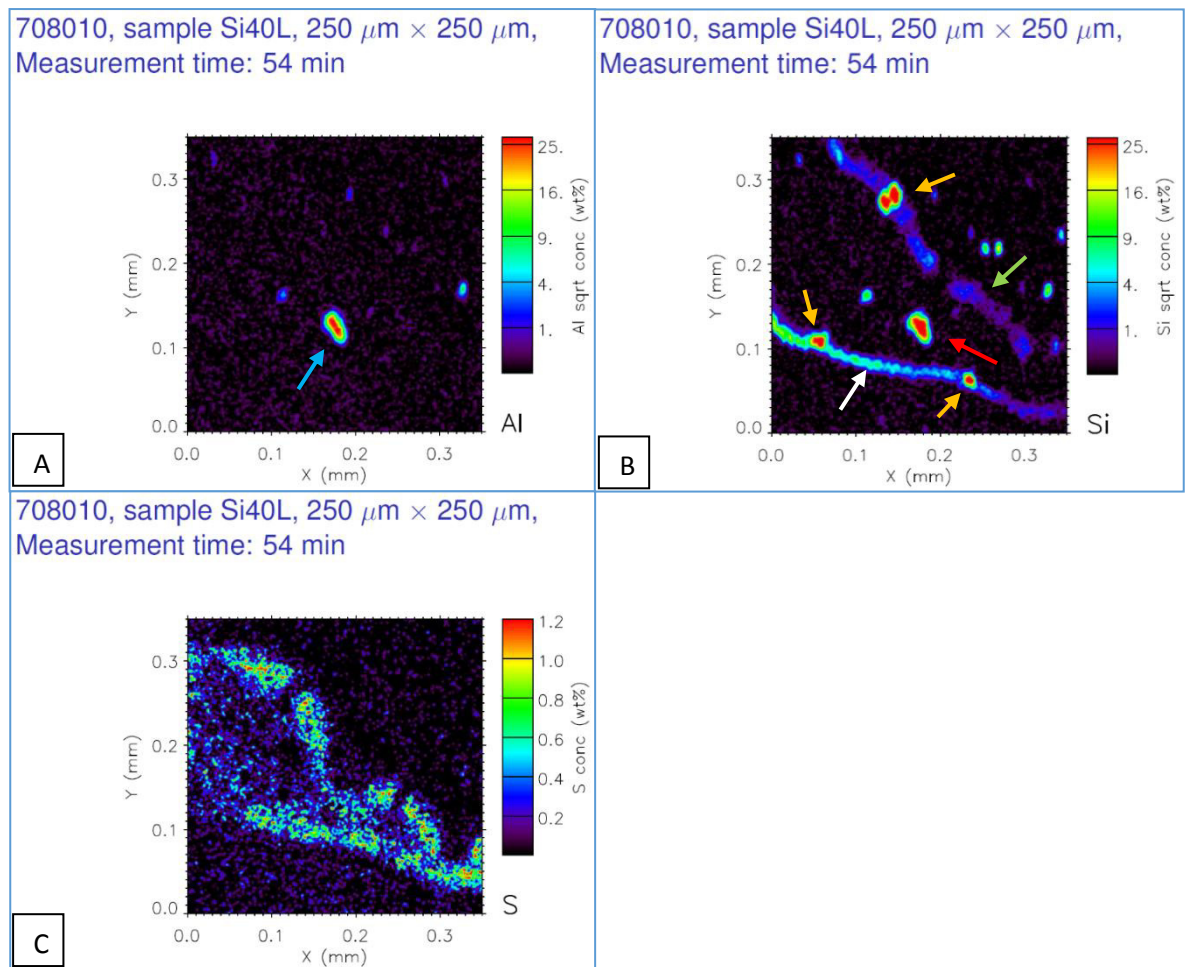


Figure 3.7 Micro-PIXE images showing aluminium (A), silicon (B) and sulphur (C) detection in rice leaf tissue from Silicon + group plant 40. Arrows label areas of note, discussed in text.

One large aluminium signal was detected within the tissue (Fig 3.7A) (see blue arrow). This aluminium signal is co-localised with a silicon signal, also peaking at 25% weight (Fig 3.7B) (see red arrow). This co-localised signal is located at the lower epidermis of the leaf within a recess, an area we would expect to find bulliform cells.

There is a consistent silicon signal seen across the upper and lower epidermis of the leaf (Fig 3.7B) (see white and green arrows respectively). The upper epidermis layer gives a stronger signal, peaking at 16% weight in places. The lower epidermis signal is weaker, only breaching 4% weight in small areas, usually peaking at 3% weight. The epidermal silicon layers are periodically broken by strong silicon signals, peaking at 25% weight (Fig 3.7B) (see gold arrows). These silicon signals

are located above vascular bundles, where silica cells are found. The distinctive dumbbell shape of silica cells can be seen in the silica cell at the lower epidermis.

Plant 42 – Rice Leaf – Sample 21 (708011):

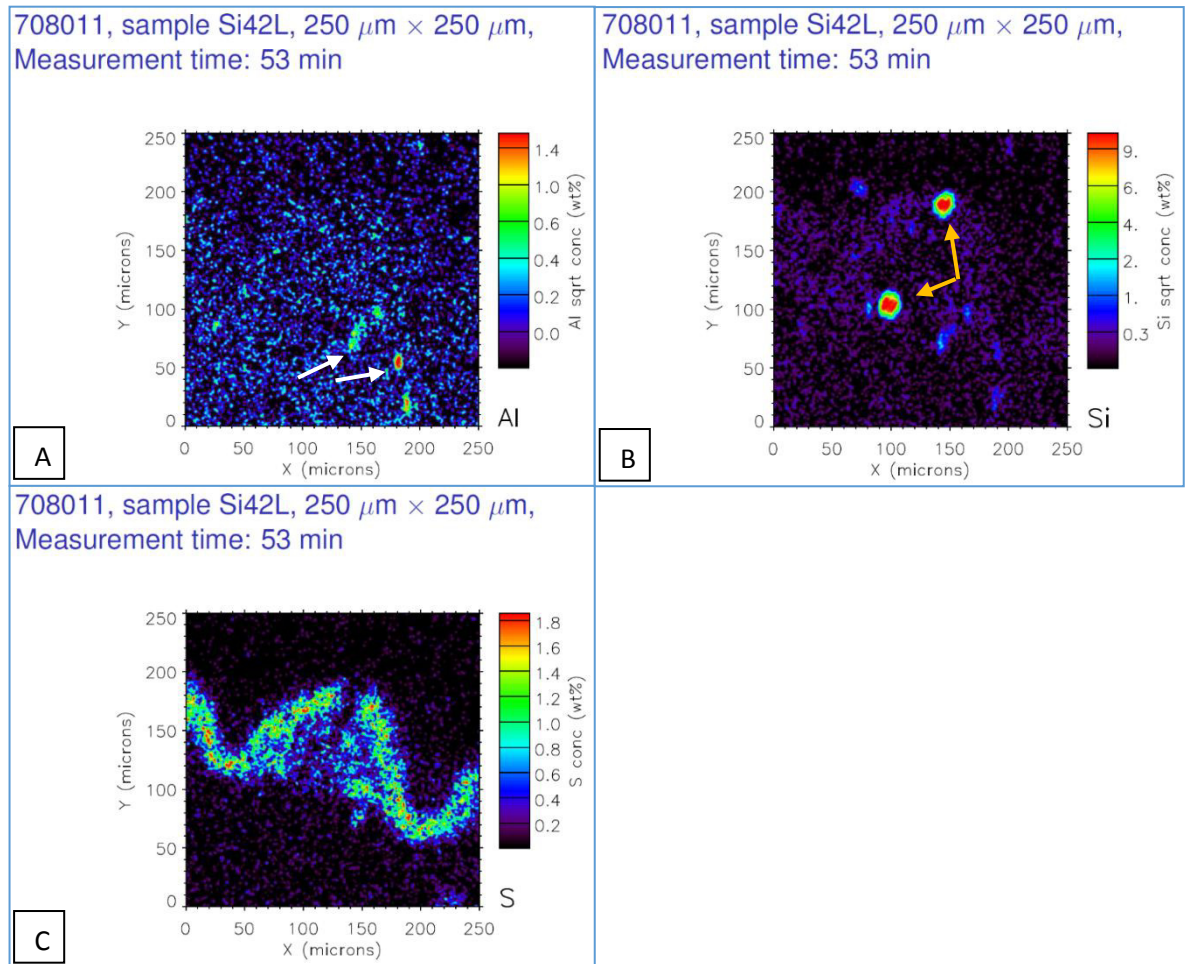


Figure 3.8 Micro-PIXE images showing aluminium (A), silicon (B) and sulphur (C) detection in rice leaf tissue from Silicon + group plant 42. Arrows label areas of note, discussed in text.

This sample contains two small areas of aluminium detection at the upper epidermis, peaking at 1.4% weight (Fig 3.8A) (see white arrows). There is no observable layer of silicon at the epidermis in this sample, but two strong silicon signals peaking at 10% weight are seen above the vascular bundle in the location of silica cells (Fig 3.8B) (see gold arrows). The characteristic dumbbell shape of silica cells can be seen in these images.

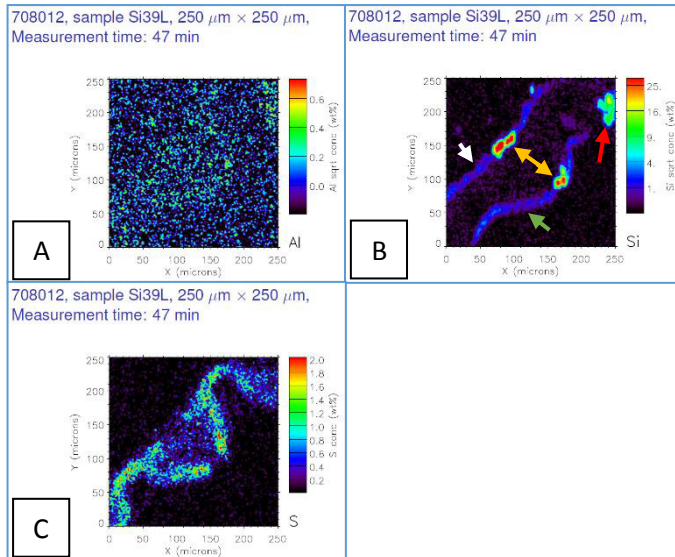


Figure 3.9 Micro-PIXE images showing aluminium (A), silicon (B) and sulphur (C) detection in rice leaf tissue from Silicon + group plant 39. Arrows label areas of note, discussed in text.

There is a faint but consistent silicon signal at both the upper and lower epidermis, consistently reading at 3% weight (Fig 3.9B) (see white and green arrow respectively). There are strong silicon signals both above and below the vascular bundle peaking at 25% weight, indicative of silica cells (Fig 3.9B) (see gold arrows). There faint signs of aluminium detection (Fig 3.9A) beyond the background reading in line with the sulphur map (Fig 3.9C).

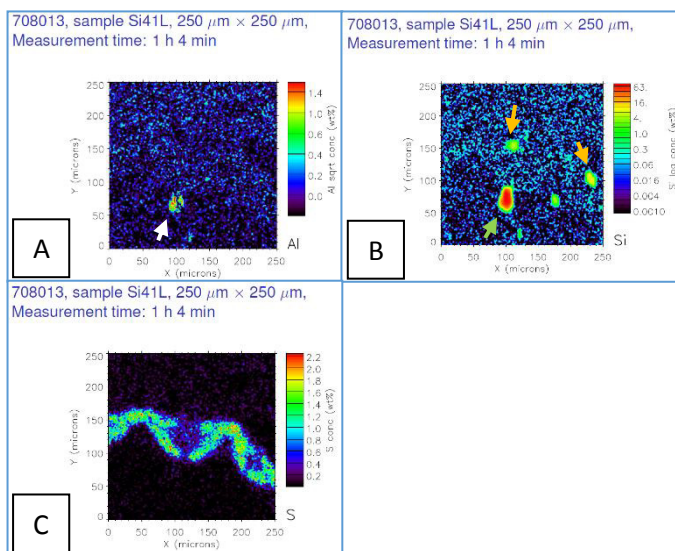


Figure 3.10 Micro-PIXE images showing aluminium (A), silicon (B) and sulphur (C) detection in rice leaf tissue from Silicon + group plant 41. Arrows label areas of note, discussed in text.

One area of aluminium detection outside the sample tissue, peaking at 1.4% weight (Fig 3.10A) (see white arrow). This aluminium signal is co-localised with a large silicon signal, peaking at 53% weight (Fig 3.10B) (see green arrow). No other signs of aluminium in sample tissue. There are two other silicon signals within the sample peaking at around 15% weight within the region silica cells would be located (Fig 3.10B) (see gold arrows).

Summary

Two of the sample groups contained small areas of aluminium detection, one at the location of bulliform cells (Fig 3.7A) and one at the epidermis (Fig 3.8A). Another sample showed a faint background level of aluminium throughout the tissue (Fig 3.9A). Beyond these instances, there was no evidence of aluminium in this sample group.

All four samples showed evidence of silicon deposition at the silica cells, whilst two of them showed further evidence of a silicon layer at the upper and lower epidermis (Fig 3.7B & Fig 3.9B). The silicon signal at the silica cells was consistently stronger than the signal at the epidermis. One strong silicon signal was found in the location of bulliform cells (Fig 3.7B).

This sample group is clean with the sulphur maps showing no damage to the tissue. In addition, only a few minor hotspots for silicon or aluminium appear outside the plant tissue.

3.3.1.3 Micro-PIXE Images of Rice Leaf Tissue – Aluminium +

This sample group is comprised of cross-sectioned leaf tissue from the aluminium + sample group; plants grown in the presence of added aluminium, but the absence of silicon in their growth solution. Only three samples were run in this group, rendering a compact display of some images unnecessary.

Plant 43 – Rice Leaf – Sample 28 (708018):

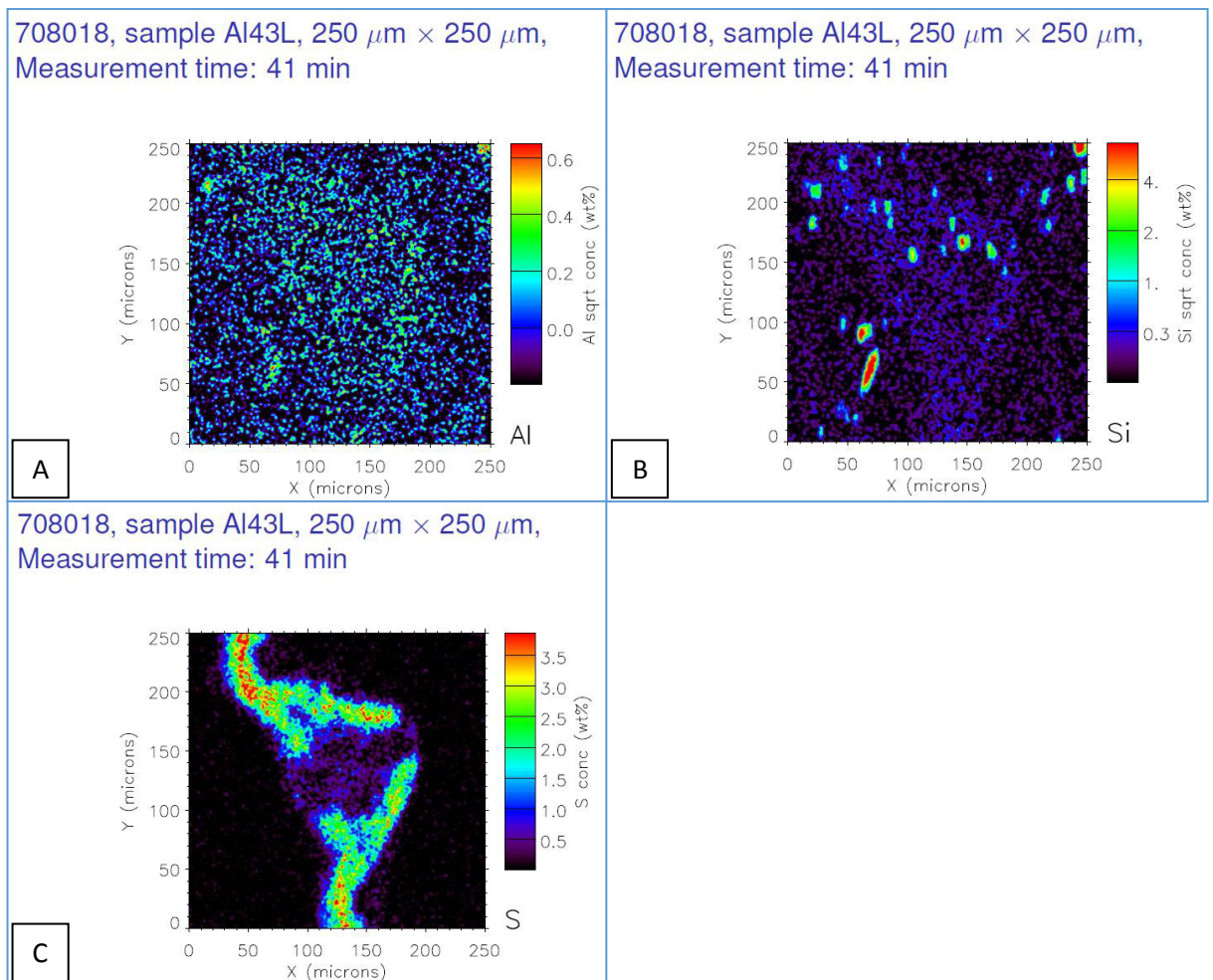


Figure 3.11 Micro-PIXE images showing aluminium (A), silicon (B) and sulphur (C) detection in rice leaf tissue from Aluminium + group plant 43.

There are multiple silicon readings scattered across the sample, peaking at 5% weight (Fig 3.11B).

These silicon signals are located both inside and outside the plant tissue and co-localise with several other elements including sodium and magnesium (see supplementary data). There are signs of aluminium detection throughout the plant tissue (Fig 3.11A) noted by a green signal mirroring the shape of the plant tissue shown in the sulphur map (Fig 3.11C).

Plant 45 – Rice Leaf – Sample 29 (708019):

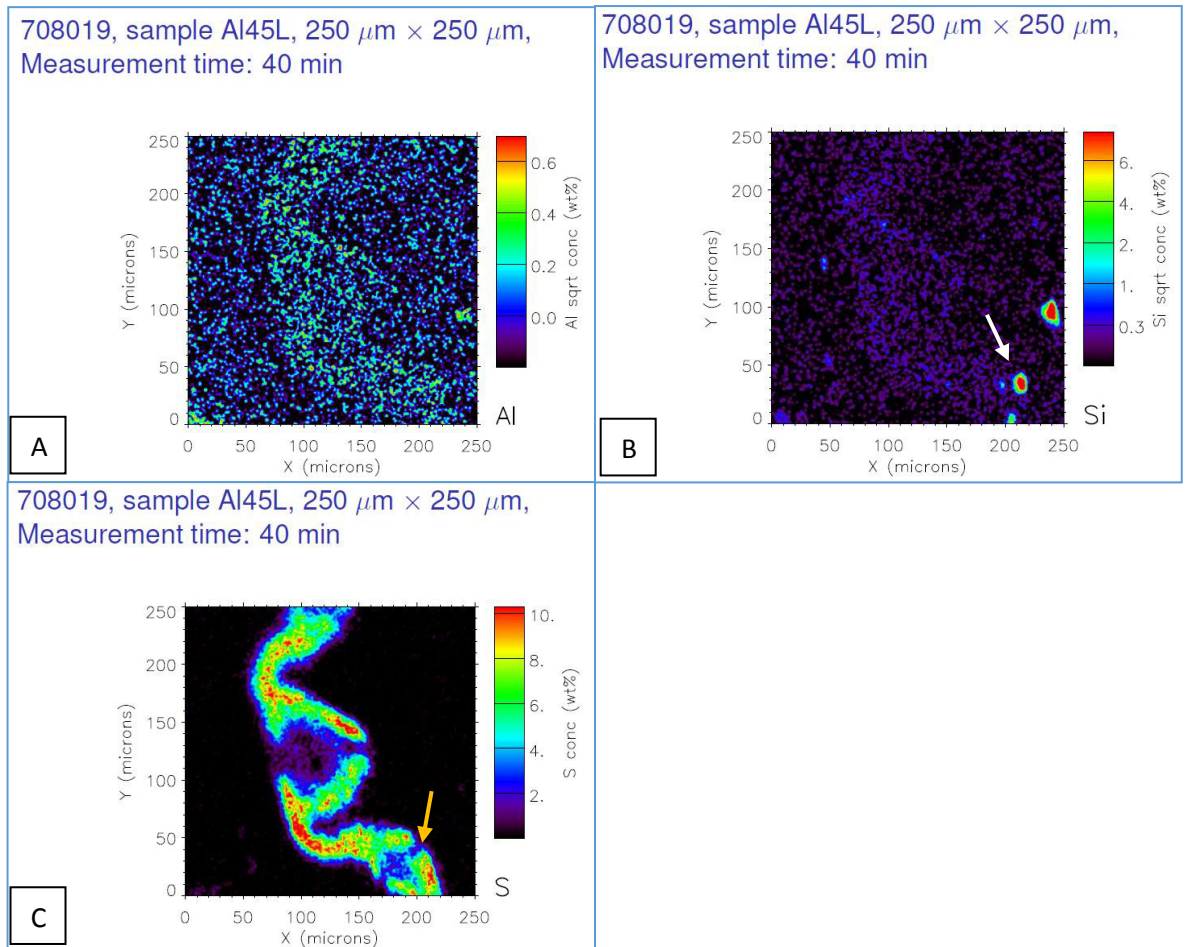


Figure 3.12 Micro-PIXE images showing aluminium (A), silicon (B) and sulphur (C) detection in rice leaf tissue from Aluminium + group plant 45. Arrows label areas of note, discussed in text.

Two silicon signals both peaking at just over 6% weight, one outside the sample tissue and the other at the lower epidermis (Fig 3.12B) (see white arrow), in proximity to the expected location of silica cells, shown in the sulphur map (Fig 3.12C) (see gold arrow). There are signs of aluminium detection throughout the plant tissue noted by a light blue/green signal (Fig 3.12A) mirroring the shape of the plant tissue shown in the sulphur map (Fig 3.12C).

Plant 46 – Rice Leaf – Sample 30 (708020):

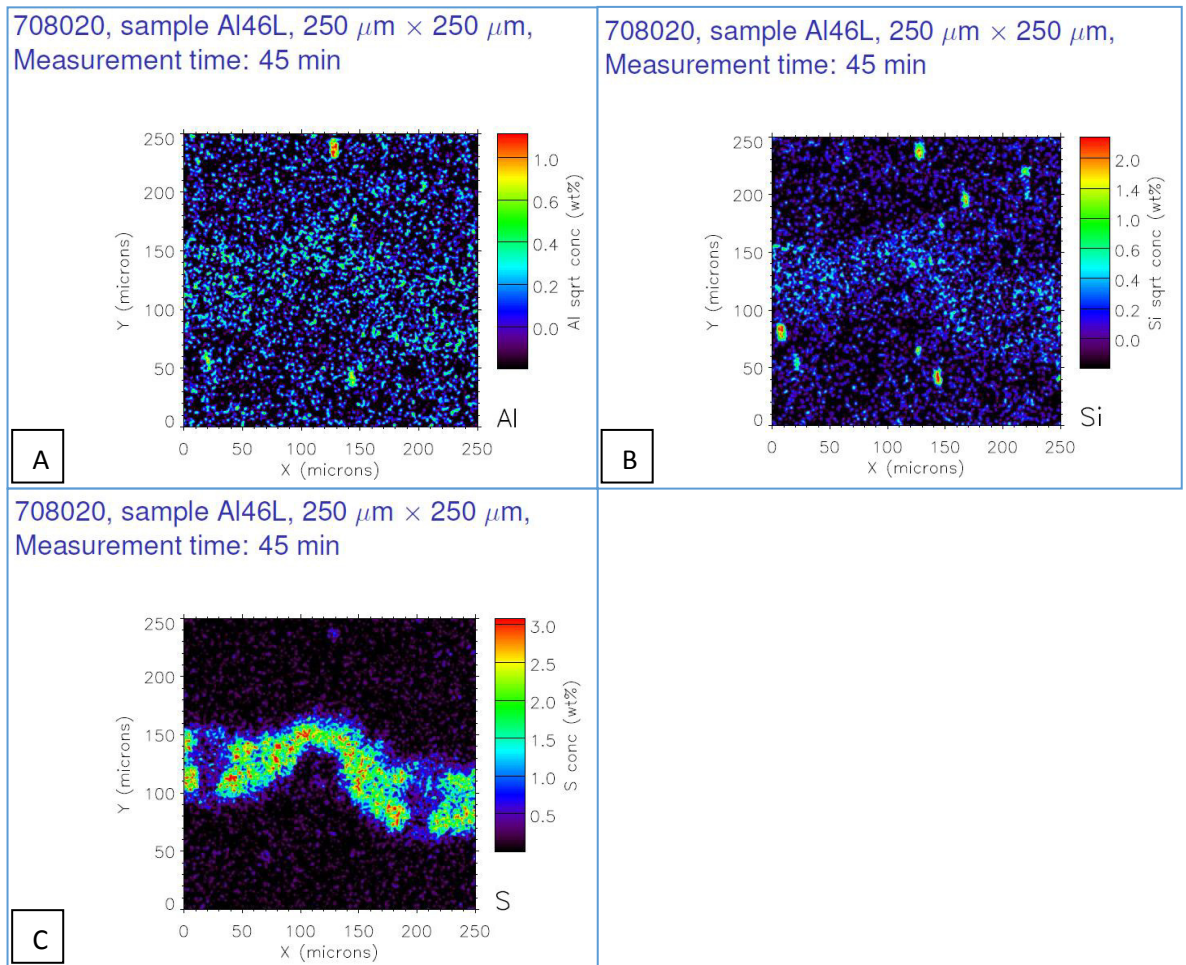


Figure 3.13 Micro-PIXE images showing aluminium (A), silicon (B) and sulphur (C) detection in rice leaf tissue from Aluminium + group plant 46.

There are signs of aluminium detection throughout the plant tissue noted by a light blue/green signal (Fig 3.13A) mirroring the shape of the plant tissue shown in the sulphur map (Fig 3.13C). There are larger external silicon hotspots but nothing notable within or bordering the plant tissue (Fig 3.13B). There are signs of silicon detection throughout the sample tissue by a light blue signal (Fig 3.13B) mirroring the shape of the plant tissue shown in the sulphur map (Fig 3.13C).

Summary

In all three samples, aluminium is detected throughout the sample tissue as evidenced by the brighter aluminium signal that corresponds with the tissue outline in the sulphur maps. This is strong evidence for increased aluminium in the leaf tissue when compared with the control

group. The aluminium is not found in any large desposits, but rather as a diffuse presence throughout the tissue.

One of the samples shows a diffuse silicon presence throughout the sample tissue (Fig 3.13B). All three samples show small, scattered silicon signals both in and outside the sample tissue. There is very little evidence of silicon deposition within this sample group.

3.3.1.4 Micro-PIXE Images of Rice Leaf Tissue – Aluminium and Silicon +

This sample group is comprised of cross-sectioned leaf tissue from the aluminium and silicon + sample group; plants grown in the presence of added silicon and aluminium in their growth solution. Of the four samples, two representative samples were chosen for a detailed analysis here, the other two samples from this group are displayed below them in more compact images.

Plant 34 – Rice Leaf – Sample 27 (708017):

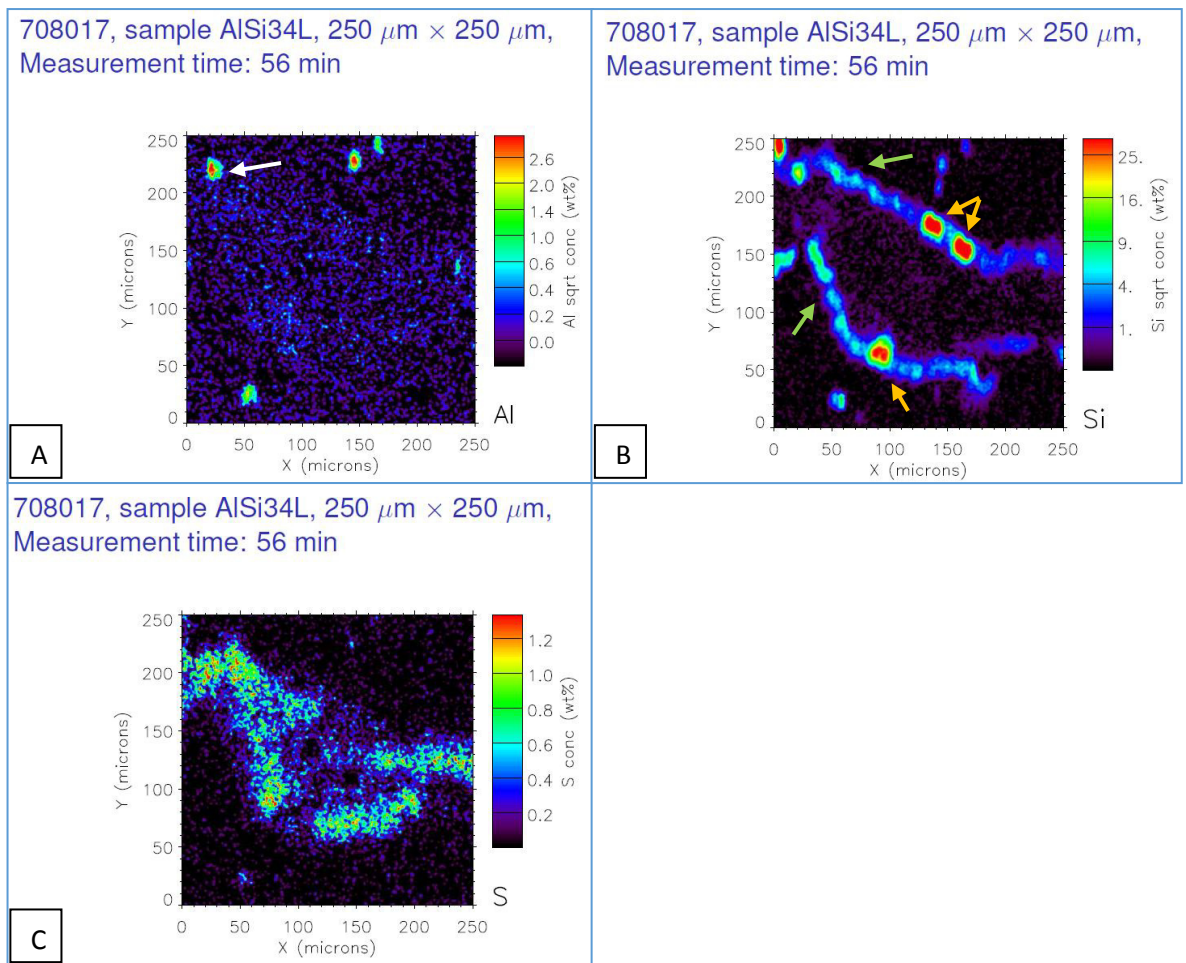


Figure 3.14 Micro-PIXE images showing aluminium (A), silicon (B) and sulphur (C) detection in rice leaf tissue from Aluminium/Silicon + group plant 34. Arrows label areas of note, discussed in text.

There was one area of aluminium detection within the sample tissue, peaking at 3% weight, located at the upper epidermis (Fig 3.14A) (see white arrow). Silicon was detected at three silica cell locations at the epidermis, surrounding the vascular bundle, peaking at 28% weight in these regions. (Fig 3.14B) (see gold arrows). Silicon was also detected at the upper and lower epidermis (Fig 3.14B) (see green arrows). There are also several hotspots located outside of the sample tissue for both silicon and aluminium.

Plant 31 – Rice Leaf – Sample 24 (708014):

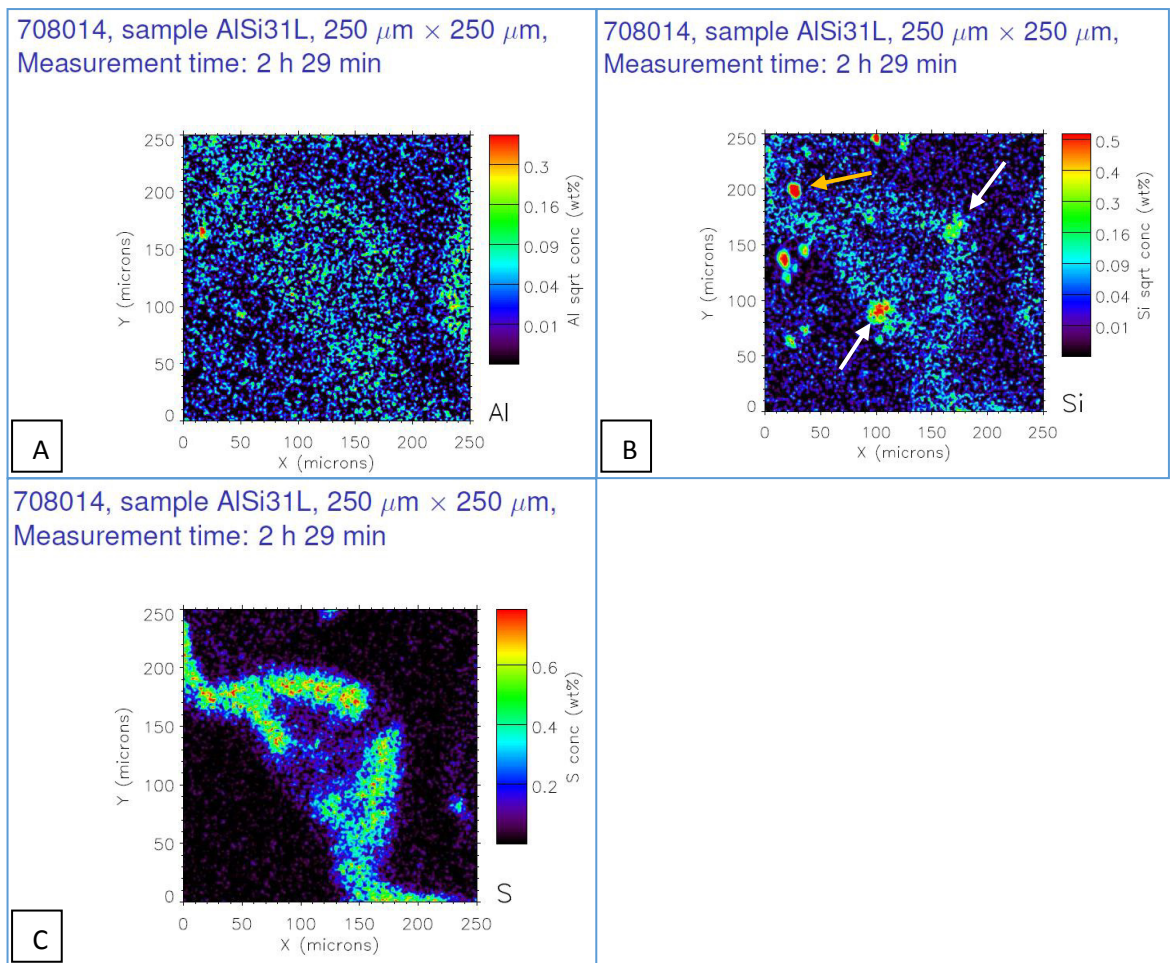


Figure 3.15 Micro-PIXE images showing aluminium (A), silicon (B) and sulphur (C) detection in rice leaf tissue from Aluminium/Silicon + group plant 31. Arrows label areas of note, discussed in text.

There are signs of aluminium detection throughout the plant tissue noted by a light blue/green signal (Fig 3.15A) mirroring the shape of the plant tissue shown in the sulphur map (Fig 3.15C). Silicon was detected above and below the vascular bundle at the epidermis where silica cells are found (Fig 3.15B) (see white arrows). Silicon was also found in one area of the epidermis (Fig 3.15B) (see gold arrow) and throughout the sample in low concentrations, mirroring the shape of the plant tissue shown in the sulphur map (Fig 3.15C). All three element maps show extremely low concentrations of their respective elements.

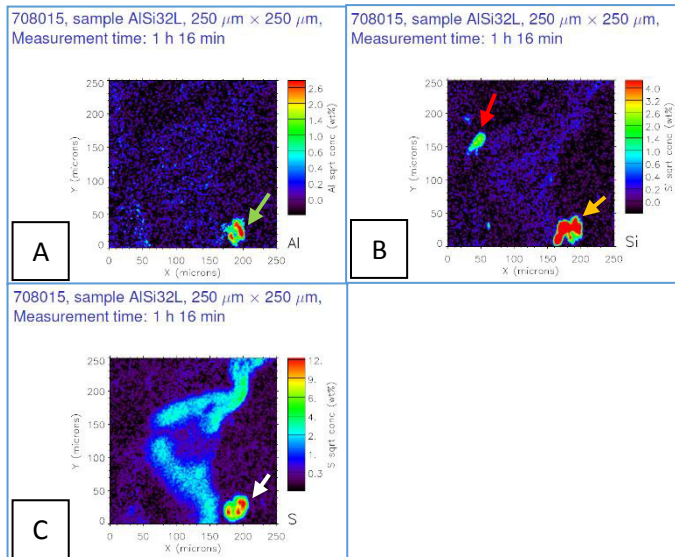


Figure 3.16 Micro-PIXE images showing aluminium (A), silicon (B) and sulphur (C) detection in rice leaf tissue from Aluminium/Silicon + group plant 32. Arrows label areas of note, discussed in text.

There is a large hotspot below the sample which shows detection for aluminium (Fig 3.16A) (see green arrow) at 2.6% weight, silicon at 4% weight (Fig 3.16A) (see gold arrow) and sulphur (Fig 3.16C) (see white arrow), as well as several other elements (see supplementary data). There is also a silicon signal at the lower epidermis of the leaf tissue (Fig 3.16B) (see red arrow). There are signs of aluminium (Fig 3.16A) and silicon (Fig 3.16B) detection throughout the sample tissue shown by a blue signal mirroring the shape of the plant tissue in the sulphur map (Fig 3.16C).

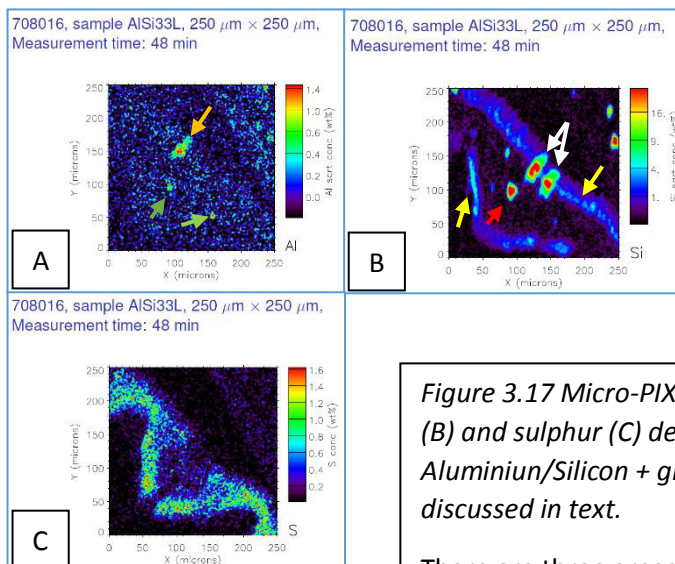


Figure 3.17 Micro-PIXE images showing aluminium (A), silicon (B) and sulphur (C) detection in rice leaf tissue from Aluminium/Silicon + group plant 33. Arrows label areas of note, discussed in text.

There are three areas of aluminium detection within the plant tissue. The first aluminium signal (Fig 3.17A) (see gold arrow) crosses the upper epidermis into the mesophyll. The other two aluminium signals (Fig 3.17A) (see green arrows) are both located within the mesophyll tissue, in proximity to the vascular bundle, peaking at 1.4% weight. There are also very faint signs of aluminium detection throughout the plant tissue, noted by a light blue/green signal. Silicon was detected above the vascular bundle at the site of silica cells, peaking at 25% weight (Fig 3.17B) (see white arrows). Silicon is also found at the vascular bundle, the signal peaking at 25% weight (Fig 3.17B) (see red arrow) and at the upper and lower epidermis, between 3-9% weight (see yellow arrows).

Summary

Three of the four samples show evidence of aluminium detection throughout the plant tissue (Fig 3.15A, Fig 3.16A & Fig 3.17A). Beyond this there were a few small areas of aluminium detection in greater concentrations in two samples (Fig 3.14A & Fig 3.17A). These aluminium signals were not found to be distributed in any pattern or specifically at certain regions of the plant tissue.

Three of the four samples showed silicon deposition at the known location of silica cells (Fig 3.14B, Fig 3.15B & Fig 3.17B). Two of the samples showed silicon deposition at the upper and lower epidermis (Fig 3.14B & Fig 3.17B). Other than two areas of silicon and aluminium signals being found in close proximity (Fig 3.14 & Fig 3.17), there is no evidence of co-localisation between the two elements.

3.3.1.5 Micro-PIXE Images of Rice Root Tissue – Control Group

This sample group is comprised of cross-sectioned root tissue from the control sample group; plants exposed to neither added silicon nor aluminium in their growth solution. Two representative samples were chosen for a detailed analysis here, the other samples from this group are displayed below them in more compact images.

Plant 37 – Rice Root – Sample 5 (707004):

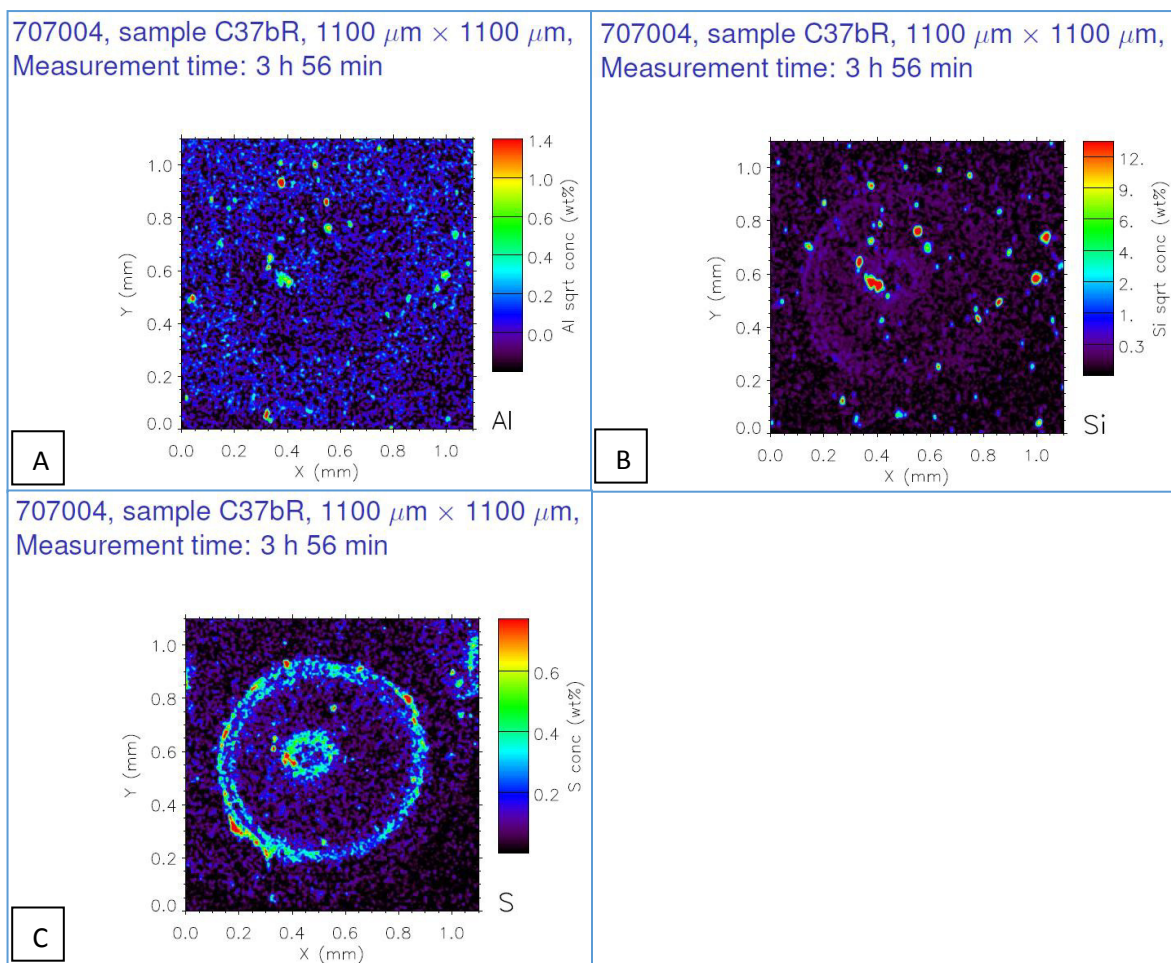


Figure 3.18 Micro-PIXE images showing aluminium (A), silicon (B) and sulphur (C) detection in rice root tissue from control group plant 37 sample b.

There are sporadic readings for aluminium (Fig 3.18A) and silicon (Fig 3.18B) throughout, both inside and outside the plant tissue. These scattered readings are co-localised with several other elements (see supplementary data). Beyond these scattered readings, there is no sign of aluminium in this sample. There is some evidence of low silicon concentrations throughout the root tissue (Fig 3.18B), mirroring the shape of the plant tissue shown in the sulphur map (Fig 3.18C).

Plant 36 – Rice Root – Sample 6 (707005):

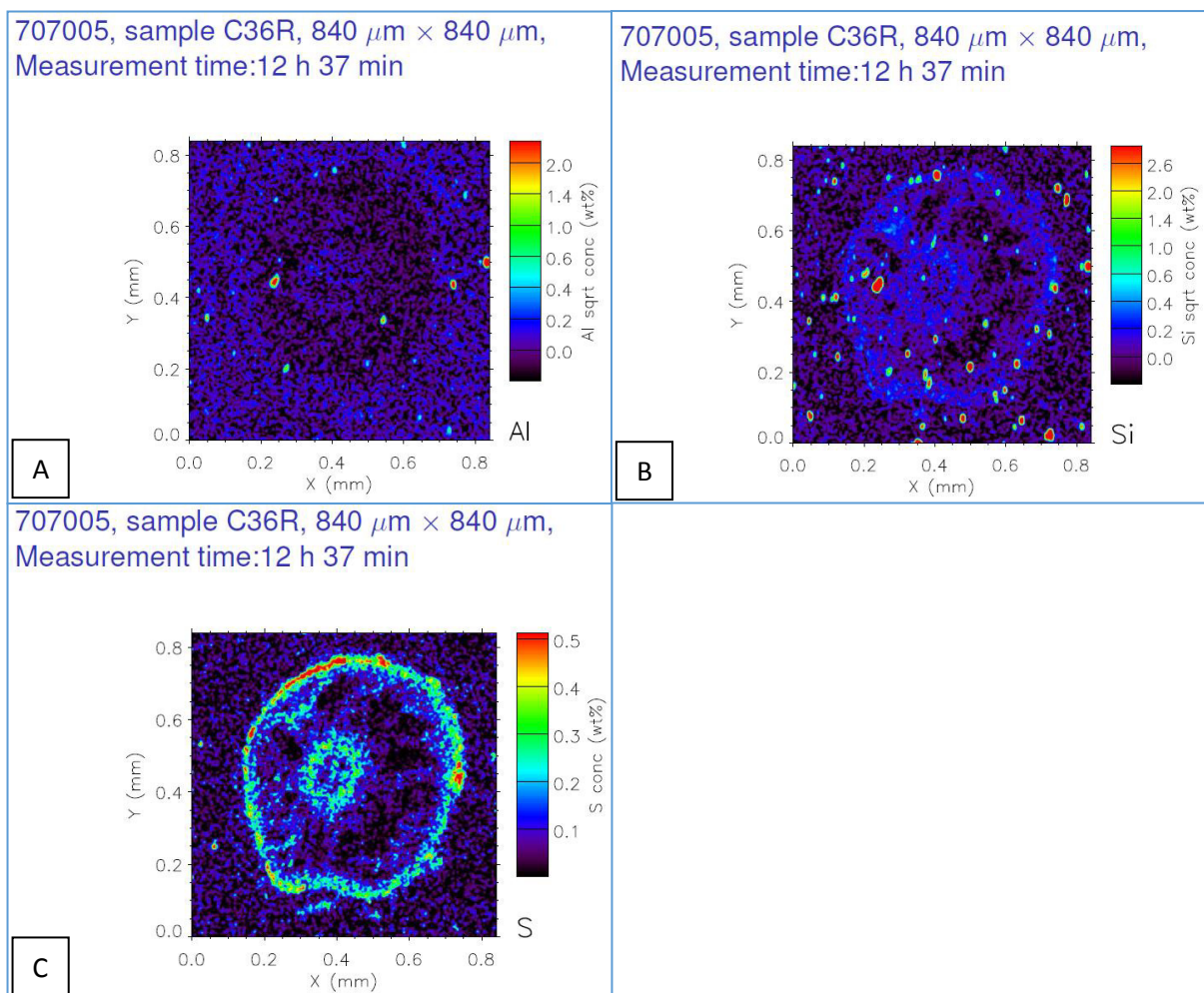


Figure 3.19 Micro-PIXE images showing aluminium (A), silicon (B) and sulphur (C) detection in rice root tissue from control group plant 36.

There are sporadic readings for aluminium (Fig 3.19A) and silicon (Fig 3.19B) throughout the sample, both inside and outside the plant tissue (Fig 3.19). These readings are co-localised with several other elements (see supplementary data). Beyond these scattered readings, there is no sign of aluminium in this sample. There is some evidence of low silicon concentrations throughout the root tissue (Fig 3.19B), mirroring the shape of the plant tissue shown in the sulphur map (Fig 3.19C).

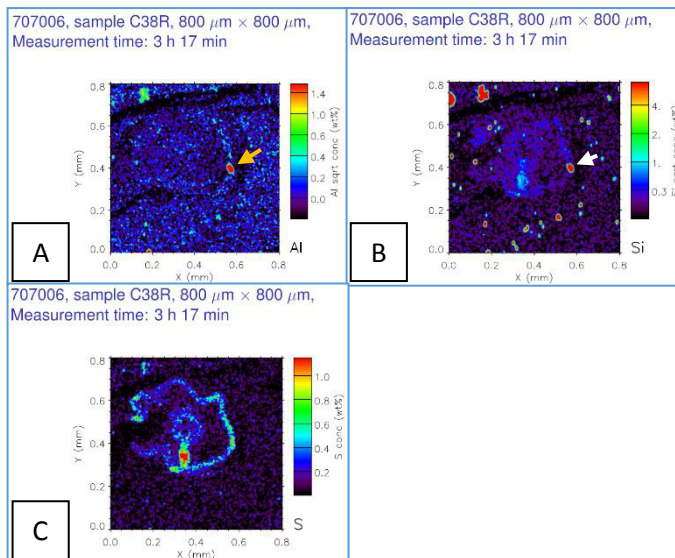


Figure 3.20 Micro-PIXE images showing aluminium (A), silicon (B) and sulphur (C) detection in rice root tissue from control group plant 38. Arrows label areas of note, discussed in text.

There is one area of aluminium detection, peaking at 1.5% weight (Fig 3.20A) (see gold arrow). This aluminium signal is co-localised with a silicon signal, peaking at 6% weight (Fig 3.20B) (see white arrow). This area also gives a signal for chlorine, iron, potassium and sodium (see supplementary data). There are multiple other hotspots for both silicon and aluminium outside the plant tissue within this sample. The sulphur map shows that the root appears to have suffered severe damage during either the fixation or sectioning process (Fig 3.20C).

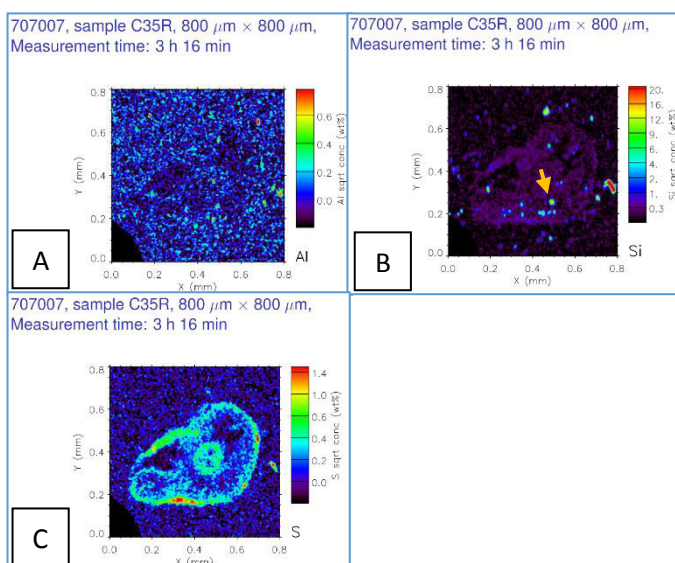


Figure 3.21 Micro-PIXE images showing aluminium (A), silicon (B) and sulphur (C) detection in rice root tissue from control group plant 35. Arrows label areas of note, discussed in text.

There is no evidence of aluminium within the plant tissue (Fig 3.21A). There are several small silicon signals within the cortex, peaking at 20% weight (Fig 3.21B) (see gold arrow). This area also shows detection for multiple other elements including titanium and iron (see supplementary data). There are several silicon readings detected outside the sample tissue. The sulphur map shows that the root appears to have suffered damage during either the fixation or sectioning process (Fig 3.21C).

Summary

All four samples in this group showed sporadic readings for silicon and aluminium, both inside and outside the sample in the form of small hotspots. The readings within the sample tissue have no consistent localisation. Other than these readings, there is no evidence of either silicon or aluminium deposition in this sample group.

3.3.1.6 Micro-PIXE Images of Rice Root Tissue – Silicon +

This sample group is comprised of cross-sectioned root tissue from the silicon + sample group; plants grown in the presence of added silicon in their growth solution, but not added aluminium. Of the four samples, two representative samples were chosen for a detailed analysis here, the other two samples from this group are displayed below them in more compact images.

Plant 42 – Rice Root – Sample 17 (707016):

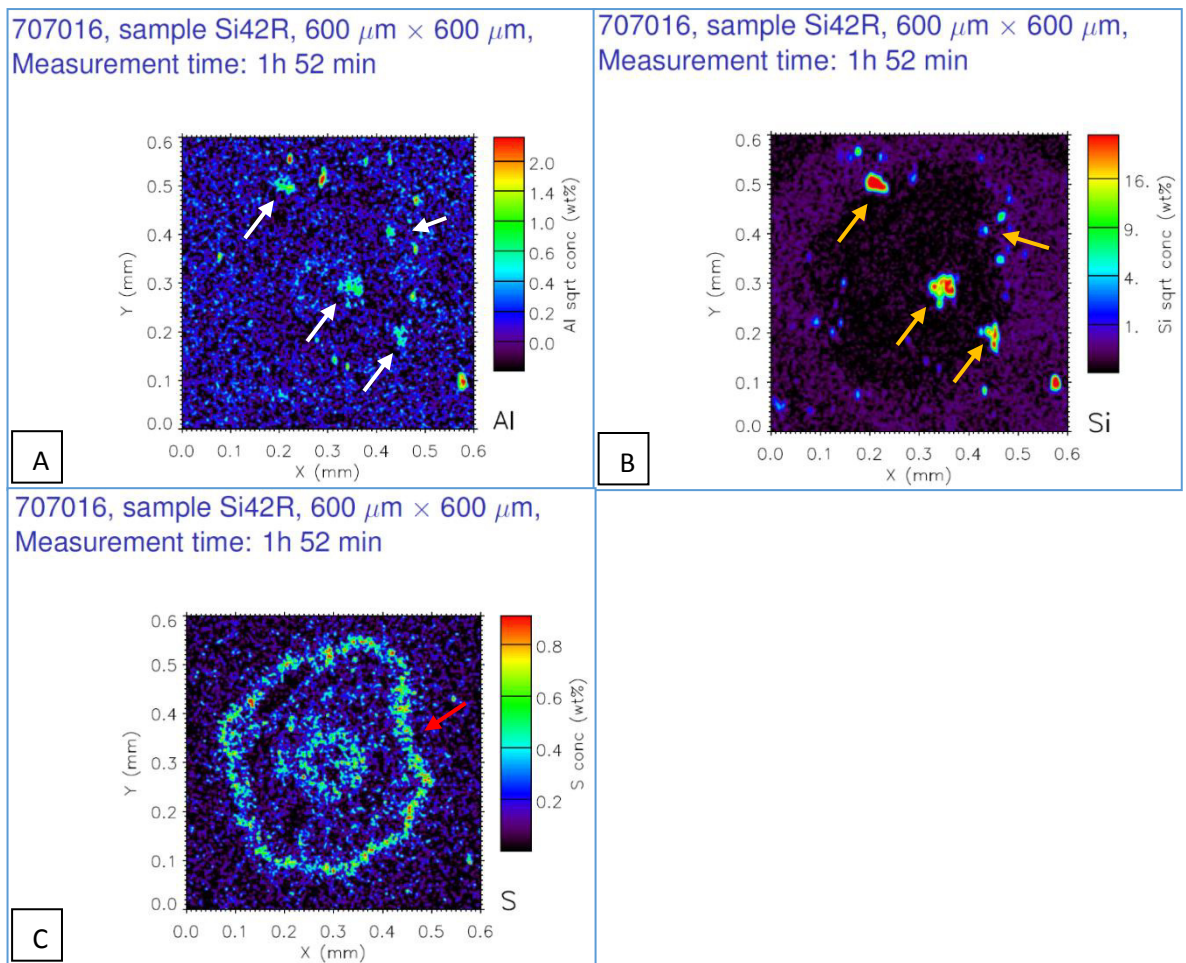


Figure 3.22 Micro-PIXE images showing aluminium (A), silicon (B) and sulphur (C) detection in rice root tissue from Silicon + group sample 42. Arrows label areas of note, discussed in text.

Multiple aluminium readings were detected in this sample at numerous points across the rhizodermis, with one reading within the vascular tissue at the sample's centre (Fig 3.22A) (see white arrows). These aluminium signals are co-localised with silicon readings consistently throughout this sample (Fig 3.22B) (see gold arrows). These areas also show signals for calcium, sodium, iron and magnesium (see supplementary data). The sulphur map shows that the rhizodermis of this root sample is deformed or damaged, likely as a result of tissue processing or sectioning (Fig 3.22C).

Plant 41 – Rice Root – Sample 19 (707018):

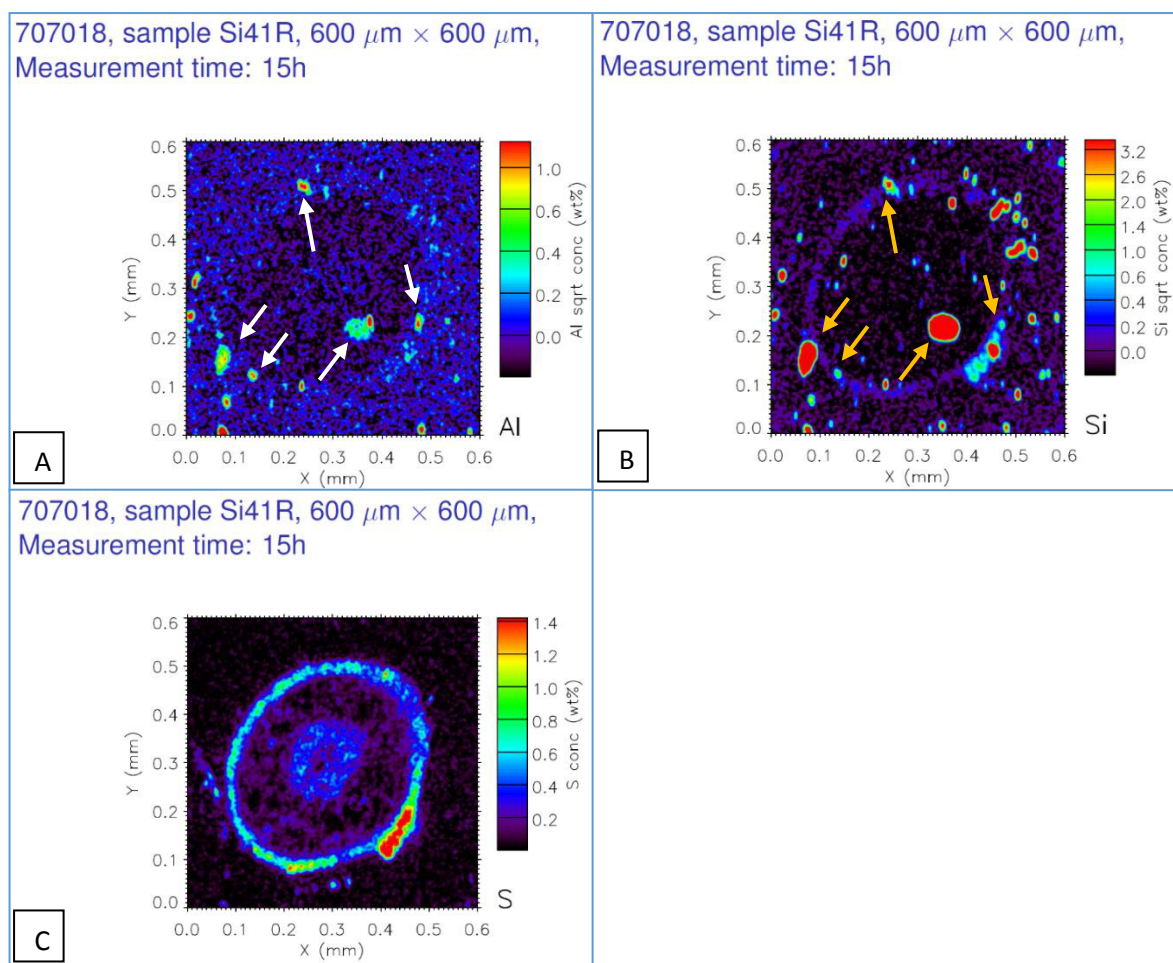


Figure 3.23 Micro-PIXE images showing aluminium (A), silicon (B) and sulphur (C) detection in rice root tissue from Silicon + group sample 41. Arrows label areas of note, discussed in text.

There were multiple aluminium readings at the rhizodermis, with one large reading within the cortex peaking at around 1% weight (Fig 3.23A) (see white arrows). These readings are co-localised with silicon readings peaking at 3.2% weight (Fig 3.23B) (see gold arrows). In addition to these readings, there are multiple silicon signals scattered throughout the sample both inside and outside the tissue, though within the plant tissue they are mostly contained to the rhizodermis and are co-localised with calcium, magnesium and iron (see supplementary data).

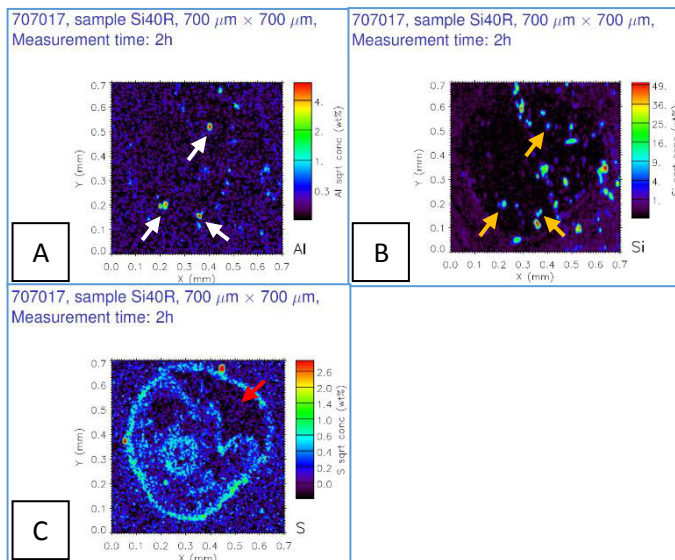


Figure 3.24 Micro-PIXE images showing aluminium (A), silicon (B) and sulphur (C) detection in rice root tissue from Silicon + group sample 40. Arrows label areas of note, discussed in text.

This is a heavily damaged root section, in which much of the cortex has come away from the rhizodermis internally (Fig 3.24C) (see red arrow). There are several aluminium readings within the cortex peaking at 6% weight (Fig 3.24A) (see white arrows), these are co-localised with silicon signals peaking at around 16% weight (Fig 3.24B) (see gold arrows). In addition to these signals, there are numerous silicon readings focused mainly in the damaged region of the root cortex, peaking at 49% weight (Fig 3.24B). All silicon locations are co-localised with sodium, magnesium and calcium readings (see supplementary data).

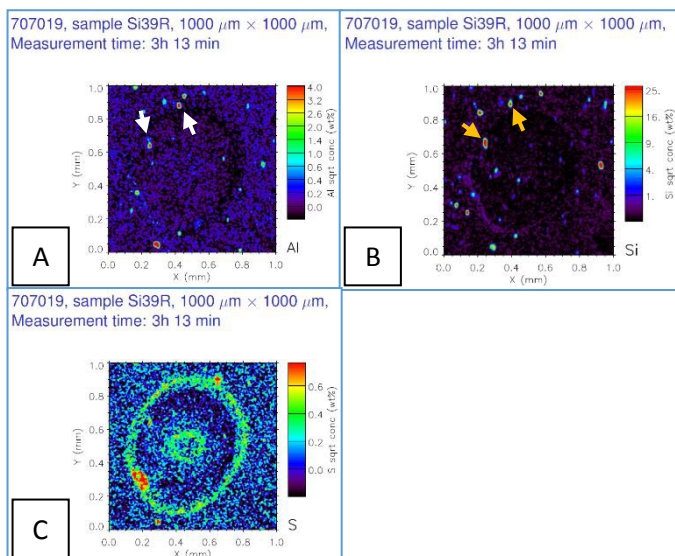


Figure 3.25 Micro-PIXE images showing aluminium (A), silicon (B) and sulphur (C) detection in rice root tissue from Silicon + group sample 39. Arrows label areas of note, discussed in text.

There are a few scattered aluminium and silicon signals, mostly external to the sample. There are two small areas of aluminium detection within the sample, peaking at 4% weight (Fig 3.25A) (see white arrows) which are co-localised with silicon readings, peaking at 25% weight (Fig 3.25B) (see gold arrows). These readings, as well as those external to the sample, are co-localised with calcium, magnesium and iron (see supplementary data). The sulphur map shows this sample to be intact (Fig 3.25C)

Summary

Three of the samples in this group are littered with aluminium and silicon hotspots, both inside and outside the sample (Fig 3.22, Fig 3.23 & Fig 3.24). Silicon and aluminium are co-localised at almost all of these hotspots, along with other elements such as calcium and magnesium. The widespread nature of these hotspots both inside and outside the plant tissue in this sample group makes it difficult to come to definitive conclusions based on these results.

3.3.1.7 Micro-PIXE Images of Rice Root Tissue – Aluminium +

This sample group is comprised of cross-sectioned root tissue from the aluminium + sample group; plants grown in the presence of added aluminium in their growth solution, but not silicon. Of the four samples, two representative samples were chosen for a detailed analysis here, the other two samples from this group are displayed below them in more compact images.

Plant 43 – Rice Root – Sample 9 (707008):

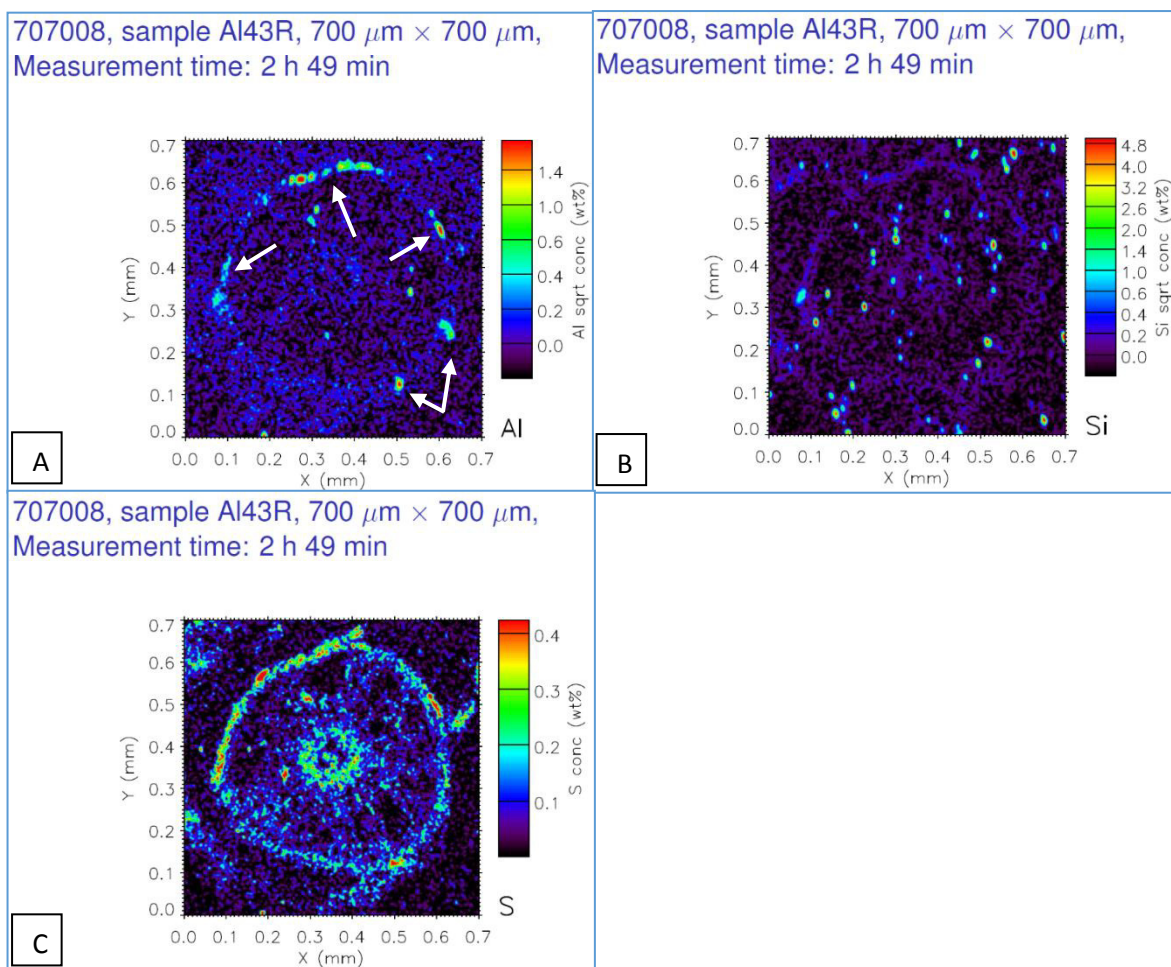


Figure 3.26 Micro-PIXE images showing aluminium (A), silicon (B) and sulphur (C) detection in rice root tissue from aluminium + group plant 43. Arrows label areas of note, discussed in text.

There is an aluminium signal intermittently at the rhizodermis of the root tissue, peaking at 1.8% weight (Fig 3.26A) (see white arrows). There are silicon hotspots interspersed throughout the sample, both in and outside the root tissue (Fig 3.26B). Whilst the sulphur map shows no signs of damage (Fig 3.26C), the chlorine map shows some minor structural damage at the top of the sample (see supplementary data).

Plant 46 – Rice Root – Sample 12 (707011):

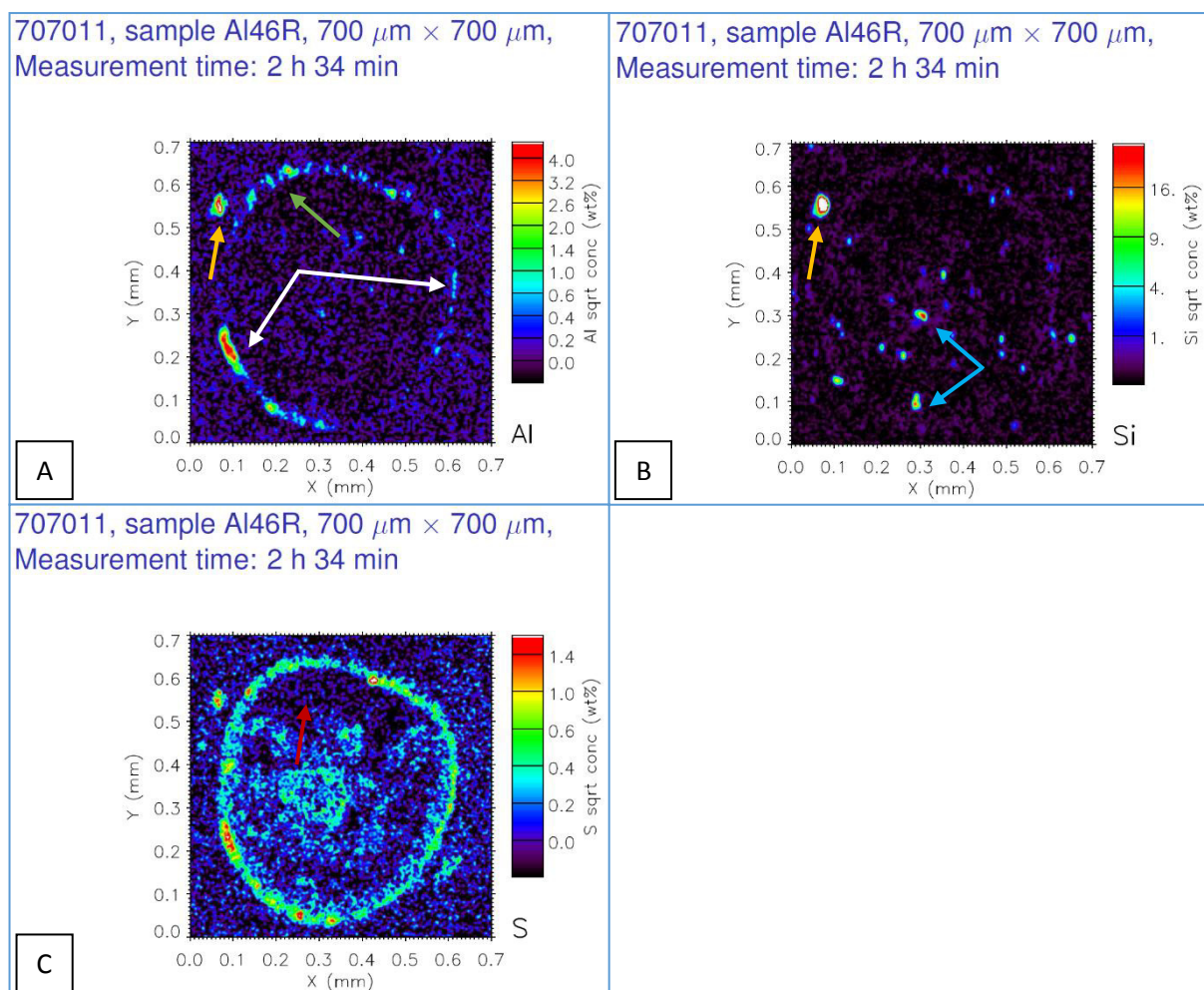


Figure 3.27 Micro-PIXE images showing aluminium (A), silicon (B) and sulphur (C) detection in rice root tissue from aluminium + group plant 46. Arrows label areas of note, discussed in text.

There is significant damage to the sample on the sulphur map (Fig 3.27C) (see red arrow). This damage is more clear in the sodium and chlorine images (see supplementary data). Aluminium can be seen at the rhizodermis of the plant tissue, with the signal strength peaking at 4% weight both in undamaged (Fig 3.27A) (see white arrows) and damaged areas of the sample (see green arrow). There is a large hotspot for silicon (Fig 3.27A) and aluminium (Fig 3.27B) outside the plant tissue (see gold arrows). There are several other small silicon readings within the undamaged tissue of the root (Fig 3.27B) (see blue arrows) co-localised with calcium (see supplementary data).

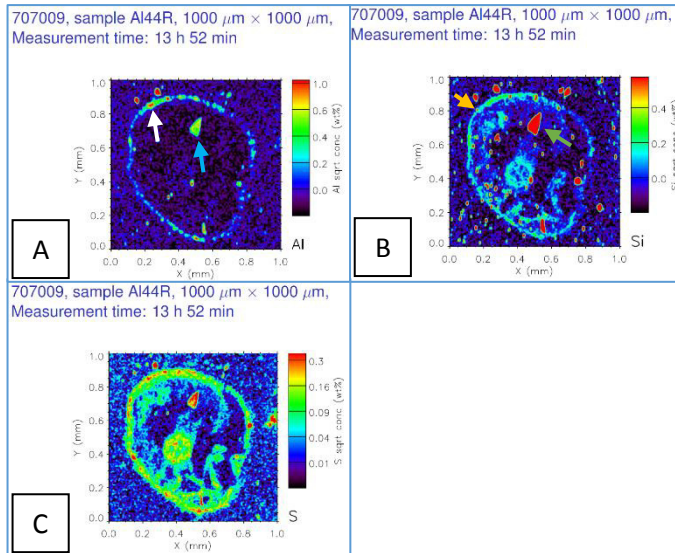


Figure 3.28 Micro-PIXE images showing aluminium (A), silicon (B) and sulphur (C) detection in rice root tissue from aluminium + group plant 44. Arrows label areas of note, discussed in text.

There is an aluminium signal consistently at the rhizodermis of the root tissue, peaking at 1.0% weight (Fig 3.28A) (see white arrow). In addition, there is a large aluminium hotspot within the cortex (see blue arrow), co-localised with a silicon signal (Fig 3.28B) (see green arrow). There is a weak silicon signal at the rhizodermis (Fig 3.28B) (see gold arrow), but the scale shows that the maximum detected silicon here was at 0.2% weight, which is at around the background level for silicon detection in other samples. Even the largest silicon hotspot only peaks at 0.6% weight (Fig 3.28B) (see green arrow). The sulphur map appears to give a strong reading, but the scale shows that it peaks at 0.3% weight (Fig 3.28C).

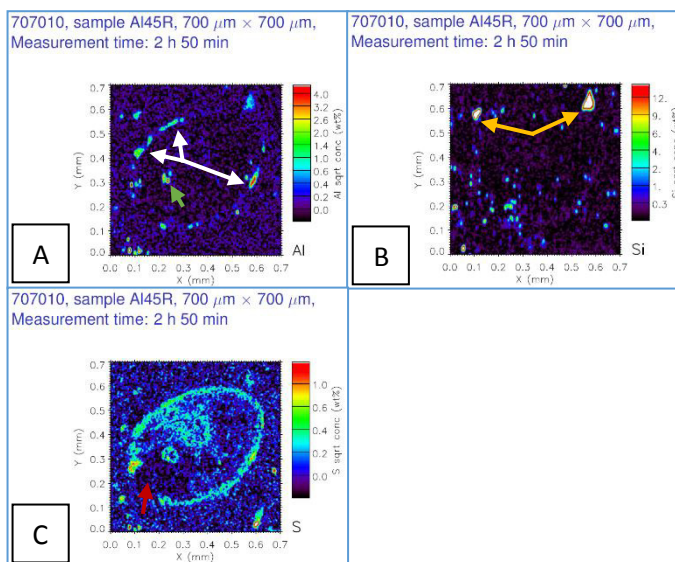


Figure 3.29 Micro-PIXE images showing aluminium (A), silicon (B) and sulphur (C) detection in rice root tissue from aluminium + group plant 45. Arrows label areas of note, discussed in text.

There is an aluminium signal intermitantly at the rhizodermis of the root tissue, peaking at 4% weight (Fig 3.29A) (see white arrows). There is also an aluminium signal at the vascular bundle (see green arrow), however, the sulphur map shows that the sample is damaged in this area (Fig 3.29C) (see red arrow). This damage is even more apparent in the chlorine and potassium maps (see supplementary data). The only major silicon readings outside of this damaged quadrant are large hotspots outside the root tissue (Fig 3.29B) (see gold arrows).

Summary

Aluminium was detected consistently at the rhizodermis in all samples in this group (Fig 3.26A – Fig 3.29A). Silicon hotspots were common across all samples, showing co-localisation with aluminium and other elements (Fig 3.26B – Fig 3.29B). The aluminium signal found at the rhizodermis does not have a co-localised silicon signal associated with it, unlike the scattered aluminium hotspots found elsewhere. One of the samples appears to be heavily damaged, which can be seen in the sulphur map (Fig 3.28C).

3.3.1.8 Micro-PIXE Images of Rice Root Tissue – Aluminium and Silicon +

This sample group is comprised of cross-sectioned root tissue from the aluminium and silicon + sample group; plants grown in the presence of added silicon and aluminium in their growth solution. Of the four samples, two representative samples were chosen for a detailed analysis here, the other two samples from this group are displayed below them in more compact images.

Plant 32b – Rice Root – Sample 13 (707012):

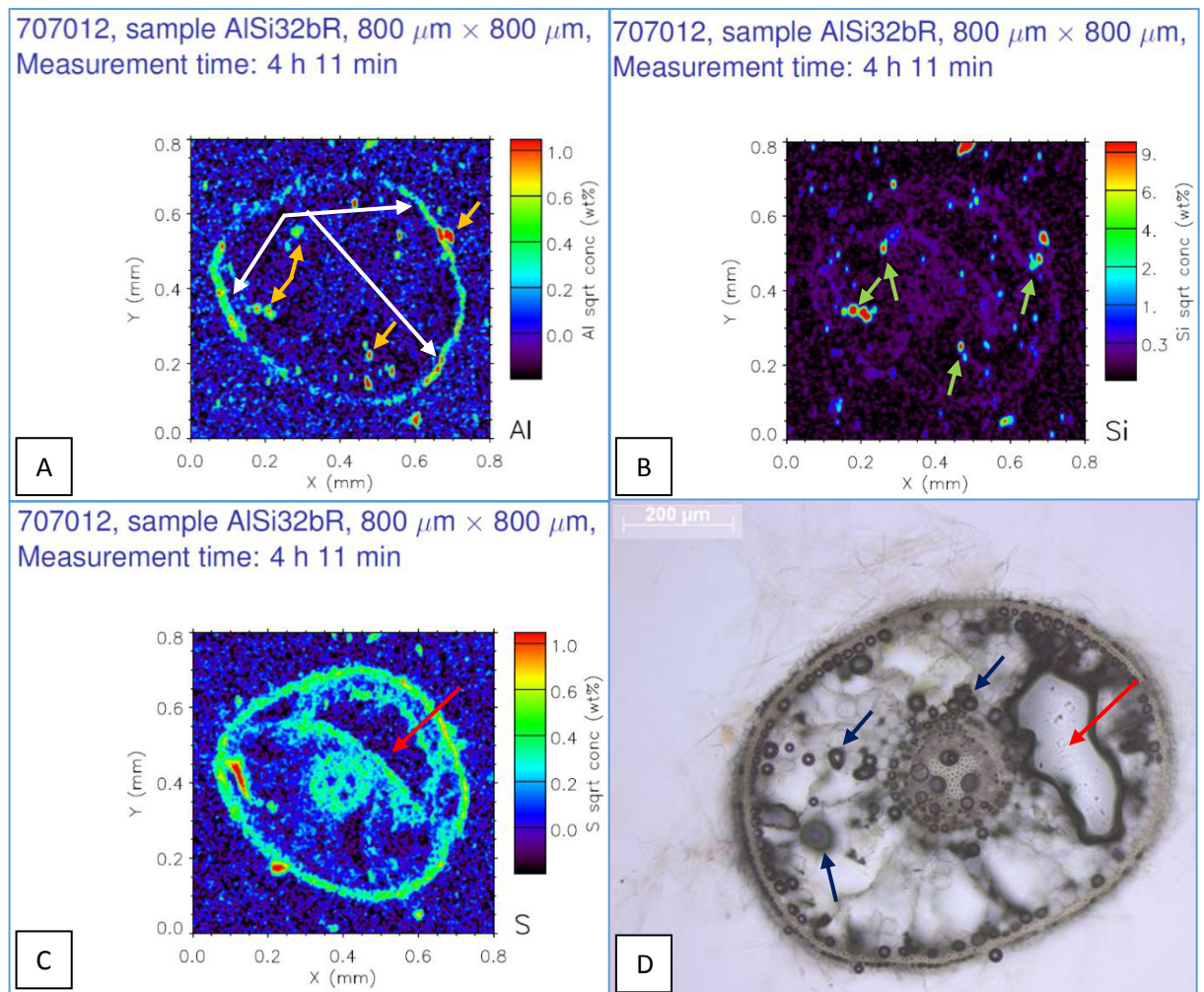


Figure 3.30 Micro-PIXE images showing aluminium (A), silicon (B) and sulphur (C), and light microscope image (D)* in rice root tissue from Aluminium/Silicon + group plant 32 sample b. Arrows label areas of note, discussed in text. *The light microscope image comes from the same sample as the Micro-PIXE images, but is not the same section.

There is a consistent aluminium reading at the rhizodermis, peaking at 1 % weight (Fig 3.30A) (see white arrows). There are multiple aluminium signals within the cortex (Fig 3.30A) (see gold arrows). These aluminium signals are co-localised with silicon signals, peaking at 9% weight (Fig 3.30B) (see green arrows) as well as calcium, potassium, phosphorus, sodium and magnesium (see supplementary data). There is a large damaged area of the cortex (Fig 3.30C & D) (see red arrows), though the rhizodermis surrounding this area seems to be intact. On the light microscope image, bubbles are found in similar areas of the sample and with similar frequency to the silicon and aluminium readings found in the Micro-PIXE images (Fig 3.30D) (see dark blue arrows).

Plant 33 – Rice Root – Sample 16 (707015):

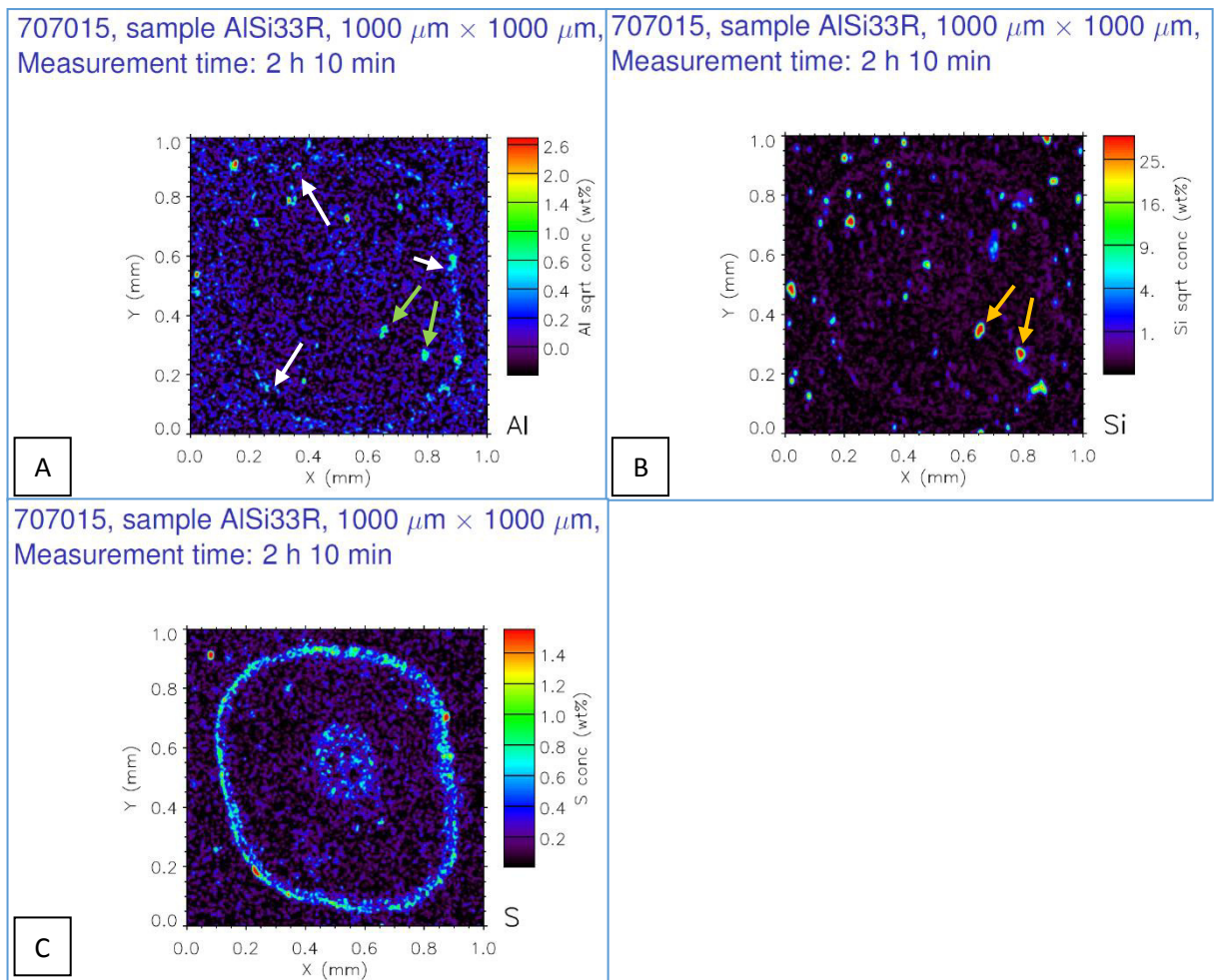


Figure 3.31 Micro-PIXE images showing aluminium (A), silicon (B) and sulphur (C) detection in rice root tissue from Aluminium/Silicon + group plant 33. Arrows label areas of note, discussed in text.

There is a sparse but visible aluminium signal at the rhizodermis, peaking at around 1% weight (Fig 3.31A) (see white arrows). There are also several small aluminium hotspots within the cortex, peaking at 1.4% weight (see green arrows). These areas are co-localised with silicon readings peaking at 30% weight (Fig 3.31B) (see gold arrows). There are other sparse, scattered signals for both aluminium (Fig 3.31A) and silicon (Fig 3.31B), both inside and outside the sample tissue.

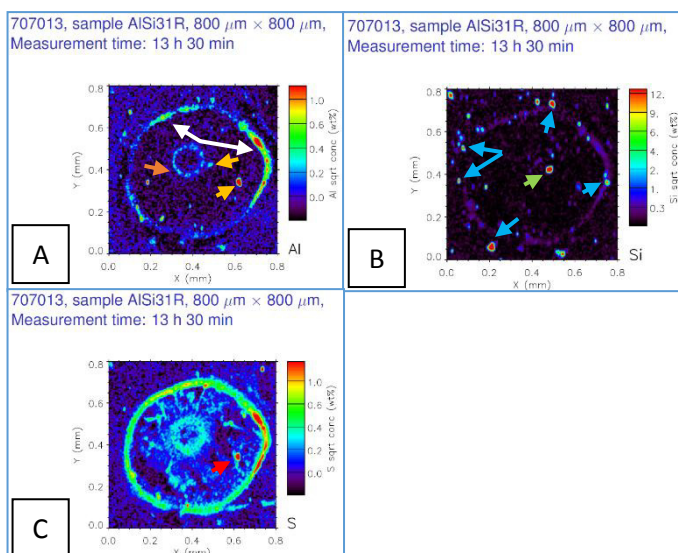


Figure 3.32 Micro-PIXE images showing aluminium (A), silicon (B) and sulphur (C) detection in rice root tissue from Aluminium/Silicon + group plant 31. Arrows label areas of note, discussed in text.

There is an intermittent aluminium reading at the rhizodermis, peaking at 1 % weight (Fig 3.32A) (see white arrows). There are also aluminium readings within the cortex of the root tissue (see gold arrows) and at the endodermis (see orange arrow). There are multiple silicon readings at the rhizodermis of the root (Fig 3.32B) (see light blue arrows). There is a large silicon hotspot within the cortex (see green arrow) which is co-localised with an aluminium signal. There is a large hotspot for sulphur (Fig 3.32C) (see red arrow) which is co-localised with both silicon and aluminium.

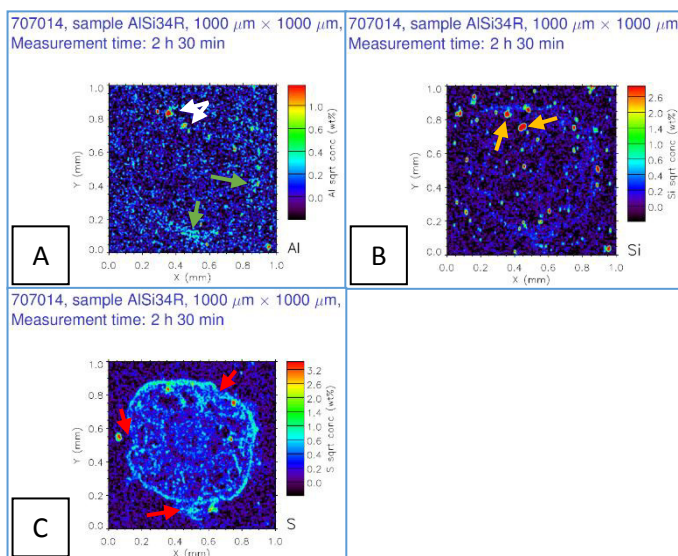


Figure 3.33 Micro-PIXE images showing aluminium (A), silicon (B) and sulphur (C) detection in rice root tissue from Aluminium/Silicon + group plant 34. Arrows label areas of note, discussed in text.

There is a faint and scattered, but still noticeable, aluminium signal at the rhizodermis, peaking at around 0.6% weight (Fig 3.33A) (see green arrows). There are a few isolated hotspots of aluminium within the cortex, peaking at 1.4% weight (see white arrows). These aluminium hotspots are co-localised with silicon readings peaking at 3% weight (Fig 3.33B) (see gold arrows). There are numerous silicon readings throughout the sample, both inside and outside the the plant tissue. Many silicon readings are co-localised with calcium (see supplementary data). The sulphur map shows damage to the structure of the root tissue, with a distorted rhizodermis (Fig 3.33C) (see red arrows).

Summary

Aluminium was detected at the rhizodermis of all samples in this group, though two samples showed heavier aluminium deposition (Fig 3.30A & Fig 3.32A), whilst the other two samples had sparser aluminium signals (Fig 3.31A & Fig 3.33A). Aluminium hotspots were also common through the sample, both inside and outside the plant tissue (Fig 3.30A – Fig 3.33A). Silicon hotspots were common across all samples, showing co-localisation with aluminium hotspots and other elements (Fig 3.30B – Fig 3.33B). The aluminium signal found at the rhizodermis does not have a consistent co-localised silicon signal associated with it.

One of the samples showed significant signs of damage on both the sulphur map (Fig 3.30C) and the light microscope image (Fig 3.30D). Another sample showed signs of minor damage at the rhizodermis (Fig 3.33C).

3.3.2 Micro-PIXE Quantitative Data

The following graphs show the quantitative measurements for silicon and aluminium within the sample tissue. The leaf was separated into the epidermis, mesophyll and invaginations as well as a total reading for both silicon and aluminium. The root tissue was separated into rhizodermis and cortex, as well as a total reading for both silicon and aluminium.

3.3.2.1 Total Leaf Silicon Content

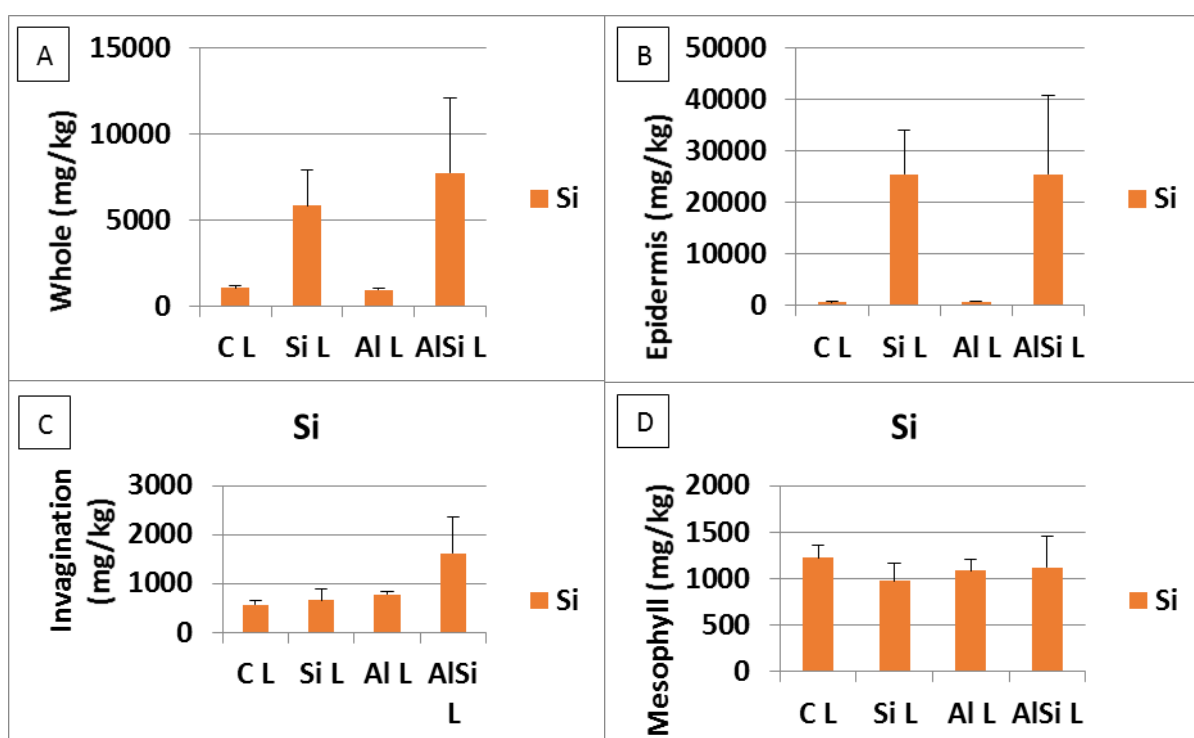


Figure 3.34 Total leaf silicon concentrations for the four sample groups: control (C L), Silicon + (Si L), Aluminium + (Al L) and Silicon/Aluminium + (AlSi L). **A:** Total silicon as mg/kg in the whole leaf sample. **B:** Total silicon as mg/kg in the leaf epidermis. **C:** Total silicon as mg/kg in the leaf invaginations. **D:** Total silicon as mg/kg in the leaf mesophyll sample.

Total silicon concentration was significantly higher in the leaf tissue of rice plants in the presence of added silicon, groups Si & AlSi, than in the silicon-deplete groups, C and Al (Fig 3.34A). In these silicon-replete groups, the vast majority of silicon was detected in or around the epidermis of the leaf tissue (Fig 3.34B). The area marked as invaginations are in fact the locations of bulliform cells; motor cells which can contract, folding the leaf to reduce water loss (Fig 3.34C). Silicon was detected in the mesophyll of the rice tissue in much smaller quantities; interestingly, silicon was

detected at comparable levels in the mesophyll amongst all four sample groups, regardless of whether they were grown in added silicon or not (Fig 3.34D).

3.3.2.2 Total Leaf Aluminium Content

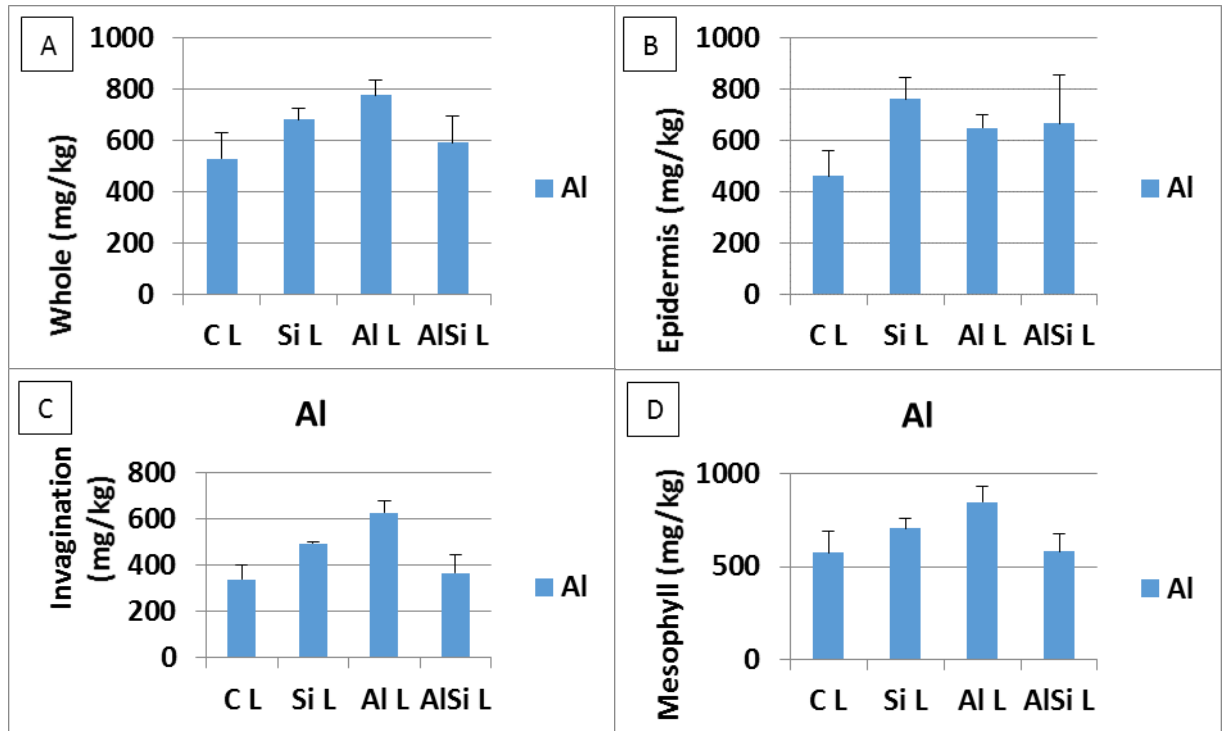


Figure 3.35 Total leaf aluminium concentrations for the four sample groups: control (C L), Silicon + (Si L), Aluminium + (Al L) and Silicon/Aluminium + (AlSi L). **A:** Total aluminium as mg/kg in the whole leaf sample. **B:** Total aluminium as mg/kg in the leaf epidermis. **C:** Total aluminium as mg/kg in the leaf invaginations. **D:** Total aluminium as mg/kg in the leaf mesophyll sample.

Total aluminium concentrations in the leaf tissue were comparable and low in all four sample groups with none of the groups measuring higher than 800 mg/kg (Fig 3.35A). Aluminium levels in the epidermis were lower in the control group, peaking at just over 400 mg/kg, whilst the other three groups all ranged between 600–800 mg/kg (Fig 3.35B). In the invaginations, the control and Aluminium/silicon + groups both peaked just under 400 mg/kg, whilst the silicon group was higher at 500 mg/kg and the aluminium group higher still at 600 mg/kg (Fig 3.35C). The mesophyll showed a similar pattern with the control and aluminium/silicon + groups giving the lowest concentrations at around 500 mg/kg, whilst the silicon and aluminium groups were higher at 700 and 800 mg/kg respectively (Fig 3.35D).

3.3.2.3 Leaf Silicon and Aluminium Comparison

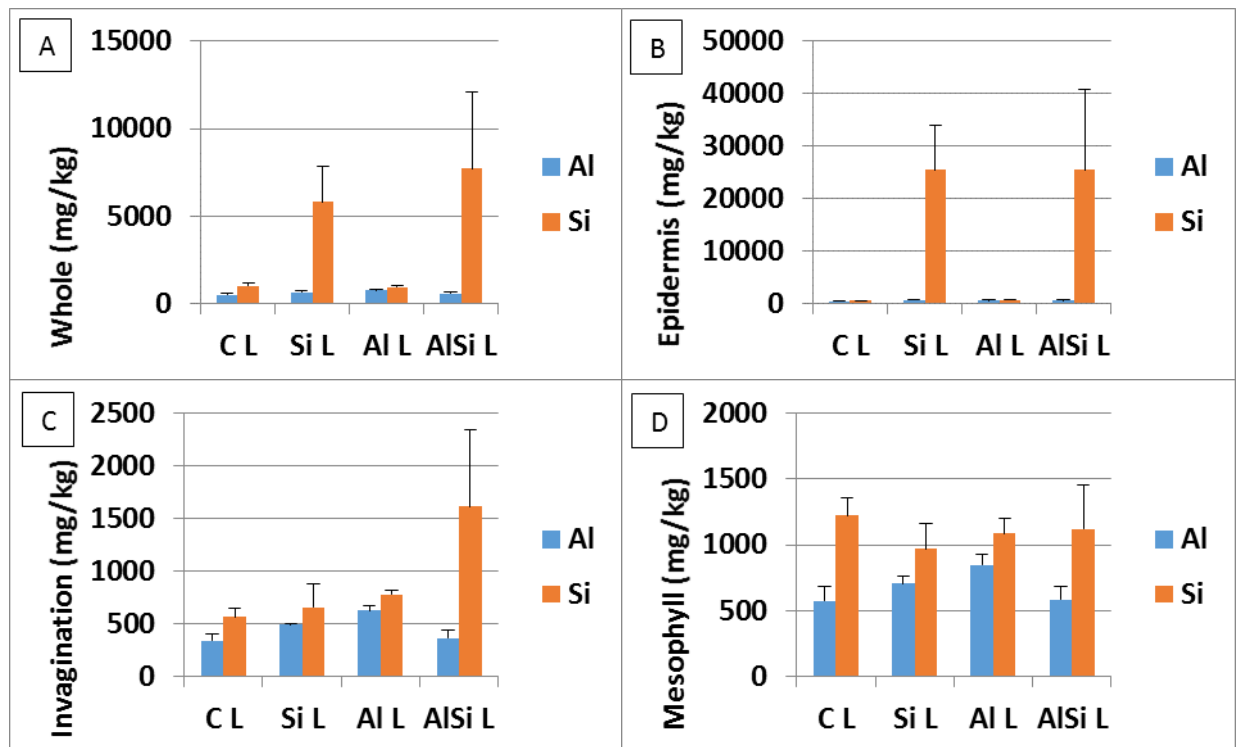


Figure 3.36 Total leaf silicon and aluminium concentrations for the four sample groups: control (C L), Silicon + (Si L), Aluminium + (Al L) and Silicon/Aluminium + (AlSi L). **A:** Total silicon and aluminium as mg/kg in the whole leaf sample. **B:** Total silicon and aluminium as mg/kg in the leaf epidermis. **C:** Total silicon and aluminium as mg/kg in the leaf invaginations. **D:** Total silicon and aluminium as mg/kg in the leaf mesophyll sample.

The comparisons of both total silicon and aluminium, along with the breakdowns by region, within the plant tissue show no correlation between the higher silicon levels in the silicon and silicon/aluminium groups and any corresponding difference in aluminium levels (Fig 3.36).

3.3.2.4 Rice Root Silicon Content

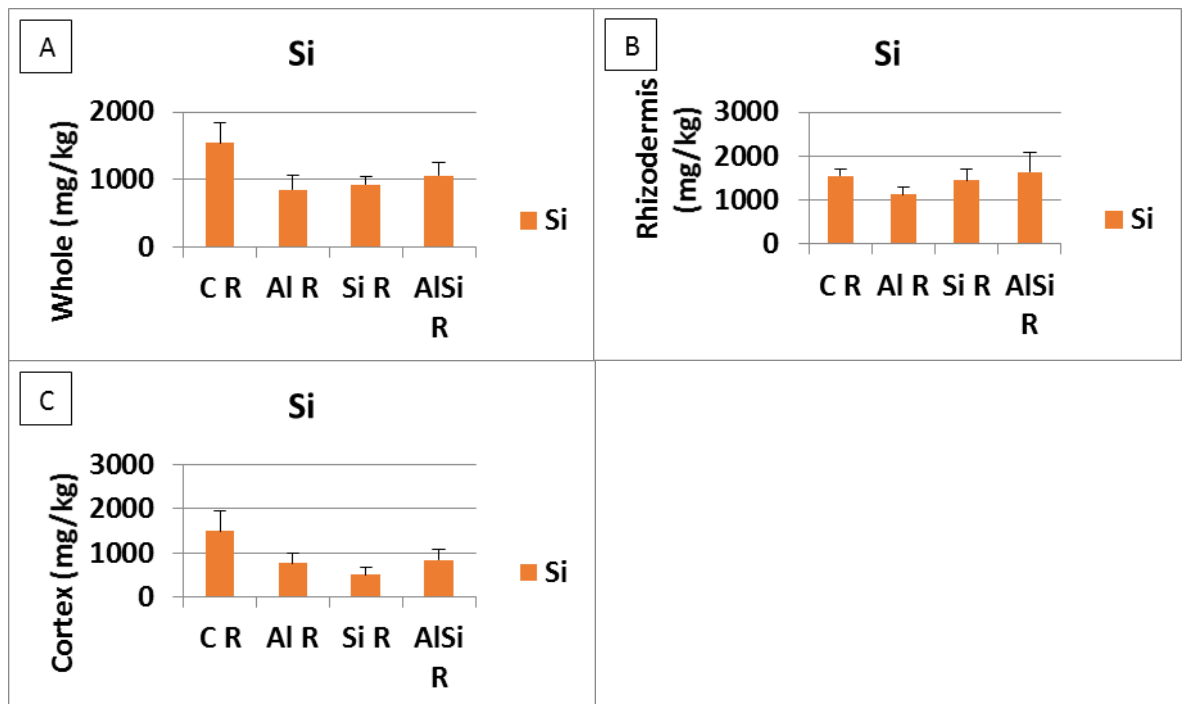


Figure 3.37 Total root silicon concentrations for the four sample groups: control (C L), Silicon + (Si L), Aluminium + (Al L) and Silicon/Aluminium + (AlSi L). **A:** Total silicon as mg/kg in the whole root sample. **B:** Total silicon as mg/kg in the root rhizodermis. **C:** Total silicon as mg/kg in the root cortex.

Total silicon levels were highest in the control group at around 1,500 mg/kg, whilst the other three groups were lower and at similar levels, between 800–1,000 mg/kg (Fig 3.37A). The control group's silicon levels were not disproportionately higher than the other groups at the rhizodermis (Fig 3.37B), however, the silicon levels in the cortex were much higher than the other groups (Fig 3.37C).

3.3.2.5 Rice Root Aluminium Content

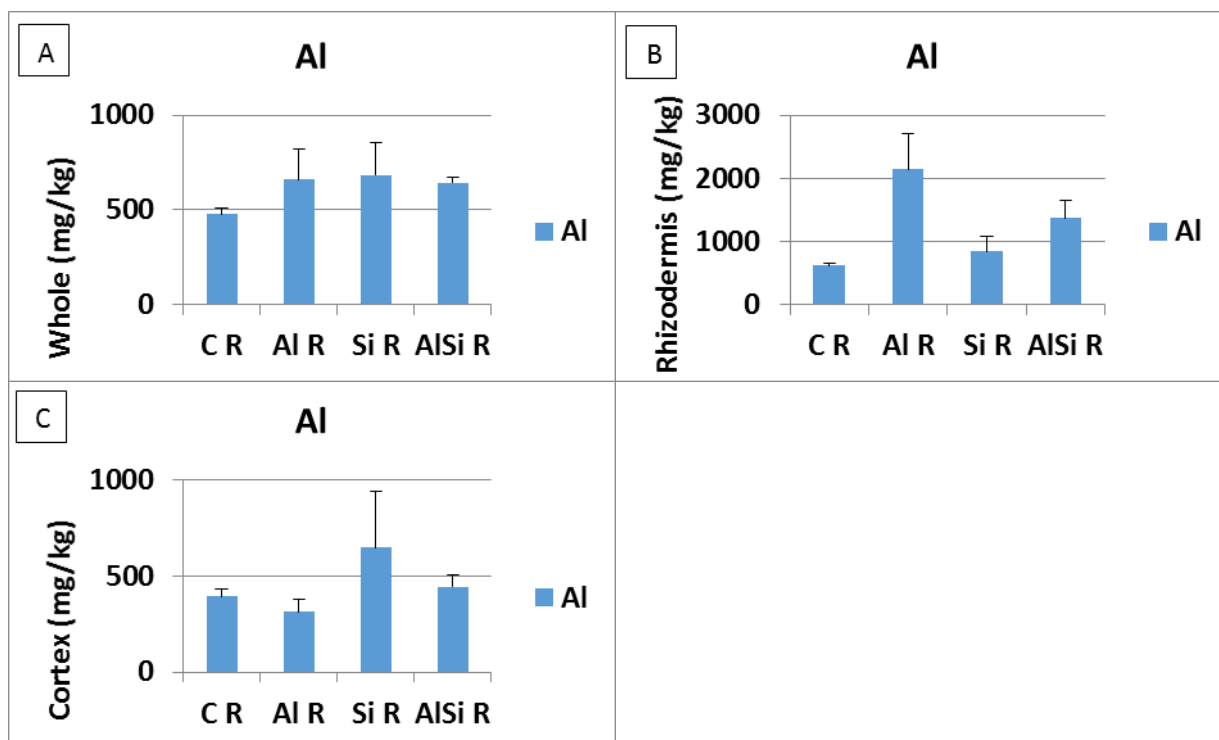


Figure 3.38 Total root aluminium concentrations for the four sample groups: control (C L), Silicon + (Si L), Aluminium + (Al L) and Silicon/Aluminium + (AlSi L). **A:** Total aluminium as mg/kg in the whole root sample. **B:** Total aluminium as mg/kg in the root rhizodermis. **C:** Total aluminium as mg/kg in the root cortex.

Total aluminium levels were higher in the aluminium, silicon and silicon/aluminium than in the control group (Fig 3.38A). At the rhizodermis, aluminium levels were significantly higher in the aluminium group, peaking at just over 2,000 mg/kg (Fig 3.38B). The next highest group was the silicon/aluminium group at around 1,400 mg/kg, followed by the control and silicon groups which were below 1,000 mg/kg. In the cortex, the silicon group had significantly higher aluminium levels than the others, though there is a huge margin for error in the reading (Fig 3.38C). The other three groups show similar aluminium levels below 500 mg/kg.

3.3.2.6 Root Silicon/Aluminium Comparison

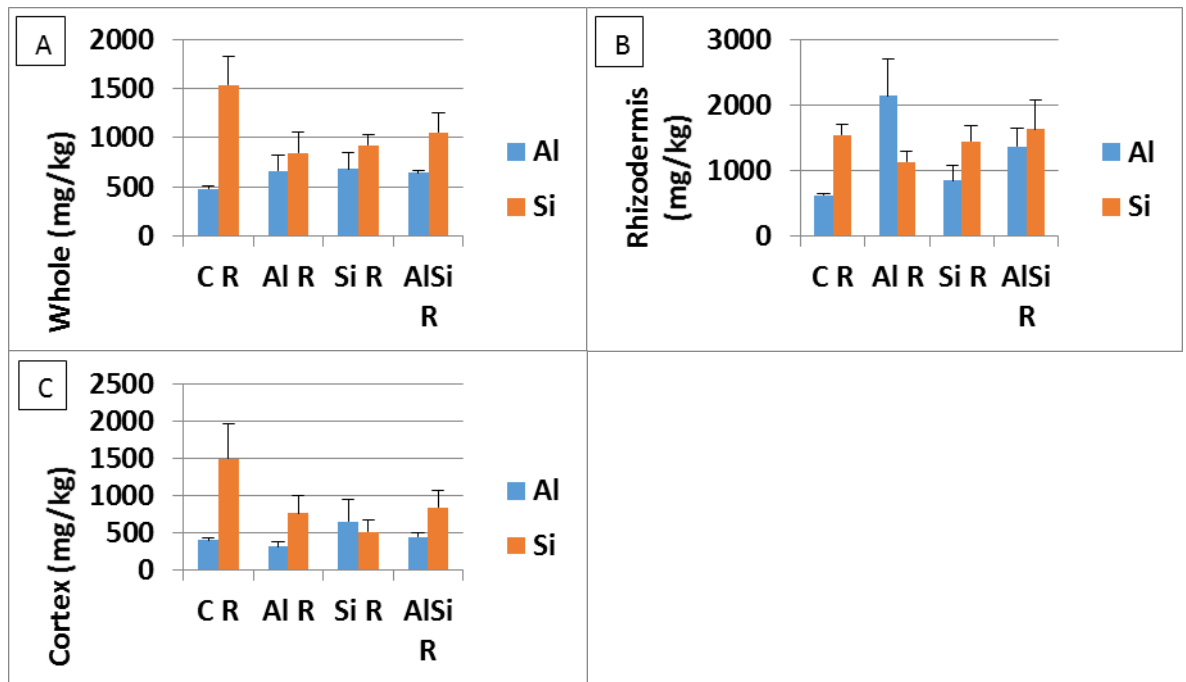


Figure 3.39 Total root silicon and aluminium concentrations for the four sample groups: control (C L), Silicon + (Si L), Aluminium + (Al L) and Silicon/Aluminium + (AlSi L). **A:** Total silicon & aluminium as mg/kg in the whole root sample. **B:** Total silicon & aluminium as mg/kg in the root rhizodermis. **C:** Total silicon & aluminium as mg/kg in the root cortex.

The comparisons of both total silicon and aluminium, along with the breakdowns by region within the plant tissue, show no correlation between the higher silicon levels in the silicon and silicon/aluminium groups and any corresponding difference in aluminium levels (Fig 3.39).

3.3.3 LEXRF Imaging

LEXRF images were taken for oxygen, aluminium and silicon; whilst oxygen is not relevant to this study, the image provides a useful overview of the plant tissue. Light microscope images and areal density maps are also displayed here to give the LEXRF images context.

Light microscope images show the relative location of the LEXRF images within the greater structure of the plant tissue, highlighted by a red box. The areal density map shows the calculated mass relative to the area, displayed in $\mu\text{g cm}^{-2}$; the whiter an area appears on the image, the denser the mass of area is.

LEXRF images show the amount of the relevant element (oxygen, aluminium or silicon) in $\mu\text{g cm}^{-2}$. The colour scale on the right side of each image shows the percentage weight detection of each element in that region of the sample. It is important to note that the scale varies between images. Within each image's colour scale: dark blue shows that there is no element detection; the lower end of the scale is represented by lighter blues, greens and yellow; and orange and red represent the highest levels of element detection within the sample.

3.3.3.1 Silicon + Leaf Tissue

The first sample group is comprised of cross-sectioned leaf tissue from the silicon + sample group; plants grown in the presence of added silicon but not aluminium in their growth solution.

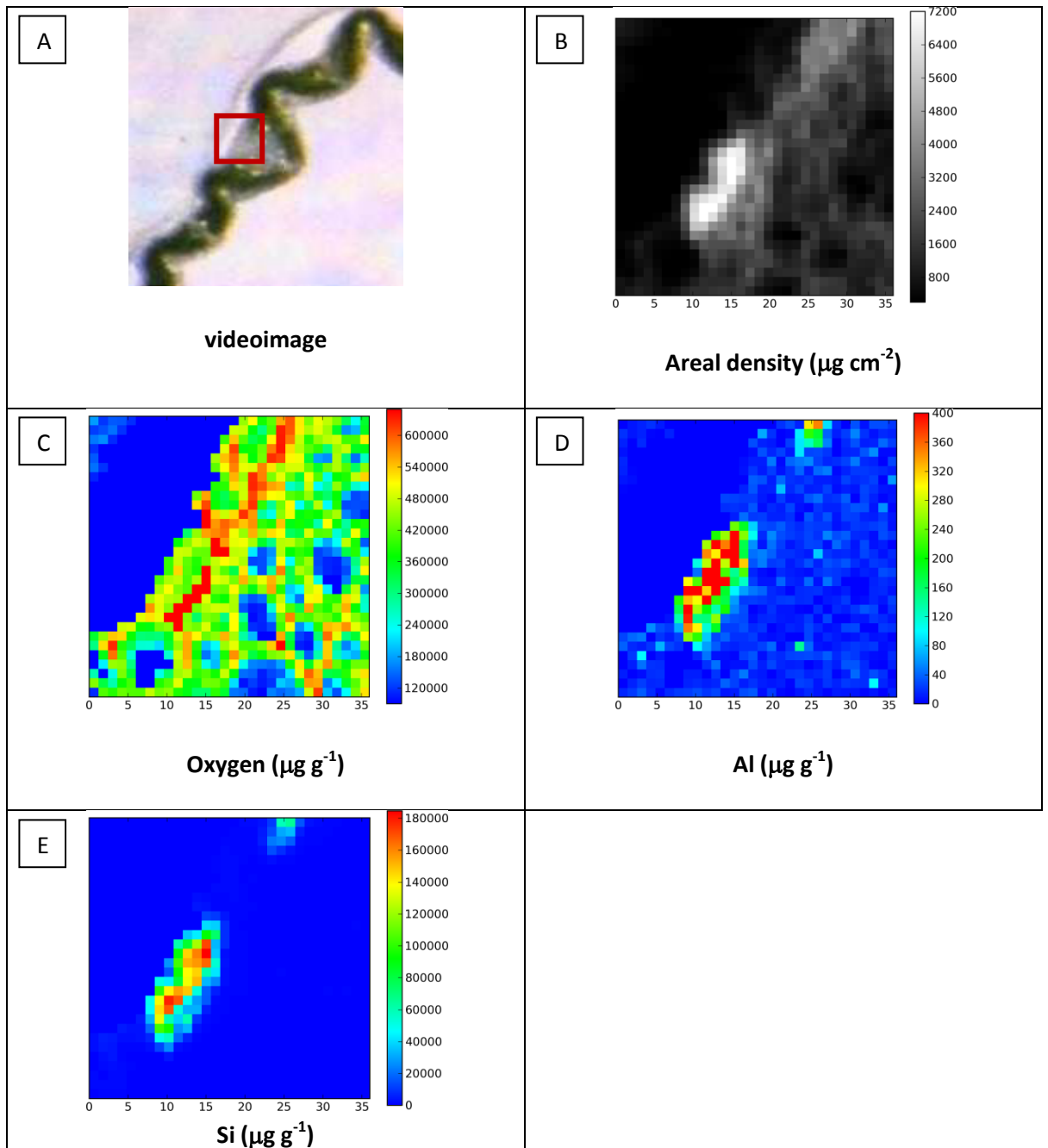


Figure 3.40 LEXRF imaging of Silicon + Group Leaf Tissue. **A:** Light microscope image showing rice leaf sample; red box highlights area of LEXRF imaging sample area. **B:** Areal density image of sample area. **C:** LEXRF detection of oxygen. **D:** LEXRF detection of aluminium. **E:** LEXRF detection of silicon.

This LEXRF image is taken from the upper epidermis of the leaf tissue, above a large vascular bundle (Fig 3.40A). Silicon was detected at two locations above the vascular bundle, in the known location of silica cells, with a signal strength peaking at around 180 mg/g, which equates to around 18% weight (Fig 3.40E). This silicon signal at the silica cells is co-localised with an aluminium signal, peaking at around 0.4 mg/g or around 0.04% weight (Fig 3.40D). There is also

some evidence of a diffuse aluminium presence as evidenced by the lighter blue areas throughout the sample. The areal density image shows a much higher mass density at the area of silicon and aluminium detection, peaking at $7,200 \mu\text{g cm}^{-2}$, at least two or three times higher than the surrounding tissue (Fig 3.40C).

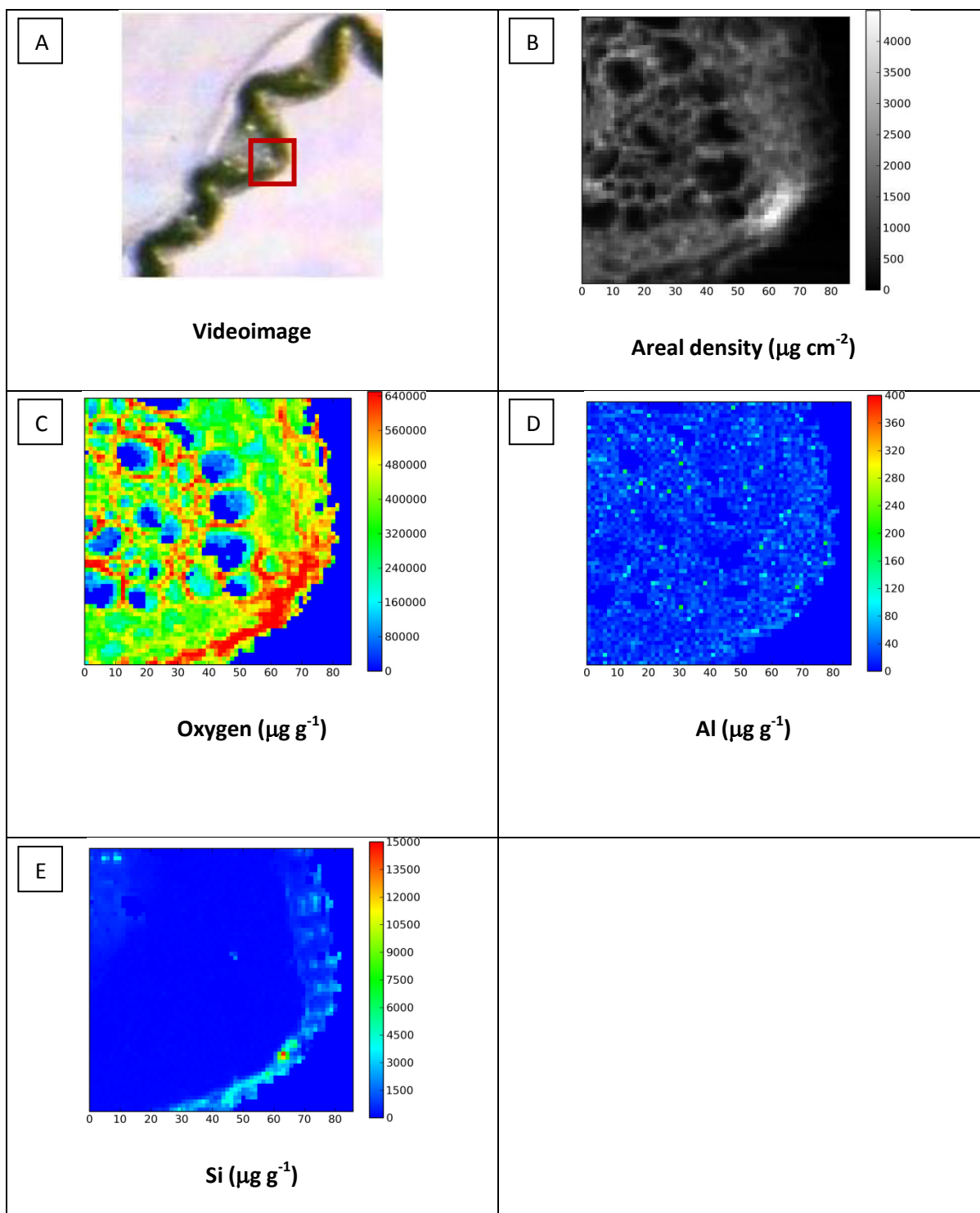


Figure 3.41 LEXRF imaging of Silicon + Group Leaf Tissue. **A:** Light microscope image showing rice leaf sample; red box highlights area of LEXRF imaging sample area. **B:** Areal density image of sample area. **C:** LEXRF detection of oxygen. **D:** LEXRF detection of aluminium. **E:** LEXRF detection of silicon.

The LEXRF images were taken from the lower epidermis of the leaf tissue, below a large vascular bundle (Fig 3.41A). Silicon was detected at the lower epidermis of the plant tissue in this sample, peaking at around 150 mg/g in one spot, but generally reading at around 4 mg/g along the silicon

layer (Fig 3.41E). There is evidence of a diffuse aluminium presence as evidenced by the lighter blue areas throughout the sample, but there is no sign of co-localisation between aluminium and the silicon layer at the epidermis (Fig 3.41D). The areal density image shows a higher mass density than the surrounding tissue at the area of highest silicon concentration at the lower epidermis (Fig 3.41B).

3.3.3.2 Silicon/Aluminium + Group Leaf Tissue

This sample group is comprised of cross-sectioned leaf tissue from the aluminium and silicon + sample group; plants grown in the presence of added silicon and aluminium in their growth solution.

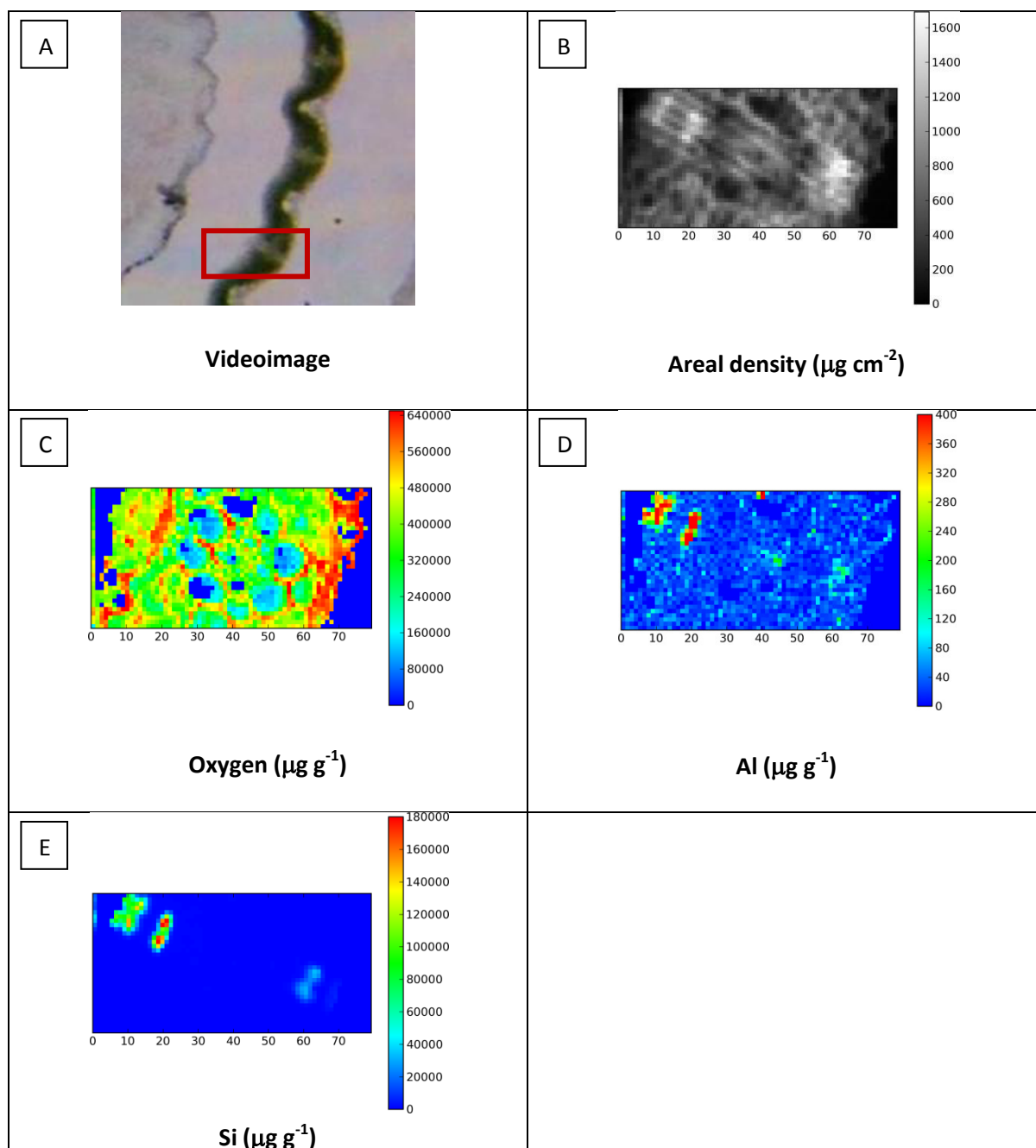


Figure 3.42 LEXRF imaging of Silicon/Aluminium + Group Leaf Tissue. **A:** Light microscope image showing rice leaf sample; red box highlights area of LEXRF imaging sample area. **B:** Areal density image of sample area. **C:** LEXRF detection of oxygen. **D:** LEXRF detection of aluminium. **E:** LEXRF detection of silicon.

The LEXRF images were taken from a cross section that extends across the width of the leaf tissue, encompassing both the upper and lower epidermis as well as the vascular bundle beneath them (Fig 3.42A). Silicon was detected at two locations above the vascular bundle and one below, in the known location of silica cells, with a signal strength peaking at around 180 mg/g above the vascular bundle, which equates to around 18% weight (Fig 3.42E). The silicon signal is weaker at the signal below the vascular bundle, peaking at around 50 mg/g, or 5% weight. This silicon signal at the silica cells is co-localised with an aluminium signal, peaking at around 0.4 mg/g or around 0.04% weight above the vascular bundle and around 0.2 mg/g or 0.02% weight below (Fig 3.42D). There is also evidence of a diffuse aluminium presence as evidenced by the lighter blue areas throughout the sample. The areal density image shows a higher mass density than the surrounding tissue at the areas of silicon and aluminium detection, both above and below the vascular bundle (Fig 3.42B).

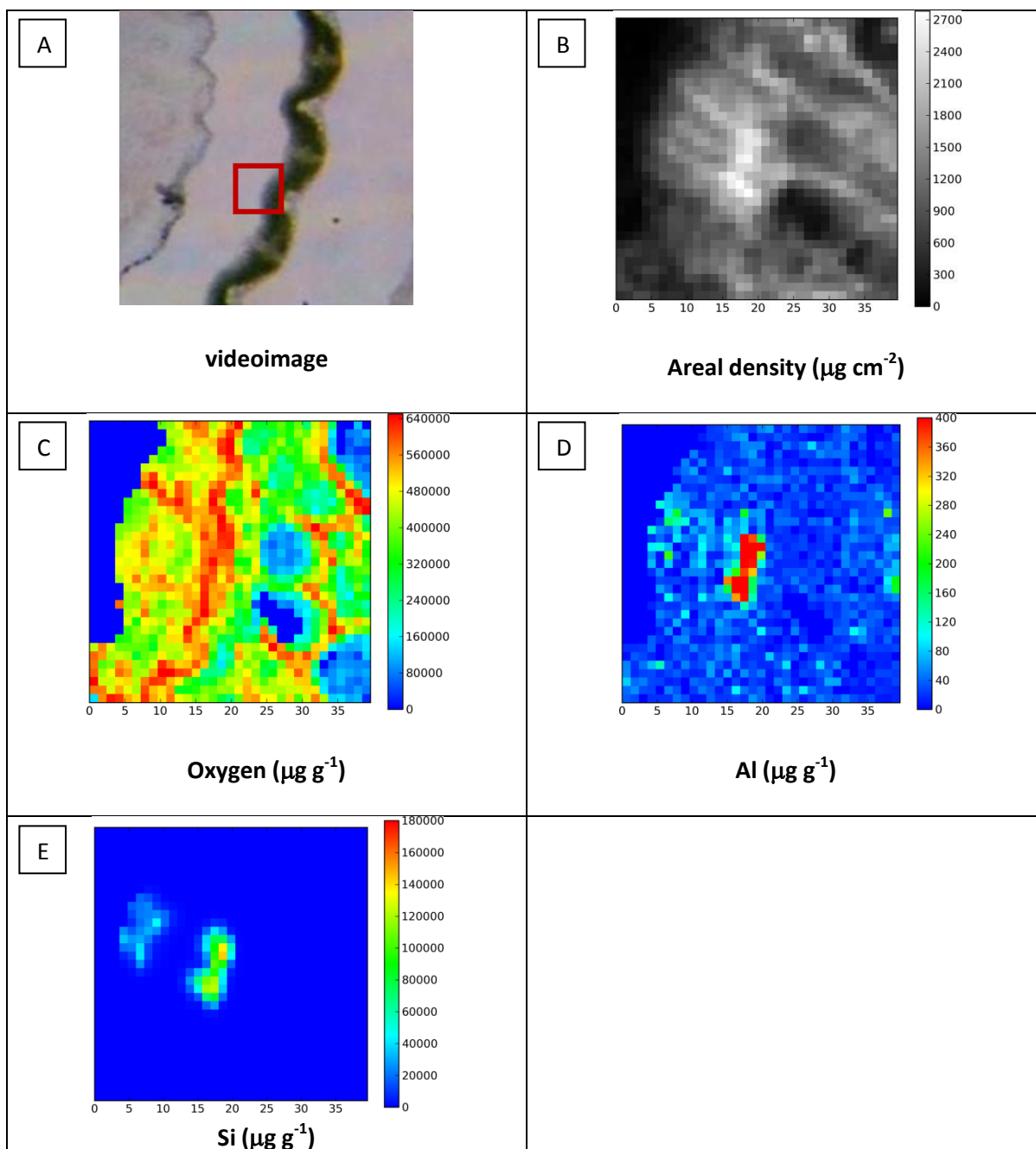


Figure 3.43 LEXRF imaging of Silicon/Aluminium + Group Leaf Tissue. **A:** Light microscope image showing rice leaf sample; red box highlights area of LEXRF imaging sample area. **B:** Areal density image of sample area. **C:** LEXRF detection of oxygen. **D:** LEXRF detection of aluminium. **E:** LEXRF detection of silicon.

The LEXRF images were taken from the upper epidermis of the leaf tissue, above a collection of bulliform cells (Fig 3.43A). Silicon was detected at two locations above the vascular bundle, in the known location of silica cells, with a signal strength peaking at around 180 mg/g, which equates to around 18% weight (Fig 3.43E). This silicon signal at the silica cells is co-localised with an aluminium signal, peaking at around 0.4 mg/g or around 0.04% weight at the lower of the two

silica cells, but only around 0.2 mg/g or 0.02% weight at the higher silica cell (Fig 3.43D). There is also evidence of a diffuse aluminium presence as evidenced by the lighter blue areas throughout the sample. The areal density image is somewhat out of focus, but still shows a higher mass density than the surrounding tissue at the areas of silicon and aluminium detection (Fig 3.43B).

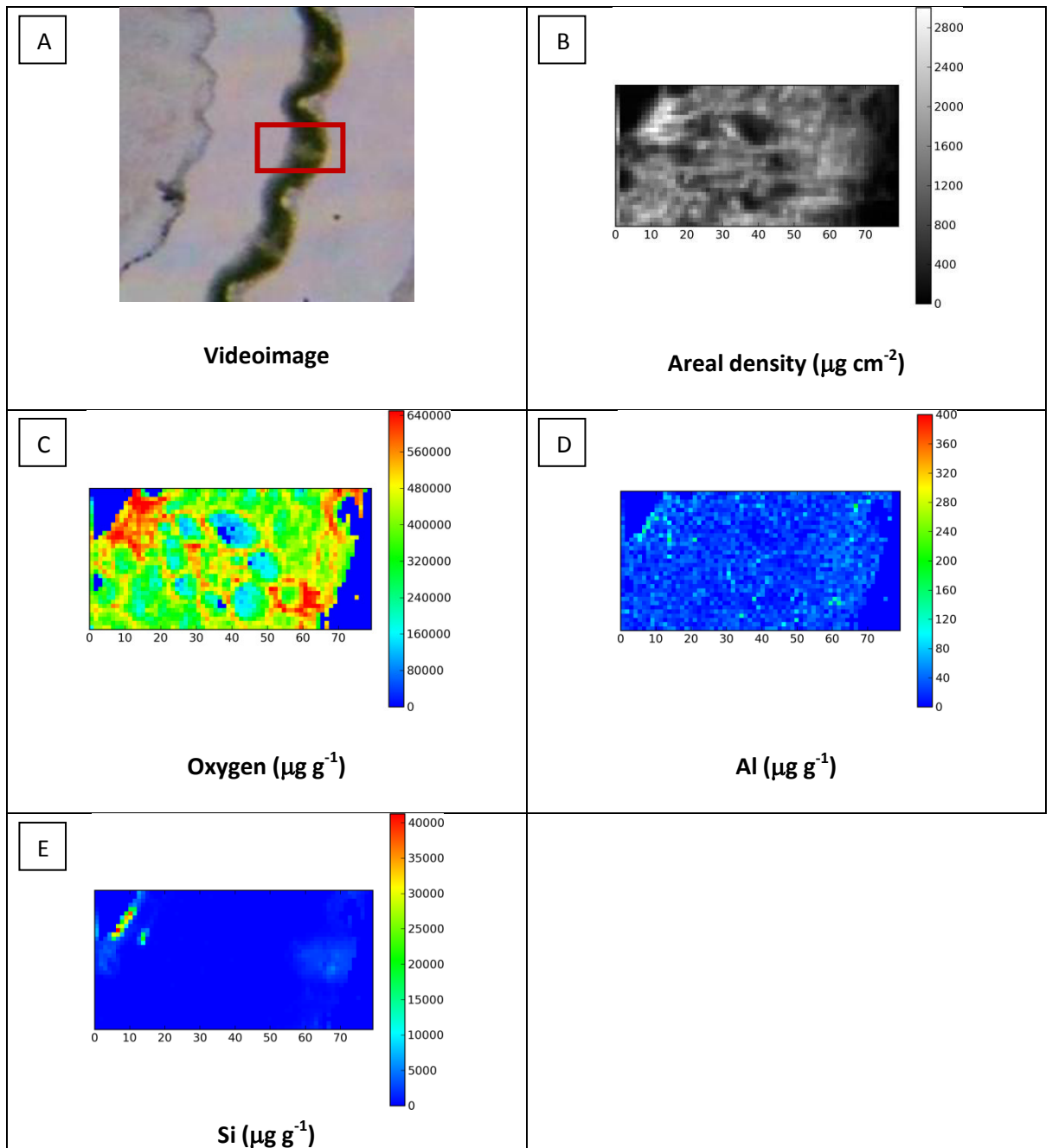


Figure 3.44 LEXRF imaging of Silicon/Aluminium + Group Leaf Tissue. **A:** Light microscope image showing rice leaf sample; red box highlights area of LEXRF imaging sample area. **B:** Areal density image of sample area. **C:** LEXRF detection of oxygen. **D:** LEXRF detection of aluminium. **E:** LEXRF detection of silicon.

The LEXRF images were taken from a cross section that extends across the width of the leaf tissue, encompassing both the upper and lower epidermis as well as the vascular bundle beneath them (Fig 3.44A). Silicon was detected above the vascular bundle, in the known location of silica cells, peaking at around 41 mg/g or 4% weight (Fig 3.44E). There is also a faint silicon presence at the lower epidermis of the leaf tissue, reading below 5 mg/g or 0.5% weight. There is evidence of a

diffuse aluminium presence as evidenced by the lighter blue areas throughout the sample, but there is no sign of co-localisation between aluminium and the silicon at the epidermis (Fig 3.44D). The areal density image is somewhat out of focus, but still shows a higher mass density than the surrounding tissue at the areas of silicon at the upper epidermis, though not the lower epidermis (Fig 3.44B).

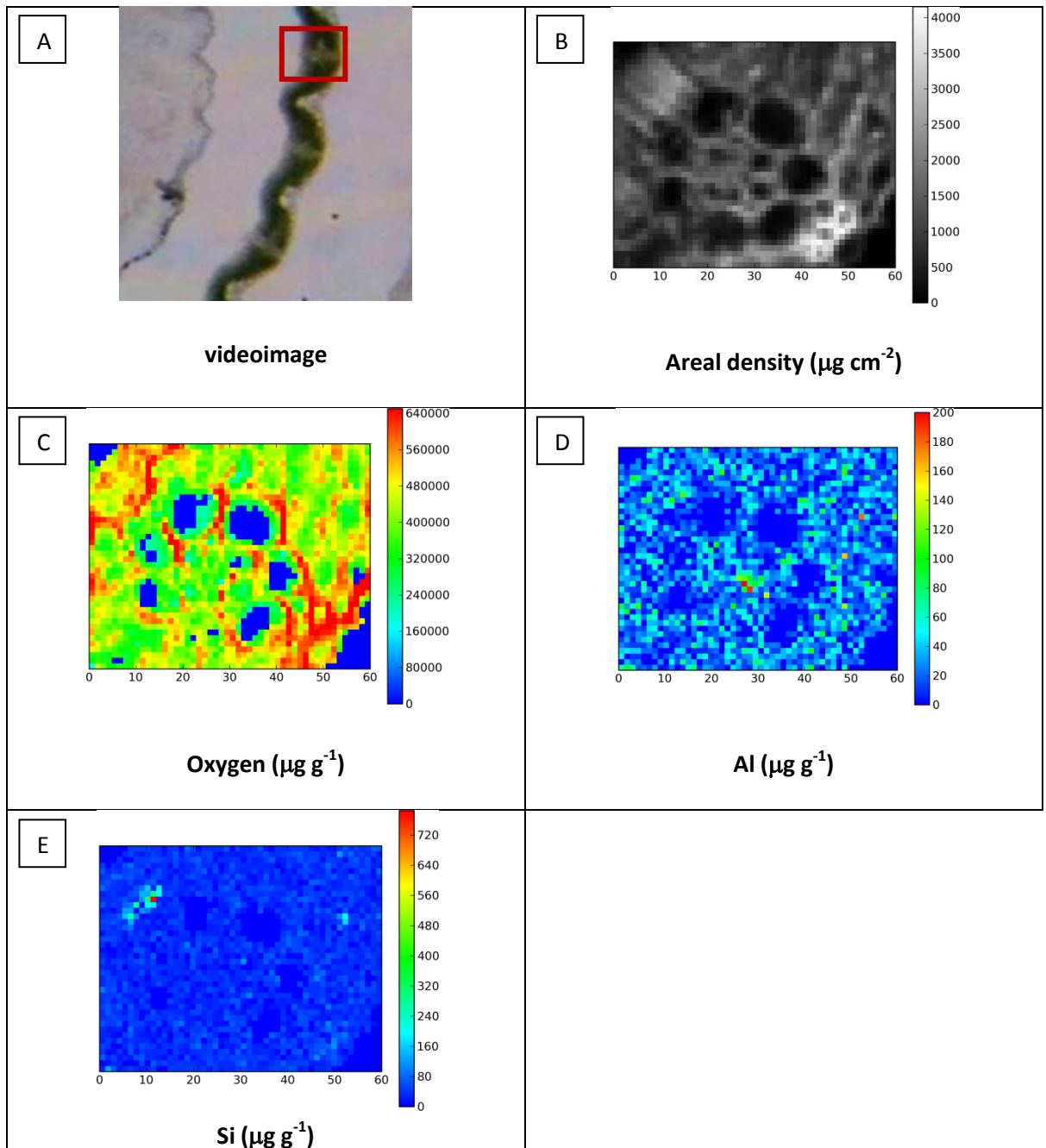


Figure 3.45 LEXRF imaging of Silicon/Aluminium + Group Leaf Tissue. **A:** Light microscope image showing rice leaf sample; red box highlights area of LEXRF imaging sample area. **B:** Areal density image of sample area. **C:** LEXRF detection of oxygen. **D:** LEXRF detection of aluminium. **E:** LEXRF detection of silicon.

The LEXRF images were taken from a cross section that extends across the width of the leaf tissue, encompassing both the upper and lower epidermis as well as the vascular bundle between them (Fig 3.45A). There is evidence of a diffuse aluminium presence as evidenced by the lighter blue areas throughout the sample (Fig 3.45D). There is evidence of a diffuse silicon presence in this sample and one small area of higher silicon accumulation, but reading at only 0.7 mg/g at its peak (Fig 3.45E). The areal density image shows a higher mass density than the surrounding tissue below the vascular bundle, but there is no correlation with aluminium or silicon deposition seen (Fig 3.45B).

3.4 Discussion

3.4.1. Micro-PIXE Image Analysis

The results of each individual sample group will be discussed, followed by a general discussion of the method and the findings of this research.

3.4.1.1 Control Leaf: Grown in the Absence of Added Silicon or Aluminium

The control group leaf samples showed very little evidence of silicon or aluminium within the leaf tissue, much as we would expect. There were no readings indicative of a silica layer at the epidermis, nor of the highly silicified silica cells above the vascular bundles. Large hotspots for silicon were present in two samples (Fig 3.2 & Fig 3.4), but these hotspots were mostly external to the plant tissue. Both of these samples came from the same plant, control group plant 37, and the fact that these hotspots were prevalent even after a second sample was taken from this plant suggests that the embedded sample itself was either damaged or contaminated. Hotspots for aluminium and silicon could be clay-like particles, especially when the other elements associated with them are taken into account.

With the exception of the external hotspots, there is some evidence of silicon and aluminium within the plant tissue in one sample (Fig 3.6). Two small aluminium signals, peaking at 2% weight, along with four silicon readings within the plant tissue, peaking at 4% weight, are seen. However, given the seemingly random localisation of these readings within the mesophyll and epidermis, along with the appearance of similar readings in the same sample external to the plant tissue, it is unlikely that they are actually representative of silicon or aluminium within the plant tissue.

The control group showed what we would have hoped and expected to see, little to no evidence of silicon or aluminium within the plant tissue in known areas of silicon deposition. The control group readings provide a reliable point of reference for the other sample groups.

3.4.1.2 Silicon + Leaf: Grown in the Presence of Added Silicon

The silicon + group samples showed strong evidence for silicon at known sites of silicon deposition above the vascular bundles at the location where we would expect to find silica cells. Signal strength varied between samples, with two samples peaking at 25% weight (Fig 3.7 & 3.9), a third giving a signal peaking at around 15% (Fig 3.10) and the final sample reading at 9% weight (Fig 3.8), which is still considerably higher than the background levels detected in the control samples.

One sample shows a large silicon and aluminium reading directly below the lower epidermis (Fig 3.10). This signal's positioning suggests it could be a silica cell which was dislodged during the sectioning process, however this region also shows detection for multiple other elements, including potassium, titanium and iron, suggesting contamination as a more likely source (see supplementary data).

Though all four samples showed evidence of silicon at the silica cells, only two showed evidence of silicon at the leaf edge, both at the upper and lower epidermis. Sample 22 (Fig 3.9B) shows a weaker signal, never rising above 4% weight along the edge of the epidermis. This signal is also present in another sample, however there is also a thicker band of silicon found at the upper epidermis, ranging from 4–16% weight (Fig 3.7B). It is interesting to note that this thicker band of silicon is found directly above the largest vascular bundle in this sample leaf, considering the role of the xylem in the transport of silicic acid through the plant. If silicic acid is being transported through the xylem and then deposited at the end of the transpiration stream, this area is where we would expect to see the largest silicon deposition.

There were no signs of aluminium detection beyond a few isolated and easily discounted hotspots. One strong signal present at the location of bulliform cells shows a strength of 25% weight aluminium, far higher than any reading in any of the groups, even those that were grown in the presence of aluminium (Fig 3.7A).

The silicon + group showed strong evidence for silicon accumulation and deposition at the silica cells and epidermis, which are known areas of silicon deposition. There was no consistent or sizeable evidence of aluminium detection. These results are within expectations of the sample group and demonstrate Micro-PIXE's use in localising silicon within rice tissue.

3.4.1.3 Aluminium + Leaf: Grown in the Presence of Added Aluminium

Although there was no evidence of aluminium deposition in any specific areas, all three samples showed a diffuse aluminium presence within their tissue, peaking at around 0.6% weight which is higher than that of the background reading found throughout the sample (Fig 3.11–3.13).

One sample shows what appears to be scattered silicon signals, however these are randomly distributed and localised both inside and outside plant tissue (Fig 3.11). This reading is likely the result of dust contamination on the surface of the sample. Another sample shows a small silicon signal around the area where a silica cell is localised, however its placement is not actually in line with the silica cell's expected location (Fig 3.12). There is also another similar silicon hotspot nearby located outside the sample tissue, suggesting that these are merely contaminants.

The aluminium + group showed a diffuse but noticeable signal for aluminium throughout the sample tissue. Whilst this is not evidence for co-localisation between silicon and aluminium, it does show that the aluminium from the growth solution penetrated beyond the roots and into the higher plant tissue. It also demonstrates Micro-PIXE's usefulness in detecting low levels of an element. Although the aluminium signal is too small and diffuse to be accurately quantified, we can at least qualitatively identify its presence in the tissue.

3.4.1.4 Aluminium/Silicon + Leaf: Grown in the Presence of Added Aluminium and Silicon

Much like the silicon + group, the aluminium/silicon + group shows strong evidence of silicon detection in multiple areas that we would expect to find silica deposition. All four samples (Fig

3.14B–3.17B) show strong silicon detection in the region of the epidermis above the vascular bundles where we would expect to find silica cells.

In addition to the localisation of silicon at the silica cells, two samples also show a signal for silicon at both the upper and lower epidermis, ranging between 4–16% weight in one sample (Fig 3.14B) and 3–9% in the other (Fig 3.17B). This is consistent with the layer of silica we would expect to find covering the epidermis of rice leaf tissue.

What is surprising is that two out of the four samples show no sign of this epidermal layer of silica (Fig 3.15B & Fig 3.16B). This could be the result of this leaf tissue being taken from a younger, less developed leaf which had not accumulated this silicon layer. Another possible explanation could lie with the brittle nature of the silica layer, which could have shattered when the leaf section was cut with a microtome.

Three of the four samples showed evidence of aluminium throughout the sample tissue, much like the aluminium + group (Fig 3.15A–3.17A). However, the aluminium signal in these samples is lower when observed against the background levels of aluminium found throughout the sample, peaking at 0.3% weight in two samples (Fig 3.15A & Fig 3.16A) and 0.4% in the final sample (Fig. 3.17A). This visual observation suggests a lower aluminium concentration throughout the sample tissue in the aluminium/silicon + group when compared to the aluminium group. There is significant evidence in the literature to suggest that silicon's presence in plant tissue alleviates aluminium toxicity. Aluminium added at 50 μM concentration has been shown to decrease rice seedling growth rates and increase aluminium accumulation in the plant tissue, but the addition of 10 μM silicon resulted in alleviation of aluminium's effects and a reduction in aluminium accumulation (Singh et al., 2011).

3.4.1.5 Control Root: Grown in the Absence of Added Aluminium or Silicon

The Micro-PIXE readings for the control root sections consistently showed sporadic hotspot readings for both silicon and aluminium (Fig 3.18–3.21). Whilst the consistent detection of these readings across all samples suggests their legitimacy, their seemingly random localisation, both within sample tissue and outside it, suggests otherwise. This being the control group, the presence of any significant levels of silicon or aluminium would be unexpected.

These hotspot readings could be the result of sample contamination, however their consistency amongst the control root samples, as well as the root samples in the other three groups, suggests that these readings are present as a result of the conditions in the root tissue sample itself.

There are no signs of a consistent aluminium or silicon signal anywhere throughout the samples which would suggest deposition sites.

3.4.1.6 Silicon + Root: Grown in the Presence of Added Silicon

The silicon + rice root samples were perhaps the most disappointing sample group due to the sample tissue damage. Two samples show signs of significant structural damage, most certainly a result of the cryofixation and/or sectioning of the samples (Fig 3.22 & Fig 3.24). In addition to the structural damage, all samples are once again contaminated with hotspots for silicon and aluminium detection. As with the control root samples, these hotspots appear both inside and outside the sample tissue with a seemingly random distribution and can most likely be attributed to damage or dust contamination of the sample (Fig 3.22–3.25).

Beyond the ever-present hotspots, there were no reliable or consistent areas of silicon or aluminium detection in this sample group. Given silicon's known accumulation in the upper plant tissue, the stem and leaf, the lack of silicon detection in this sample group is not unexpected and without the addition of aluminium to this groups nutrient solution, its presence was not expected either.

3.4.1.7 Aluminium + Root: Grown in the Presence of Added Aluminium

Micro-PIXE readings for the aluminium + root were much more promising, showing a reliable signal for aluminium accumulation at the rhizodermis of the root in all samples (Fig 3.26–3.29), ranging between 0.5–4% weight. Whilst the resolution and magnification available in these images is not sufficient to state this with certainty, aluminium appears to penetrate the rhizodermis but not the exodermis below it. Work on *Bracharia* species has shown evidence of the exodermis' role in alleviating aluminium toxicity by acting as an apoplastic barrier to the metal's entry (Arroyave et al., 2013).

In addition to the consistent signal at the rhizodermis, there are once again sporadic, co-localised hotspots for aluminium and silicon throughout the sample, both internal and external to the rice root tissue. The lack of consistency in their location, along with their localisation inside and outside the sample, allows us to identify and eliminate these hotspots from our observations. Silicon's presence is not expected in these samples in any significant amount, further putting their veracity into doubt.

The consistent detection of the aluminium at the root rhizodermis is an expected result, especially given the low levels of aluminium detected in the leaf tissue of aluminium-exposed plants. The rhizodermis is the outermost layer of cells in the plant root, acting as a barrier to apoplastic transport and is directly exposed to the aluminium-containing nutrient solution. Experiments with wheat have shown that aluminium is concentrated in the rhizodermis and the layer of cortex directly beneath it, but that it does not penetrate further than this (Delhaize et al., 1993). Whilst the result has precedent, it does mean that the co-localisation of aluminium and silicon within leaf tissue cannot be detected if the aluminium itself does not penetrate past the roots in significant quantities.

Despite the lack of aluminium detection beyond the rhizodermis of the roots, the reliable detection of aluminium at the rhizodermis does show the effectiveness of Micro-PIXE in localising

aluminium in rice root tissue. Whilst the presence of the hotspots is unfortunate, they are relatively easy to identify due to their random distribution, along with the co-localisation of readings for aluminium with other metals such as iron.

3.4.1.8 Silicon/Aluminium + Root: Grown in the Presence of Added Aluminium and Silicon

Aluminium was detected at the rhizodermis of all samples, but two samples showed heavier deposition (Fig 3.30 & Fig 3.32), whilst the other two samples had a sparser but still easily identifiable aluminium signal (Fig 3.31 & Fig 3.33). Aluminium was deposited in a similar distribution to the aluminium + sample group, with a band of aluminium at the rhizodermis, however, at a lower concentration ranging between 0.3–1% weight, as opposed to the higher readings of up to 4% weight in the aluminium + group.

Overall, we see a lower aluminium detection both in % weight and in distribution when compared with the aluminium + group, though still significantly higher than the control and silicon + groups. Given the only difference in growth conditions between the silicon/aluminium + group and the aluminium + group is the presence of silicon in the former, the difference in aluminium levels between samples could be the result of silicon's presence. Silicon and aluminium were made available to the rice plants at differing stages so as to avoid the interaction between silicon, aluminium and other nutrients in the nutrient solution. Therefore, silicon's influence on this reduced aluminium level in the silicon/aluminium + group could only be as a result of silicon's effect on the plant itself and not due to interactions between silicon and aluminium in the nutrient solution.

However, we see no evidence of silicon accumulation in the root tissue at the rhizodermis or beyond the hotspots which litter the rice root samples (Fig 3.30B–3.33B). These hotspots show no consistency and show up both inside and outside plant tissue.

Though there are no large areas of aluminium deposition in the leaf tissue, there is a noticeable aluminium signal throughout the sample tissue. This signal is less prominent in the aluminium/silicon + group when compared with the aluminium + group, suggesting silicon's presence reduced the aluminium levels in both the leaf and the root of the aluminium/silicon + group plants (See section 3.4.1.4 Aluminium/Silicon + Leaf: Grown in the Presence of Added Aluminium and Silicon). These results suggest that silicon's presence in the plant reduces the amount of aluminium that enters the plant, but any influence that silicon has on the accumulation of aluminium in this sample group is not the result of silicon deposition in the root tissue, but rather an altered physiological state which reduces uptake by the roots.

As with all root samples, sporadic and randomly distributed silicon readings were detected in this sample group, but are unlikely to be accurate representations of silicon distribution and much more likely the result of dust contamination.

3.4.2 Micro-PIXE Quantitative Analysis

The quantitative analysis of leaf tissue results shows significantly higher levels of silicon in the silicon + and aluminium/silicon + groups when compared to groups not grown in the presence of added silicon, supporting the Micro-PIXE images (Fig 3.34). We also see the vast majority of the silicon detected in the epidermis, with both silicon replete groups averaging over 20,000 mg/kg at the epidermis, compared to sub-1,500 mg/kg for the mesophyll and invaginations (Fig 3.34). Furthermore, silicon levels are consistent in the mesophyll and invaginations across all sample groups, with only the epidermis showing significantly increased silicon levels in silicon replete groups.

The aluminium/silicon + group appears to have an increased silicon content within the invagination region when compared with the other groups, but there is a large margin of error here, suggesting a single anomalous reading is affecting the result (Fig 3.34C). One sample within the aluminium/silicon + group shows a thick silicon layer at the epidermis, which when cross-

referenced with the image maps used to define epidermis and invagination shows that the silicon layer from the epidermis overlaps into the area identified as invagination, causing the elevated reading for this group (Fig 3.46) (see gold arrows).

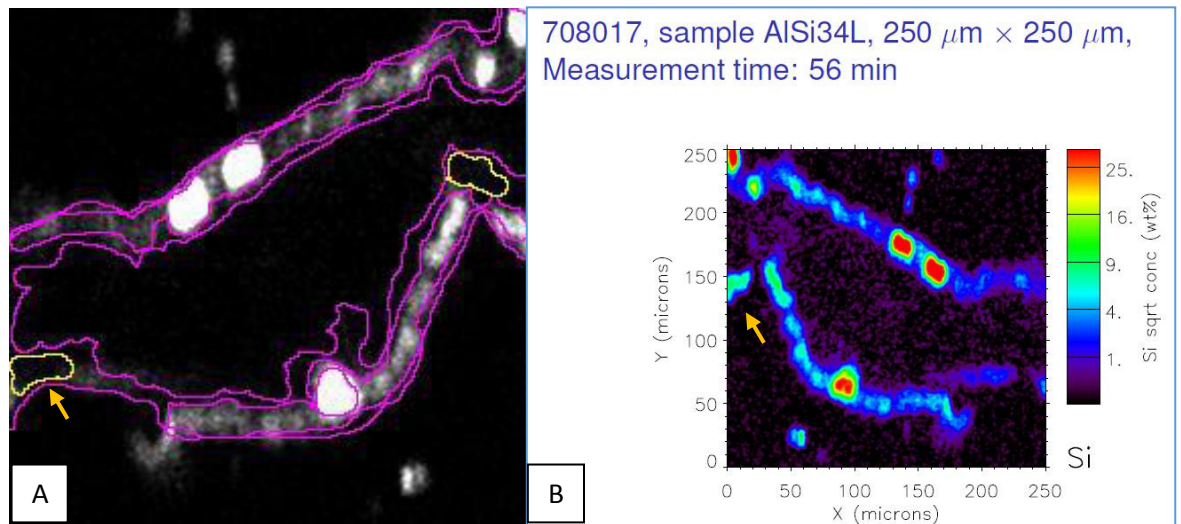


Figure 3.46 Image comparison between image used to determine regions for quantitative analysis (A) and Micro-PIXE image of the same region (B). **Image A:** The purple lines mark out the epidermis, whilst the yellow lines identify the invaginations.

Aluminium levels were consistent across all four sample groups, though slightly higher in the aluminium + group than the others (Fig 3.35A). Within specific areas, the aluminium group showed higher aluminium levels in the mesophyll and invaginations than the other groups (Fig 3.35C & 3.35D). This result fits with observations of the Micro-PIXE images which appeared to show slightly higher aluminium concentrations throughout the mesophyll in the aluminium + group when compared with the aluminium/silicon + group (see section 3.4.1.8 Silicon/Aluminium + Root: Grown in the Presence of Added Aluminium and Silicon). The comparison between silicon and aluminium levels within the leaf tissue shows no correlation between the two elements quantitatively (Fig 3.36).

Within the root tissue, silicon levels were perplexingly the highest in the control group, with the other three groups showing similar low silicon levels (Fig 3.37). However, when looking over the Micro-PIXE images we see that the control root samples are littered with hotspots for silicon, but show no other sign of silicon deposition (Fig 3.18B–3.21B). Silicon is taken up by the roots,

however it is transported through the xylem into the higher plant and as such is not expected to accumulate in the roots in any significant amount.

Aluminium levels are apparently fairly uniform across the silicon +, aluminium + and aluminium/silicon + groups according to the quantitative analysis, however this is in conflict with direct observation of the Micro-PIXE images (Fig 3.22A–3.25A). The aluminium + and aluminium/silicon + groups clearly show a ring of aluminium at the rhizodermis not found in the other sample groups. Micro-PIXE images of the root sections are littered with hotspots of varying sizes and whilst the larger of these can be excluded from quantitative analysis, drawing the line on what to include and what to exclude is arbitrary. For this reason, quantitative analysis of the silicon and aluminium levels in the root tissue is of limited use in samples with such hotspots.

3.4.3 LEXRF Image Analysis

Due to beamline time restraints, LEXRF imaging was only performed on two sample groups, the silicon + group and the aluminium/silicon + group. Samples in both the silicon + and the aluminium/silicon + groups showed evidence of silicon deposition at the silica cells, with a signal strength consistently peaking at around 180 mg/g, which equates to 18% weight (Fig 3.40E, 3.42E, 3.43E & 3.44E). Silicon was also found deposited at the epidermis of one sample in the silicon + group (Fig 3.41E), but not in any of the aluminium/silicon + group samples.

Aluminium was also detected consistently at the silica cells, perfectly co-localised with silicon in all samples which encompassed silica cells (Fig 3.40D, 3.42D, 3.43D & 3.44D). Aluminium levels are low when compared with silicon, peaking at 0.4 mg/g or around 0.04% weight in areas of aluminium and silicon co-localisation. Aluminium is also found as a diffuse presence throughout the sample tissue in both sample groups, although visual observations suggest that the aluminium presence is sparser in the silicon + group when compared with the aluminium/silicon + group.

Co-localisation of silicon and aluminium at the silica cells is an intriguing and novel result, however the levels of aluminium found at the silica cells are consistent between the silicon + group and the aluminium/silicon + group, suggesting that the extremely low levels of aluminium present in the aluminium deplete group were sufficient for this level of aluminium accumulation. Additionally, increased aluminium exposure in the aluminium/silicon + group did not increase aluminium deposition in these regions.

Whilst these results suggest silicon and aluminium have some interaction at the silica cells, there is no evidence that this co-localisation is involved in the amelioration of aluminium toxicity.

3.4.4 General Discussion

Hotspots are a common issue with the Micro-PIXE imaging method, affecting all sample groups to varying degrees. Hotspots are areas of element detection that do not fit with our knowledge of the sample, are external to the sample or are otherwise suspiciously positioned to the point that they are not assumed to give an accurate depiction of the sample's makeup. It is possible to discount hotspots by cross-referencing multiple maps together to identify co-localisation with certain elements. Numerous hotspots also appear outside the sample tissue itself, which can obviously be discounted as not part of the sample.

Prime examples of this can be seen in the control group leaf samples (Fig 3.2Bb–3.6B) which show large areas of silicon detection at high concentrations, peaking at 16% weight in several areas of one sample (Fig 3.2B). However, the sulphur map highlights the structure of the leaf tissue and clearly demonstrates that these readings occur outside the plant tissue itself (Fig 3.2C). These hotspots can be removed from statistical analysis when calculating quantitative elemental levels in samples, and indeed many have, but the issue of where to draw the line on what can be discounted and what cannot hampers the usefulness of this method for quantitative analysis of silicon and aluminium levels in rice tissue.

It can be difficult to visualise the morphology of the plant tissue sample based on the aluminium or silicon maps due to the relatively small and localised areas in which these elements are found. Several other element maps are useful for this purpose though, including sulphur, phosphorus and chlorine. The sulphur map was displayed alongside the aluminium and silicon maps due to sulphur's absence in key areas where silica cells are found, above the vascular bundles, making for a more effective visual contrast between these two images (Fig 3.47) (see gold arrows).

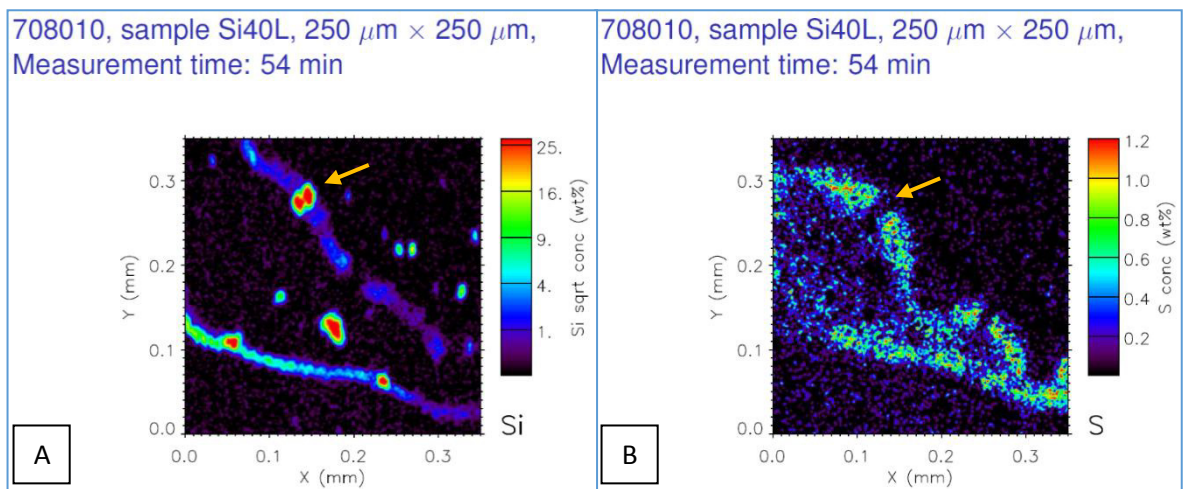


Figure 3.47 Micro-PIXE image comparison showing the sulphur (A) and silicon (B) element maps. Arrows label areas of note, discussed in text.

The size of the sample area scanned varied between samples slightly depending on the sample's size and morphology. Most rice leaf samples scanned were 250 μm x 250 μm , though some larger samples were scanned at 300 μm x 300 μm . For root tissue there were more variances depending on the radius of the root itself, with samples ranging from 600 μm x 600 μm , up to 1,100 μm x 1,100 μm . The size of each scan is displayed in the image for each section. These sample sizes were chosen to give a broader overview of the distribution of silicon and aluminium within the plant tissues, rather than a detailed look at their structure. Therefore, these images are useful for determining where silicon and aluminium are within the structure of the plant, but not, for example, their distribution within a cell.

Micro-PIXE is more than capable of detecting both aluminium and silicon, but its detection limits are worse for these elements than heavier elements. Micro-PIXE cannot be used to measure

elements lighter than fluorine, most notably carbon and oxygen (Orlić, 1999). Micro-PIXE's sensitivity for lighter elements above this limit, such as silicon and aluminium, is not as high as other methods such as LEXRF. In practice, we see these sensitivity limitations in the form of a background level of aluminium and silicon which is detected, scattered throughout the sample both within and without tissue. These readings are low level, typically below 0.2% weight for aluminium and 0.4% weight for silicon, though it varies between images and must be accounted for on a case by case basis. As a result, concentrations of aluminium or silicon close to or below this detection level cannot be reliably identified in these rice samples.

Micro-PIXE has proved to be a useful method for the localisation of aluminium and silicon in rice tissue. In leaf tissue, silicon was identified consistently at the leaf epidermis where it is known to accumulate as a layer of amorphous silica. Silicon signals were most strongly detected at the known locations of silica cells, which are the highly silicified cells which are found above and below the vascular bundles of leaf tissue. No evidence was found for the silicification of either the xylem or the phloem, nor of the bulliform cells, all other areas which have shown evidence of silicification. There was also no evidence of silicon accumulation in the root tissue, though the prevalence of hotspots throughout the root tissue samples makes this conclusion difficult to confirm with any degree of certainty.

Aluminium detection at the root rhizodermis was expected, given the root's role in protecting the plant from the uptake of toxic metals. There was no reliable detection of aluminium within the root cortex or vascular tissue, suggesting that the vast majority of the aluminium that contacted the plant did not make it past the root rhizodermis. There was no evidence of aluminium accumulation in specific areas of the leaf tissue using Micro-PIXE imaging, however, the aluminium replete groups did show aluminium detection throughout their leaf tissue as a diffuse presence. Interestingly, this aluminium presence was greater in the aluminium + group than compared to the aluminium/silicon + group, suggesting that the presence of silicon within its

tissue reduced the rice plants uptake of aluminium, supported by both visual observation and quantitative data (see sections 3.4.1.8 Silicon/Aluminium + Root: Grown in the Presence of Added Aluminium and Silicon & 3.4.2 Micro-PIXE Quantitative Analysis).

The results of LEXRF imaging provide further confirmation for observations seen in the Micro-PIXE images, as well as bringing their own unique results. Silicon was detected consistently at the location of silica cells in both the silicon replete sample groups in LEXRF imaging, much like in the Micro-PIXE images (see section 3.4.3 LEXRF Image Analysis).

Aluminium was found as a diffuse presence throughout the sample tissue, much like in the Micro-PIXE results. However, unlike the Micro-PIXE results, LEXRF revealed a co-localised aluminium signal at the silica cells in both the silicon + group and the aluminium/silicon + group, seemingly unaffected by the addition of aluminium to the plants growth solution. The aluminium signal is weak, peaking at only 0.04% weight, far below the 18% weight silicon signal consistently seen in multiple samples (Fig 3.40, 3.42 & 3.43). Whilst this is evidence of silicon and aluminium co-localisation, the aluminium signal does not vary between rice plants grown in the presence of aluminium and those which are not, suggesting this co-localisation is not a tolerance mechanism within the rice plant for dealing with aluminium toxicity. This co-localisation of aluminium with silicon at the silica cells of rice has not been previously reported to our knowledge.

4. Callose Detection in Rice Using Fluorescence Microscopy

4.1 Introduction

Of the known silicifiers in the plant kingdom, two have been studied more extensively than the rest; horsetails and rice. Horsetails are a 'living fossil', which is to say that their genus, *Equisetum*, is the only remaining extant genus of the entire *Equisetopsida/Sphenopsida* class (Guillon, 2004). Whilst intriguing from a scientific perspective, horsetail is not an economically important plant, unlike the other well-studied silicifer, rice.

Even between the extensive research into biosilicification in both rice and horsetail, there are huge gaps in our knowledge of the processes and mechanisms involved. Significant work has been done on the localisation of silica deposition within plant tissues and identifying the structures formed during this process (Holzhüter et al., 2003; Ueno & Agarie, 2005; Currie & Perry, 2007; Law & Exley, 2011). The uptake of silicic acid from soil solution and its movement throughout the plant has also been studied extensively, though the processes involved are still not fully understood (Ma et al., 2006; Ma et al., 2007; Yamaji et al., 2008). One area of biosilicification in plants that is often left by the wayside when it comes to research is the actual process of biosilification – the conversion of silicic acid taken up from the soil into silica at the deposition site. The general assumption is that once silicic acid reaches the terminus of the transpiration stream, the water it was carried in evaporates, increasing the concentration past the point of saturation at which point silica forms. Whilst this is a simple and tidy assumption, it does not explain why certain structures are more heavily silicified than others, such as the silica cells in rice. Nor does it explain how silica so perfectly replicates the surface structures of the cells it covers, with many examples of intricate silica structures found in numerous plants, including horsetail and rice, which simply cannot be the result of the random dumping of silicic acid at the leaf's surface (Currie & Perry, 2007; Law & Exley, 2011).

In a recent study into horsetails, it was suggested that a hemicellulose, mixed-linkage (1→3, 1→4)-β-D-glucan (MLG) could act as a template for silica deposition in multiple *Equisetum* species (Fry et al., 2008). Continuing on from Fry's study, further research into silica structures in *Equisetum arvense* showed that silica deposition at the stomata exactly mirrored the known locations of callose deposition in the same region (Law & Exley, 2011). It was also shown that callose can induce the polymerisation of silicic acid into silica in an under-saturated solution (< 2 mM) of silicic acid; this is the first evidence of an under-saturated solution of silicic acid being induced to form silica under normal conditions, with only the addition of a biomolecule.

The hemicellulose callose is a polysaccharide in the form of β -1,3 - glucan with some β -1,6 – branches which is found in numerous areas throughout many plant tissues, including the cell walls and plasmodesmata (Chen & Kim, 2009). Callose has also been shown to play a vital role in stomatal pore formation in *Asplenium nidus*, participating in guard cell wall thickening (Apostolakos et al., 2009).

Two of the most prominent methods of identifying callose in plant tissue are through aniline blue staining and through immunofluorescence labelling. Aniline blue is a biological stain which reacts with (1→3)-β-glucans to give a yellow fluorescence under UV light. The advantage of this method is its simplicity: samples are cut and immersed in a working solution of aniline blue for 30 minutes, after which they are ready to be viewed by fluorescence microscopy.

Immunofluorescence labelling involves using a commercially available antibody against callose, with a fluorescent marker attached to it to bind to callose within the plant tissue. Of the two staining methods, immunofluorescence is more sensitive, but also more labour intensive (Pendle & Benitez-Alfonso, 2015). There are two variants of immunofluorescence: primary and secondary. Primary immunofluorescence binds an antibody conjugated with a fluorophore directly to the target site, whilst secondary immunofluorescence binds an unconjugated primary antibody to the site, then binds a second antibody, conjugated with a fluorophore, to the primary antibody

(Vancells, 2014). Secondary, or indirect immunofluorescence, can provide stronger staining signals than its primary counterpart, as the binding of multiple secondary antibodies to a single primary antibody will amplify the signal.

The present research aims to further this new avenue of research into silica deposition in plants, with the focus shifted primarily to rice to determine if callose could also play a role in its silica deposition. Through collaboration with the University of Athens, our aim was to determine the locations of callose deposition in rice leaf tissue using aniline blue and secondary immunofluorescence techniques, and to compare this data with the known sites of silica deposition in rice (*Oryza sativa*).

4.2 Method

4.2.1 Rice Plant Hydroponic Growth

Rice plants were grown hydroponically to an age of one month for use in this experiment. Rice was grown in silicon replete conditions in the presence of 2 mM silicic acid. For full details on hydroponic growth setup, see section Hydroponic Rice Culture.

Further to this, a group of younger rice plants were grown on site in Athens. These rice seedlings were grown to an age of one week from germination.

4.2.2 Aniline Blue Staining Protocol

Rice leaf samples were cut using a small scalpel blade to be as thin as possible, with sub-1 mm being the ideal size to ensure maximum stain penetration. Once cut, the samples were placed inside an Eppendorf tube with an aniline blue staining buffer.

Aniline Blue Staining Buffer (Stock):

- 0.07M K_2HPO_4 at pH 8.0.
- 0.05% aniline blue.

The aniline blue staining buffer is made from a 10x dilution of the stock solution, diluted with 0.07M K_2HPO_4 to give a final concentration of 0.005% aniline blue. The samples inside the Eppendorf were then submerged in 1 mL of the aniline blue staining buffer and left for 30 minutes at room temperature. After the incubation, the staining buffer was pipetted away and replaced with 0.07M K_2HPO_4 at pH 8.0 to rinse the samples.

Individual rice leaf samples were then placed onto glass slides using a thin paintbrush to avoid damaging the sample. The sample was then covered with a small amount of K_2HPO_4 and a cover slip was placed on top, avoiding air bubbles as the cover was lowered. The amount of K_2HPO_4 required varied slightly depending on the thickness of the sample.

4.2.3 Immunofluorescence Protocol

Rice leaf samples were cut using a small scalpel blade to be as thin as possible, with sub-1 mm being the ideal size to ensure antibody penetration. Once cut, the samples were placed inside an Eppendorf tube with 1 mL of a fixation buffer. The fixation buffer consists of 8% paraformaldehyde in a PEM buffer at 1x concentration. The PEM buffer itself is formed of PIPES, EGTA and magnesium sulphate, and was created in a stock solution at 2x concentration.

PEM Stock Solution (2x concentration):

- 500 mL ultrapure water (water conductivity <0.067 $\mu\text{S}/\text{cm}$).
- Add 15.12 g PIPES.
- Add 1.9 g EGTA.
- Add 1.24 g MgSO_4 .
- Stir with magnetic stirrer bar.
- Adjust pH to 6.8 with potassium hydroxide.

Fixation Buffer:

- Dilute PEM buffer to 1x concentration by 1/1 mixture with ultrapure water (100 mL total).
- Add 8 mL paraformaldehyde.
- Stir with magnetic stirrer bar.

Samples were left in the fixation buffer for one hour. After the hour was up, the fixation buffer was pipetted out of the Eppendorf tube, being careful not to remove the samples with it. The Eppendorf containing the samples was then filled with 1 mL of 1x concentration PEM and left for 10 minutes – this PEM rinse was repeated three times. The next stage was enzyme digestion, which breaks down the cellulose present in the plant cell wall.

1% Cellulase Solution:

- Adjust PEM to pH 5.6 using potassium hydroxide.
- Dilute PEM buffer to 1x concentration by 1/1 mixture with ultrapure water (1 mL total).
- 0.01 g cellulase (Onozuka R-10, Yakult Pharmaceuticals, Japan).

The final rinse of PEM was removed and 0.5 mL of 1% cellulase solution was added to the Eppendorf. The sample was then placed inside an incubator at 25°C for 30 minutes. After the 30 minutes were up, the 1% cellulase solution was pipetted away, again ensuring the samples were not accidentally taken along with it. The Eppendorf containing the samples was then filled with 1 mL of 1x concentration PEM and left for 10 minutes – this PEM rinse was repeated three times. The next stage after this is the extraction stage, which requires the use of an extraction buffer.

Extraction Buffer:

- Add 30 µL Triton X-100 to an Eppendorf.
- Add 50 µL DMSO.
- Add 920 µL PBS Buffer and vortex the Eppendorf to mix the solution.
- Leave to stand for two hours to allow the Triton X-100 to dissolve completely.

Once the extraction buffer was completed, the last PEM rinse was removed and then 0.5 mL of the extraction buffer was added to the Eppendorf containing the rice tissue samples and left for one hour. After the hour was up, the extraction buffer was pipetted away, again ensuring the samples were not accidentally taken along with it. The Eppendorf containing the samples was then filled with 1 mL of 1x concentration PEM and left for 10 minutes – this PEM rinse was repeated three times. The samples are then ready for the primary antibody stage.

Primary Antibody Solution:

- Add 1 mL PBS to an Eppendorf.
- Add Anti – (1-3) β – D – glucan monoclonal antibody from mouse at 1/40 ratio.
- Agitate the Eppendorf to mix the solution.

Once the primary antibody solution was completed, the last PEM rinse was removed and then 100 μ L of primary antibody solution was pipetted into the Eppendorf, ensuring complete coverage of the rice tissue samples. The Eppendorf containing the samples was then left overnight at room temperature. The next day, the primary antibody solution was pipetted away, again ensuring the samples were not accidentally taken along with it. The Eppendorf containing the samples was then filled with 1 mL of 1x concentration PBS and left for 10 minutes – this PBS rinse was repeated three times. The samples are then ready for the secondary antibody stage.

Secondary Antibody Solution:

- Add 1 mL PBS to an Eppendorf.
- Add Anti-Mouse IgG-Fluorescein Isothiocyanate Conjugated (FITC) antibody from mouse at 1/40 ratio.
- Agitate the Eppendorf to mix the solution.

Once the secondary antibody solution was completed, the last PBS rinse was removed and then 100 μ L of secondary antibody solution was pipetted into the Eppendorf, ensuring complete coverage of the rice tissue samples. The Eppendorf containing the samples was then left for two hours in the dark in an incubator at 37°C. The secondary antibody solution was pipetted away, again ensuring the samples were not accidentally taken along with it. The Eppendorf containing the samples was then filled with 1 mL of 1x concentration PBS and left for 10 minutes – this PBS rinse was repeated three times. The samples are then ready for the DNA counterstain.

DNA Counterstain:

- Add 1 mL PBS into an Eppendorf.
- Add 10 mg HOECHST 33258.
- Agitate the Eppendorf to mix the solution.

After the final PBS rinse was removed, the Eppendorf containing the samples was then filled with 1 mL DNA counterstain and left at room temperature for 10 minutes. The DNA counterstain was then pipetted away, again ensuring the samples were not accidentally taken along with it. The Eppendorf containing the samples was then filled with 1 mL of 1x concentration PBS and left for 10 minutes – this PBS rinse was repeated twice. At this point the samples can either be stored in a refrigerator in their final PBS wash for later use or mounted with a mounting medium.

Mounting Medium (15 mL):

- Add 5 mL PBS to a small, sealable container.
- Add 10 mL Glycerol.
- Add 0.015 g P-Phenyldiamine.
- Agitate the container to mix the solution.

Samples were mounted individually on glass slides. Each sample was moved from the PBS onto a slide using a fine brush to avoid damage. The sample was then covered with a small amount of mounting medium and a cover slip was placed on top, avoiding air bubbles as the cover was lowered. The amount of mounting medium required varied slightly depending on the thickness of the sample.

4.2.4 Fluorescence Microscopy

All plant tissue sections were viewed with a Zeiss Axioplan microscope and images were captured using a Zeiss Axiocam MRc5 digital camera. The microscope was equipped with 20x, 40x and 100x objectives.

- Aniline blue imaging and the appropriate autofluorescence images were taken using a UV Filter Cube #487902 (Exciter Filter: G 365, Beam Splitter: FT 395, Barrier Filter: LP 420).
- Immunofluorescence imaging and the appropriate autofluorescence images were taken using a Blue Filter Cube #487910 (Exciter Filter: BP 450-490, Beam Splitter: FT 510, Barrier Filter: BP 515-565).

4.3 Results

The resulting images from both aniline blue staining and immunofluorescence, as well as the appropriate autofluorescence images, are displayed below with figure headings and arrows denoting areas of interest.

4.3.1 Aniline Blue Imaging

This section contains the aniline blue and corresponding autofluorescence images. Figure headings display the magnification of each image, along with a scale bar attached to the image. Arrows label areas of interest which are described in text.

4.3.1.1 Autofluorescence of Rice Leaf Samples

Autofluorescence images were taken of unstained rice leaf samples using the UV filter cube in order to ascertain the levels of fluorescence given off by the plant tissue itself. These images provide a baseline against which the stained samples can be compared.

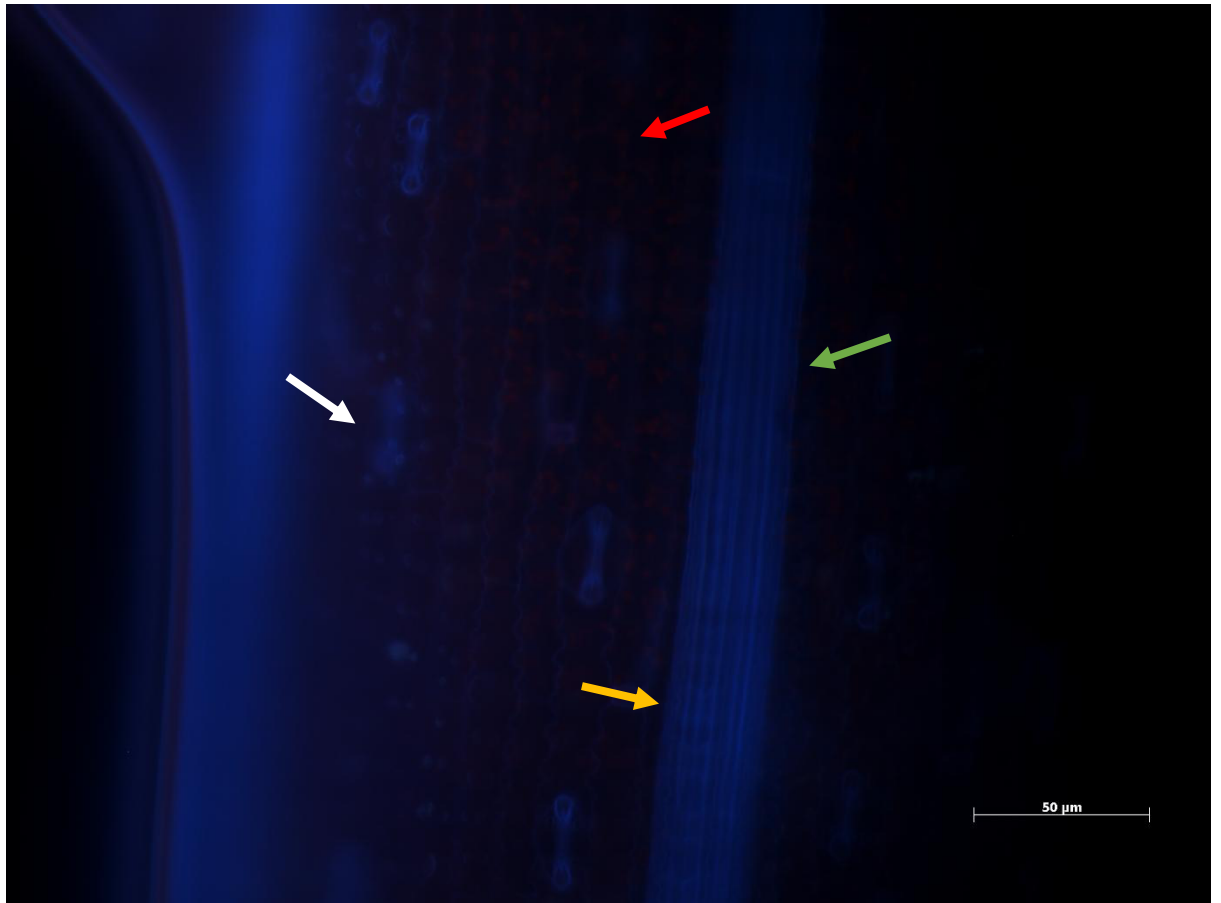


Figure 4.1 Fluorescence microscopy image of unstained rice leaf tissue shows autofluorescence levels at 40x magnification. The rice plant this tissue was taken from was approximately one month old.

The epidermis of the rice leaf tissue gives off autofluorescence in several areas through the UV filter (Fig 4.1). The red spots visible throughout the epidermis are chloroplasts within the epidermal cells (see red arrow). The large blue column moving across the leaf sample is the band of fibre that runs over the top of vascular bundles (see green arrow). Silica cells are visible in this fibre band, though difficult to make out as they are on a different plane of focus (see gold arrow). Stomata are also visible across the leaf's surface, identifiable by a blue fluorescence where the guard cells meet (see white arrow).

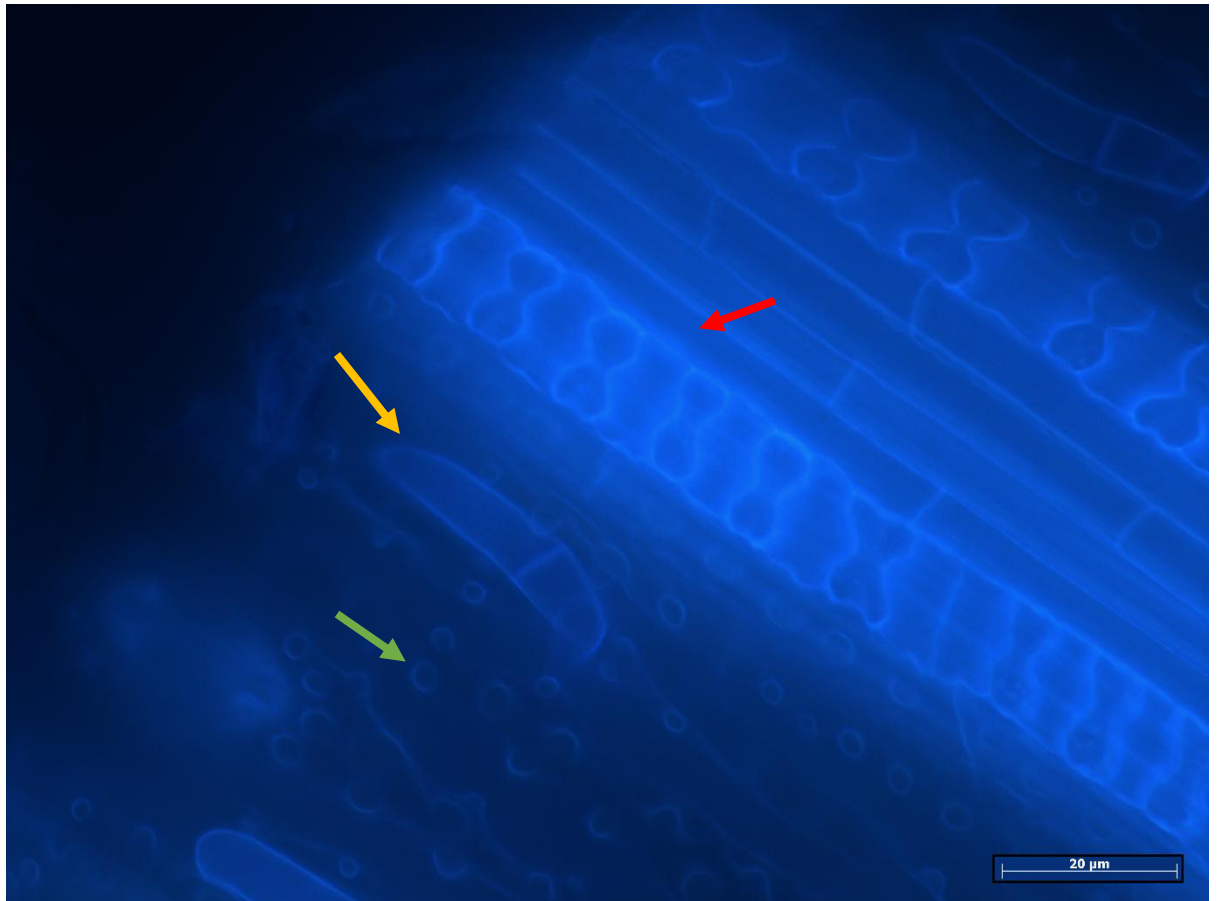


Figure 4.2 Fluorescence microscopy image of unstained rice leaf tissue shows autofluorescence levels at 100x magnification. The rice plant this tissue was taken from was approximately one month old.

At higher magnifications the blue autofluorescence is more prominent, especially around the fibres that cover the vascular bundle (Fig 4.2)(see red arrow). Edges of structures and cells have definition, but there is no distinct fluorescence emanating from them. Papilla are visible here showing no fluorescence beyond the dull blue of the rest of the sample (see green arrows). Several trichomes can also be seen, again showing no distinct fluorescence (see gold arrows).

Overall the rice leaf tissue shows limited autofluorescence in several areas. The red signal from chloroplasts is easily identifiable and of little concern. The edges of structures pick up a slight glow which could be mistaken for fluorescence in stained samples, though this fluorescence is faint and uniform throughout similar cells.

4.3.1.2 Aniline Blue Stained Rice Leaf

The following images are of aniline blue stained rice leaf samples taken using the UV filter cube. A yellow/cyan fluorescence indicates the presence of callose.

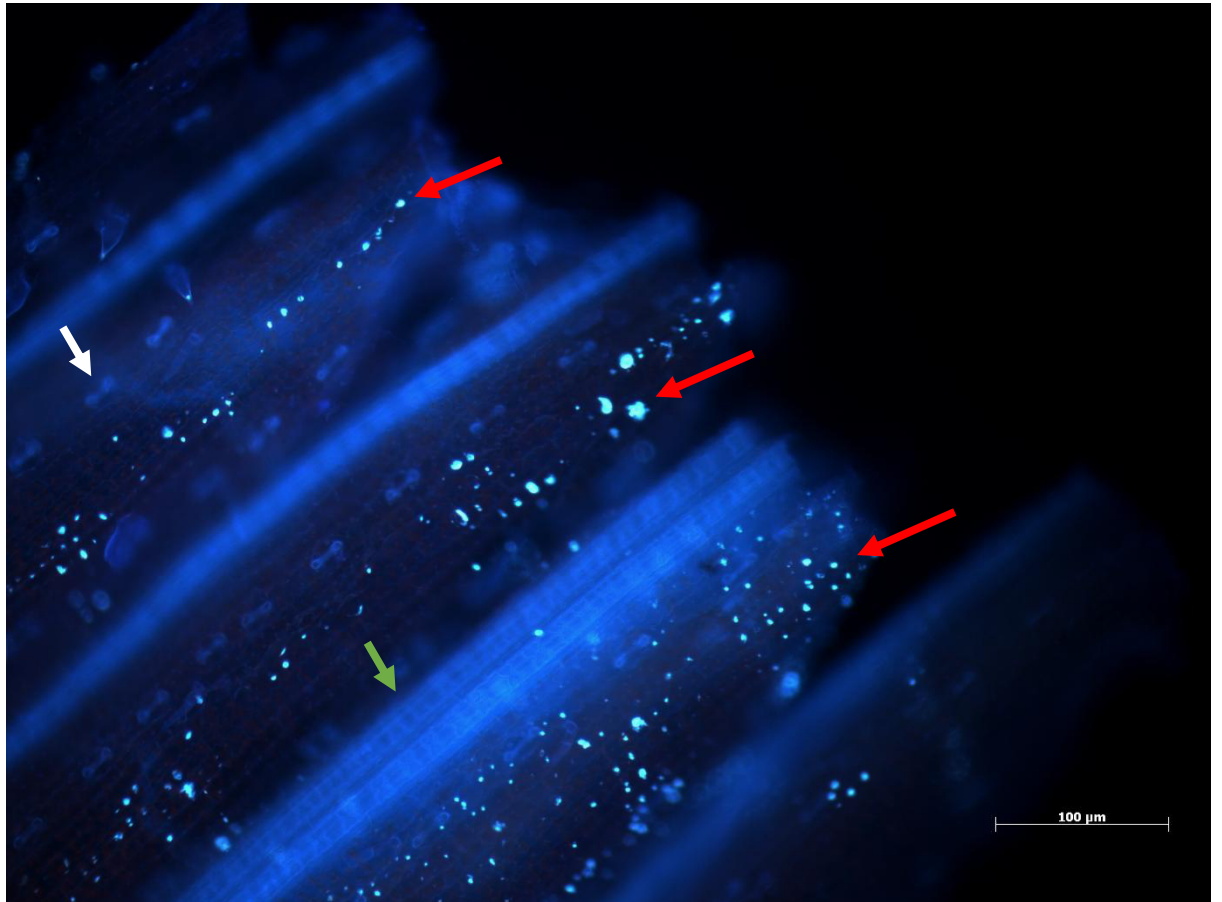


Figure 4.3 Fluorescence microscopy image of aniline blue stained rice leaf tissue shown at 20x magnification. The rice plant this tissue was taken from was approximately one month old.

At lower magnifications callose can clearly be detected across the surface of the leaf epidermis in punctate deposits which give off a strong cyan/yellow fluorescence (Fig 4.3)(see red arrows). These deposits are likely the sites of papilla across the surface of the epidermal cells, though at this magnification it is not possible to determine. Other signals seen in the autofluorescence images are also still clearly present, including the stomata (see white arrow) and fibre bands (see green arrow). Due to the morphology of the leaf sample, it was not possible to keep all areas of the sample in focus in lower magnification images.

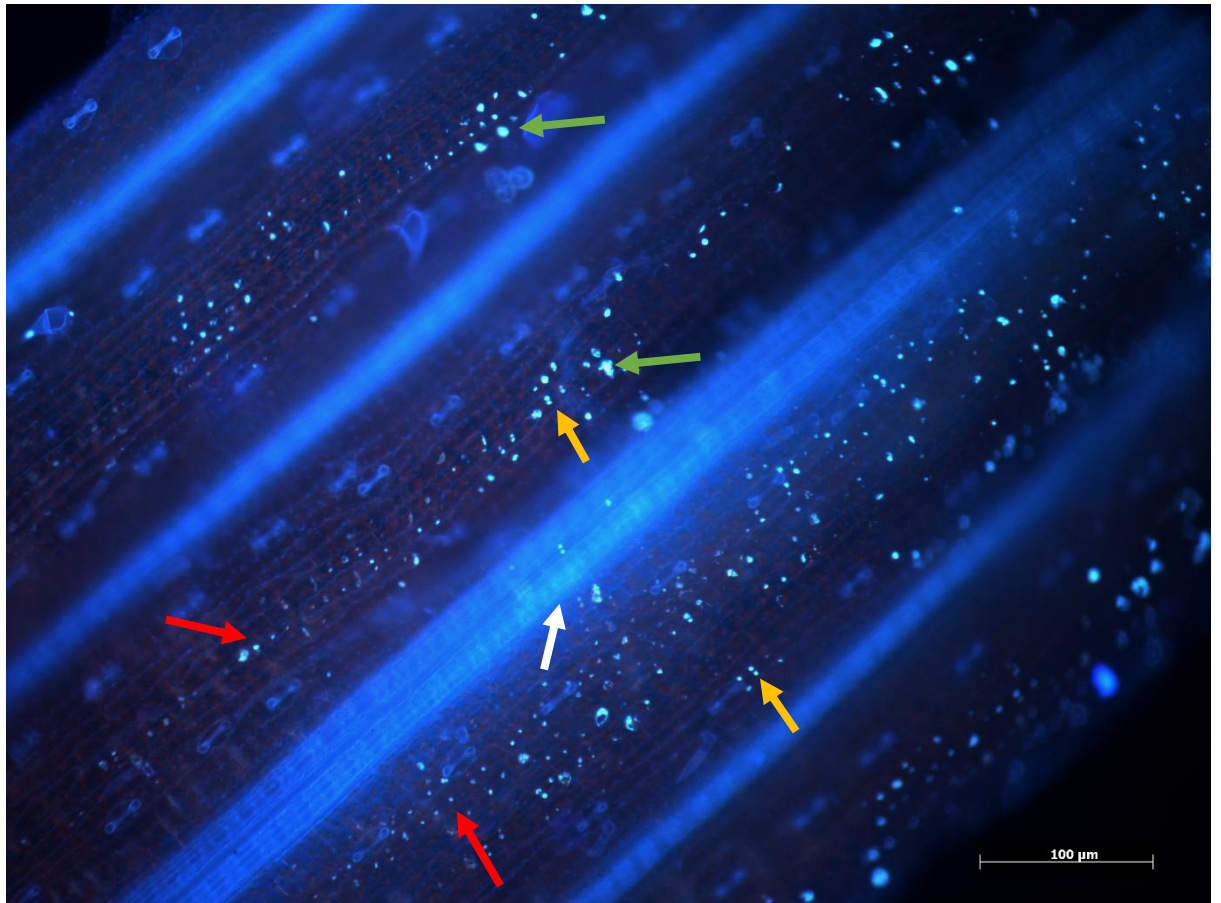


Figure 4.4 Fluorescence microscopy image of aniline blue stained rice leaf tissue shown at 20x magnification. The rice plant this tissue was taken from was approximately one month old.

The callose signal seen across the leaf epidermis becomes easier to localise (see Fig 4.4). Clear deposits of callose are visible at regular intervals across the surface of individual epidermal cells in the locations of papilla (see red arrows). Papilla are sometimes localised in clustered groups of two or three, which can be seen in the callose staining at various locations (see gold arrows). There is a light blue glow emanating from a group of silica cells in the middle of the sample, however it is difficult to distinguish this from the general autofluorescence that this region gives off (see white arrow). Callose is typically stained yellow by aniline blue under autofluorescence and a yellow signal can be seen at the centre of many of the larger papilla (see green arrows).

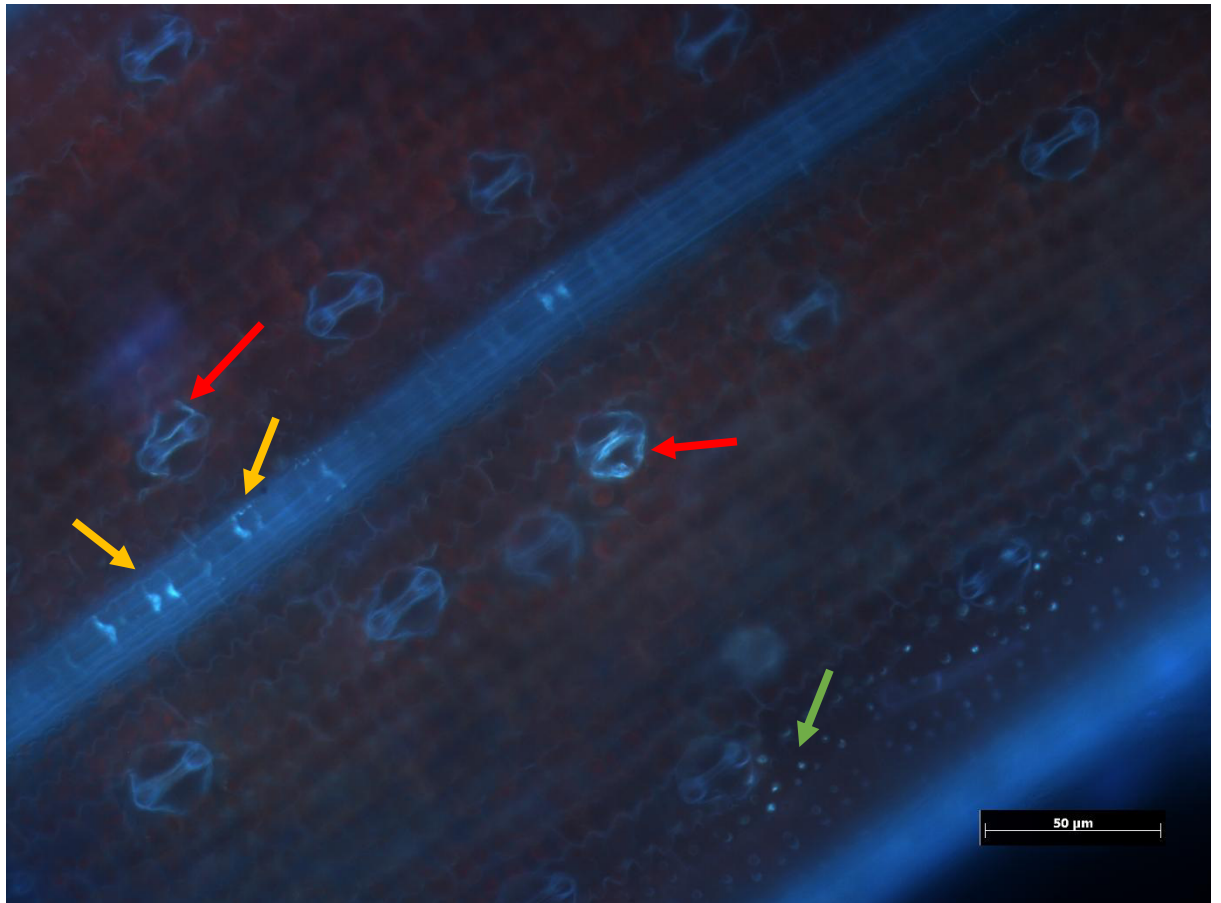


Figure 4.5 Fluorescence microscopy image of aniline blue stained rice leaf tissue shown at 40x magnification. The rice plant this tissue was taken from was approximately one month old.

At higher magnifications, callose deposits become visible in several areas other than the papilla (Fig 4.5). Callose can be seen clearly surrounding areas of the guard cells at two separate stomata, identifiable by the cyan fluorescence which is easily distinguished from the stomata's own dull blue autofluorescence (see red arrows). Callose can also be seen at the edges of several silica cells, which are located above the fibre bands that cover the vascular bundles (see gold arrows). A few papilla show a callose signal at the lower edge of the image (see green arrow); more are not visible due to the focus of the image being on the raised area above the vascular bundle.

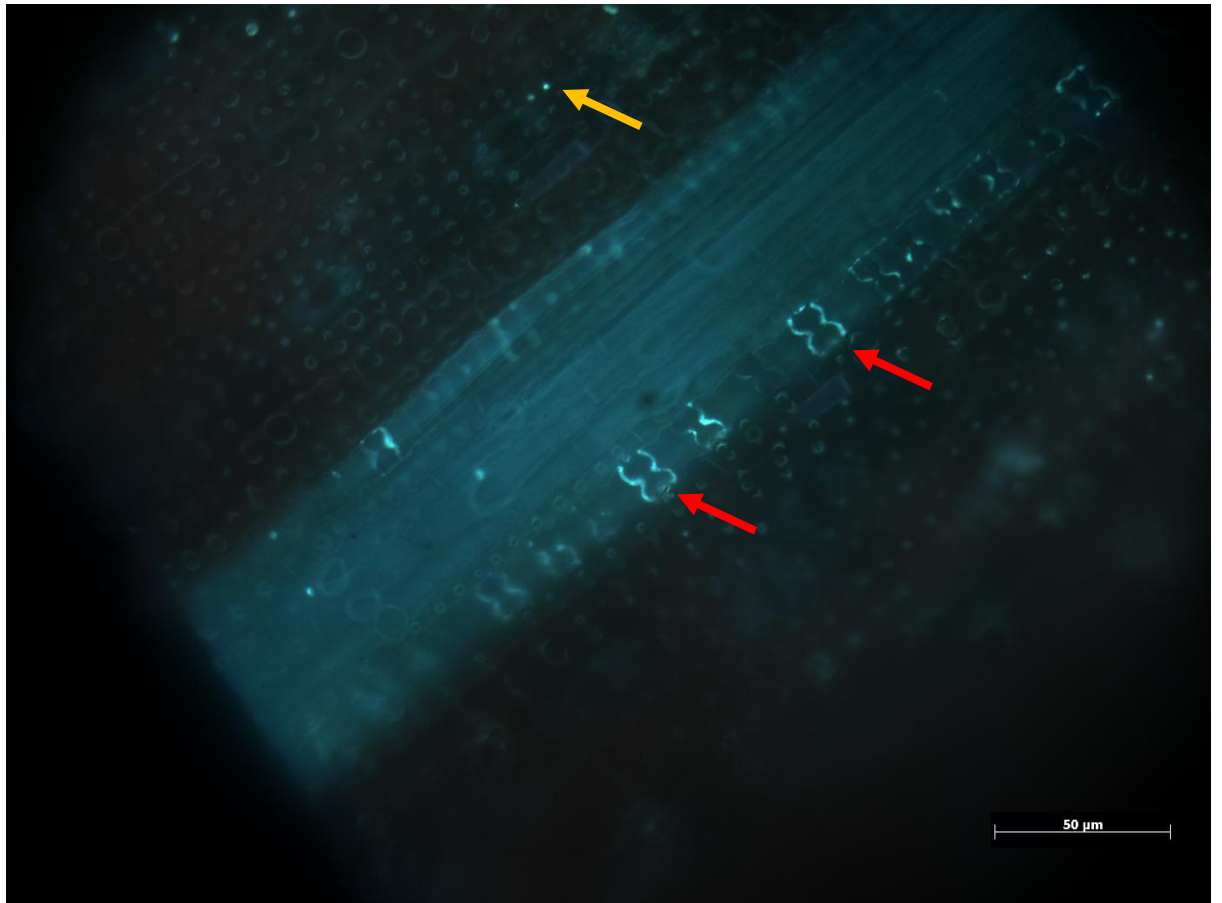


Figure 4.6 Fluorescence microscopy image of aniline blue stained rice leaf tissue shown at 40x magnification. The rice plant this tissue was taken from was approximately one month old.

Callose can be seen at the edges of multiple silica cells running over the top of the fibre band (Fig 4.6). Several silica cells are completely surrounded by callose deposits (see red arrows). No callose deposits are visible in this sample at the stomata, though some small signals can be seen at the papilla (see gold arrows).

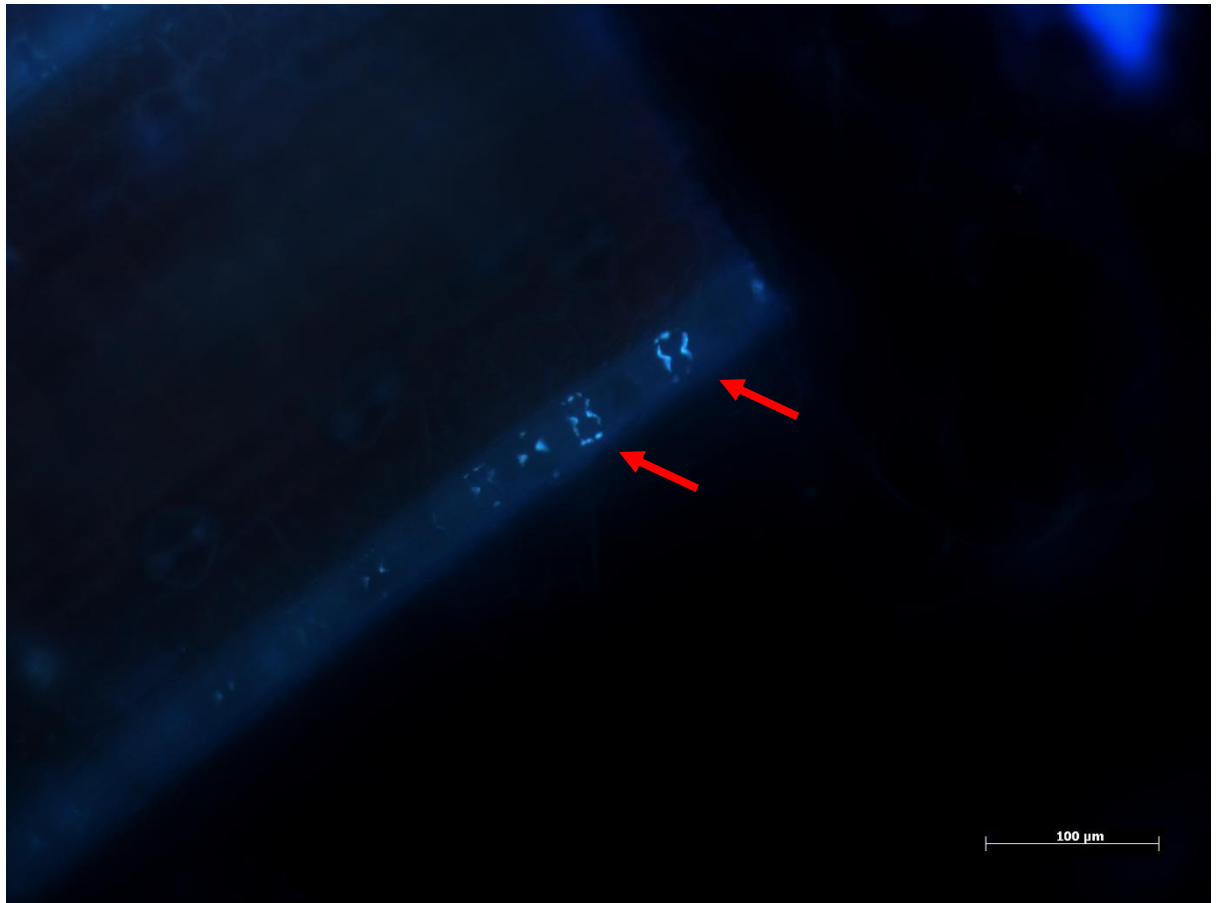


Figure 4.7 Fluorescence microscopy image of aniline blue stained rice leaf tissue shown at 20x magnification. The rice plant this tissue was taken from was approximately one month old.

Once again, callose can be seen at the edges of multiple silica cells running over the top of the fibre band (Fig 4.7). Several silica cells are completely surrounded by callose deposits (see red arrows), whilst others show only occasional callose deposits around them. No other callose deposits can be seen in this area of the sample, though the focus of the image is on the fibre band that covers the vascular bundle and away from the papilla on the epidermal cells.

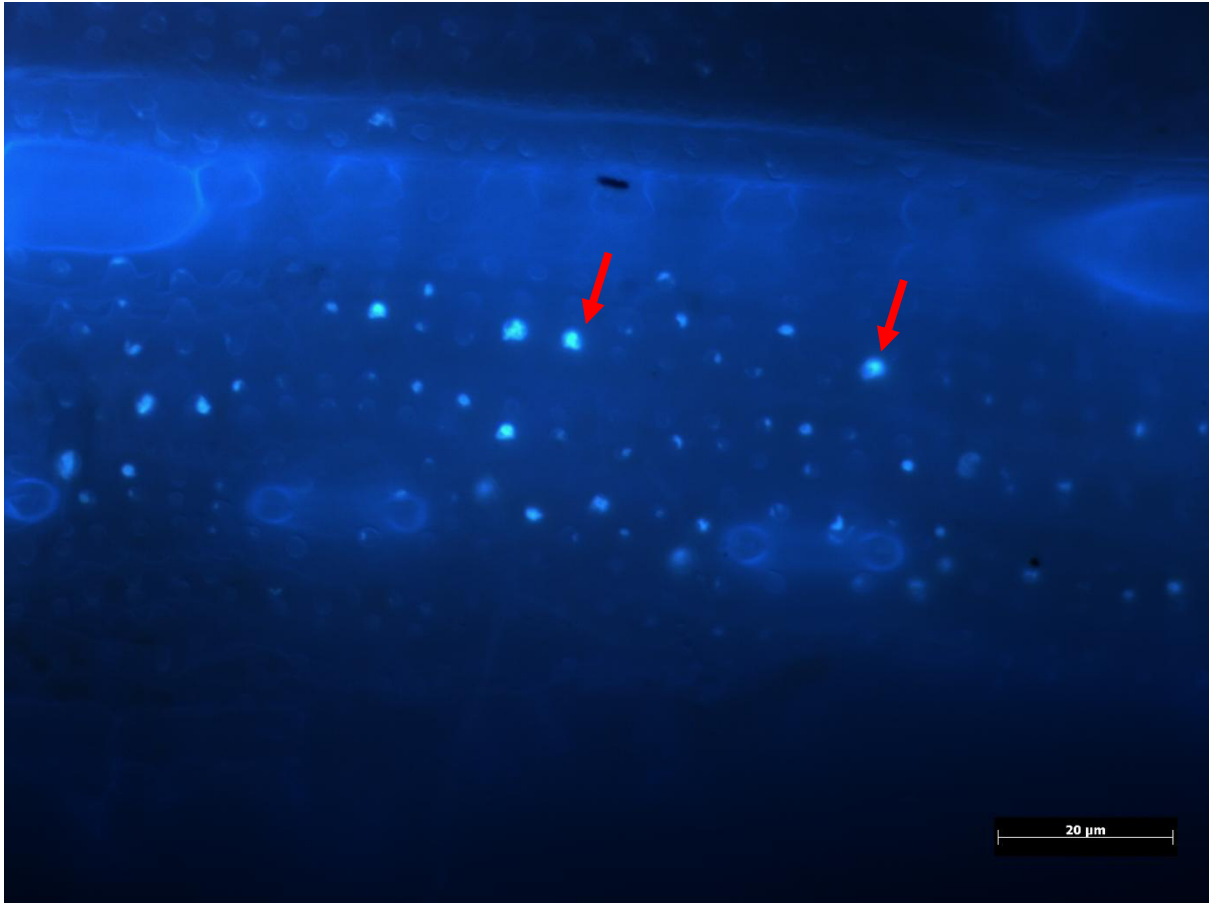


Figure 4.8 Fluorescence microscopy image of aniline blue stained rice leaf tissue shown at 100x magnification. The rice plant this tissue was taken from was approximately one month old.

Callose deposits can clearly be seen at the papilla, giving off a clear cyan fluorescence that is identifiable even against the heavily bleached background (Fig 4.8). The blue haze seen in the image is a result of multiple areas of heavy autofluorescence in this sample. Despite this interference, the callose signal is still easily visible at the papilla (see red arrows), though not at the silica cells in this sample.

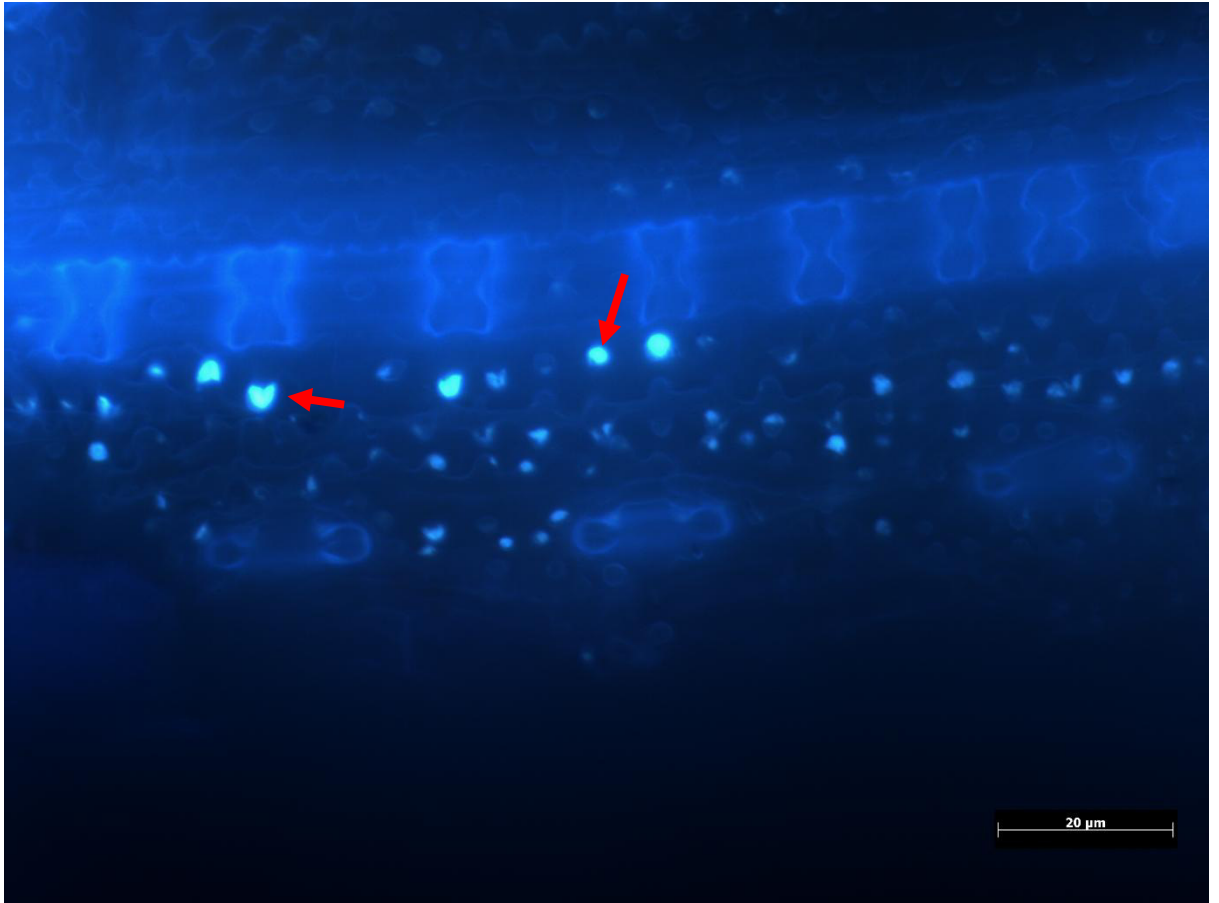


Figure 4.9 Fluorescence microscopy image of aniline blue stained rice leaf tissue shown at 100x magnification. The rice plant this tissue was taken from was approximately one month old.

Once again a callose signal is clearly visible at the papilla of the epidermal cells, identified by their cyan/yellow fluorescence (Fig 4.9)(see red arrows). Stomata and silica cells are also visible in this sample, though they show no evidence of callose deposition in this area of the sample.

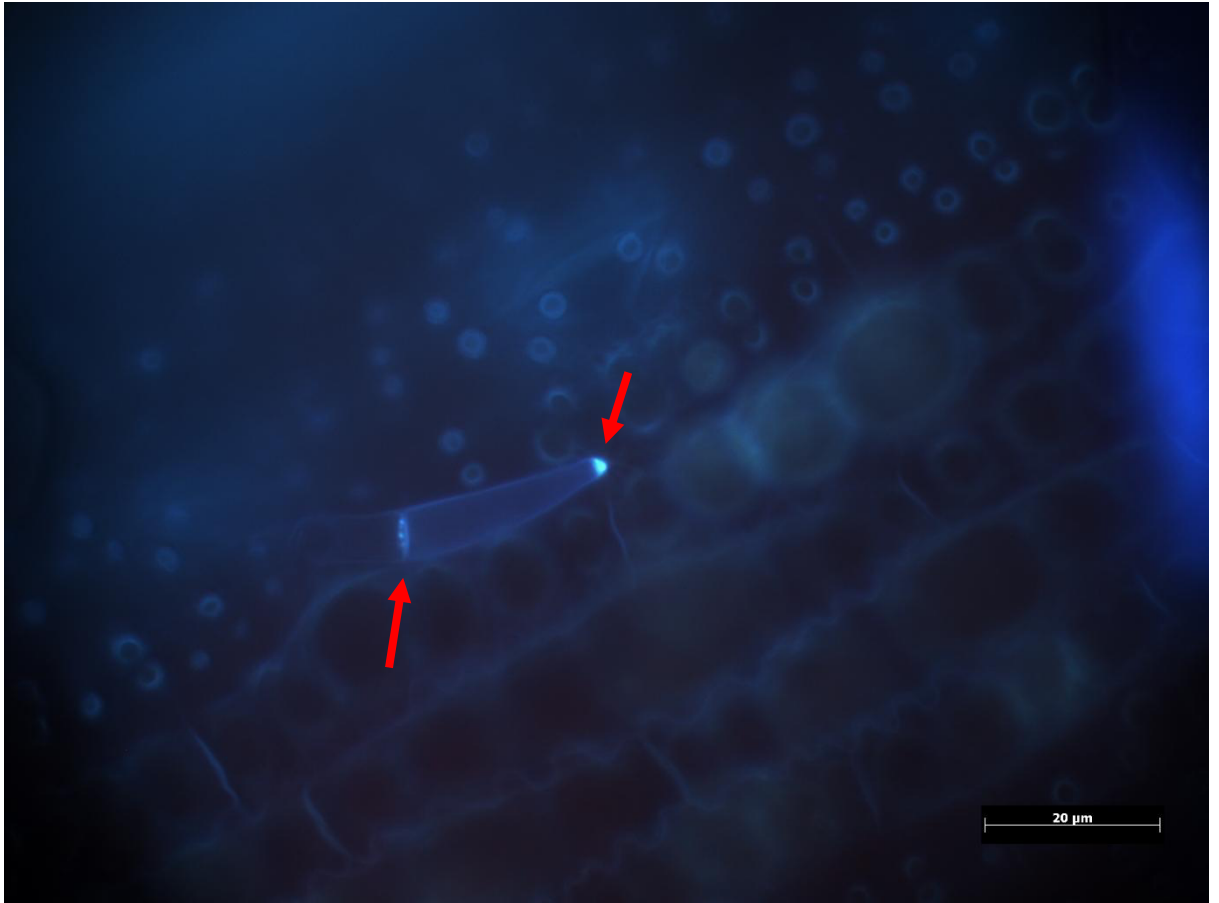


Figure 4.10 Fluorescence microscopy image of aniline blue stained rice leaf tissue shown at 100x magnification. The rice plant this tissue was taken from was approximately one month old.

At the highest magnifications callose deposits can be seen at the trichomes (Fig 4.10). Callose is localised at the tip of the trichome as well as at the base, but not throughout the main body (see red arrows). No other callose deposits can be seen in this area of the sample.

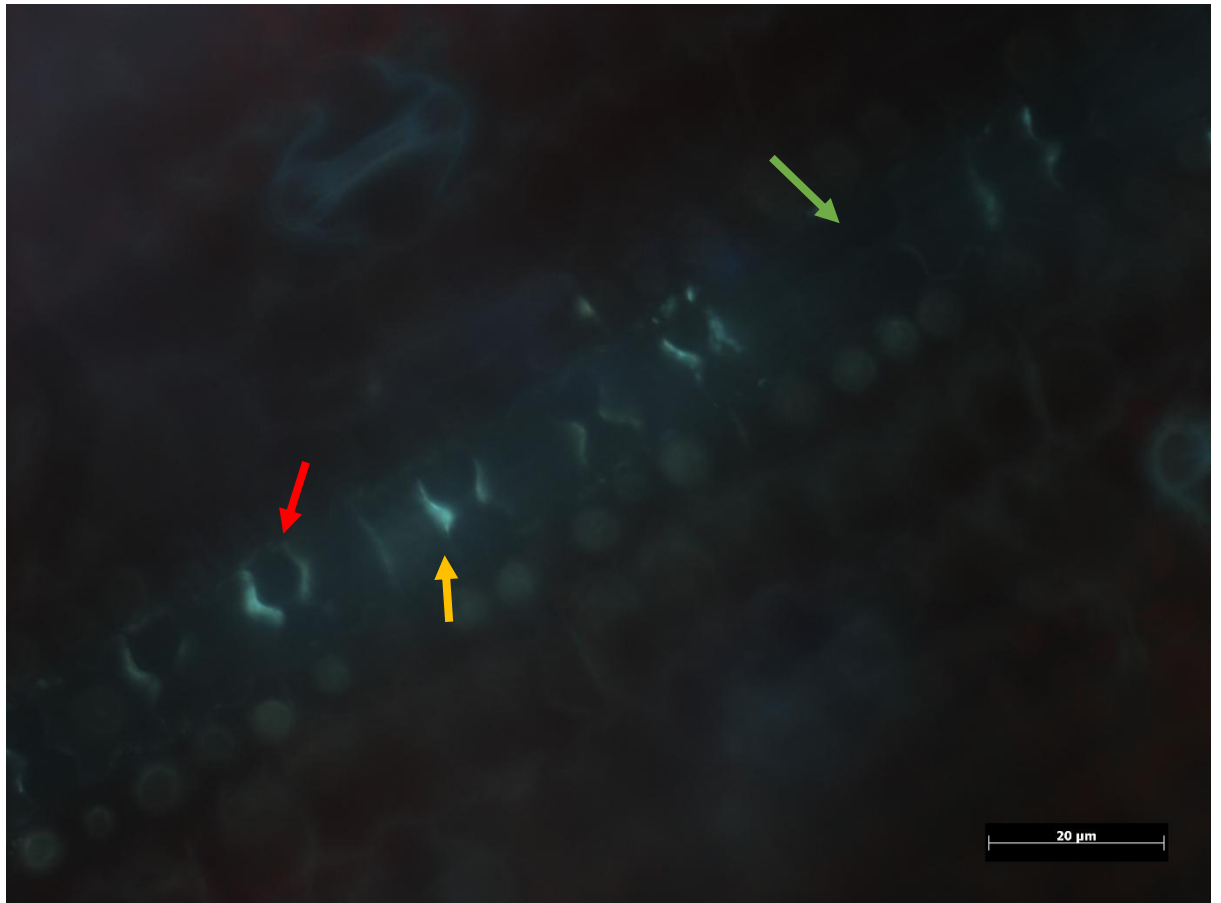


Figure 4.11 Fluorescence microscopy image of aniline blue stained rice leaf tissue shown at 100x magnification. The rice plant this tissue was taken from was approximately one month old.

At the highest magnifications the callose deposits surrounding the silica cells can be identified more clearly (Fig 4.11). Silica cells are easily identifiable by their characteristic dumbbell shape (see red arrow). Callose is not evenly deposited around the silica cells, with some areas showing thicker bands of callose (see gold arrow) whilst other areas show no signal at all (see green arrow).

4.3.2 Immunofluorescence Imaging Results

This section contains the immunofluorescence and corresponding autofluorescence images.

Figure headings display the magnification of each image, along with a scale bar attached to the image. Arrows label areas of interest which are described in the text.

4.3.2.1 Autofluorescence of Rice leaf Tissue

Autofluorescence images were taken of unstained rice leaf samples using the blue filter cube in order to ascertain the levels of fluorescence given off by the plant tissue itself. These images provide a baseline against which the stained samples can be compared.



Figure 4.12 Fluorescence microscopy image of unstained rice leaf tissue shown at 20x magnification presenting autofluorescence under the immunofluorescence filter. The rice plant this tissue was taken from was approximately one month old.

Under the blue filter without staining rice leaf tissue gives off very little autofluorescence (Fig 4.12). The entire sample is visualised as a dull green with few areas of definition, though individual structures such as papilla and trichomes are still clearly discernible. Trichomes have an elevated fluorescence at their edges when compared with the rest of the sample (see red arrow).

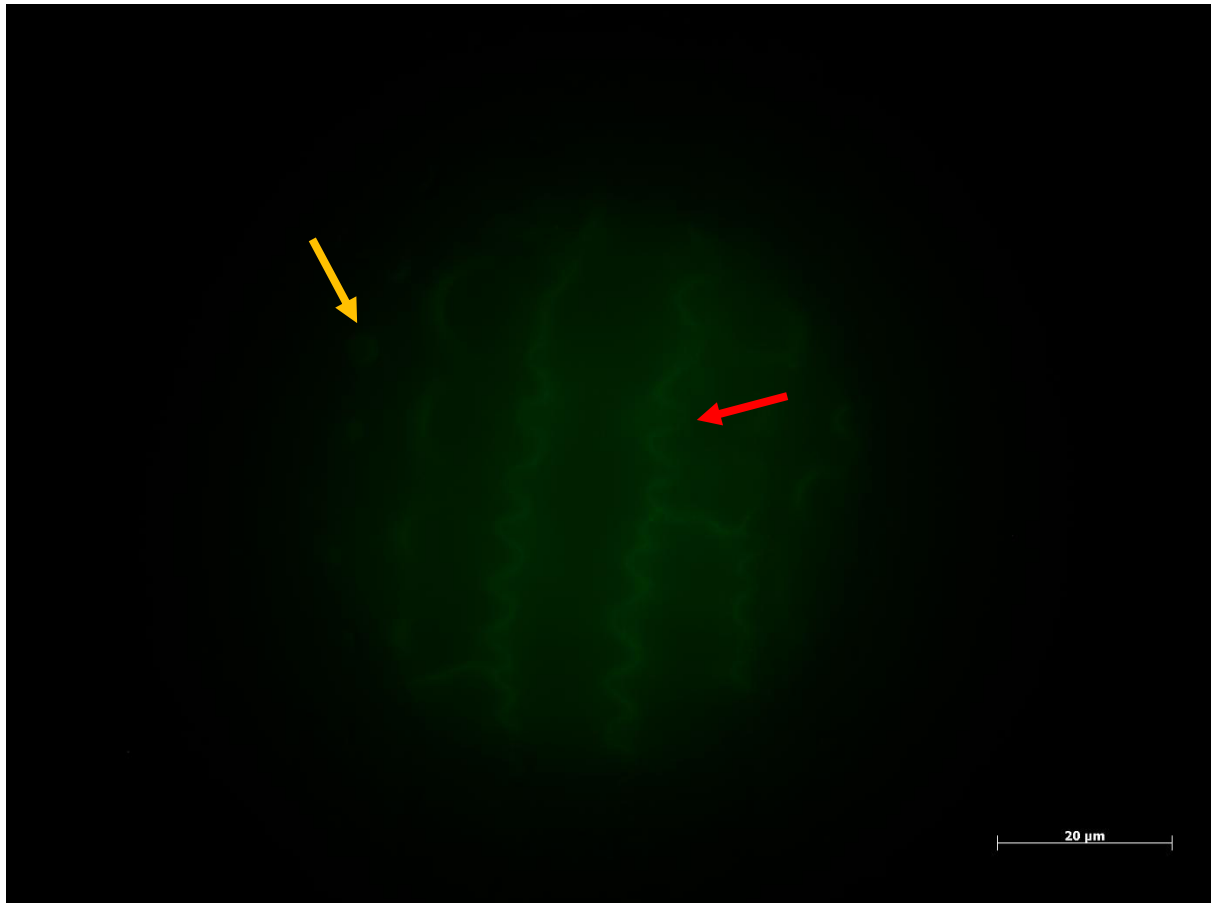


Figure 4.13 Fluorescence microscopy image of unstained rice leaf tissue shown at 100x magnification presenting autofluorescence under the immunofluorescence filter. The rice plant this tissue was taken from was approximately one month old.

Epidermal cells can be identified, with their structure and borders clearly defined, although they give no enhanced fluorescence signal beyond the dull green (Fig 4.13). The characteristic sinuate, or wave-like, structure of the epidermal cells edges can be seen (see red arrow). Papilla can also be seen at the edge of the visible circle, again showing no noticeable fluorescence (see gold arrow).

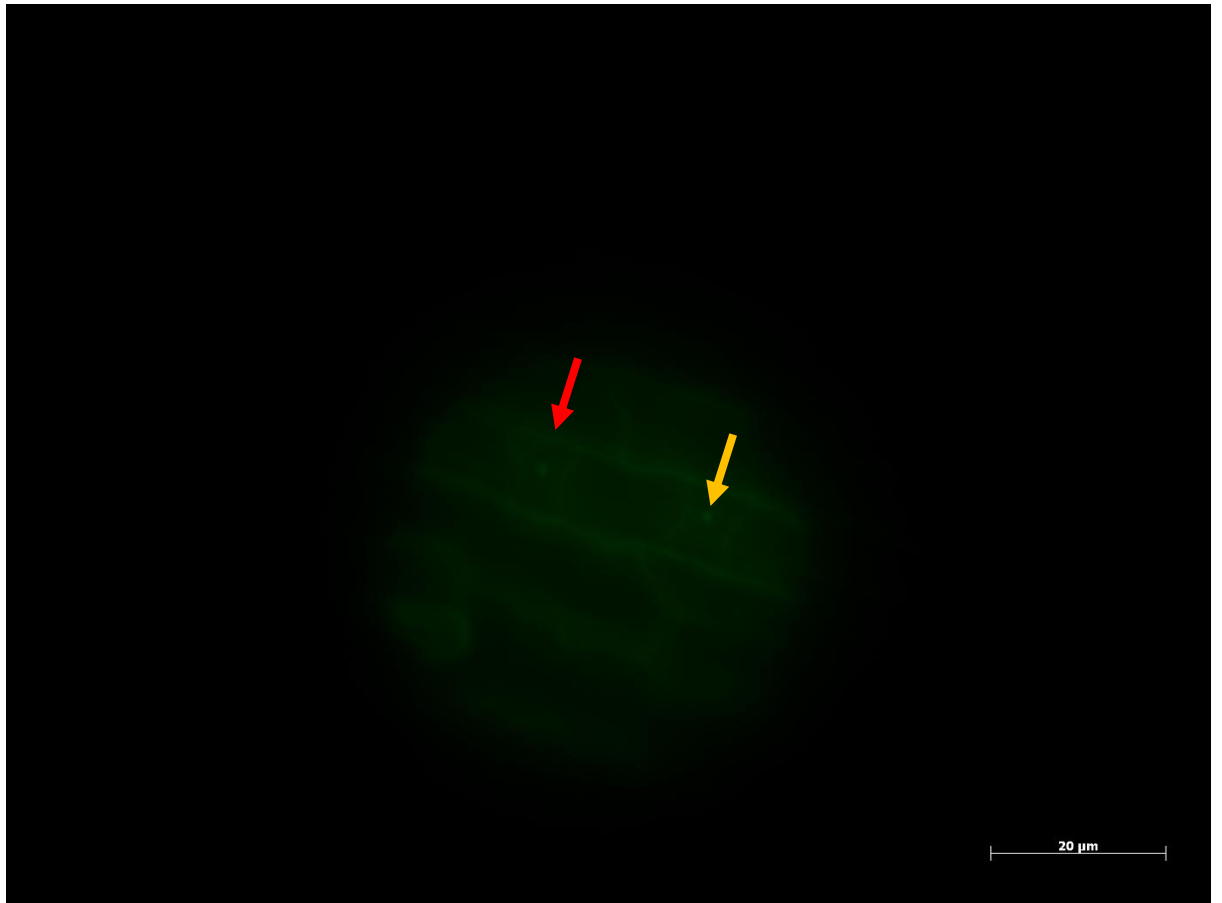


Figure 4.14 Fluorescence microscopy image of unstained rice leaf tissue shown at 100x magnification presenting autofluorescence under the immunofluorescence filter. The rice plant this tissue was taken from was approximately one month old.

Silica cells can be seen, identified by their characteristic dumbbell shape, running in a column between epidermal cells (Fig 4.14) (see red arrow). Though the silica cells give off no enhanced autofluorescence when compared with the rest of the sample tissue, small silica bodies contained within the cell are visible under the blue filter cube (see gold arrow).

4.3.2.2 Immunofluorescence Stained Rice Leaf Tissue

With the sample autofluorescence levels established, the immunofluorescence stained samples were then analysed under the blue filter cube. Bright green fluorescence indicates the presence of callose.

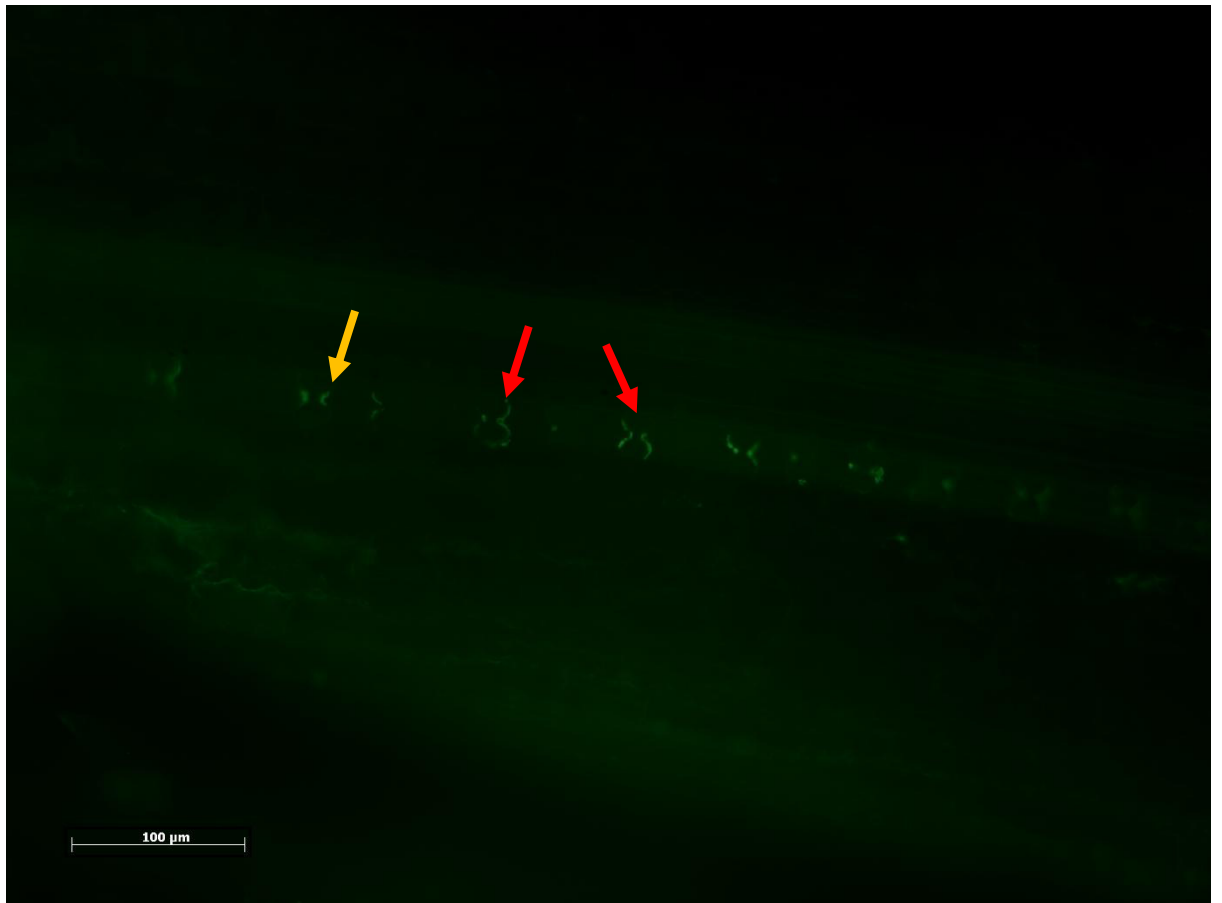


Figure 4.15 Fluorescence microscopy image of immunofluorescence stained rice leaf tissue shown at 20x magnification. The rice plant this tissue was taken from was approximately one month old. At the leaf epidermis layer callose can be clearly seen at the epidermis of the silica cells, the signal identifiable by a bright green fluorescence (Fig 4.15). Multiple silica cells exhibit this callose signal to varying degrees: some are almost completely surrounded (see red arrow) whilst others show intermittent callose detection (see gold arrow). The silica cells are raised above a vascular bundle, leaving the rest of the leaf epidermis out of focus.

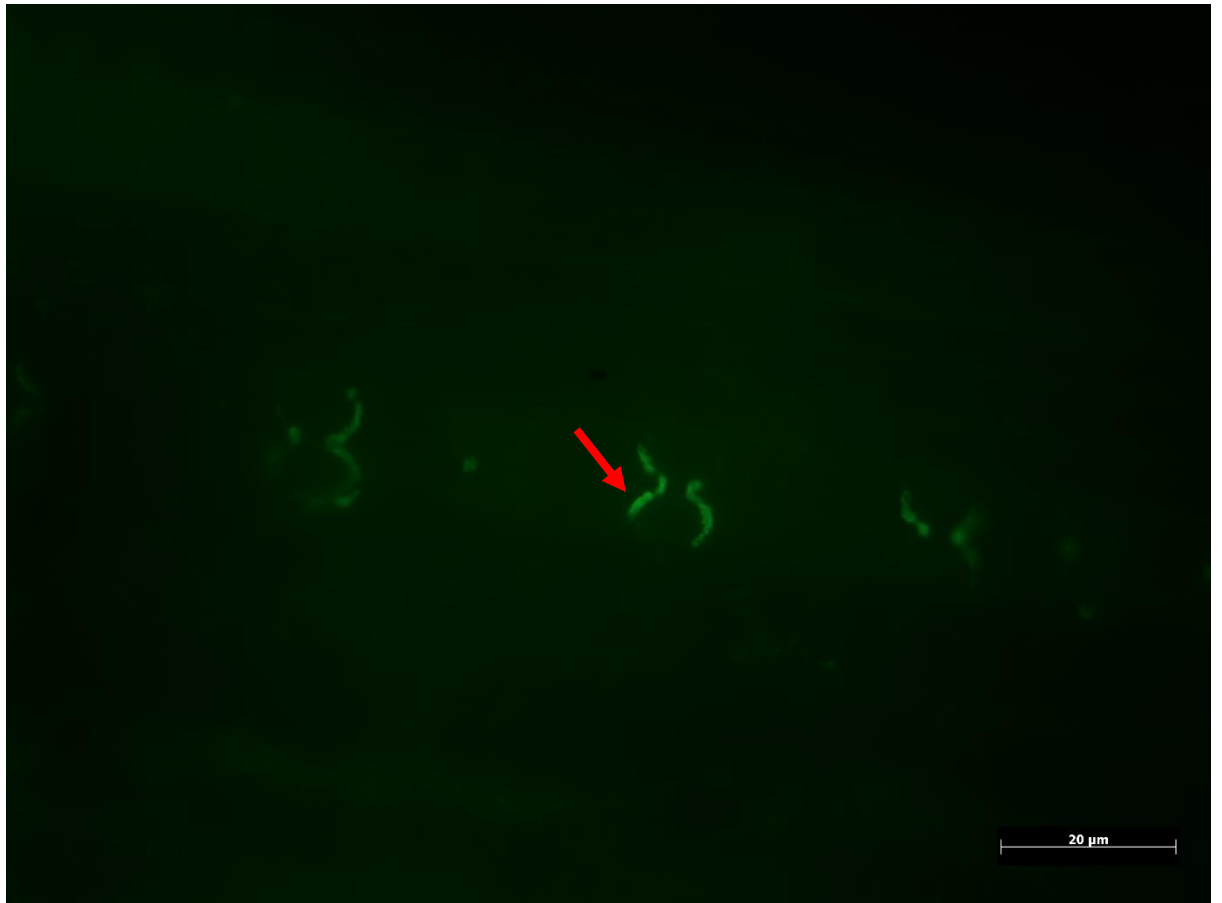


Figure 4.16 Fluorescence microscopy image of immunofluorescence stained rice leaf tissue shown at 100x magnification. The rice plant this tissue was taken from was approximately one month old.

At the highest magnifications the silica cells are more clearly identifiable with their characteristic dumbbell shape (Fig 4.16). The callose signal is only detected at the edges of the silica cells, though it is not possible to determine if the signal comes from the silica cells themselves or the epidermal cells bordering them (see red arrow).

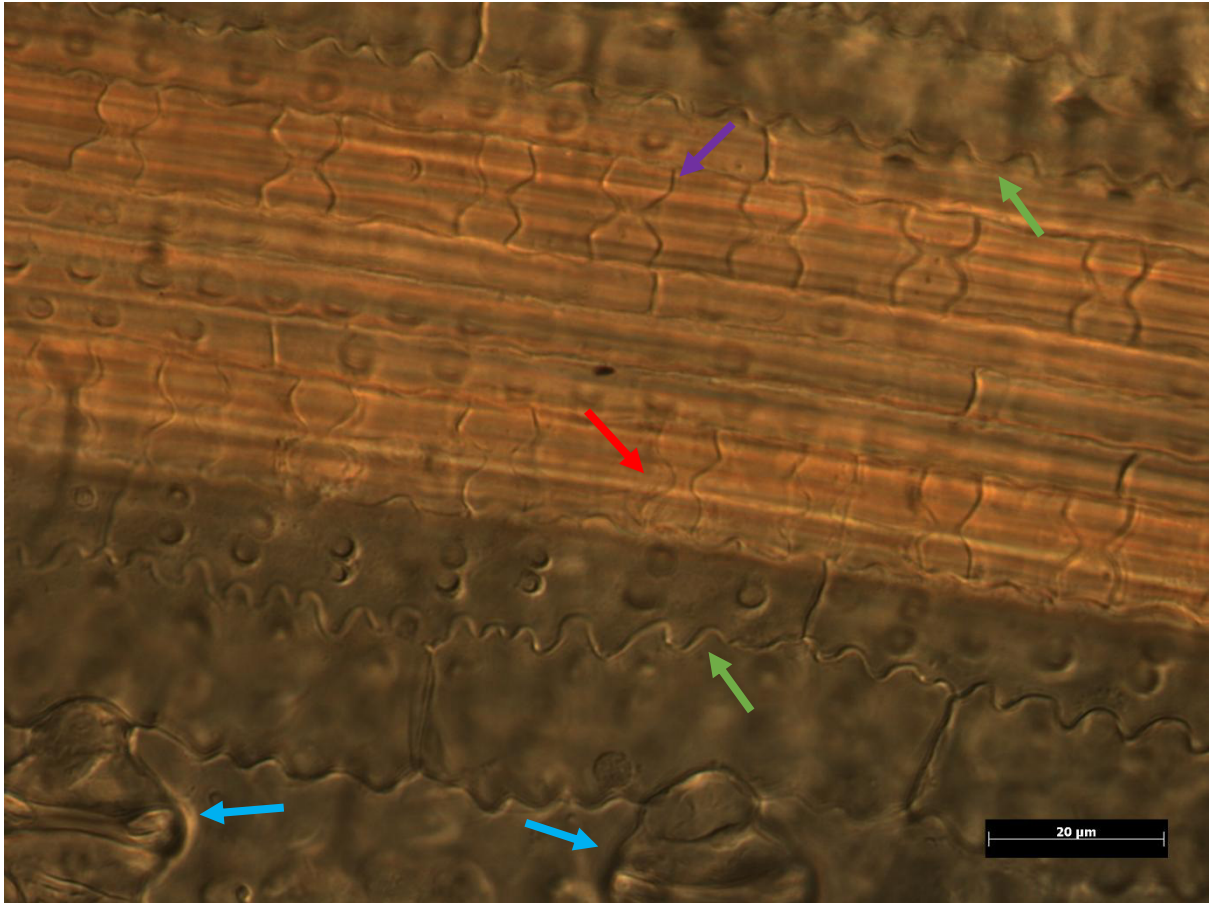


Figure 4.17 Light microscopy image of immunofluorescence stained rice leaf tissue shown at 100x magnification. This image is of the same region shown in figure 4.16. The rice plant this tissue was taken from was approximately one month old.

Light microscope images of the stained tissue reveals more about the surrounding area (Fig 4.17) as much detail is lost to the dull green autofluorescence in some of the fluorescence images (Fig 4.16). The row of silica cells that showed a strong callose signal can be seen (see red arrow) bordering another row of silica cells above them (see purple arrow). The upper silica cell row did not show any signs of callose detection under fluorescence imaging (Fig 4.16). The surrounding tissue can be seen more clearly, with epidermal cells bordering both sides of the silica cell rows (see green arrows). Multiple stomata are also visible (see blue arrows), showing no sign of callose under staining (Fig 4.16).

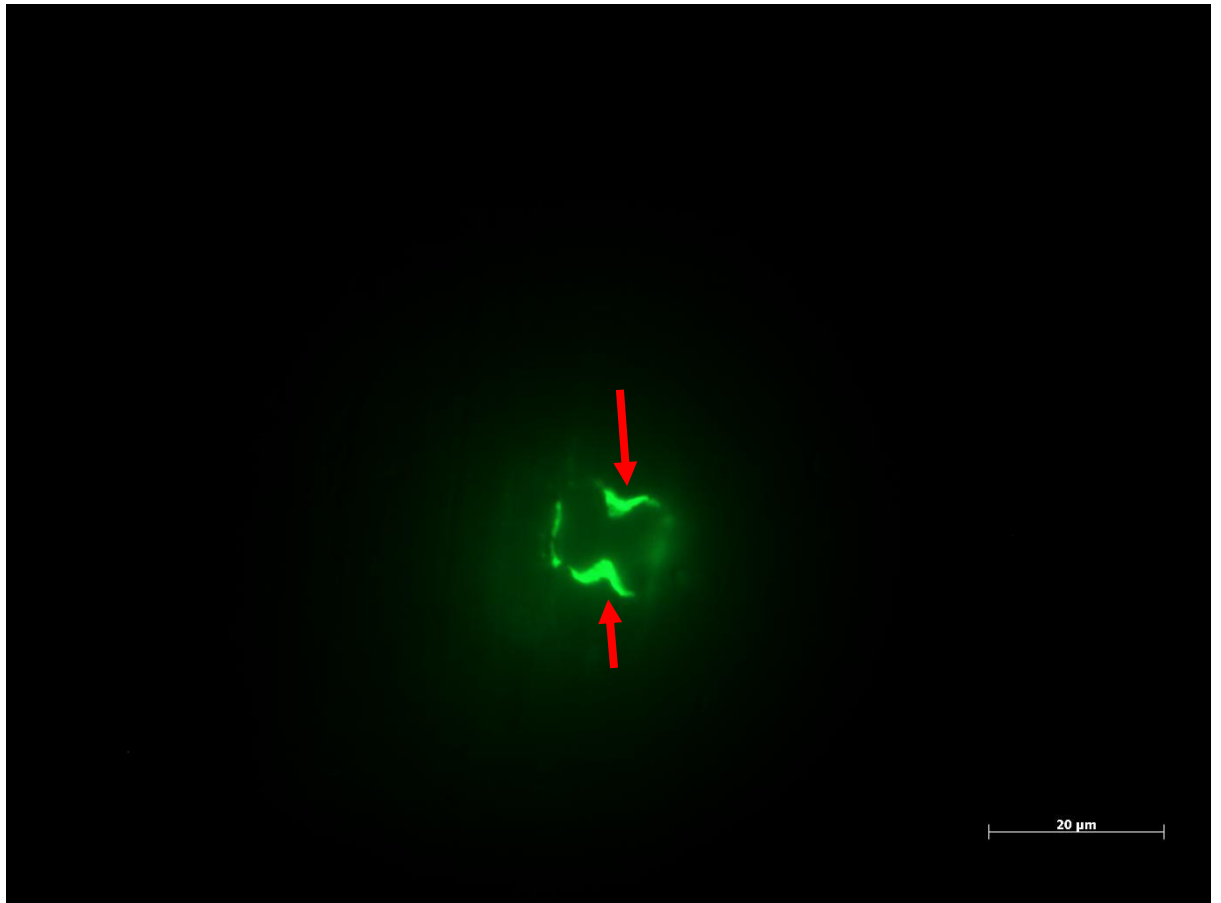


Figure 4.18 Fluorescence microscopy image of immunofluorescence stained rice leaf tissue shown at 100x magnification. The rice plant this tissue was taken from was approximately one month old.

Reducing the field of view removes much of the background fluorescence given off by neighbouring structures and gives a much clearer image of individual structures, such as a silica cell (Fig 4.18). Callose is more heavily localised at the sides of the silica cell, with thick bands of fluorescence seen where the dumbbell curves inwards (see red arrows).

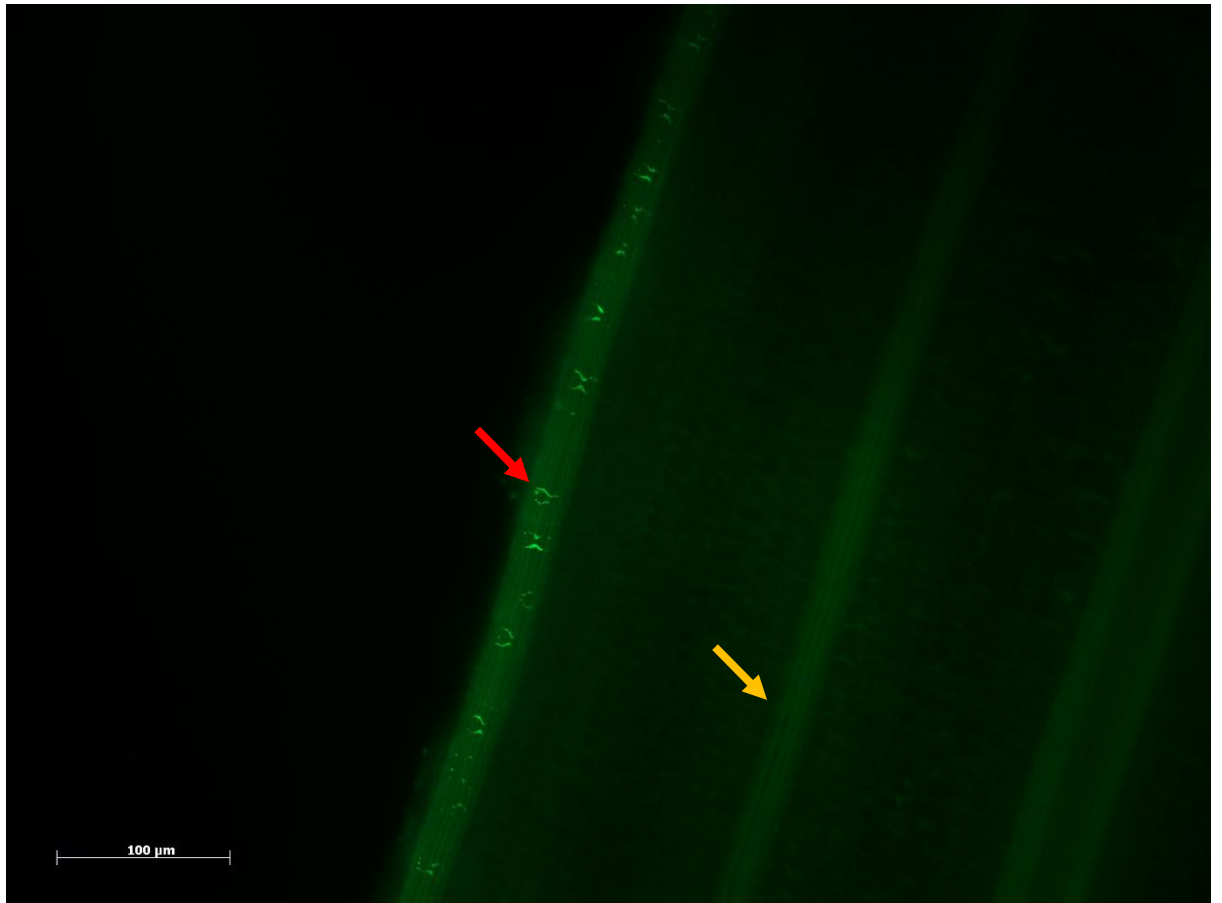


Figure 4.19 Fluorescence microscopy image of immunofluorescence stained rice leaf tissue shown at 20x magnification. The rice plant this tissue was taken from was approximately one month old. Antibody penetration into the tissue was variable, but staining was more consistently successful at the edges of the sample which provided a greater surface area for the antibodies to infiltrate (Fig 4.19). Silica cells can be seen clearly stained for callose at the edges of the leaf tissue sample (see red arrow), but similar structures deeper in the middle of the tissue sample do not show any similar fluorescence (see gold arrow).

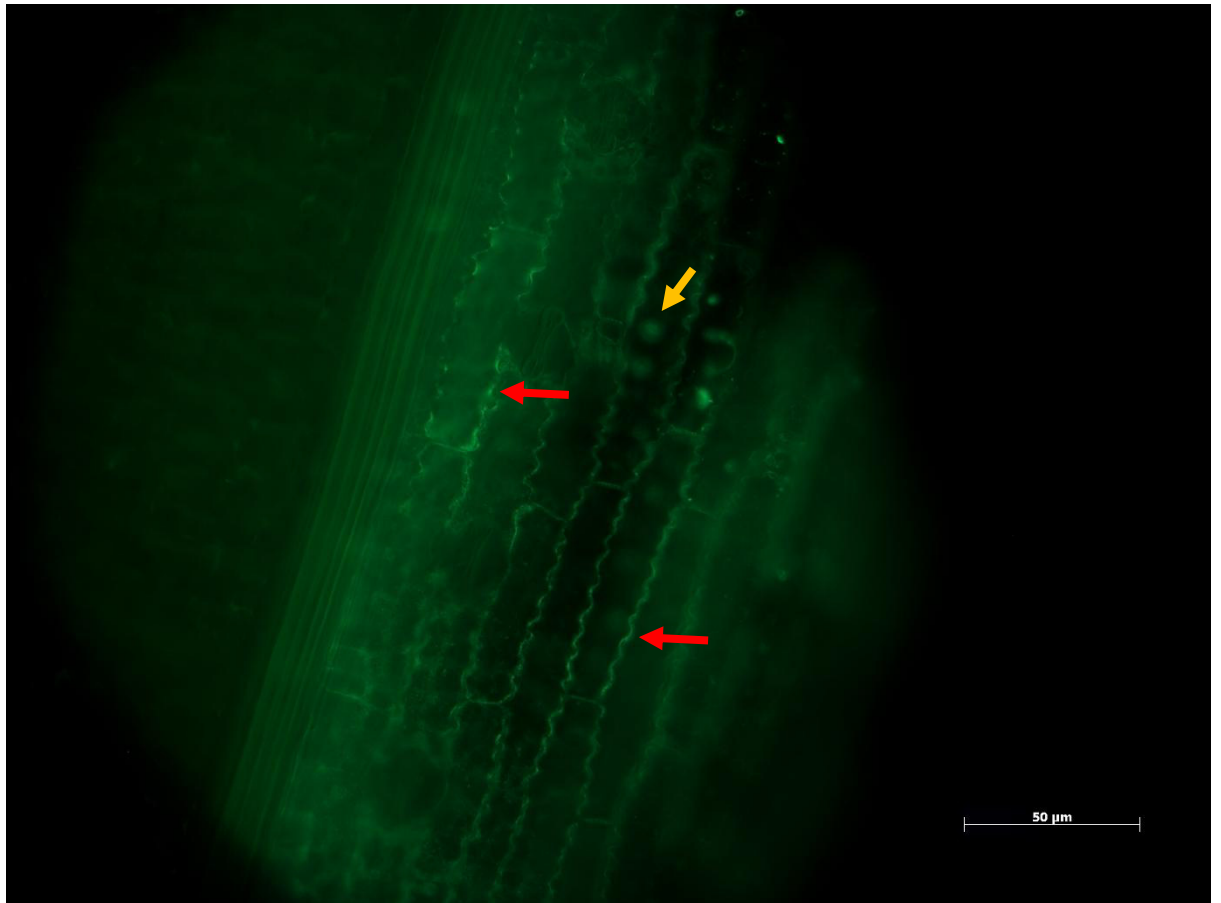


Figure 4.20 Fluorescence microscopy image of immunofluorescence stained rice leaf tissue shown at 40x magnification. The rice plant this tissue was taken from was approximately one month old.

Callose-induced fluorescence can be seen at the cell walls of epidermal cells across the leaf surface (Fig 4.20). The sinuate outer walls of the epidermal cells show significant fluorescence at the peaks and troughs of the wave-like structure, with reduced fluorescence seen at the transitional areas (see red arrows). The focus of this image is on the epidermal cell walls themselves which leaves the papilla on these cells largely out of view, though some can still be seen (see gold arrow).

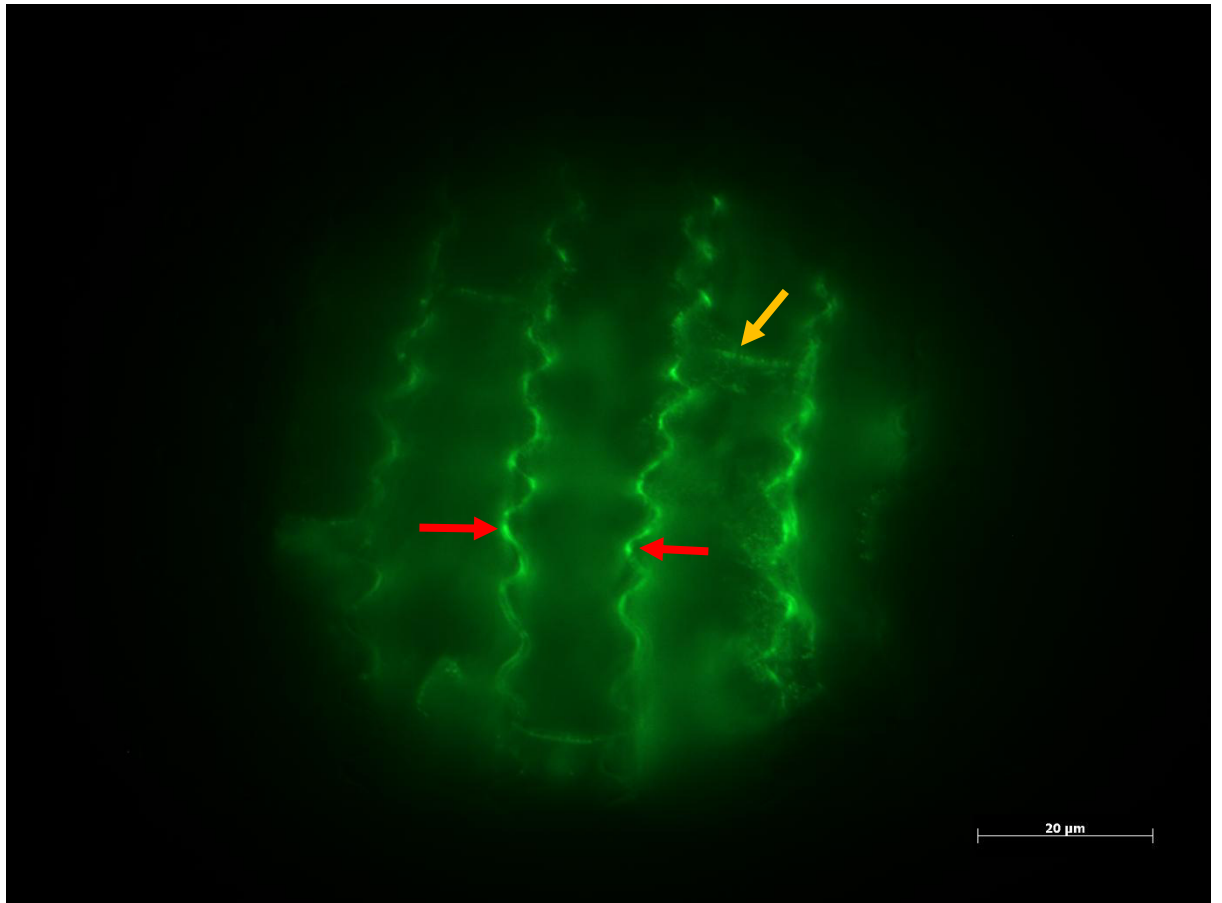


Figure 4.21 Fluorescence microscopy image of immunofluorescence stained rice leaf tissue shown at 100x magnification. The rice plant this tissue was taken from was approximately one month old. Higher magnification images of the epidermal cell walls confirm the presence of callose (Fig 4.21). As before, the sinuate outer walls of the epidermal cells show significant fluorescence at the peaks and troughs of the wave-like structure, with reduced fluorescence seen at the transitional areas (see red arrows). Where two epidermal cells meet at their short edge, callose induced fluorescence is present although it is not as prominent as at the sinuate peaks and troughs (see gold arrow).

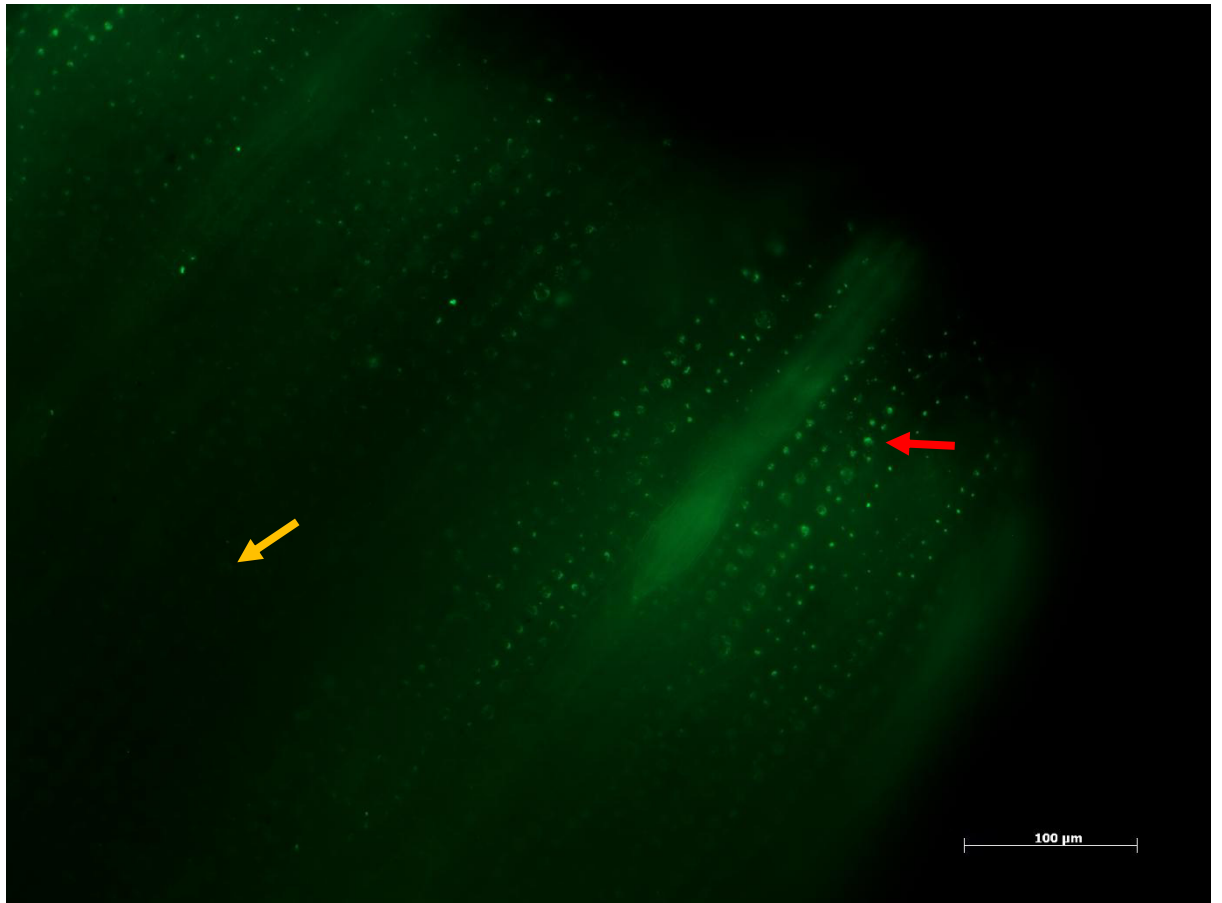


Figure 4.22 Fluorescence microscopy image of immunofluorescence stained rice leaf tissue shown at 20x magnification. The rice plant this tissue was taken from was approximately one month old.

Even at low magnification fluorescence identifying callose at the papilla of epidermal cells is evident, shown by the light green fluorescence against the dull green background of the surrounding tissue (Fig 4.22) (see red arrow). Papilla further into the plant tissue sample are visible but show a reduced fluorescence when compared with those closer to the sample edge suggesting that the antibodies did not penetrate deeper into the tissue in this sample (see gold arrow).

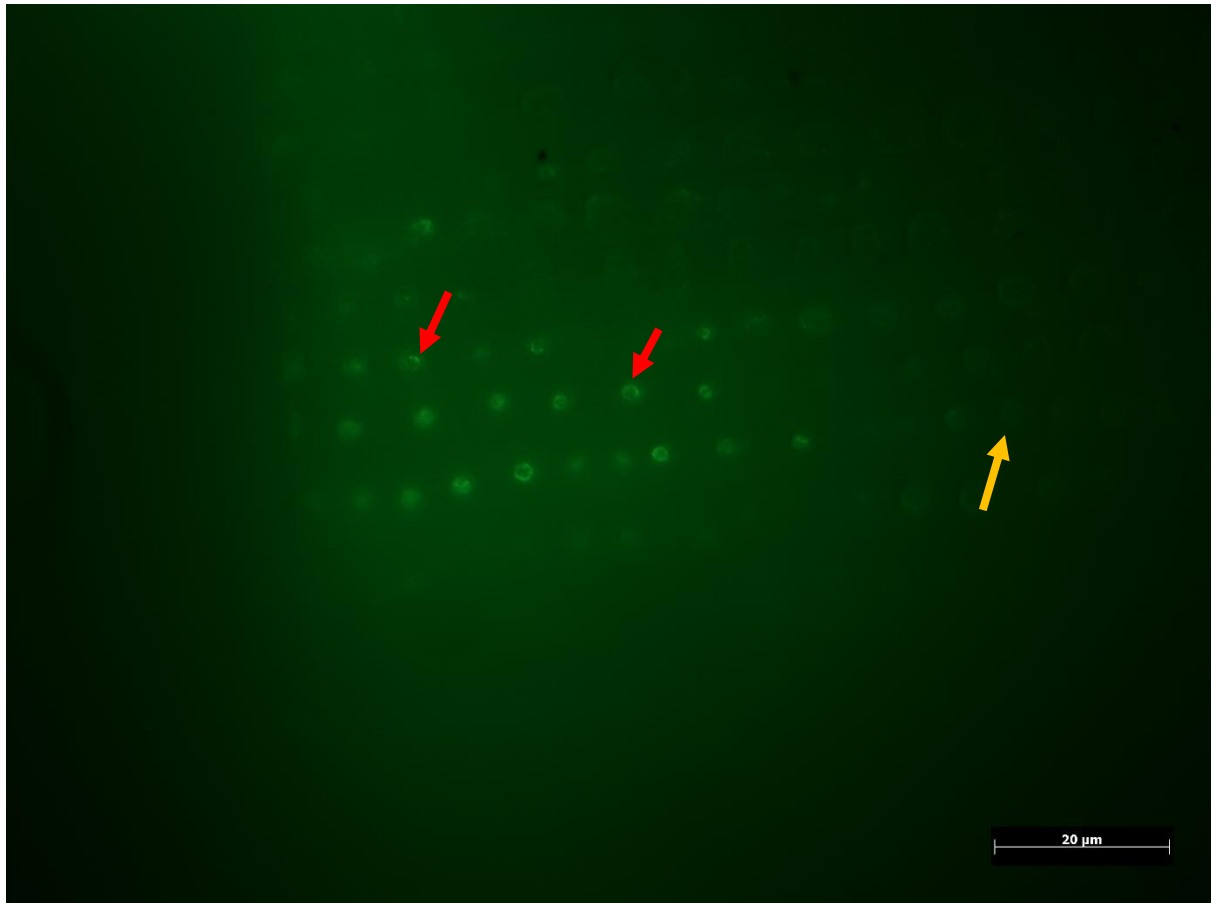


Figure 4.23 Fluorescence microscopy image of immunofluorescence stained rice leaf tissue shown at 100x magnification. The rice plant this tissue was taken from was approximately one month old.

At the highest magnifications the dull green autofluorescence of the sample tissue can drown out a lot of the finer detail of the sample (Fig 4.23). Despite this interference, the papilla of the epidermal cells can be seen to give off a distinguishable fluorescence signal for callose (see red arrows). Papilla closest to the edge of the sample fluoresce, whilst those deeper into the sample do not (see gold arrow).

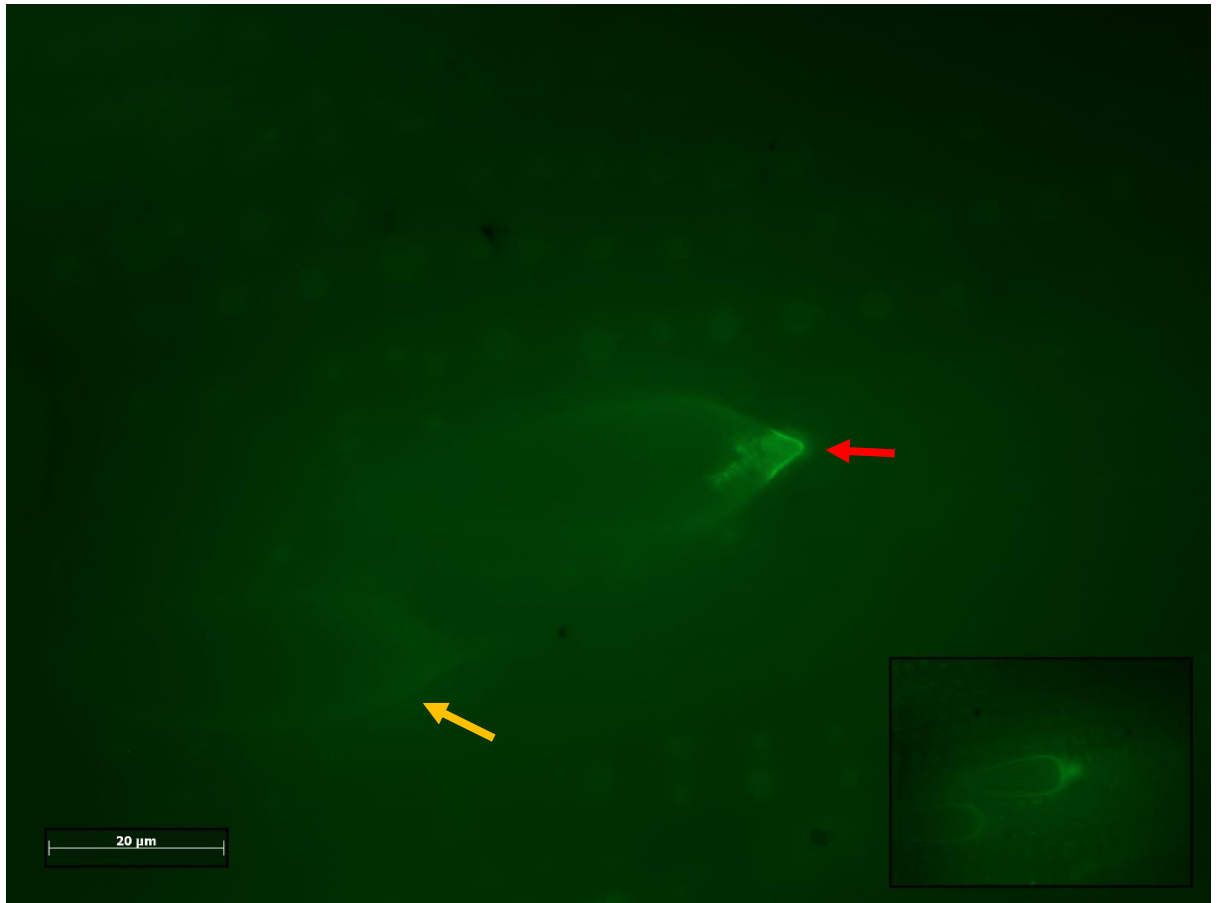


Figure 4.24 Fluorescence microscopy image of immunofluorescence stained rice leaf tissue shown at 100x magnification. The insert shows the same region at a different level of focus. The rice plant this tissue was taken from was approximately one month old.

Callose-induced fluorescence was seen at the trichomes, centred at the tip of the trichome (Fig 4.24) (see red arrow). Whilst the tip shows a strong signal, the main body of the trichome shows no sign of callose deposition (Fig 4.24 – see insert). Not all trichomes showed this callose signal as evidenced by the neighbouring trichome which shows no fluorescence signal at all (see gold arrow). The dull green autofluorescence of the sample again obscures some detail of the surrounding sample tissue.

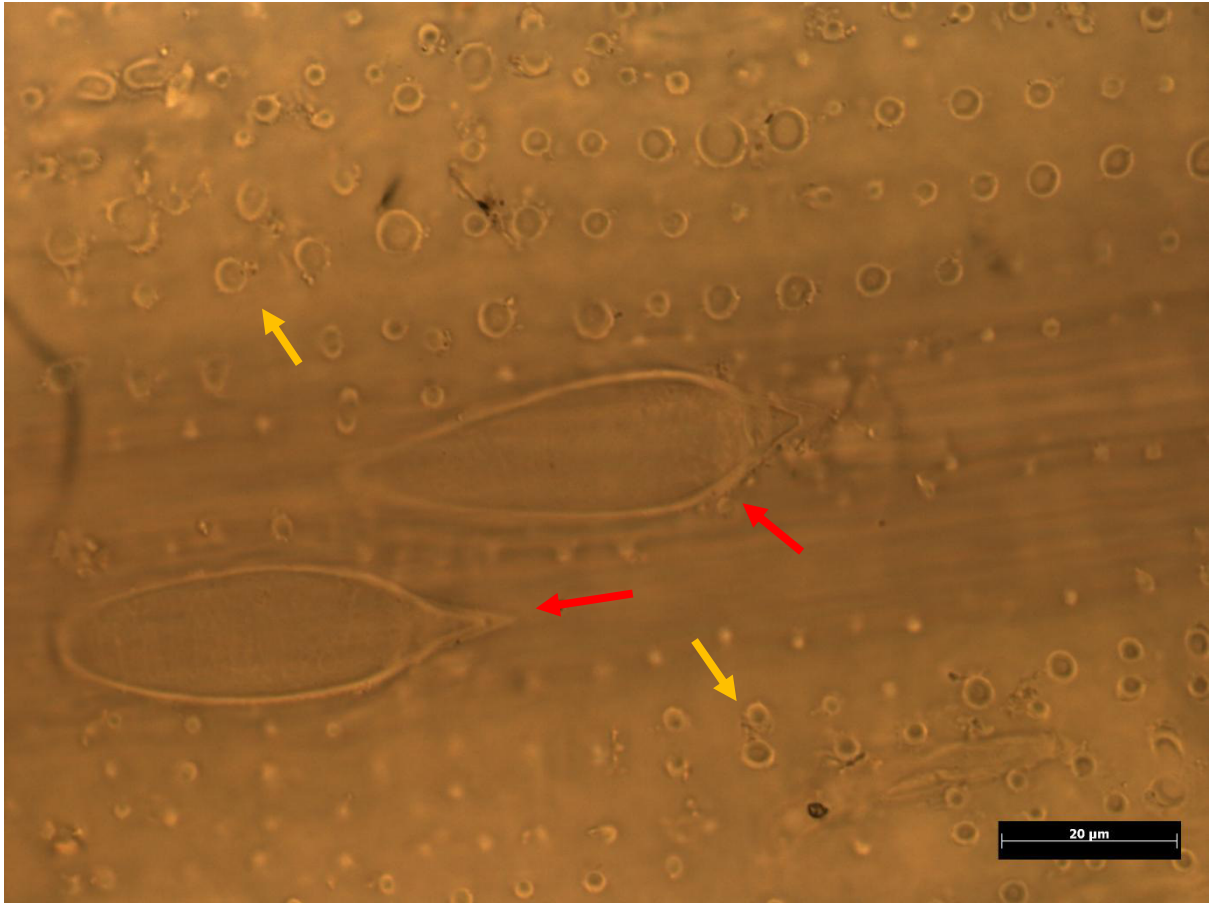


Figure 4.25 Light microscopy image of immunofluorescence stained rice leaf tissue shown at 100x magnification. This image is of the same region shown in figure 4.24. Arrows label areas of note, discussed in the text below.

Light microscope images of the stained tissue reveals more about the surrounding area (Fig 4.25) as much detail is lost to the dull green autofluorescence in some of the fluorescence images (Fig 4.24). Two trichomes can be seen clearly (see red arrows) with epidermal cells surrounding them, covered with papilla (see gold arrows).

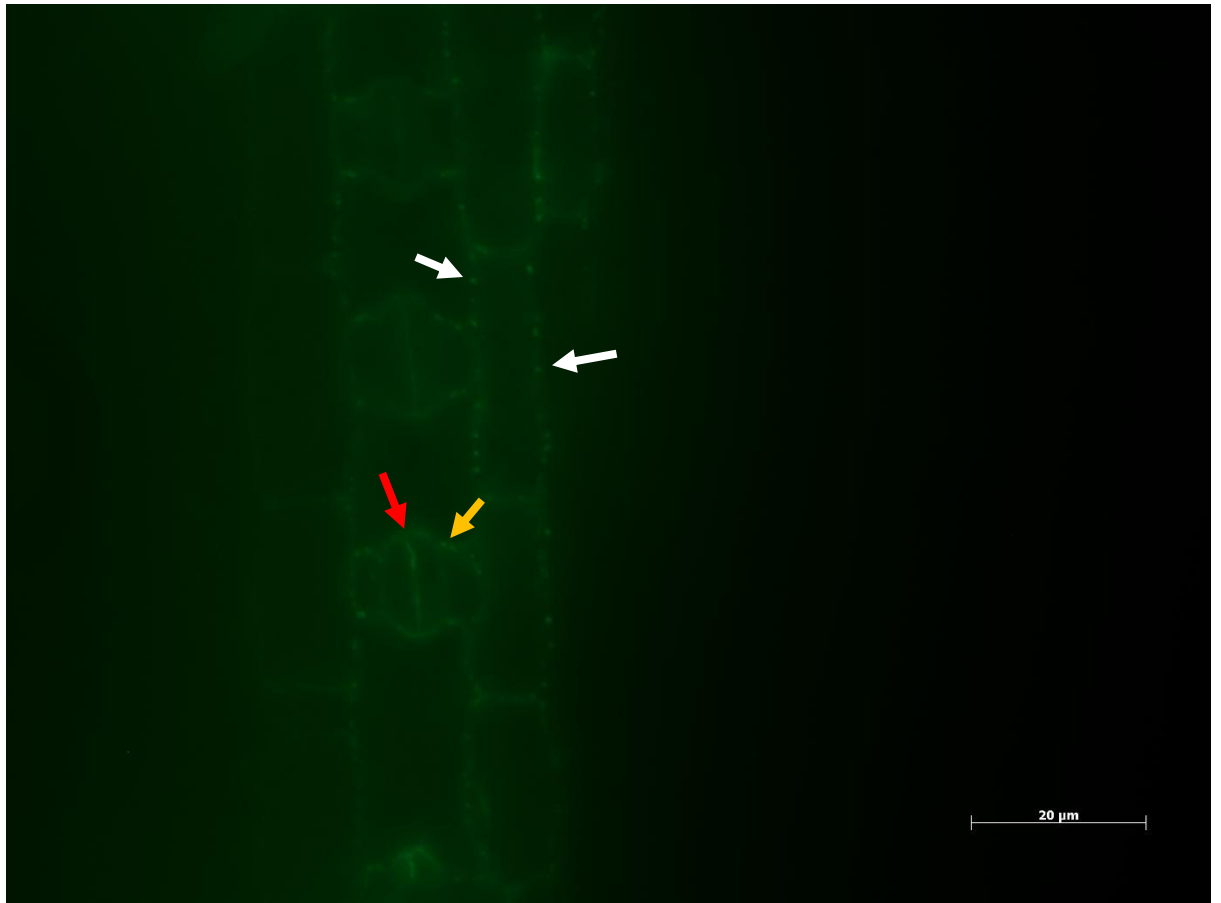


Figure 4.26 Fluorescence microscopy image of immunofluorescence stained rice leaf tissue shown at 100x magnification. The rice plant this tissue was taken from was approximately one week old.

Stomata were consistently stained for callose in younger plants whose leaves were still developing (Fig 4.26). Callose can be seen clearly at the inner walls of the guard cells bordering the stomatal aperture (see red arrow). Callose can also be detected to a lesser degree surrounding the rest of the guard cells and the surrounding epidermal cells (see gold arrow). Callose staining can also be seen at the surrounding epidermal cells, with intermittent punctate deposits of callose at various points around each epidermal cell (see white arrows).

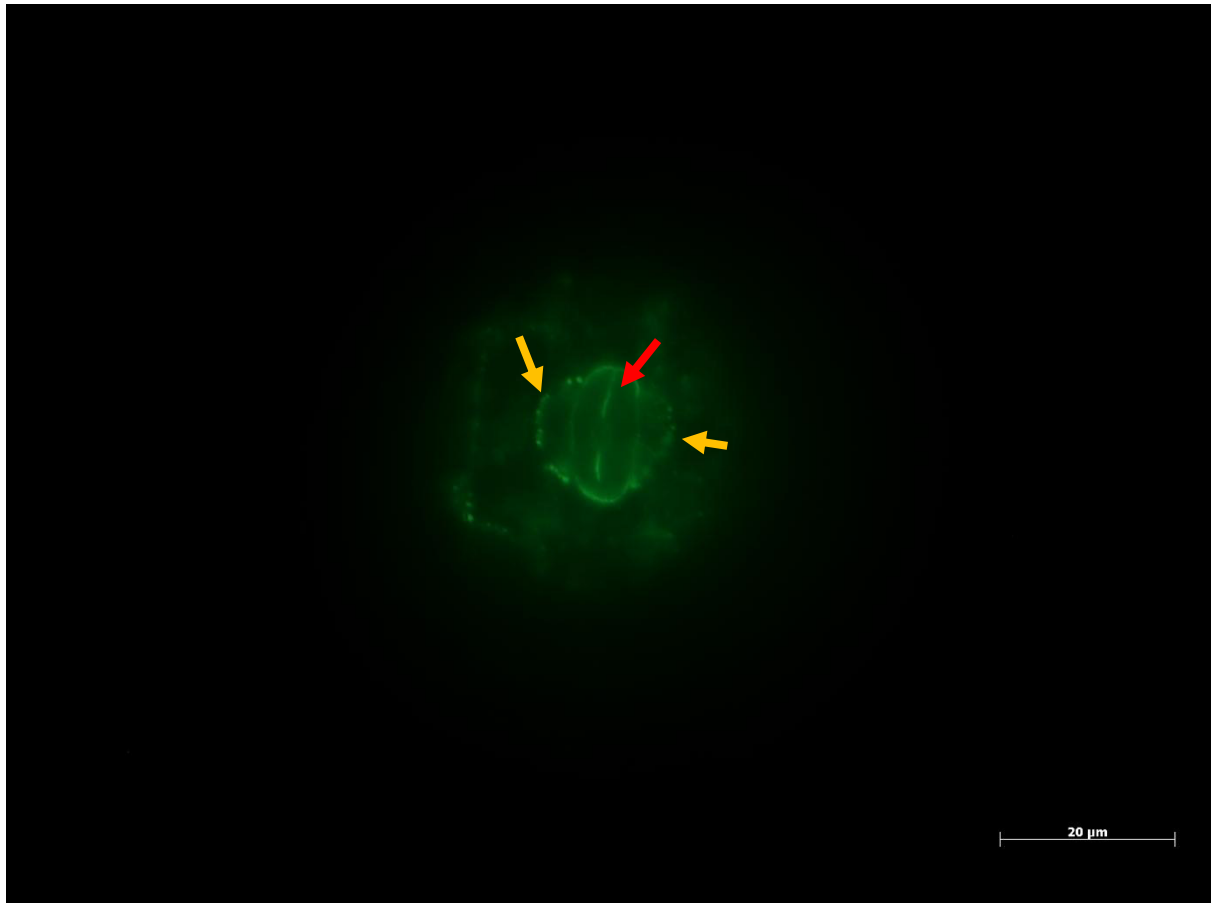


Figure 4.27 Fluorescence microscopy image of immunofluorescence stained rice leaf tissue shown at 100x magnification. The rice plant this tissue was taken from was approximately one week old.

Reducing the field of view removes much of the background fluorescence given off by neighbouring structures and gives a much clearer image of individual structures, such as a stomata (Fig 4.27). Callose can be seen clearly at the inner walls of the guard cells, though it does not extend to the centre of the stomatal aperture (see red arrow). Callose can also be detected surrounding the rest of the guard cells and the two neighbouring subsidiary cells (see gold arrows).

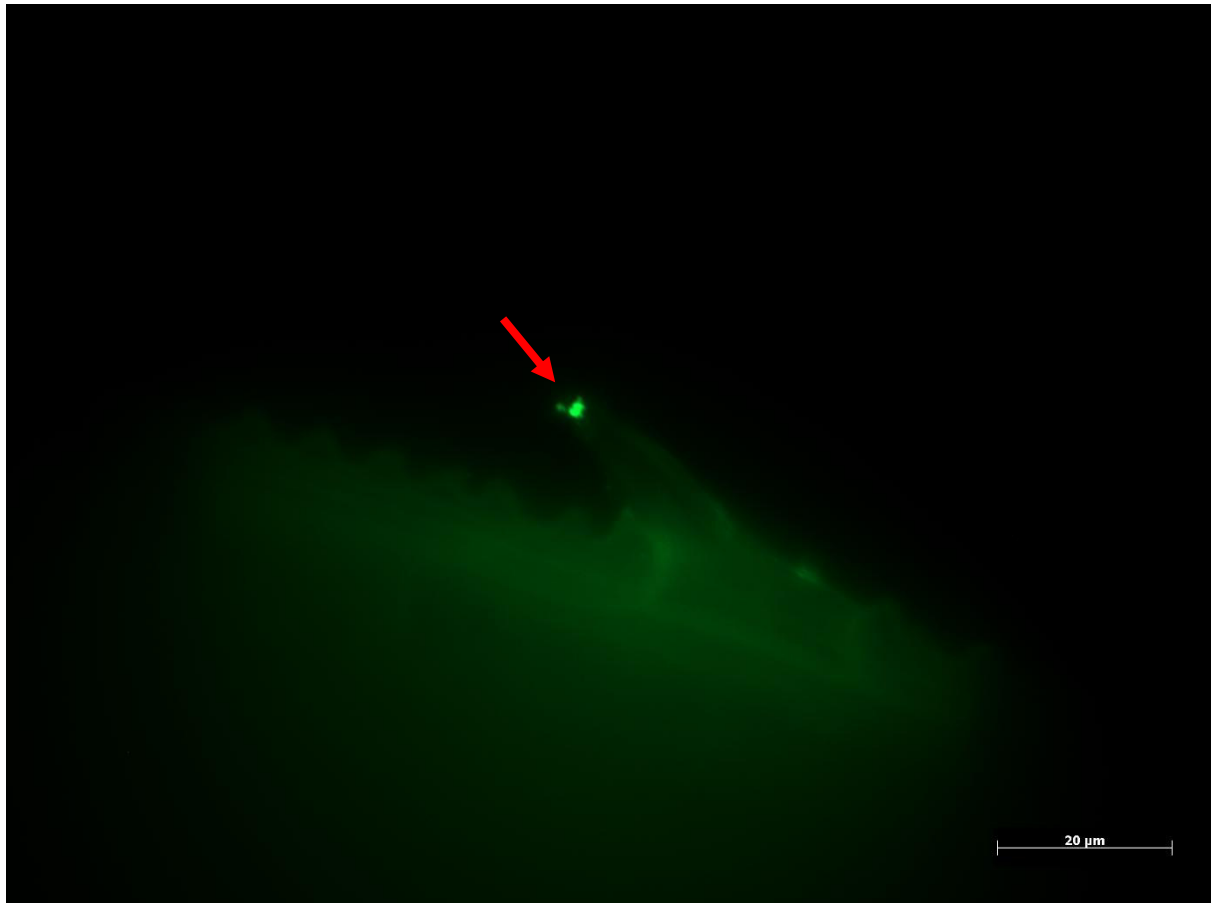


Figure 4.28 Fluorescence microscopy image of immunofluorescence stained rice leaf tissue shown at 100x magnification. The rice plant this tissue was taken from was approximately one week old. Callose-induced fluorescence can be clearly seen again at a trichome, orientated to give a side-on view of the structure; fluorescence is again concentrated at the tip of the trichome (Fig 4.28 – see red arrow). Whilst the tip shows a strong signal, the main body of the trichome shows no sign of callose deposition. There is no sign of callose deposition at the papilla of the bordering epidermal cells.

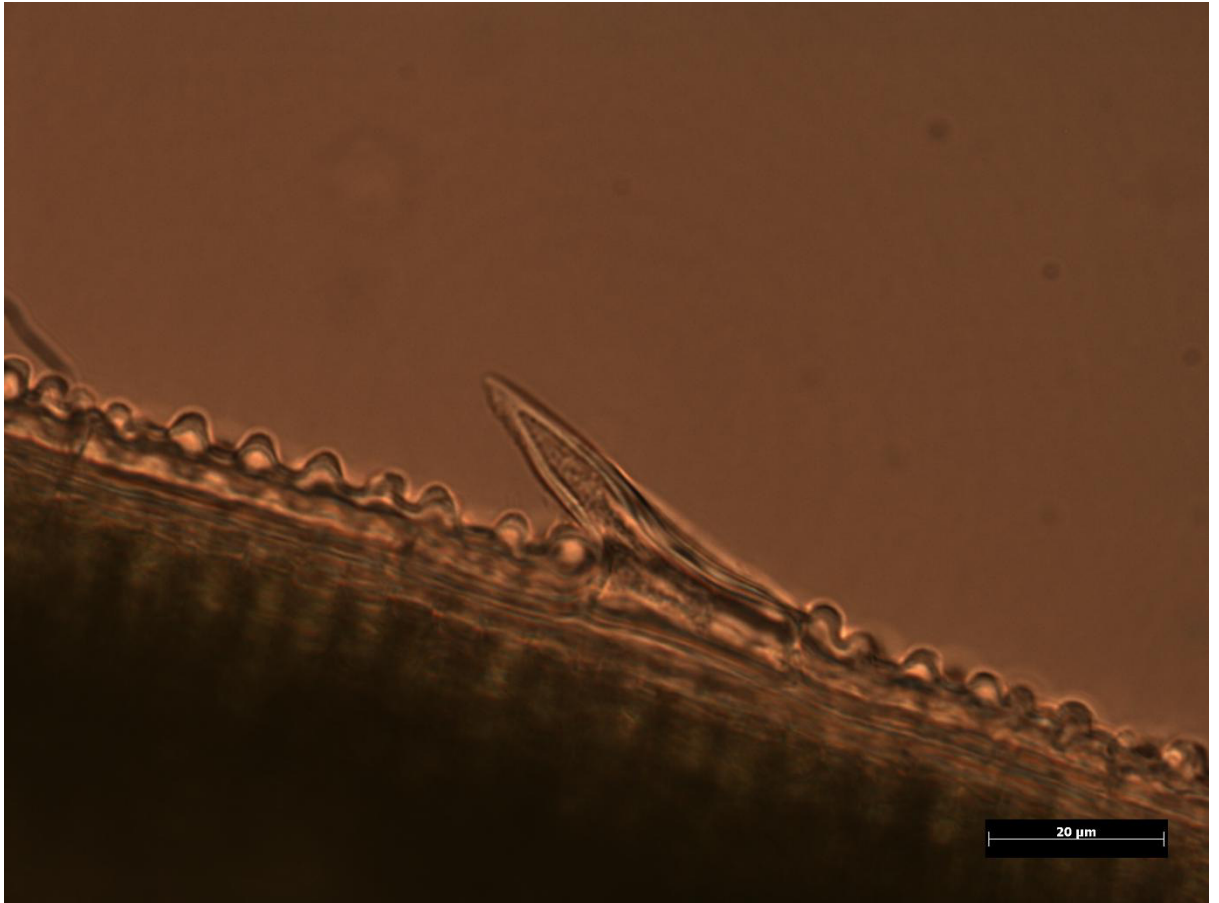


Figure 4.29 Light microscopy image of immunofluorescence stained rice leaf tissue shown at 100x magnification. This image is of the same region shown in figure 4.26. Arrows label areas of note, discussed in the text below.

Light microscope images of the stained tissue reveal more about the surrounding area, showing the full structure of the trichome and the surrounding epidermal cells and their papilla (Fig 4.29).

4.4 Discussion

4.4.1 Aniline Blue Autofluorescence

When compared with the autofluorescence images, the aniline blue stained samples showed clear differences to their unstained counterparts. Chloroplasts within cells showed up red under the UV fluorescence filter (Fig 4.1), whilst almost all other structures (epidermal cell walls, silica cells, stomatal openings, trichomes and the lignified fibres below the silica cells) gave off a dull, dark blue fluorescence (Fig 4.1 & Fig 4.2). By contrast, aniline blue stained samples showed multiple areas of light blue/cyan fluorescence in specific areas, indicating the presence of callose (see section 4.3.2). When stained with aniline blue, callose is often described as giving off a yellow fluorescence under UV excitation rather than the cyan colour primarily observed here (Rost, 1995). Interference from the dull blue autofluorescence given off by almost all cellular structures in the rice tissue is the culprit for this colour shift; the mixture of the yellow fluorescence and the blue autofluorescence combined to give off the cyan colour observed. In multiple areas of strong enough staining it is possible to see the yellow fluorescence overpowering the blue background – this effect is most noticeable on the larger stained papilla, where the centre of the nodule is yellow, shifting towards cyan at the edges (Fig 4.4).

4.4.2 Immunofluorescence Autofluorescence

Autofluorescence images also taken under the blue filter cube were used for the immunofluorescence staining. Rice leaf tissue is observable as a dull green colour with few areas of definition, though individual structures such as trichomes and papilla are still clearly visible (Fig 4.12). At higher magnifications individual structures, such as the epidermal cell walls, are distinct, but show no sign of increased fluorescence from the surrounding tissue (Fig 4.13). Silica cells similarly do not show signs of autofluorescence beyond the dull green background, though their borders are clearly visible, along with small punctate deposits inside the individual cells (Fig 4.14).

4.4.3 Callose Seen at Silica Cells in Both Aniline Blue and Immunofluorescence

Both the aniline blue and immunofluorescence staining of the rice tissue provided striking images showing callose detection at multiple sites of known silicification. Through aniline blue staining callose was shown to deposit at the edges of silica cells, the dumbbell-shaped cells running in columns along the veins of leaves (Fig 4.5, Fig 4.6, Fig 4.7 & Fig 4.11). Callose at the silica cells was identified by a strong, cyan-yellow coloured fluorescence concentrated at the edge of the silica cells, easily discernible from the darker blue background fluorescence. Only some of the observable silica cells were stained for callose, with some areas of silica cells showing no sign of staining (Fig 4.8), whilst other areas showed intermittent staining of some silica cells in a column, but not others (Fig 4.5, Fig 4.6 & Fig 4.7). Whilst it is possible that callose was simply not present at all silica cell boundaries, it is more likely that the aniline blue stain did not penetrate all areas of the sample tissue at a constant rate.

Immunofluorescence staining showed a similar pattern of callose deposition at the edges of silica cells, with columns of silica cells showing a clear bright green fluorescence at their borders; the signal was extremely distinct from the dull green background given off by all tissue when viewed under the blue filter (Fig 4.15, Fig 4.16, Fig 4.18 & Fig 4.19). The small punctate deposits seen in the autofluorescence were not seen in the stained images. As seen in the aniline blue staining, not all silica cells were stained for callose, and those silica cells which were stained were rarely entirely surrounded by callose. Antibody penetration seemed to be most efficient at the edges of the sample, with silica cells near the edges showing strong staining whilst those further into the sample showed no signs of callose staining (Fig 4.19).

Silica cells, as their name would suggest, are well known to accumulate silica in high concentrations when rice is grown in the presence of silicic acid (Ma, 1990). The callose staining data shows strong evidence for significant deposition of callose at the edges of the silica cells, with both staining methods showing similar results.

4.4.4 Callose Seen at Papilla in Both Aniline Blue and Immunofluorescence

The papilla, the raised nodules which cover the surface of the leaf epidermal cells, showed strong signals for callose deposition across multiple samples in both the aniline blue and immunofluorescence staining methods.

Aniline blue staining showed callose detection, visible by a cyan-yellow coloured fluorescence at the papilla, with the strong yellow signal emanating from the centre of the papilla, fading to cyan around the edges (Fig 4.3, Fig 4.4, Fig 4.5, Fig 4.8 & Fig 4.9). As seen previously with the silica cells, not all papilla were stained due to the variation in different areas of tissue's permeability to the stain; even at higher magnifications unstained papilla are visible in proximity to their stained counterparts (Fig 4.8 & Fig 4.9).

Immunofluorescence showed similar results, with papilla showing clear staining for callose, identifiable by the bright green fluorescence at the peak of the nodules (Fig 4.22 & Fig 4.23). Not all papilla were stained, with an increase in antibody penetration at the corners of the sample tissue where the surface to volume ratio is higher (Fig 4.22).

Papilla are known areas of silica deposition in rice, with a study into the effects of silicon fertilisation of rice growth showing that the size of papilla increased under silicon replete conditions (Ning et al., 2014).

4.4.5 Callose Seen at Trichomes in Both Aniline Blue and Immunofluorescence

Trichomes are hair or spine-like features which cover the surface of leaves in some plant species, including important crops like rice and wheat. Trichomes are defence mechanisms for the plant, providing a barrier against herbivory. Whilst the physical role of these rough spines is obvious, they may also play a chemical role as trichomes in tomatoes have been shown to express protein inhibitors during insect feeding (Tian et al., 2012).

Aniline blue staining showed callose localised at the tip of the trichome as well as at the base, but not throughout the main body (Fig 4.10). The callose signal was larger at the tip of the trichome, giving off a strong yellow/cyan fluorescence, whereas the base showed only a few intermittent specs of cyan fluorescence along the joining point between the trichome and the epidermal cell. Immunofluorescence imaging revealed strong callose signals at multiple trichomes, once again focused at the tip of the spine-like protrusion with no callose signal found anywhere else in the structure (Fig 4.24 & 4.28).

Trichomes are known to be silicified in several plant species, including wheat (Rafi et al., 1997) and rice (Simpson & Volcani, 1981). The localisation of callose only at the tip of the trichome could be an indication that silicification of trichomes is basipetal, working its way from the tip to the base. This is not without precedent, as basipetal secretions of pyrethrins, chemicals used in plant defence, have been shown to occur in *Tanacetum cinerariifolium* (Ramirez et al., 2012). Indeed, the callose signal seen in one trichome appears to fade out as it moves further down the base of the trichome, rather than remaining as a punctate deposit purely at the tip (Fig 4.24).

4.4.6 Callose Seen at Stomata in Both, Though Only in Young Tissue for Immunofluorescence

Stomata are the pore-like openings, flanked by two guard cells, which regulate gas exchange in the plant. Only one sample showed callose staining using aniline blue staining, though immunofluorescence provided much better results on this front but only in the younger tissue samples; stomata were not found to be stained for callose in the one-month old plants.

The majority of stomata seen in the aniline blue staining showed no sign of callose detection, except one sample in which two stomata showed a definite signal for callose (Fig 4.5). The first of the stained stomata showed callose surrounding one of its guard cells completely, with a signal at only the inner wall of the opposing guard cell. The second of the stained stomata showed one guard cell completely surrounded by callose, but no signal at the opposing guard cell.

Immunofluorescence in the one-month old rice tissue showed no signs of callose staining at the stomata; stomata were clearly visible and observed but showed no elevated fluorescence when compared with their surroundings or the autofluorescence readings (Fig 4.20). Under the advice of our colleagues from the University of Athens, younger rice samples were grown for analysis and in rice seedlings aged one week from germination, stomata were stained readily (Fig 4.26 & Fig 4.27). Multiple stomata were observed alongside developing epidermal cells, showing intermittent callose staining at both the guard cells and the subsidiary cells which border them (Fig 4.26). When examining individual stomata in more detail it was observed that callose was deposited at the inner walls of the guard cells, where the pair meet to cover the stomatal aperture. However, the callose did not extend to the centre of the guard cells (Fig 4.27). Callose was not found at the anticlinal walls of the guard cells, where the guard cell and subsidiary cell are connected, but rather it is deposited in such a way as to surround both cells in a single callose layer (Fig 4.26 & Fig 4.27).

Stomata and their associated cells are known areas of silicification in rice leaves and it has in fact been shown that rice plants grown in the absence of silica have delayed responses with regards to the opening of stomatal pores (Agarie et al., 1998). Investigation into silica deposition at the stomata performed using transmission electron microscopy found that silica is deposited at all walls of the guard cells except for the anticlinal wall between the guard cell and the subsidiary cell (Ueno & Agarie, 2005). The immunofluorescence imaging shows the same pattern of deposition in callose at the guard cells, with callose not found at the anticlinal walls but present at the remaining areas of the guard cell wall, providing further evidence for a connection between silica deposition and callose.

Callose is known to deposit in the stomata of other plant species, at the guard and subsidiary cells. In the fern *Asplenium nidus* callose was shown to be deposited in differing patterns throughout the stomata depending on its developmental stage, and it was found to be essential in

the development of stomatal pore openings and playing a role in guard cell wall thickening (Apostolakos et al., 2009). The similarities between the callose detection observed in rice (Fig 4.26 & 4.27) and the callose detection found in *Asplenium nidus* (Fig 4.30) are striking, suggesting a similar role for callose in the development of rice stomata and guard cell formation.

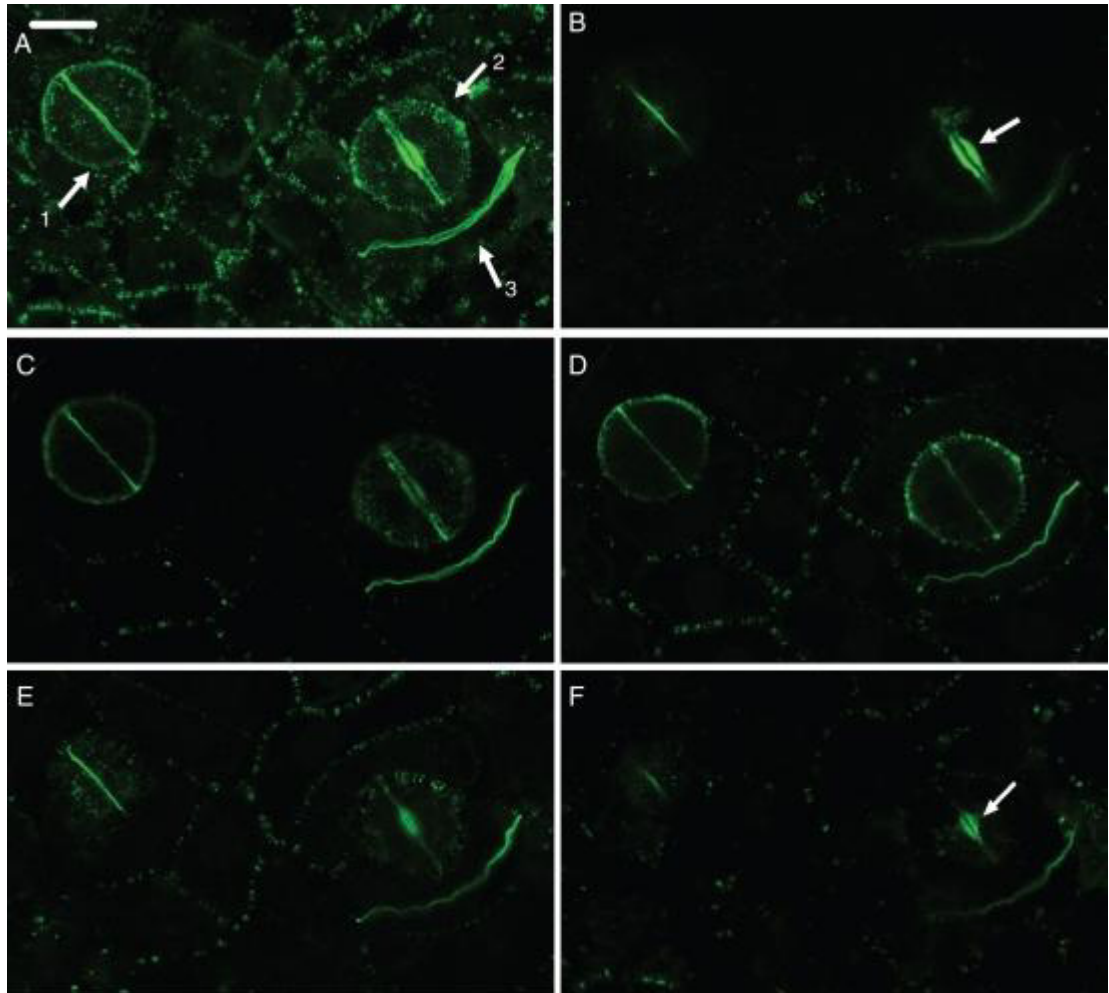


Figure 4.30 Callose staining of stomata in *Asplenium nidus* using the same immunofluorescence techniques used in the current study (Apostolakos et al., 2009).

Thanks to the similarities between callose stained stomata found in *Asplenium nidus* and the images of silica stained stomata found in *Equisetum arvense* further research into callose and its interactions with silicic acid was performed and it was found that callose can induce the formation of silica in under-saturated solutions of silicic acid, providing further evidence for its role in templating silica deposition in plants (Law & Exley, 2011).

4.4.7 Callose Seen at Epidermal Cell Walls in Immunofluorescence

Callose staining was not observed at the epidermal cell walls through aniline blue staining, however, immunofluorescence found evidence of callose at the epidermal cell walls in both the one-week and one-month old plant tissue (Fig 4.20, Fig 4.21 & Fig 4.26). In one-month old leaf tissue, callose-induced fluorescence can be seen at the boundaries of the epidermal cells, showing a bright green fluorescence against the dull green autofluorescence seen throughout the sample (Fig 4.20). At higher magnifications the callose staining can be seen to be concentrated at the peaks and troughs of the sinuate border of the epidermal cells (Fig 4.21). At the connections between vertically stacked epidermal cells the callose signal is still present, however it is less pronounced than at the lateral, sinuate sides (Fig 4.21).

In the one-week old tissue, an earlier stage of epidermal cell was stained for callose, lacking the sinuate shape and papilla which cover the surface in fully developed leaf epidermal cells (Fig 4.26). The callose signal found in these samples was not a complete layer around the cell, but rather punctate deposits of callose found intermittently at various points around the cell wall.

Callose staining in the epidermal cells showed a remarkable similarity to the staining of silica structures obtained from horsetail epidermal structures using PDMPO (Fig 4.31). Silica is most heavily deposited at the edges of the epidermal cells, which corresponds with the heaviest areas of callose deposition in the current work.

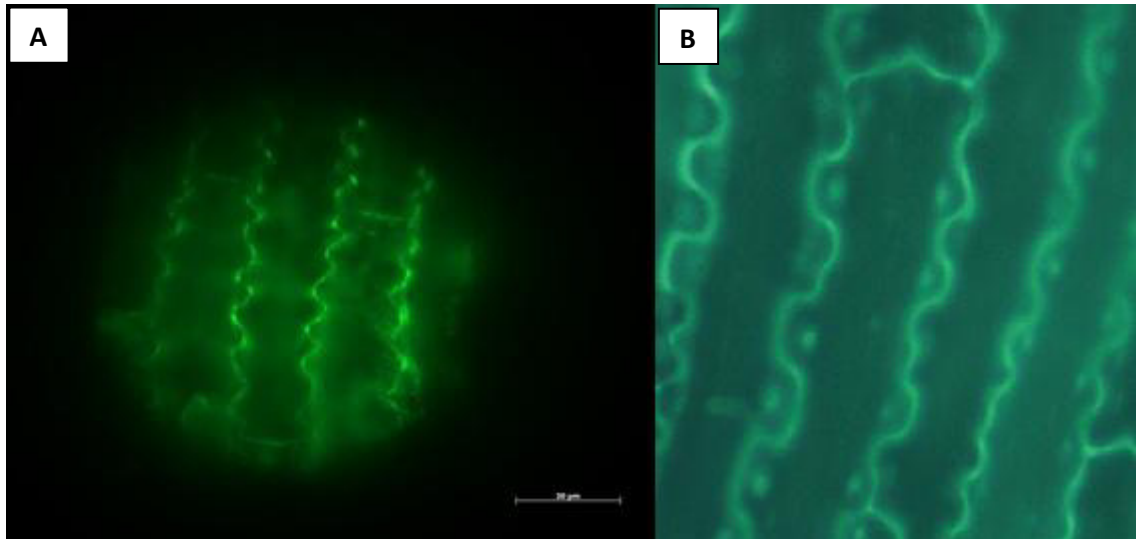


Figure 4.31 Comparison of callose stained epidermal cells from rice (A) and PDMPO stained silica structure from the epidermal cells of horsetail (B) (Law & Exley, 2011).

4.4.8 These Callose Locations are All Known Sites of Silica Deposition in Rice

Every site of callose deposition found through both aniline blue staining and immunofluorescence corresponded with known areas of silica deposition in rice. Those cells which are known to be the most heavily silicified, the silica cells, also showed the most consistent and largest callose deposits surrounding their cell walls, whilst other well-known areas of silicification such as the epidermal cells (and their associated papilla), trichomes and stomata all showed definite signs of callose deposition. Areas of specific cells which are known not to accumulate silica, like the anticlinal walls of stomatal guard cells, were also shown to not accumulate callose in this region. This further strengthens the hypothesis that callose templates for silica deposition.

Strong evidence has been found for a connection between callose and silica deposition, however the next step will be elucidating the mechanisms behind the interactions that occur between callose and silicic acid.

5. Investigation into the Effects of Sample Preparation Procedure on Silica Morphology through SEM Imaging

5.1 Introduction

Many areas of the upper plant are known to be silicified in rice, with the primary destination for silica deposition being found at the terminus of the transpiration stream; a 2.5 μm silica layer is formed in the gap between the leaf epidermis and the 0.1 μm thick cuticle which covers it (Yoshida, 1965). In addition to this layer of silicon, more specific silicification of certain cell types occurs, such as at the silica cells and the bulliform cells. Silica cells are dumbbell-shaped cells which are found covering the veins of the leaf epidermis in a ladder-like formation, whilst the bulliform cells are motor cells responsible for the curling of the leaf during drought conditions, which reduces water loss (Ma & Takahashi, 2002).

During the course of my experiments with PDMPO, several unexpected silica structures were found which resembled xylem vessels (see section 7.3.1.5). Xylem is not typically considered a site for silica deposition in rice and no evidence of the previous discovery of these structures could be found.

The most pertinent question when considering the silicification of the xylem in plants is could the xylem still function under conditions of silicification, and if so at what level of impediment? The cells which form the xylem vessels are dead in mature xylem, functioning only as a vessel through which water is moved primarily via gradients in hydrostatic pressure as water evaporates from the leaves, resulting in an upwards pull force acting on the water in the xylem; root pressure plays a role in forcing water upwards, but this is secondary to the much stronger forces of hydrostatic pressure (Myburg et al., 2013). Without any real purpose other than to act as a hydrophobic tube for the transport of water, it is possible that the silicification of these structures would not prevent their function, though it would certainly impede it to a varying degree depending on the thickness of the silica layer.

Assuming a mature xylem vessel of typical size, roughly 30 µm in diameter, with a layer of silica covering its internal surface at the same thickness found at the leaf epidermis, 2.5 µm, then the internal volume of that xylem vessel would have decreased by roughly 30%. The presence of silicon has been shown to reduce the transpiration rate in rice on numerous occasions (Okuda & Takahashi, 1961; Ma, 1988). Rice supplied with silicon at 100ppm in the culture solution showed a reduction in transpiration rate of between 27 – 29% (Okuda & Takahashi, 1961). Similarly another study showed that the transpiration rate of the rice plants was negatively correlated with the silica content of the shoot, with a 13.22% silica concentration in the shoot resulting in a 27% drop in transpiration rate over a silica free shoot (Ma, 1988). Interestingly, in both cases this reduction in transpiration was exclusively ascribed to the silica deposited at the surface of the leaves, when in fact silicification of the xylem could also play a role in this reduction in transpiration capacity.

Biogenic silica in rice and other plants has been shown to exist in a form similar to silica gel and that this silica gel accounts for upwards of 90% of the total silicon within the plant (Ma, 1990). Silica gel is a highly porous, amorphous form of silica which is commonly used as a desiccant due to its ability to adsorb water through its porous structure. Whilst it can be used as a desiccant under relatively dry conditions, in a water-saturated environment like the lumen of a xylem vessel, silica gel would be nothing more than another porous layer which water had to pass through in order to leave the xylem and as such, would not prevent xylem function.

Whilst the xylem is known to be vital in the transport of silicic acid from the roots up to areas of silica deposition, it is not thought of as an area of silica deposition itself. There is some evidence of silica deposition in the xylem of certain species, with an analysis of phytolith morphology in wild rice (*Zizania palustris*) finding xylem silica phytolith structures (Yost & Blinnikov, 2011). To obtain these phytoliths, an extensive preparation procedure was performed on the harvested plant tissue before it was ashed and analysed through light microscopy; ½ inch to 1 inch samples

of leaf tissue were treated with a cleaning agent called Liquinox, sonicated and then dried overnight at 80°C.

Silicic acid in the xylem is known to be super-saturated, at least transiently with concentrations well in excess of the 2 mM necessary for silica polymerisation under normal conditions (Casey et al, 2003; Mitani et al, 2005). However the xylem is a relatively enclosed biological system and it has also been shown that once xylem sap is removed from that enclosed system, it quickly begins to polymerise into silica (Mitani et al, 2005). As soon as the leaf tissue is cut, the xylem system is no longer a closed system and the xylem sap still contained within could very quickly polymerise into silica, especially given the large delay (over two days) between cutting of the samples and the digestion of the organic component in the wild rice experiment (Yost & Blinnikov, 2011).

Silicic acid has been used in spruce (*Picea abies*) and birch (*Betula verrucosa*) trees as a method of mapping the ultrastructure of the xylem (Persson et al., 2004). Wood samples were impregnated with a silica sol-gel and heated to produce a silica-cast replica of the xylem structure. This process shares many similarities with our own acid digestion method preparation; samples are cut and then dried out in an incubator at 37°C until they reach a dry weight (see section 2.2 Microwave Acid Digestion & Filtration). This application of heat to the sample, which includes xylem vessels filled with sap containing a potentially super-saturated silicic acid concentration could easily result in the polymerisation of silicic acid into silica in the xylem. Even ignoring the addition of heat to the sample, xylem vessels are severed in the samples harvested for acid digestion, with leaves being cut into roughly 1 cm pieces; this eliminates the closed nature of the xylem system and leaves the super-saturated silicic acid susceptible to polymerisation as the tissue samples are dried out.

Whilst the xylem could still theoretically function whilst silicified, its capacity to transport water would be significantly reduced. Given that the evidence for the silicification of the xylem comes from techniques which could themselves be causing the formation of silica, an experiment was

devised to determine whether the techniques themselves had caused these results. Rice plants were grown hydroponically and when matured, split into two groups: the first group would be dried out to a constant weight and then acid digested, whilst the second group would be acid digested at their wet weight immediately after harvesting. The silica structures found in both groups would then be analysed by scanning electron microscopy (SEM) to determine if certain structures, including xylem silica structures were only found in the dried group.

5.2 Method

Methods and instruments specific to this chapter are described here. For general techniques used throughout this thesis, see section 2. Materials and Method.

5.2.1 Hydroponic Growth of Rice Samples

Rice plants were grown hydroponically to an age of one month for use in this experiment. Rice was grown in silicon replete conditions in the presence of 2 mM silicic acid. For full details on hydroponic growth setup, see section 2.1 Hydroponic Growth of Plants.

5.2.2 Wet Digest vs Dry Digest Preparation

Once grown to an age of one month, rice plants were harvested and separated into two groups; wet and dry digest. The wet digest group was weighed, separated into stem and leaf before being cut into roughly 1cm sections and then immediately digested using the standard acid digest procedure (see section 2.2 Microwave Acid Digestion & Filtration). The dry digest group was weighed, separated into stem and leaf before being cut into roughly 1 cm sections and then stored inside an incubator at 37°C. The dry digest samples were periodically weighed until they reached a constant dry weight. At this point, the dried samples were then acid digested using the standard acid digest procedure.

Both sample groups were filtered after digestion to harvest their silica using the standard digest filtration procedure and stored in an incubator at 37°C until the silica was dried. Samples can be

stored indefinitely in this state, provided they are kept within the incubator to prevent moisture build-up.

5.2.3 Scanning Electron Microscopy

Two different SEMs were used to analyse the rice silica digests: A Hitachi TM3000 Tabletop Microscope and a Hitachi S-4500 Scanning Electron Microscope.

The Hitachi TM3000 is a compact, tabletop microscope designed with ease of use in mind and as such it requires minimal training and sample preparation in order to use. The TM3000 has a magnification range of between 15 – 30,000 times and a resolution of 30 nm. In addition to this, the use of the charge reduction mode and high pressure chamber allow for the imaging of uncoated samples. The TM3000 uses backscattered electrons to image the specimen, rather than secondary electrons, which require more precise vacuum conditions.

The Hitachi S-4500 Scanning Electron Microscope is a more traditional scanning electron microscope with a magnification range of between 20 – 500,000 times and a resolution of less than 1.5 nm. Samples must be coated before imaging using the S-4500.

5.2.3.1 Sample Preparation

Silica residue from the acid digests was mounted onto 12mm sticky back carbon tabs (Agar Scientific) affixed to 15mm x 6mm stubs (Agar Scientific). A small amount of silica was added to the tab which was then gently agitated and rotated to spread the silica around whilst avoiding damaging larger silica structures. A 1mm exclusion zone was maintained on the carbon tab, where no silica was placed to keep the sample contained. The stubs were lightly shaken to remove any unfixed silica and then stored in a specially designed storage box until needed for analysis.

5.2.3.2 TM-3000 Tabletop SEM

Sample stubs are attached to the sample holder, using a height reference standard to ensure the correct working distance; the stub should come up to within 1 mm of the reference bar.

Afterwards the sample holder and affixed stub were placed inside the vacuum chamber of the TM-3000 and screwed into place. The vacuum chamber is then sealed and pressurised.

After a brief set-up period, the TM-3000 is ready for image analysis, with the controls being operated, for the most part, from within the QUANTAX 70 software on the adjoining computer. The exception is the sample movement, which is operated by two dials which control horizontal and vertical movement of the sample holder within the vacuum chamber.

5.2.3.3 S-45000 SEM

Before sample stubs could be analysed using the S-4500, they were gold plated using an EM scope FD 500 sputter coating unit. This process is required because the samples must be electrically conductive for analysis using this type of SEM, otherwise the images will become charged and distorted.

The sample was then attached to the stage using a height reference standard to ensure the correct working distance. Once attached, the sample was then placed into the vacuum chamber using a loading rod to avoid contamination of the chamber. The chamber was then sealed, brought to vacuum conditions and the electron beam was activated. After optimisation of the imaging conditions, the sample was ready for imaging.

5.2.4 Thermogravimetric Analysis

Thermogravimetric Analysis (TGA) was performed on dried silica samples using a STA S-1500 Simultaneous Thermogravimetric Analyser at Keele University. TGA measures the weight change of a sample as it is heated to high temperature. In a typical experiment, a sample was placed in a pre-weighed crucible suspended inside a furnace and attached to a micro-balance. The sample was then heated to 800°C at 10°C/min in the flow of nitrogen, during which time the changing weight of the sample was recorded.

5.2.5 Fourier Transform InfraRed (FTIR)

Fourier Transform InfraRed (FTIR) is a method of spectroscopy whereby IR radiation is passed through a sample. Some of the infrared radiation is then absorbed by the sample, whilst the rest is transmitted through the sample. The resulting spectrum of molecular absorption and transmission provides a molecular fingerprint of the sample which can be compared with known spectra to determine to composition of that sample. FTIR was performed at Keele University using a Nicolet iS10 FT-IR Spectrometer.

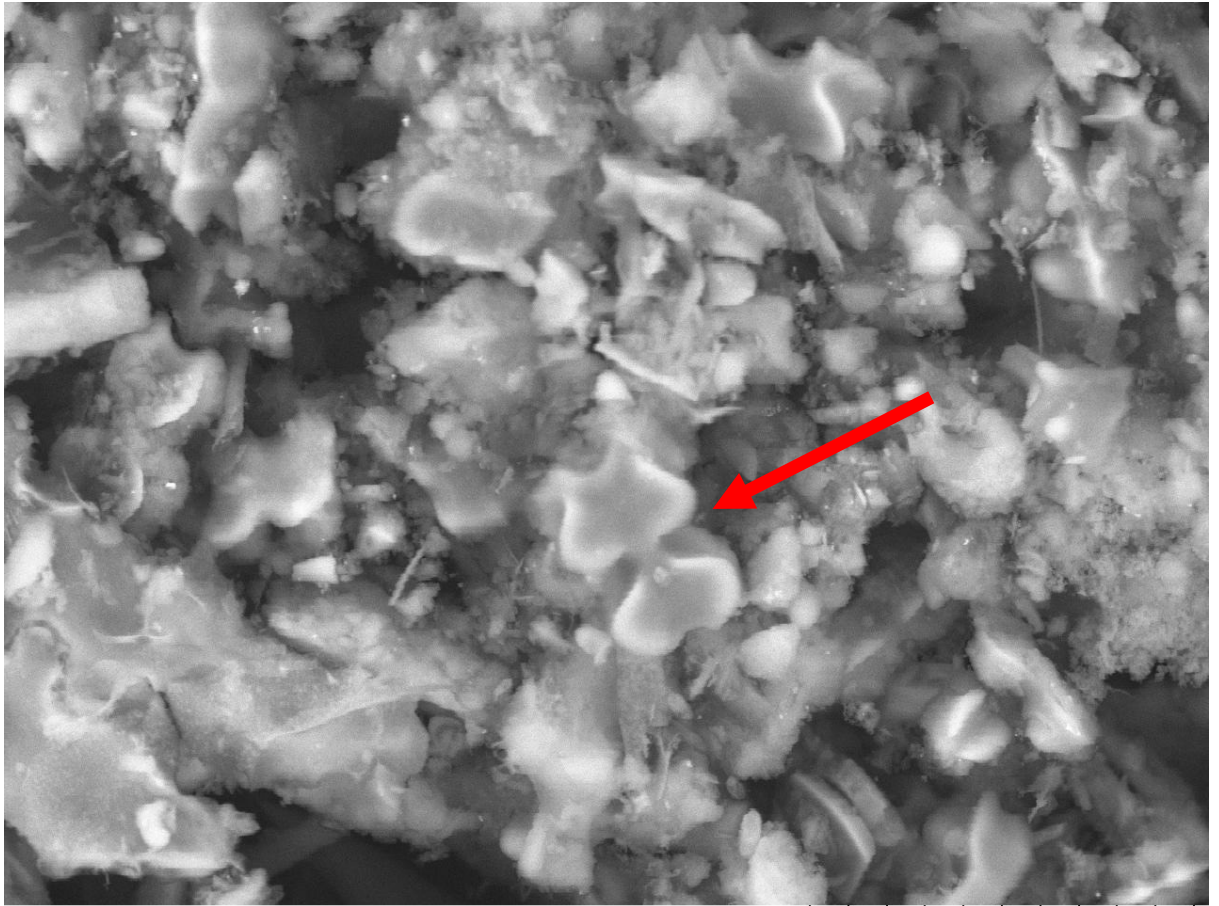
5.3 Results

5.3.1 TM3000 Tabletop Microscope

The following SEM images were obtained using the TM3000 tabletop microscope. The appropriate scale bar is located in the bottom right corner of each image. Each image is described briefly below.

5.3.1.1 Wet-Digested Rice Leaf

Samples in this group were taken from rice leaf tissue which was acid digested at its wet weight. Image magnification is displayed in the bottom right of the image along with an appropriate scale bar.



LeafWetRic0003

NL D4.4 x2.0k 30 um

Figure 5.1 SEM image of silica structures taken from a wet digested rice leaf at 2000 x magnification. Arrows label areas of interest, discussed in text.

Scattered shards of silica make up the majority of the sample and it can be impossible to identify their original morphology and location based on what remains (Fig 5.1). Certain structures are abundant throughout the sample, such as silica cells which are identified by their characteristic dumbbell shape (see red arrow).

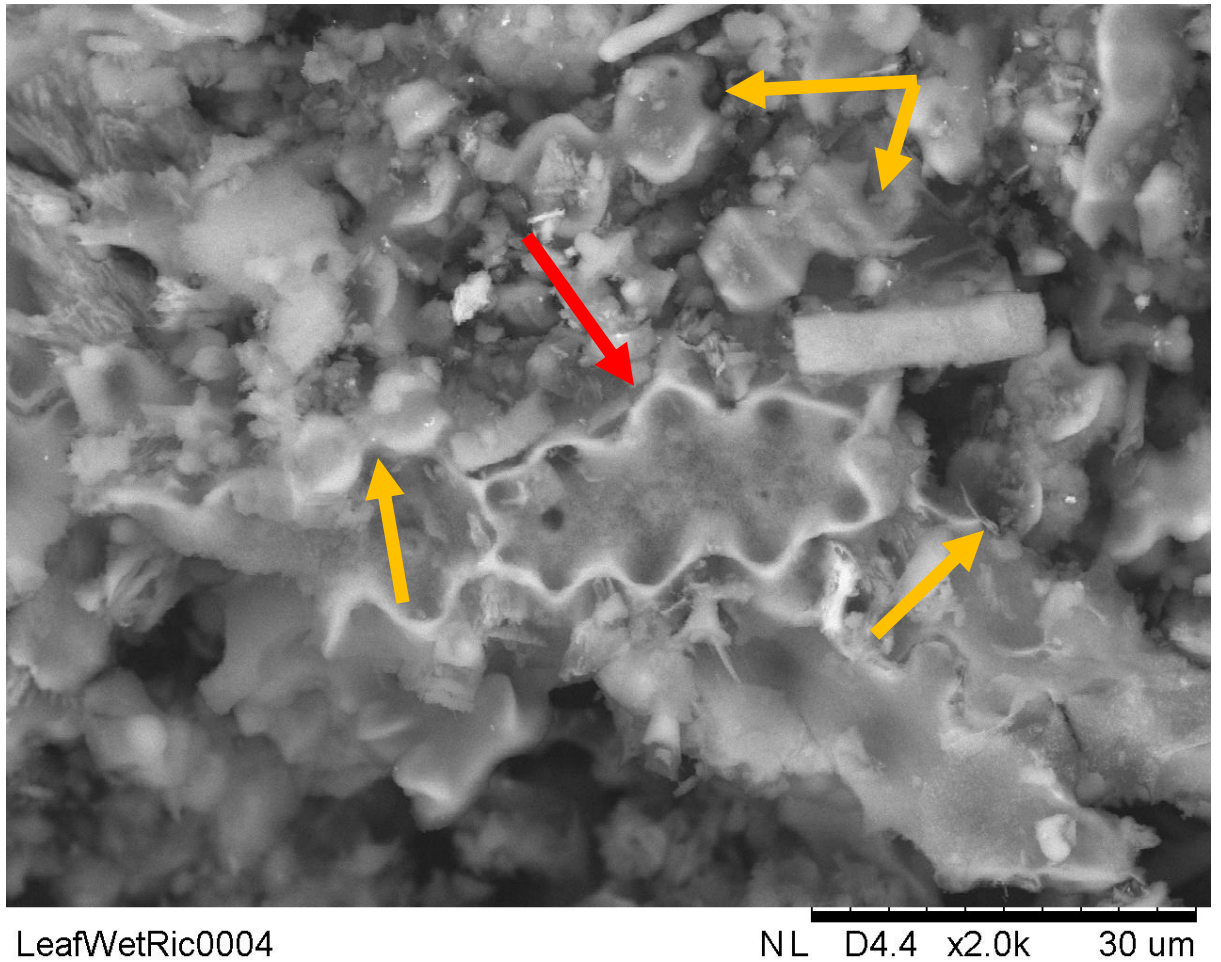


Figure 5.2 SEM image of silica structures taken from a wet digested rice leaf at 2000 x magnification. Arrows label areas of interest, discussed in text.

The orientation of the silica structures on the SEM stub is beyond control, which leads to some structures being viewed from their underside (Fig 5.2). The silica that covers an epidermal cell is usually observed by its distinctive papilla which cover the surface, however here we see the underside of the silica; the part which was in contact with the epidermal cell (see red arrow). Multiple silica cells are also found scattered throughout this image (see gold arrows). From the orientation of these silica cells, we can observe that they are entirely silicified, unlike the epidermal cells which only have their outward-facing surface silicified.



LeafWetRic0011

NL D4.3 x2.0k 30 um

Figure 5.3 SEM image of silica structures taken from a wet digested rice leaf at 2000 x magnification. Arrows label areas of interest, discussed in text.

Their distinctive mushroom-shaped morphology makes identification of bulliform cells easy to identify (Fig 5.3) (see red arrow). Bulliform cells appear to be entirely silicified much like silica cells, rather than just covered with a surface layer of silica like epidermal cells.

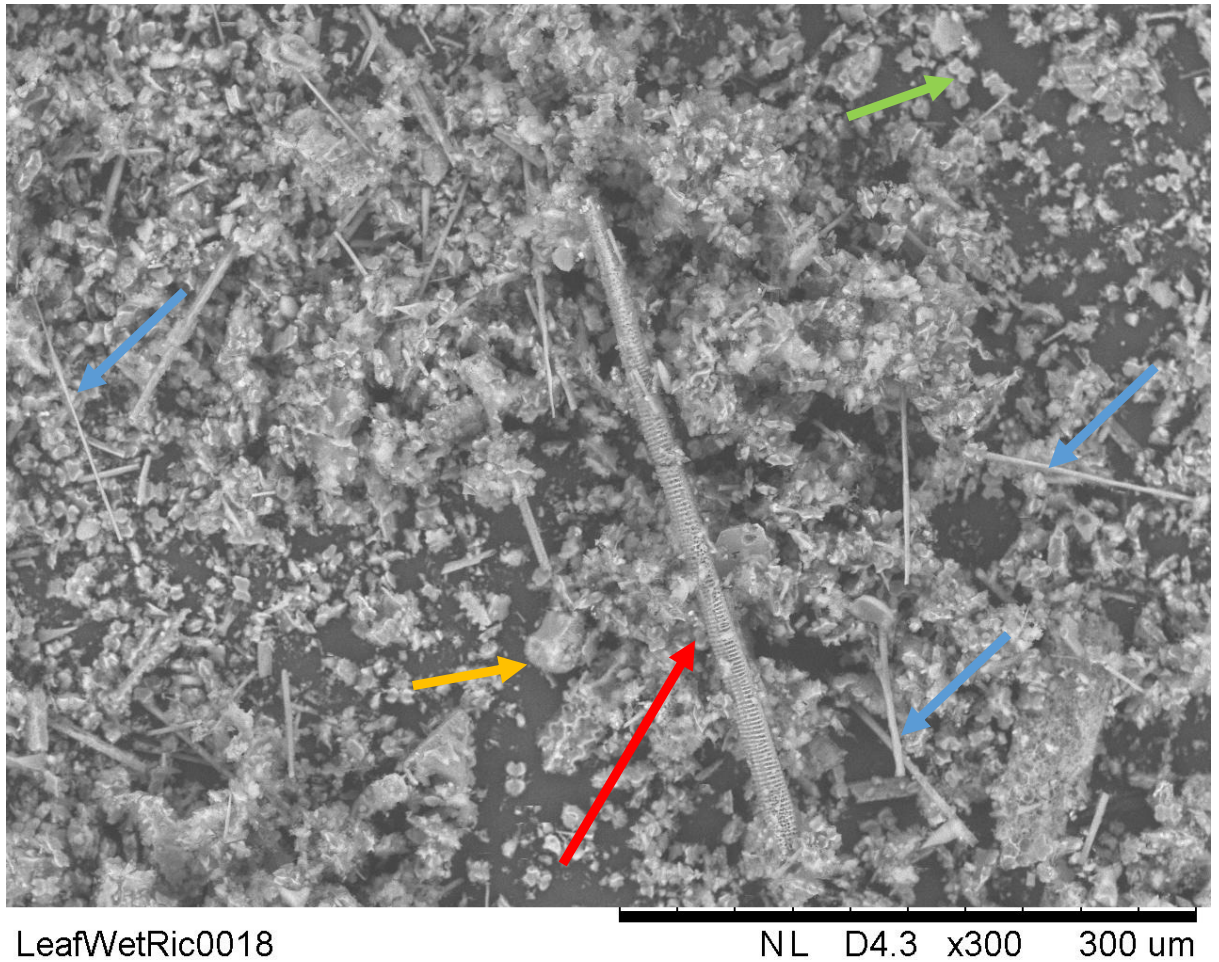


Figure 5.4 SEM image of silica structures taken from a wet digested rice leaf at 300 x magnification. Arrows label areas of interest, discussed in text.

At lower magnifications, an overview of the general landscape of silica structures visible throughout the samples can be observed (Fig 5.4). Whilst much of the silica in view is damaged and unidentifiable, multiple distinct structures are visible. A silica structure which can be identified as having come from inside a xylem vessel is the largest and most intact structure found in this sample group (see red arrow). The xylem silica structures measures over 360 μm in length and is approximately 16 μm wide with distinctive ridges running around the cylinder up its whole length. Numerous silica cells are visible throughout the sample (see green arrow). Another bulliform cell is visible here (see gold arrow), though it is orientated on its side rather than lying flat like the previous specimen (Fig 5.3). This sideways orientation provides more evidence that the entire bulliform cell is silicified, rather than just the exposed surface. Long, thin silica spines

can be observed strewn across the sample (see blue arrows). These spines do not share the characteristic ridging of the xylem structures.

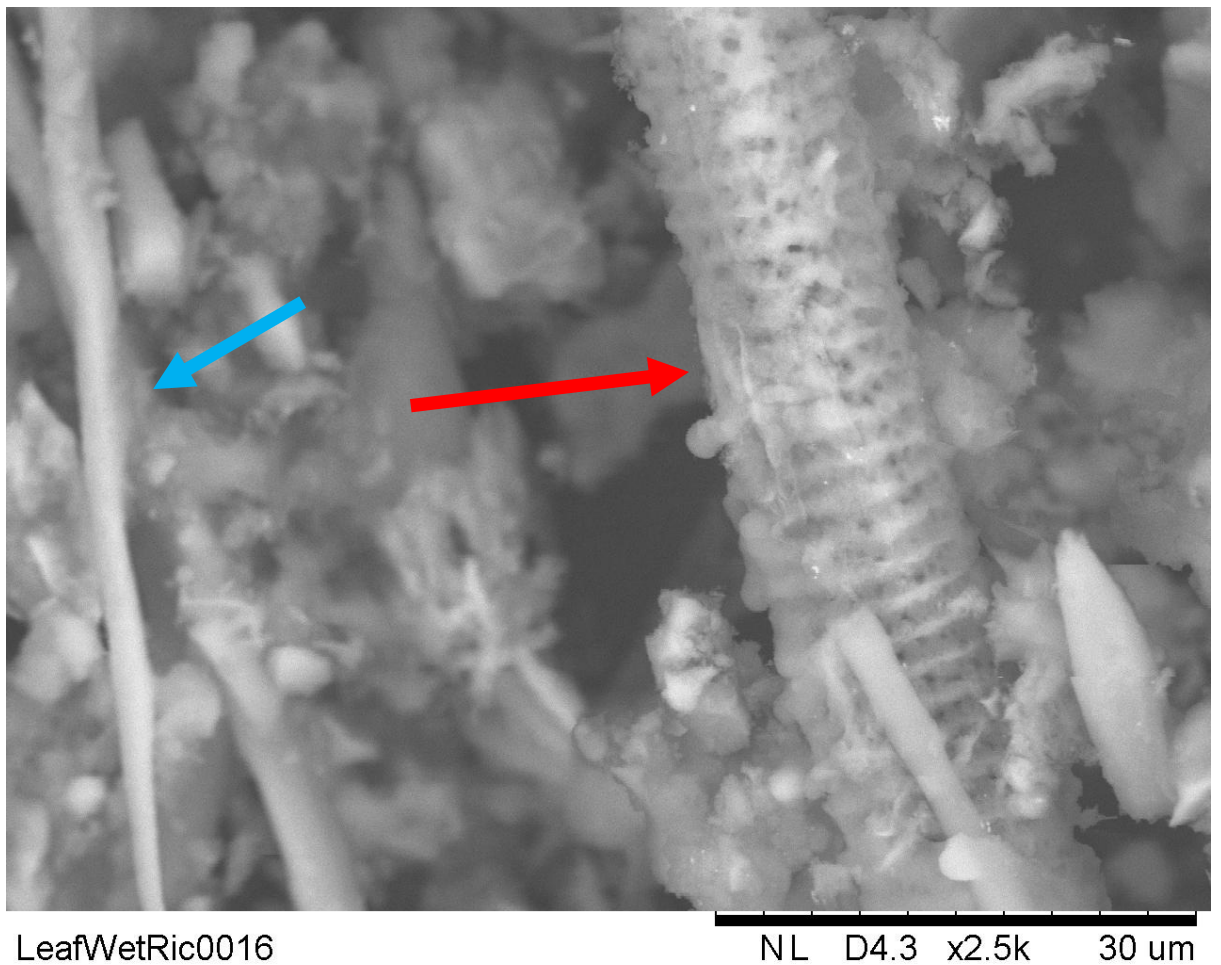


Figure 5.5 SEM image of silica structures taken from a wet digested rice leaf at 2500 x magnification. Arrows label areas of interest, discussed in text.

A closer image of a xylem silica structure, clearly showing the ridged pattern that runs up the length of the structure (Fig 5.5) (see red arrow). A closer view of one of the silica spines that are strewn across the sample can also be seen, showing a smooth surface unlike the xylem (see blue arrow).

5.3.1.2 Wet-Digested Rice Stem

Samples in this group were taken from rice stem tissue which was acid digested at its wet weight. Image magnification is displayed in the bottom right of the image along with an appropriate scale bar.

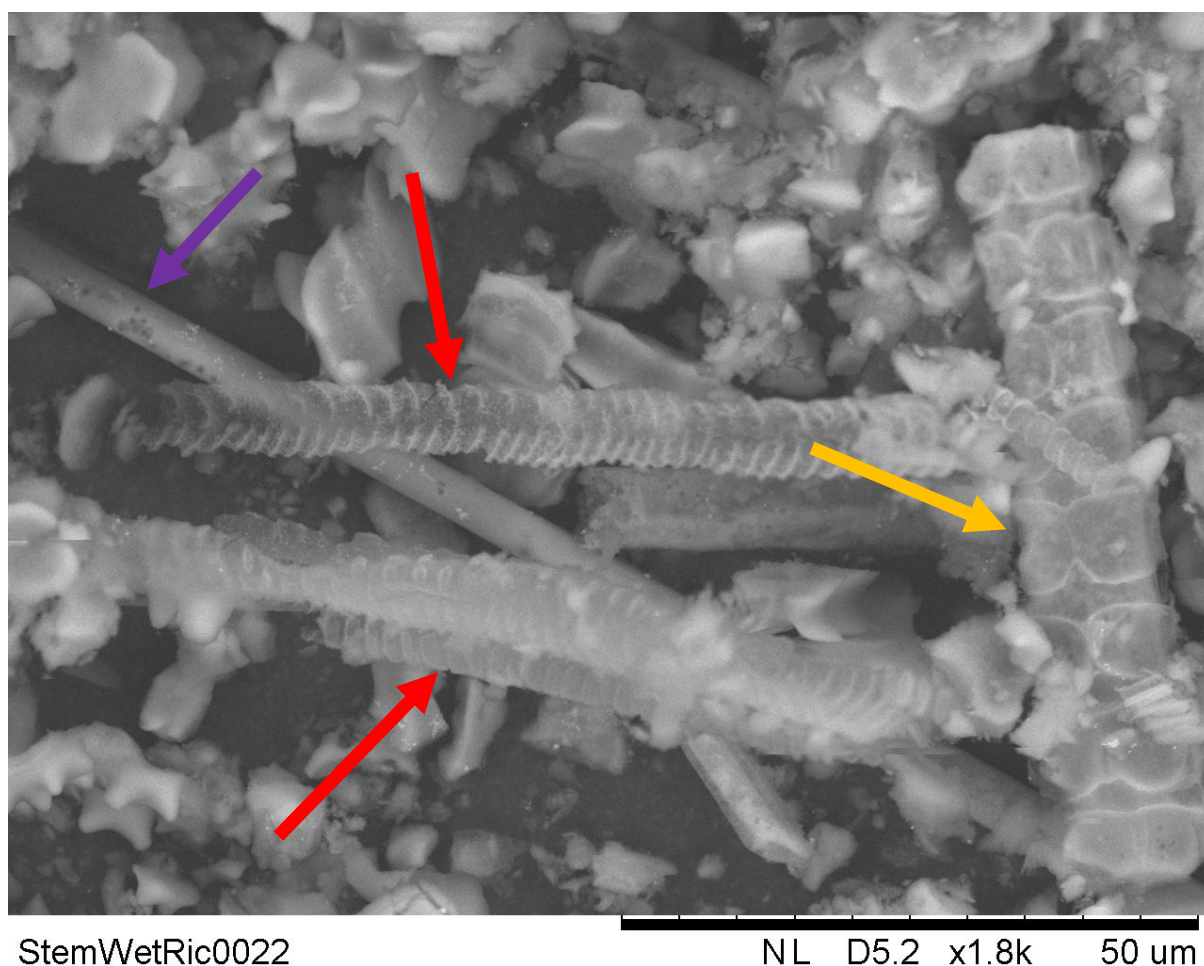


Figure 5.6 SEM image of silica structures taken from a wet digested rice stem at 1800 x magnification. Arrows label areas of interest, discussed in text.

Ridged structures similar to the xylem structures found in the leaf tissue can be observed (Fig 5.6) (see red arrows), however those found in the stem have a smaller width, around 6-8 μm compared with the 16 μm found in the leaf (Fig 5.4 & 5.5). Several of these structures are connected together but still clearly represent individual tubes. The characteristic ridging seen in other silica xylem structures can be observed. Another long cylindrical structure can be observed behind the xylem tubes (see purple arrow). This structure appears to be no more than 4 μm in

width and lacks the distinctive ridges of the xylem, however it is too smooth and rounded for a shard of broken silica from another structure. The familiar dumbbell shape of the silica cells can be seen up the length of a large silica piece, however rather than the cells themselves, here we see an imprint of where the silica cells were seated (see gold arrow).

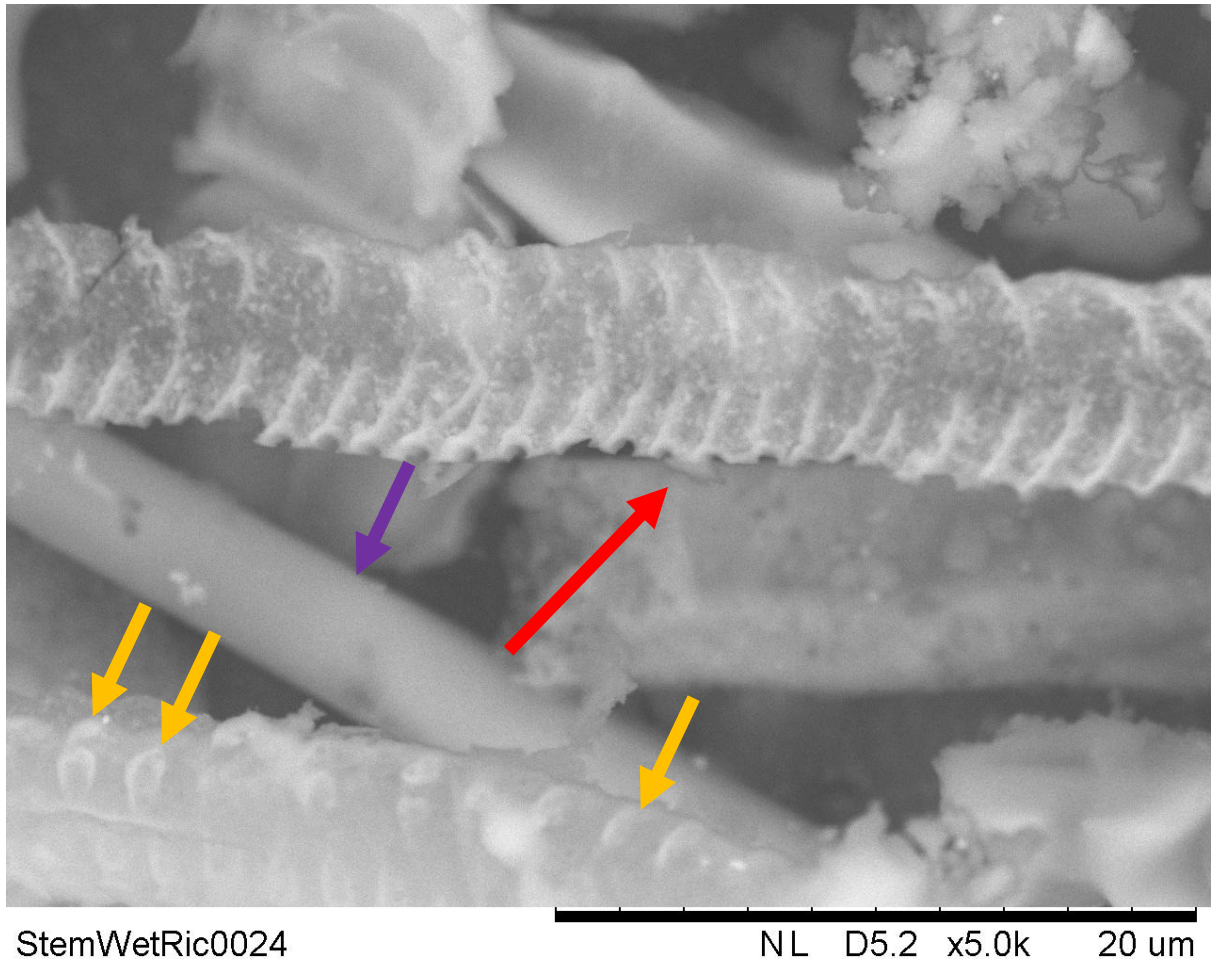


Figure 5.7 SEM image of silica structures taken from a wet digested rice stem at 5000 x magnification. Arrows label areas of interest, discussed in text.

A closer image of a xylem silica structure, clearly showing the ridged pattern that runs up the length of the structure (Fig 5.7) (see red arrow). The ridges on this structure are different in morphology to those seen on previous xylem structures (Fig 5.5). The xylem structure below shows a more typical ridging, with thicker, raised silica ridges as opposed to the thin, tapering ridges of the upper structure (see gold arrows). A close up of the smooth cylindrical structure

seen previously (Fig 5.6) confirms it lacks any ridging or other distinctive features seen in the xylem silica structures (see purple arrow).

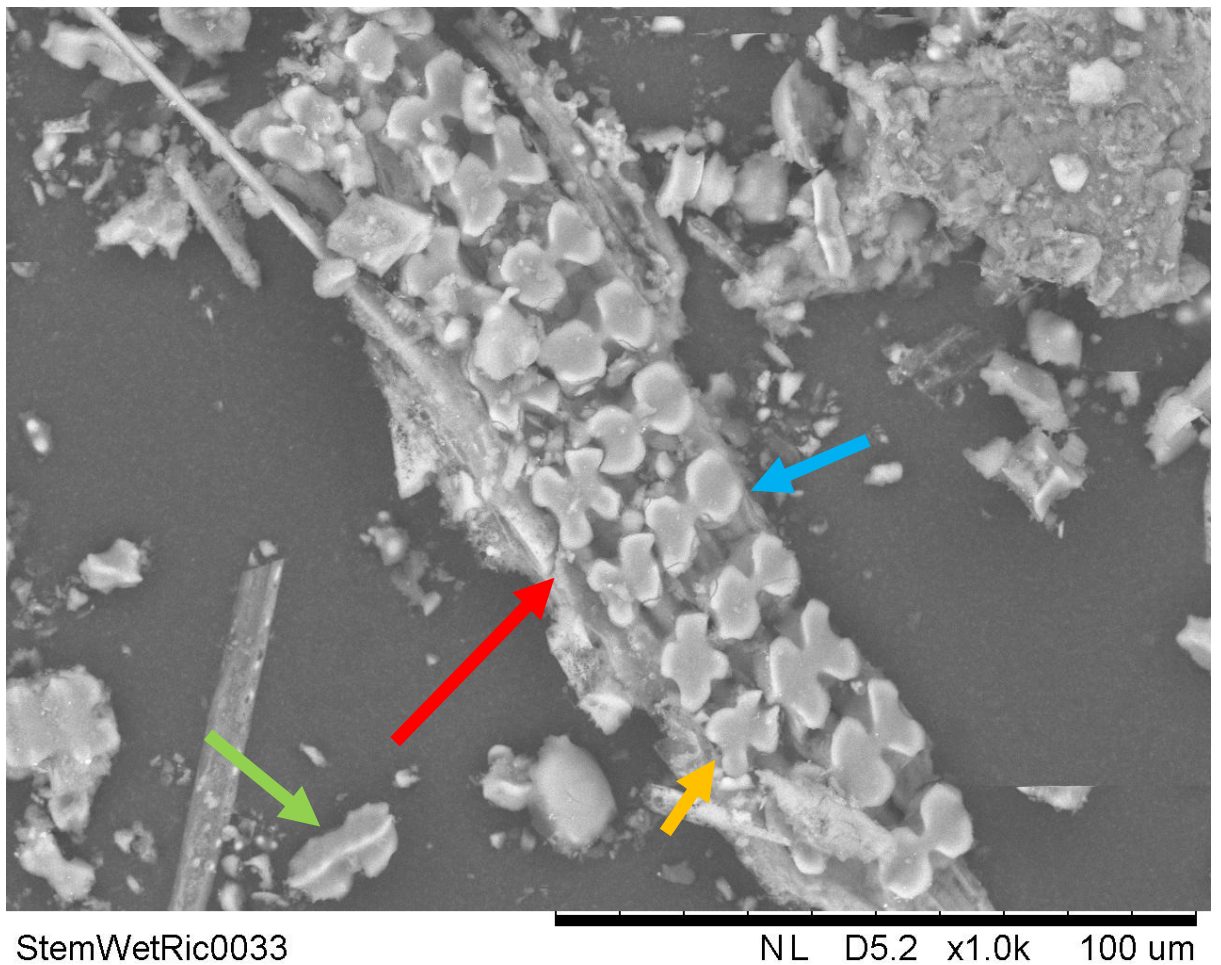
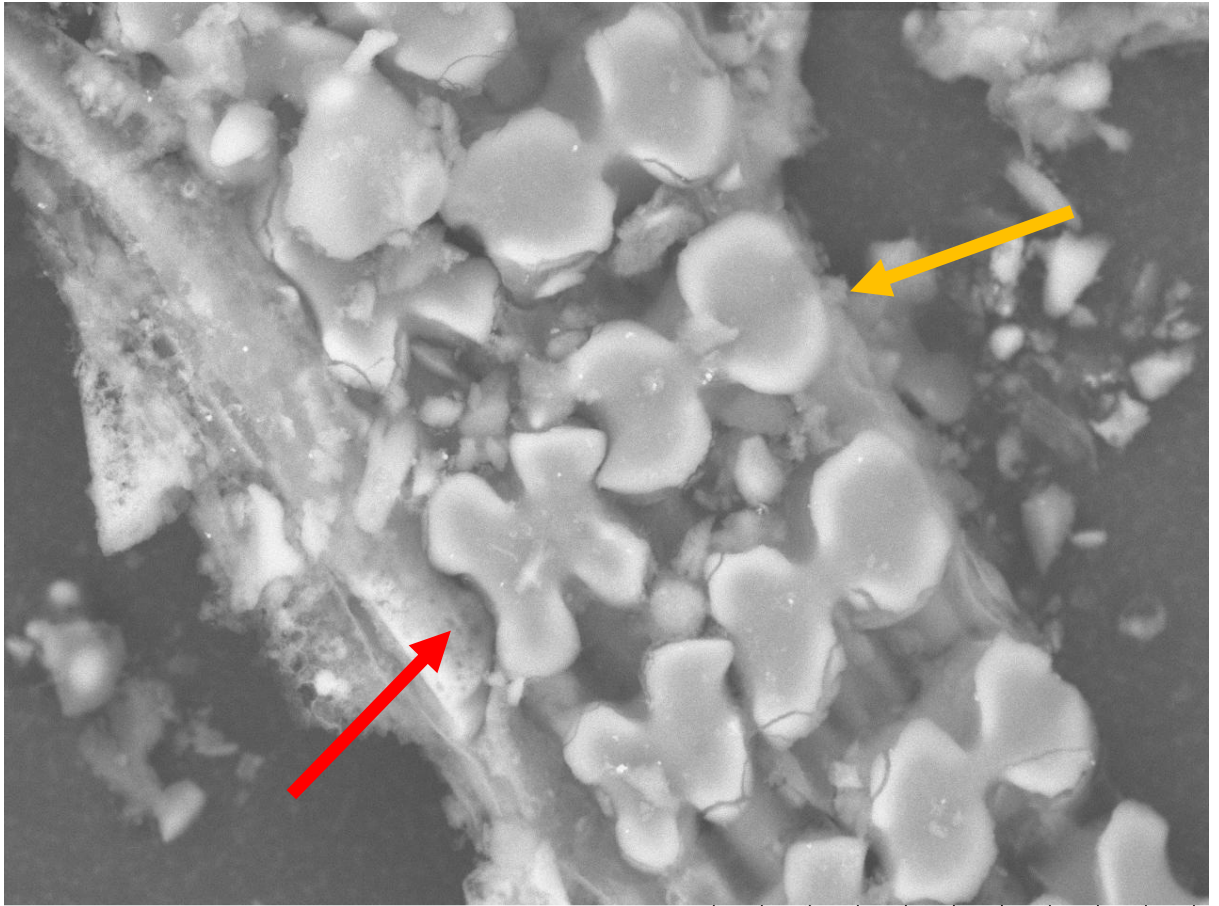


Figure 5.8 SEM image of silica structures taken from a wet digested rice stem at 1000 x magnification. Arrows label areas of interest, discussed in text.

A dual-layer of silica cells can be observed, with two columns of horizontally-orientated silica cells running up each column (Fig 5.8) (see red arrow). The silica cells in the leftmost column have a more distorted morphology when compared with those in the right column, appearing to be crushed and misshapen (see gold arrow), whilst those on the right are more rounded in their appearance (see blue arrow). It should be noted though that there is a great degree of variation in the size and shape of individual silica cells seen across both columns. A loose silica cell can be seen, orientated on its side showing that the entire cell is silicified (see green arrow).



StemWetRic0032

NL D5.2 x2.5k 30 um

Figure 5.9 SEM image of silica structures taken from a wet digested rice stem at 2500 x magnification. Arrows label areas of interest, discussed in text.

A higher magnification image of the dual-layer of silica cells, once again showing the two columns of silica cells which would typically be found above and below a vascular bundle (Fig 5.9). The left column of silica cells is distorted with the individual cells appearing compressed (see red arrow).

The right column of silica cells are longer and more rounded (see gold arrow).

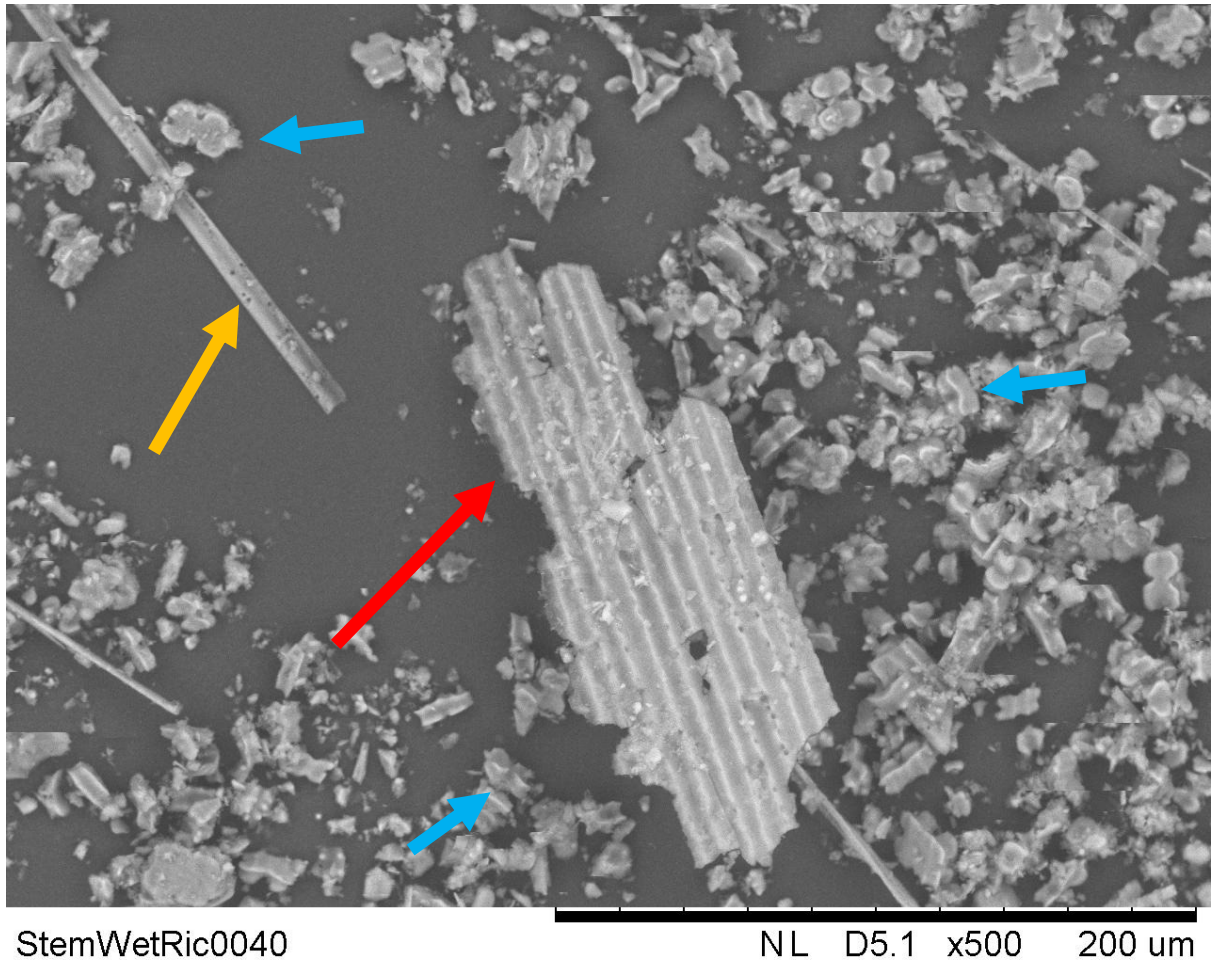


Figure 5.10 SEM image of silica structures taken from a wet digested rice stem at 500 x magnification. Arrows label areas of interest, discussed in text.

A large silica structure can be observed, at almost 200 μm in length which bares the appearance of corrugated metal sheeting (Fig 5.10) (see red arrow). This structure is the silica layer from above the epidermis of the stem. Unlike epidermal cells in the leaf, the stem epidermis is not covered with small nodules called papilla. The lack of these defining marks makes the orientation of this silica structure difficult to determine; the visible side could be the outer or inner surface of the silica sheet. A corrugation has broken off from the main structure but it is still intact and identifiable (see gold arrow). Silica cells are seen strewn throughout the image (see blue arrows).

5.3.1.3 Dry-Digested Rice Leaf

Samples in this group were taken from rice leaf tissue which was dried to a constant weight before acid digestion. Image magnification is displayed in the bottom right of the image along with an appropriate scale bar.

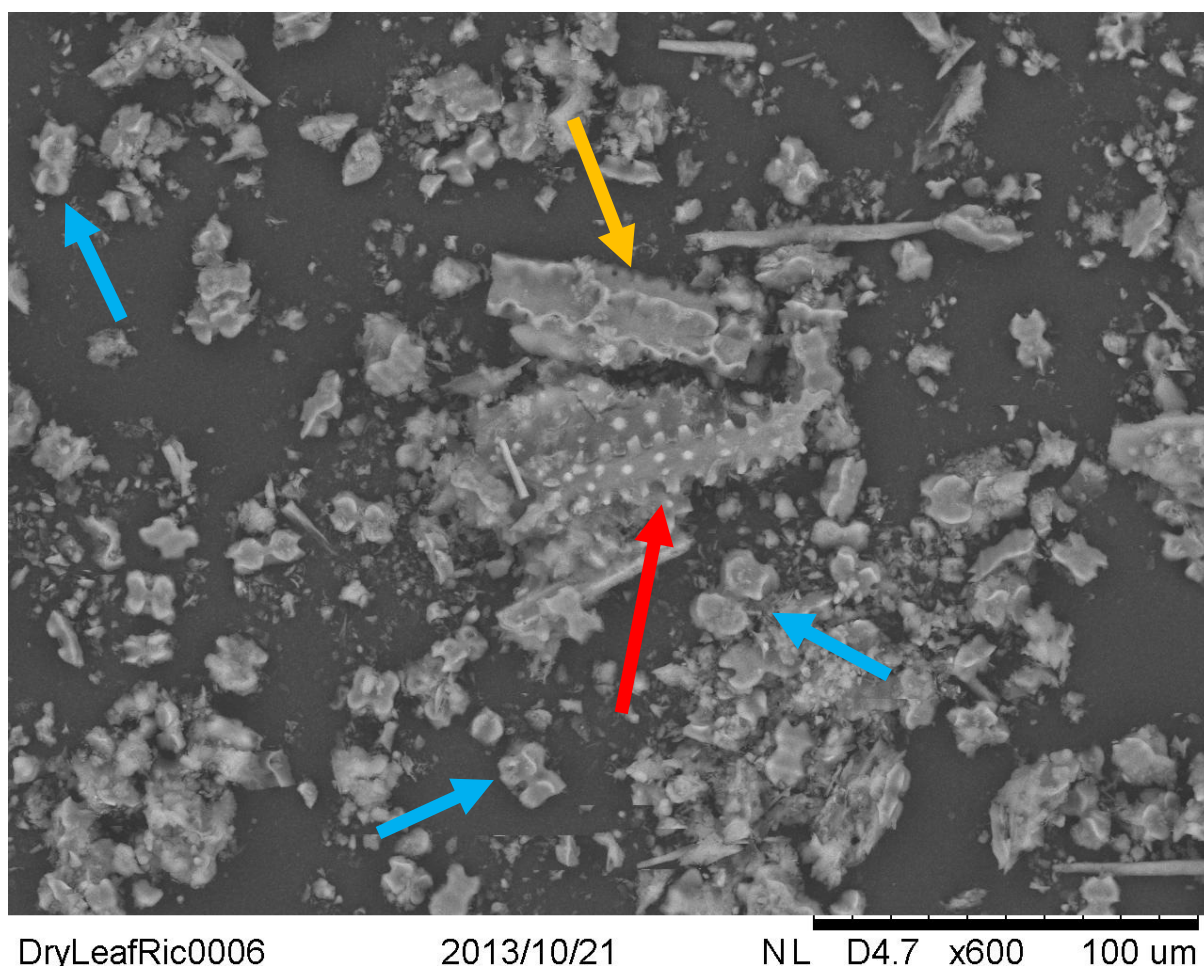


Figure 5.11 SEM image of silica structures taken from a wet digested rice stem at 5000 x magnification. Arrows label areas of interest, discussed in text.

Both orientations of silica structures from the epidermal silica layer can be observed side-by-side (Fig 5.11). One structure shows the silica covering of multiple epidermal cells, complete with their distinctive papilla extending outwards (see red arrow). Above it lays another silica structure from epidermal cells, this time with the surface which contacted the epidermal cells themselves showing (see gold arrow). Silica cells are strewn throughout the sample (see blue arrows).

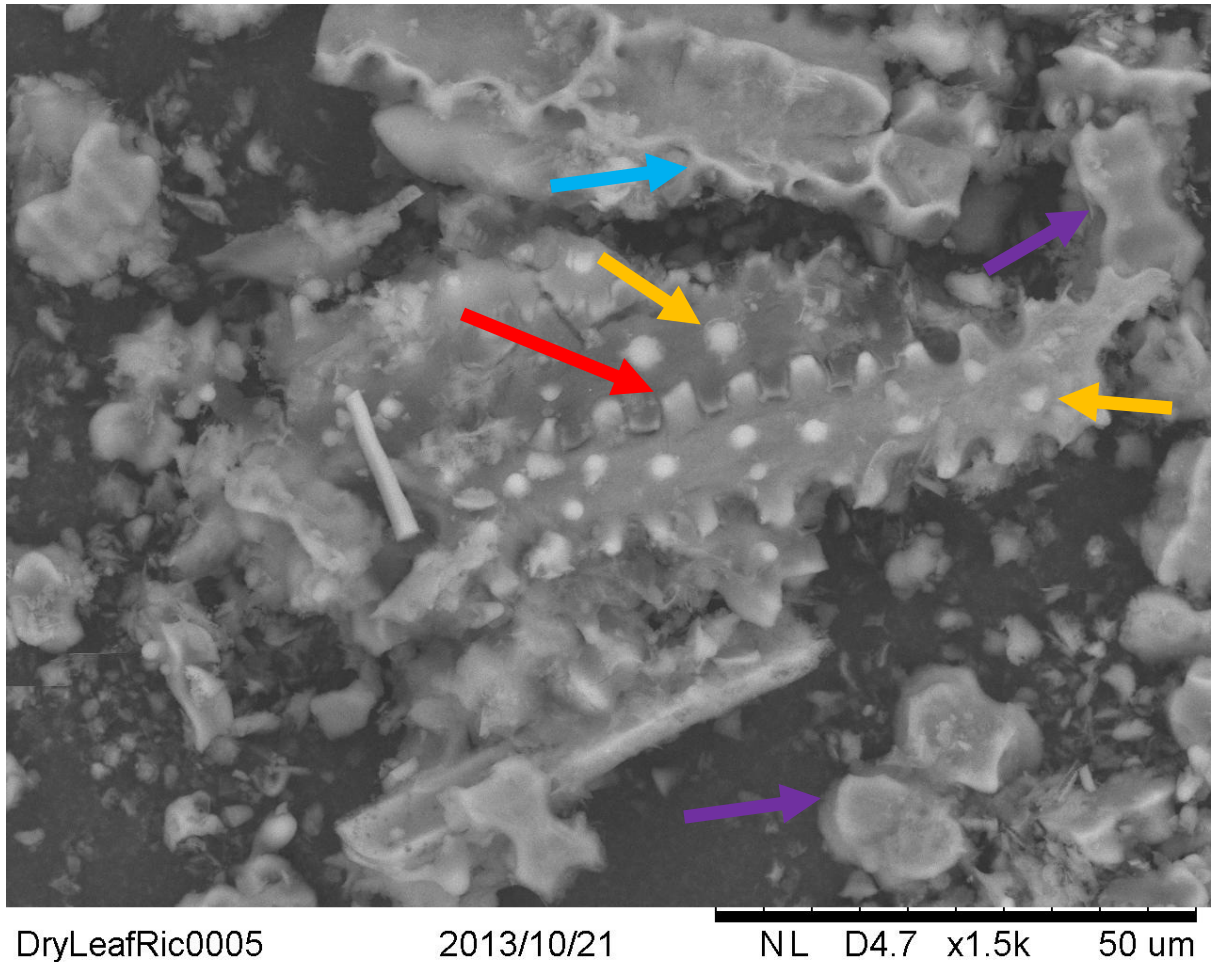


Figure 5.12 SEM image of silica structures taken from a wet digested rice stem at 1500 x magnification. Arrows label areas of interest, discussed in text.

A higher magnification image of the epidermal silica structures seen previously, showing both the top and bottom orientations of the structure (Fig 5.12). In the silica structure which is orientated top side up, the interlocking structure of the epidermal cells can be clearly observed (see red arrow). The surface of the epidermal cells is covered with papilla which extend outwards from the rest of the cell (see gold arrows). In the silica structure which is orientated bottom side up, the edges of the silica clearly extend further out than the centre, leaving a hollowed-out silica cell (see blue arrow). This hollow area was filled with living tissue as the silica layer covered and enveloped the exposed surface of the epidermal cell. Several silica cells can be clearly observed throughout the image (see purple arrows).

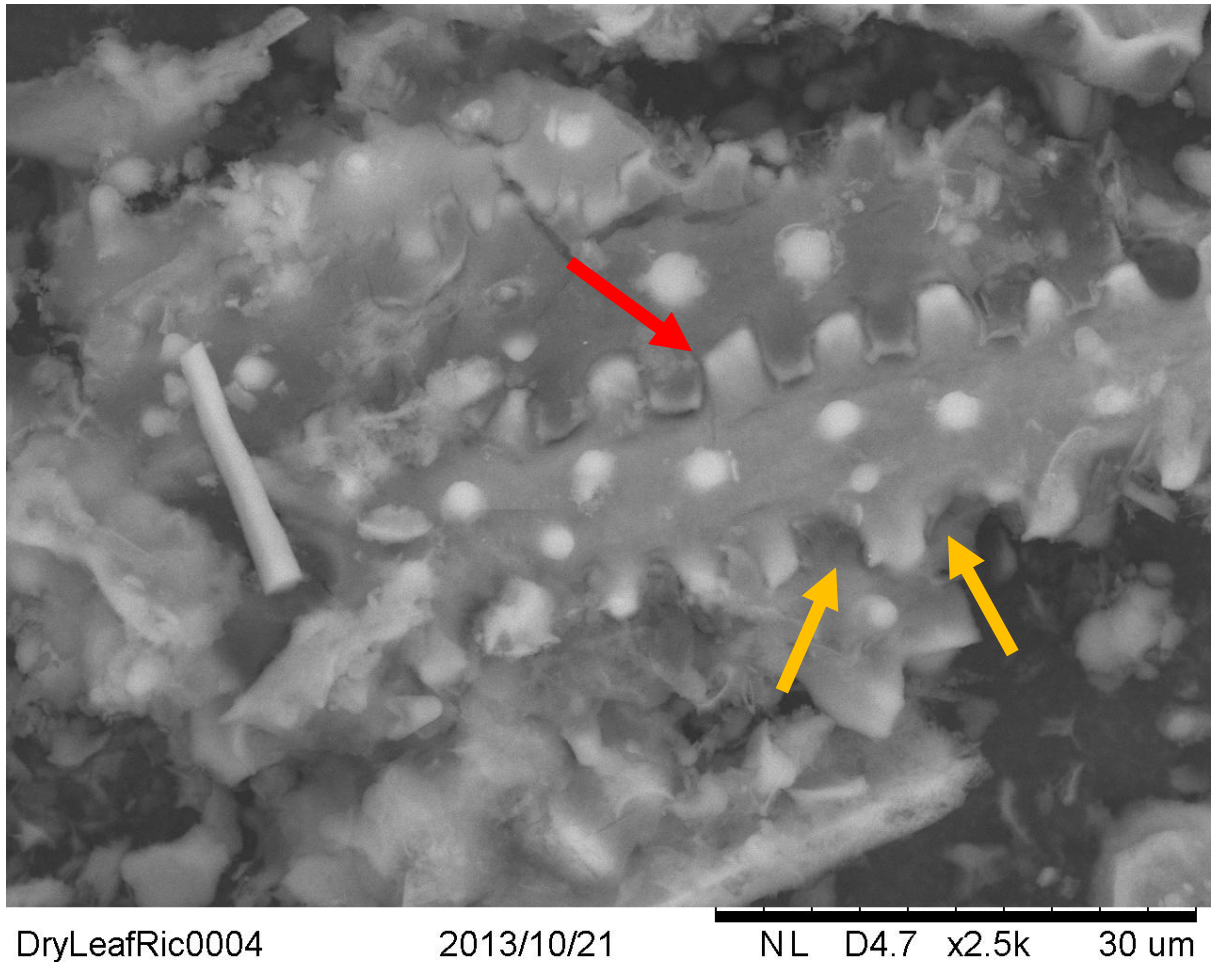


Figure 5.13 SEM image of silica structures taken from a wet digested rice stem at 2500 x magnification. Arrows label areas of interest, discussed in text.

The interlocking connection between two epidermal cells is clearly replicated in the silica structure which covered them (Fig 5.13). Whilst the silica layer over the epidermis is one large structure, it does not simply coat the surface with silica; instead individual cells are recognisable at their boundaries (see red arrows). On the other side of the epidermal cell, where no neighbouring cell is found in this sample, the contours of the epidermal cell are still replicated by the silica, giving evidence that each cell is silicified individually (see gold arrows).

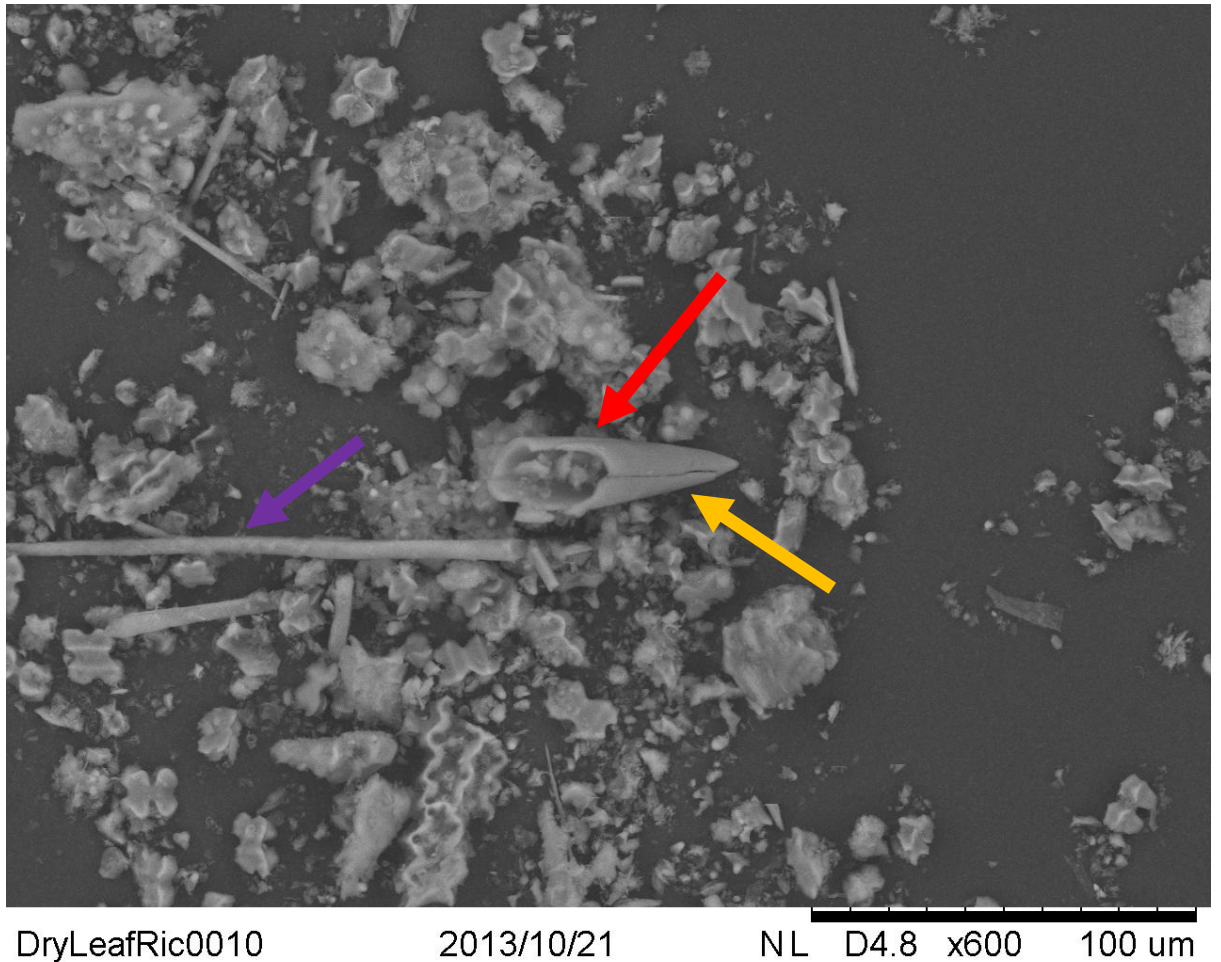
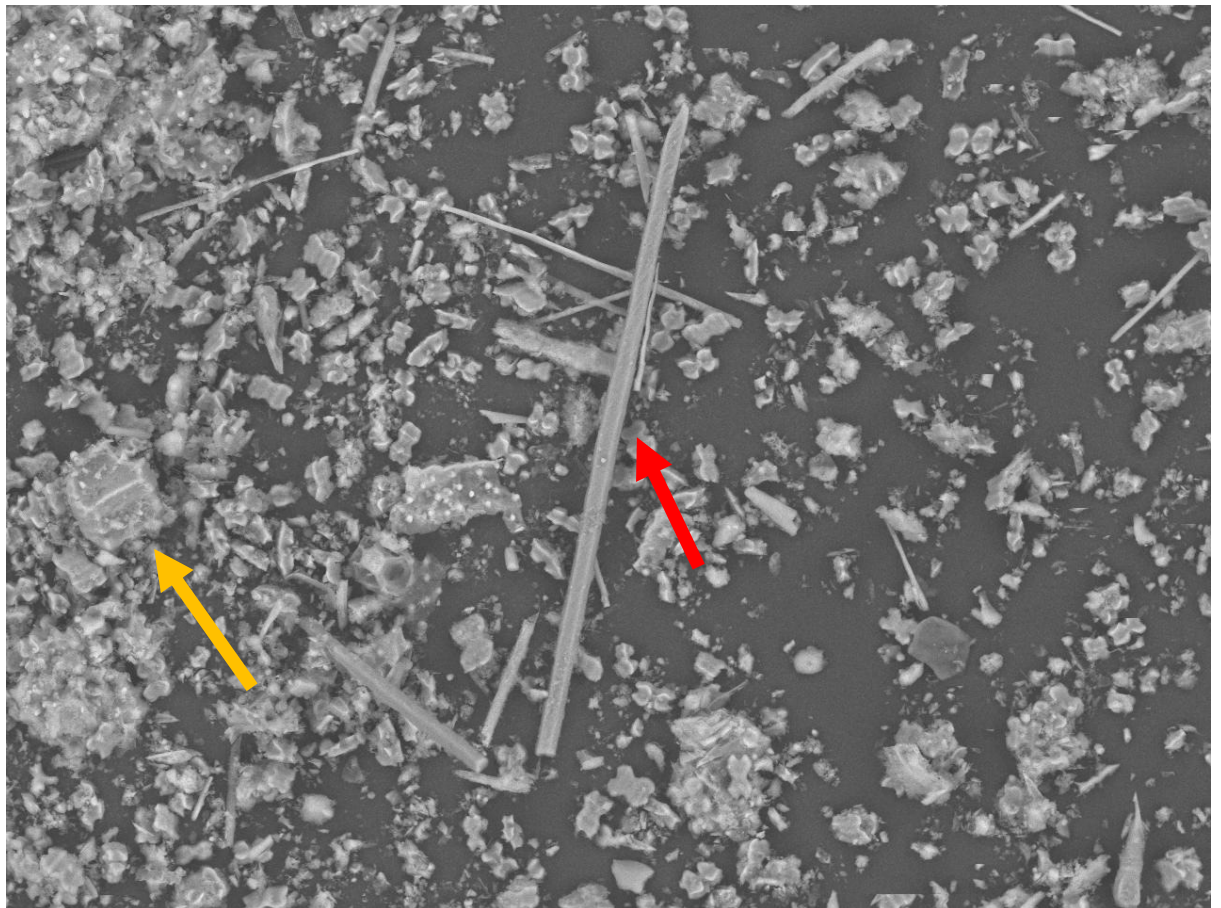


Figure 5.14 SEM image of silica structures taken from a wet digested rice stem at 600 x magnification. Arrows label areas of interest, discussed in text.

A silica structure of around 60 μm in length can be observed with a wide base which tapers to a point, giving the structure a spike or spine-like appearance (Fig 5.14) (see red arrow). The structure appears to be hollow, though some silica debris from the rest of the sample rests inside it. A hairline fracture along the spine's underside is clearly visible (see gold arrow). A silica tube-like structure is also visible, smooth with no distinctive features or ridges (see purple arrow). This tube like-structure could potentially represent a silicified phloem vessel, as phloem tubes are smaller but more numerous than xylem.



DryLeafRic0002

2013/10/21

NL D4.8 x400 200 μ m

Figure 5.15 SEM image of silica structures taken from a wet digested rice stem at 400 x magnification. Arrows label areas of interest, discussed in text.

A long, thin silica structure measuring approximately 260 μ m in length and 10 μ m in width can be observed, with flat edges giving the structure a cuboid shape (Fig 5.15)(see red arrow). This structure lacks the distinctive ridge-like markings of the xylem structures seen previously (Fig 5.4).

A bulliform cell can be seen in the neighbouring silica debris, identified by its distinctive mushroom shape (see gold arrow).

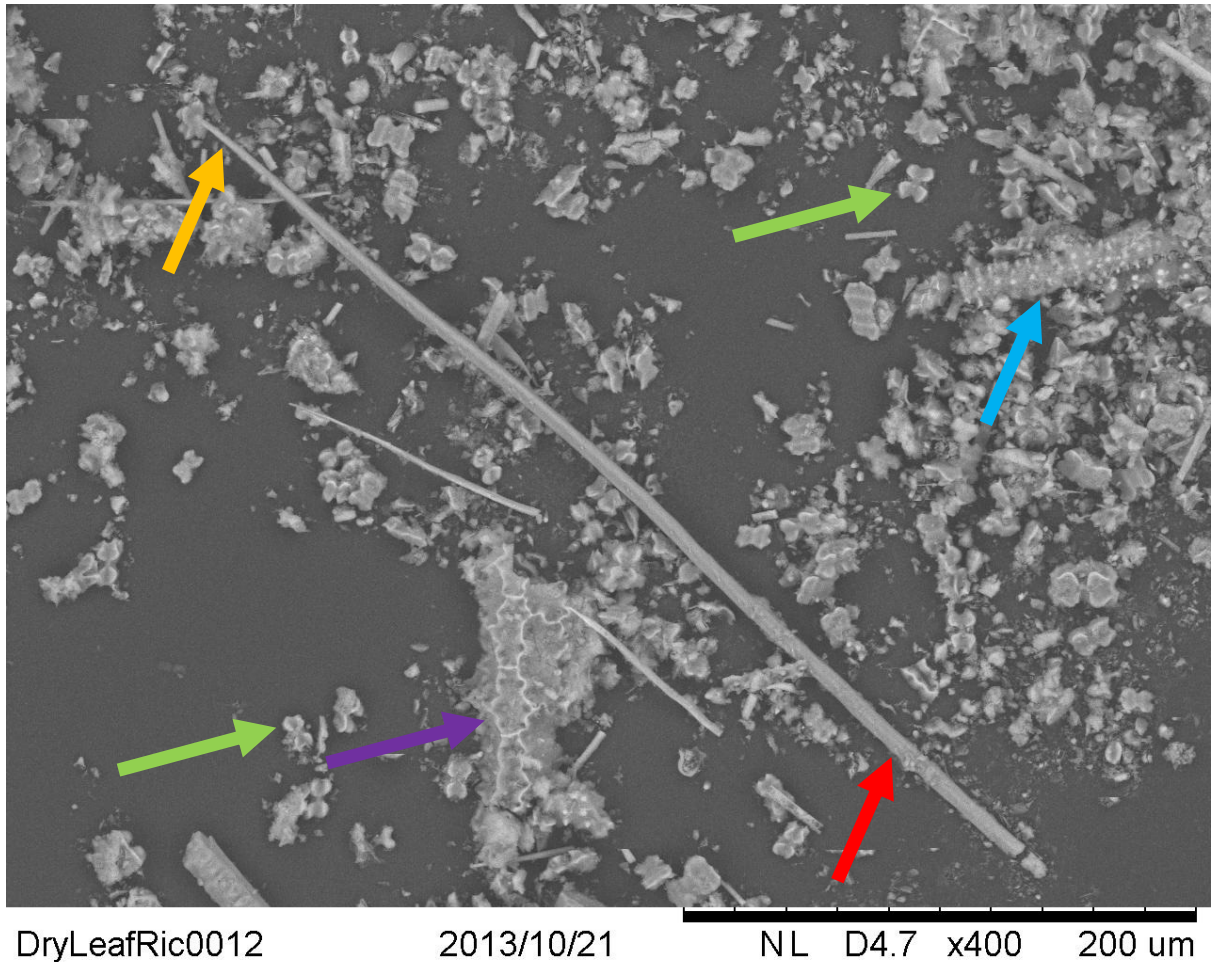


Figure 5.16 SEM image of silica structures taken from a wet digested rice stem at 400 x magnification. Arrows label areas of interest, discussed in text.

A large silica spine structure can be observed measuring over 430 μm in length (Fig 5.16) (see red arrow). The structure has a width of approximately 30 μm , though it tapers off to a point at one end (see gold arrow). None of the defining characteristics of the xylem structures previously observed are present in this spine; it has no ridges or raised structures extending from it. Silica structures from the epidermal cells are visible throughout the sample, both right-side up (see blue arrow) and inverted (see purple arrow). Silica cells are strewn throughout the sample (see green arrows).

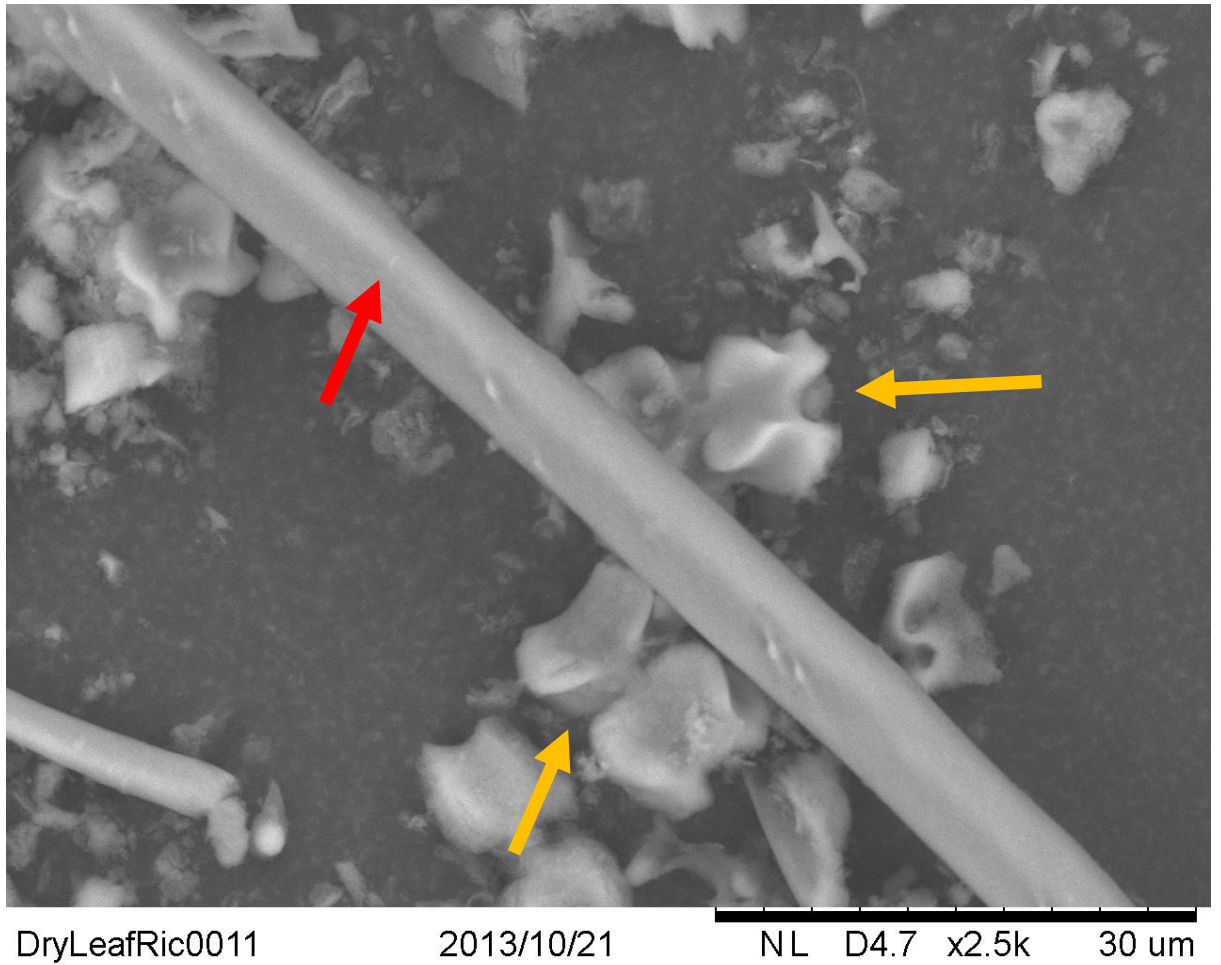
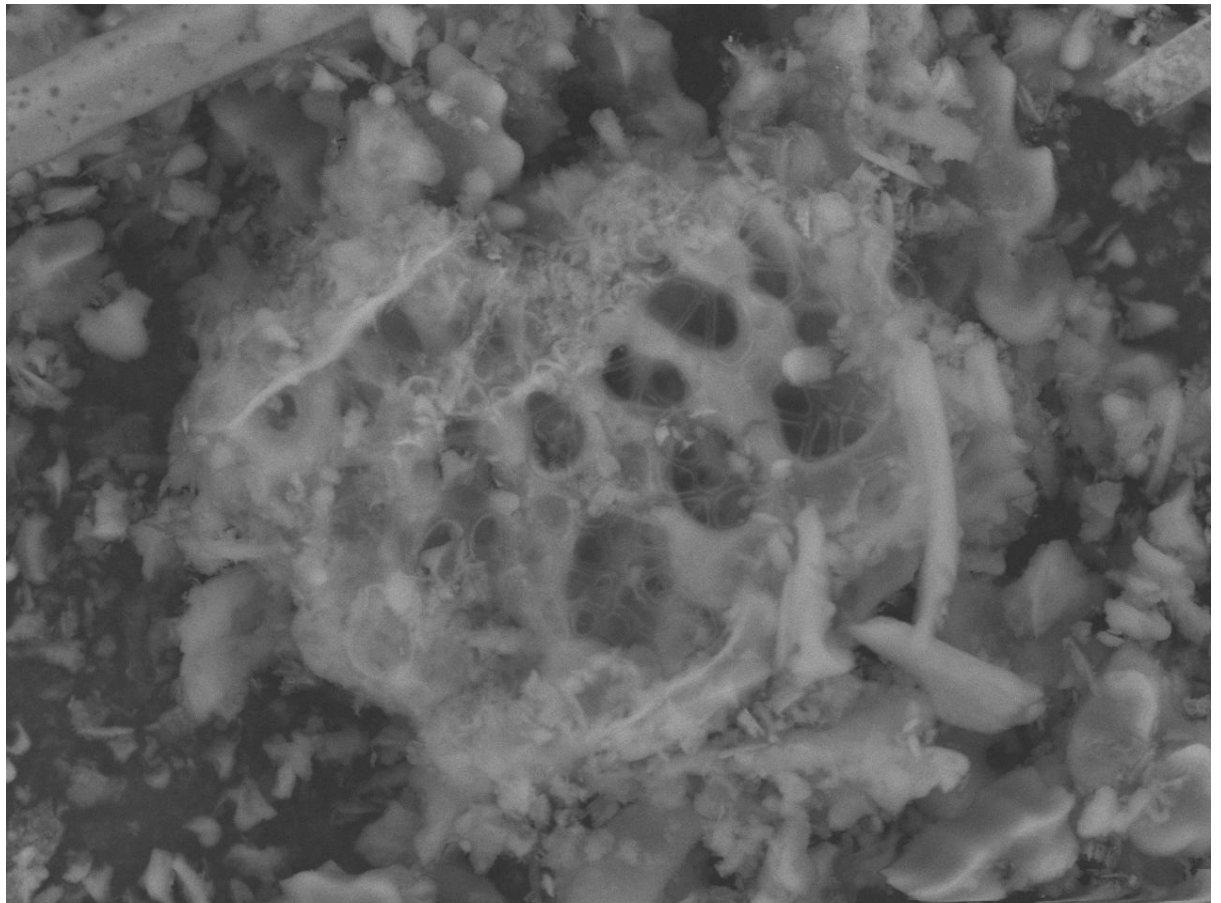


Figure 5.17 SEM image of silica structures taken from a wet digested rice stem at 2500 x magnification. Arrows label areas of interest, discussed in text.

A higher magnification image of the long silica structure seen previously (Fig 5.17). The structure does not appear to be cylindrical as clear edge lines are visible down its length, however these edges are soft and rounded (see red arrow). The shape of the structure is difficult to determine from this angle. Several silica cells nearby provide a point of reference for the size of the structure (see gold arrows).



DryLeafRic0024

2013/10/21

NL D4.8 x2.0k 30 um

Figure 5.18 SEM image of silica structures taken from a wet digested rice stem at 3000 x magnification. Arrows label areas of interest, discussed in text.

An unidentified silica structure which appears to be a hollowed spherical shape, the walls of which are composed of a mesh of silica with holes of varying shapes and sizes throughout (Fig 5.18). It has not been possible to identify which region of the plant tissue this structure originated from. The holes on the upper surface of the structure appear to be larger than those on the inner visible surface, however this could be an illusion based on the surfaces different proximity to the camera. Whilst other images are representative of structures found throughout the sample, this structure was only observed once, and only in this sample group.

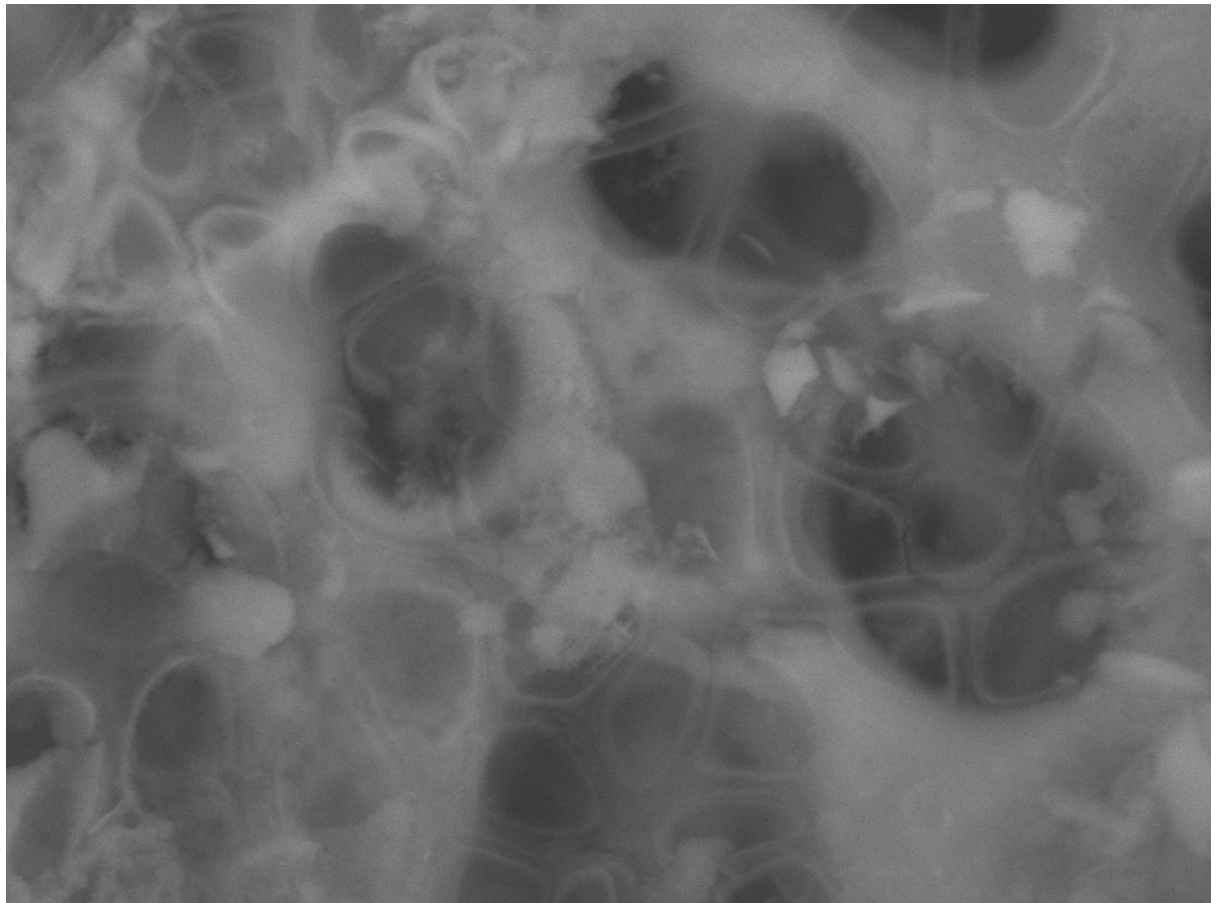


Figure 5.19 SEM image of silica structures taken from a wet digested rice stem at 3000 x magnification. Arrows label areas of interest, discussed in text.

Higher magnification image of the unidentified silica structure seen previously (Fig 5.19). The focus of this image is on the inner layer of silica within the structure. The holes that cover the surface of this structure make up the vast majority of its surface with each hole measuring around 3-4 μm across, whilst the silica supports between them are only around 1 μm in thickness. There is no apparent pattern to the holes distribution, though they interlock in a mosaic pattern without leaving large areas of silica.

5.3.1.4 Dry-Digested Rice Stem

Samples in this group were taken from rice stem tissue which was dried to a constant weight before acid digestion. Image magnification is displayed in the bottom right of the image along with an appropriate scale bar.

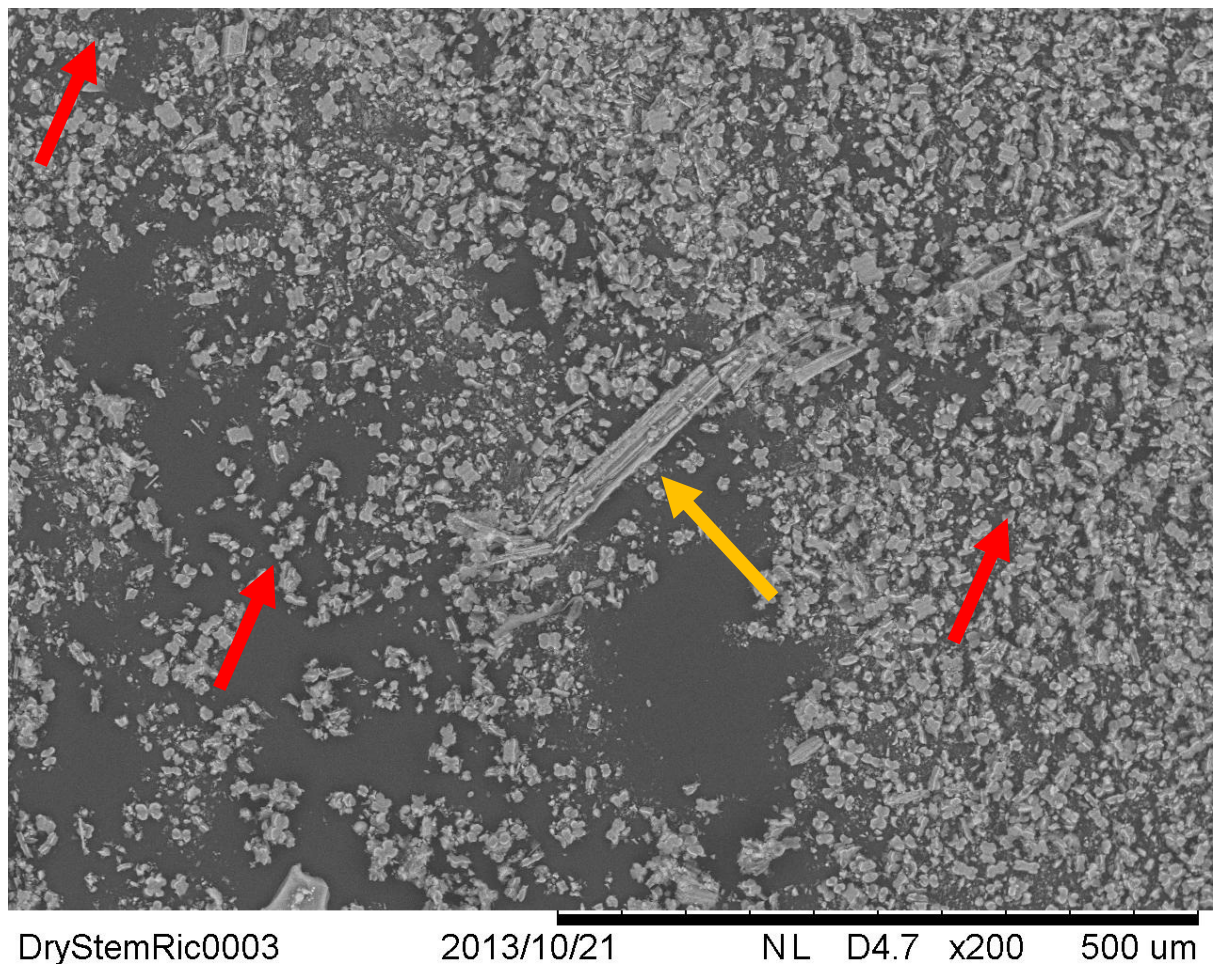
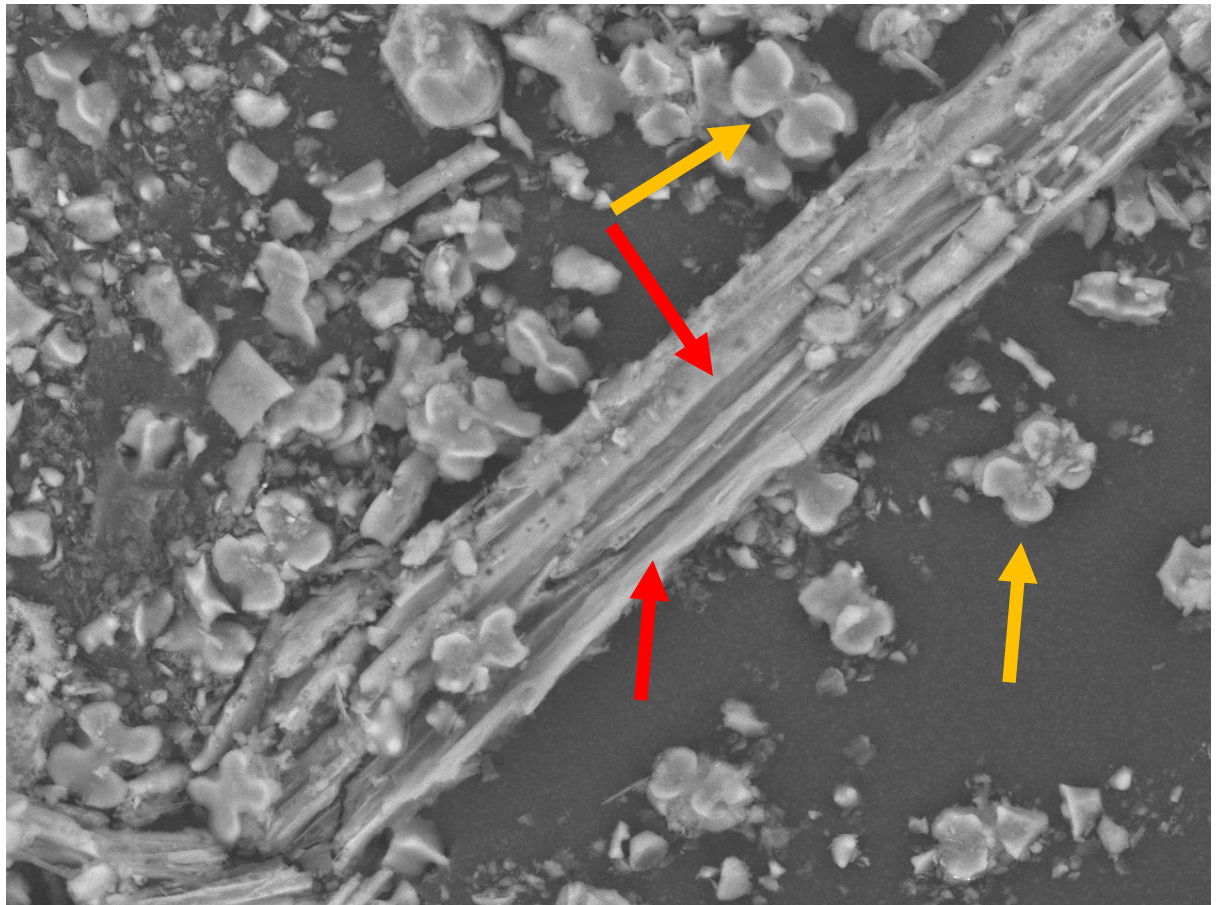


Figure 5.20 SEM image of silica structures taken from a dry-digested rice stem at 200 x magnification. Arrows label areas of interest, discussed in text.

Low magnification images were taken to give an overview of the silica structures that will typically be found in silica digests of rice stem tissue (Fig 5.20). Much of the sample is comprised of silica cells which can be seen strewn throughout the images (see red arrows). Larger, more complex structures are also visible, though sometimes difficult to identify at lower magnifications (see gold arrow).



DryStemRic0002

2013/10/21

NL

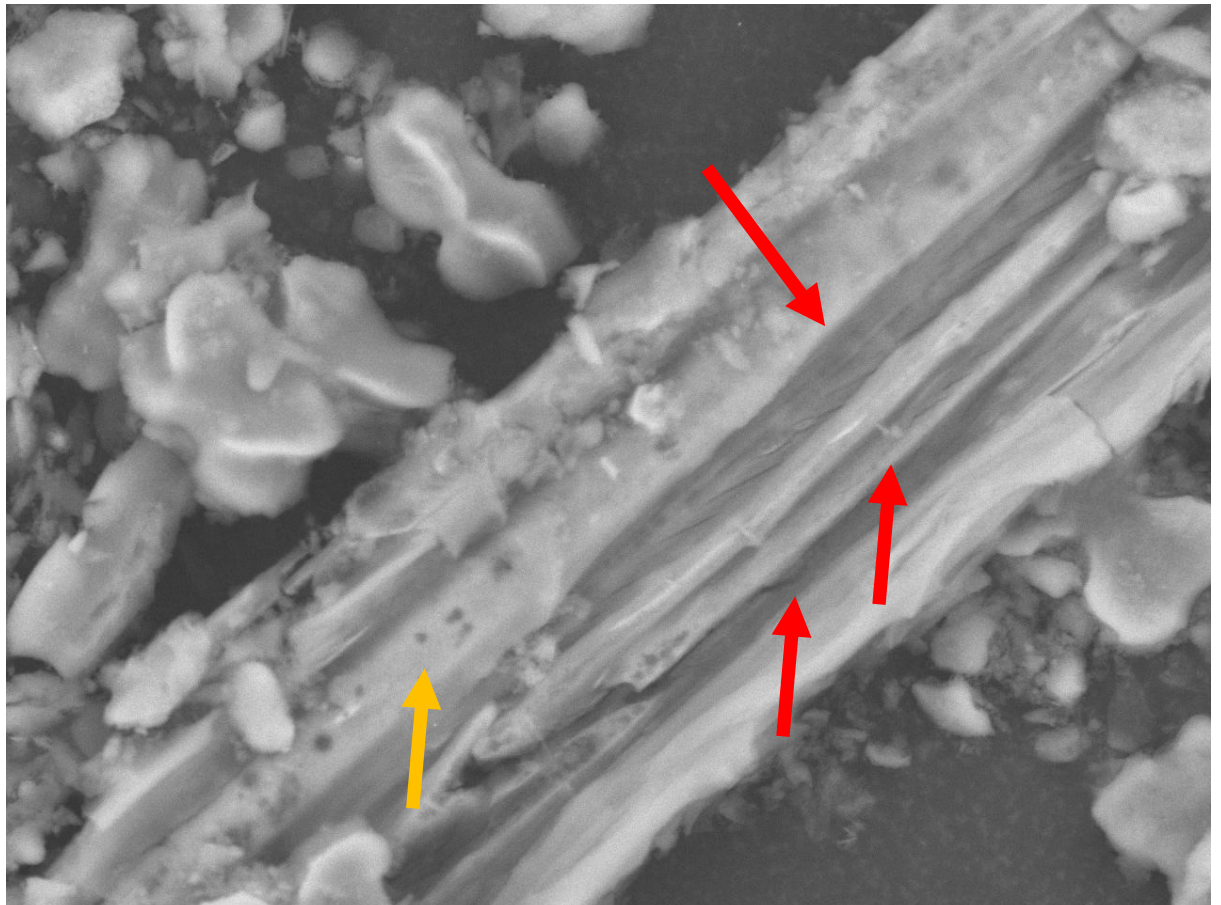
D4.7

x1.0k

100 μ m

Figure 5.21 SEM image of silica structures taken from a dry-digested rice stem at 1000 x magnification. Arrows label areas of interest, discussed in text.

A large unidentified silica structure measuring approximately 200 μ m in length and 25 μ m in width can be observed (Fig 5.21). The structure is scored by channels running down its vertical axis (see red arrows). The origins of the structure are unknown and our view is limited to what is obviously the internal facing side of the structure which contacts with the plant tissue. Silica cells are visible throughout the sample (see gold arrows).



DryStemRic0001

2013/10/21

NL

D4.7

x2.5k

30 um

Figure 5.22 SEM image of silica structures taken from a dry-digested rice stem at 2500 x magnification. Arrows label areas of interest, discussed in text.

A higher magnification image of the unidentified silica structure seen previously (Fig 5.22). The channels which run down its vertical axis are more clearly visible, showing multiple grooves and ridges of varying size (see red arrows). There are also small holes visible in the walls of these channels (see gold arrow).

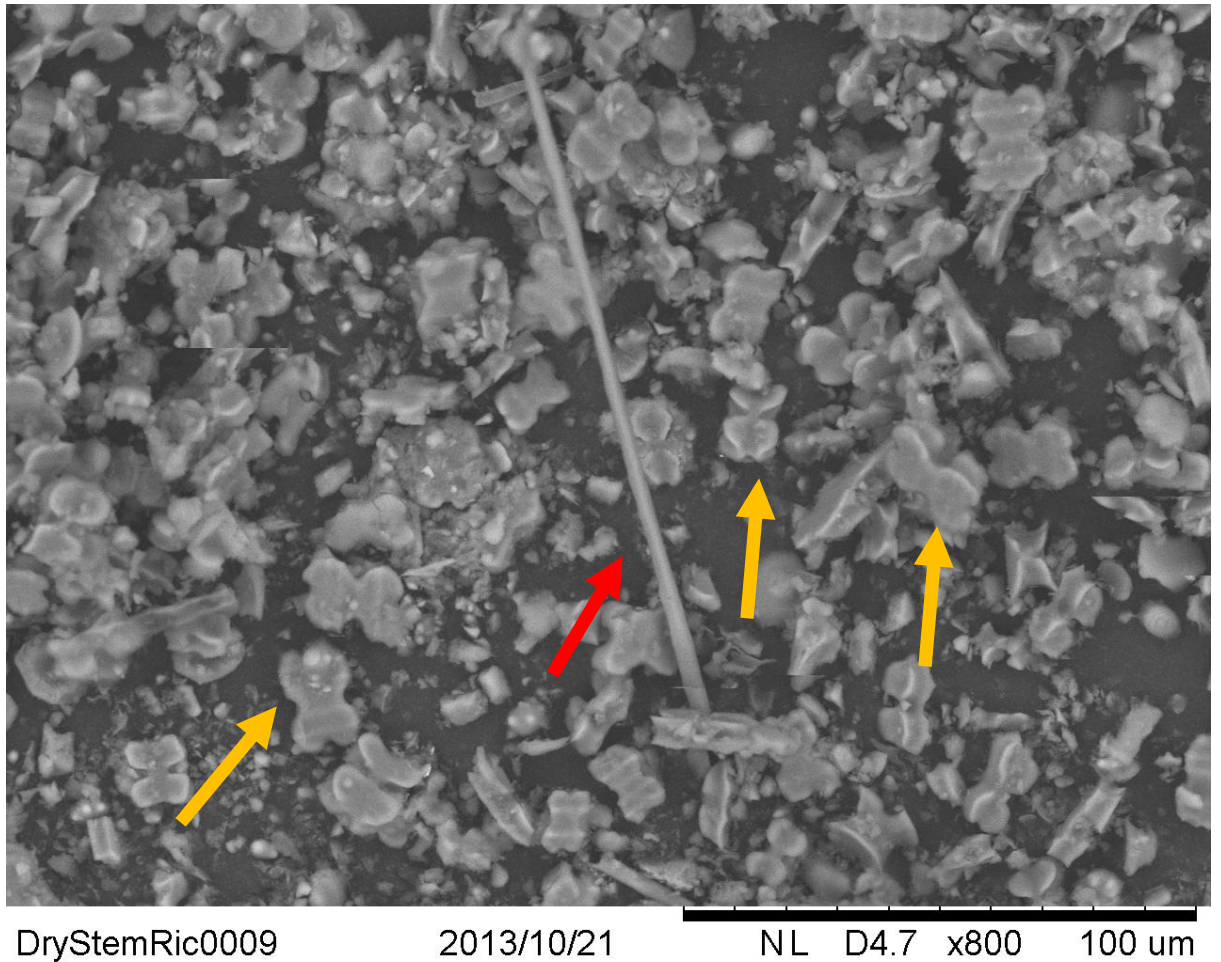


Figure 5.23 SEM image of silica structures taken from a dry-digested rice stem at 800 x magnification. Arrows label areas of interest, discussed in text.

A silica tube, possibly representing a silicified phloem tube is visible measuring over 100 μm in length but only approximately 4 μm in width (Fig 5.23). The silica tube has a smooth surface devoid of any distinguishing features (see red arrow). In the surrounding silica debris, multiple silica cells are visible (see gold arrows).

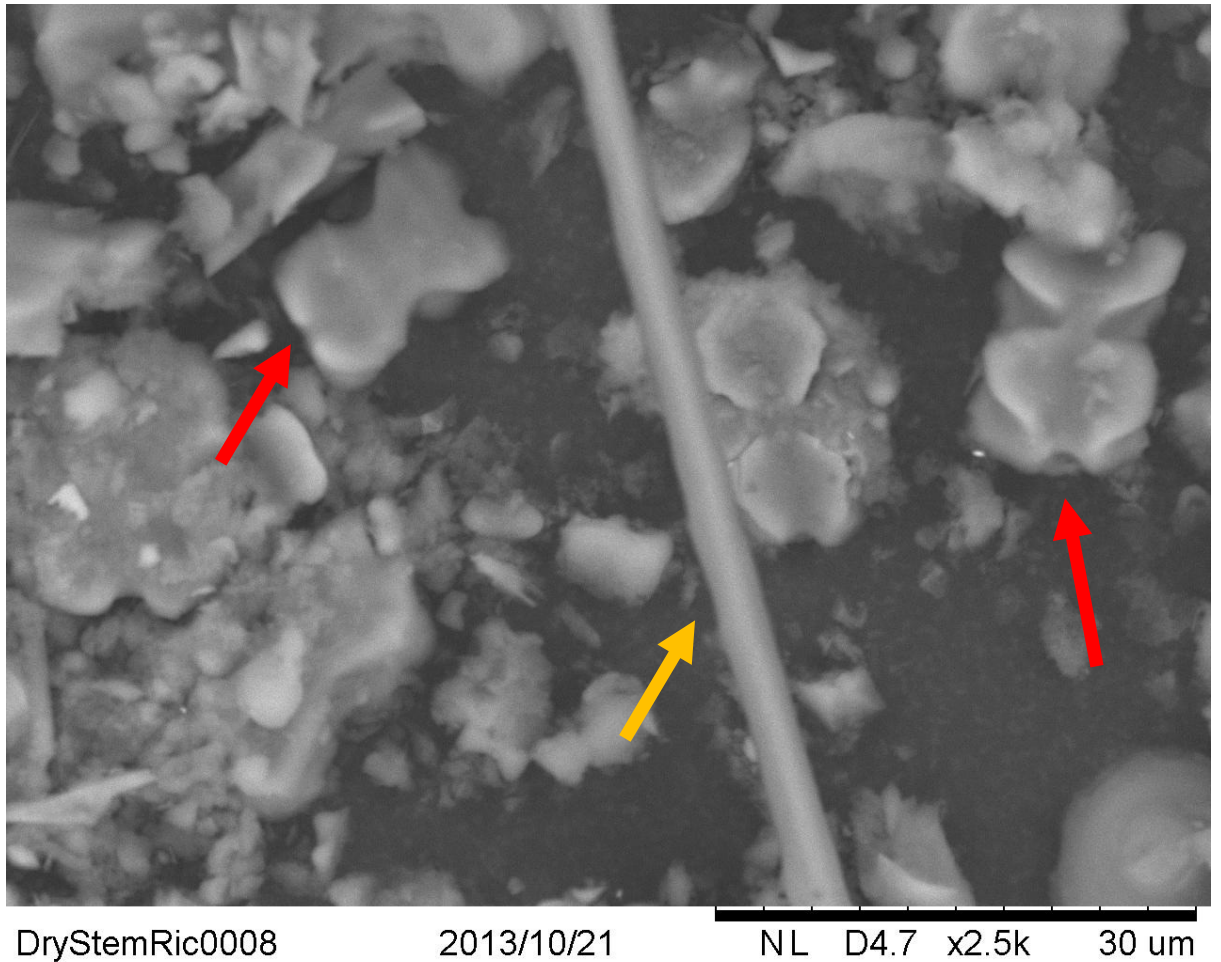


Figure 5.24 SEM image of silica structures taken from a dry-digested rice stem at 2500 x magnification. Arrows label areas of interest, discussed in text.

A higher magnification image of the silica phloem tube seen previously confirms the earlier observations with a complete lack of detail of structure along the tube's smooth surface (Fig 5.24). The tube is approximately 3 μm thick (see gold arrow). Silica cells can be observed on either side of the silica tube (see red arrows).

5.3.2 Hitachi S-4500 Scanning Electron Microscope

The following SEM images were obtained using the Hitachi S-4500 Scanning Electron Microscope. The appropriate scale bar is located in the bottom right corner of each image. Each image is described briefly below.

5.3.2.1 Wet-Digested Rice Leaf

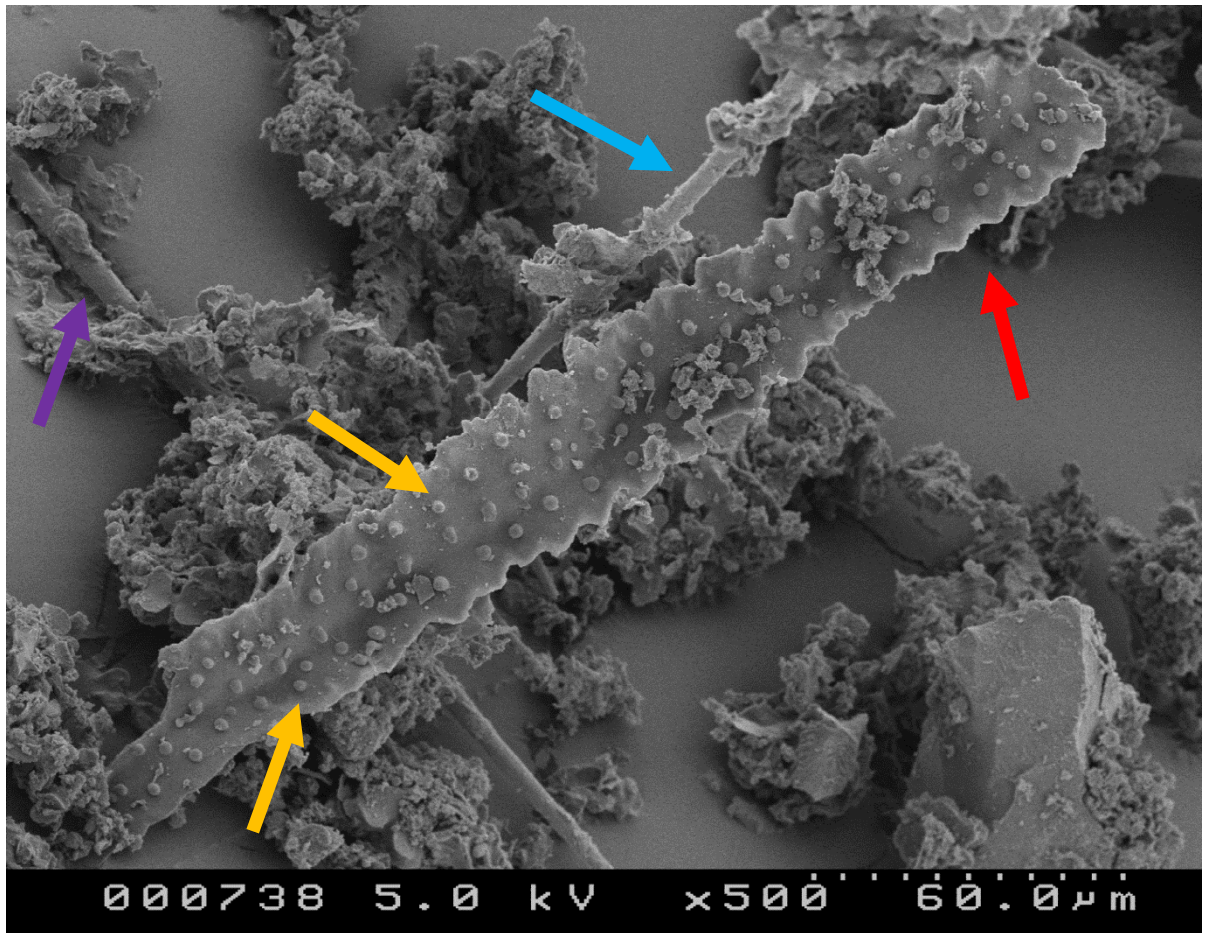


Figure 5.25 SEM image of silica structures taken from a wet-digested rice leaf at 500 x magnification. Arrows label areas of interest, discussed in text.

A large piece of silica which covered epidermal cells at the leaf's surface (Fig 5.25). Though this sample is much larger than any individual epidermal cell thus far observed, there are no obvious signs of individual epidermal cells boundaries within the sample. The edges of the structure show the characteristic sinuate, or wave-like edges of the epidermal cell (see red arrow). Papilla cover the surface of the structure in uniform rows, with regular intervals between each papilla (see gold arrows). Two silica spines or tubes are visible running across the image, one running parallel to the epidermal structure (see blue arrow) and another running perpendicular to it (see purple arrow). The tubes themselves appear to be smooth and devoid of distinguishing features, though they have silica structures on them which could be part of their structure, or merely debris which is in contact with them.

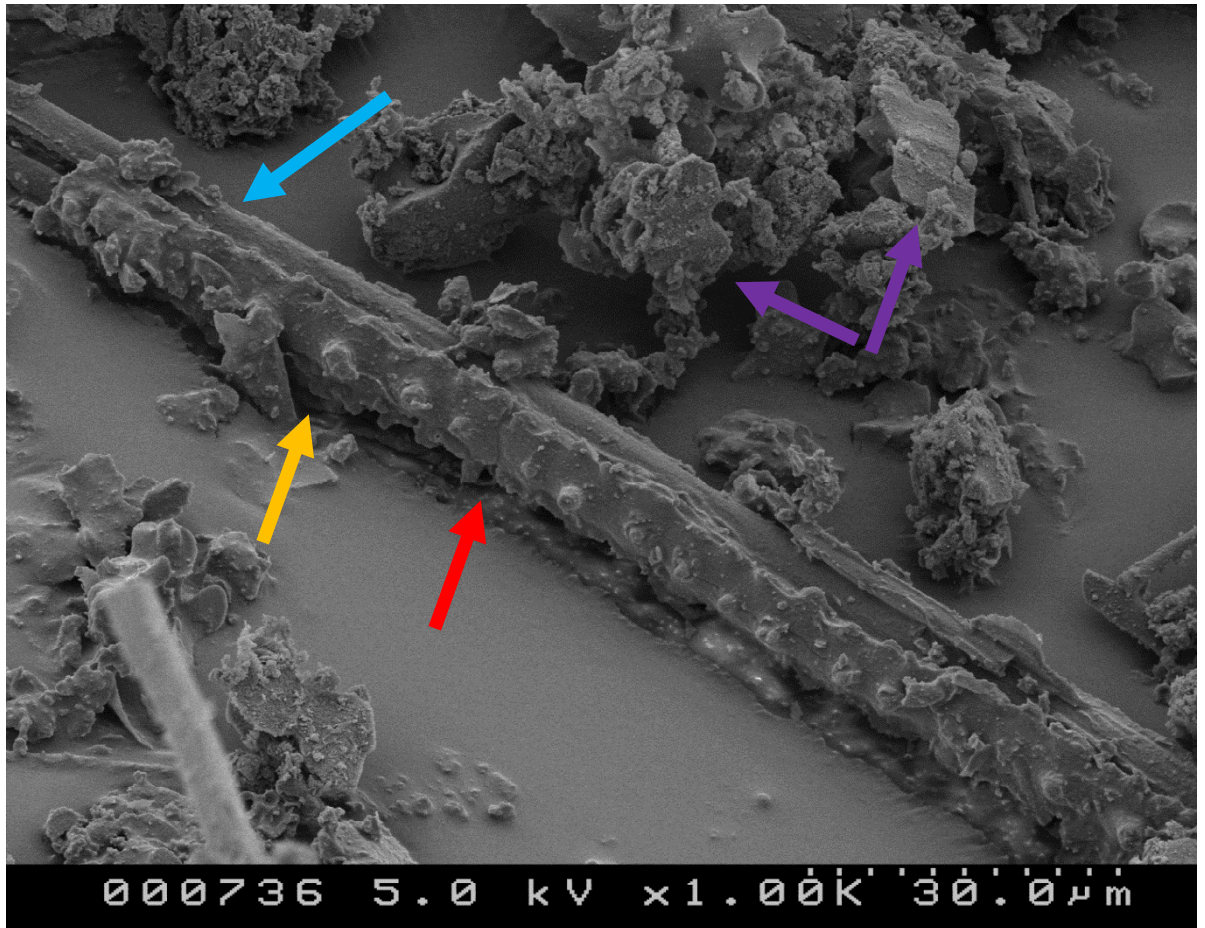


Figure 5.26 SEM image of silica structures taken from a wet-digested leaf stem at 1000 x magnification. Arrows label areas of interest, discussed in text.

A silica structure from the epidermis of the rice leaf showing a single row of epidermal cells (Fig 5.26). The divide between individual cells can be observed at one point along the structure's length (see red arrow). A single column of papilla runs down the length of the structure across the surface of the epidermal cells (see gold arrow). The structure appears to sit above two silica tubes which run parallel to the epidermal cells with a noticeable gap between the two separate tube-like structures (see blue arrow). Both the epidermal and tube-like structures have been observed in other samples, but not together in this orientation. The tubes have a smooth surface with no distinguishable features. Several silica cells are visible amongst other silica debris, identifiable by their distinctive dumbbell shape (see purple arrows).

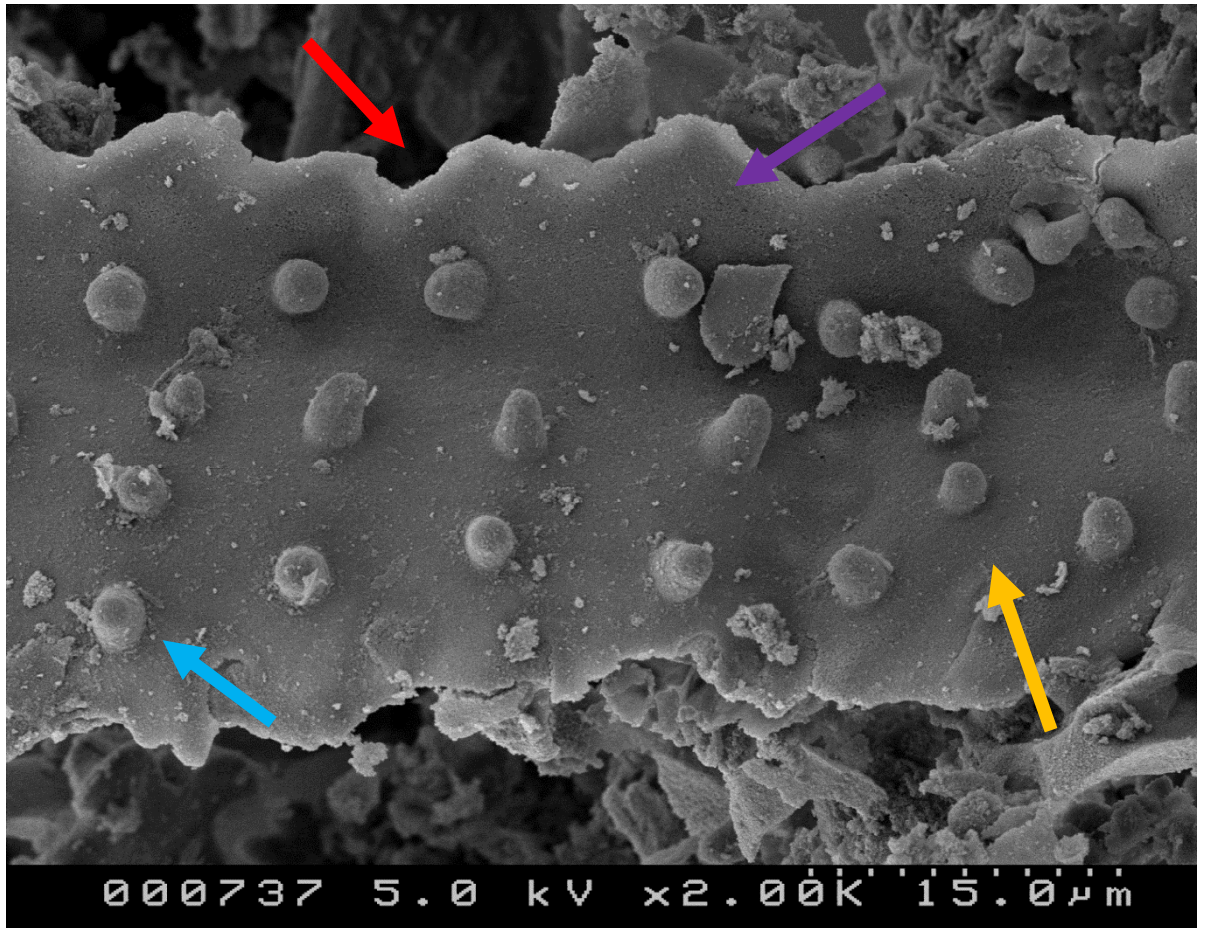


Figure 5.27 SEM image of silica structures taken from a wet-digested leaf stem at 2000 x magnification. Arrows label areas of interest, discussed in text.

A high magnification image of a silica structure from the epidermis of the rice leaf (Fig 5.27).

There is no divide along the structure that would indicate multiple cells, suggesting this is in fact one large epidermal cell. The edges of the structure show the characteristic sinuate, or wave-like edges of the epidermal cell (see red arrow). Papilla are visible across the surface of the structure, presented as three distinct columns in most areas, however at several points this uniform order is broken and either two (see gold arrow) or four papilla (see blue arrow) are observed side by side. The surface of the silica and the papilla themselves gives an appearance of porous rock, with small holes visible throughout the structure (see purple arrow).

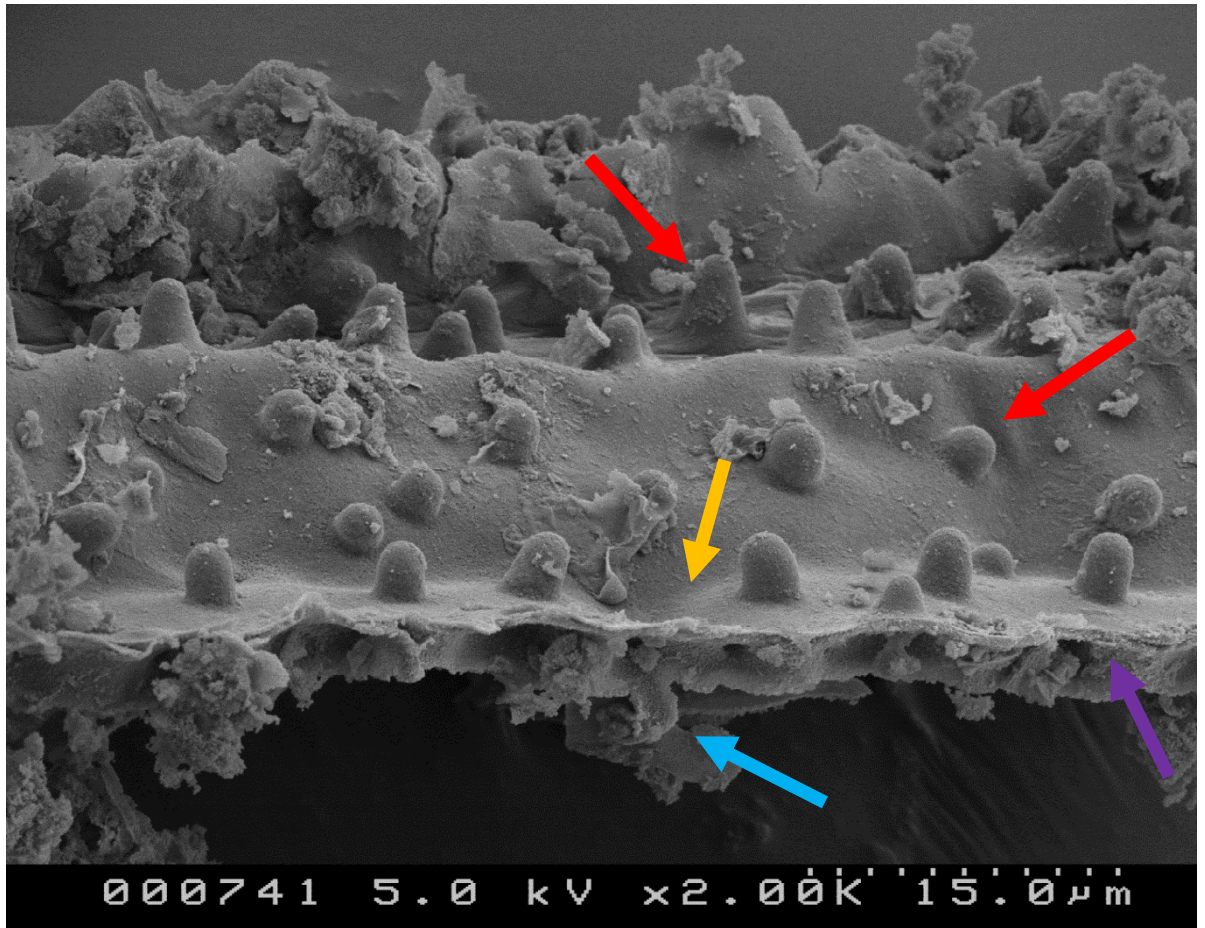


Figure 5.28 SEM image of silica structures taken from a wet-digested leaf stem at 2000 x magnification. Arrows label areas of interest, discussed in text.

High magnification image of a silica structure from the leaf epidermis, orientated at a side-on angle (Fig 5.28). The angle of observation allows observation of not only the surface layer of silica, but also the silica layer's thickness. Papilla cover the surface of the epidermal structure, varying in size significantly between individual papilla (see red arrows). The gap where two epidermal cells meet can be seen by a depressed valley in the silica layer on the surface (see gold arrow), further confirmed by a silica wall extending deep underneath the sample (see blue arrow). The silica layer that covers the majority of the epidermal cell can be seen to be less than 1 μm thick at the edge (see purple arrow), though it is thicker around the edges of the epidermal cells where the silica layer extends down between them.

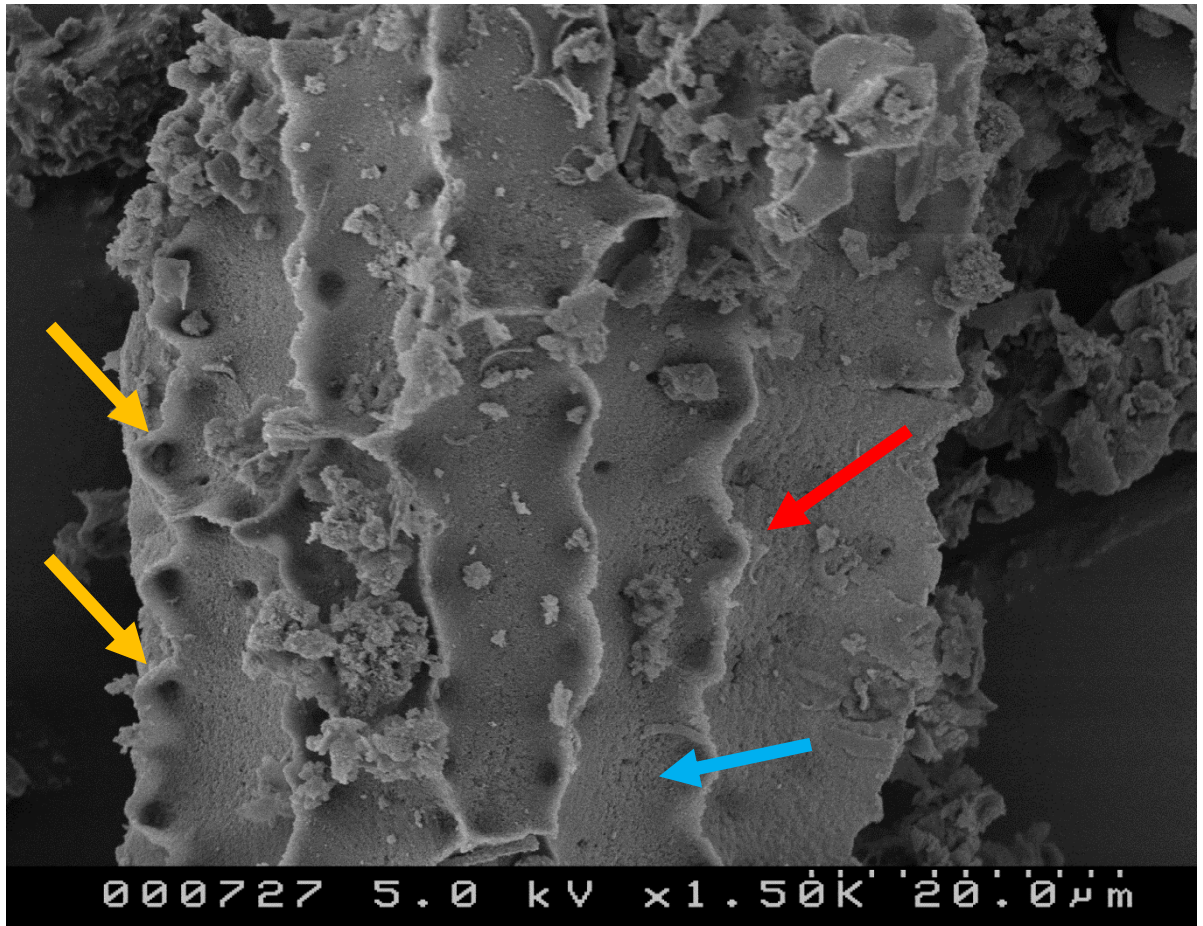


Figure 5.29 SEM image of silica structures taken from a wet-digested leaf stem at 1500 x magnification. Arrows label areas of interest, discussed in text.

The underside of an epidermal silica structure, showing the outlines of multiple individual epidermal cells (Fig 5.29). The silica layer which covers the surface of the leaf epidermis extends down into the gap between individual cells, creating a replica of the upper half of the cell, though it does not penetrate further to cover the underside of the epidermal cell (see red arrow). Round recesses into the silica can be observed indicating the location of the papilla which cover the upper surface of the epidermis (see gold arrows). The silica layer itself does not appear entirely solid, but rather shows the appearance of a porous rock, with tiny holes throughout its structure (see blue arrow).

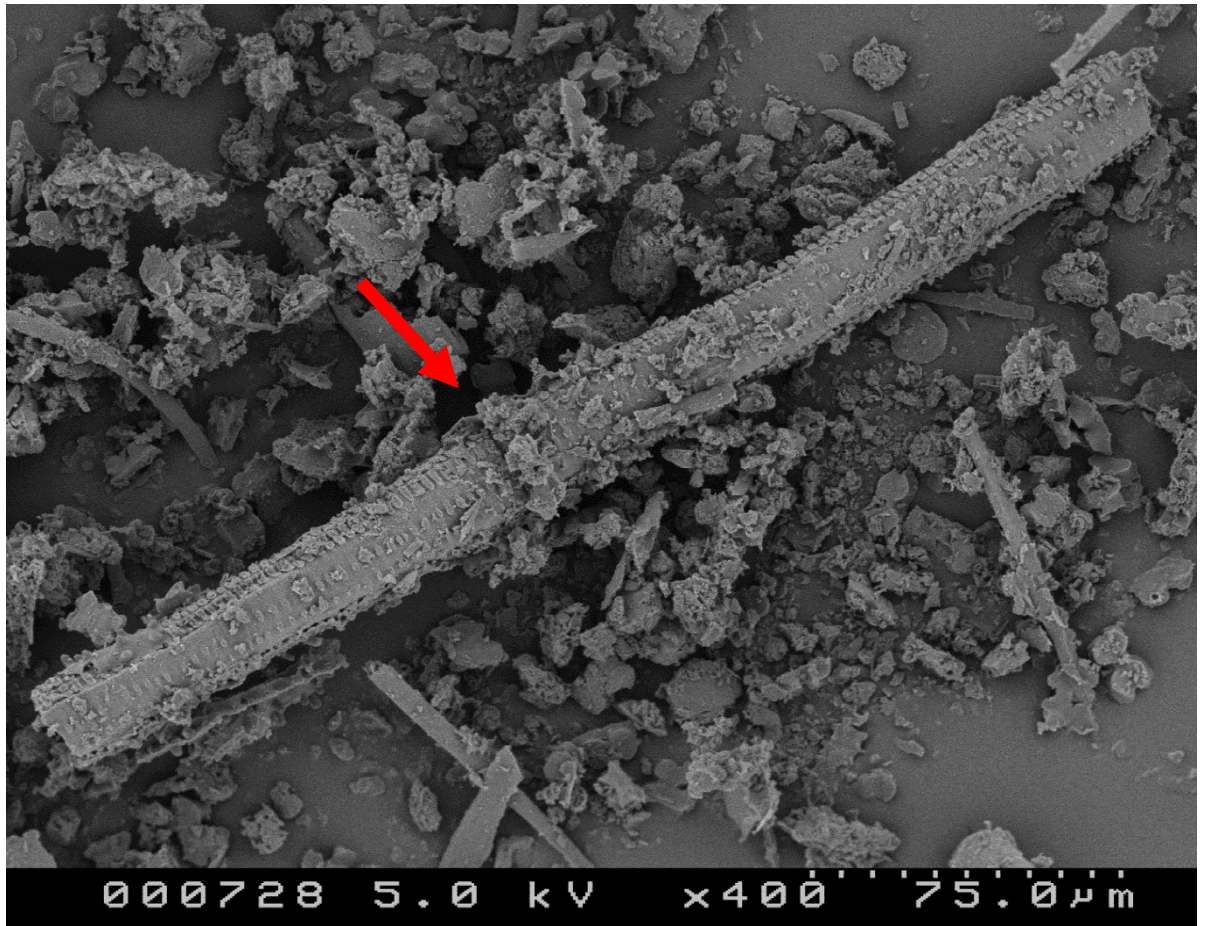


Figure 5.30 SEM image of silica structures taken from a wet-digested leaf stem at 400 x magnification. Arrows label areas of interest, discussed in text.

A large tube-like structure from the xylem of the rice leaf can be observed, identified by both its size and shape, as well as the distinctive ridges which cover its surface (Fig 5.30). The structure measures just under 300 μm in length with a width of approximately 30 μm . Silica debris from elsewhere in the sample can be seen laying on top of the larger structure in places, however this debris is distinct from the raised ridges (see red arrow).

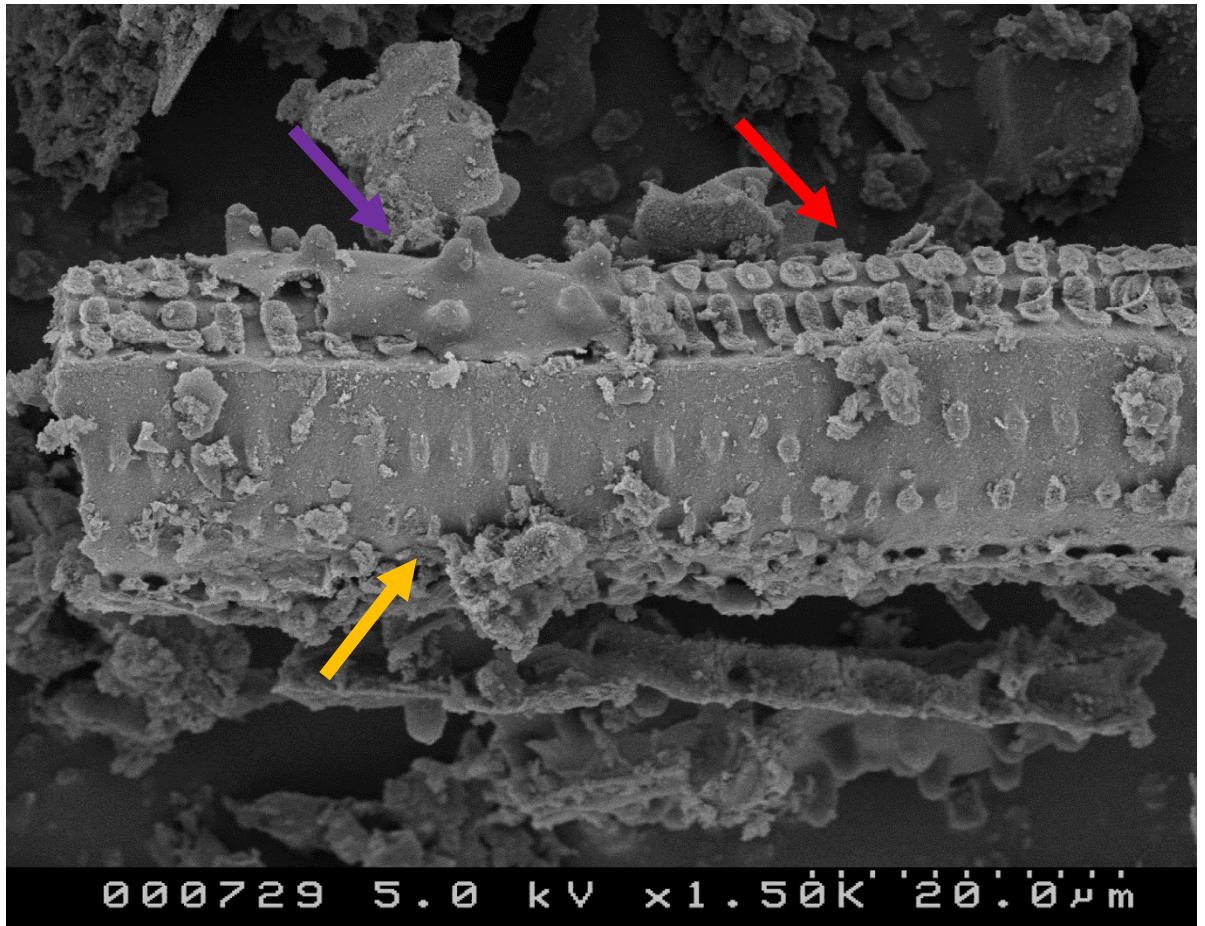


Figure 5.31 SEM image of silica structures taken from a wet-digested leaf stem at 1500 x magnification. Arrows label areas of interest, discussed in text.

Higher magnification of the end of a silica structure from the xylem (Fig 5.31). The ridges which appeared to surround the entire tube structure in lower magnification images can be seen to be formed from multiple individual raised areas of silica (see red arrows). The surface of the xylem tube facing the camera appears thicker than those around the sides, with less pronounced ridges which only extend partially out of the main body of silica (see gold arrow). A small area of the xylem is covered with a piece of epidermal silica which has broken off from a larger structure (see purple arrow).

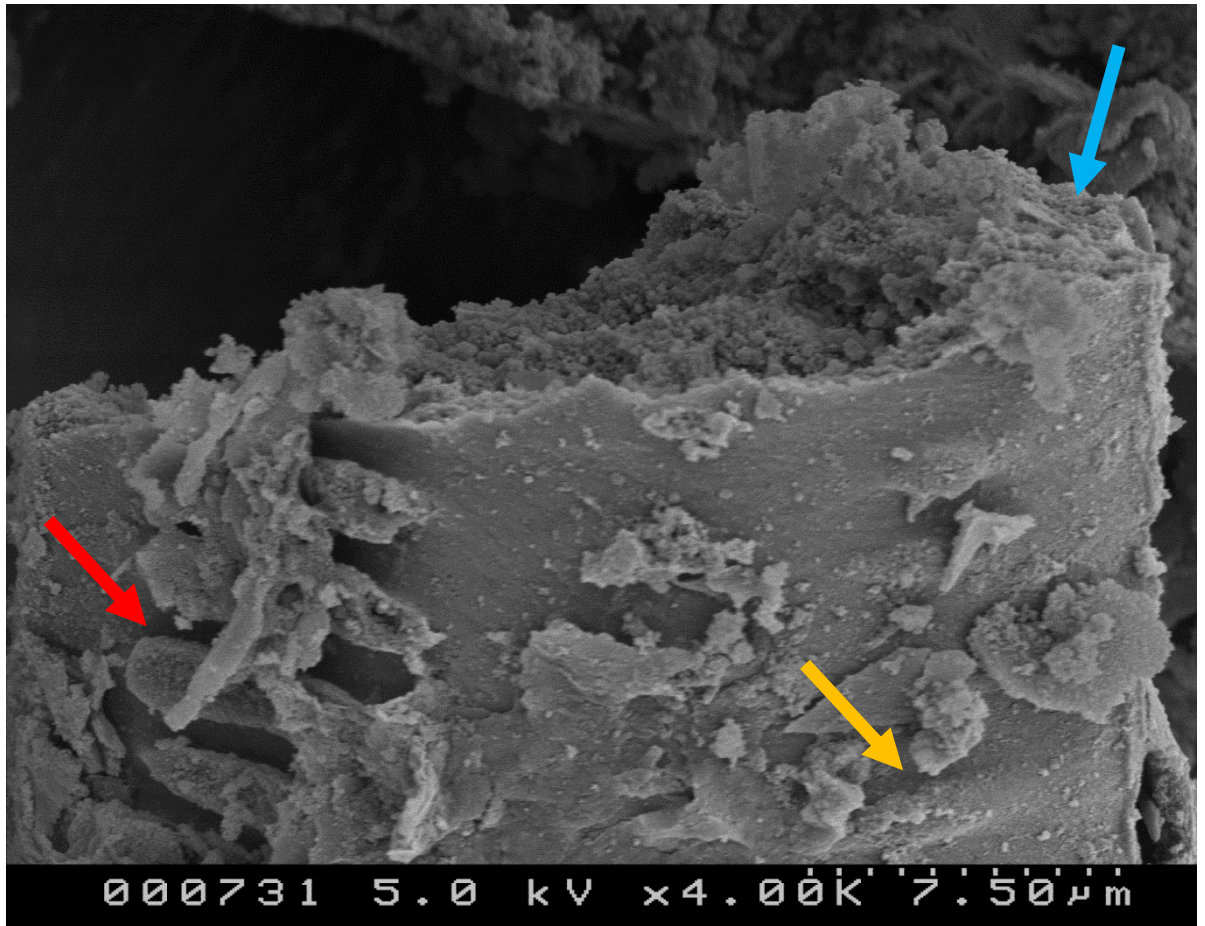


Figure 5.32 SEM image of silica structures taken from a wet-digested leaf stem at 4000 x magnification. Arrows label areas of interest, discussed in text.

Higher magnification of the end of a silica structure from the xylem, with the platform rotated in order to give a best possible view of the inside of the tube (Fig 5.32). The ridges at the outer edges of the xylem tube can be seen clearly on one facing (see red arrow), though they are less pronounced on another (see gold arrow). Despite the best attempts, it was not possible to view the end of the tube any more clearly than this, meaning we cannot determine if the xylem silica structure is hollow or no. It can be determined that if the tube is indeed hollow, its walls are thick relative to its diameter, reducing the overall capacity of the xylem tube significantly (see blue arrow).

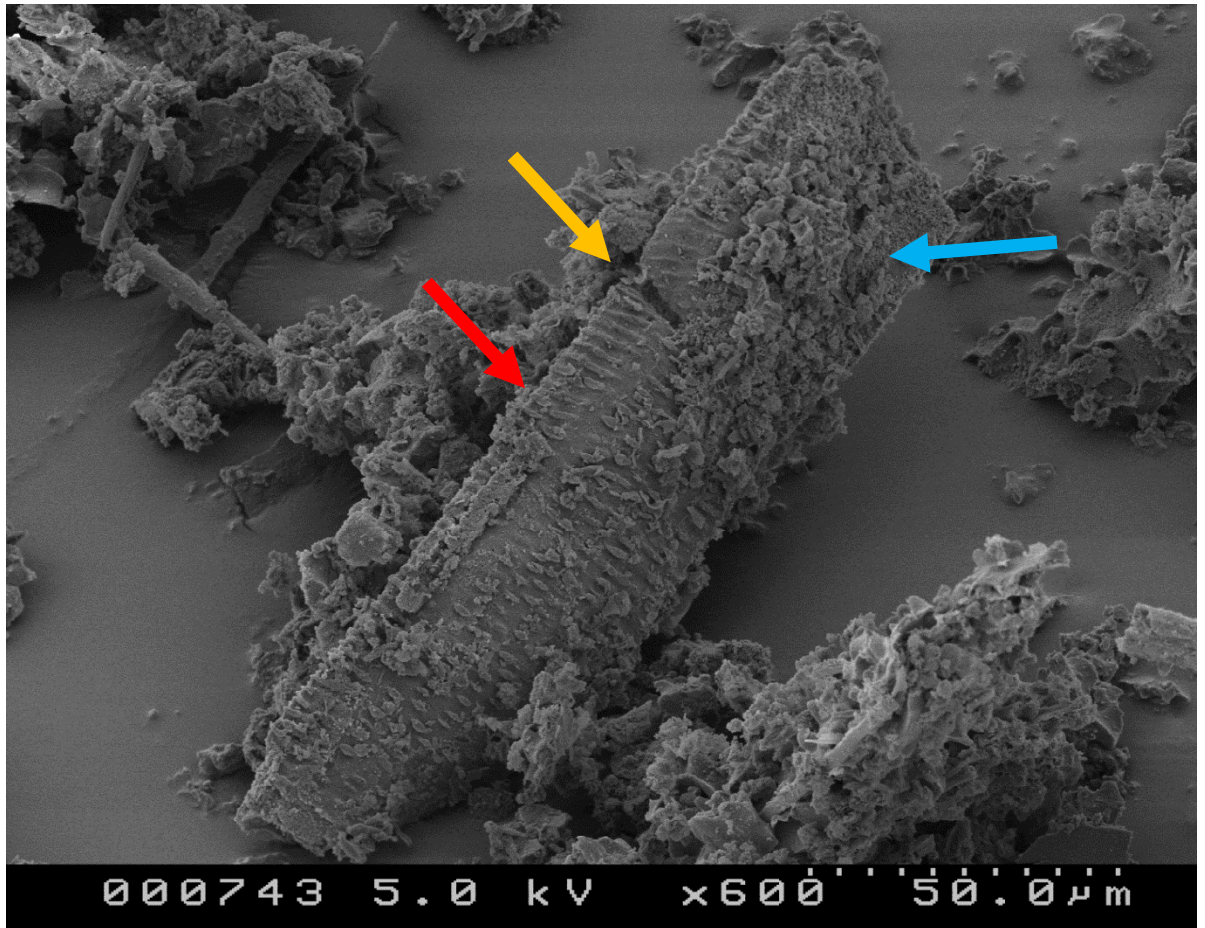


Figure 5.33 SEM image of silica structures taken from a wet-digested leaf stem at 600 x magnification. Arrows label areas of interest, discussed in text.

Another silica structure from the leaf xylem tissue, shorter but wider this time measuring approximately 160 μm in length and 40 μm in width (Fig 5.33). The distinctive ridges which surround the xylem structure are visible, with clear gaps between individual columns of ridges (see red arrows). The xylem structure appears to be damaged with a large gap cutting into its side (see gold arrows). Large areas are covered with silica debris from elsewhere in the sample, covering much of the surface detail of the xylem structure (see blue arrow).

5.3.2.2 Dry-Digested Leaf Tissue

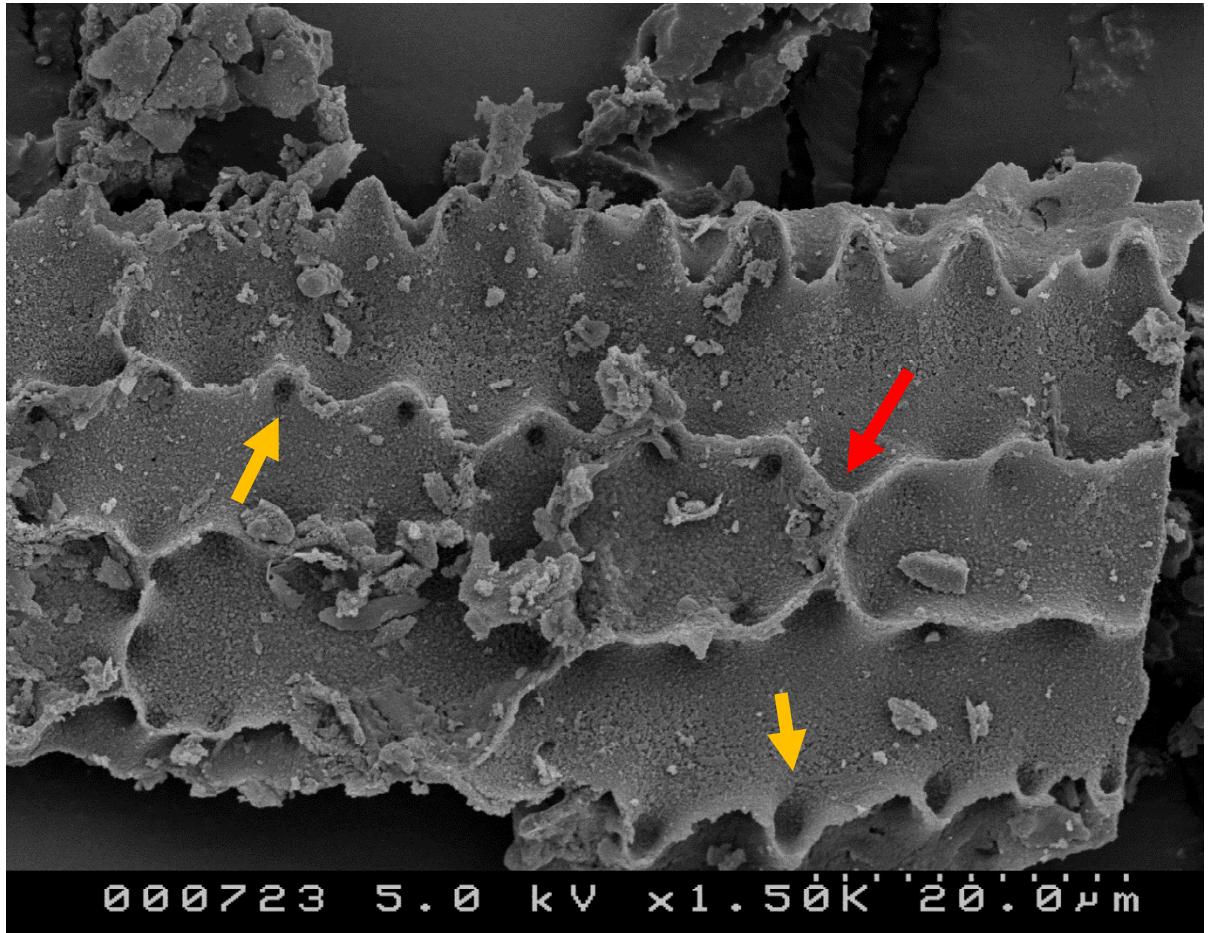


Figure 5.34 SEM image of silica structures taken from a dry-digested leaf stem at 1500 x magnification. Arrows label areas of interest, discussed in text.

The underside of an epidermal silica structure, showing the outlines of multiple individual epidermal cells (Fig 5.29). The silica layer which covers the surface of the leaf epidermis extends down into the gap between individual cells, creating a replica of the upper half of the cell, though it does not penetrate further to cover the underside of the epidermal cell (see red arrow). Small recesses into the silica can be observed showing the location of the papilla which cover the upper surface of the epidermis (see gold arrows). The silica layer itself does not appear entirely solid, but rather shows the appearance of a porous rock, with tiny holes throughout its structure. These observations are identical to those of a similar structure found in the wet-digest group (Fig 5.29).

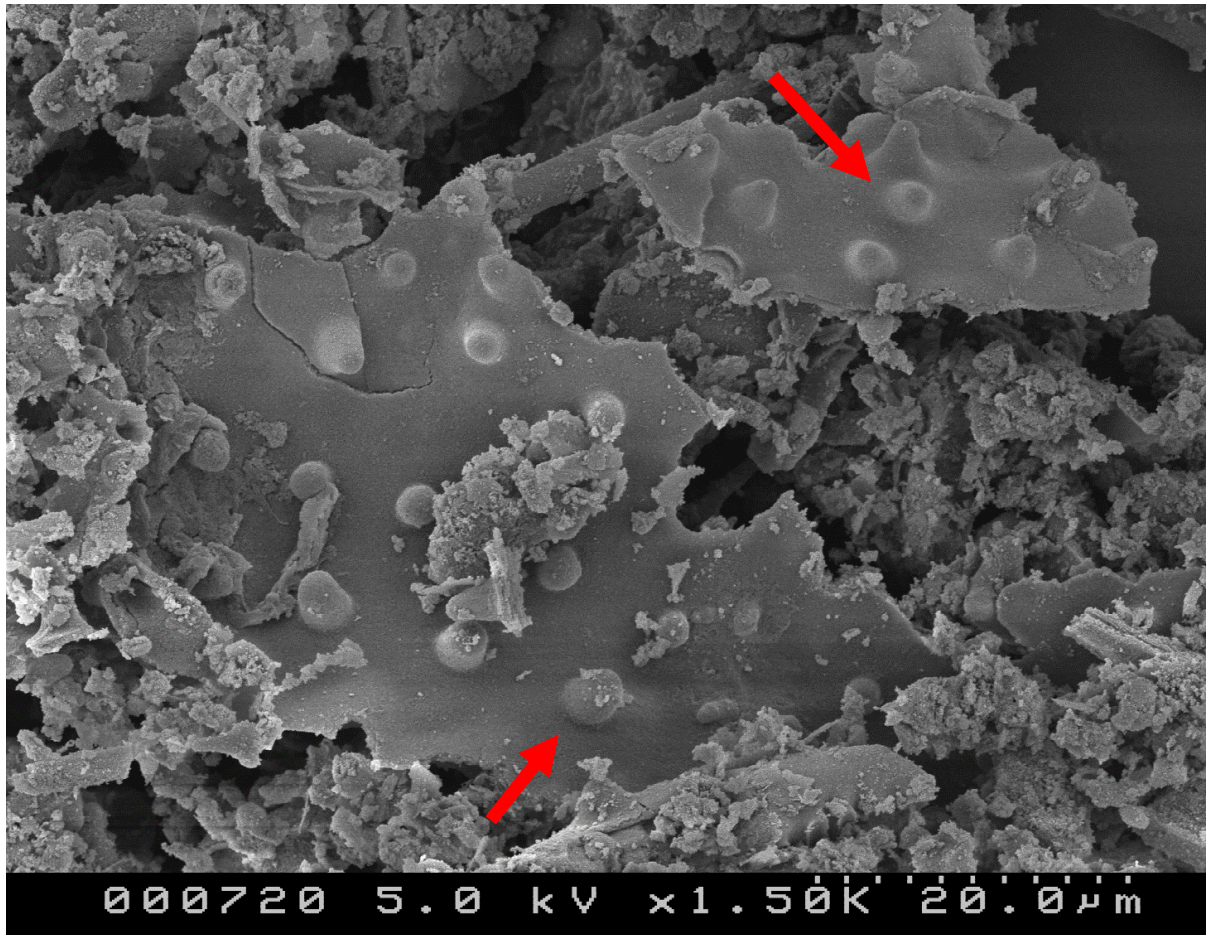


Figure 5.35 SEM image of silica structures taken from a dry-digested leaf stem at 1500 x magnification. Arrows label areas of interest, discussed in text.

Fragmented pieces of a silica structure from the epidermis of the rice leaf (Fig 5.35). There are no gaps or recesses into the silica that would represent where two epidermal cells meet, suggesting this sample could be representative of a single large epidermal cell or that the divide between cells is not always as prominent. Papillas can be observed covering the surface of the silica structure (see red arrows).

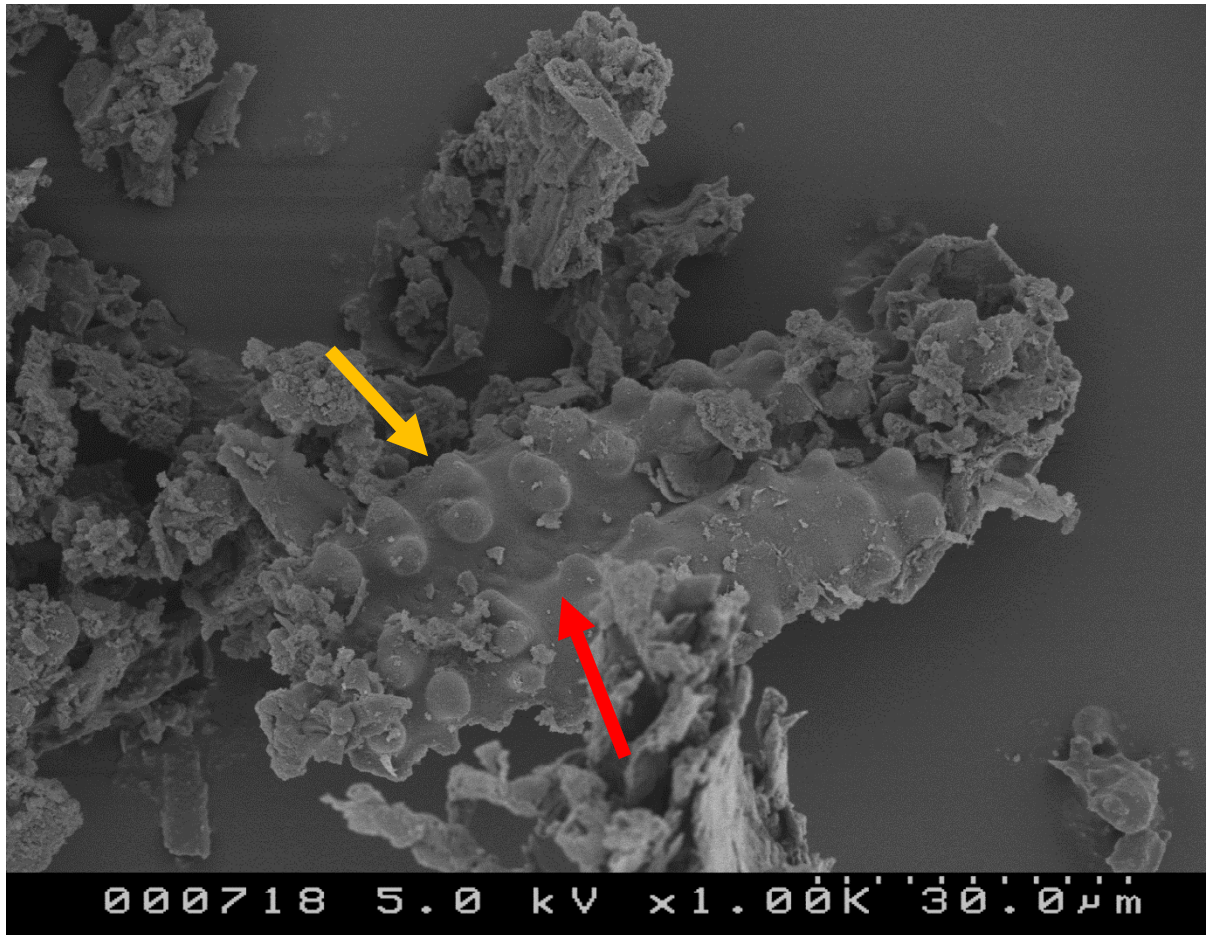


Figure 5.36 SEM image of silica structures taken from a dry-digested leaf stem at 1000 x magnification. Arrows label areas of interest, discussed in text.

A silica structure from the epidermis of the rice leaf tissue (Fig 5.36). Though not as obvious due to the angle of observation, the interlocking sinuate, or wave-like edges of the two individual epidermal cells can be observed in the recess between the two peaks that represent each cell (see red arrow). Papilla can be observed covering the surface of the silica structure, with some papillas gathered closely together, appearing as a single, double peaked structure (see gold arrow).

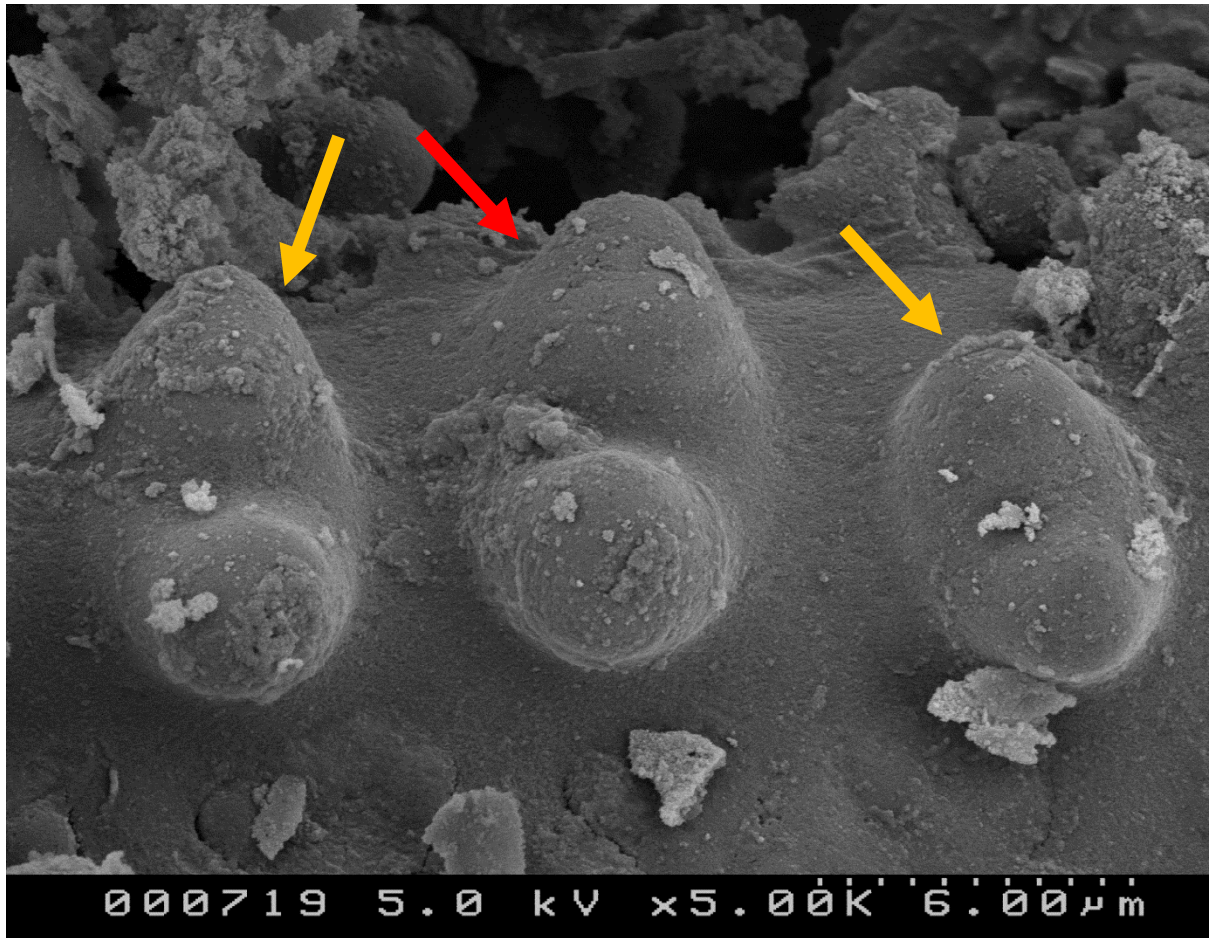


Figure 5.37 SEM image of silica structures taken from a dry-digested leaf stem at 5000 x magnification. Arrows label areas of interest, discussed in text.

Observing the papilla under a higher magnification reveal that in some cases, two or even three papilla are joined together to form a multi-peaked structure on the surface of the epidermal cells (Fig 5.37). Whether there papilla are actually connected or merely adjacent to each other is difficult to determine, as the silica layer could mask the gaps between them. Of the three papilla groups observed, one is formed of three individual peaks (see red arrow) whilst the other two are formed of two peaks (see gold arrows).

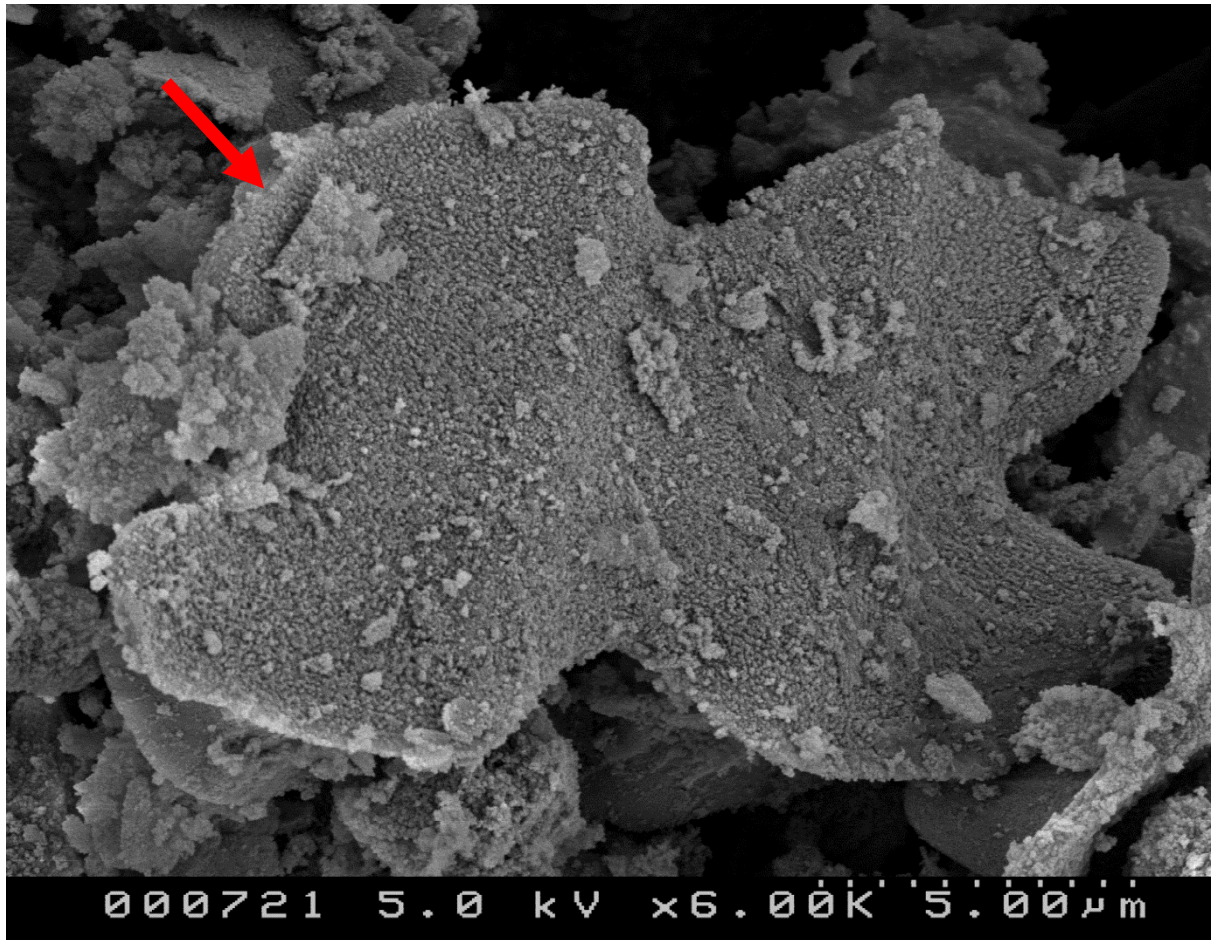


Figure 5.38 SEM image of silica structures taken from a dry-digested leaf stem at 6000 x magnification. Arrows label areas of interest, discussed in text.

A silica cell can be observed at high magnification, identified by its dumbbell shape but showing a rough textured surface which has not been observed in previous images (Fig 5.38). The silica cell surface's appearance is most reminiscent of sandstone. Whilst it is possible the surface is merely covered in debris from elsewhere in the sample, the rough texture is uniform across the cell's surface and other debris fragments are observable, looking distinctly different from the surface texture (see red arrow).

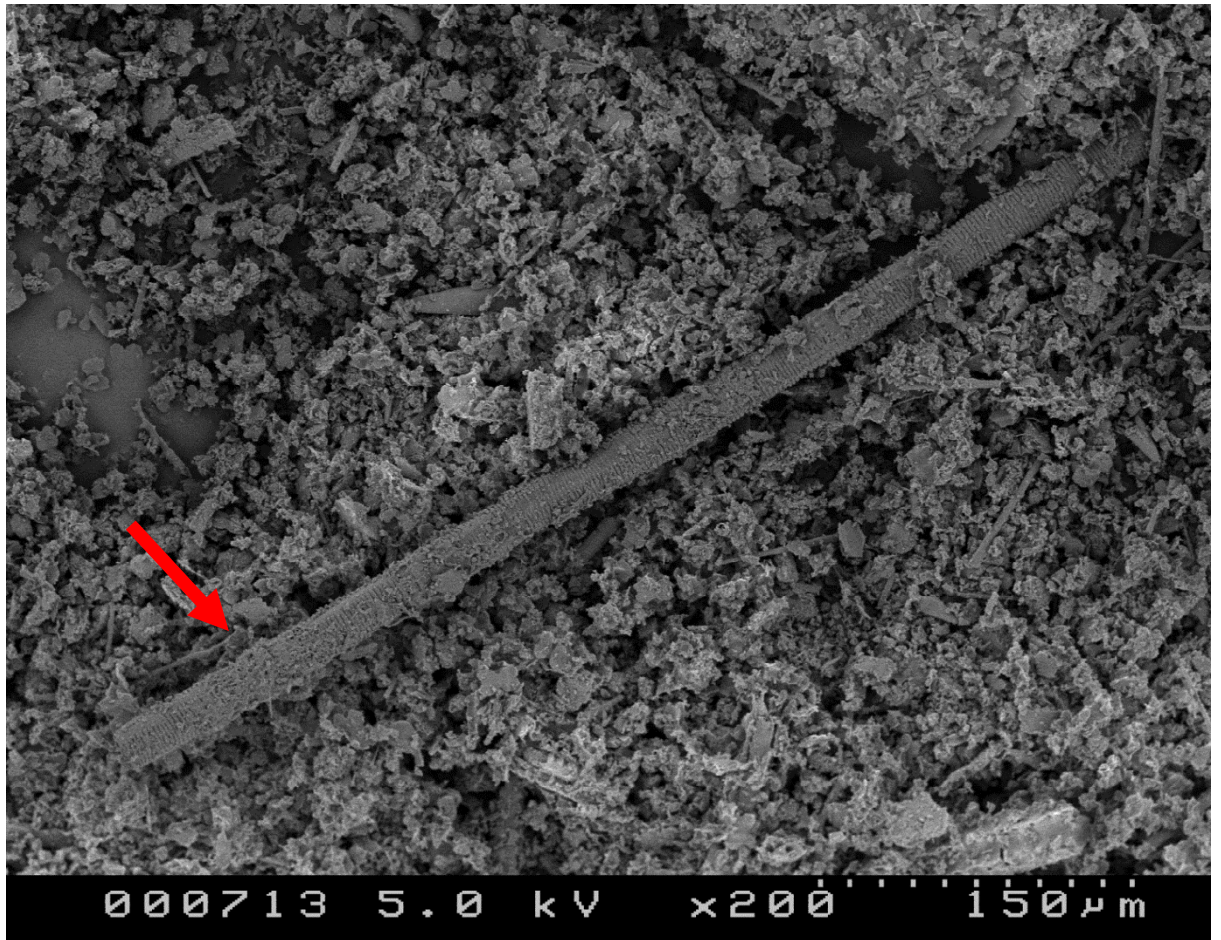


Figure 5.39 SEM image of silica structures taken from a dry-digested leaf stem at 200 x magnification. Arrows label areas of interest, discussed in text.

A large tube-like structure from the xylem of the rice leaf can be observed, identified by both its size and shape, as well as the distinctive ridges which cover its surface (Fig 5.39). The structure measures almost 600 μm in length with a width of approximately 30 μm (see red arrow). This is the longest intact xylem structure found in any of the sample groups.

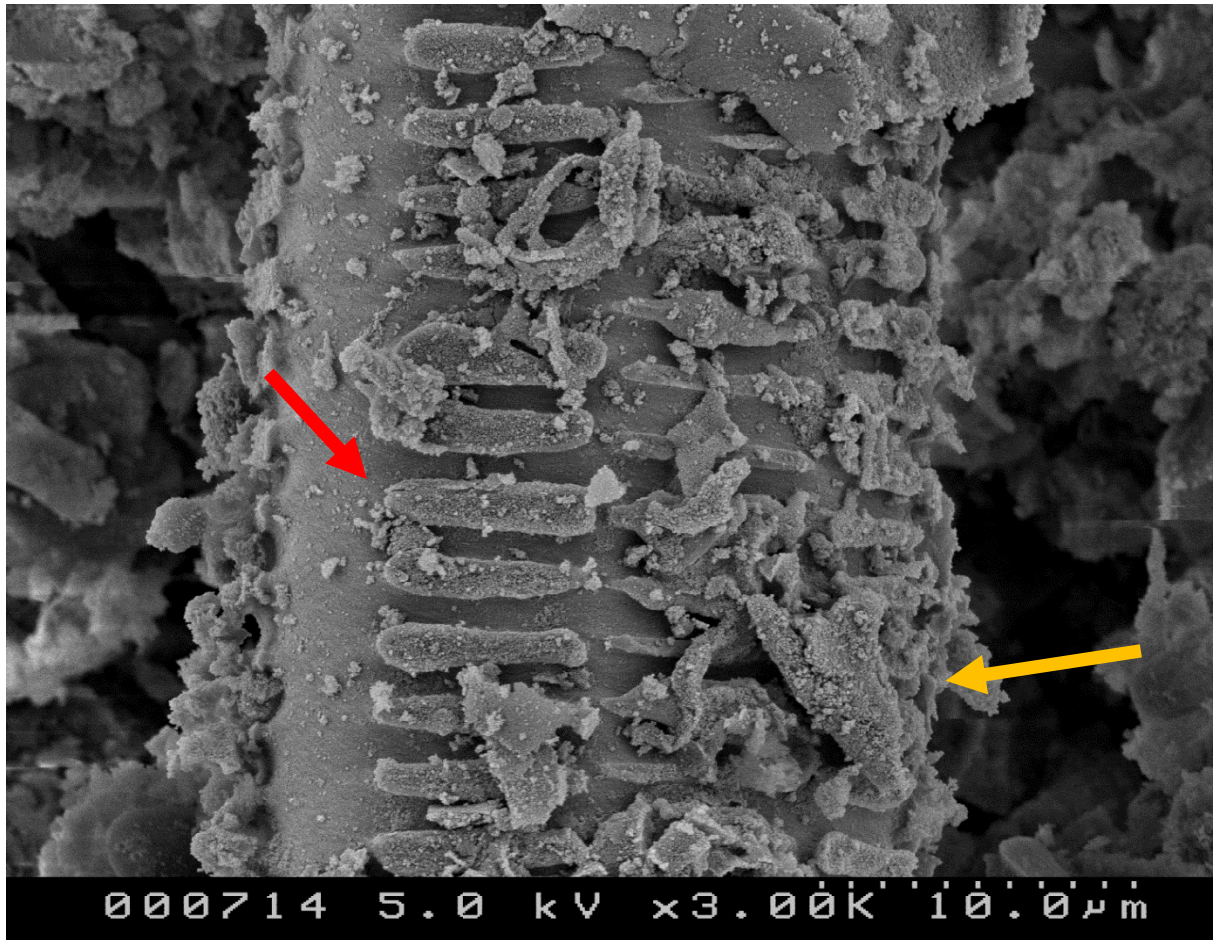


Figure 5.40 SEM image of silica structures taken from a dry-digested leaf stem at 3000 x magnification. Arrows label areas of interest, discussed in text.

A higher magnification image of the xylem structure seen previously, showing the detailed ridges that surround its cylindrical shape (Fig 5.40). Each ridge is around 7 μm in length, in a rectangular shape though the edges are rounded (see red arrow). These individual ridges are stacked in columns which run up the length of the xylem silica structure, with multiple columns running alongside each other, surrounding the structure to create the ridged effect seen at lower magnifications. Silica debris from elsewhere in the sample covers some areas of the structure, but this debris is easily recognised as separate from the main body (see gold arrow).

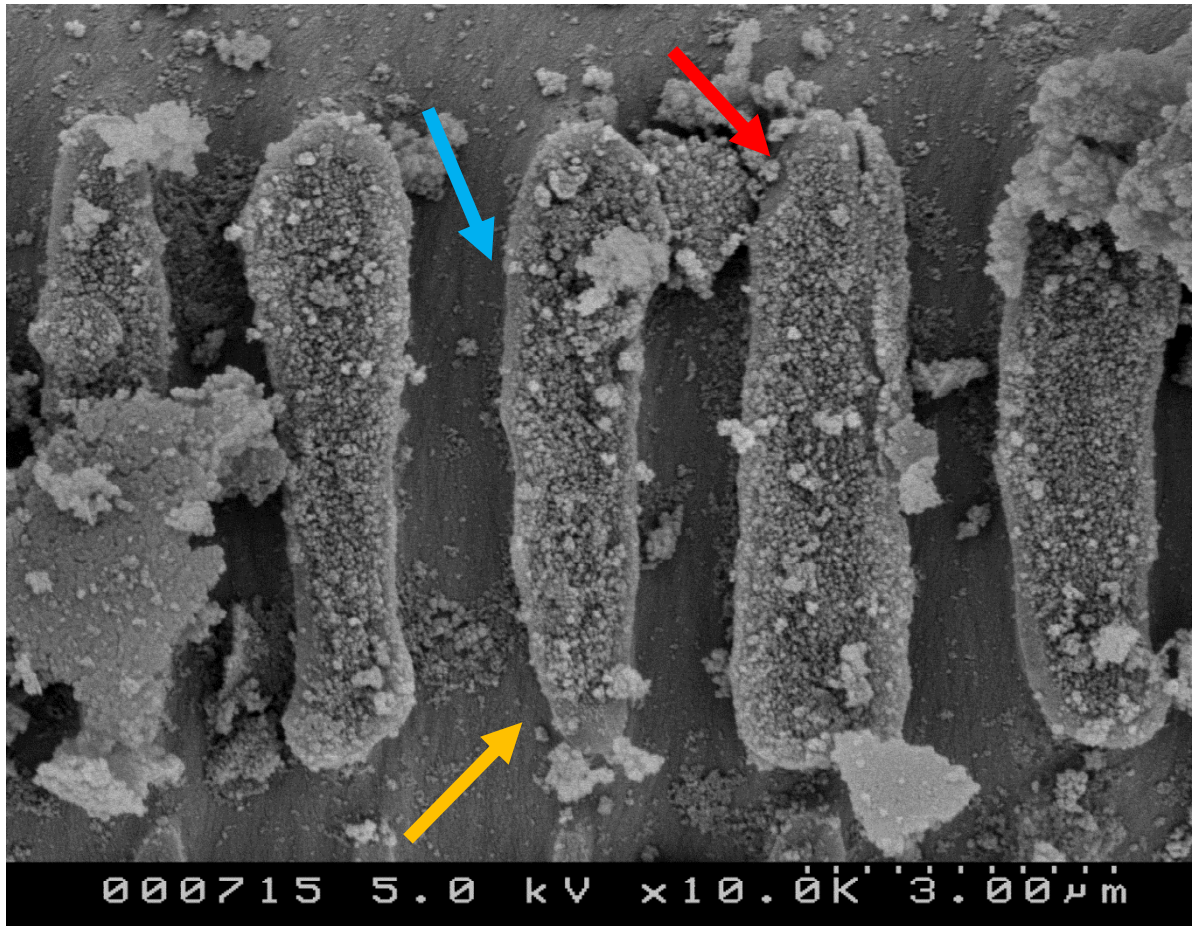


Figure 5.41 SEM image of silica structures taken from a dry-digested leaf stem at 10,000 x magnification. Arrows label areas of interest, discussed in text.

High magnification image of the silica ridges which cover the surface of the xylem silica structure (Fig 5.41). Each individual silica ridge varies in shape and width, with some ridges maintaining a rectangular shape (see red arrow) whilst others taper at one end (see gold arrow). The surface of the ridges has a rough texture, as if covered with fine particulates whilst the underlying xylem structure has a much smoother texture. The rough texture on the ridges appears to fade towards to edges, giving way to the smoother texture of the rest of the xylem structure on the side of the ridge (see blue arrow).

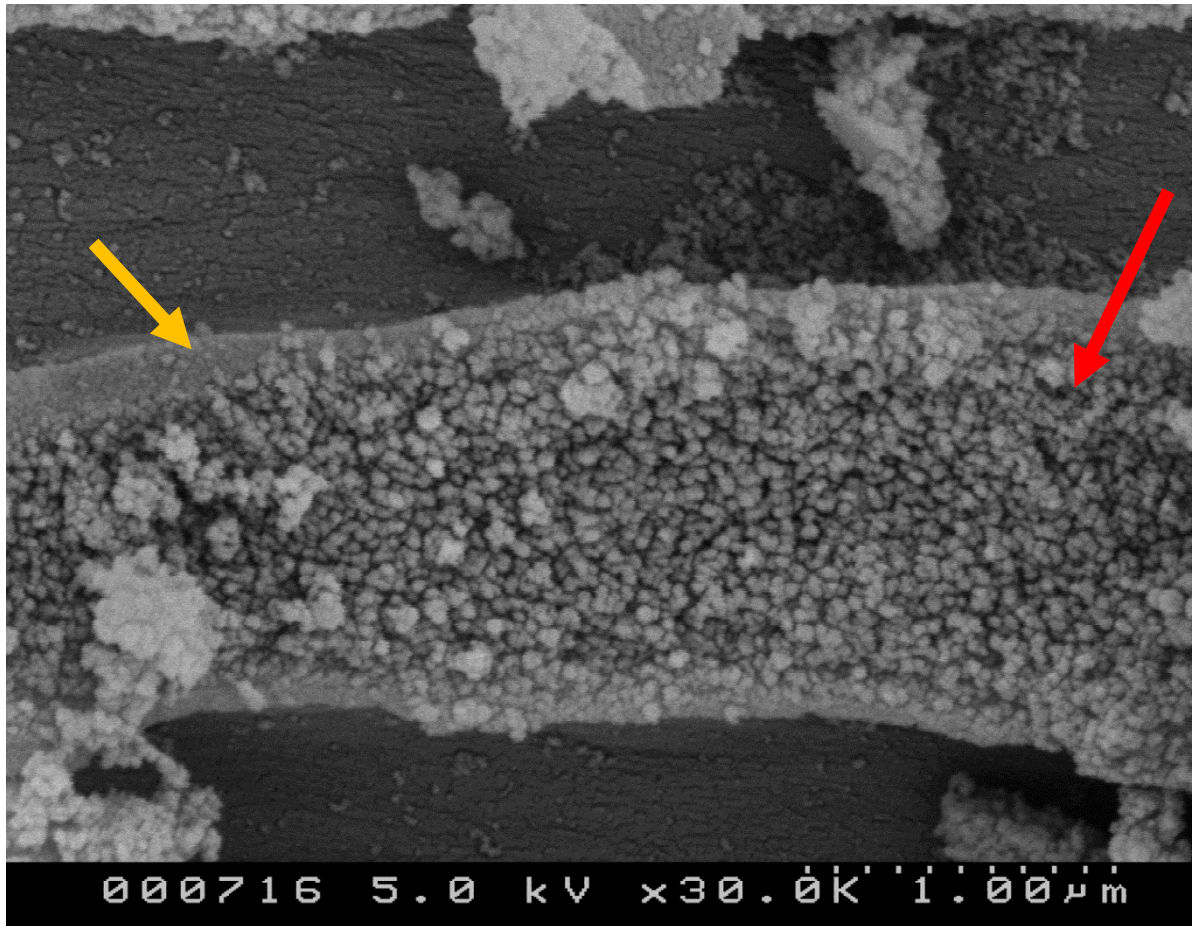


Figure 5.42 SEM image of silica structures taken from a dry-digested leaf stem at 30,000 x magnification. Arrows label areas of interest, discussed in text.

High magnification image of a single ridge from the xylem silica structure seen previously (Fig 5.42). The rough texture of the surface of these ridges can be seen clearly, resembling sandstone with numerous particulate silica formations across its surface of varying sizes (see red arrow). The sides of the ridge do not share this rough texture, but are smooth like the rest of the xylem silica structure (see gold arrow). It is not possible from these images to determine if the silica particles covering the surface are a result of debris from the sample sticking to these areas, or if they represent a part of the structure of the ridges themselves.

5.3.3 Thermogravimetric Analysis

Silica samples from both the wet and dry digest groups were analysed by Thermogravimetric Analysis (TGA). Two separate samples from different plants in each group were analysed. TGA measures the weight lost by the sample as it is heated.

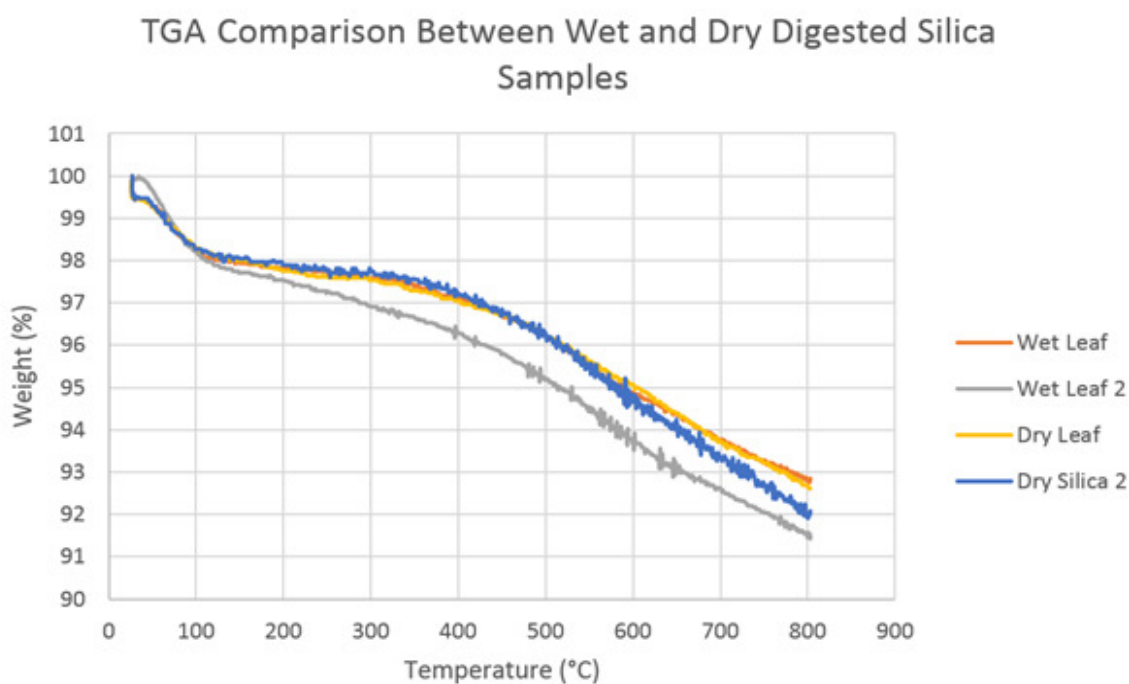


Figure 5.43 Thermogravimetric analysis of silica samples obtained from acid digestion of rice tissue in both the wet and dry digest groups.

A simple TGA analysis revealed similar profiles of weight loss across the silica samples in both the wet and dry digest groups (Fig 5.43). The weight loss detected is as a result of water removal from the sample, with between 7-9% weight loss detected across all samples. This result shows the vast majority of the weight of the digest samples is in fact silica, not undigested organic matter.

5.3.4 Fourier-Transformed Infrared Spectroscopy

Fourier transformed infrared spectroscopy (FTIR) was used to analyse silica samples obtained from both the wet and dry digest groups. FTIR is a technique used to measure the infrared spectrum of absorbance of a sample, in this case biogenic silica.

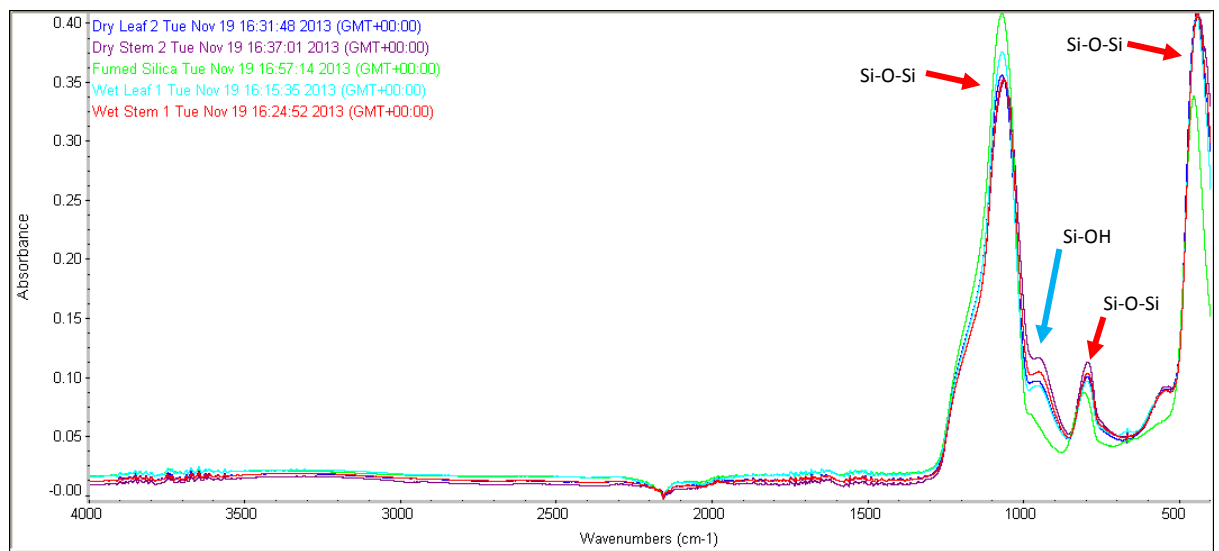


Figure 5.44 FTIR absorbance measurements of silica obtained from both the wet and dry digests, as well as fumed silica. Arrows label absorbance peaks, labelling them based on known FTIR absorbance readings for silicon bonds (Al-Maliki, 2012).

FTIR showed relatively consistent absorbance readings across the silica samples obtained from the wet and dry digests, as well as the fumed silica (Fig 5.44). The fumed silica has a lower peak associated with Si-OH bonds, suggesting that the fumed silica was less hydrated than the biogenic silica samples (see blue arrow). There was no evidence of any organic tissue remaining in the FTIR spectra of the silica samples, with only the peaks associated with Si-O-Si (see red arrows) or Si-OH (see blue arrow) detected.

5.4 Discussion

5.4.1 Comparison between TM3000 SEM and S-4500 SEM Images

Two variations of SEM were employed in this research project: a tabletop SEM designed for ease of use and minimal sample preparation and a more conventional SEM. The TM3000 tabletop microscope has a maximum magnification of 30,000 times and a spatial resolution of 30 nm and whilst the conventional Hitachi S-4500 was never taken beyond 30,000 times magnification, it is capable of 500,000 times magnification with a spatial resolution of 1.5 nm. The difference in the spatial resolution is clear when analysing images taken using the two different microscopes, with the S-4500 providing much clearer images and showing more of the structural details of the silica sample (Fig 5.43).

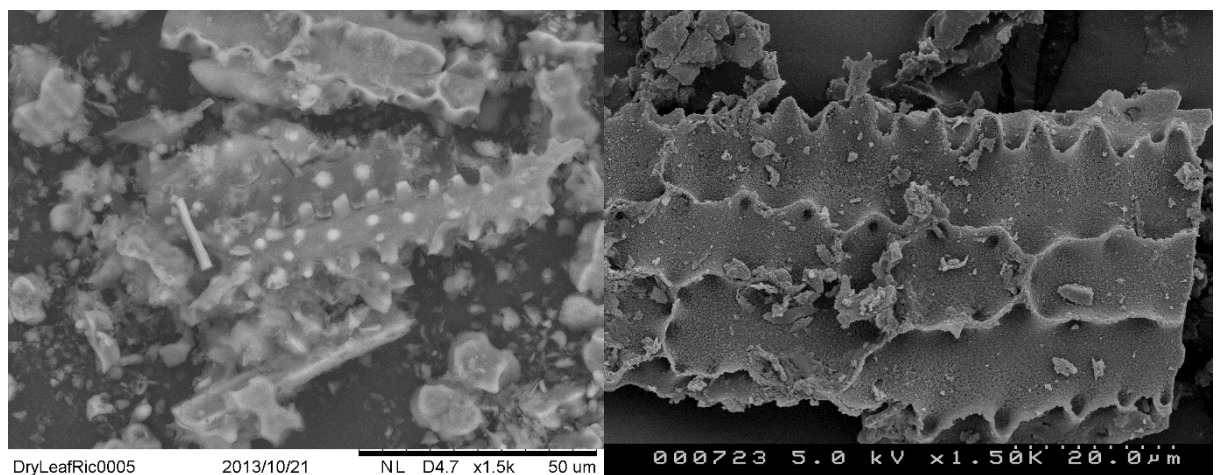


Figure 5.43 Comparison between images taken by the TM3000 SEM (A) and the S-4500 SEM (B), both at a magnification of 1,500 x and both showing the reverse side of a leaf epidermal silica structure.

The difference in image quality is staggering, but expected given the difference in resolution between the two devices. Where the TM3000 comes into its own is in its ease of use and lack of sample preparation; silica is merely mounted on a sticky tab attached to a stub, fixed within the vacuum chamber, sealed and then imaged using a simple and intuitive software system. By comparison, samples must be gold-plated before being imaged using the S-4500 and the

procedure for actually using the larger SEM is more complicated and required the assistance of a trained staff member.

The two different approaches to SEM imaging can complement each other however, with each device covering for the short-comings of each other, especially considering that samples which have been imaged using the TM3000 are compatible with the S-4500. The easy to use TM3000 can be used to quickly scan over multiple samples, identifying structures of interest which can then later be analysed using the higher resolution S-4500. The TM3000 sample stubs are compatible with the S-4500, so samples of interest merely need to be gold-plated and they can be transferred to the higher resolution device. By combining the two instruments, the ease and simplicity of the TM3000 can be used to analyse large quantities of digested silica, whilst the higher resolution and better image quality of the S-4500 can be used to image key structures.

5.4.2 TGA & FTIR

Thermogravimetric analysis of the silica samples showed similar results across all four samples from both the wet and dry digest groups (Fig 5.43). Between 7-9% weight loss was observed across the samples indicating the presence of water within the samples, however given the knowledge that biogenic silica is the most hydrated form of silica observed in nature, this observation is to be expected (Street-Perrott & Barker, 2008). No large drops in weight were observed, which would have indicated that the samples were formed of organic tissue in addition to silica.

FTIR showed consistent absorbance readings across the silica samples obtained from both the wet and dry digests, as well as the fumed silica (Fig 5.44). The fumed silica has a lower peak associated with Si-OH bonds, suggesting that the fumed silica was less hydrated than the biogenic silica samples. Again, given that biogenic silica is known to be hydrated, it would be expected that fumed silica would contain less water (Street-Perrott & Barker, 2008). There was no evidence of any biological compounds, specifically carbon bonds which would allude to the possibility of

organic matter remaining in the silica samples. The FTIR and TGA data support the research by emphasising that after the acid digestion of either wet or dried rice tissue, the only remaining component is hydrated biogenic silica and that all traces of the organic portion of the plant has been removed.

5.4.4 Differences between Silica Samples Obtained from Wet and Dry Digestion of Rice Tissue

Similar silica structures were found in both the wet and dry digested rice samples, using both the TM3000 and S-4500 SEMs.

Typical epidermal cell structures were observed in wet digested rice, showing their characteristic sinuate shape, with silica from the surface of multiple interlocking epidermal cells (Fig 5.2, Fig 5.25-29). Nodules called papilla are visible at the surface of these epidermal silica structures, with higher magnifications revealing variation in the height and thickness of these nodules (Fig 5.27 & Fig 5.28). When viewing these epidermal structures from underneath, at the side where they contacted the organic tissue of the rice leaf, it can be observed that the papilla had an organic component, evidenced by the holes in the silica indicating a papilla's presence on the surface of the structure (Fig 5.29). Similar epidermal structures were identified in the dry digest samples, with interlocking sinuate epidermal cells and surface papilla seen from both their surface and underside orientations (Fig 5.11-13 & Fig 5.34-37). At high magnifications, papilla can be seen in pairings of two or three, running down the length of an epidermal cell (Fig 5.37).

Silica cells were another common structure across both the wet and dry digest groups and both imaging methods. Silica cells in the wet digest were found predominantly as individual scattered silica structures (Fig 5.1, Fig 5.2, Fig 5.4, Fig 5.6, Fig 5.8 & Fig 5.26). A single intact silica structure was found which demonstrated the ladder-like structures which silica cells occupy over the veins of leaves (Fig 5.8 & Fig 5.9). In the dry digest tissue, silica cells were again commonly distributed throughout the sample as individual silica structures, though none were observed as part of intact ladder-like structures (Fig 5.11, Fig 5.12, Fig 5.16, Fig 5.17, Fig 5.20-24 & Fig 5.38). The lack of

images of a ladder-like silica cell structure in the dry sample group is a consequence of the fragility of these structures, which are rarely found intact in silica digests. At high magnifications using the S-4500 SEM, the surface of an individual silica cell was more closely observed, revealing a rough texture similar to sandstone in appearance (Fig 5.38).

Bulliform cells, also known as motor cells, were seen in both samples, identified by their distinctive mushroom-like shape in both the wet digest group (Fig 5.3 & Fig 5.4) and the dry digest group (Fig 5.15). Unlike the epidermal cells, which were merely covered in a layer of surface silica, bulliform cells appeared to be completely silicified, like the smaller silica cells.

These structures are typical of the cell types that would be expected to be silicified in rice plants. Silicon is known to be primarily deposited as a 2.5 μm thick layer of silica beneath the cuticle but above the leaf epidermis (Yoshida, 1965). Silica cells are the dumbbell shaped cells which cover are located at surface of the veins in leaves, arranged in ladder-like structures above the vascular bundles and, as their name would suggest, these cells are known to be amongst the first cells to become silicified when a rice plant is exposed to silicic acid (Ma & Takahashi, 2002). In the same study it was identified that bulliform cells are also silicified, though this process occurs later in the plants development than the silicification of the silica cells.

Given the known deposition of silica at these sites, it was not expected that the differing sample preparation protocols between the wet and dry digest groups would alter these structures.

Where a difference between the wet and dry digests was expected was in the xylem-like structures; these silicified xylem vessels were theorised to be formed by the tissue drying procedure and not be representative of the actual state of xylem vessels in living plants. This theory was almost immediately disproven by the presence of silicified xylem structures in the wet and dry digest groups.

Silicified xylem vessels of varying sizes were found in the wet digest group, identified as long cylindrical tubes of silica with raised ridges running around the cylinder, down its entire length

(Fig 5.4-7 & Fig 5.30-33). The xylem vessels varied greatly in diameter, with the smallest measuring around 6-8 μm in width (Fig 5.7), whilst the largest was 40 μm (Fig 5.33). Structures varied greatly in length with the longest measuring over 360 μm in length (Fig 5.4) though the ends of the xylem structures showed clear signs of having snapped or broken, indicating that they are much longer than the fragments observed here.

Xylem silica structures were also observed in the dry digest samples, showing the same distinctive morphology of a long cylinder covered with raised ridges (Fig 5.39-42). In the higher resolution S-4500 images, from both wet and dry sample groups it became apparent that each ridge which appeared to circle the entire cylinder was actually formed over multiple individual raised ridges, with gaps in between them at intervals (Fig 5.31, Fig 5.32 & Fig 5.40). These ridges are in fact silica moulds of the bordered pits, structures used by the plant to transport water between xylem vessels and prevent gas embolisms from blocking water flow through the xylem (Atwell et al, 1999). A comparison between the internal structure of a rice xylem vessel and the silica structure obtained from acid digestion of a rice plant confirms the identity of these silica structures as silicified xylem vessels (Fig 5.43).

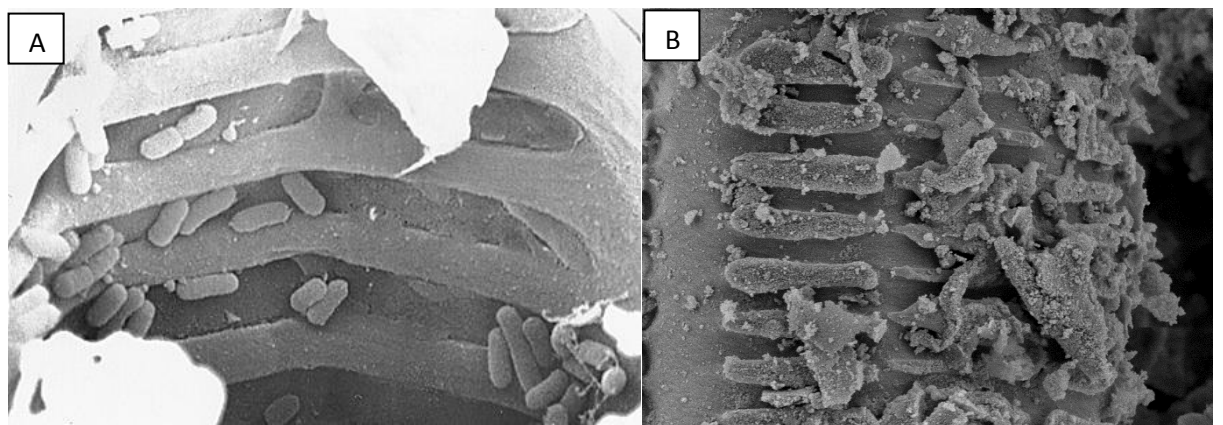


Figure 5.43 Comparison between SEM image of bordered pits in rice xylem (A)(American Phytopathological Society, 2015) and the raised ridges found on silica structures from within the xylem (B).

The presence of silicified xylem vessels in both the wet and dry digests shows that the drying procedure was not responsible for their formation and suggests that these structures are present

in living rice plants. In order to determine if these silica xylem structures were hollow or solid silica, the platform was rotated to give the optimal viewing angle at the edge of a xylem vessel (Fig 5.32). It was not possible to determine if the structure is completely solid, however it can at least be determined that the walls of the xylem are thickly deposited with silica, which would drastically reduce the efficiency with which they could transport water by severely reducing the diameter of the lumen.

It is well established that silicic acid is transported through the xylem up to the surface of the upper plant where it forms silica (Tamai & Ma, 2003). Reported concentrations of silicic acid in the xylem have reached as high as 18 mM in rice, far beyond the 2mM saturation point at which silicic acid usually begins to polymerise into silica at (Mitani et al., 2005). It would be expected that silicification of the xylem vessels would take place and yet it is not considered a known site for silica deposition. The only evidence of silicification of the xylem vessels found previously was in a phytolith study performed on wild rice (Yost & Blinnikov, 2011). Whilst the process for acquiring these phytoliths was not entirely similar to the acid digestion method used in the current study, it does share one important quality, heat.

Acid digestion is performed in a microwave, accelerating the digestion process considerably whilst tissue ashing procedure used in the wild rice study involved both the drying of tissue samples and the subsequent ashing of the organic matter in a muffle furnace at 500°C for six hours (Yost & Blinnikov, 2011). High temperatures have been shown to cause the polymerisation of silicic acid, indeed this method is used to form silica replicas of the inside of xylem vessels in spruce and birch trees (Persson et al., 2004). It is possible that the heat from the digest process is responsible for the formation of the xylem silica structures in the wet digest group, whilst the dry group xylem silica structures are formed as was first suspected; a combination of the evaporation of water and heat of the incubator during the drying process.

Given the limitations that having such a heavily silicified xylem system would have on a living rice plant, it seems almost impossible that xylem vessels could be silicified to the extent we have seen evidence for here. Whilst the drying procedure has been ruled out as the sole cause of xylem silica structure formation, other less-avoidable steps in the acid digestion procedure could be responsible for their formation. A slow, none-microwave assisted acid digestion program would be the next logical course of action with regards to determining the origin of these xylem silica structures.

6. Investigation into Silicic Acid Uptake in Rice

6.1 Introduction

Not all plants are silicon accumulators, and those that are accumulate silicon at different rates.

Any plant which accumulates silicon does so via the uptake of silicic acid, $\text{Si}(\text{OH})_4$, from the soil solution, after which the silicic acid is translocated throughout the plant to various sites of deposition (Currie & Perry, 2007). It has been proposed that there are three uptake methods which plants can employ – active, passive or rejective – and that these uptake methods determine whether a plant is a silicon accumulator or not (Takahashi et al., 1990).

Passive transport occurs via diffusion of a solute across the lipid component of cell membranes from an area of high concentration on one side of the membrane to an area of low concentration on the opposite side (Raven, 2001). Active uptake is recognised as the movement of silicic acid from an area of lower concentration to an area of high concentration via an energy dependent process. Rejective uptake refers to uptake in which a plant actively rejects some or all of the silicic acid in the solution, taking it up at a lower rate than its concentration within the external solution.

Rejective can immediately be ruled out as a contender for silicic acid in rice due to its significant levels of silica accumulation, which leaves active and passive. Again, given the accumulation of silica, active uptake seems to be the obvious answer but silica accumulation at such high levels, up to 10% shoot dry weight in some cases, is possible through passive transport (Epstein, 1994).

However, silica accumulation within plant tissue is not reliant on active transport and can in fact occur through purely passive uptake of silicic acid.

Several silica transporters have been reported in recent years, such as proteins in the aquaporin family which appear to be involved in silicic acid transport. The aquaporin Lsi1 was found to be expressed primarily in the roots of rice and its suppression via RNA interference led to a reduction in silicic acid uptake, whilst not affecting water transport (Ma et al., 2006). That water's uptake is

unaffected by the aquaporin's suppression, but silicic acid's uptake is, which lends credence to the theory that Lsi1 is a transporter for silicic acid and not a channel which water can pass through that silicic acid follows.

Sadly the data for water transport is not shown, but the claim that water transport between the control group and the Lsi1-suppressed plants was unchanged is not unexpected, for several reasons. A recent study identified 34 separate aquaporins in rice, and it is not unreasonable to expect there are more than that (Nguyen et al., 2013). If, for example, only three of these aquaporins are permeable to silicic acid and one of them is suppressed, a noticeable decrease in silicic acid uptake would be observable; a 33% decrease assuming all three silicic acid permeable aquaporins are equal. However, if all 34 aquaporins allowed the movement of water then the decrease in water uptake would be much lower (around 2.9%) which is much harder to detect, especially between multiple plants whose uptake of water would vary considerably between individuals. Whilst there is no doubt that Lsi1 is an aquaporin permeable to silicic acid, there is yet no evidence to suggest that it is anything more than a passive transport channel of water which allows silicic acid through as well.

Under regular conditions, silicic acid will not polymerise into silica unless it reaches a saturation point, a concentration of around 2 mM. However, silicic acid follows the transpiration stream and as such reaches its terminus at the leaf surface, whereupon the water from the xylem sap will evaporate but the silicic acid will not, eventually leading to the 2 mM silicic acid concentration required for polymerisation. Even without the silicic acid concentration hitting the saturation point, silicic acid could still polymerise into silica with the assistance of other compounds found at the leaf surface. It was recently shown that major sites of silica deposition in horsetail mirror the known locations of callose, a hemicellulose found in plant cell walls (Law & Exley, 2011).

Different methods have been used to determine that silicic acid uptake in silicon accumulating plants is achieved via active transport rather than passive, with measuring the silicic acid content

of the xylem used in several studies (Casey et al., 2003; Mitani et al., 2005). Many studies neglect the simplest method of determining the uptake rate of a solute in a solution though: measuring the concentration of that solute in the external solution over time.

To determine whether the transport of silicic acid into rice through the roots is achieved by passive or active transport, a simple experiment was devised. If silicic acid is taken into the plant through active transport then the concentration of silicic acid in the external growth solution would be expected to fall over time. Conversely, if silicic acid is taken into the roots passively along with water, then the concentration of silicic acid in the solution should remain constant over time even as its volume decreases due to the plant taking water up through transpiration. Though not expected for rice, a known silicon accumulator, the third possibility would be an increase in silicon concentration, which would suggest rejective uptake.

Evaporation of water from the growth solution's surface would alter the result of these readings, seemingly elevating the silicic acid concentration over time as water was removed. To address this issue a thin layer of oil was used to cover the surface of the growth solution, preventing evaporation from the solution's surface. Several oils were tested for their ability to block evaporation of water, along with ensuring the oils themselves did not leach silicon into the solution. The four oils tested were linseed oil, rapeseed oil, mineral oil and liquid paraffin.

6.2 Materials and Method

6.2.1 Oil Suitability Tests: Evaporation Prevention and Silicon Leaching

The oil used in the final experiment would need to prevent evaporation from the surface of the solution it covered as efficiently as possible. It was also important to determine which of the oils would leach the lowest amount of silicon into a solution it was in contact with. To this end, a simple preliminary experiment was devised.

25 plastic 15 mL capacity tubes were used and split into five groups with five replicates in each group: control (no oil), linseed oil, rapeseed oil, mineral oil and liquid paraffin. Each of the 15 mL sample tubes were filled with 15 mL 500 μ M calcium chloride (CaCl_2) solution with 0.1 mM silicic acid ($\text{Si}(\text{OH})_4$). Samples were sealed and allowed to rest for 30 minutes. After this time, a 5 mL sample was taken from each tube and stored for analysis of silicon concentration analysis via GFAAS (see section 2.4).

2 mL of the appropriate oil was then pipetted onto the surface of the CaCl_2 solution, ensuring it formed a layer completely covering the solution. The control layer did not have any oil covering it.

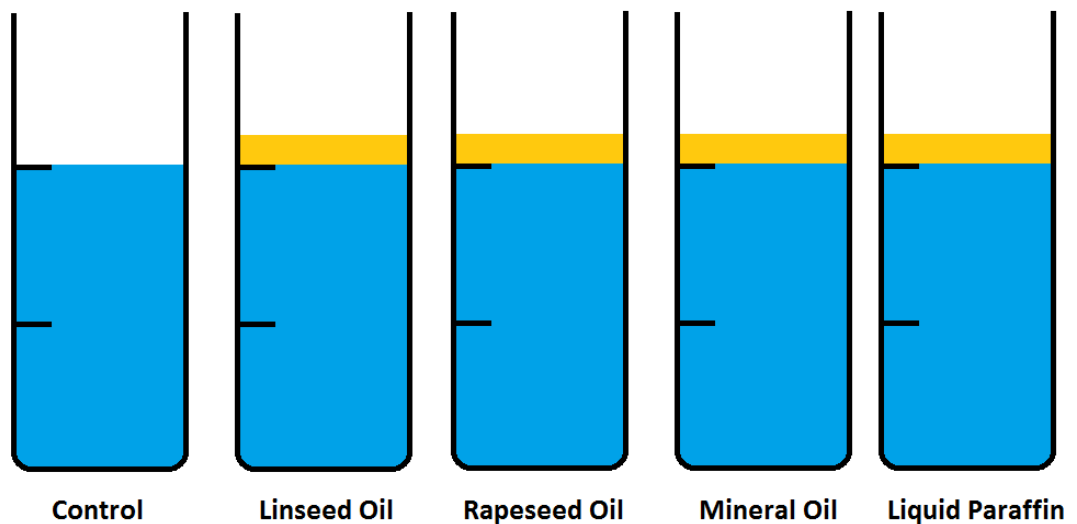


Figure 6.1 Diagram showing the experimental setup for the oil suitability tests.

Each sample tube was then weighed and the water level within the tube for both the solution and the oil layer were recorded. The tubes were then placed under a fluorescent growth light for seven days. After seven days, the sample tubes had their water levels measured and were weighed again. A negative change in weight or water level would mean that water was lost from the tube via evaporation.

Once weighed, the oil layer was removed and a 5 mL sample was taken from each of the tubes for silicon concentration analysis via GFAAS (see section 2.4) and Molybdenum Blue Assay (see section 2.5).

6.2.2 Transpiration Experiment

This experiment consisted of 20 plastic 15 mL capacity tubes separated into two groups: plant and control. Tubes from both groups were filled with 10 mL 500 μM CaCl_2 solution containing 1 mM $\text{Si}(\text{OH})_4$. Tubes from the control group then had 2 mL of linseed oil pipetted onto the surface of the solution, ensuring complete coverage.

Tubes from the plant group each had a single rice plant added to the tube, ensuring the roots were completely submerged. Rice plants were grown hydroponically to an age of one month for use in this experiment. Rice was grown in silicon replete conditions in the presence of 2 mM silicic acid. For full details on hydroponic growth setup, see section 2.1 Hydroponic Rice Culture. With the plants in place, 2 mL of linseed oil was pipetted onto the surface of the solution, ensuring complete coverage whilst minimising the oil's contact with the plant.

Finally, three samples were taken from the remaining CaCl_2 stock solution for silicon concentration measurement via molybdenum blue assay. These samples served as a baseline result for the solution's silicon concentration before the experiment began. The control and plant groups were then weighed and the water level observed and recorded before being moved under a fluorescent growth light where they were left for five days.

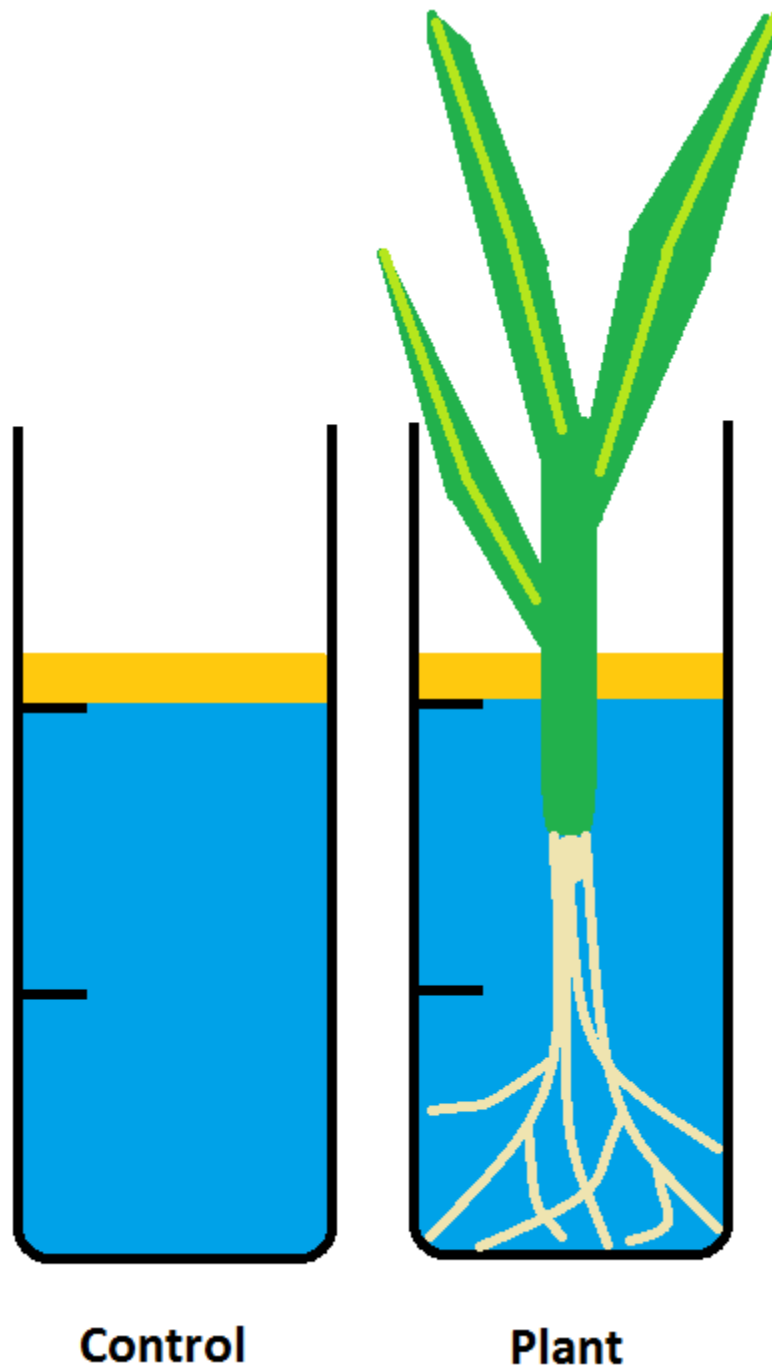


Fig 6.2 Diagram showing experimental setup of transpiration experiment. Control group consists of CaCl₂ solution with 1 mM silicic acid covered with a 2 mL layer of linseed oil. Plant group was identical except for the presence of a one month old rice plant which was submerged past root level into the solution.

After five days the control and plant tubes were once again weighed and had their water levels observed and recorded. The oil layer was removed via pipetting and samples of the CaCl₂ solution were taken from each tube in both the control and plant groups for silicon concentration analysis via molybdenum blue assay.

6.3 Results

6.3.1 Oil Suitability Tests: Evaporation Prevention

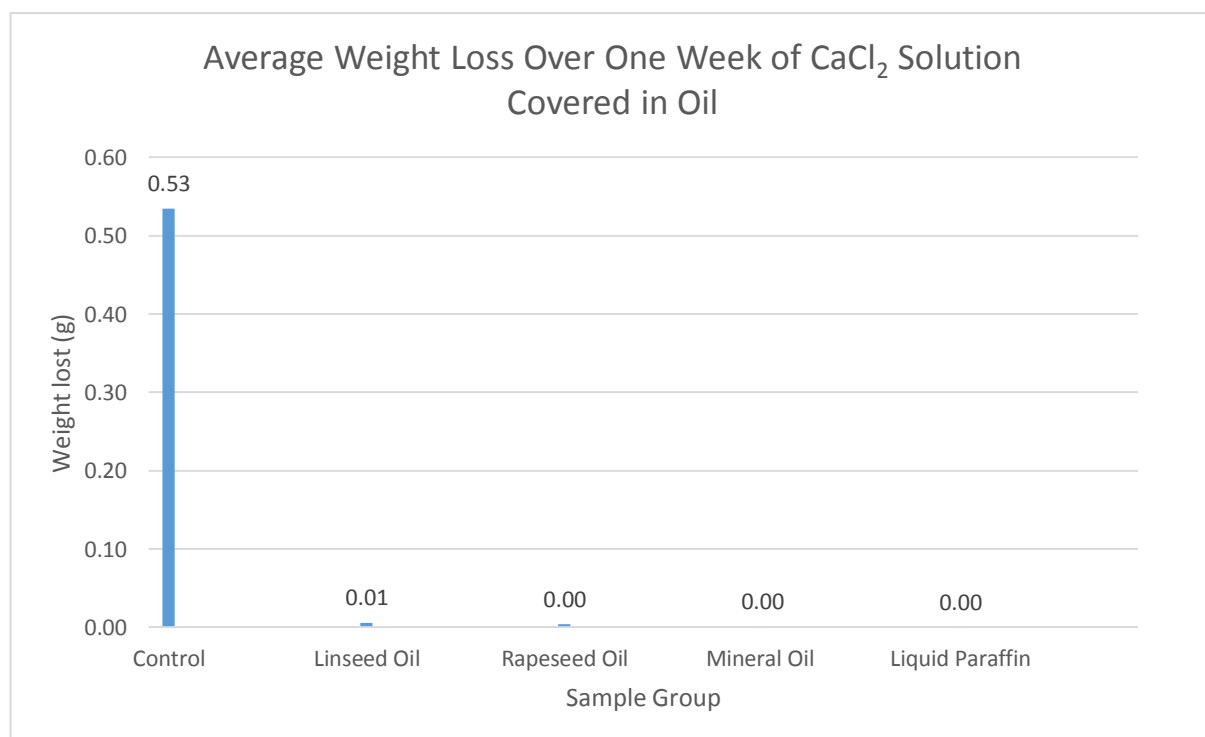


Figure 6.3 Graph showing the average weight loss of sample tubes filled with CaCl₂ solution. The loss in weight represents the loss of water via evaporation.

The control group lost 0.53 g in weight over the course of one week through evaporation. Linseed oil groups showed a negligible change in weight over the same period of time, only 0.01 g. The other three oils – rapeseed oil, mineral oil and liquid paraffin – showed no change in weight at all (Fig 6.3).

6.3.2 Oil Suitability Tests: Silicon Leaching

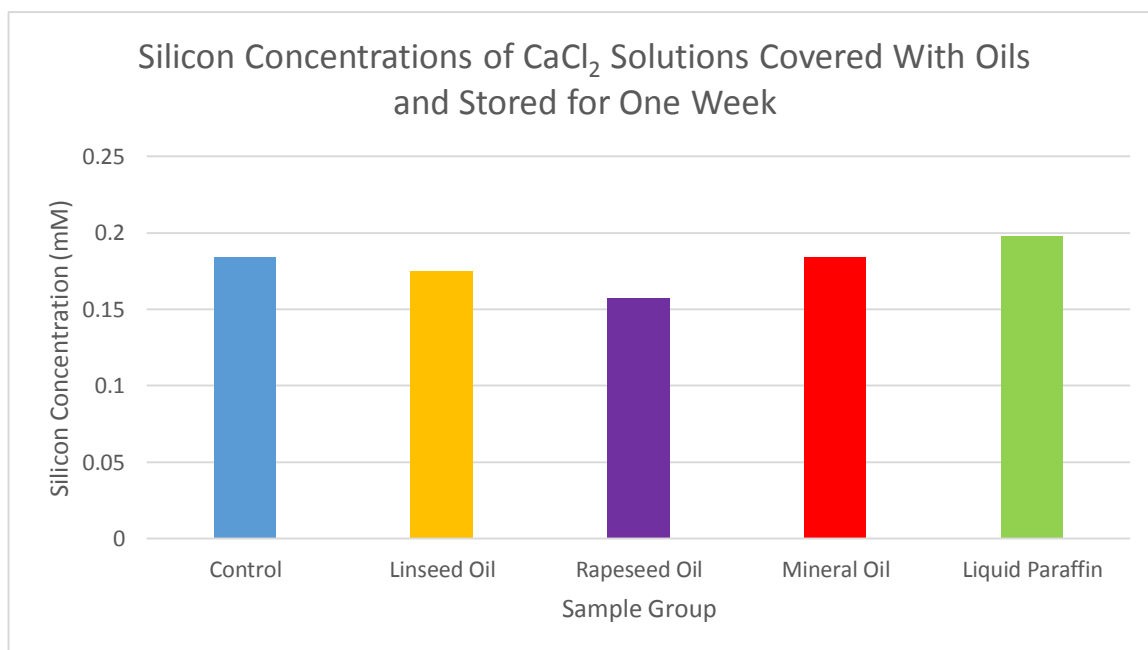


Figure 6.4 Graph showing silicon concentration of CaCl_2 solutions covered with various oils. The control group was not covered with oil. Linseed oil, rapeseed oil, mineral oil and liquid paraffin were used to cover the other four solutions.

Though no silicon was added to the CaCl_2 solutions in this experiment, silicon's presence can still be detected in low levels due to its rather ubiquitous nature; though not listed as an ingredient in CaCl_2 , silicon can still be found as a low level contaminant. The control group represents a solution that had no contact with an oil, which gave a silicon concentration of 0.18 mM. Linseed oil, mineral oil and liquid paraffin were all within 0.01 mM of this reading, whilst rapeseed oil showed a lower silicon concentration of 0.15 mM (Fig 6.4).

6.3.3 Oil Properties and Selection

In addition to its properties with regards to evaporation prevention and silicon leaching, other considerations were made when choosing an oil to use in the transpiration experiment. The viscosity of the oil affected how easy the substance was to pipette, with the more viscous oils dripping from the pipette almost immediately after uptake. Linseed oil was found to be the least viscous and therefore the easiest to work with from a pipetting standpoint.

All of the oils used showed negligible evidence of allowing evaporation to pass through it (Fig 6.3) and no evidence of leaching silicon into a solution it is placed in contact with (Fig 6.4). Whilst all of the oils were equal in these qualities, linseed oil was found to be the easiest to work with due to its lower viscosity when compared with the others. As a result, linseed oil was used in the transpiration experiment.

6.3.4 Transpiration Experiment

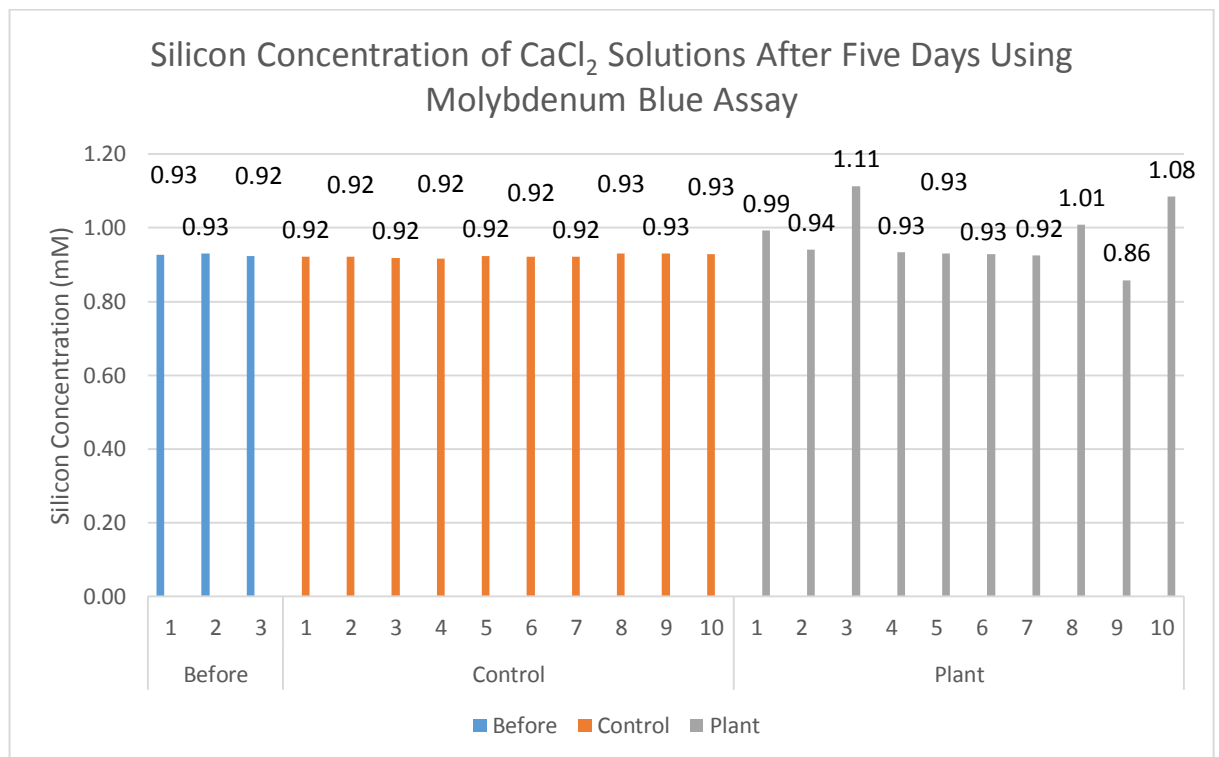


Fig 6.3 Graph showing the silicon concentrations of CaCl_2 solutions from three groups. 'Before' represents samples of the solution taken before the experiment. 'Control' represents CaCl_2 solutions covered with linseed oil. 'Plant' represents CaCl_2 solutions with a rice plant submerged to the stem in the solution and the solution covered with linseed oil.

All sample groups used a $500 \mu\text{M}$ CaCl_2 solution with 1 mM silicic acid added, of which one batch was created and used for all sample groups. The before group represents three separate samples of this solution which were taken before the experiment began to identify the solution's silicon concentration before the experiment began. All three samples within the before sample group gave a consistent reading of $0.92/0.93 \text{ mM}$ silicon concentration before the experiment began (Fig 6.3 – see before group).

The control group had its CaCl_2 solution covered with a layer of linseed oil, but did not contain a rice plant. The control group mirrored the before group, giving consistent readings of 0.92/0.93 mM silicon concentration across all samples, showing no change in silicon levels after five days (Fig 6.3 – see control group).

The plant group had a one month old rice plant placed root deep into the CaCl_2 solution and it was covered with a layer of linseed oil. This group showed more variation, with four of the ten samples showing a marked increase in silicon concentration, up to 1.11 mM silicon in the highest sample (Fig 6.3 – see plant group). One sample showed a reduction in silicon concentration, down to 0.86 mM. Half of the sample within the plant group showed silicon concentrations mirroring the before and control group results, between 0.92/0.94 mM.

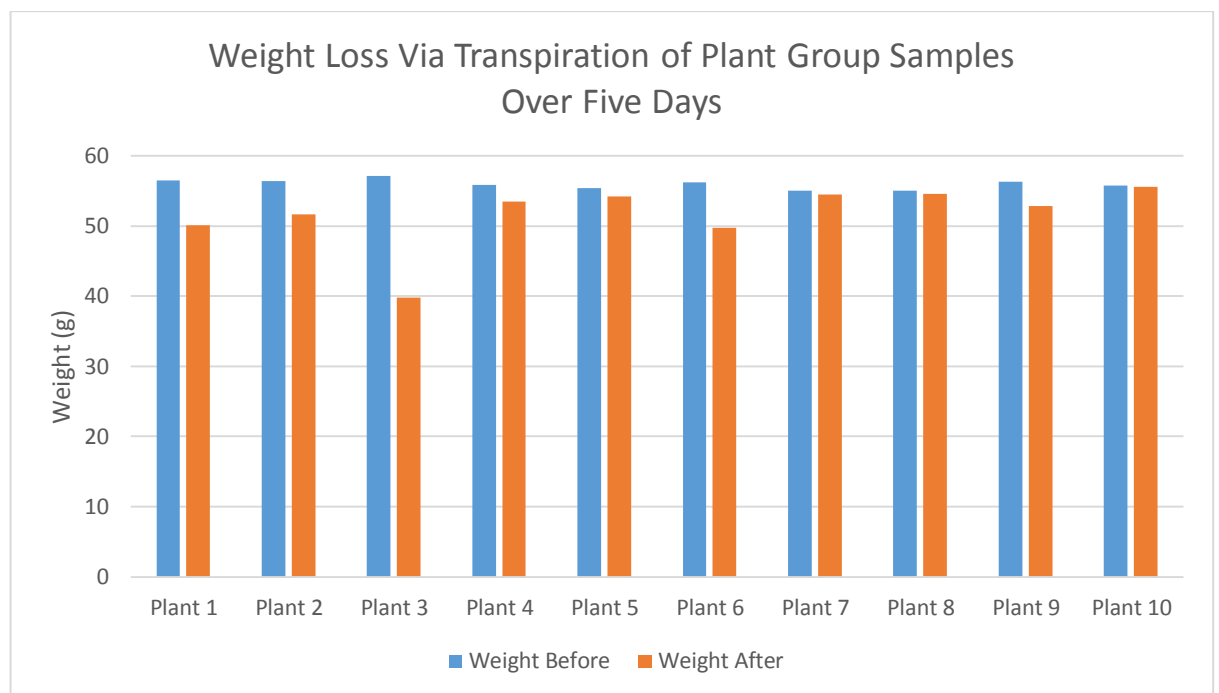


Fig 6.4 Graph showing the weight of sample tubes from the plant group before and after the five day experiment.

The oil layer above the CaCl_2 solution prevents evaporation, therefore any weight loss in the plant group samples is due to transpiration, the plant taking up water before it reaches the leaves and evaporates away there. Despite efforts to ensure that plants used were of the same size and age, the rate of transpiration varies from plant to plant. Weight loss varied from between 0.27 g in

plant 10 to 17.29 g in plant 3 (Fig 6.4). All samples did show a noticeable weight loss, confirming transpiration was taking place in all plants.

6.4 Discussion

In the transpiration experiment, samples taken from the CaCl_2 solution before the experiment showed readings of 0.92/0.93 mM when analysed using a molybdenum blue assay, slightly below the 1 mM concentration that had been aimed for, but consistent at this level (Fig 6.3). The control group showed no variation from the before sample group, with consistent readings for silicic acid at 0.92/0.93 mM. These readings confirm that the presence of the linseed oil layer covering the CaCl_2 solution did not impact the solution's silicic acid concentration.

The plant group showed more variation in its readings: four samples showed a noticeable increase in silicic acid concentration within the solution, five samples showed no marked change and one sample showed a reduction in silicic acid concentration (Fig 6.3). An increase in silicic acid concentration within the solution is an unexpected result with two probable causes. The first explanation for this result could be that these rice plants were taking up silicic acid at a slower rate than water, which would imply some capacity to block silicic acid's passage into the plant. The second explanation is that silicic acid concentrations were higher within the plant than outside it, which caused silicic acid to leach back out of the plant and into the CaCl_2 solution. The rice plants used in this experiment were taken from a growth tank containing 1 mM silicic acid, which could have resulted in the silicic acid concentration within their transpiration stream being higher than that of the 0.92 mM solution outside. In retrospect, growing plants in the absence of silicon before their use in the experiment would have been prudent to avoid this outcome.

Despite the unusual results shown from several of the plants, only one of the ten solutions showed a decrease in silicic acid concentration (Fig 6.3). Plant 9 did show a noticeable decrease in silicic acid concentration down to 0.86 mM which may suggest active uptake of silicic acid. Active transport can be most simply defined as the movement of a substance against a concentration

gradient, from an area of lower concentration to higher (Datnoff et al., 2001). If rice plants take up silicic acid via active transport against a concentration gradient, then a decrease in silicic acid concentration within the growth solution would be expected over time, a result only observed in one sample out of ten.

The weight change data for samples before and after the five day experiment shows that all ten of the plant group samples lost weight, though to varying degrees (Fig 6.4). No plant tissue was observed to have fallen from any of the sample groups and the oil layer prevents the loss of water via evaporation, leading to the conclusion that all ten plants took up the solution via transpiration. The variance in weight loss, and by extension the rate of transpiration, within the plants can be attributed to the variances between individual rice plants. Whilst all rice plants were of the same age, and plants of a similar size were chosen for the experiment, their root systems varied in size more extensively than their shoots. Regardless of these variances, all the plants were transpiring during the experiment meaning they were capable of taking up not only water but also silicic acid.

It is often taken as fact that for a plant like rice to accumulate such large quantities of silica that the uptake and transport of silicic acid into and through the plant must be the result of an active transport mechanism. However, the saturation and subsequent polymerisation of silicic acid into silica does not necessarily require the active uptake of silicic acid. Silicic acid following water up the transpiration stream will invariably accumulate at the transpiration stream's terminus, the leaf surface. Whilst the water will then evaporate from the leaf's surface, the silicic acid will remain and accumulate until it reaches its saturation point of 2 mM, at which point it will polymerise into silica (Ma et al., 2001). This silica formation will in turn reduce the silicic acid concentration in the xylem of the upper plant, maintaining a concentration gradient which brings a continuous flow of silicic acid up the xylem to the leaves.

Other researchers have found evidence of active transport of silicic acid in rice through other means, such as investigating the silicic acid concentrations present in freshly extracted xylem sap.

One study showed that silicic acid levels within the xylem of rice plants reached 18 mM after just 30 minutes exposure to a 0.5 mM silicic acid solution (Mitani et al., 2005). No evidence of any compounds which could prevent the polymerisation of silicic acid within the xylem was found. Once removed from the xylem, the silicic acid concentration within the xylem sap began to fall, though the total silicon content did not, suggesting that silicic acid began to polymerise into silica after being removed from the xylem. It was also confirmed that monosilicic acid was the only form of silicon detected within the xylem sap, disproving the hypothesis that silicic acid is converted into another form during its transport through the xylem. Such high levels of silicic acid within the xylem could only be the result of active transport, though several questions remain over these findings.

A similar study was performed on wheat, another crop plant which is known to accumulate silica, and it was found that the xylem sap contained in excess of 8 mM silicic acid, far above the 0.02 mM concentration of the growth solution after only 30 minutes exposure (Casey et al., 2003). This would mean that silicic acid concentrations within wheat would be 400 times higher than that of the external solution and as the researchers themselves point out, the uptake ratios would be even higher than that because of the progressive depletion of the silicic acid in the solution. Uptake rates such as these seen in both the experiments with rice and wheat would result in a rapid decrease in the silicic acid concentration of a solution, a result we did not observe in our own experiments.

Active transport of silicic acid into the plant is not the only explanation for the demonstrated super-saturation of silicic acid seen in both rice and wheat xylem. Whilst silicic acid behaves like water in the same system, it is a significantly larger molecule. As a result, not all channels through which water can flow will allow silicic acid. If 100% of the water channels allow silicic acid into the xylem but only 10% allow it to leave, then silicic acid will accumulate in the xylem. This is because water transport through the xylem is not only regulated by osmosis, but also by hydrostatic

pressure caused by transpiration (Passioura, 2010). In this scenario, water and silicic acid are pulled into the xylem at the same rate, but silicic acid cannot leave at the same rate, resulting in the accumulation of silicic acid over time. The hyper-accumulated silicic acid within the xylem will then begin to diffuse out of the xylem into the surrounding tissue due to the altered concentration gradient now present between the xylem and its exterior.

7. PDMPO Staining of Mature Rice Silica

7.1 Introduction

Rice is a known biosilicifier, taking up silicic acid from the soil and depositing it within its shoot and leaves as amorphous silica (Ueno & Agarie, 2005). The primary site of silica deposition in rice is at the leaves, beneath the cuticle but above the epidermal cells, where silica forms a roughly 2.5 μm thick layer over the surface of the leaf (Yoshida, 1965). Other sites of prominent silicification are at the silica cells and bulliform cells, both of which are completely silicified, unlike the epidermis which is just covered by a surface layer of silica (Ma, 1990). Silica has been shown to accumulate in the cell walls of guard cells at rice stomata, with the exception of the anticlinal walls adjacent to the subsidiary cells (Ueno & Agarie, 2005).

Various imaging methods are used to study the silica structures found in rice, with the earliest work relying on a mixture of tissue ashing, toluidine blue staining and mounting using a medium of differing refractive index, which resulted in silica being visible under light microscope (Blackman, 1969). This method was somewhat effective, but not specific to silica and could easily flag up false positives for silica detection.

More recently a specific fluorescent tracer for silica was discovered in the form of 2-(4-pyridyl)-5-((4-(2-dimethylaminoethylaminocarbonyl)methoxy)phenyl)oxazole (PDMPO) which was found to bind with silica and give off a bright green fluorescence (Shimizu et al., 2001). PDMPO has been used in numerous studies to stain for silica in diatoms (Shimizu et al., 2001; Znachor & Nedoma, 2008; Leng et al., 2015). Whilst investigating silicification in horsetail (*Equisetum arvense*), PDMPO was used to stain silica obtained from hydroponically grown plant tissue via microwave acid digestion and subsequent filtration (Law & Exley, 2011). This is the first, and at time of writing, only published case of PDMPO being used to study biogenic silica which originated within plant tissue.

Aluminium toxicity is a major limiting factor in crop production, inhibiting root growth and nutrient uptake for plants grown in acidic soils, such as those where rice production predominantly takes place (Ma & Takahashi, 2002). However, the presence of silicon, as silicic acid, in the growth solution has been shown to alleviate the toxic effects of aluminium, reducing root growth inhibition (Ma et al., 1997). Silicon and aluminium co-deposition in plant tissue is rare and most cases of colocalisation of the two elements take place in the roots (Hodson & Evans, 1995). PDMPO staining is ill equipped to determine the presence of aluminium in silica structures, however, what it can uncover is changes in the morphology of silica structures deposited in rice tissue after exposure to aluminium, when compared with samples which were not exposed to the toxin.

The aims of this study are threefold:

- To evaluate PDMPO staining and subsequent fluorescence microscopy as a method for identifying silica structures found in rice tissue.
- To analyse biogenic silica structures found in rice, determine their point of origin within the living plant and cross-reference this with known sites of silicon deposition. This will determine if PDMPO staining can reveal anything new about silicification in plants which previous methods have overlooked.
- To determine if the addition of aluminium to a plant's growth solution post silicification results in any alterations to the silica structures found in rice tissue digests.

To this end, several batches of rice plants were grown hydroponically under varying conditions. Once matured, these plants were harvested, acid digested and then stained with PDMPO. The resulting solution was then analysed with fluorescence microscopy and images analysed.

7.2 Method

7.2.1 Hydroponic Growth of Rice Plants

Rice plants were grown hydroponically to an age of six weeks for use in this experiment. Rice was grown in either in the presence or absence of 2 mM silicic acid. A further group of rice plants, taken from the original group grown in the presence of silicic acid, were grown for two weeks in 0.5 mM or 500 μ M CaCl_2 containing 100 μ M aluminium. For full details on hydroponic growth setup, see section 2.1 Hydroponic Rice Culture.

7.2.2 Acid Digestion and Filtration

Once the growth period of six weeks was over, rice plants were harvested. Each plant was separated into stem, leaf and root before being cut into roughly 1 cm sections. The leaf, stem and root sections were then weighed before being stored inside an incubator at 37°C to dry them. The plant samples were periodically weighed until they reached a constant dry weight. At this point, the dried samples were then acid digested using the standard acid digest procedure.

Samples were filtered after digestion to harvest their silica using the standard digest filtration procedure and stored in an incubator at 37°C until the silica was dried. Samples can be stored indefinitely in this state, provided they are kept within the incubator to prevent moisture build-up. For full details on the acid digestion and filtration procedure, see section 2.2 Microwave Acid Digestion and Filtration.

7.2.3 PDMPO Staining

After harvesting and acid digestion, silica samples were stained using 0.125 μ M PDMPO in 20 mM PIPES at pH7 and stored in a refrigerator for 48 hours to allow the fluorophore to bind with the sample. For further details on the PDMPO staining see section 2.2.4 PDMPO Staining.

7.2.4 Fluorescence Microscopy

After the binding period, samples were ready for viewing under fluorescence microscopy. Due to the aqueous nature of the sample, 25 μL of the silica/PDMPO suspension was pipetted into a cavity slide and viewed using an Olympus BX50 with a BXFLA fluorescent lamp. Images were taken under the U-MWU filter cube using a Colourview III digital camera using the CELL imaging software. For further details on fluorescence microscopy see section 2.3 Light & Fluorescence Microscopy.

7.3 Results

The following images were obtained through the PDMPO staining of silica obtained by acid digestion of plants grown under varying conditions. The green fluorescence indicates PDMPO binding with silica. It is important to point out that no organic component of the plant remains; the structures observed are composed entirely of biogenic silica unless otherwise stated.

7.3.1 Silicon Replete Rice

The following images were taken from PDMPO silica digests obtained from the acid digestion of rice plants grown in the presence of added silicic acid.

7.3.1.1 Epidermal Cells

The following images display silica structures from the epidermal layer of silica which covers the leaf in rice. Scale bars are located in the bottom right corner of the images and arrows denote areas of interest, described in the text.

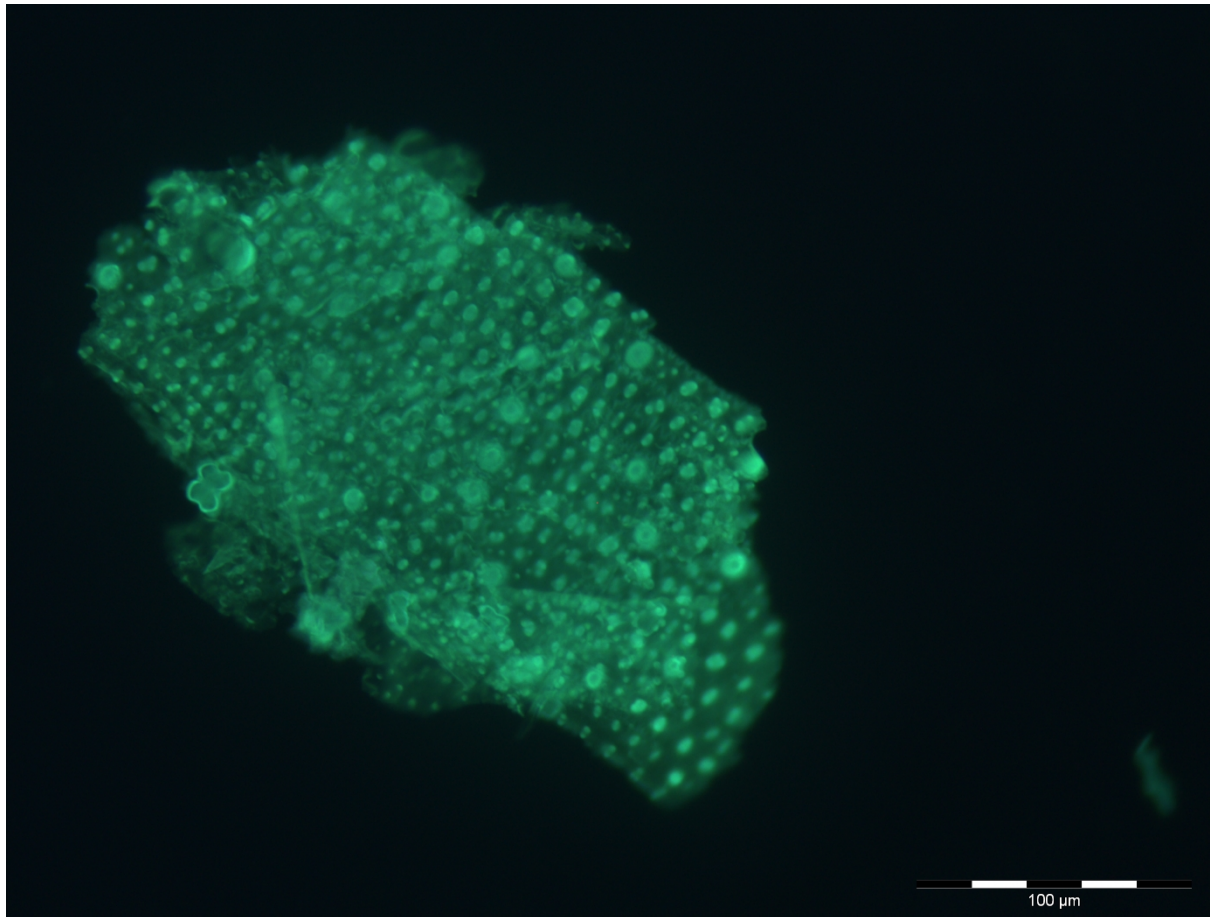


Figure 7.1 PDMPO stained silica from rice leaf epidermis, viewed under fluorescence microscopy. Scale bar is present in the bottom right corner of the image.

The most common large silica structures found in PDMPO staining originate from the leaf epidermis, where large sheets of silica which covered the epidermal cells can be seen (Fig 4.1).

Due to the nature of microscopy and the morphology of the sample only certain areas can be kept in focus in a single image; the focal point of this image is centred on the papilla, the raised nodules which cover the epidermal cells (see red arrows). As a result, the divides between the individual epidermal cells cannot be seen clearly. A silica cell is also visible in this image, affixed to an epidermal cell; this edge likely attached to a ladder-like column of silica cells, however, only a single cell remained attached to this piece (see gold arrow).

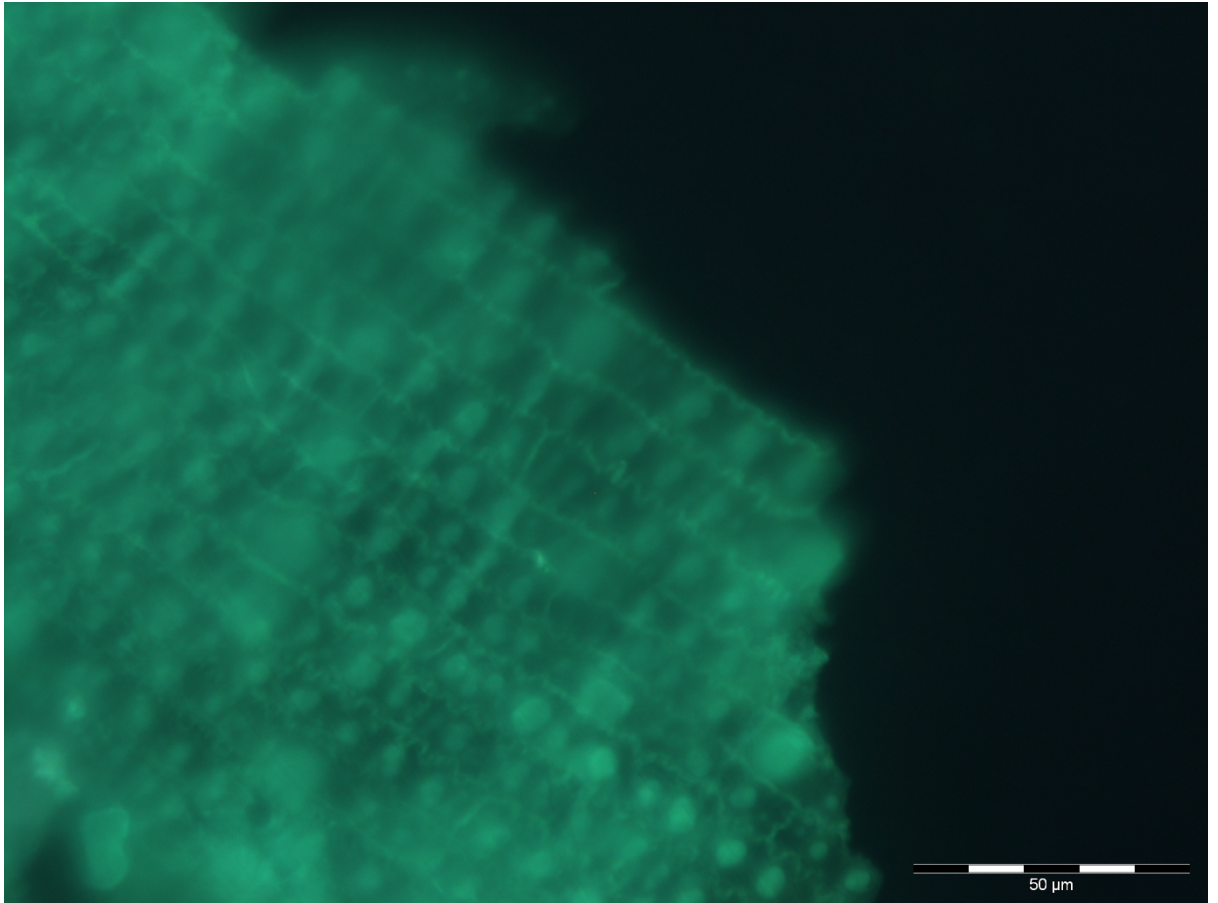


Figure 7.2 PDMPO stained silica from rice leaf epidermis, viewed under fluorescence microscopy. This image is of the same silica fragment as shown in Fig 7.1 but at a higher magnification. Scale bar is present in the bottom right corner of the image.

At a higher magnification and with the focal point of the image adjusted, the individual borders of each epidermal cell in the silica structure can be observed (Fig 7.2). The long edges of each epidermal cell are sinuate, with the peaks and troughs of each wave interlocking with the neighbouring cell (see red arrow). The short edges of each epidermal cell are straight, lacking the sinuate formation of the long edges (see gold arrow). Papilla can still be observed, though they are out of focus (see white arrow). At higher magnifications the strong fluorescence from large silica pieces can create a green haze, resulting in a reduced clarity when compared with lower magnification images.

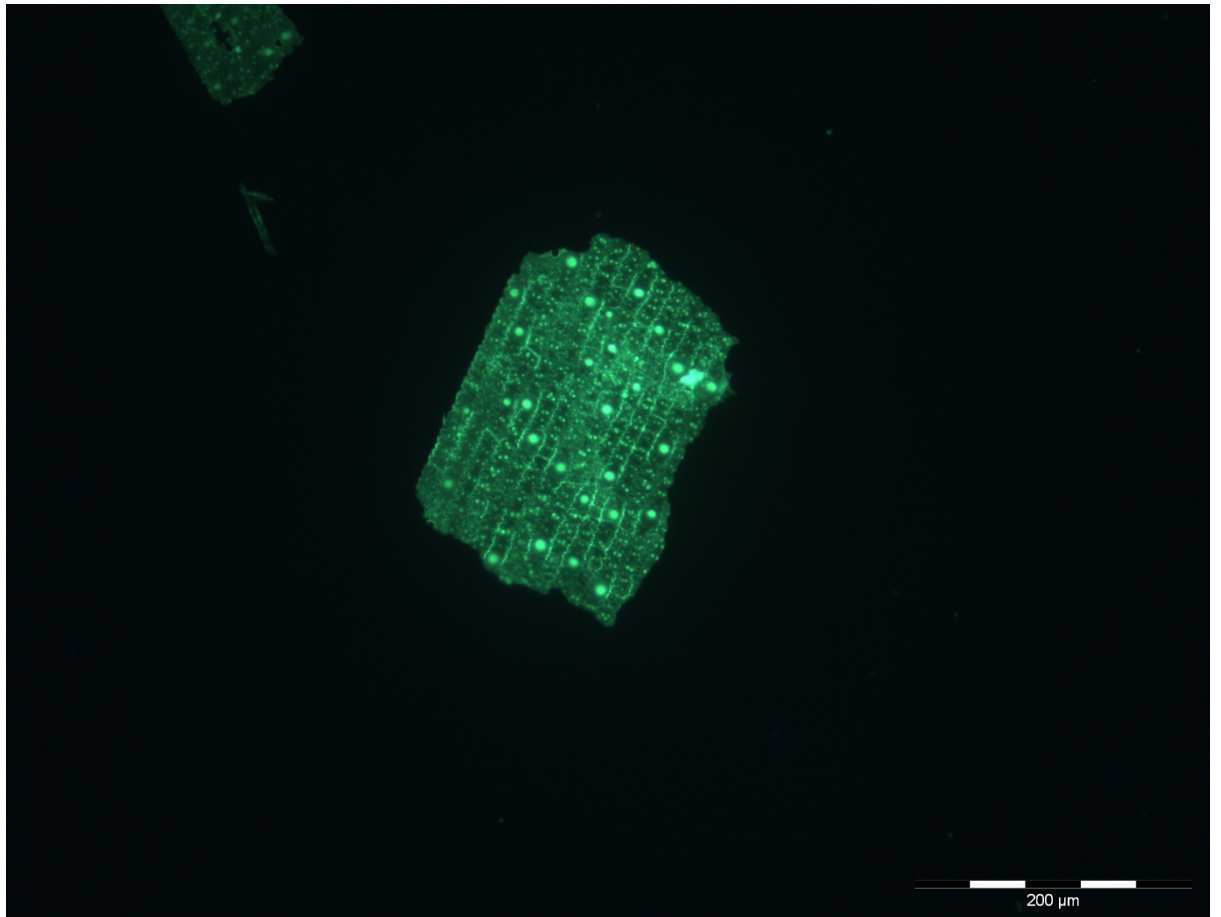


Figure 7.3 PDMPO stained silica from rice leaf epidermis, viewed under fluorescence microscopy. Scale bar is present in the bottom right corner of the image.

The epidermal cells have various types of papilla and nodules which can cover their surface, with various patterns of distribution between them. Smaller papilla are visible along the surface of the cells, running down the length of the epidermal cells in primarily in pairs (see red arrow), but also occasionally as a trio (see gold arrow). Larger nodules are interspersed between the more common papilla, giving off a strong fluorescence signal (see white arrow). The edges of individual epidermal cells are visible, though at lower magnifications it is difficult to observe the sinuate shape.

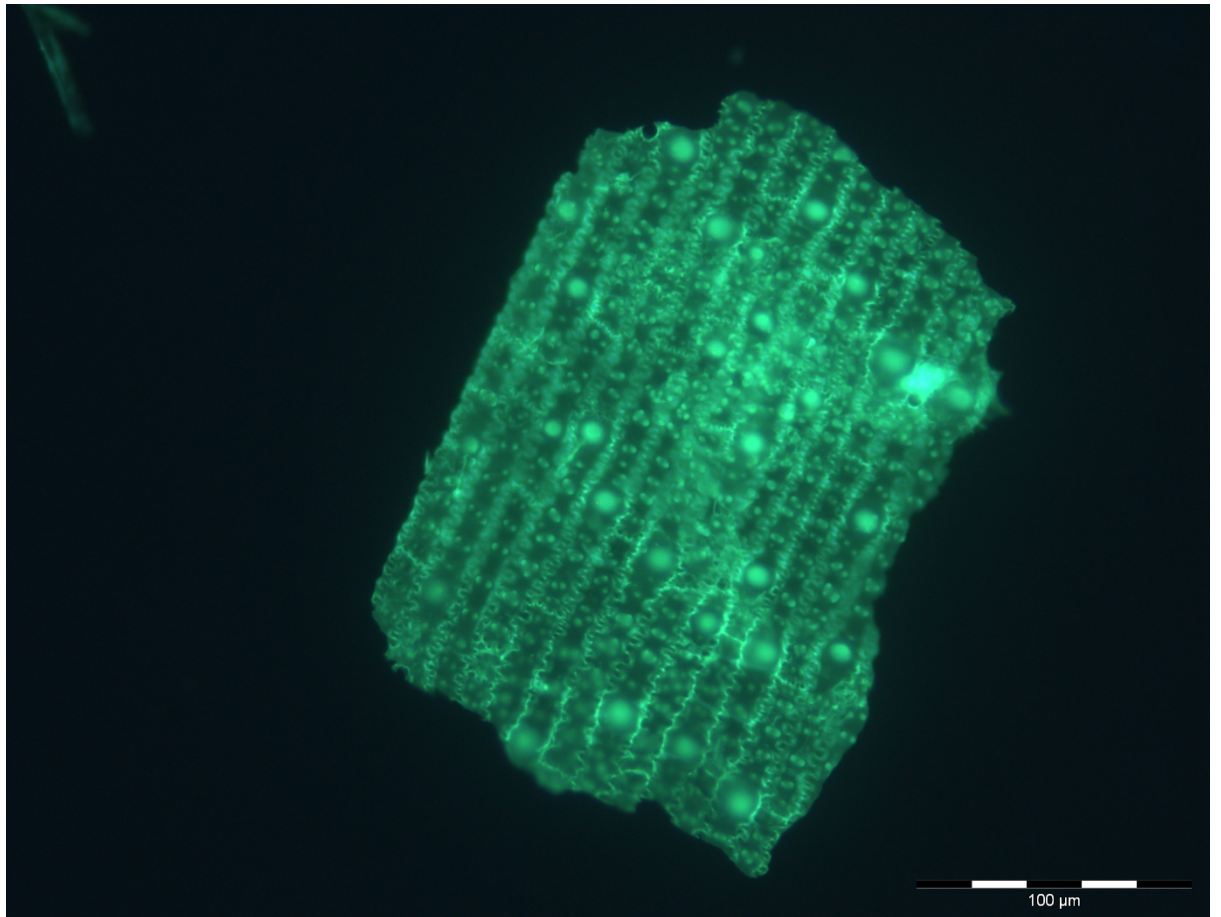


Figure 7.4 PDMPO stained silica from rice leaf epidermis, viewed under fluorescence microscopy. This image is of the same silica fragment as shown in Fig 7.3 but at a higher magnification. Scale bar is present in the bottom right corner of the image.

At higher magnifications the large nodules along the surface of the epidermal cells seem out of focus (this is due to their morphology) (Fig 7.6). They are large, spherical and featureless protrusions of silica which are stained more strongly by PDMPO than the surrounding structures, suggesting a more dense silica deposition at these sites (see red arrow). The regular papilla can be seen clearly, running down the length of the epidermal cells in pairs (see gold arrows) or threes (see white arrows). The interlocking sinuate pattern of the epidermal cells can also be clearly observed at this magnification, showing the almost mosaic-like structure of this silica fragment (see purple arrow). The larger nodules are sufficiently different in morphology to the regular papilla, enough to suggest that they are a different structure altogether.

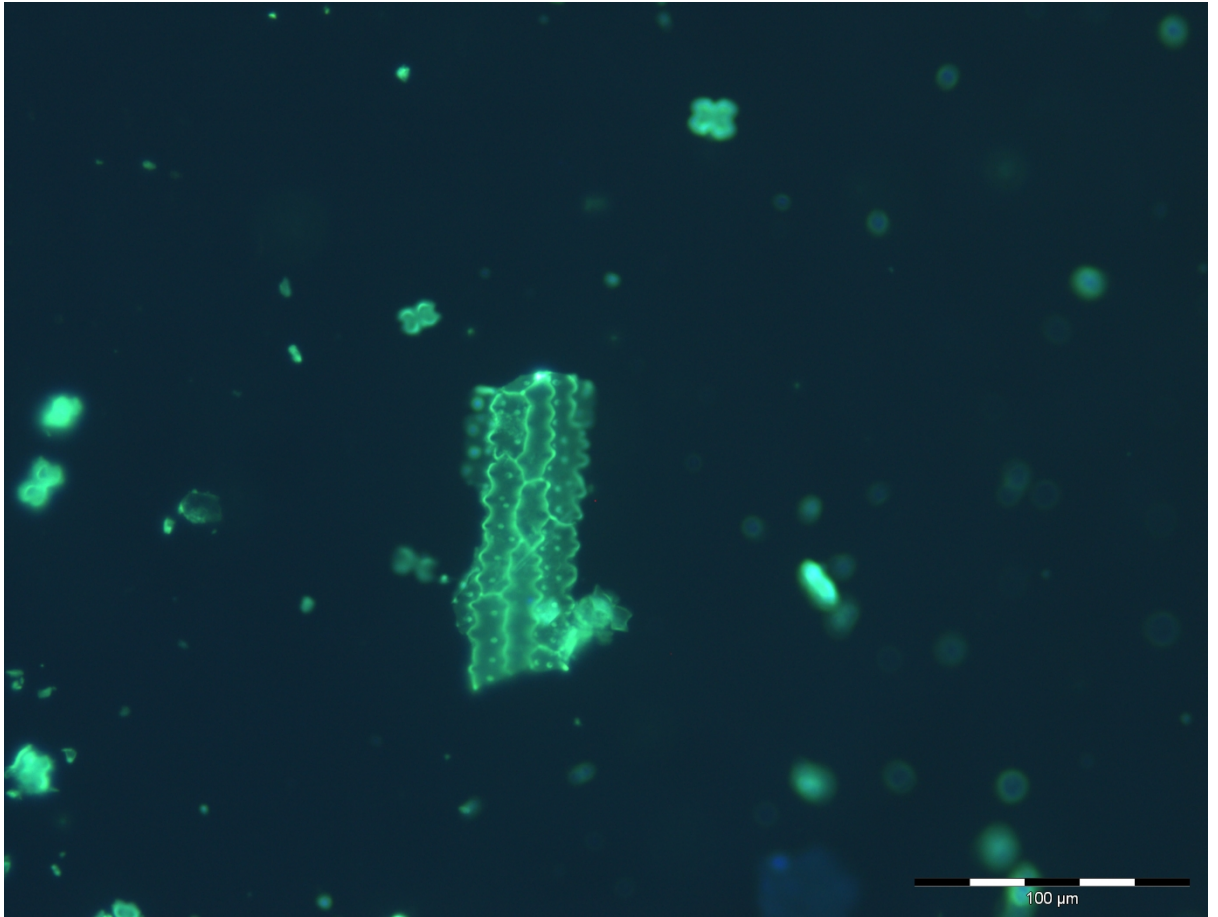


Figure 7.5 PDMPO stained silica from rice leaf epidermis, viewed under fluorescence microscopy. Scale bar is present in the bottom right corner of the image.

Silica structures from the epidermis are not always in such large fragments, with smaller shards of silica often making up much of the sample (Fig 7.5). These smaller fragments of silica can be useful for acquiring more detailed images of the structures, as the reduced fluorescence when compared with larger samples results in a reduction of the green haze seen elsewhere. Several epidermal cells can be observed interlocking, with papilla covering their surface (see red arrows).

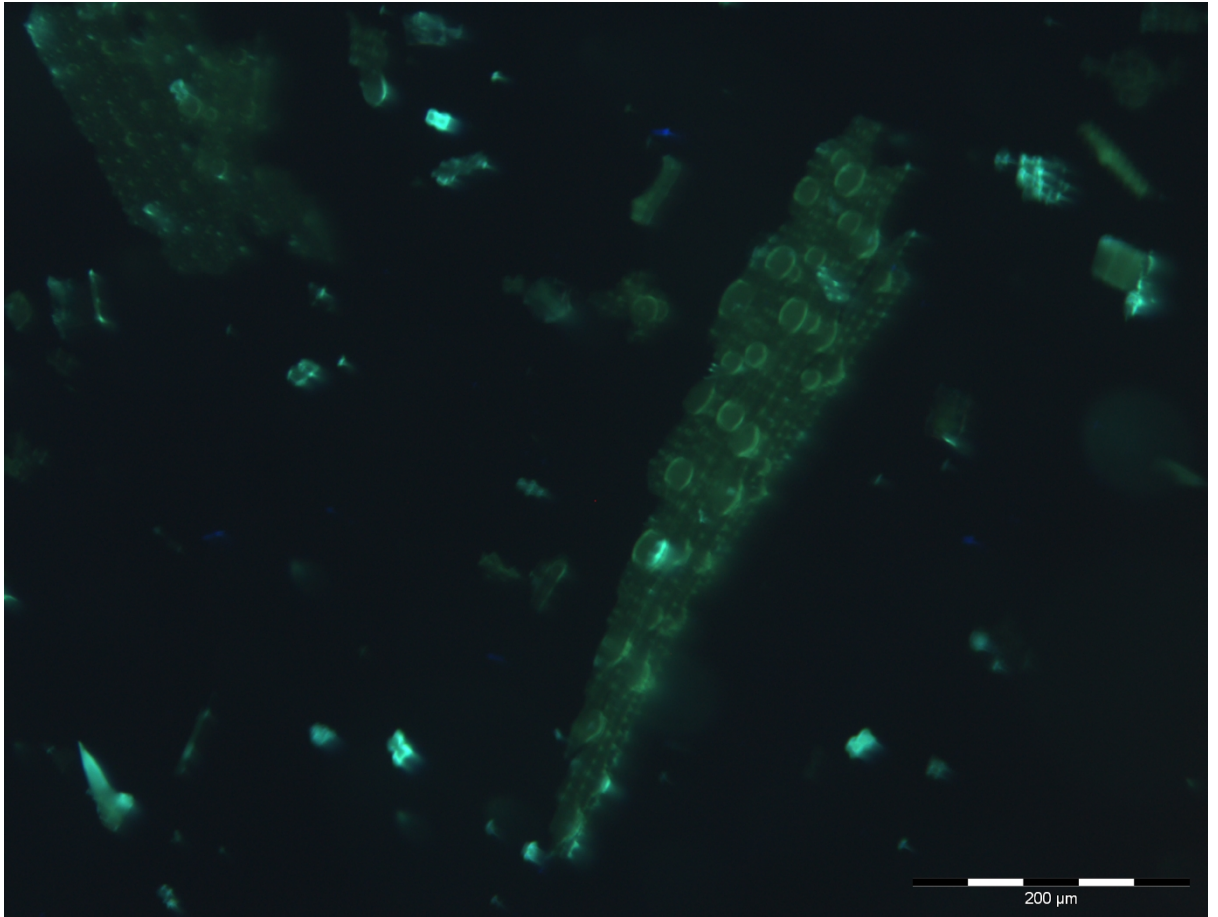


Figure 7.6 PDMPO stained silica from rice leaf epidermis, viewed under fluorescence microscopy. Scale bar is present in the bottom right corner of the image.

As the leaf develops, large nodules begin to appear intermittently along the epidermal cells, taking the place normally occupied by pairs of papilla (Fig 7.6). These nodules can be wider than the epidermal cell beneath them in some cases, causing the epidermal cell to swell around the nodule (see red arrow). The usual rows of papilla can still be seen covering the epidermal cells in between the larger nodules (see gold arrow).

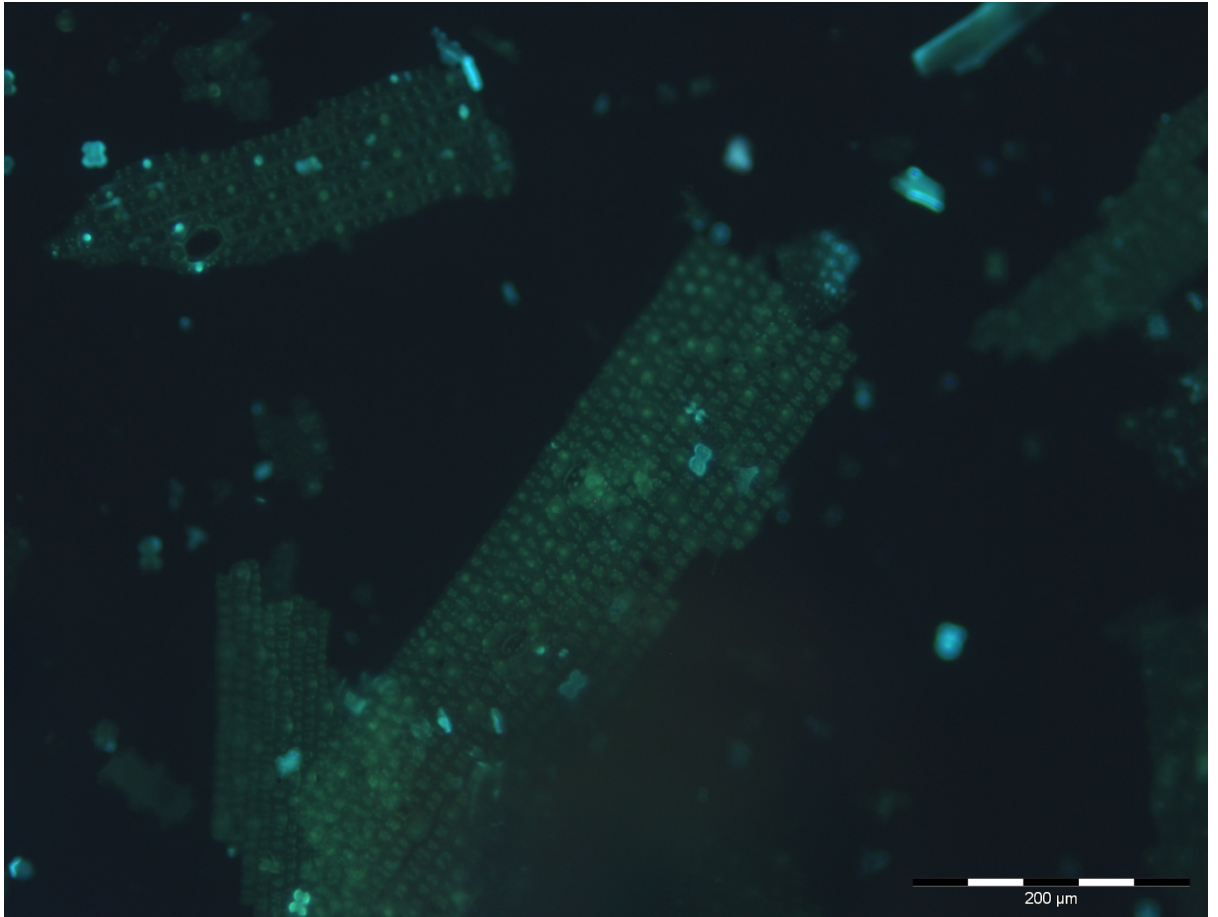


Figure 7.7 PDMPO stained silica from rice leaf epidermis, viewed under fluorescence microscopy. Scale bar is present in the bottom right corner of the image.

Several large epidermal silica structures can be observed with a more varied papilla distribution (Fig 7.7). Whilst papillas were typically seen in pairs or threes in previous samples, there are groupings of four and five papilla present in the largest silica fragment (see red arrow). Several stomata can also be seen within the largest silica sample with the guard cells still visible (see gold arrows). In another silica fragment a large aperture can be seen, this could either be a stomata without its guard cells or possibly the location of a trichome which has become separated from the main silica structure (see white arrow). Several silica cells can also be seen floating above the larger silica fragments (see purple arrows).

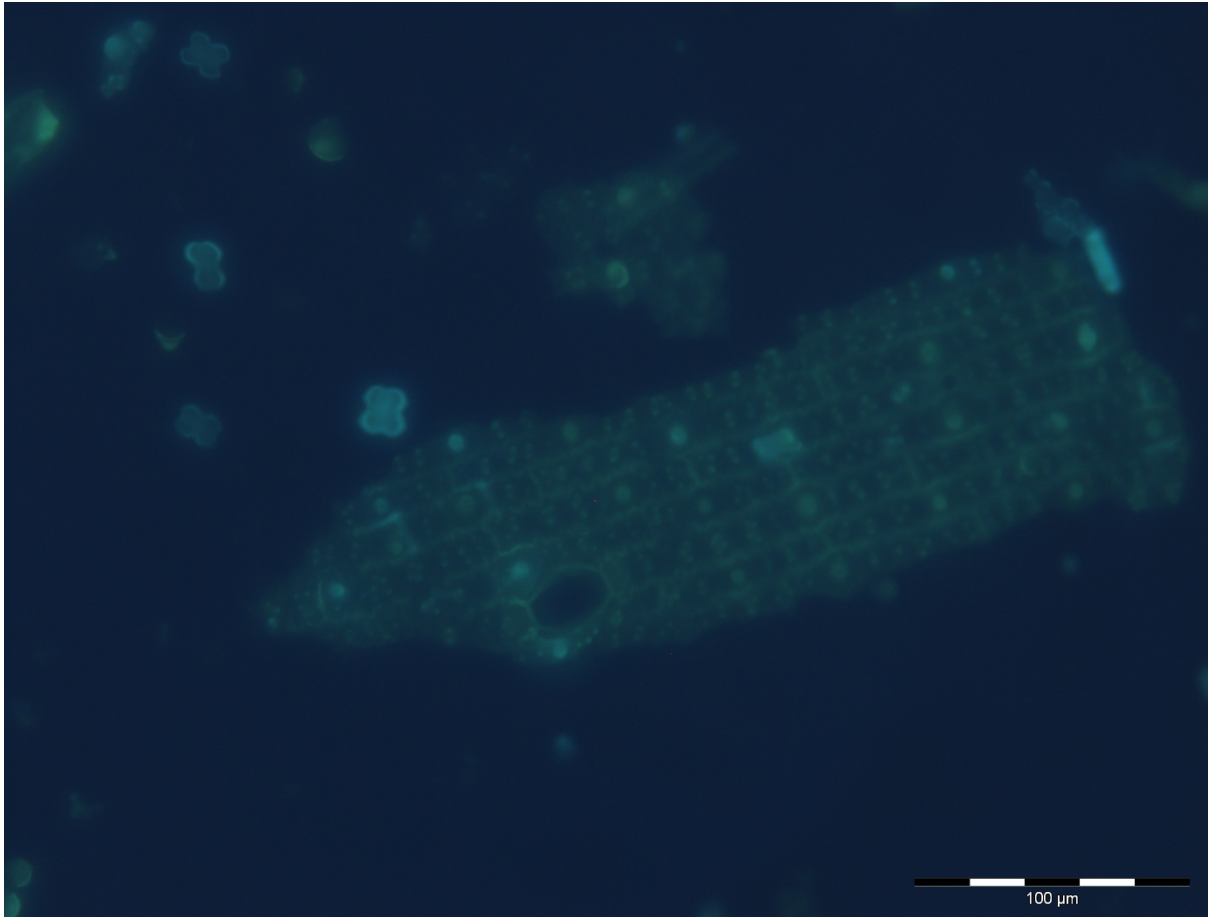


Figure 7.8 PDMPO stained silica from rice leaf epidermis, viewed under fluorescence microscopy. Scale bar is present in the bottom right corner of the image.

At a higher magnification the surrounding cells which form the gap in the silica can be clearly seen (Fig 7.8). Though this gap in the silica appeared to be a stomatal aperture at lower magnification, it can be more clearly identified as where a trichome once sat due to the lack of supporting cells which surround the two main guard cells in a stomata (see red arrow).

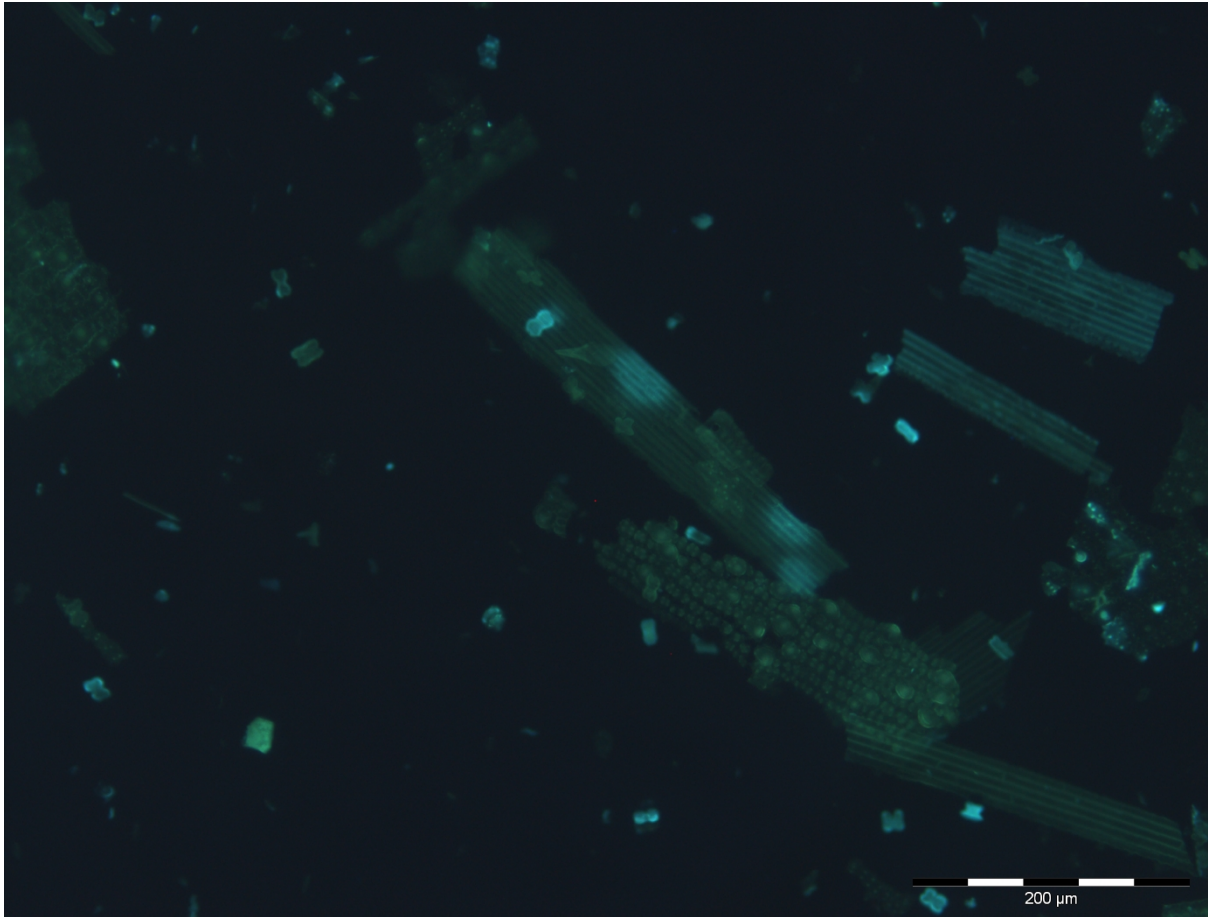


Figure 7.9 PDMPO stained silica from rice leaf epidermis, viewed under fluorescence microscopy. Scale bar is present in the bottom right corner of the image.

In addition to the sinuate epidermal cells, there is also a secondary type of epidermal cell present (Fig 7.9). These secondary epidermal cells are roughly the same size and shape as their primary counterparts, but lack the sinuate edges and papilla which define the primary epidermal cells (see red arrows). Two silica structures consisting of primary epidermal cells are located neighbouring the secondary epidermal cells, providing an excellent juxtaposition of the two structures (see gold arrows).

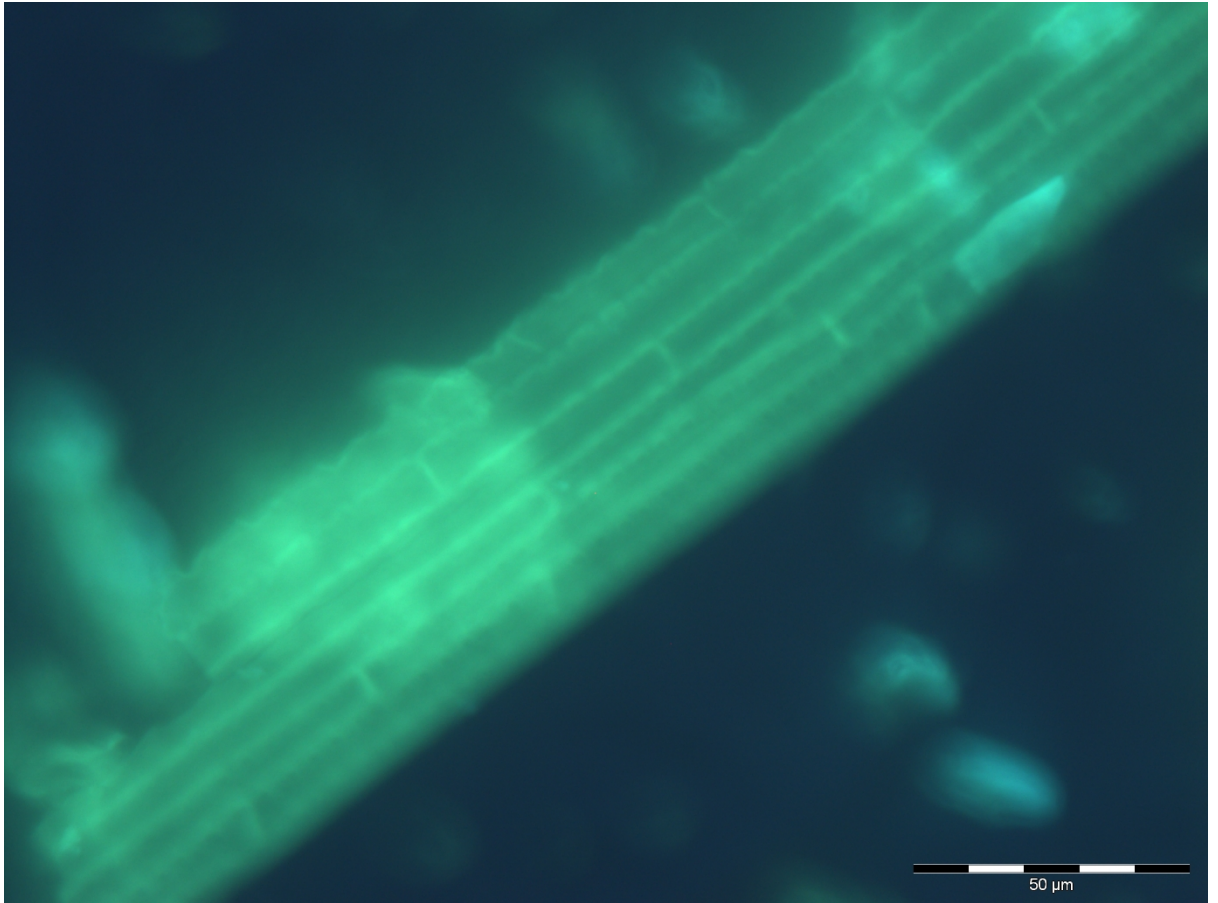


Figure 7.10 PDMPO stained silica from rice leaf epidermis, viewed under fluorescence microscopy. Scale bar is present in the bottom right corner of the image.

When viewed under higher magnifications the secondary epidermal cells are revealed to have more detail in their structure than was first thought (Fig 7.10). The edges of the secondary epidermal cells are not straight as they appeared previously, but rather they share the sinuate shape of the primary epidermal cells but in a much less pronounced manner (see red arrow). Again, due to the high magnification and large silica sample, a green haze from the excess of fluorescence signal in the area removes some clarity from the image, but the details are still clearly visible.

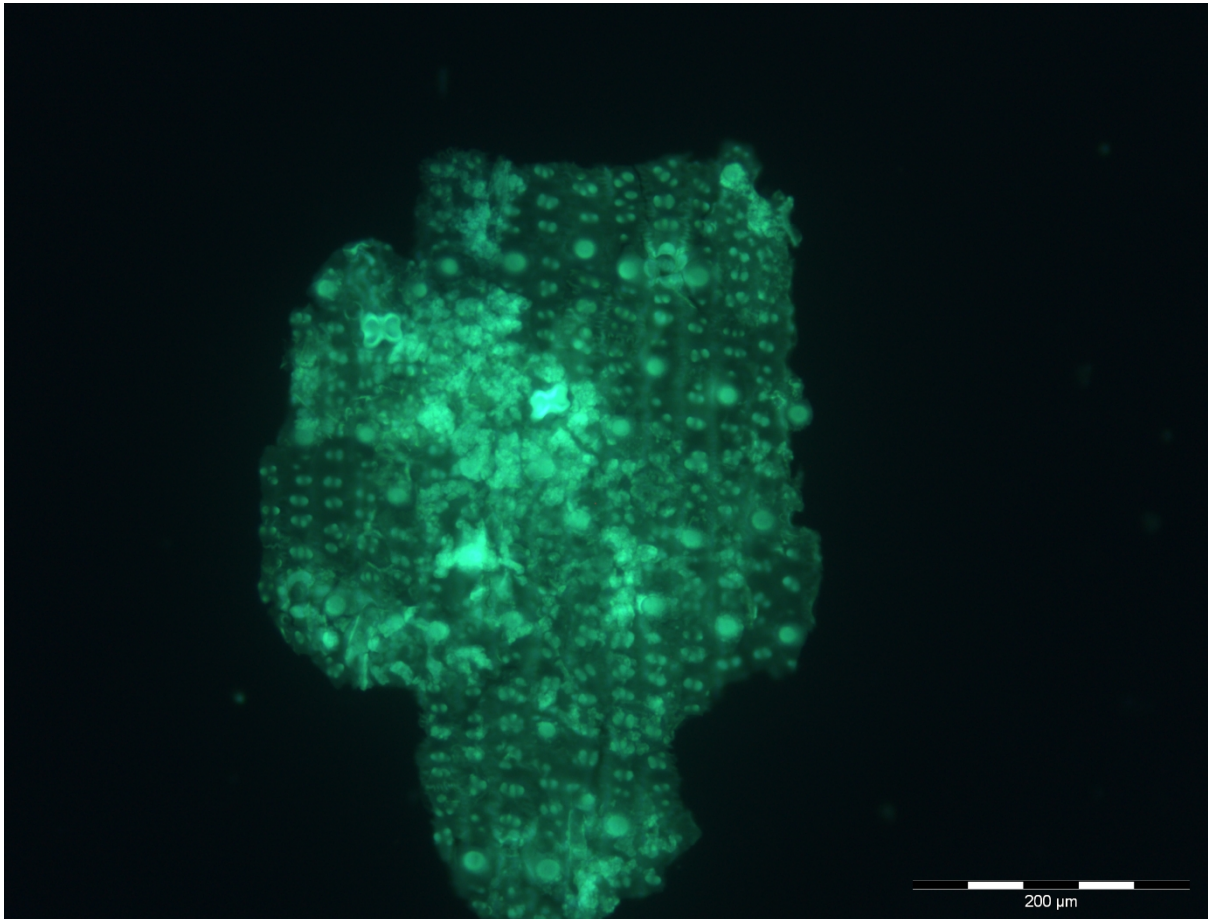


Figure 7.11 PDMPO stained silica from rice leaf epidermis, viewed under fluorescence microscopy. Scale bar is present in the bottom right corner of the image.

Another large fragment of epidermal silica can be seen showcasing the differing types of nodules which cover the epidermal cell surface (Fig 7.11). The most common formation is the papilla, located in pairs or threes running up the length of the epidermal cells (see red arrow). Larger formations of papilla in groups of four or five can be seen, joined at the base by a silica mound. This mound likely appears as increasing amounts of silica are deposited at the papilla causing neighbouring structures to bleed into each other (see gold arrow). Finally the larger, single nodules can be seen interspersed between the papilla with bulbous, featureless surfaces (see white arrow).

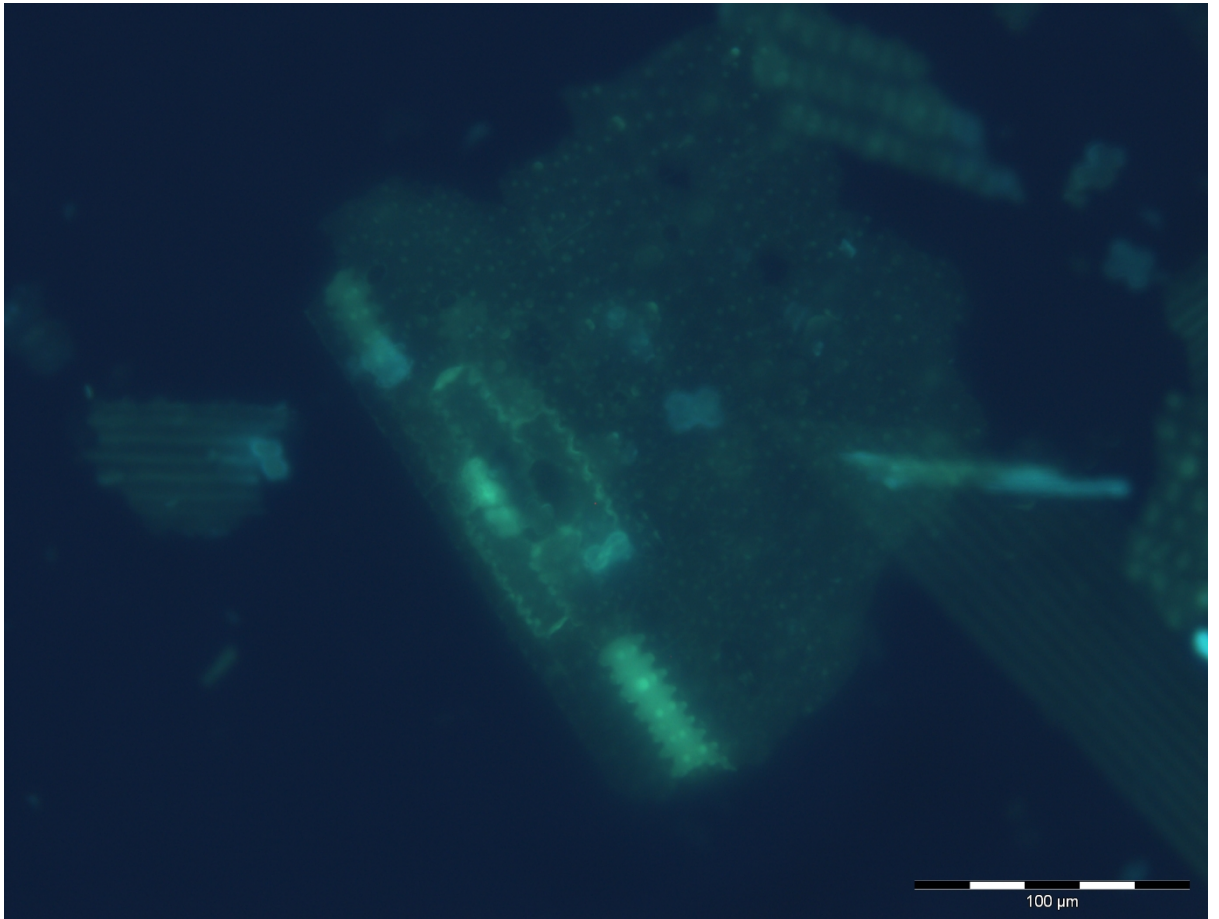


Figure 7.12 PDMPO stained silica from rice leaf epidermis, viewed under fluorescence microscopy. Scale bar is present in the bottom right corner of the image.

Several epidermal cells were observed with much stronger PDMPO staining than the surrounding silica (Fig 7.12). Three neighbouring epidermal cells showed increased PDMPO fluorescence at their outer edges, though not at the internal neighbouring edges or at the papilla across their surface (see red arrow). In addition to this grouping, a single epidermal cell nearby showed a stronger PDMPO fluorescence across its entire surface, including its papillas (see gold arrow).

7.3.1.2 Silica Cells

The following images display silicified silica cells which cover the veins of leaves in rice. Scale bars are located in the bottom right corner of the images and arrows denote areas of interest, described in the text.

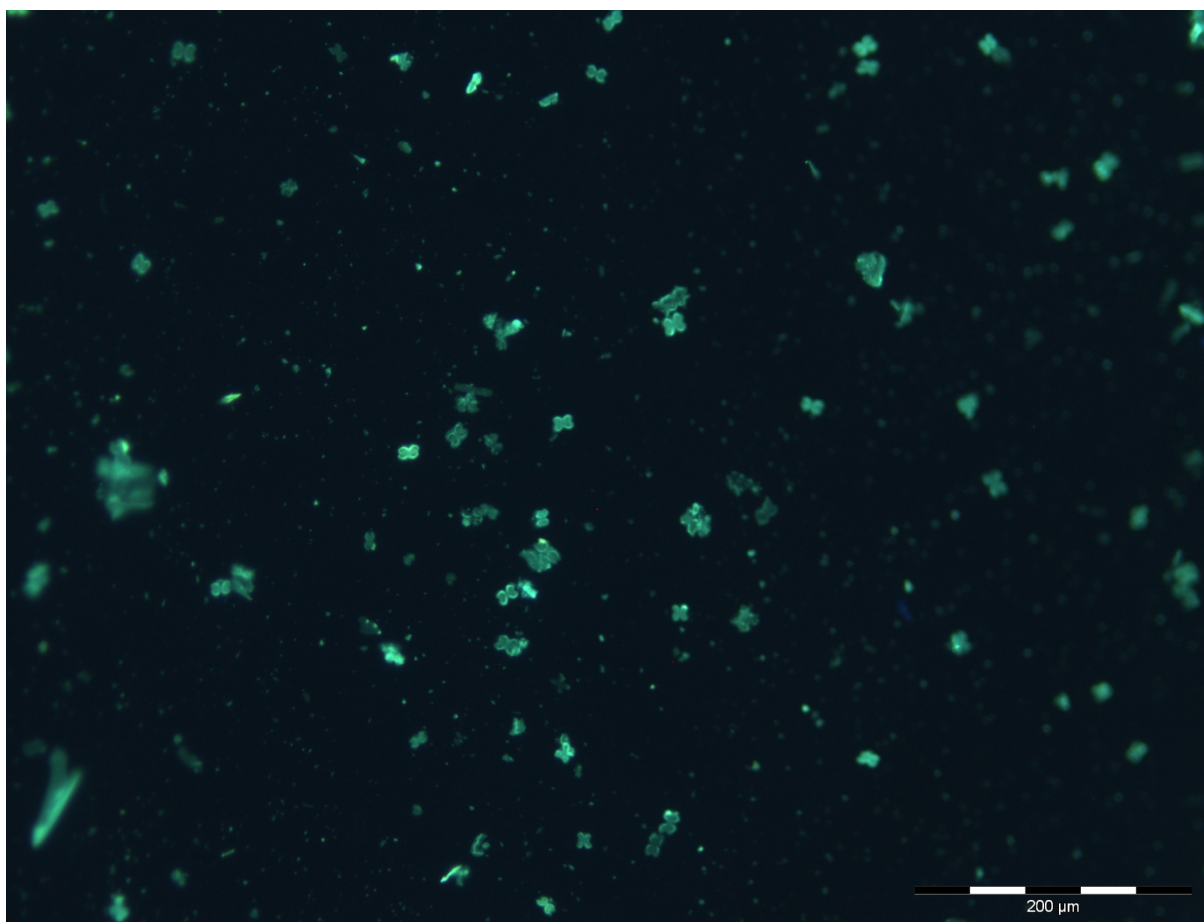


Figure 7.13 PDMPO stained silica from rice leaf epidermis, viewed under fluorescence microscopy. Scale bar is present in the bottom right corner of the image.

Dumbbell-shaped silica cells were incredibly common within the rice leaf and stem digests, with individual cells scattered across almost all samples (Fig 7.13). Silica cells usually appear brighter than the larger pieces of silica, either a result of their floating higher within the liquid medium or as a result of a denser silica deposition at these cells compared to the epidermal cells (see red arrows). Other small fragments of silica can be seen floating amongst the silica cells, likely broken shards from much larger silica structures; these shards cannot be identified due to their small size relative to the structures they originated from (see gold arrow).

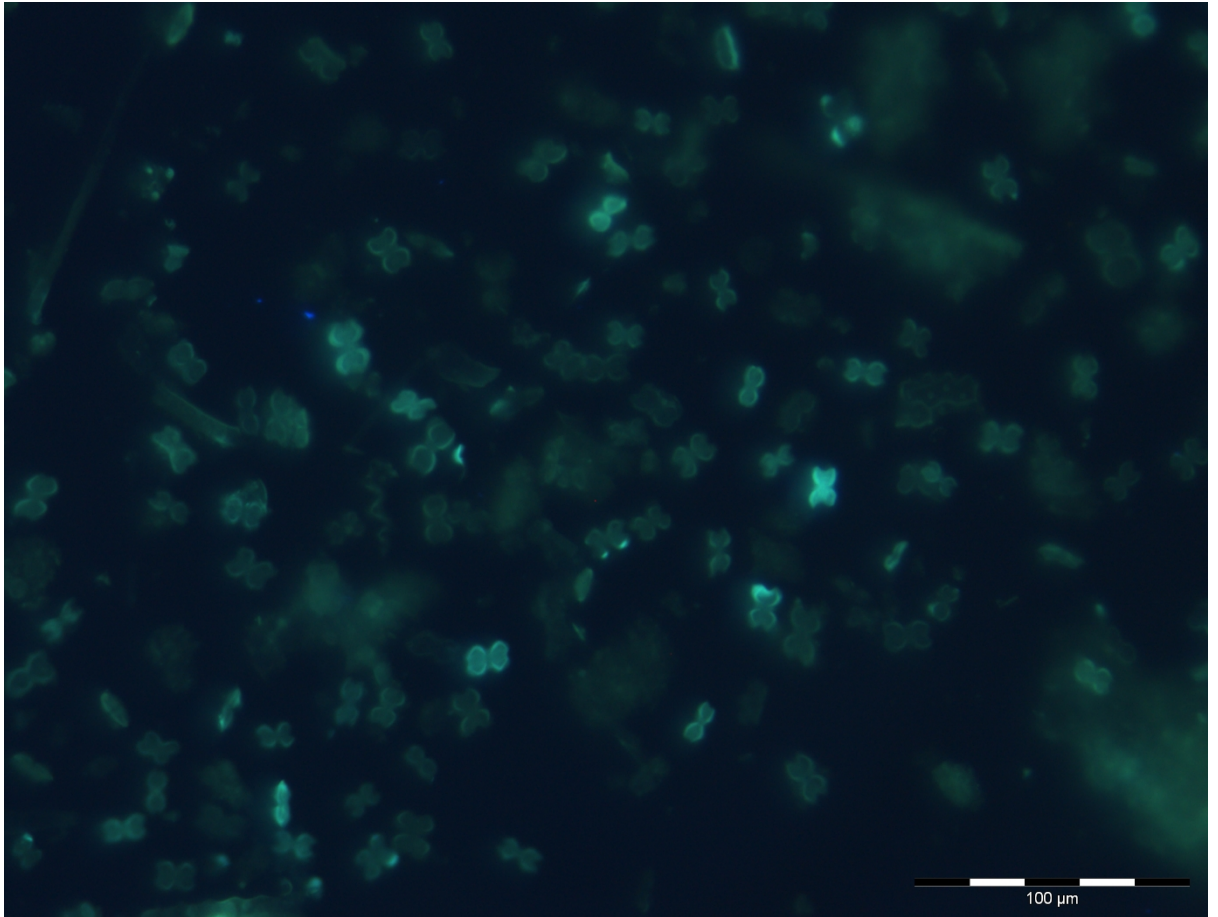


Figure 7.14 PDMPO stained silica from rice leaf epidermis, viewed under fluorescence microscopy. Scale bar is present in the bottom right corner of the image.

Numerous silica cells can be observed with varying levels of fluorescence intensity (Fig 7.14).

Whilst some of the silica cells fluoresce brightly (see red arrows), most of the cells present have the more typical green fluorescence exhibited by larger silica samples suggesting that the brighter fluorescence seen in some cells is most likely the result of their position within the liquid medium, with higher samples fluorescing brighter. A significant degree of variation in the shape of silica cells can be seen, though all of them share the same general dumbbell-shape.

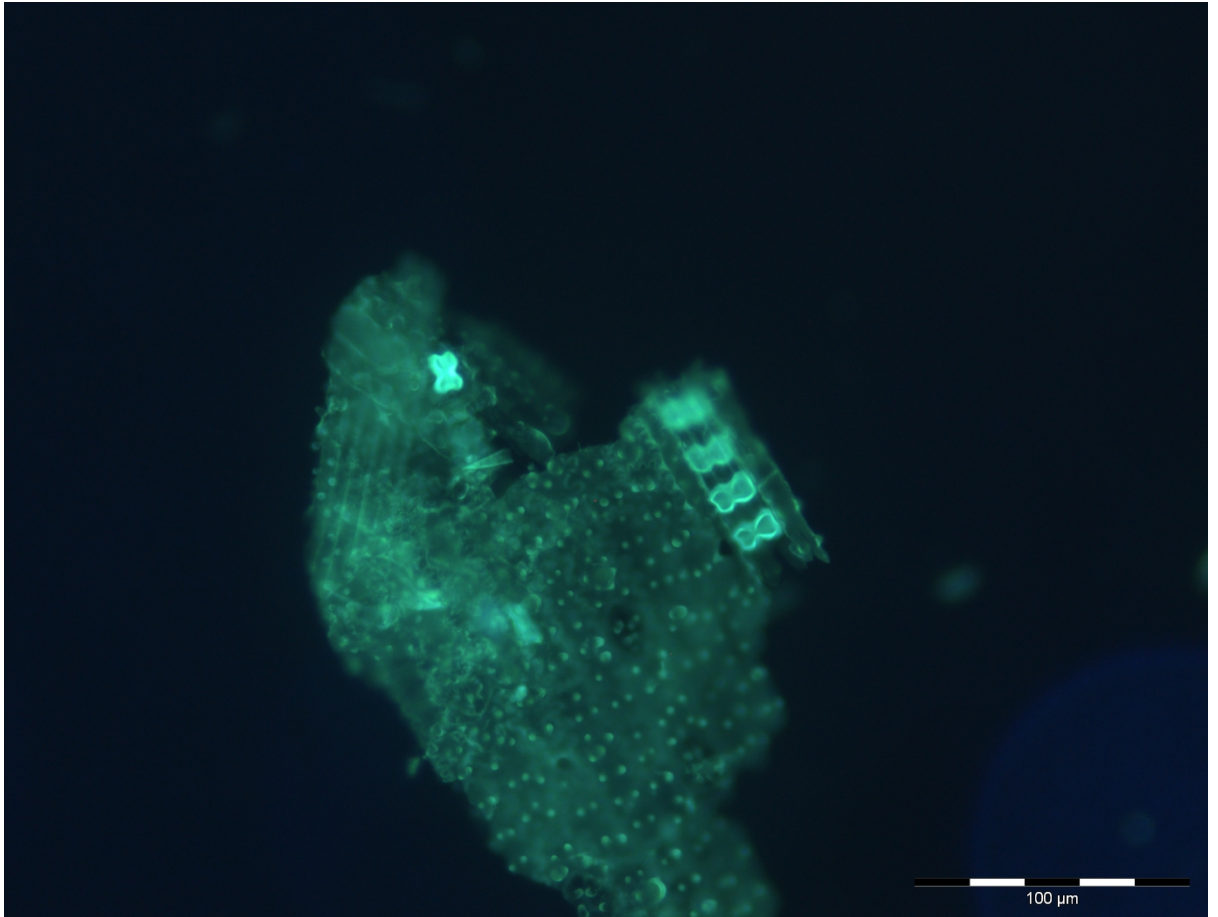


Figure 7.15 PDMPO stained silica from rice leaf epidermis, viewed under fluorescence microscopy. Scale bar is present in the bottom right corner of the image.

Several silica cells can be seen attached to a large epidermal cell structure (Fig 7.15). Silica cells are found in ladder-like structures running along the surface of the leaf over the veins, which contain the vascular bundles – these structures are commonly seen on the surface of the leaf but do not usually survive the digest process intact. Four silica cells can be seen in a row, with cork cells in between them and epidermal cells flanking both sides (see red arrows). The silica cells fluoresce brighter than the surrounding silica, suggesting a denser deposition of silica in these cells. The epidermal cells surrounding this silica cell structure are primary epidermal cells as evidenced by the papilla which cover their surface (see gold arrows). Stomata are also visible in the epidermal structure at several points, though they are difficult to make out as they are sunken into the main body of silica (see white arrows).

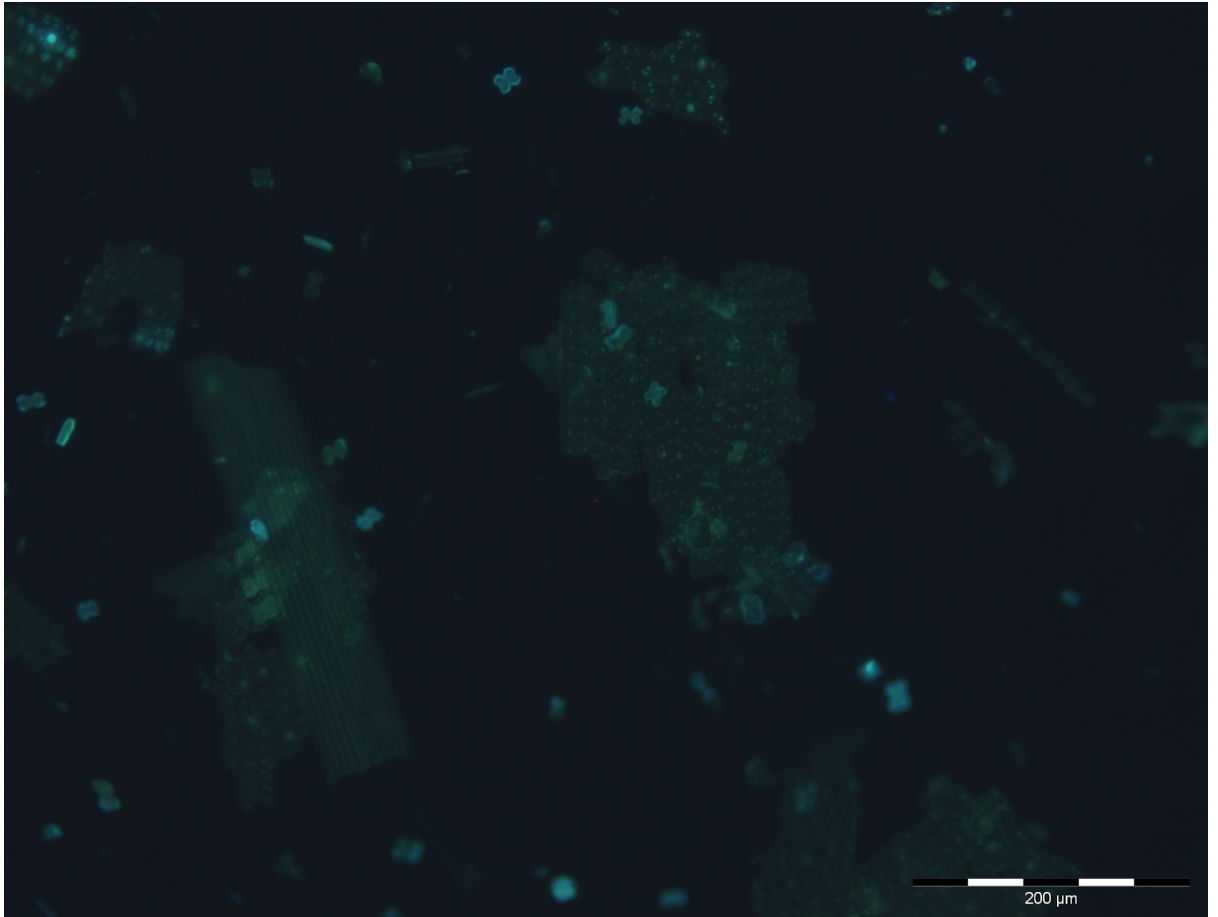


Figure 7.16 PDMPO stained silica from rice leaf epidermis, viewed under fluorescence microscopy. Scale bar is present in the bottom right corner of the image.

Another small segment of a silica cell ladder-like structure can be seen, flanked on both sides by epidermal cells (Fig 7.16). Three silica cells are arranged in a row with their long edges running parallel to each other and cork cells located between them (see red arrow). The ladder-like structure is flanked by secondary epidermal cells this time, lacking the defined sinuate shape or papilla (see gold arrows). The silica cells are once again more heavily stained than the surrounding silica. Another silica fragment from a section of primary epidermal cells can be seen with papilla covering its surface, providing a contrast between the two types of epidermal cell structure (see white arrow).

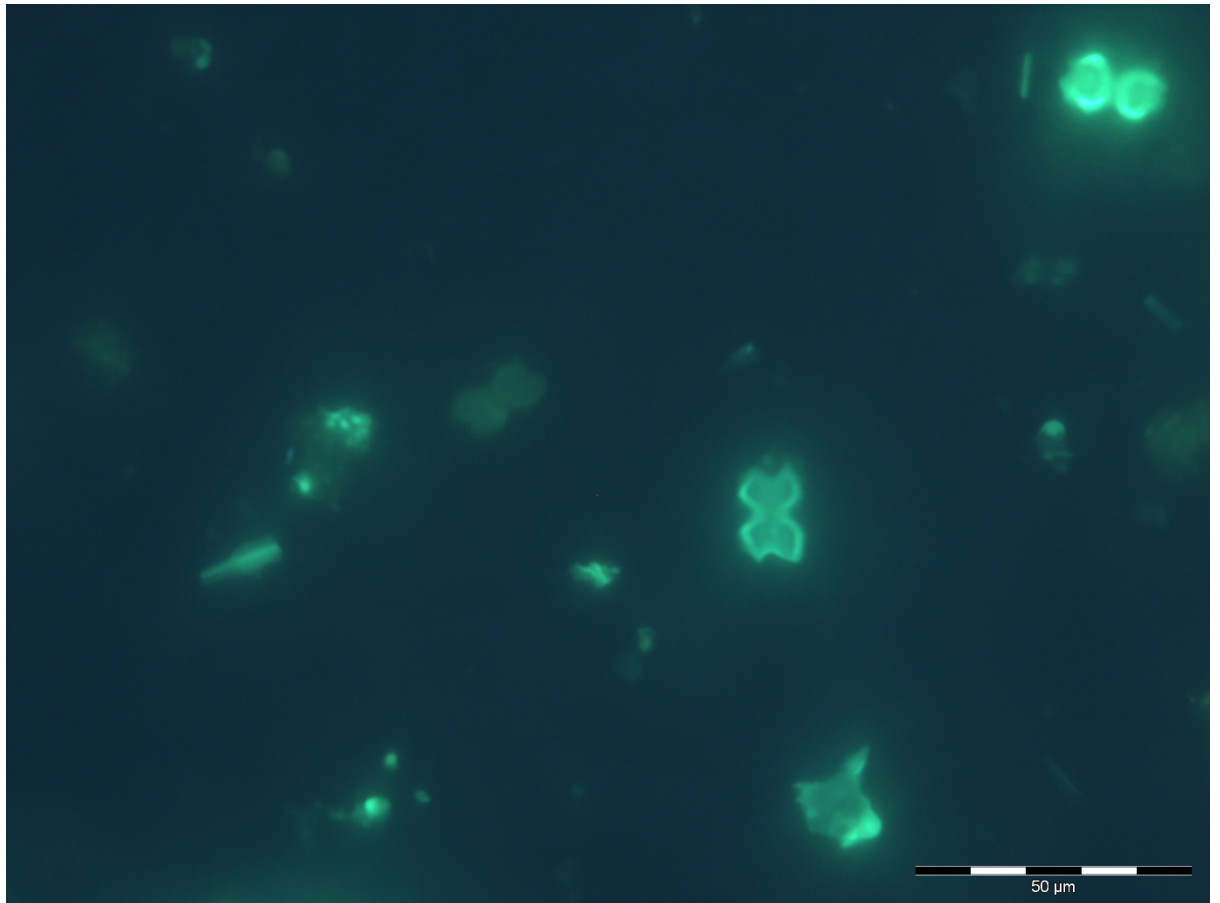


Figure 7.17 PDMPO stained silica from rice leaf epidermis, viewed under fluorescence microscopy. Scale bar is present in the bottom right corner of the image.

Under higher magnifications silica cells show variation in the PDMPO staining intensity depending on the region (Fig 7.17). The outer edges of the silica cell show more intense PDMPO staining than the internal section of the cell, suggesting a heavier silica build-up in this outer region (see red arrows). Several other silica fragments can be seen in this sample, having broken away from larger sections (see gold arrows).

7.3.1.3 Bulliform Cells

The following images display silicified bulliform cells which are located at pivot points in the leaf where it is required to bend. Scale bars are located in the bottom right corner of the images and arrows denote areas of interest, described in the text.

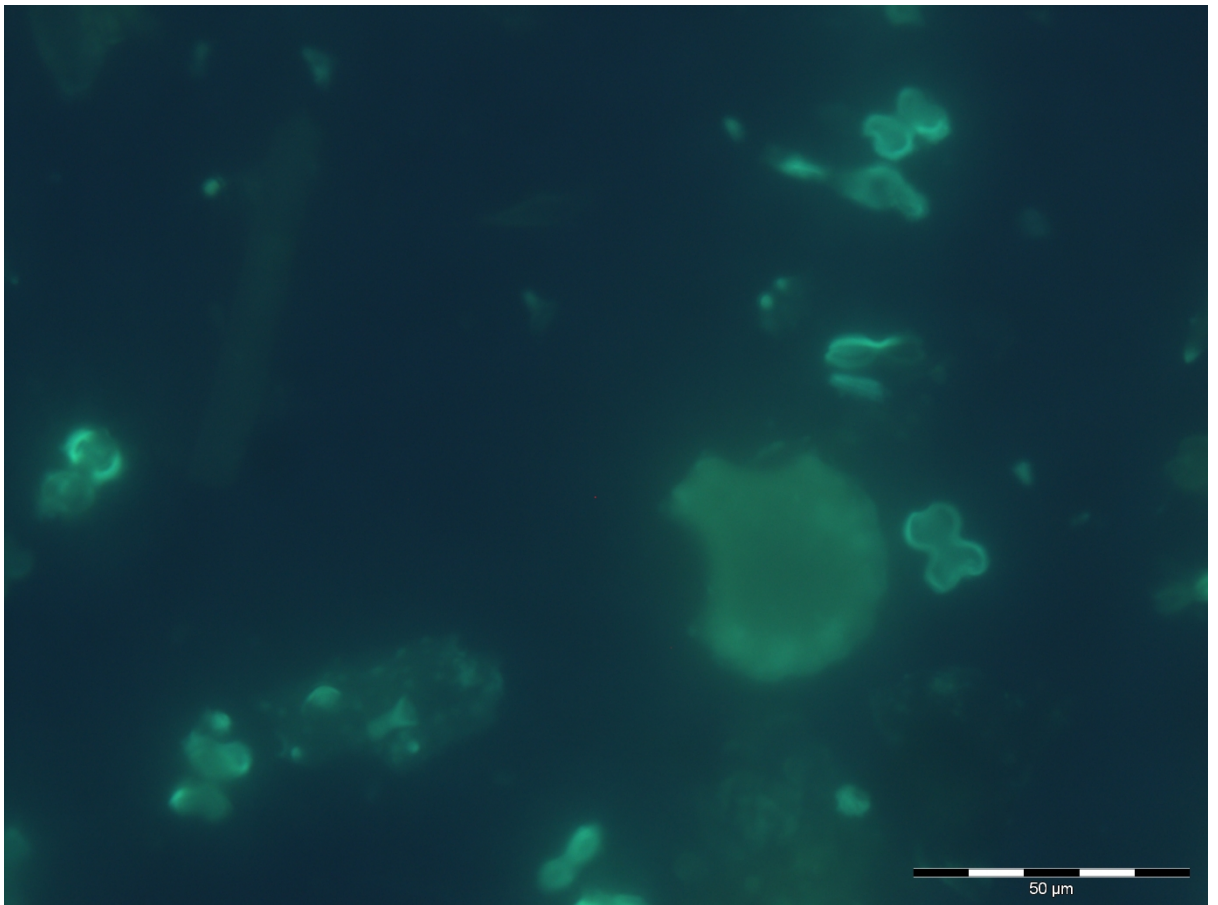


Figure 7.18 PDMPO stained silica from rice leaf epidermis, viewed under fluorescence microscopy. Scale bar is present in the bottom right corner of the image.

A large, mushroom-shaped silica structure can be observed indicating the silica which covered a bulliform cell (Fig 7.18). Bulliform cells are the motor cells found at the epidermis of the leaves in grasses which cause the leaf to curl and uncurl by changes in their turgor to regulate water loss. The mushroom shape of this particular bulliform cell indicates it was located at the pivot point around which the leaf would curl, whilst other bulliform cells on either side of this one would have a more rectangular shape (see red arrow). The bulliform cell shows slight variations in the intensity of the silica staining across its surface, but shows no sign of any distinguishing features

across its smooth surface. Several silica cells can be seen nearby, again showing a stronger PDMPO staining at their edges when compared to their main body (see gold arrows).

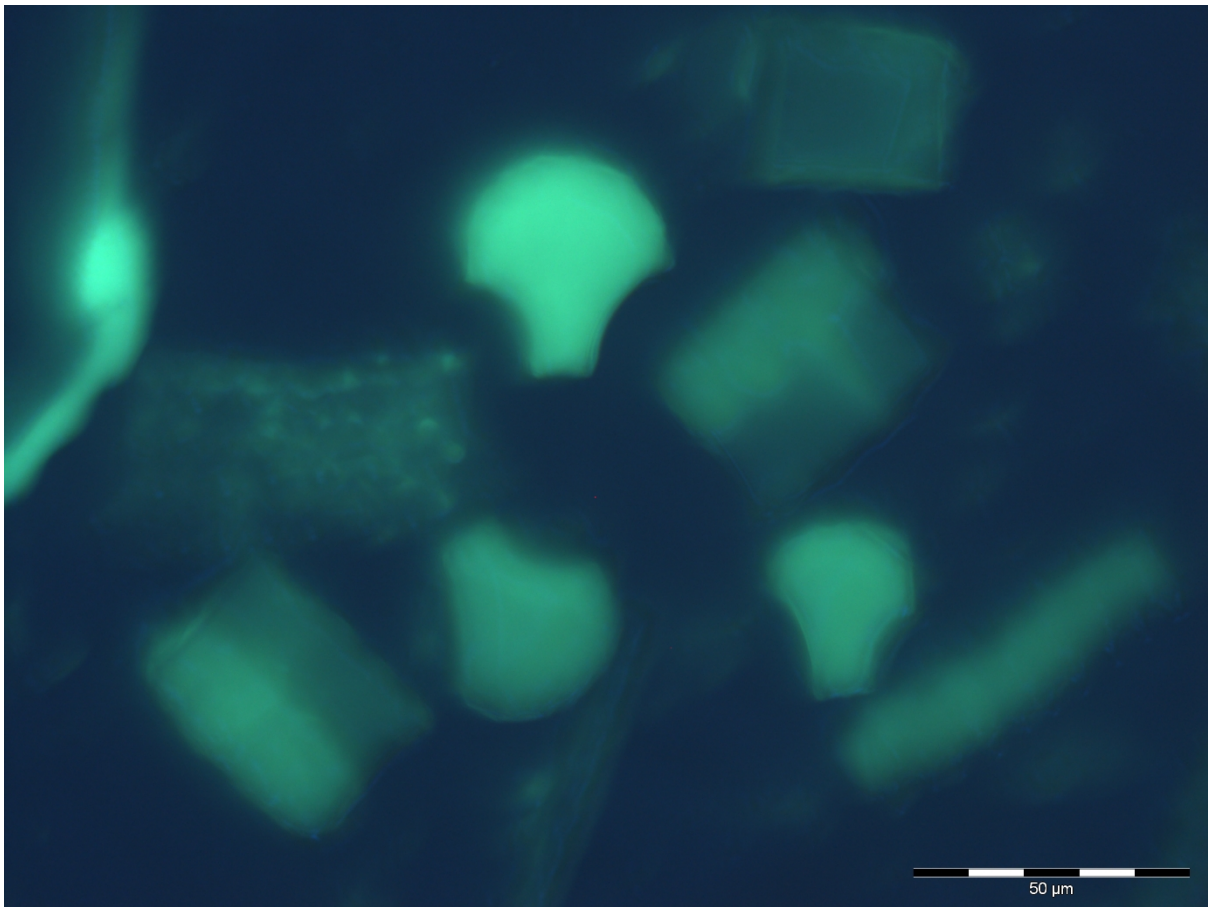


Figure 7.19 PDMPO stained silica from rice leaf epidermis, viewed under fluorescence microscopy. Scale bar is present in the bottom right corner of the image.

Numerous mushroom-shaped bulliform cells can be observed in close proximity, along with several long rectangular cells (Fig 7.19). The long rectangular cells show a distinct split running down them, one side of which has a stronger PDMPO fluorescence signal indicating heavier silica deposition at this region (see red arrows). In contrast to the rectangular cells, the mushroom-shaped cells show a relatively uniform fluorescence signal across their surface (see gold arrows). The rectangular cells could be bulliform cells which neighbour the mushroom-shaped variant on either side, though they are significantly larger than would be expected; the mushroom-shaped bulliform cell should be the largest in any given grouping. Several structures in the image are out

of focus; the focal point was chosen to give the best overall view of all silica structures, which are located at different focal points floating within the liquid.

7.3.1.4 Trichomes

The following images display silicified trichomes which are spine-like protrusions from the leaf epidermis. Scale bars are located in the bottom right corner of the images and arrows denote areas of interest, described in the text.

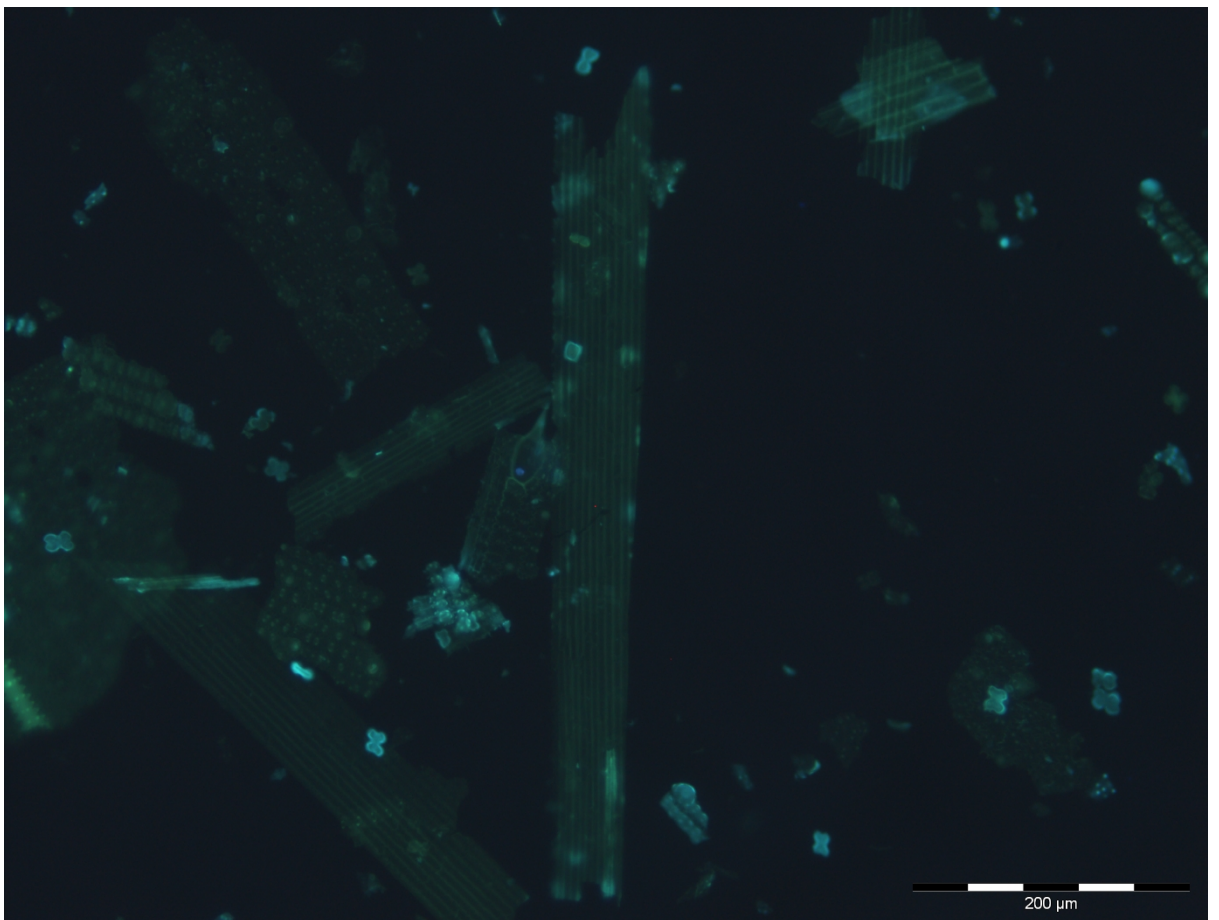


Figure 7.20 PDMPO stained silica from rice leaf epidermis, viewed under fluorescence microscopy. Scale bar is present in the bottom right corner of the image.

Numerous large shards of epidermal silica can be observed, highlighting the majority of silica structures found in one image (Fig 7.20). Multiple pieces of silica that covered the primary epidermal cells can be identified by the papilla which cover their surface (see red arrows). Within the primary epidermal structures there are several apertures indicating the presence of stomata, though the guard cells themselves are absent (see gold arrows). Alongside the primary epidermal

cells, large shards of secondary epidermal cell silica can be seen, lacking the sinuate shape and papilla of the more common primary epidermal cells (see white arrows). Loose silica cells are scattered throughout the image (see purple arrows). Finally, attached to a small shard of primary epidermal silica, a trichome can clearly be seen, identified by its bulbous base and spine-like protrusion (see light blue arrow).

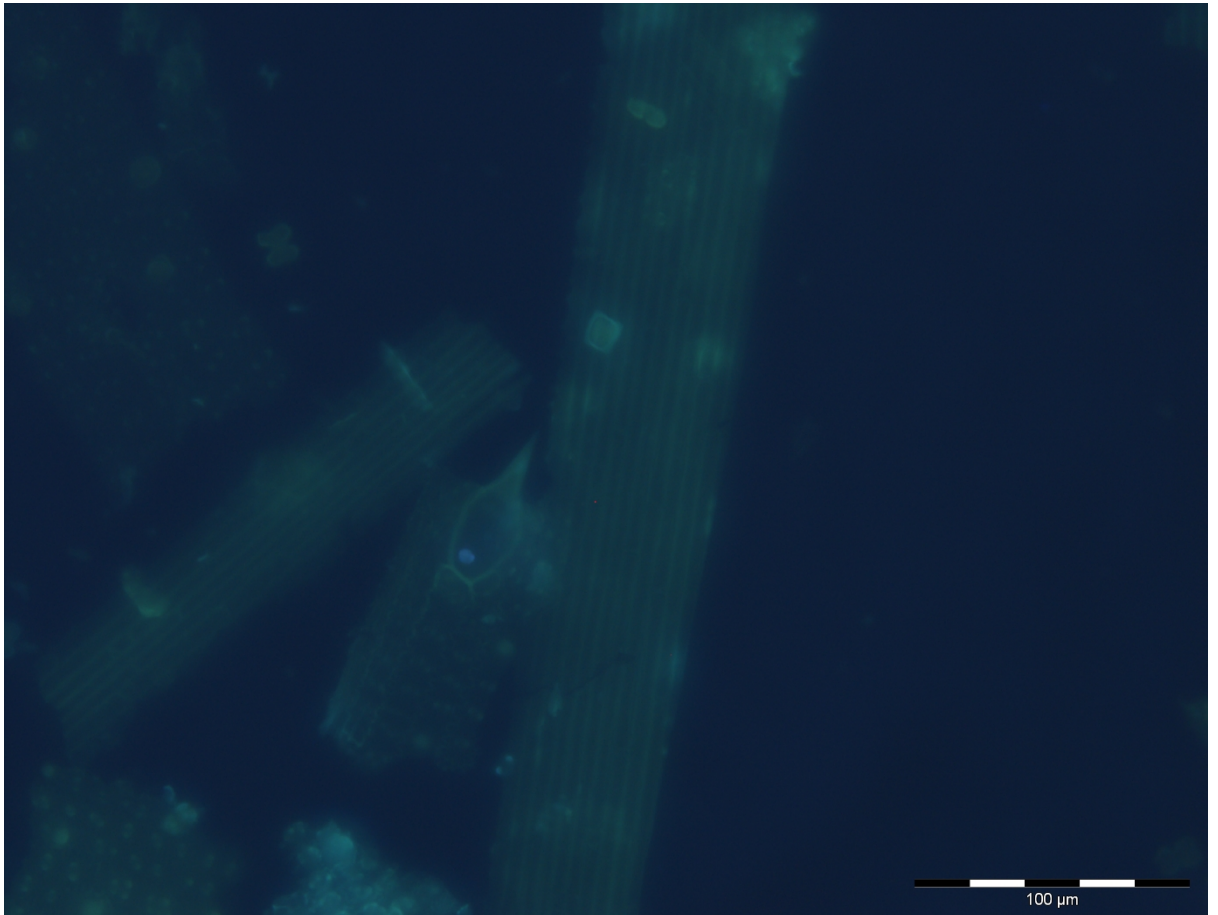


Figure 7.21 PDMPO stained silica from rice leaf epidermis, viewed under fluorescence microscopy. This image is of the same silica fragment as shown in Fig 7.20, but at a higher magnification. Scale bar is present in the bottom right corner of the image.

At a higher magnification the trichome silica structure shows heavier PDMPO staining at its outer edges when compared with the main body (Fig 7.21). The spine-like protrusion also appears to show heavier PDMPO staining, indicating heavier silica deposition at the spine when compared with the bulbous base (see red arrow). The trichome is located in a row of primary epidermal cells, seemingly taking the place of an epidermal cell in the mosaic-like silica structure, though the base of the trichome is wider than the surrounding epidermal cells (see gold arrow).

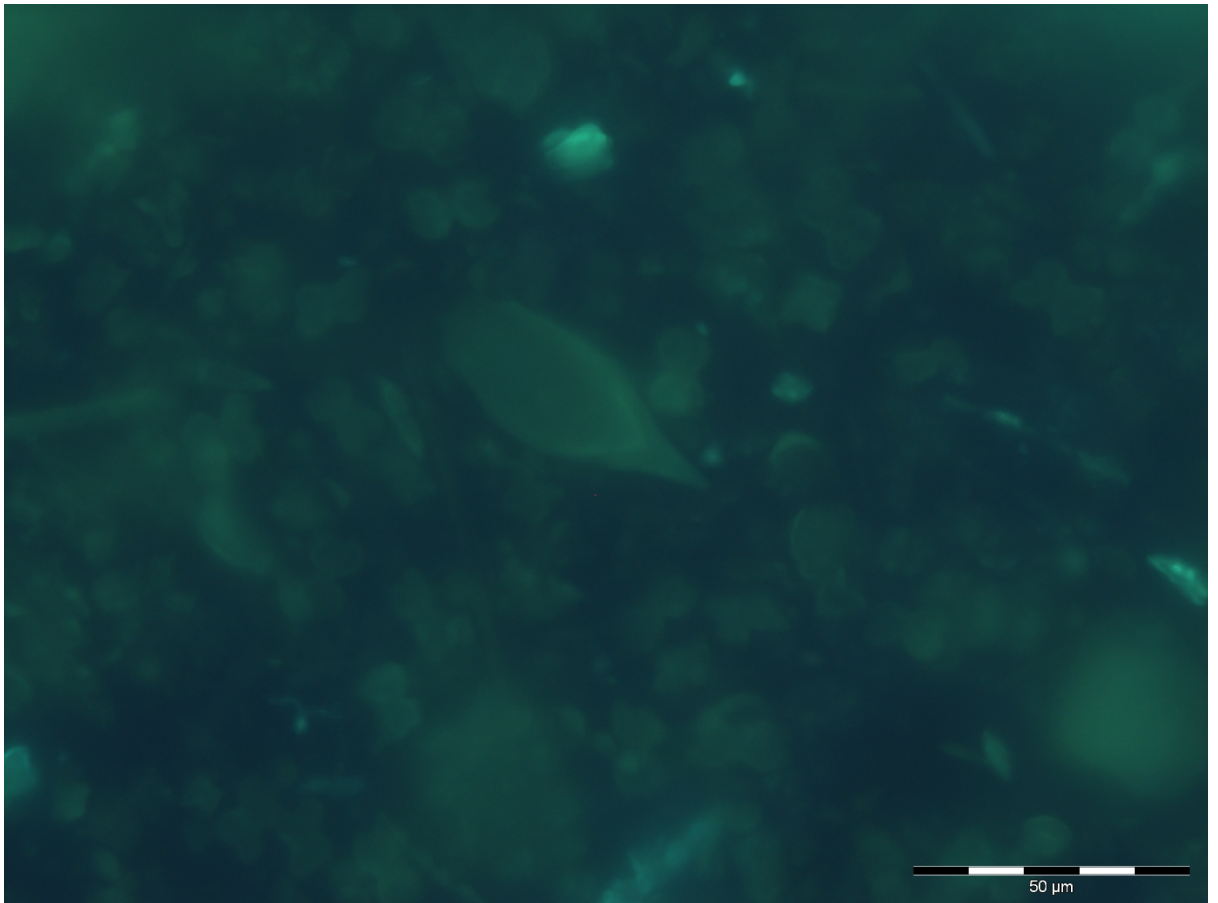


Figure 7.22 PDMPO stained silica from rice leaf epidermis, viewed under fluorescence microscopy. Scale bar is present in the bottom right corner of the image.

A trichome silica structure is found floating free from any larger epidermal structure (Fig 7.22). The trichome is viewed from its underside; the interior of the silica structure appears to be hollow, the space likely filled with the organic component of the trichome before the sample was acid digested (see red arrow). Various other fragments of silica debris are visible neighbouring the trichome, along with silica cells.

7.3.1.5 Xylem

The following images display silicified xylem vessels, which are the water transport channels within the leaf and stem. Scale bars are located in the bottom right corner of the images and arrows denote areas of interest, described in the text.

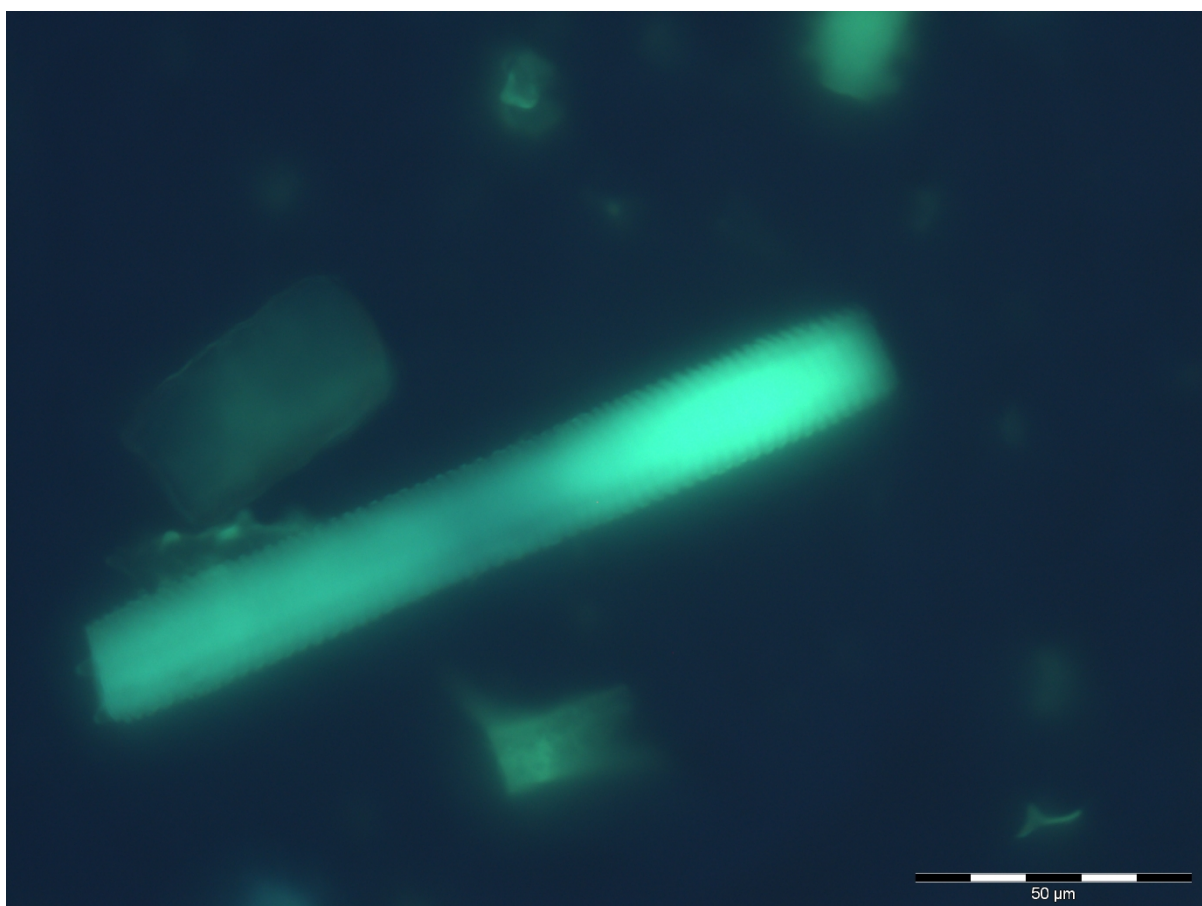


Figure 7.23 PDMPO stained silica from rice leaf epidermis, viewed under fluorescence microscopy. Scale bar is present in the bottom right corner of the image.

One of the rarer silica structures found was a tube-like structure with ridges running along its outer surface (Fig 7.23). Measuring approximately 20 μm in width, this silica structure is most reminiscent of a xylem vessel (see red arrow). Xylem vessels are the transport tubes through which water and silicic acid are transported. Xylem vessels are not typically thought of as structures prone to silicification, even though they are transporters of silicic acid themselves. No other structure or vessel within rice tissue matches the morphology of this silica structure.

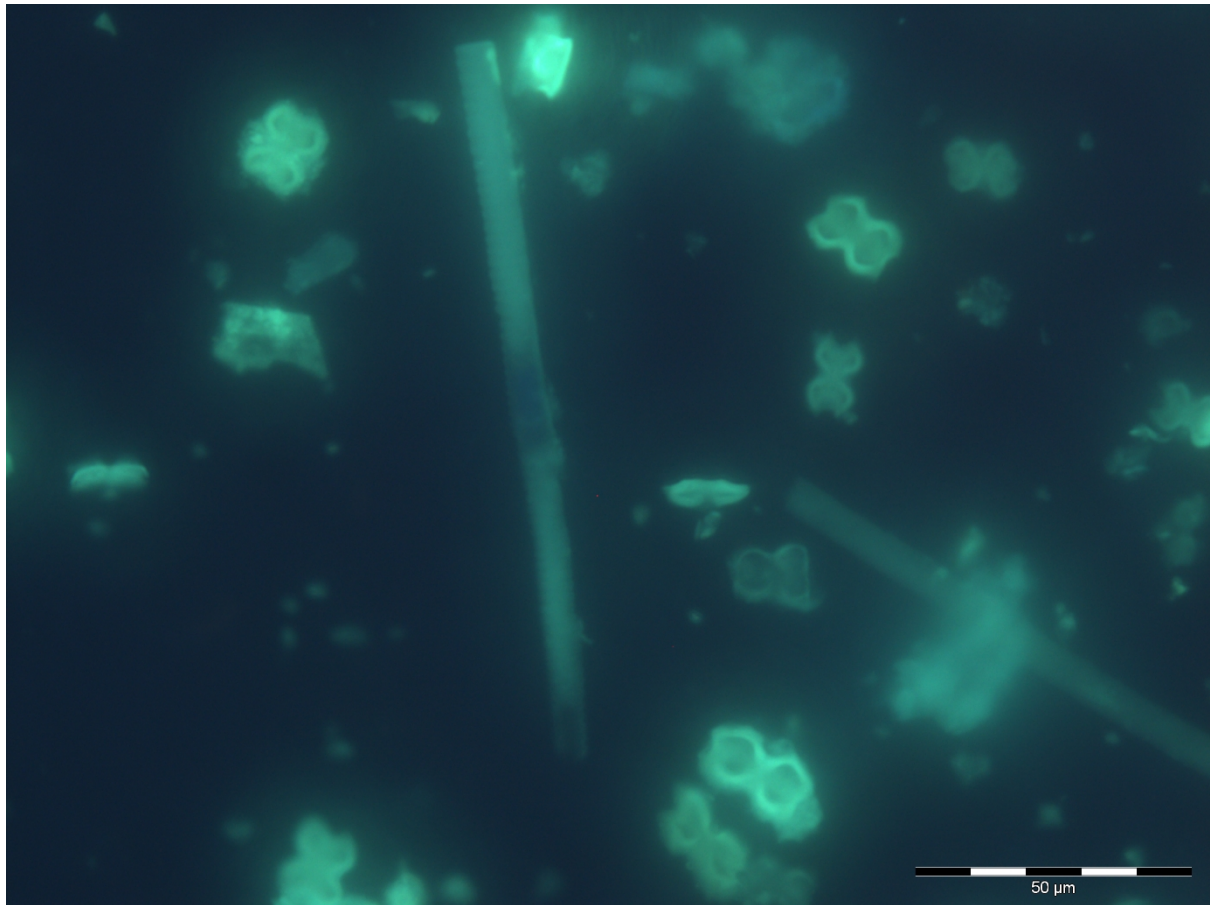


Figure 7.24 PDMPO stained silica from rice leaf epidermis, viewed under fluorescence microscopy. Scale bar is present in the bottom right corner of the image.

Another xylem-like structure was found in silica digests from rice leaf tissue, though the ridges surrounding the tube are less evident under fluorescence (Fig 7.24). The ridges which run around the tube, down its entire length, are visible at the silica tube's edge (see red arrow). The PDMPO staining is not uniform throughout the sample, with two sections appearing heavily stained (see gold arrows) whilst two sections appear to be stained only faintly (see white arrows). The xylem-like silica tube is thinner than the previously seen sample (Fig 7.23), measuring only 7-8 μm across with its width tapering slightly towards the bottom of the image. Several silica cells are visible nearby, showing strong fluorescence at their outer edges (see light blue arrows).



Figure 7.25 PDMPO stained silica from rice leaf epidermis, viewed under light microscopy. Scale bar is present in the bottom right corner of the image.

The xylem-like structure seen previously under fluorescence staining (Fig 7.24), this time viewed under light microscope (Fig 7.25). The ridges which run around the circumference of the xylem silica tube can be seen clearly here at regular intervals (see red arrow). Under light microscope the biogenic silica is shown to be colourless and translucent.

7.3.1.6 Silica Aggregation

The following images display unidentified silica aggregations from the silica obtained by acid digestion of rice. Scale bars are located in the bottom right corner of the images and arrows denote areas of interest, described in the text.

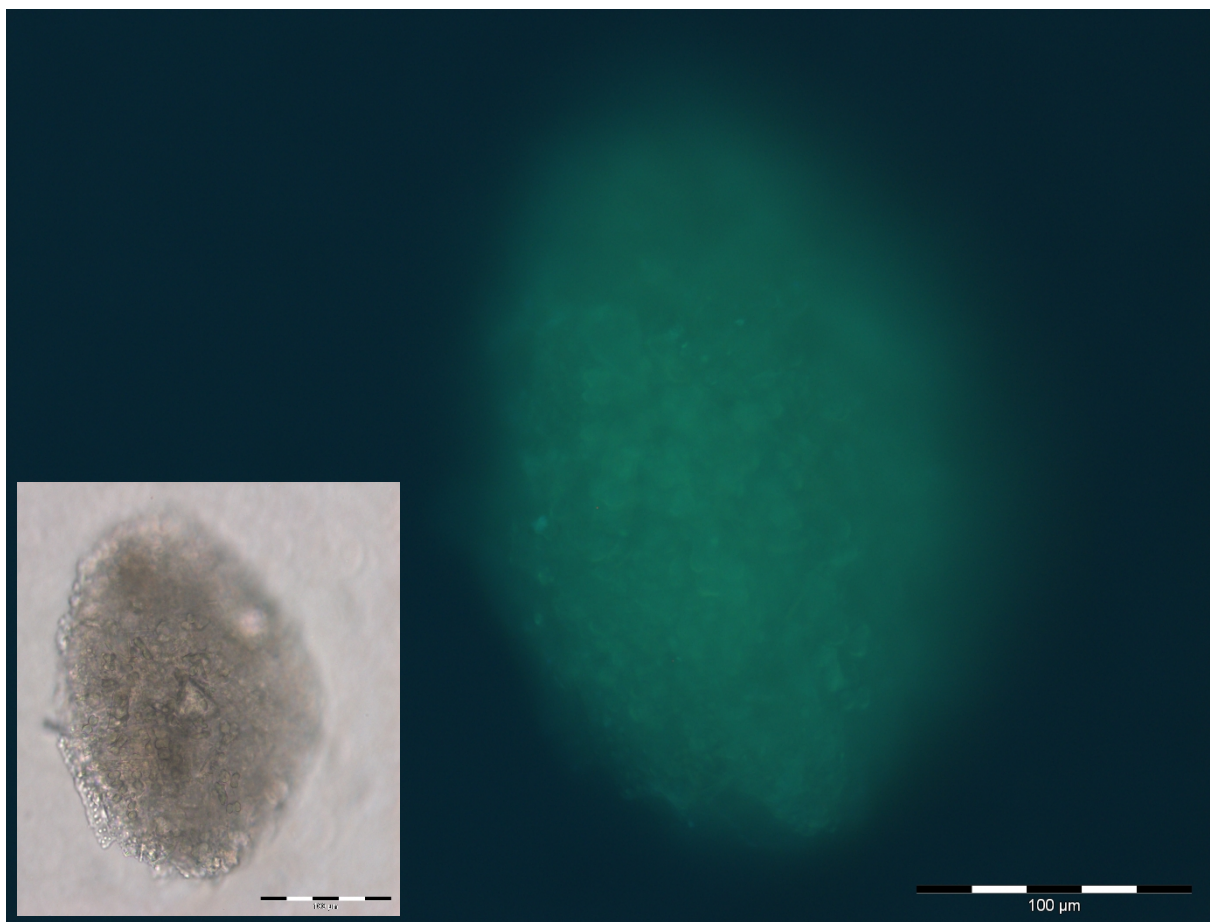


Figure 7.26 PDMPO stained silica aggregation from rice leaf epidermis, viewed under fluorescence microscopy. Insert shows the same image under light microscope. Scale bar is present in the bottom right corner of the image.

An issue with the PDMPO staining method is that the silica fragments have a tendency to aggregate together (Fig 7.26). These masses of silica give of a generic green haze, but it is almost impossible to identify any individual structures within the silica mass under PDMPO, with light microscope images proving little better (see insert in Fig 7.26).

7.3.2 Silicon Deplete Rice

The following image displays silica, or lack thereof, obtained from acid digestion of rice grown in the absence of added silicic acid. Scale bars are located in the bottom right corner of the images.

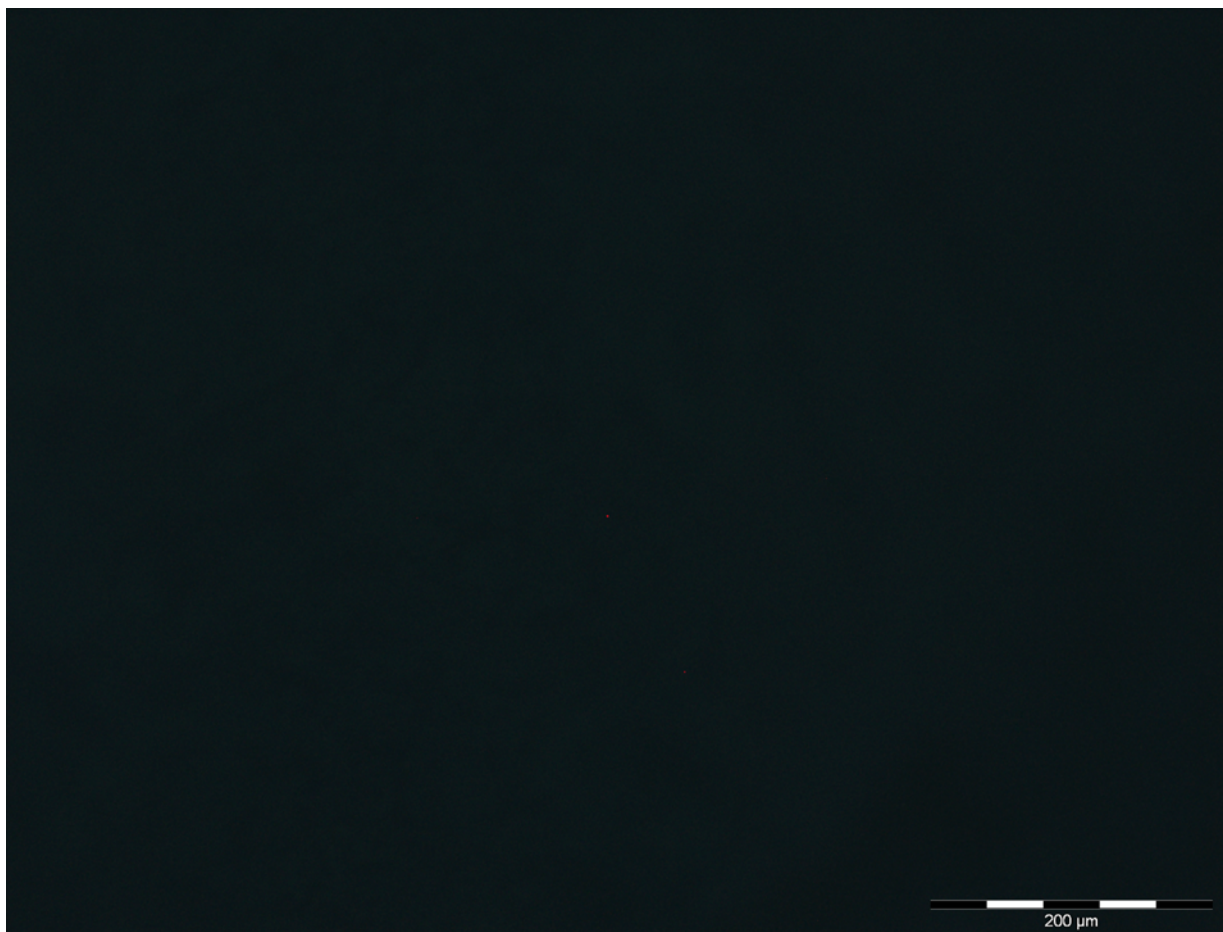


Figure 7.27 PDMPO stained silica from rice leaf epidermis of rice plants grown in the absence of silicic acid, viewed under fluorescence microscopy. Scale bar is present in the bottom right corner of the image.

Whilst this image may seem humorous, it is important to note that although no silica was obvious in the digest of the rice plants grown in the absence of silicic acid, no silica would be expected in these samples; however, silicic acid is a universal contaminant and is almost impossible to completely remove from a growth solution. Whilst the concentration of silicic acid was extremely low in the silicon deplete solutions, it is possible that over time a plant grown in such conditions could accumulate enough silicic acid to form some silica structures. As is evident from the image, no such silica structures were found (Fig 7.27).

7.3.3 Silicon and Aluminium Replete Rice

The following images were taken from PDMPO silica digests obtained from the acid digestion of rice plants grown in the presence of added silicic acid and aluminium. Scale bars are located in the bottom right corner of the images and arrows denote areas of interest, described in the text.

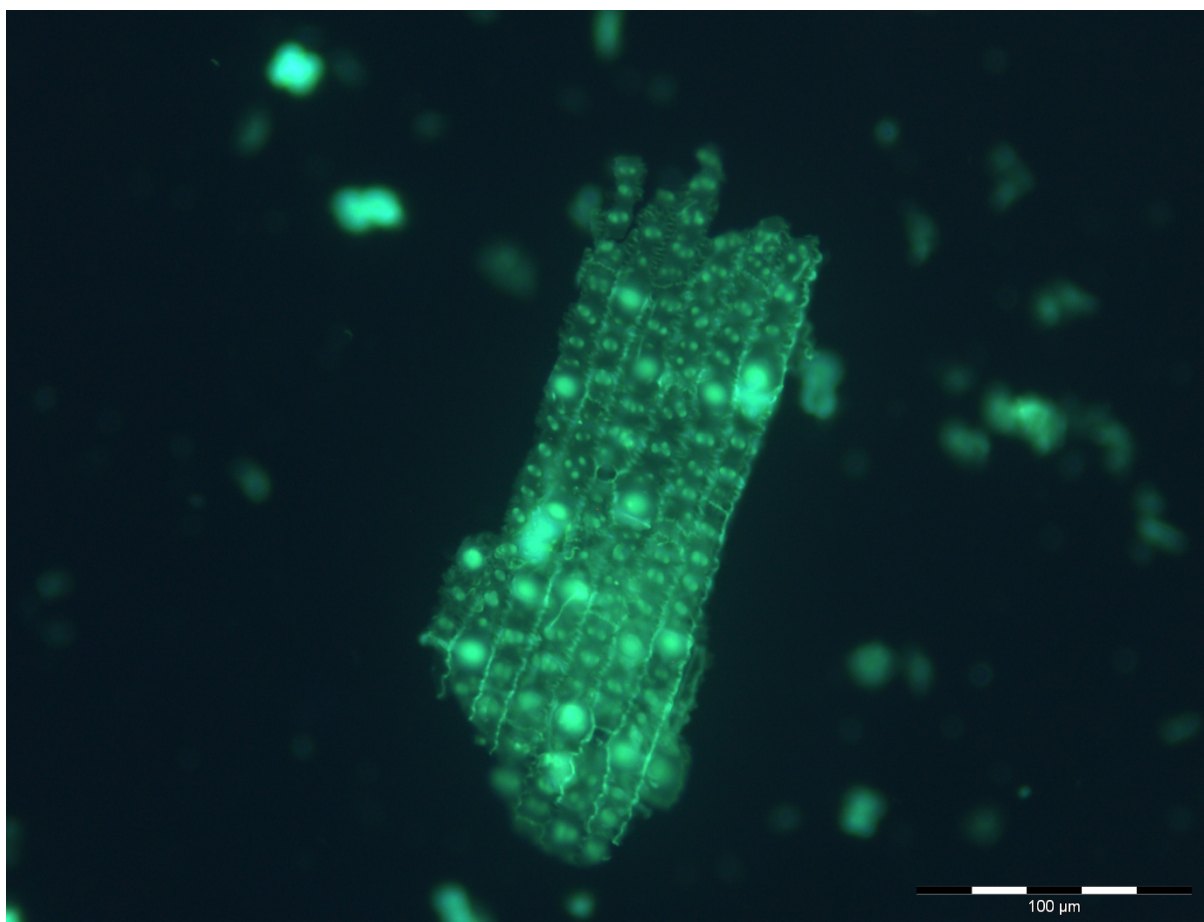


Figure 7.28 PDMPO stained silica from rice leaf epidermis of rice plants grown in the presence of silicic acid and then further grown in CaCl_2 with $100 \mu\text{M}$ aluminium for two weeks, viewed under fluorescence microscopy. Scale bar is present in the bottom right corner of the image.

Epidermal silica structures showed no variation in structure with the addition of aluminium to the plants growth solution (Fig 7.28). Primary epidermal cells were silicified in great detail, showing their sinuate edges (see red arrow) and surface papilla (see gold arrow). The larger nodules were interspersed between smaller papilla (see white arrow).

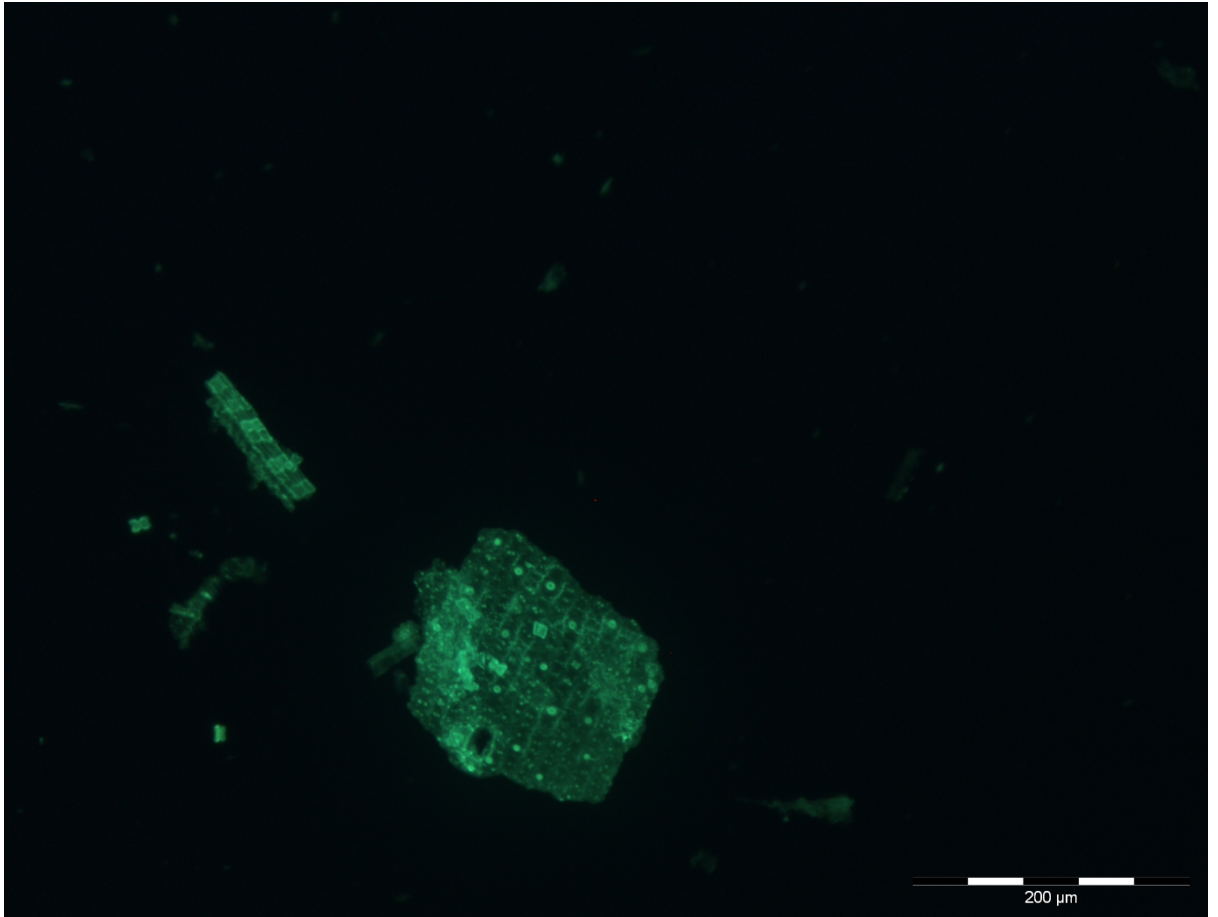


Figure 7.29 PDMPO stained silica from rice leaf epidermis of rice plants grown in the presence of silicic acid and then further grown in CaCl_2 with $100 \mu\text{M}$ aluminium for two weeks, viewed under fluorescence microscopy. Scale bar is present in the bottom right corner of the image.

A smaller section of epidermal silica was found showing an aperture indicating the previous location of a trichome, though the spine itself is not present (Fig 7.29) (see red arrow). Elsewhere in the sample, a small section of a silica cell ladder-like structure can be seen intact, but not attached to any larger epidermal structure (see gold arrow).

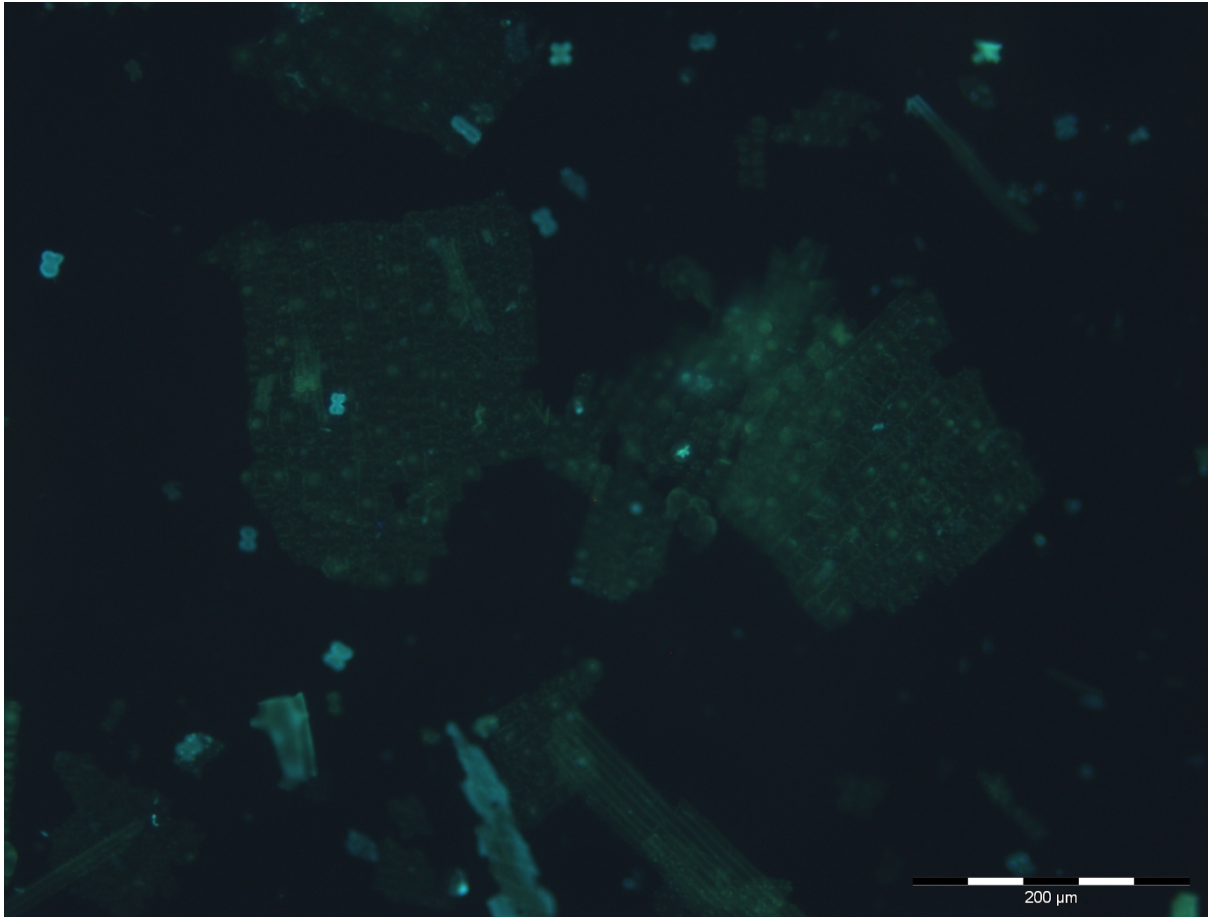


Figure 7.30 PDMPO stained silica from rice leaf epidermis of rice plants grown in the presence of silicic acid and then further grown in CaCl_2 with $100 \mu\text{M}$ aluminium for two weeks, viewed under fluorescence microscopy. Scale bar is present in the bottom right corner of the image.

Large fragments of both primary and secondary epidermal cell structures were just as common in the aluminium treatments as in the standard silica digests (Fig 7.30). Secondary epidermal cells were of a similar size and shape to the primary cells, but lacked the sinuate edges and papilla of the more common primary epidermal cells (see red arrow).

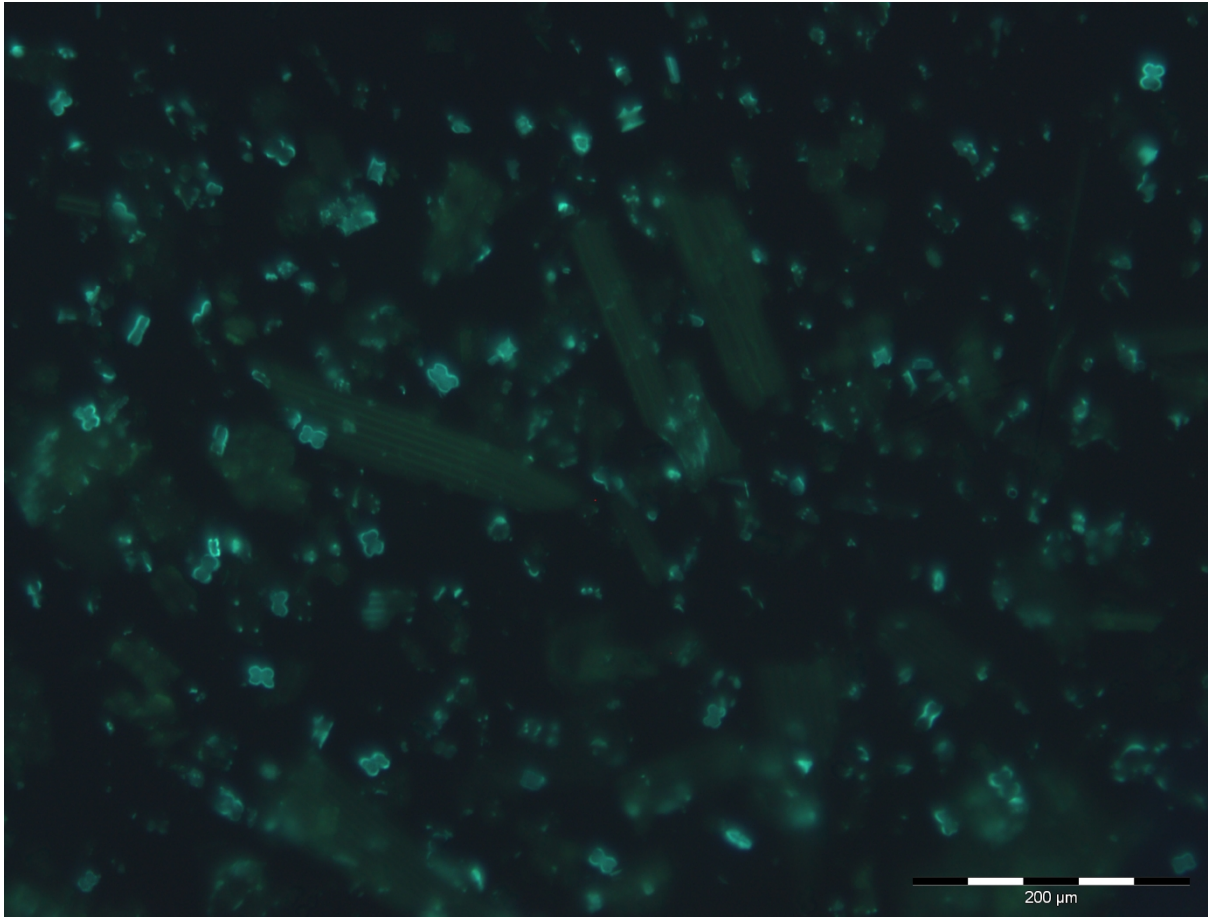


Figure 7.31 PDMPO stained silica from rice leaf epidermis of rice plants grown in the presence of silicic acid and then further grown in CaCl_2 with $100 \mu\text{M}$ aluminium for two weeks, viewed under fluorescence microscopy. Scale bar is present in the bottom right corner of the image.

In addition to the large fragments of silica, smaller broken pieces were commonplace in the digests (Fig 7.31). Silica cells were often seen floating free of any other silica structure within the sample, giving a stronger fluorescence than neighbouring silica structures (see red arrows).

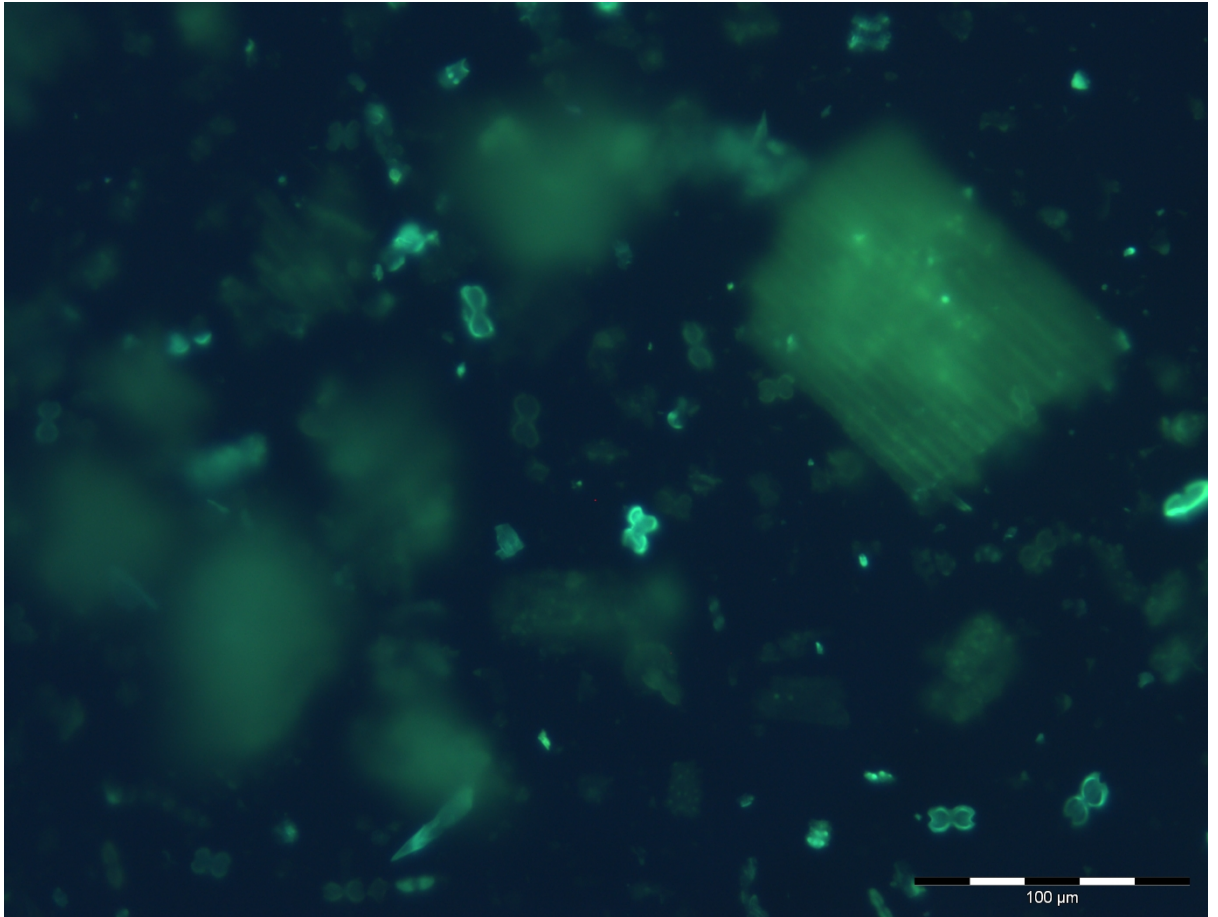


Figure 7.32 PDMPO stained silica from rice leaf epidermis of rice plants grown in the presence of silicic acid and then further grown in CaCl_2 with $100 \mu\text{M}$ aluminium for two weeks, viewed under fluorescence microscopy. Scale bar is present in the bottom right corner of the image.

At higher magnifications, silica cells can be seen to give off a stronger fluorescence signal at their outer edges than from the rest of their body (Fig 7.32). There is variation in the morphology of silica cells, with some having more rounded bulbous ends (see red arrow), whilst others have an indentation at each end (see gold arrow).

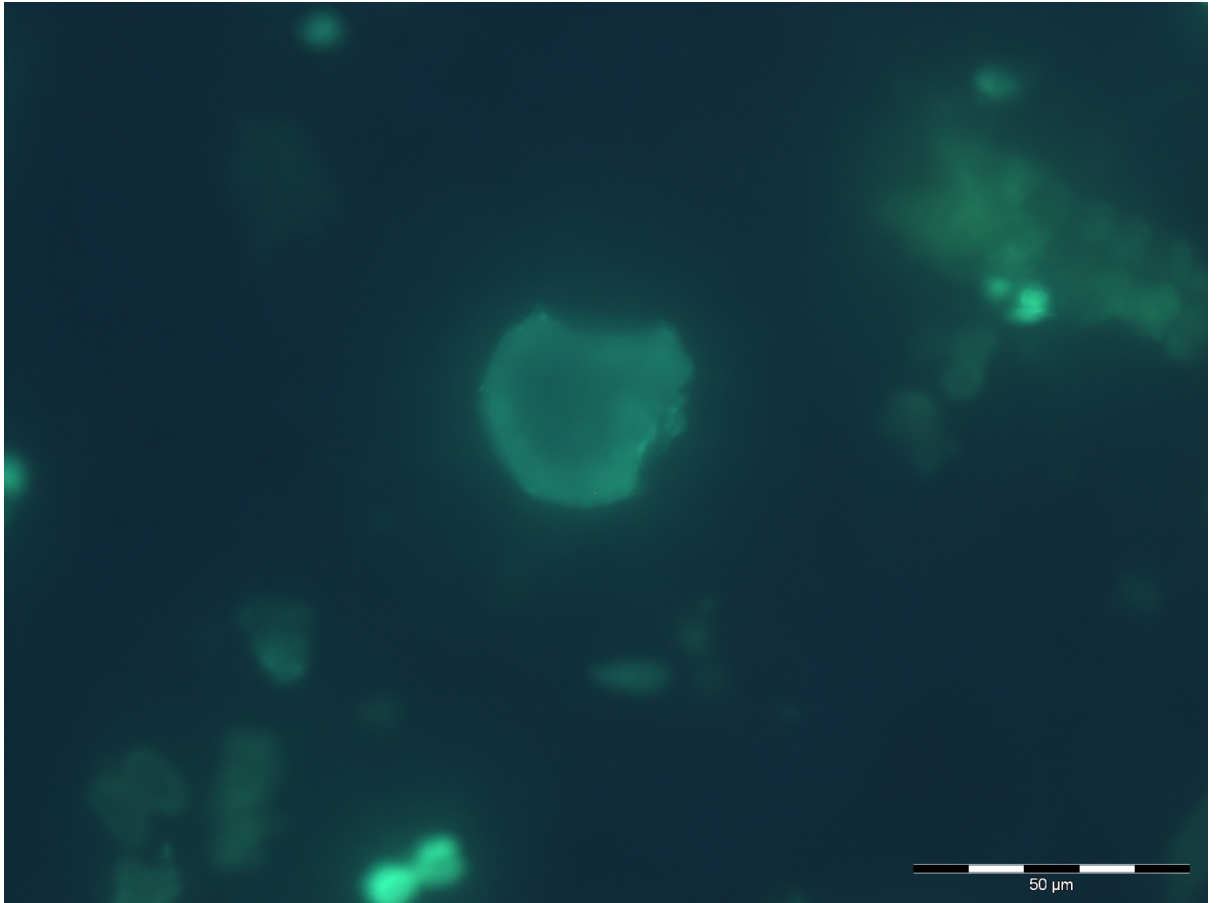


Figure 7.33 PDMPO stained silica from rice leaf epidermis of rice plants grown in the presence of silicic acid and then further grown in CaCl_2 with $100 \mu\text{M}$ aluminium for two weeks, viewed under fluorescence microscopy. Scale bar is present in the bottom right corner of the image.

Bulliform cells were observed in the aluminium treatments, though as in the previous digests only the central, mushroom-shaped cell was observed (Fig 7.33). Unlike most of the other silica structures, bulliform cells are entirely silicified instead of just being covered with a surface layer of silica (see red arrow).

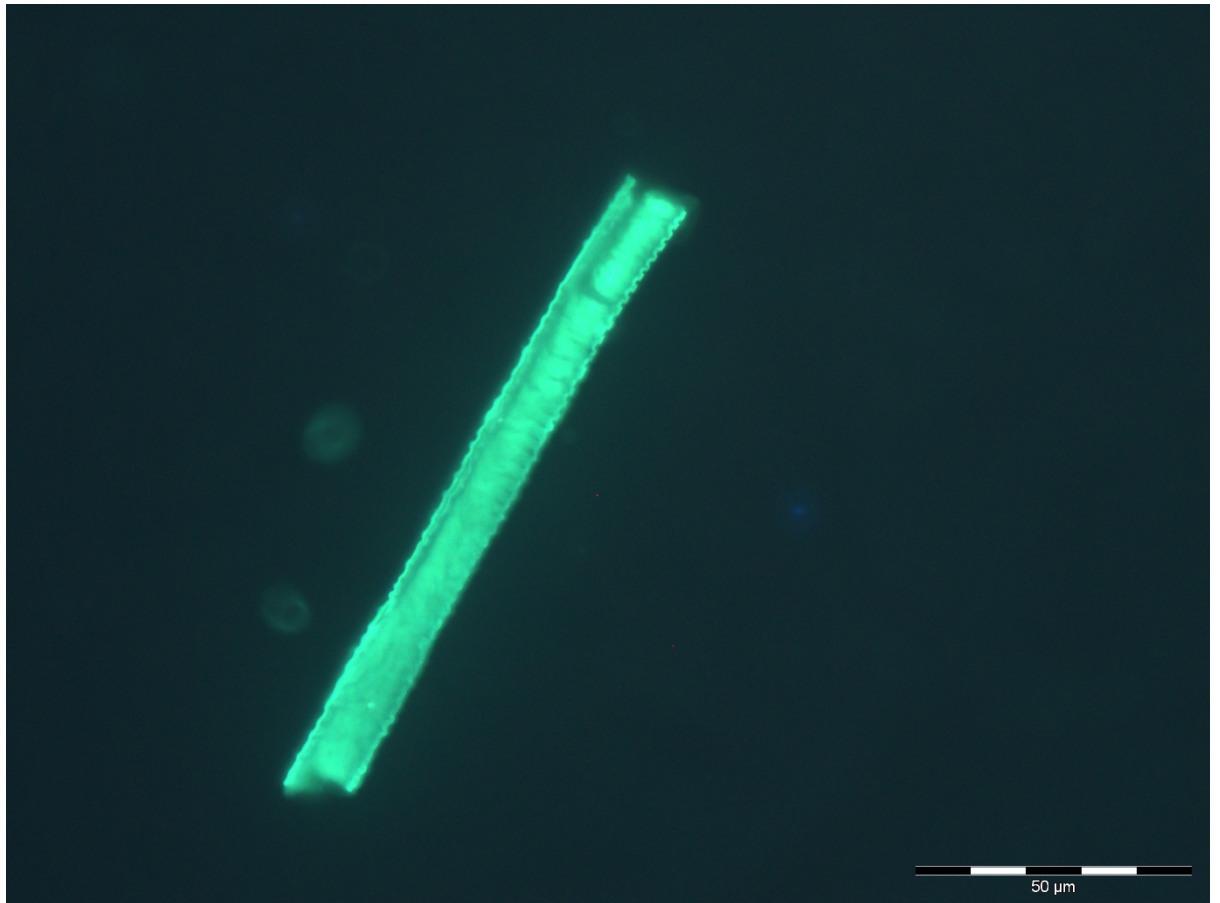


Figure 7.34 PDMPO stained silica from rice leaf epidermis of rice plants grown in the presence of silicic acid and then further grown in CaCl_2 with $100 \mu\text{M}$ aluminium for two weeks, viewed under fluorescence microscopy. Scale bar is present in the bottom right corner of the image.

The structures believed to have originated in the xylem were also present in the digests from plants grown in the presence of aluminium (Fig 7.34). The ridges which run down the length of the tube can be clearly observed (see red arrow). The whole structure gives off a strong fluorescence signal suggesting it to be densely silicified, although it is not possible to determine if the structure is hollow or solid.

7.4 Discussion

PDMPO imaging proved to be an excellent method for visualising silica structures from digested rice tissue, showing both previously identified structures as well as possibly novel silica structures.

7.4.1 Epidermal Cells and Stomata

Large sheets of silica from the epidermis of the rice leaf tissue were commonplace in the digest samples (Fig 7.1 – Fig 7.4, Fig 7.7, Fig 7.11 & Fig 7.12). The PDMPO staining of these epidermal silica structures showed intricate details, with the cell walls of individual epidermal cells being clearly visible, often showing more intense fluorescence than the surrounding silica (Fig 7.3 – Fig 7.5, Fig 7.10 & Fig 7.12). The increased fluorescence at the cell walls of epidermal cells could be the result of a denser silica deposition at these regions. It is also possible that the recessed grooves between the epidermal cells result in a greater surface area for PDMPO binding, giving the appearance of a stronger signal in these areas.

Two variations of epidermal cells were found to be silicified which have been termed primary and secondary epidermal cells. Primary epidermal cells are rectangular in shape with a sinuate border and papilla covering their surface, whilst secondary epidermal cells are rectangular but lack papilla covering their surface and their sinuate shape is less pronounced than that of the primary epidermal cells. Primary epidermal cells were the more commonly detected of the two variants, with the entire cellular structure being replicated in the silica samples including the sinuate edges and papilla (Fig 7.1 – 7.8, Fig 7.11 & Fig 7.12).

The papillas which cover the surface of the primary epidermal cells were consistently silicified, appearing brighter under fluorescence than the surrounding silica (Fig 7.1, Fig 7.3, Fig 7.4 & Fig 7.11). Given that papillas are raised nodules, a higher concentration of silica would be expected in these areas than at the flat surfaces of the epidermal cells, which would account for the stronger fluorescence signal seen.

In addition to the epidermal cells themselves, other structures at the leaf epidermis were silicified including the stomata, trichomes and silica cells. Stomata were detected on several occasions, embedded within the epidermal cell mosaic structure, although they were difficult to identify (Fig 7.7, Fig 7.15 & Fig 7.20). Two samples showed evidence of the guard cells, which cover the stomata, being silicified (Fig 7.7 & Fig 7.15), whilst the other stomata observed were merely a gap in the silica sheet representing the stomatal aperture (Fig 7.20). Stomata are required to move in living tissue, opening and closing the guard cells to regulate gas exchange, therefore it is reasonable to expect that silicified guard cells would not be attached to the larger silica sheet covering the epidermal structure as they would not be able to function. Guard cells, whilst silicified themselves, would be prone to detaching from the larger structure when the organic component of the plant was acid digested, leaving only the stomatal aperture visible in the silica in most instances. Using the PDMPO method to stain silica from horsetail (*Equisetum arvense*), silicified stomata were shown with their guard cells consistently intact and attached to larger silica structures (Law & Exley, 2011). It is possible that during the filtration and staining of the silica samples, more gentle techniques were used resulting in less damage to the silica structures, however, given that almost all other silica structures in the rice samples were found consistently intact, in large silica fragments it is more likely that the silicified stomata in horsetail are less prone to detaching than their guard cell counterparts in rice.

7.4.2 Trichomes

Trichomes, the spine-like structures which occupy the epidermal regions of rice leaves, were found to be silicified on multiple occasions (Fig 7.20 – Fig 7.22). An example of a trichome still attached to a larger epidermal silica structure was found, showing the localisation of trichomes within rows of primary epidermal cells (Fig 7.20 & Fig 7.21). The entire body of the trichome was silicified uniformly, from the bulbous base through to the spine. Although the spine appears to give a slightly stronger fluorescence than the base, this is likely due to the curved shape of the

spine giving a greater surface area for PDMPO to bind to (Fig 7.21). A detached trichome was also observed, with the bulbous base and spine still in one piece but floating free from any large silica structures (Fig 7.22). This trichome was viewed from its underside and appeared hollow due to the removal of the organic tissue which would normally be situated under the silica layer.

Interestingly, another sample showed a large epidermal silica structure with an aperture in its surface. Whilst first assumed to be a stomata, this structure is in fact a gap where a trichome had become detached (Fig 7.8). The occurrence of loose trichomes, and the gaps where they were situated in, in otherwise intact silica sections suggests that trichomes are silicified separate from the epidermal cells. Trichome development has been shown to be basipetal in other species such as *Arabidopsis*, meaning development begins at the tip of the spine and develops towards the base (Evert, 2006). Some trichomes are also known to secrete substances, including defensive compounds from their tip, acting as both a physical and chemical deterrent to predation (War et al., 2012). It is possible that silicic acid is among those substances which are secreted from the tip of the trichome, resulting in silicification happening from the tip backwards down the spine where it would adjoin to the main silica formation at the epidermis. This join would serve as a weak point in the silica layer, leaving the trichomes more susceptible to breaking away from the larger structure.

Trichomes are a common occurrence on the leaves of grass species and are hypothesised to serve a variety of roles, including temperature regulation, controlling evaporation and defence against predators, though in reality many of these hypotheses have not been tested or not conclusively proven (Callow, 2000). Trichomes are known to be silicified in rice as well as in numerous other species of grass (Kaufman et al., 1985). Kaufman and company hypothesised that the silicified trichomes could, due to their transparent properties, act as windows for light to pass through to the photosynthetic cells beneath them, however, later research disproved this theory (Agarie et al., 1996).

7.4.3 Silica Cells

Silica cells were found to be heavily stained by PDMPO when compared with the surrounding silica, implying a denser deposition of silica at these cells when compared with epidermal cells (Fig 7.13 – Fig 7.17). Silica cells were most commonly found loose from any larger silica structure, suggesting that the ladder-like formations they normally occupy are either brittle in nature or silicified in such a way as to require the organic component to maintain structural integrity (Fig 7.13, Fig 7.14 & Fig 7.17). In the few cases where sections of the ladder-like structure of silica and cork cells was silicified intact, it can be clearly seen that the silica cells give a much stronger fluorescence than the cork cells between them (Fig 7.15 & Fig 7.16).

Silica cells run in an alternating formation with cork cells to form a ladder-like structure covering the veins of rice leaves and are so called because of their high silicon content. Research has shown that these structures have a flex rigidity of over 70 times that of the surrounding leaf tissue, the researchers concluded that these structures play a role in preventing twisting torsions of the leaf (Yamanaka et al., 2009). During an investigation into silicification during growth progression, it was observed that silica cells were amongst the earliest cells to be silicified, with silica cells being present and silicified when other tissues were not (Ma, 1990). If silica cells are silicified earlier and more heavily than the intermediate cork cells, the silica structure would be littered with weak points where the less dense silica of the cork cells met the silica cells. Under normal conditions the organic matrix of the plant tissue beneath would greatly strengthen this structure, but once this component is acid digested, the entire structure would be prone to collapse.

7.4.5 Bulliform Cells

Bulliform cells were also found to be heavily silicified, though interestingly only the mushroom-shaped variants were observed in the PDMPO imaging (Fig 7.18 & Fig 7.19). Bulliform cells are located at the inner edges of a curve in the leaf; these large cells contract through water loss to curl up the leaf, thereby reducing water lost through transpiration. The largest bulliform cell is

located at the centre of the formation and is shaped somewhat like a mushroom due to its positioning (Fig 7.35)

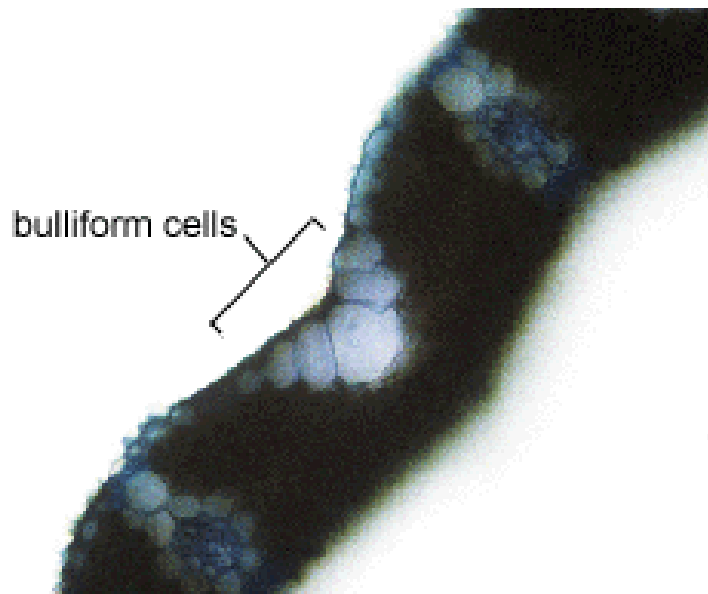


Figure 7.35 Light microscope image of a cross-sectioned rice leaf, showing the bulliform cells in formation at the inner apex of a curve in the leaf (Rost, 1997).

Unlike the previously discussed silica structures like the epidermal cells, stomata and trichomes, which were merely silica replicas of exposed surface cells, bulliform cells extend deep into the interior of the rice leaf and yet are found to be entirely silicified (Fig 7.18 & 7.19). Given the role of bulliform cells, it seems impossible that they would be able to function whilst silicified to the extent observed here; a solid silica layer surrounding the cell would certainly remove the bulliform cell's ability to expand and contract theoretically reducing the plant's ability to cope with drought conditions where it would need to conserve water. However, research into the effects of silicification shows the opposite, that silica in plants is of benefit during drought conditions as it reduces the transpiration rate (Ma, 1990). The reduction in transpiration rate in silicified plants has been ascribed to the layer of silica at the leaf epidermis and it may be that the reduction in transpiration rate that this external barrier causes outweighs the potential reductions in transpiration that the function of the bulliform cells could afford the plant. It is also possible that, through some unknown mechanism, silicification does not prevent the bulliform cells from functioning. It is feasible that the silica actually exists in a more malleable form than the solid silica

we obtain from the digests and that it is the digest procedure itself that causes the solidification into silica; almost all methods of visualising silica in plants require the plant tissue to be excised from its parent plant, at which point the controlled, relatively-contained environment maintained within the plant is disrupted. Evidence of this exists in the xylem of rice, which is capable of transporting silicic acid at super-saturated concentrations of up to 18 mM, far beyond the 2 mM required for polymerisation (Mitani et al., 2005). However, once this super-saturated solution was removed from the xylem, it quickly began to polymerise into silica, suggesting something about the internal environment of the xylem was maintaining the solution, though organic compounds or complexes with silicic acid were ruled out. Future investigation into the ability of bulliform cells to function under conditions of silicification is certainly needed, because if the curling ability of the leaves remains intact in silicified rice then the bulliform cells cannot be silicified to the extent that the PDMPO staining has shown.

7.4.6 Xylem

Whilst all of the previously discussed silica structures found in the PDMPO staining are known areas of silicification, the presence of silicified xylem vessels was an unexpected discovery. Whilst the xylem is well known as the highway through which silicic acid travels through the plant, it is not typically considered a site of silicification itself. Despite this, several structures were found which match the known morphology of xylem vessels: long cylindrical tubes with ridges running down their length (Fig 7.23 – Fig 7.25). When compared with a cross-section of plant tissue which intersects a xylem vessel, the similarity between the two structures is clear (Fig 7.36).

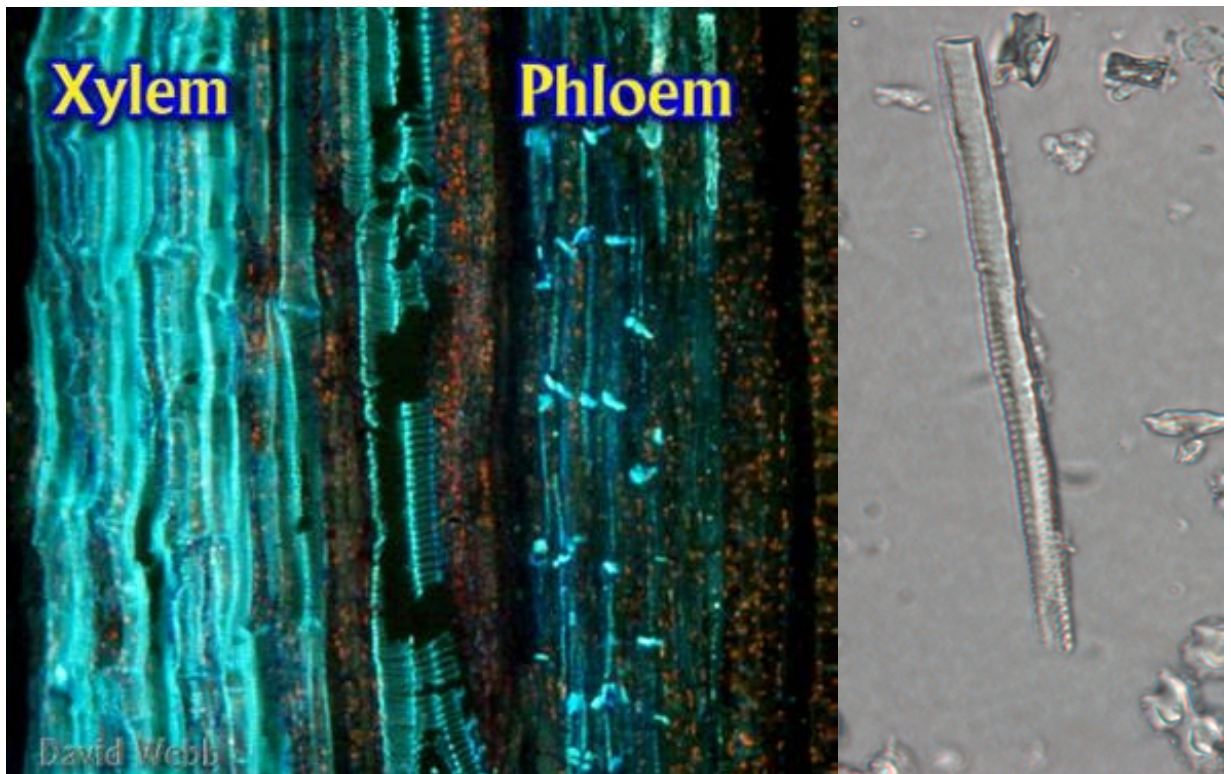


Figure 7.36 Comparison between cross-sectioned xylem vessel shown under fluorescence microscopy (A) (Valencia College, 2015) alongside a xylem silica structure under light microscope (B).

Whilst it seemed unlikely that a bulliform cell could function when silicified, it is even more bizarre to consider that a water transport channel could function unhindered by the silicification of its interior. From the PDMPO and light microscope images, it is not possible to determine if these xylem silica structures are hollow or not. If they are hollow then there is some possibility that a xylem could still transport water throughout the plant, albeit at a reduced rate due to the reduction in the diameter of its lumen. However, if the xylem silica structure is solid silica then it is simply impossible for the xylem vessel to function.

It is well known that silicic acid is transported from the roots, up through the xylem and to the surface of the upper plant where it forms silica (Tamai & Ma, 2003). As previously stated, the concentrations of silicic acid found in the xylem have exceeded the saturation point of 2 mM by a significant degree in both rice and wheat respectively (Casey et al., 2003; Mitani et al., 2005). Though maintained as silicic acid inside the xylem, once removed from the xylem these super-saturated silicic acid solutions quickly began to polymerise into silica.

Our rice samples were not immediately digested after harvesting, but were instead cut into 1 cm segments and placed in an incubator at 37°C to dry out. This drying procedure results in the removal of almost all water from the sample, which would increase the concentration of silicic acid remaining in the xylem, possibly causing the polymerisation of silicic acid into silica. This could have explained the unexpected presence of silicified xylem structures in the PDMPO stained silica samples, although later experiments performed suggested that this was in fact not the case (see 5. Investigation into the Effects of Sample Preparation Procedure on Silica Morphology through SEM Imaging).

7.4.7 Conclusions

Silica found in the plants grown in the presence of aluminium for two weeks after maturation showed no variation in structure when compared with silica found in plants grown in the absence of aluminium. Primary epidermal cells were located with sinuate shape and papilla clearly visible (Fig 7.28, Fig 7.29 & Fig 7.30), along with secondary epidermal cells (Fig 7.30 & Fig 7.31), silica cells (Fig 7.31 & Fig 7.32), bulliform cells (Fig 7.33) and xylem (Fig 7.34). Whilst there is no evidence for aluminium inducing changes in the silica deposition pattern in rice, it is still possible that aluminium is co-localised with silicon at some or all sites of deposition, though a more suitable imaging method will be required to determine this.

Unsurprisingly, there was no evidence of silica stained by PDMPO in the acid digests of rice plants grown in silicon deplete conditions (Fig 7.27). Rice plants grown hydroponically without added silicon showed no adverse effects or defects when compared with their silicon replete counterparts. As a casual observation, it was noted that the leaves of silicon deplete rice plants seemed to bend or droop over more than those in silicon replete conditions, however, this observation was not pursued experimentally. Beyond this, the lack of silica in the silicon deplete group plants merely shows that the desired growth conditions were achieved. Rice grows without

incident in the absence of silicon in laboratory conditions, though obviously many of the real-world stresses with which silicon can aid a plant would not apply under such conditions.

Despite the myriad of benefits that silicon can afford a plant grown in its presence, it is not considered to be an essential element for plant growth (Epstein, 2001). Whilst there are differences of opinion on the definition of essential amongst researchers in the field of silicification, in the broadest sense of the word essential, our work would support this non-essential view of silicon as a plant nutrient. Though certainly of benefit under real-world conditions, we were able to grow rice in the absence of silica without any ill effects when compared with their silicon replete counterparts. These silicon deplete rice plants were grown to maturity and acid digested, whereupon it was found that no silicon deposition had occurred in their tissues.

PDMPO staining is an effective method of visualising biogenic silica obtained from acid digestion of rice tissue. Not only does PDMPO staining provide striking images of the silica structures, revealing their intricate details, but because PDMPO is a specific stain for silica, we can be sure that what we are seeing is silica and not the remnants of the organic component of the plant. Where the fluorescence imaging is not clear, light microscopy can be used to supplement fluorescence microscopy, revealing certain details which may be obscured by strong PDMPO fluorescence in specific regions. The silica digests performed showed evidence of all known sites of silica deposition in rice, as well as the surprising evidence of silicification in the xylem which requires further investigation.

8. PDMPO Staining of Silica Structures in Rice through Development from Seed to Seedling

8.1 Introduction

Silica deposition in plants is the result of the uptake of silicic acid, $\text{Si}(\text{OH})_4$ from the soil solution and its subsequent polymerisation into silica (Currie & Perry, 2007). Not all plant families accumulate silica, but the Poaceae family, also known as the true grasses, are known silicon accumulators. Within the Poaceae family, rice is one of the most commonly studied silicon accumulators due to its high silica content, up to 13.13% in the leaf sheath (Lanning, 1963).

Rice is a known silica accumulator and many of the structures which silica forms within rice are well known. Silicon is primarily deposited at the leaf epidermis, between the epidermal cells and the leaf cuticle, forming a cuticle-silica double layer which acts as a physical barrier or armour for the leaf against insect and fungal attack (Ma & Yamaji, 2008). In addition to this silica layer, several specific cells are also silicified, such as bulliform cells and silica cells. Bulliform cells (also known as motor cells) are thought to be responsible for the leaf's ability to curl up when under drought conditions (Dickison, 2000). When the silica content of the rice shoot is above 5% these bulliform cells are found to be silicified, though not at lower silica concentrations (Ma et al., 2001). The other common silicified cell type is called a silica cell: dumbbell-shaped cells which occur on the leaf's surface as ladder-like structures, with alternating silica and cork cells running along the surface of the leaf epidermis above the vascular bundles (Yamanaka et al., 2009). Silica is also deposited at the epidermis and vascular tissues of the stem, leaf sheath and hull (Ma et al., 2001).

Whilst a great deal is known of where silicification occurs in rice, the question of when this process occurs and how it progresses as a rice seedling develops is still relatively unknown. Given that silica cells were found to be silicified in rice plants with silica concentrations below 5% weight, whilst bulliform cells were only silicified above 5% weight, it was proposed that

silicification occurs at the silica cells at an early stage, before progressing from the silica cells to the bulliform cells (Ma et al., 2001).

To further the knowledge of silicification in developing rice tissues, an experiment was conceived to follow the development of rice plants from seed through to the growth stages of the seedling. Rice plants were grown hydroponically and harvested at varying stages in their development for acid digestion. The silica which remained from this process was analysed using PDMPO staining and fluorescence microscopy. By analysing and comparing the varying silica structures found in rice seedlings at different stages of development it could be determined when these structures first formed and whether or not the structures found varied throughout the growth stages, which would suggest the possibility of rice being able to alter silica structures as the plant grows.

8.2 Method

8.2.1 Plants Grown Hydroponically

Rice plants were grown hydroponically for use in this experiment for 29 days. Over the course of their development, seedlings were observed and then harvested at key developmental points for acid digestion. The developmental points were:

- Un-germinated seeds (Day 0)
- Germinated Rice Seeds with Radical (Day 8)
- Germinated Seed with Radical and Shoot Apical Meristem (Day 12)
- Rice Seedling – Second Leaf Stage (Day 16)
- Rice Seedling – Third Leaf Stage (Day 22)
- Rice Seedling – Fourth Leaf Stage (Day 29)

For full details on hydroponic growth setup, see section 2.1 Hydroponic Growth of Plants.

8.2.2 Acid Digestion and Filtration

Once the growth period was over, rice plants were harvested. Each plant was separated into stem, leaf and root before being cut into roughly 1cm sections. The leaf, stem and root sections were then weighed before being stored inside an incubator at 37°C. The plant samples were periodically weighed until they reached a constant dry weight. At this point, the dried samples were then acid digested using the standard acid digest procedure.

Samples were filtered after digestion to harvest their silica using the standard digest filtration procedure and stored in an incubator at 37°C until the silica was dried. Samples can be stored indefinitely in this state, provided they are kept within the incubator to prevent moisture build-up. For full details on the acid digestion and filtration procedure, see section 2.2 Microwave Acid Digestion & Filtration.

8.2.3 PDMPO Staining and Fluorescence Microscopy

After harvesting and acid digestion, silica samples from each developmental group were stained using 0.125 μ M PDMPO in 20mM PIPES at pH7 and stored in a refrigerator for 48 hours to allow the fluorophore to bind with the sample.

After the binding period, samples were ready for viewing under fluorescence microscopy. Due to the aqueous nature of the sample, 25 μ L of the silica/PDMPO suspension was pipetted into a cavity slide and viewed using an Olympus BX50 with a BXFLA fluorescent. Images were taken under the U-MWU filter cube using a Colourview III digital camera using the CELL imaging software. For further details on the PDMPO staining and fluorescence microscopy, see sections 2.2 Microwave Acid Digestion & Filtration and 2.3 Light & Fluorescence Microscopy respectively.

8.3 Results

The following images are, unless otherwise stated, entirely formed of PDMPO stained silica viewed under fluorescence microscopy. When describing these structures, in the interest of

brevity, they shall be referred to as the cells from which they originated (e.g. epidermal cells, stomata, etc.), but they are only the silica layer which covered those cells; all organic tissue from these plant seeds and seedlings has been removed via acid digestion.

The images have a scale bar in the lower right corner of the image and have the magnification they were observed at labelled in their figure headings.

8.3.1 Un-germinated Rice Seeds

The first developmental stage of rice silica to be analysed was the un-germinated rice seeds. Rice seeds contain significant quantities of silica in their husk, the outer layer of the seed.

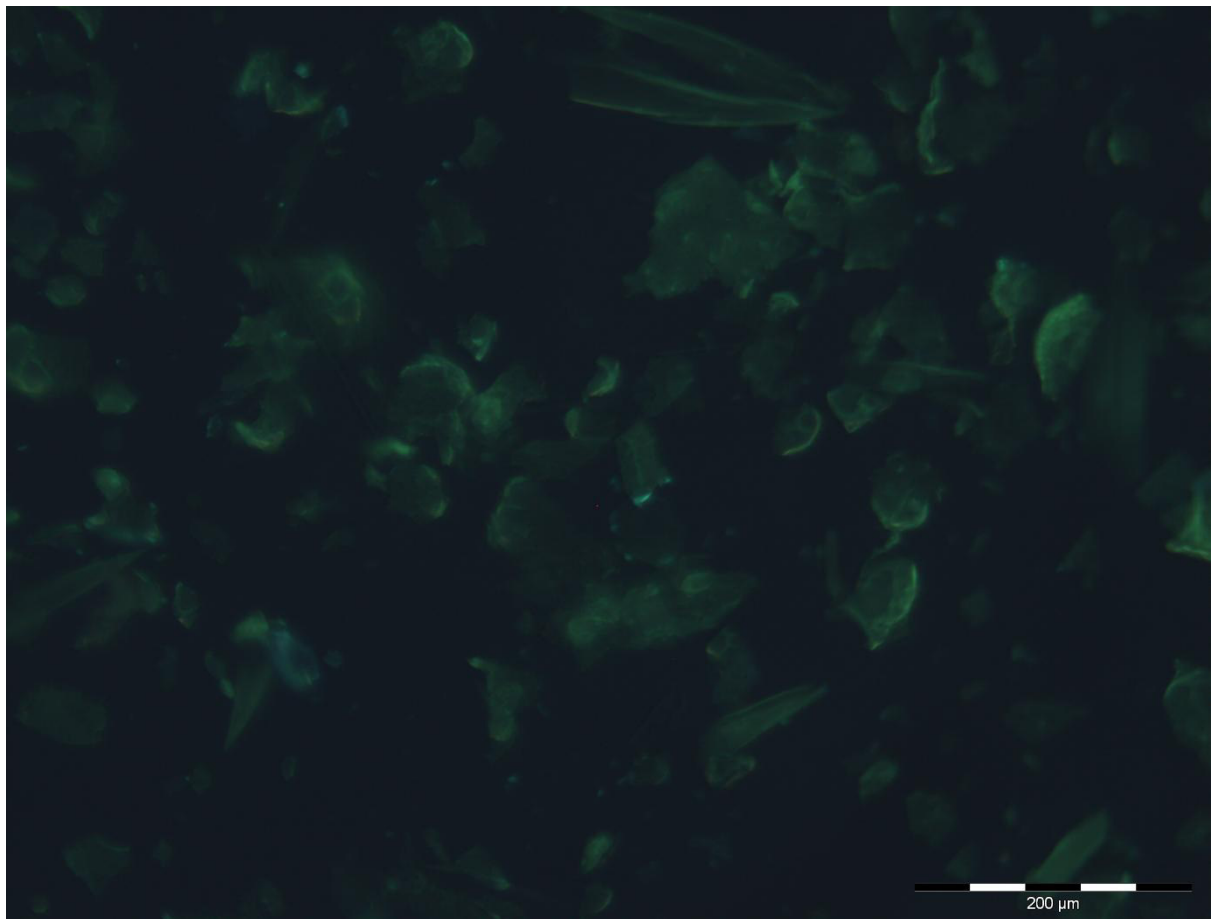


Figure 8.1 PDMPPO stained silica from acid digested rice seeds.

Amorphous shards of silica are commonplace in the silica digests from un-germinated rice seeds (Fig 8.1). Much of this silica is impossible to identify and localise from its morphology, however it does show the significant levels of silica deposition within rice seeds.

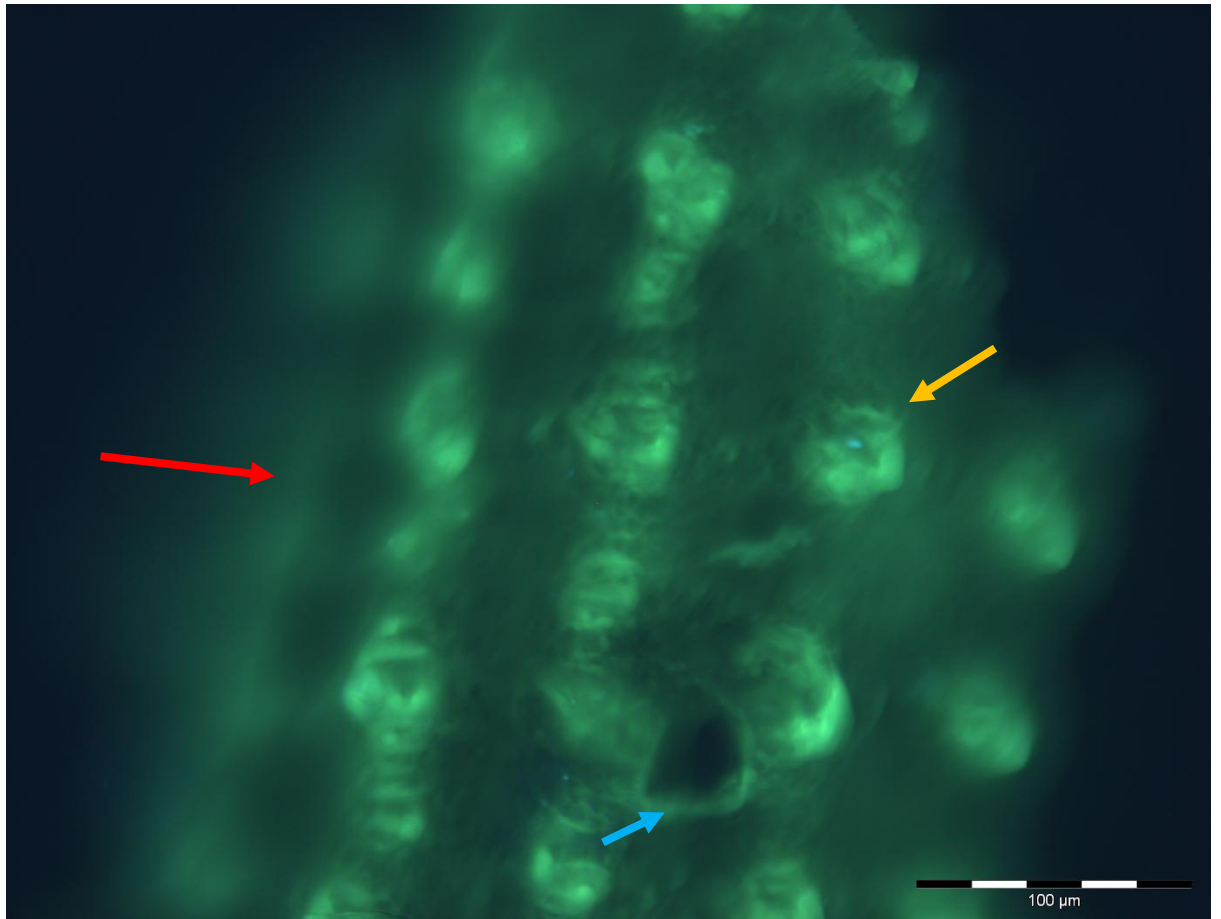


Figure 8.2 PDMPO stained silica from acid digested rice seeds. Arrows label areas of note, discussed in text.

Larger, intact silica structures are also found in the silica digests from un-germinated rice seeds (Fig 8.2). Large sheets of silica over 500 μm in length can be seen with raised nodules covering their otherwise smooth surface (see red arrow). The nodules themselves are rounded and over 40 μm in diameter with a rough texture (see gold arrows). There is also a 40 μm hole or gap visible in the silica sheet, though it is not possible to identify if this gap is part of the structure or merely a damaged area (see blue arrow).

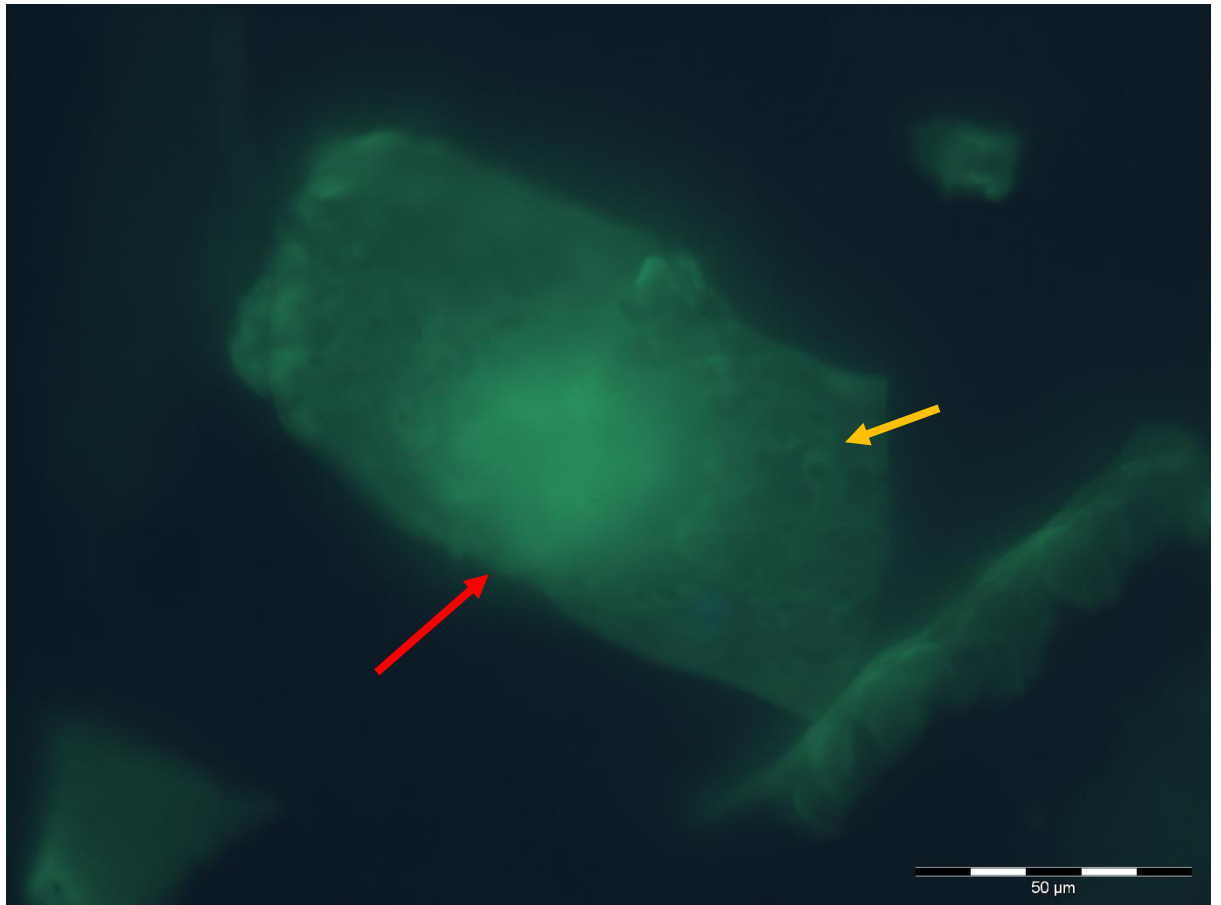


Figure 8.3 PDMPO stained silica from acid digested rice seeds. Arrows label areas of note, discussed in text.

Smaller, diffuse in appearance, sections of silica were also visible. (Fig 8.3). The silica shard is approximately 120 μ m in length with a stronger silica staining in the centre, suggesting either a thickening of the silica or a raised silica structure on the other, non-visible side of the silica piece (see red arrow). Faint outlines of what appear to be leaf epidermal cells can be observed, showing a sinuate mosaic structure where multiple interlocking cells can be seen (see gold arrow). The entire structure appears to be curved, suggesting this is a developing leaf still inside the seed.

8.3.1.1 Summary

The majority of the silica structures found in the un-germinated rice seed group originated from the rice seed husk, with large, textured silica pieces visible amongst the numerous smaller broken shards (Fig 8.1 & Fig 8.2). Evidence of a newly developing leaf within the seed was also found, showing silicification at an early stage of development (Fig 8.3).

8.3.2 Germinated Rice Seeds with Radical

The second developmental stage of rice silica to be analysed was the germinated rice seeds with their root radical formed.

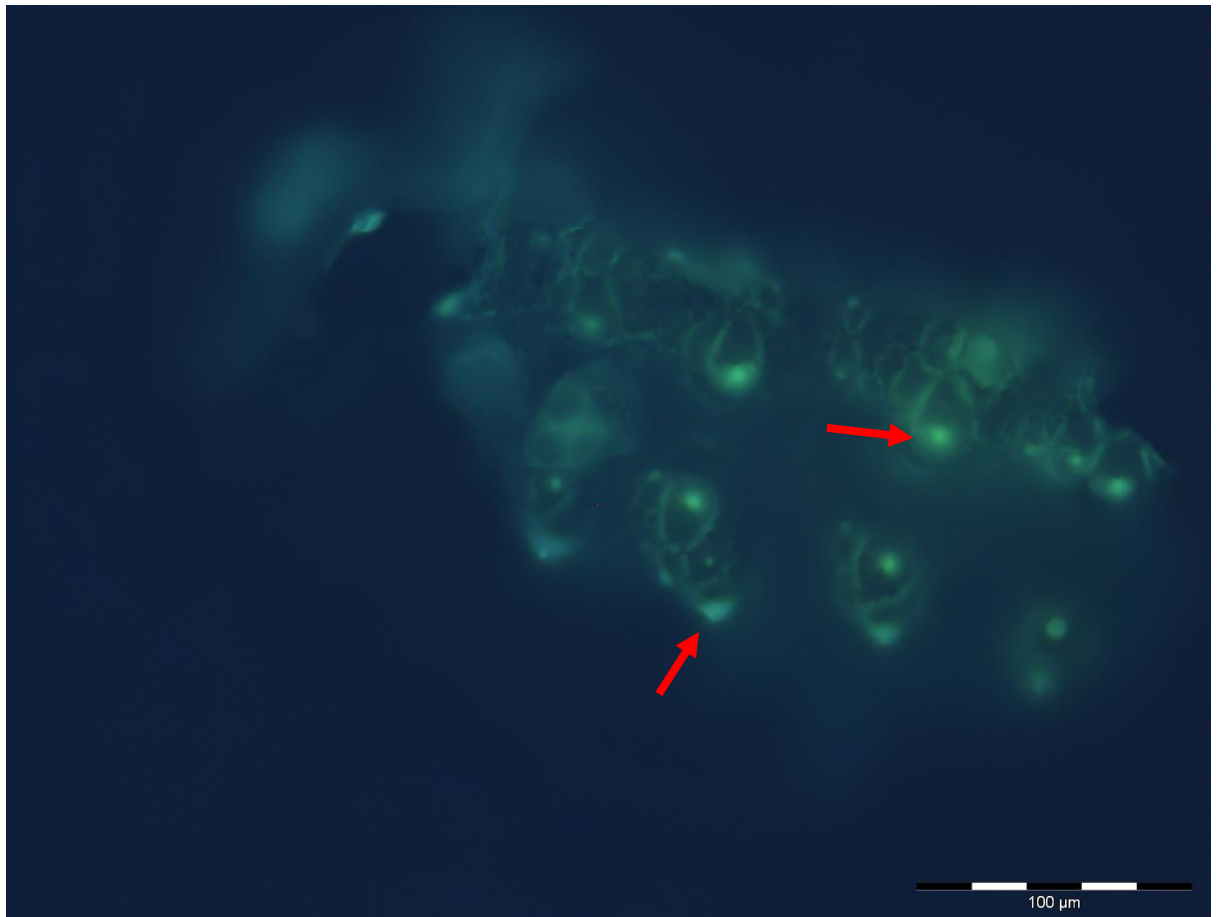


Figure 8.4 PDMPO stained silica from acid digested germinated rice seeds with radical. Arrows label areas of note, discussed in text.

Silica structures appear to be more developed in the newly germinated rice seeds (Fig 8.4). The structures seen resemble similar silica constructs found in the rice seeds (Fig 8.2), however there are several key differences. Raised nodular structures are seen both in the germinated and un-germinated seeds, however in the un-germinated seeds they have no detailed structure beyond their rough texture (Fig 8.2). In the germinated seeds, these nodules appear to be formed of multiple small cellular structures, with a heavily silicified raised bump or nodule on the surface (see red arrows). These structures could be early developments of epidermal cells, with the raised bump as an early papilla.

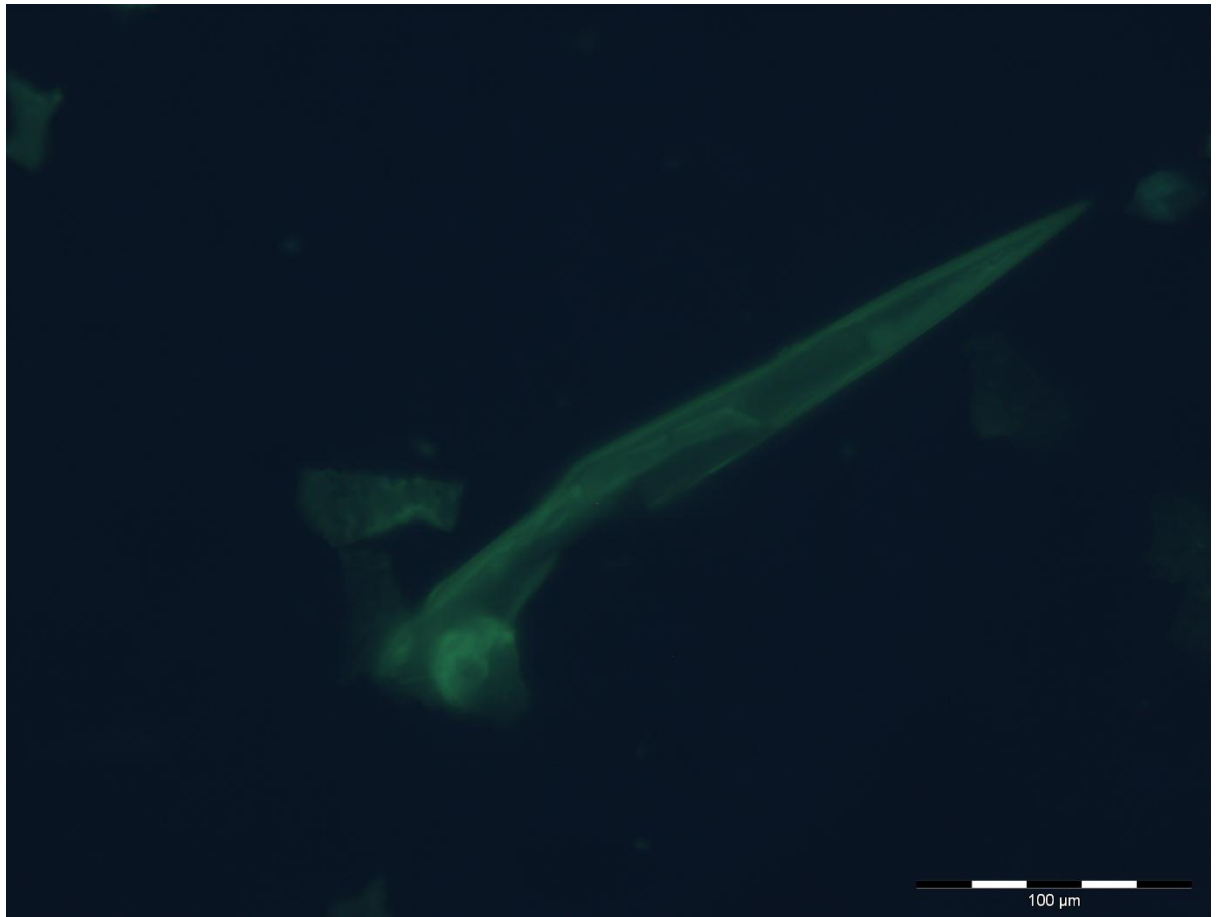


Figure 8.5 PDMPO stained silica from acid digested germinated rice seeds with radical. Arrows label areas of note, discussed in text.

A large silica shard can be seen, measuring over 300 μm in length (Fig 8.5). Whilst the shard shares the morphology of a trichome, it is far too large; trichomes average around 40-50 μm in length in one month old rice tissue. Without any obvious defining features, it is difficult to identify where this structure originated, but it is likely a shard which broke off from a much larger silica sheet from within the rice seed husk.

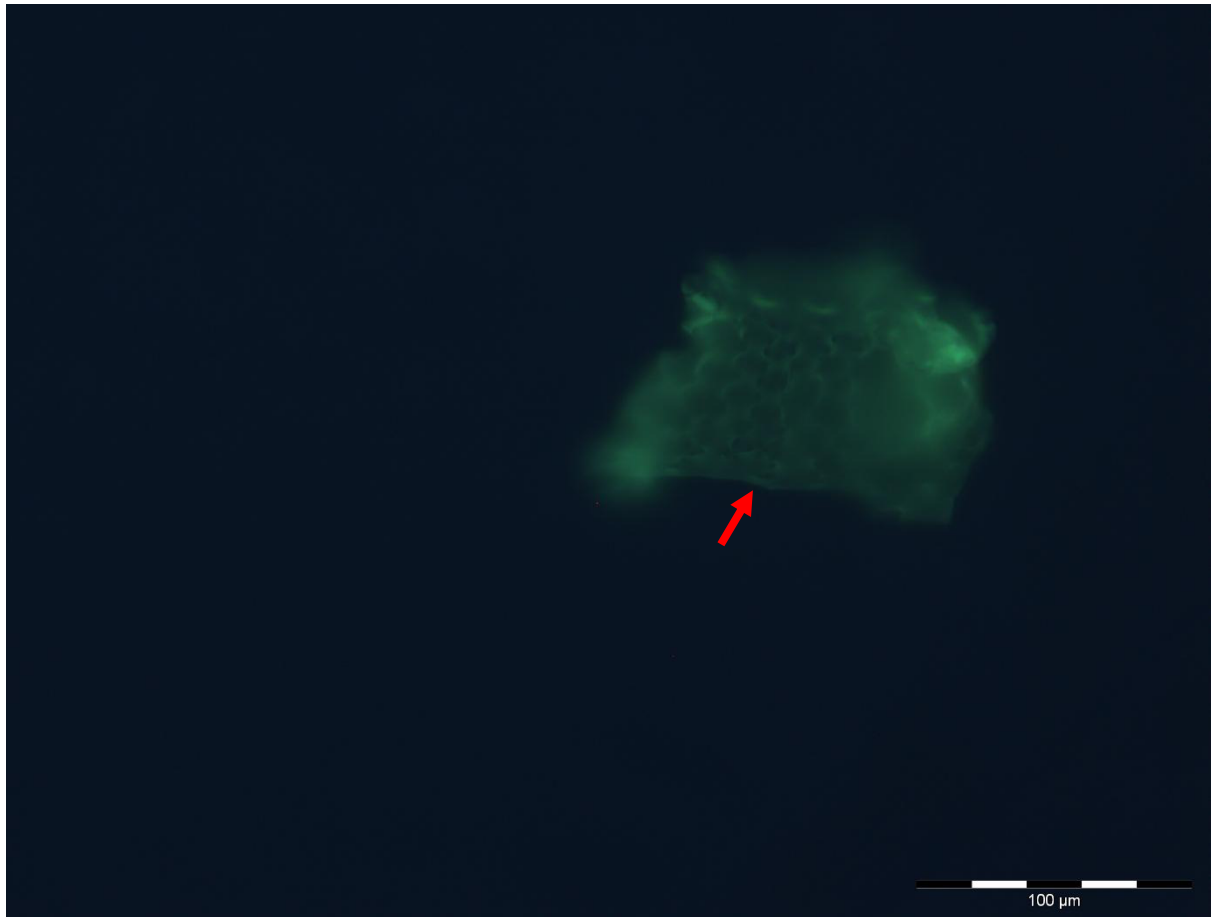


Figure 8.6 PDMPO stained silica from acid digested germinated rice seeds with radical. Arrows label areas of note, discussed in text.

The outlines of early epidermal cells can be seen within a silica sheet, identifiable by their distinctive sinuate shape (Fig 8.6). The epidermal cells do not appear to be fully developed at this stage, with the troughs of the sinuate waves almost touching at the middle of the epidermal cells (see red arrow); regular epidermal cells are much more rectangular in shape with the sinuate waves appearing only at their edges.

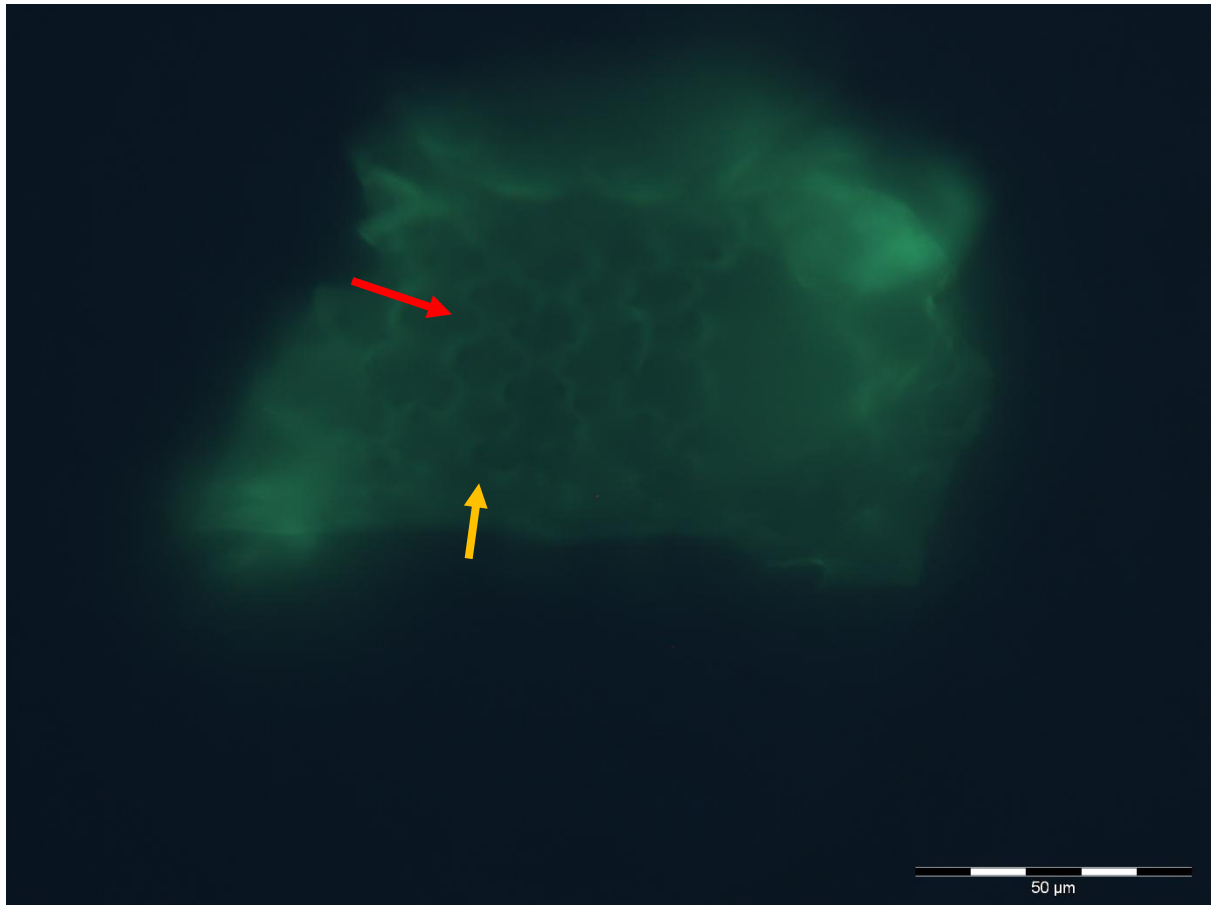


Figure 8.7 PDMPO stained silica from acid digested germinated rice seeds with radical. Arrows label areas of note, discussed in text.

A higher magnification image of the previously seen epidermal silica structure shows the epidermal cell outlines in more detail (Fig 8.7). The exaggerated sinuate shape of the developing young epidermal cells can be seen with more pronounced peaks and troughs than an epidermal cell from a more mature rice leaf (see red arrow). Darker areas are visible at some of the peaks of the epidermal cell walls, areas which would match the known locations of papilla; this sample is viewed from its underside with the papilla on the far side (see gold arrow).

8.3.2.1 Summary

The germinated seeds with radical were again dominated by silica fragments from the rice seed husk. Broken shards of much larger, brittle structures which did not survive the acid digestion and staining process intact (Fig 8.5). Several silica samples were found which indicated the growth of leaf epidermal tissue within the seed, before the formation of the apical meristem (Fig 8.4, Fig 8.6

& Fig 8.7). These samples showed structures which appear to be developing leaf epidermal cells (Fig 8.6 & Fig 8.7) as well as other unidentified structures (Fig 8.4).

8.3.3 Germinated Seed with Radical and Shoot Apical Meristem

The third developmental stage of rice silica to be analysed was the germinated rice seeds with both their root radical and shoot apical meristem formed.

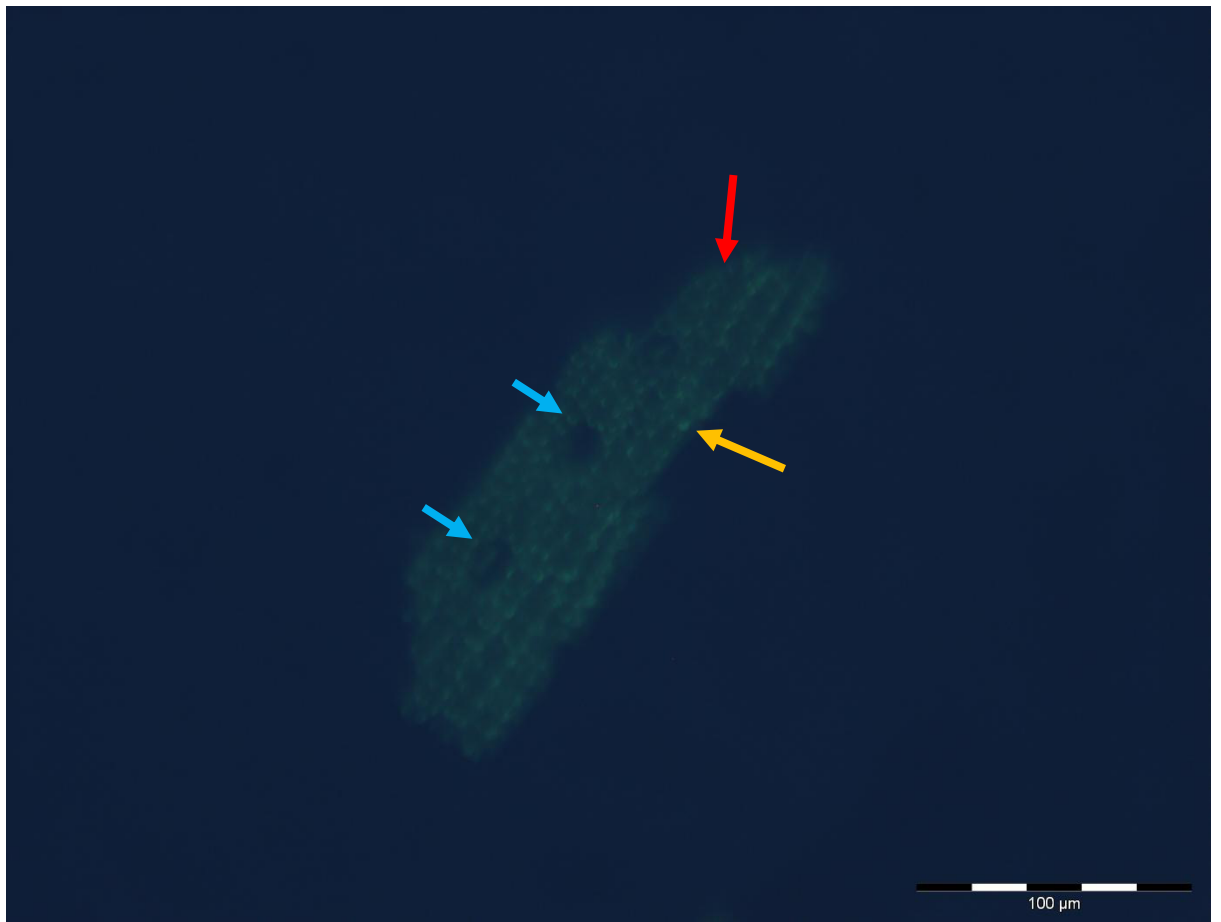


Figure 8.8 PDMPPO stained silica from acid digested germinated rice seeds with radical and shoot apical meristem. Arrows label areas of note, discussed in text.

A large silica structure from the epidermis of a rice shoot (Fig 8.8). The outlines of multiple epidermal cells are clearly visible from their interconnecting sinuate shape (see red arrow). Small nodules called papilla are also visible across the surface of the epidermal cells (see gold arrows). Two gaps in the epidermal structure are visible, measuring approximately 20 μm in diameter, though they are longer than they are wide (see blue arrows); these gaps are ghost stomata, stomatal apertures without their guard cells.

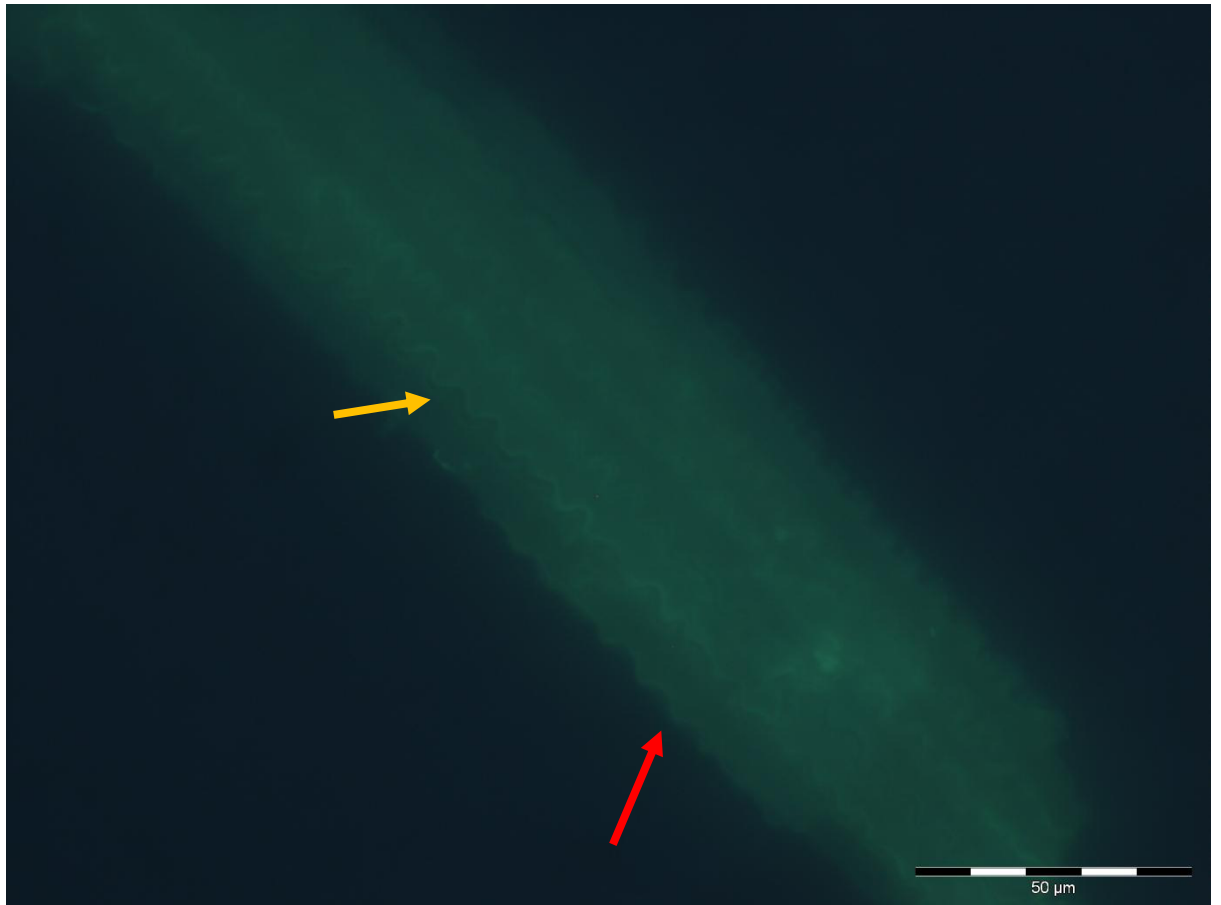


Figure 8.9 PDMPPO stained silica from acid digested germinated rice seeds with radical and shoot apical meristem. Arrows label areas of note, discussed in text.

A large silica structure on which covered multiple epidermal cells can be observed (Fig 8.9). Unlike the epidermal cells seen in the germinated seeds with radical group, these show the expected morphology for epidermal cells, with a rectangular shape and sinuate edges (see red arrow). The divides between epidermal cells joined laterally is distinctive with a noticeable gap in places (see gold arrow), however the joining point between horizontally-linked epidermal cells is more difficult to discern.

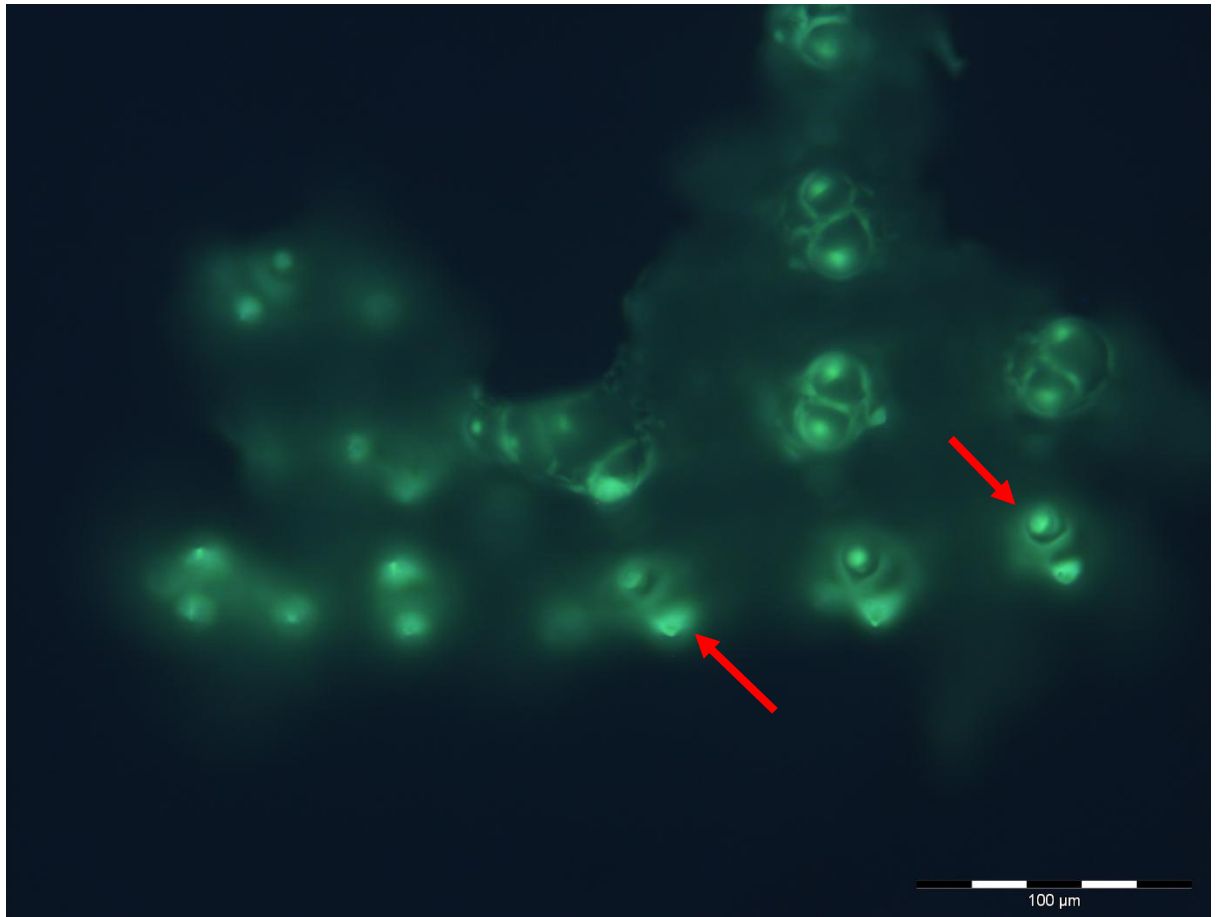


Figure 8.10 PDMPO stained silica from acid digested germinated rice seeds with radical and shoot apical meristem. Arrows label areas of note, discussed in text.

Silica structures similar to those seen in the germinated seeds with radical (Fig 8.10). Raised nodular structures are seen, formed of multiple small cellular structures, with a heavily silicified raised bump or nodule on the surface (see red arrows). These structures could be early developments of epidermal cells, with the raised bump as an early papilla, though they also bear a resemblance to the earlier silica structures from the rice seed husk (Fig 8.2).

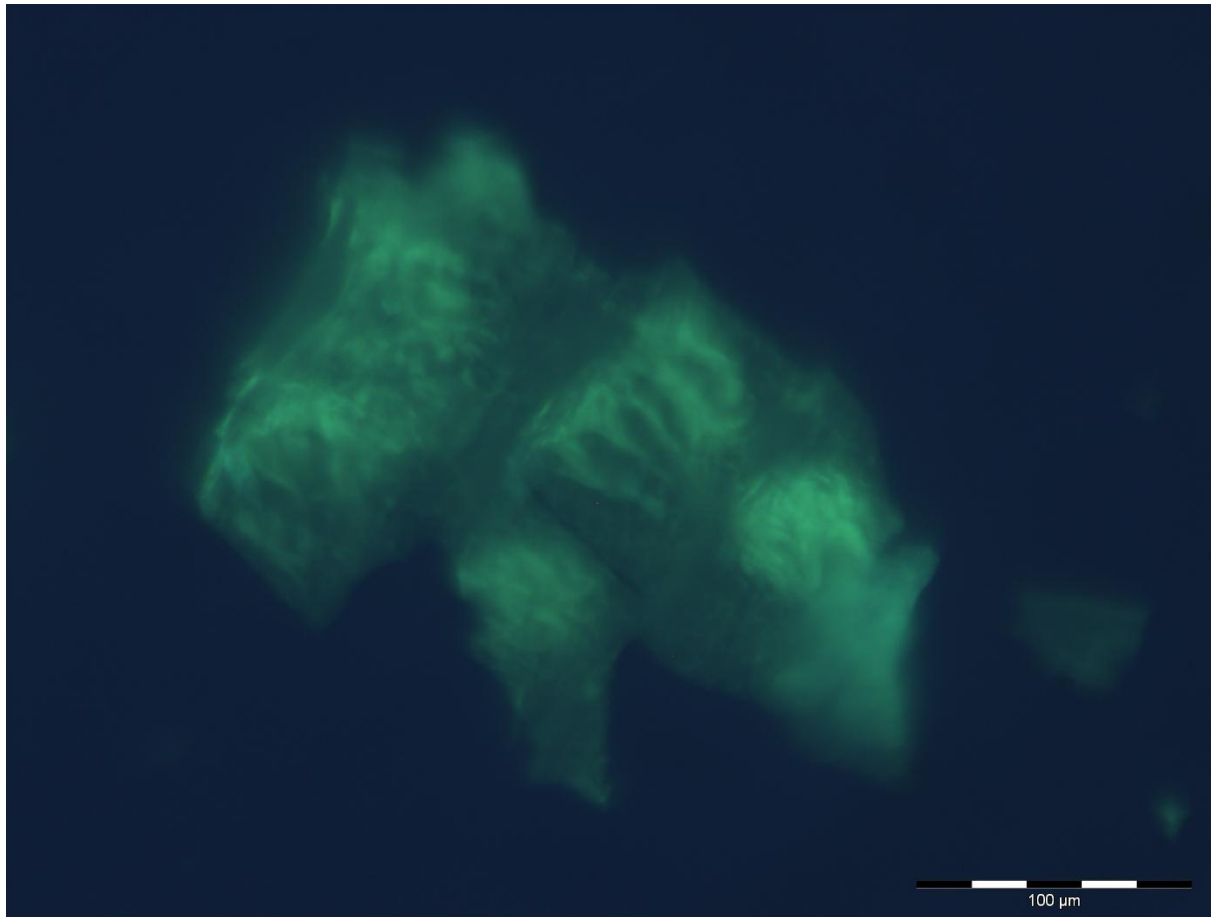


Figure 8.11 PDMPO stained silica from acid digested germinated rice seeds with radical and shoot apical meristem. Arrows label areas of note, discussed in text.

Large silica structure comprised of smoother silica punctuated with rougher, raised nodules of heavier silica deposition (Fig 8.11). This large silica structure is from the rice seed husk, meaning that the silica within the husk has not been repurposed (converted from silica to silicic acid for use in silicifying other structures) at this stage in the seedling's development.

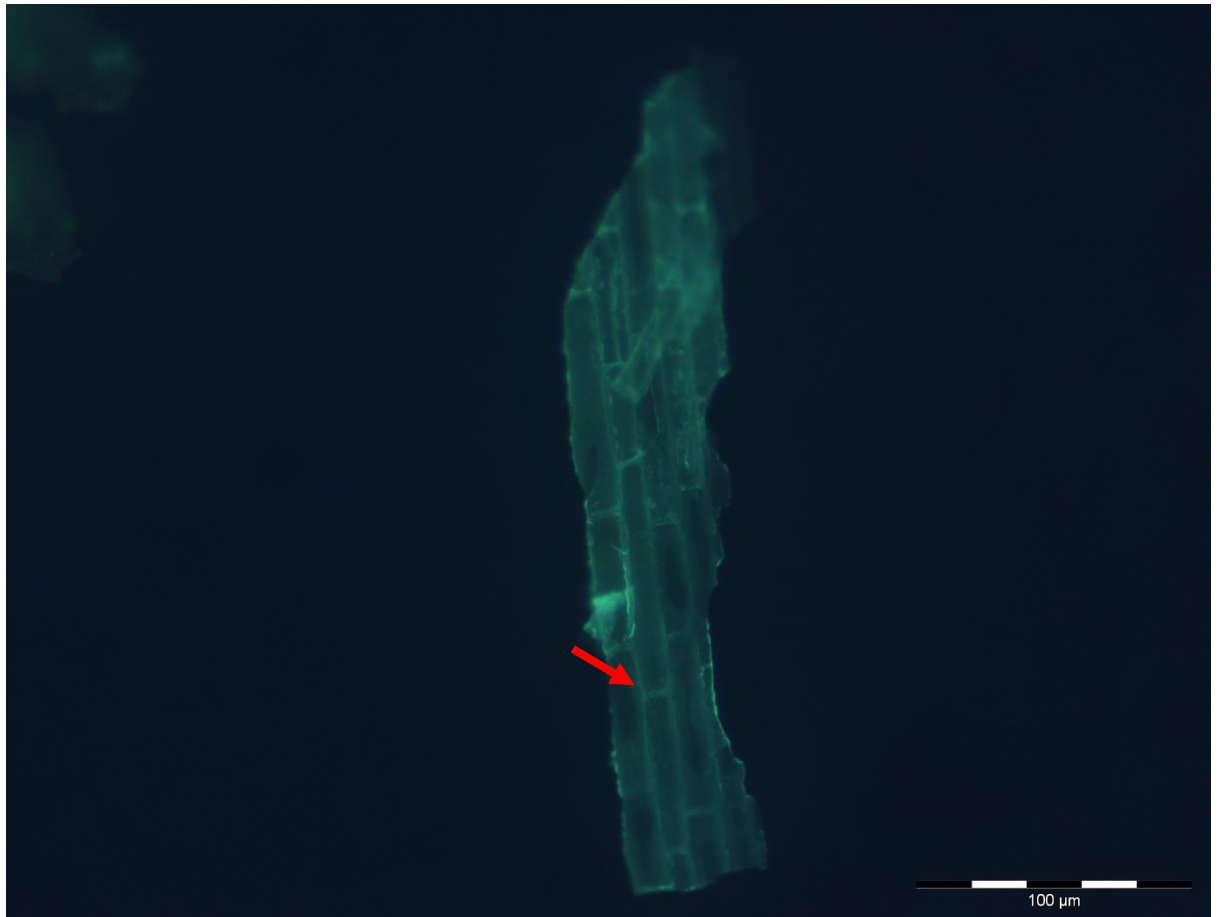


Figure 8.12 PDMPO stained silica from acid digested germinated rice seeds with radical and shoot apical meristem. Arrows label areas of note, discussed in text.

A secondary type of epidermal cells which have a different morphology to those found more commonly in the leaf tissue, lacking the sinuate edges and papillae (Fig 8.12). The epidermal cells that this silica structure covered were up to 80 μm in length and 15 μm in width, sharing the rectangular shape of the leaf epidermal cells. The divide between individual cells is clearly visible, not only in the lateral gaps but also at the horizontal joins between cells (see red arrow). These cells are either a variation on the normal epidermal cells, or an earlier stage of those epidermal cells that have not yet formed their sinuate edges and papilla.

8.3.3.1 Summary

With the formation of the shoot apical meristem, recognisable silica structures from the leaf epidermis become commonplace. Both primary and secondary epidermal cells, along with neighbouring structures such as stomata, have developed and were silicified even at the earliest

stages of the upper plant's development (Fig 8.8, Fig 8.9 & Fig 8.12). Large silica fragments from the rice seed husk were still visible at this developmental stage (Fig 8.11) along with other as yet unidentified structures (Fig 8.10).

8.3.4 Rice Seedling – Second Leaf Stage

The fourth developmental stage of rice silica to be analysed was the rice seedling when it had developed to its second leaf stage.

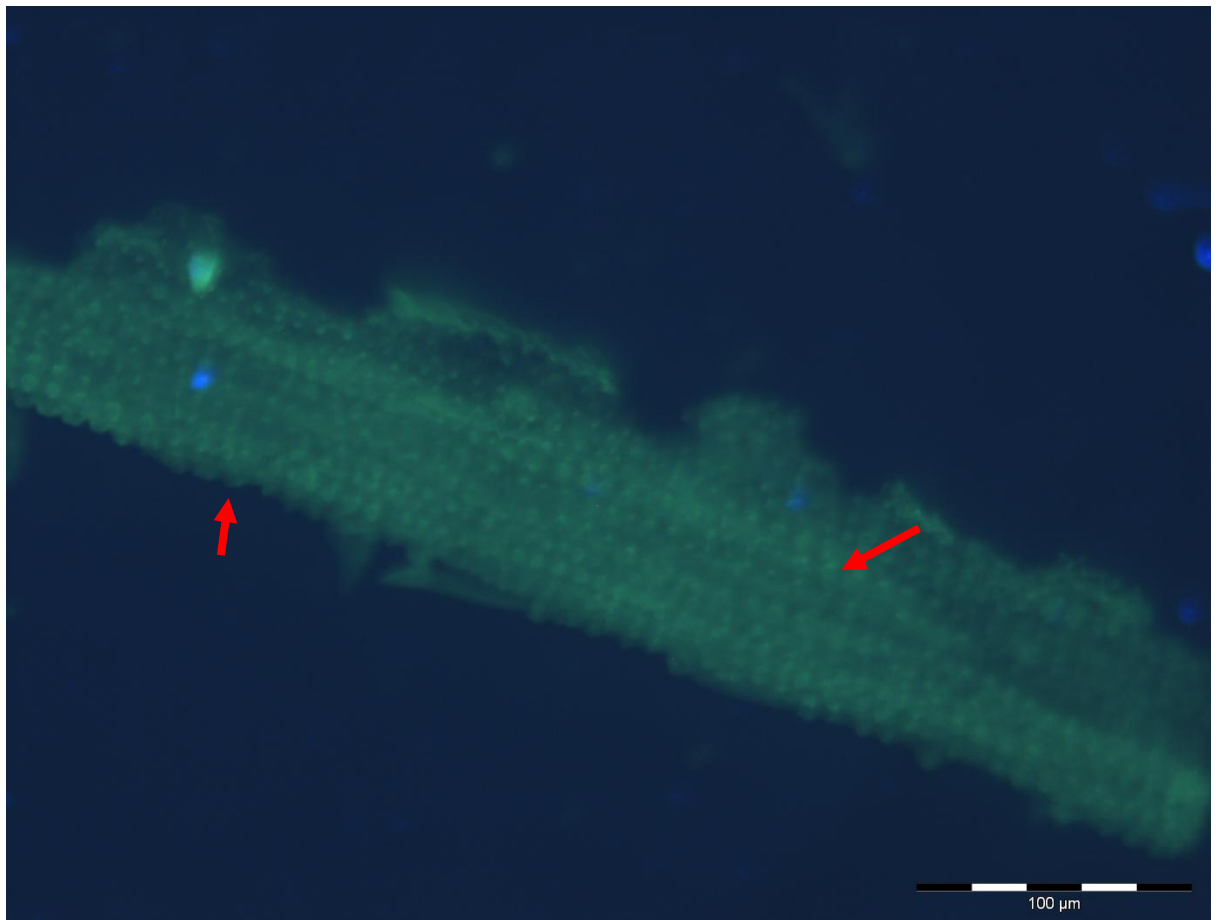


Figure 8.13 PDMPO stained silica from acid digested germinated rice seedlings at the second leaf stage. Arrows label areas of note, discussed in text.

Due to the method of visualising silica floating in a liquid, it can be difficult to orientate large silica samples in such a way as to bring the majority of the sample into focus (Fig 8.13). This silica structure from the leaf epidermis is incredibly large, over 500 μm in length, though its orientation makes it difficult to ascertain its width. This structure covered multiple epidermal cells, as evidenced by the numerous papillas or papillae visible across its length (see red arrows). Silica

covers the leaf epidermis as an almost unbroken superstructure, though the harvesting, acid digestion and PDMPO staining processes unfortunately result in the structures being broken down into smaller pieces.



Figure 8.14 PDMPO stained silica from acid digested germinated rice seedlings at the second leaf stage. Arrows label areas of note, discussed in text.

A silica structure which covered the secondary type of epidermal cells, with a gap where silica from two individual cells has come away from each other (Fig 8.14). The clear split down the gap between epidermal cells shows that the larger silicified structures are in fact multiple connected silica structures covering individual cells (see red arrow).

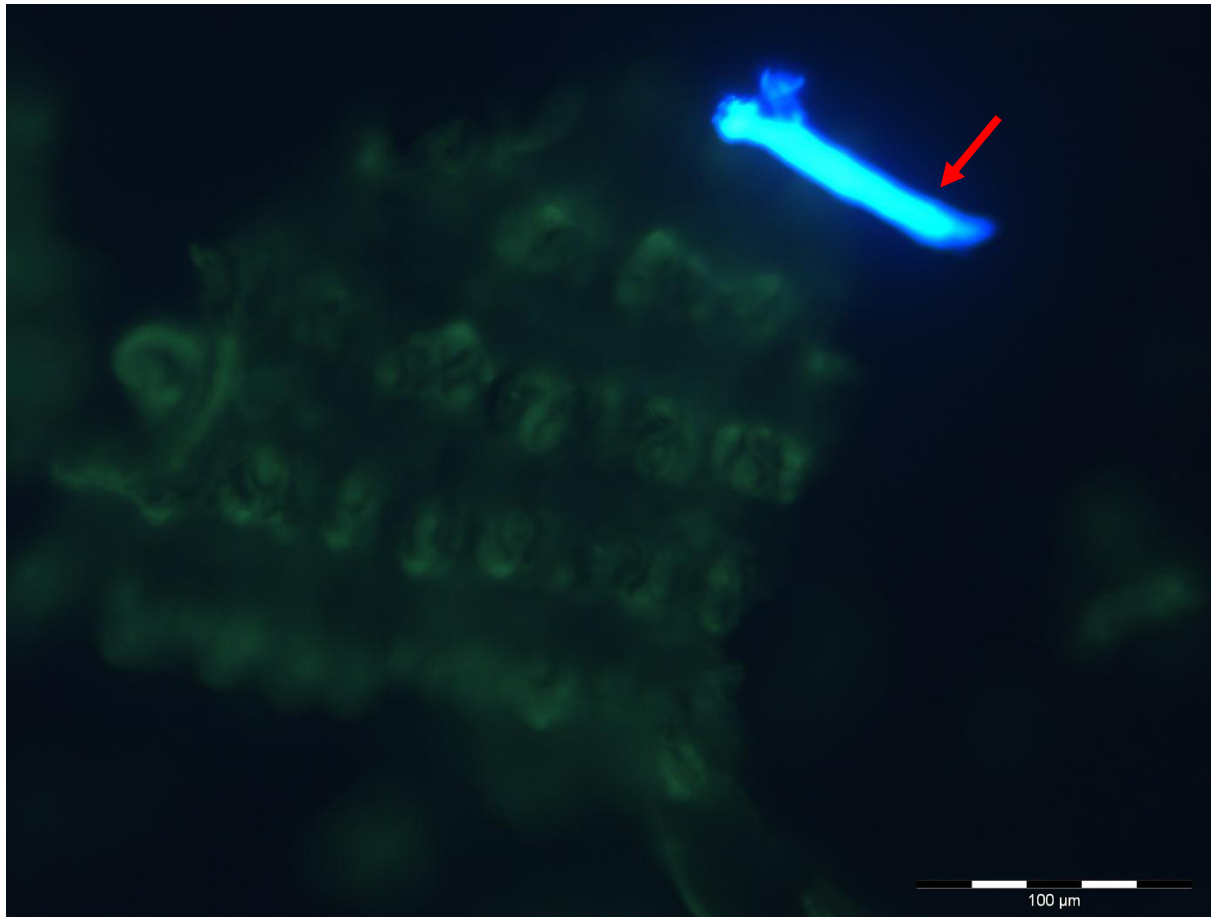


Figure 8.15 PDMPO stained silica from acid digested germinated rice seedlings at the second leaf stage. Arrows label areas of note, discussed in text.

Another large silica structure, similar to those seen in earlier sample groups, originating from the seed husk (Fig 8.15). The large blue fluorescent object visible is a contaminant, a speck of dust or hair which is easily distinguished from the stained silica samples (see red arrow). This sample shows that at the second leaf stage silica is still stored within the seed in significant quantities.

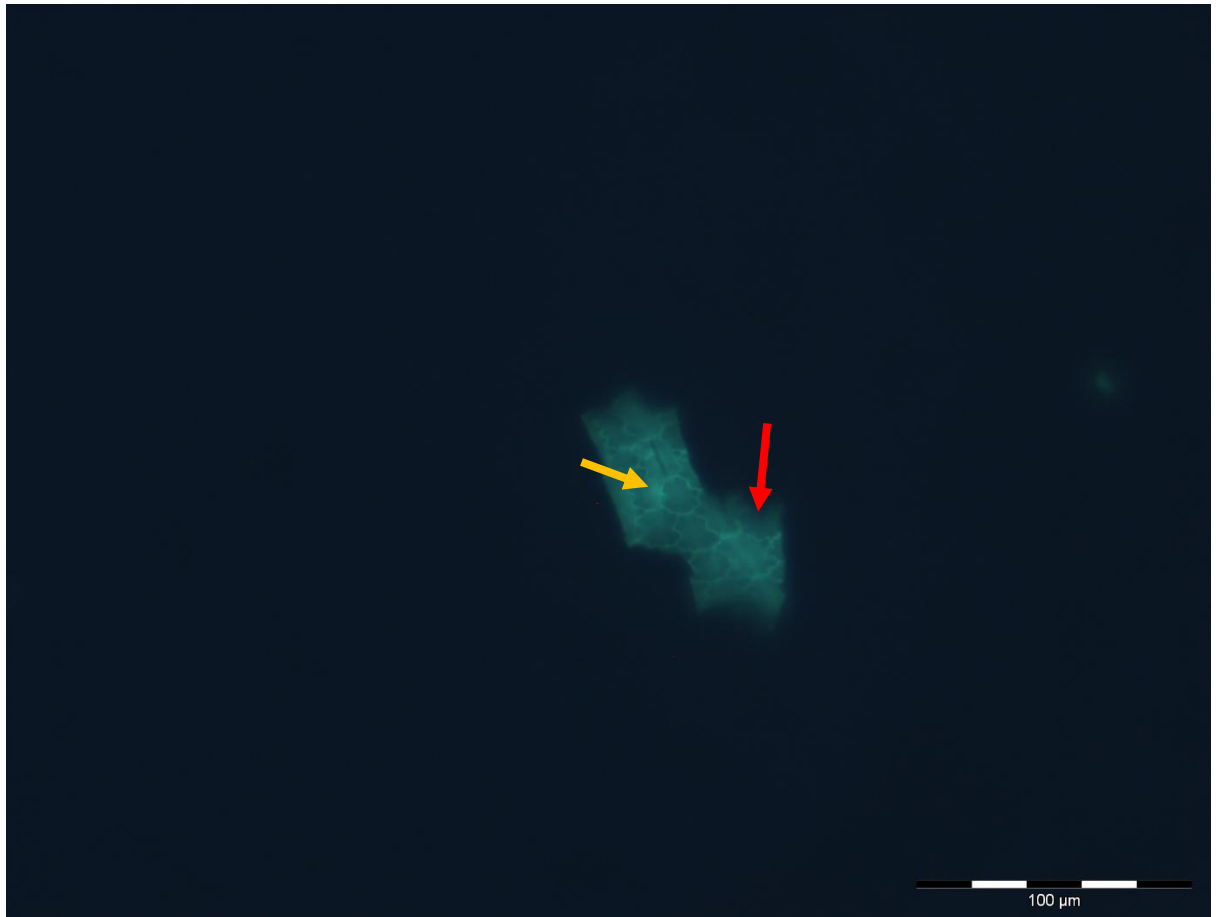


Figure 8.16 PDMPO stained silica from acid digested germinated rice seedlings at the second leaf stage. Arrows label areas of note, discussed in text.

This silica structure shows the outline of multiple small cells, presumably leaf epidermal cells due to their morphology which is similar to the sinuate shape seen in more mature epidermal cells (Fig 8.16) (see red arrow). This silica structure is possibly from the newly developing second leaf, whilst the earlier silica samples show that more mature epidermal cells would come from the first leaf. Though these cells share the wave-like outline of the older epidermal cells, they are much shorter, measuring only 10-12 μm in length, suggesting that these cells will stretch out as the leaf grows. Though there are no visible papillae, there are areas of heavier PDMPO staining that suggest heavier silica deposition on the opposite side of the structure which could indicate the presence of papillae (see gold arrow).

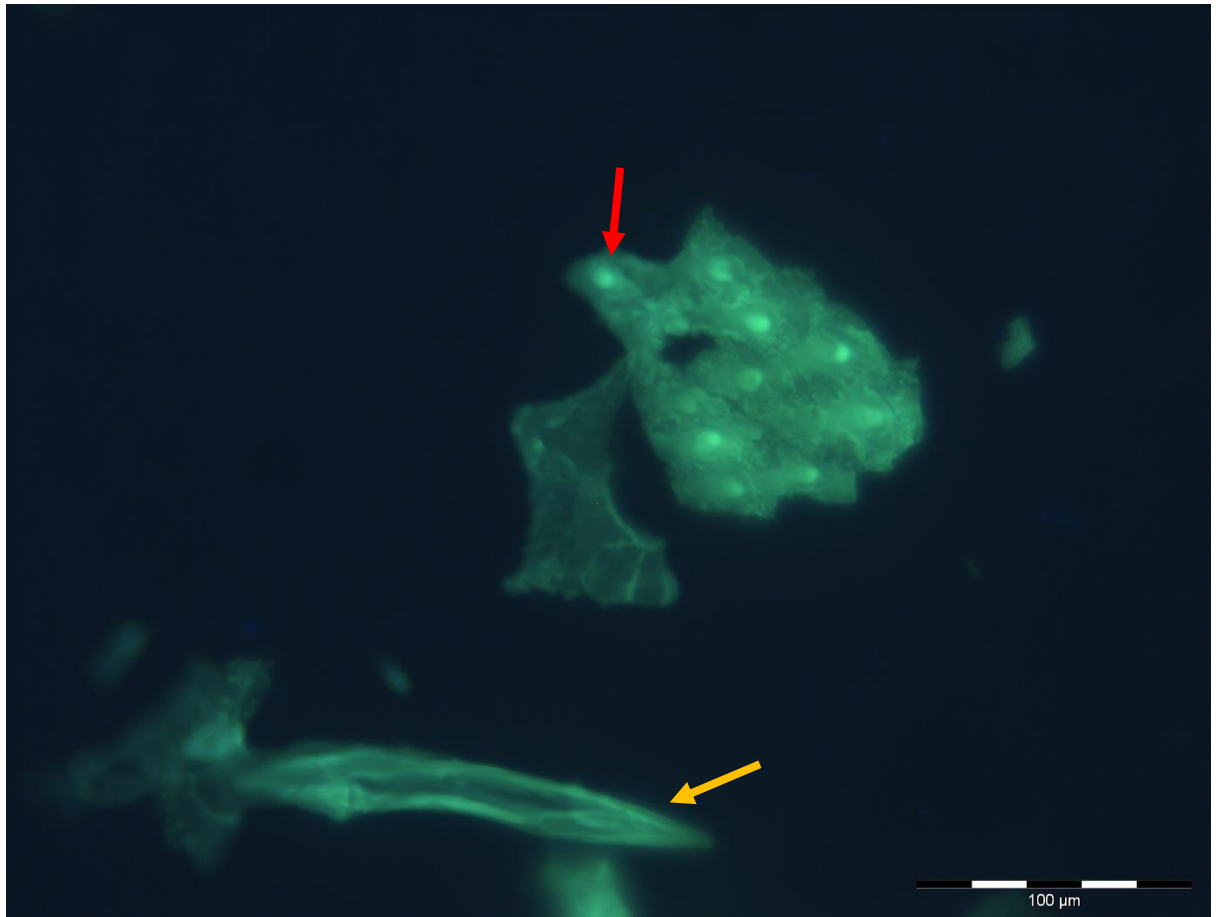


Figure 8.17 PDMPO stained silica from acid digested germinated rice seedlings at the second leaf stage. Arrows label areas of note, discussed in text.

Another silica piece from the rice seed husk is visible, along with a large spike-shaped shard of silica (Fig 8.17). The seed husk silica structure is formed of a sheet of silica covered intermittently with raised silica nodules, which show heavier PDMPO staining than the rest of the structure (see red arrow). The silica shard, like a previous similar sample (Fig 8.5), resembles a trichome but it is much too large, over 200 μm long, and is therefore likely just a shattered piece of a larger silica structure from within the seed husk (see gold arrow).

8.3.4.1 Summary

As the rice seedlings develop into the second leaf stage, significant silica deposition is occurring throughout the leaf tissue, with large silica sheets covering the entire leaf epidermal cells (Fig 8.13). Papillas have formed along the surface of the epidermal cells and these too are silicified. Secondary epidermal cells were detected for the first time at this stage; these cells have a

different morphology to the more common primary epidermal cells (Fig 8.14). Shorter sinuate cell structures were also seen, possibly identifying silicification in developing primary epidermal cells or even a third variant of epidermal cell (Fig 8.16). Silica structures from the rice seed husk were still common throughout the sample, again suggesting that this silica is not repurposed (converted from silica to silicic acid for use in silicifying other structures) in the growing seedling (Fig 8.15 & Fig 8.17).

8.3.5 Rice Seedling – Third Leaf Stage

The fifth developmental stage of rice silica to be analysed was the rice seedling when it had developed to its third leaf stage.

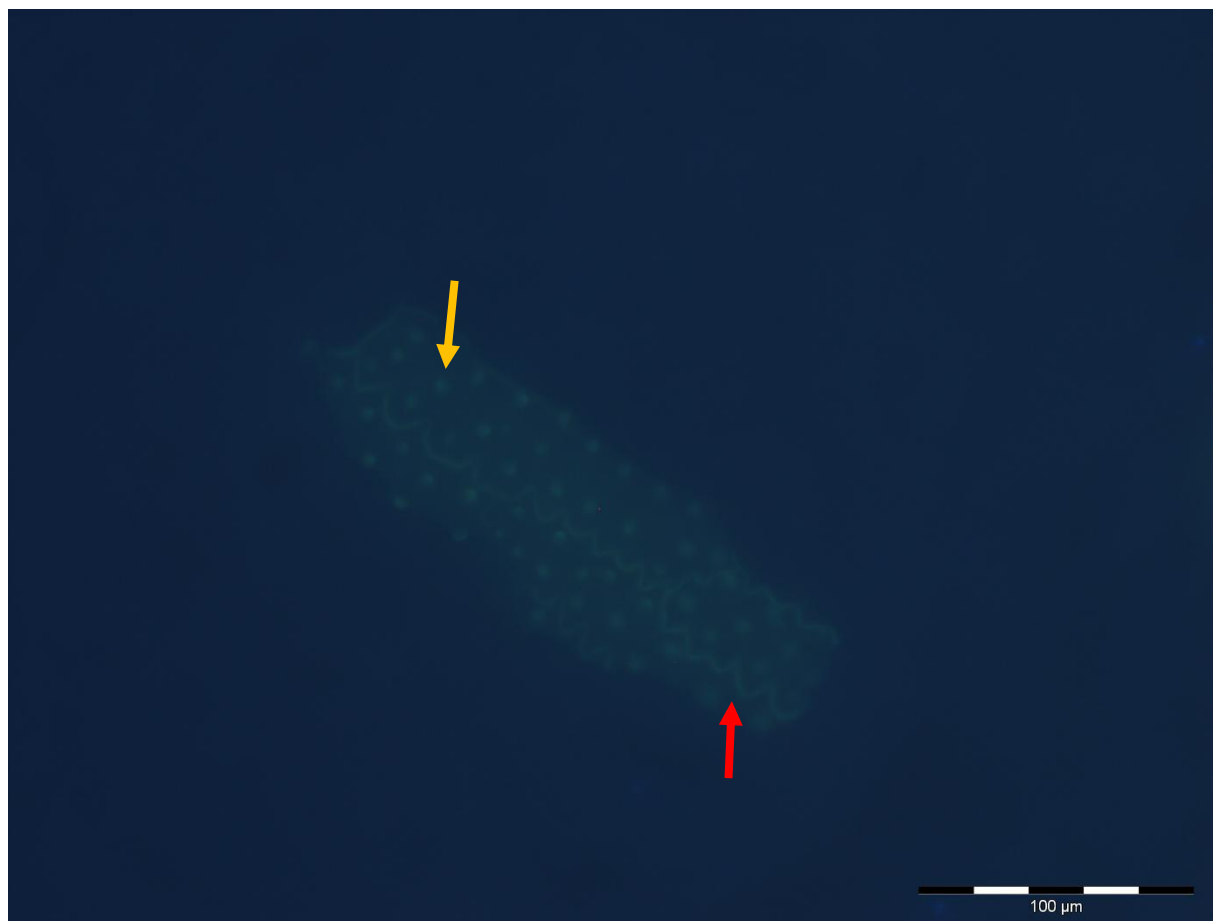


Figure 8.18 PDMPO stained silica from acid digested germinated rice seedlings at the third leaf stage. Arrows label areas of note, discussed in text.

A large silica structure which covered multiple epidermal cells can be observed, identified by their rectangular shape and sinuate edges (Fig 8.18) (see red arrow). The divide between epidermal

cells joined both laterally and horizontally is easily visible, with clear lines between the individual cells. Papillae are also visible across the surface of the epidermal cell structure as seen by the small nodules of heightened PDMPO staining (see gold arrow). Due to the advanced stage of the epidermal cells, this silica structure likely originated from one of the older leaves on the developing seedling, rather than its newer third leaf.

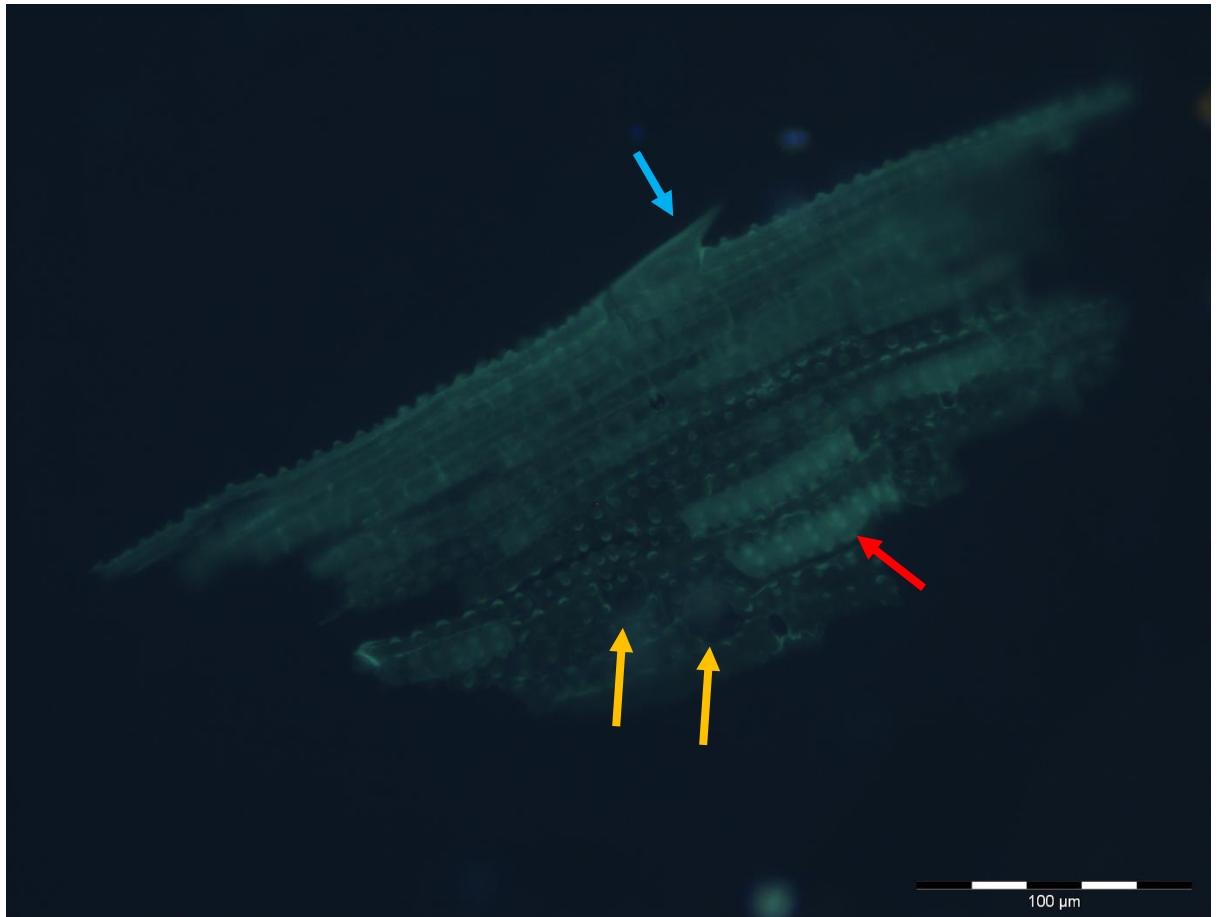


Figure 8.19 PDMPO stained silica from acid digested germinated rice seedlings at the third leaf stage. Arrows label areas of note, discussed in text.

Another large silica structure from the leaf epidermis, showing multiple, fully-developed epidermal cells connected into a large super-structure (Fig 8.19). The epidermal cells are covered with papillae, which show a heightened PDMPO staining when compared with the surrounding structure, suggesting a higher concentration of silica at the papilla (see red arrow). Two gaps in the silica structure are visible indicating the location of ghost stomata, though as in previous samples the guard cells are no longer present (see gold arrows). As the structure curves towards

over, a trichome can be seen clearly protruding out from the epidermal structure (see blue arrow).

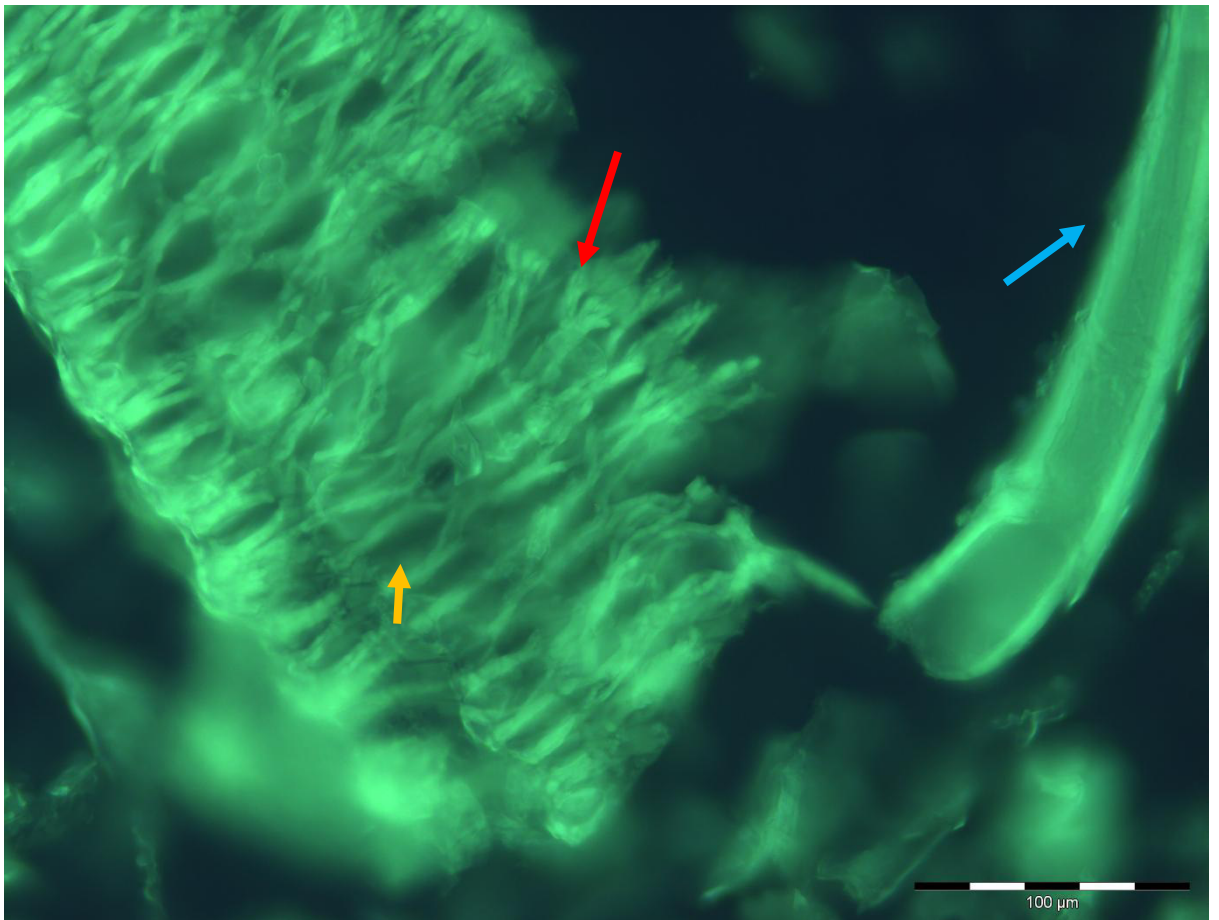


Figure 8.20 PDMPO stained silica from acid digested germinated rice seedlings at the third leaf stage. Arrows label areas of note, discussed in text.

Two large silica structures can be observed in this sample group (Fig 8.20). The larger silica structure is over 400 μm in length and 200 μm in width with filamentous strands running across its surface (see red arrow). Each strand measures approximately 5 μm in width and runs laterally across the sample, with strands either overlapping or fusing together as they intersect, leaving large gaps between the strands at intervals (see gold arrow). Given the size and shape of this silica structure, it is possible that this is the reverse view of the seed husk silica structures seen previously (Fig 8.2 & Fig 8.15). The smaller silica structure shown here is another large spine-shaped shard (Fig 8.5 & Fig 8.17), though the tip of the spine extends off the image (see blue arrow).

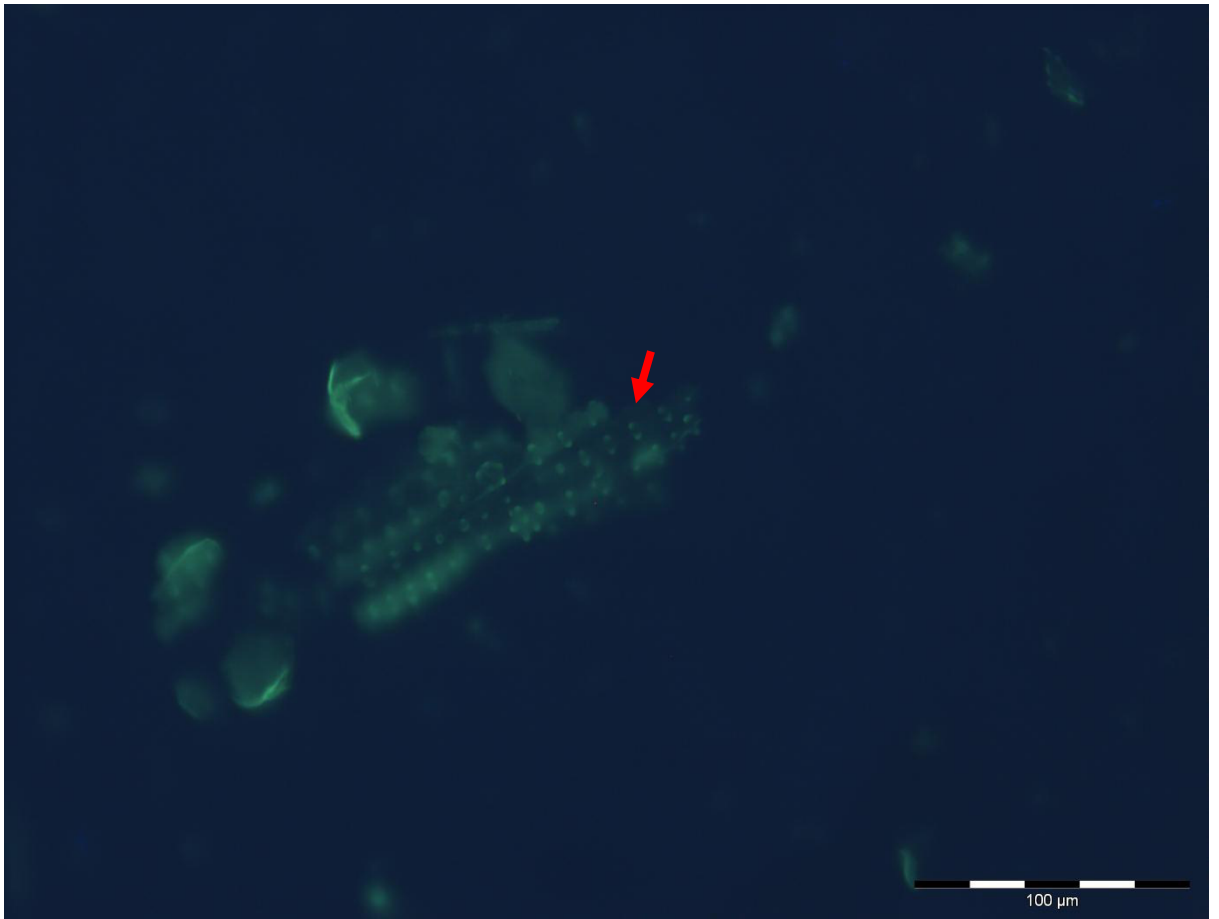


Figure 8.21 PDMPO stained silica from acid digested germinated rice seedlings at the third leaf stage. Arrows label areas of note, discussed in text.

A small piece of silica from a larger silica sheet from the leaf epidermis was seen in this sample, showing the arrangement of papilla found in mature epidermal cells (Fig 8.21). Along the sample, the papillas are primarily located in pairs running along the length of each epidermal cell (see red arrow).

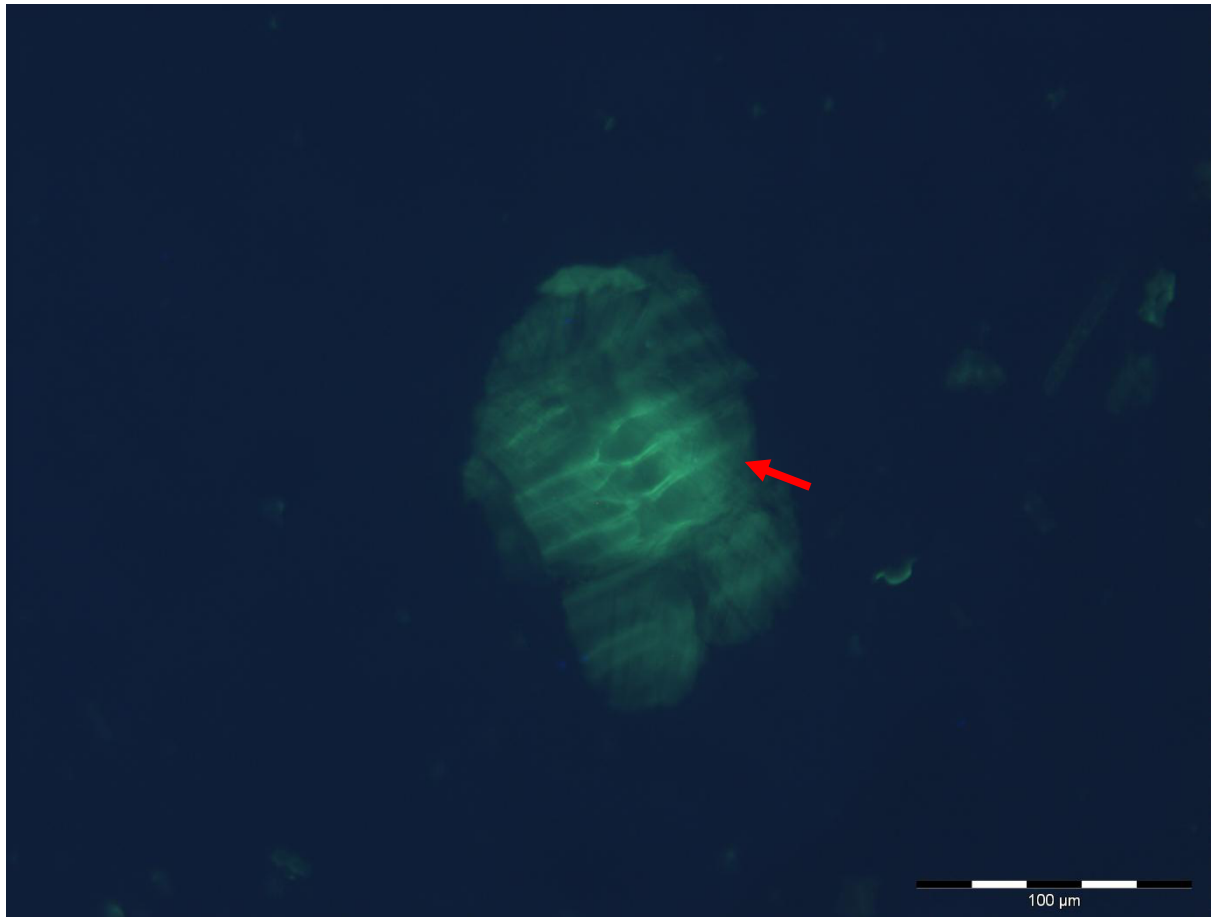


Figure 8.22 PDMPO stained silica from acid digested germinated rice seedlings at the third leaf stage. Arrows label areas of note, discussed in text.

A silica structure which covered the secondary type of epidermal cells, lacking the sinuate edges and papillae (Fig 8.22). The divisions between cells can be seen clearly across the silica structure, each individual epidermal cell has straight edges, as opposed to sinuate, and were approximately 10-12 μm in width, though no full epidermal cell can be observed in its entirety which prevents length measurements (see red arrow).

8.3.5.1 Summary

As the rice seedlings reach the third leaf stage, more epidermal structures become commonplace. In addition to both the primary and secondary epidermal cells, stomata and trichomes are also found in the silica digests (Fig 8.18, Fig 8.19 & Fig 8.21). Large silica shards from the rice seed husk are still found in this sample group, along with a new, unidentified silica structure covered in filamentous silica strands (Fig 8.20).

8.3.6 Rice Seedling – Fourth Leaf Stage

The final developmental stage of rice silica to be analysed was the rice seedling when it had developed to its fourth leaf stage.

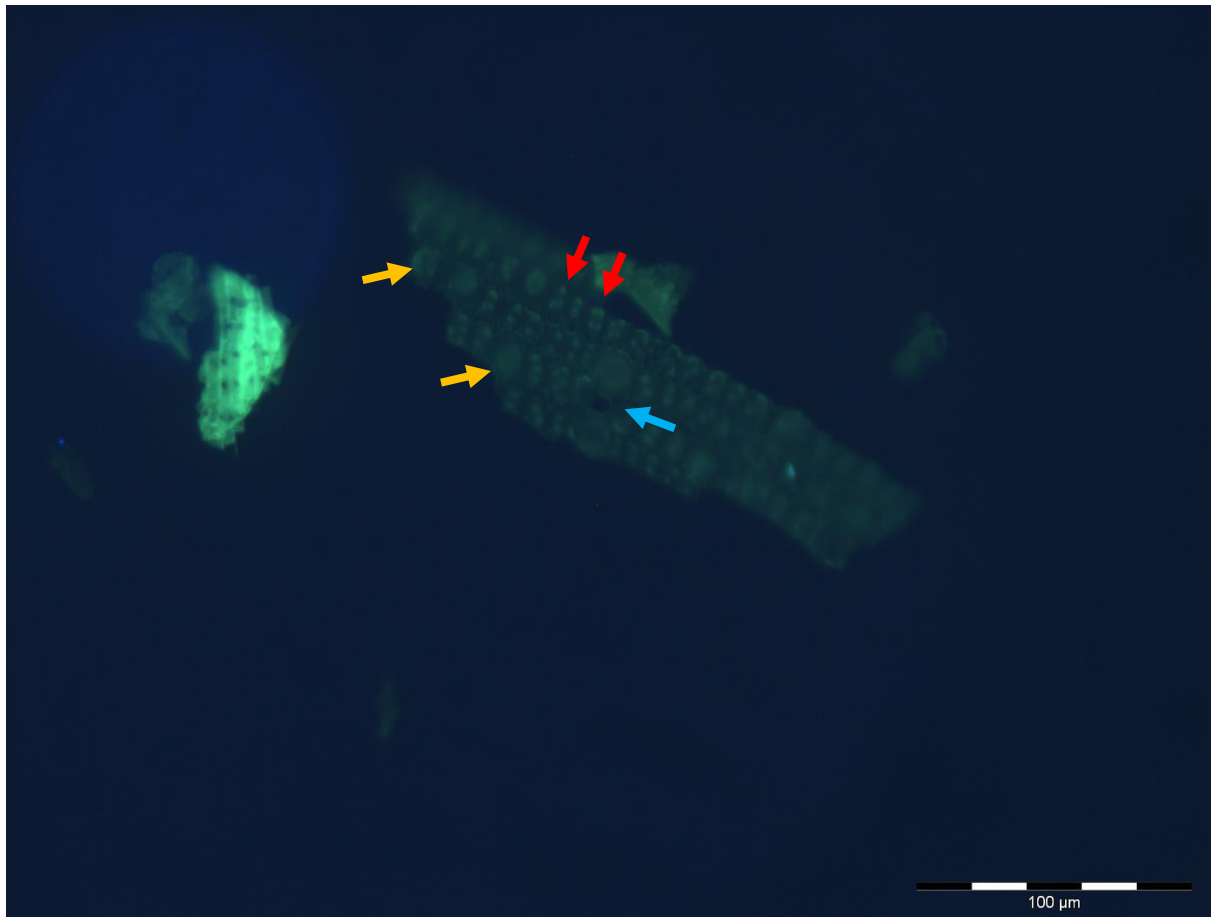


Figure 8.23 PDMPO stained silica from acid digested germinated rice seedlings at the fourth leaf stage. Arrows label areas of note, discussed in text.

In the final early developmental stage of the rice seedling, silica structures originating from the leaf epidermal tissue are frequently observed (Fig 8.23). Several columns of epidermal cells running alongside each other are visible, with each column marked out by the paired papillas which run along the top of the epidermal cells (see red arrows). At several points along the epidermal cells, the pairs of papilla are replaced with larger, bulbous nodules (see gold arrows). A gap is present within the epidermal silica structure, flanked on both sides by large, silicified structures (see blue arrow).

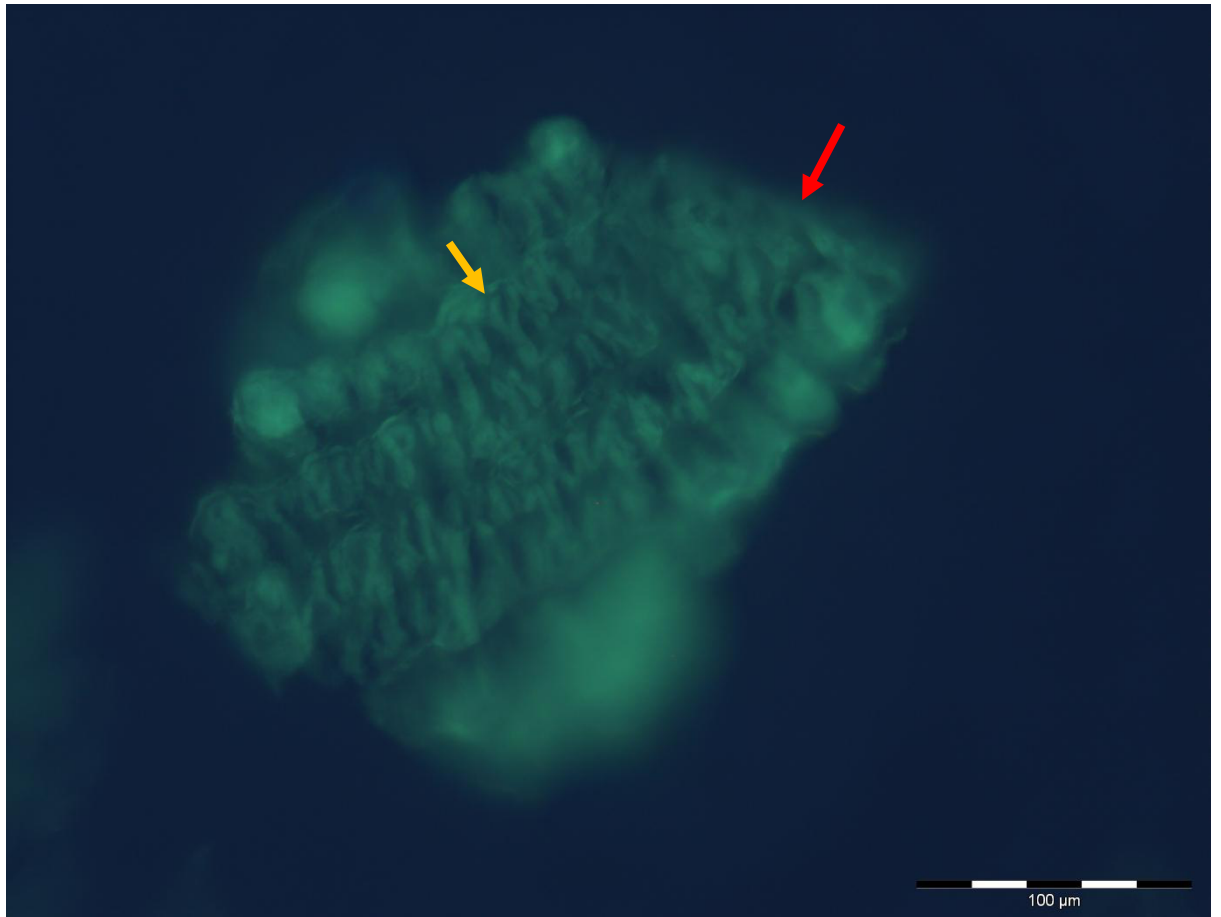


Figure 8.24 PDMPO stained silica from acid digested germinated rice seedlings at the fourth leaf stage. Arrows label areas of note, discussed in text.

A large silica structure with filamentous strands running across its surface can be observed in the fourth leaf stage sample (Fig 8.24) (see red arrow), the same structure observed in the third leaf stage (Fig 8.20). Individual strands vary in width from 3-8 μm in width and running laterally across the sample, with strands running in pairs in an appearance that resembles the structure of chromosomes, though obviously much larger (see gold arrow). The structure does not resemble any observable structure within the rice plant tissue, though it could be the reverse view of the seed husk silica structures seen previously (Fig 8.2 & Fig 8.15).

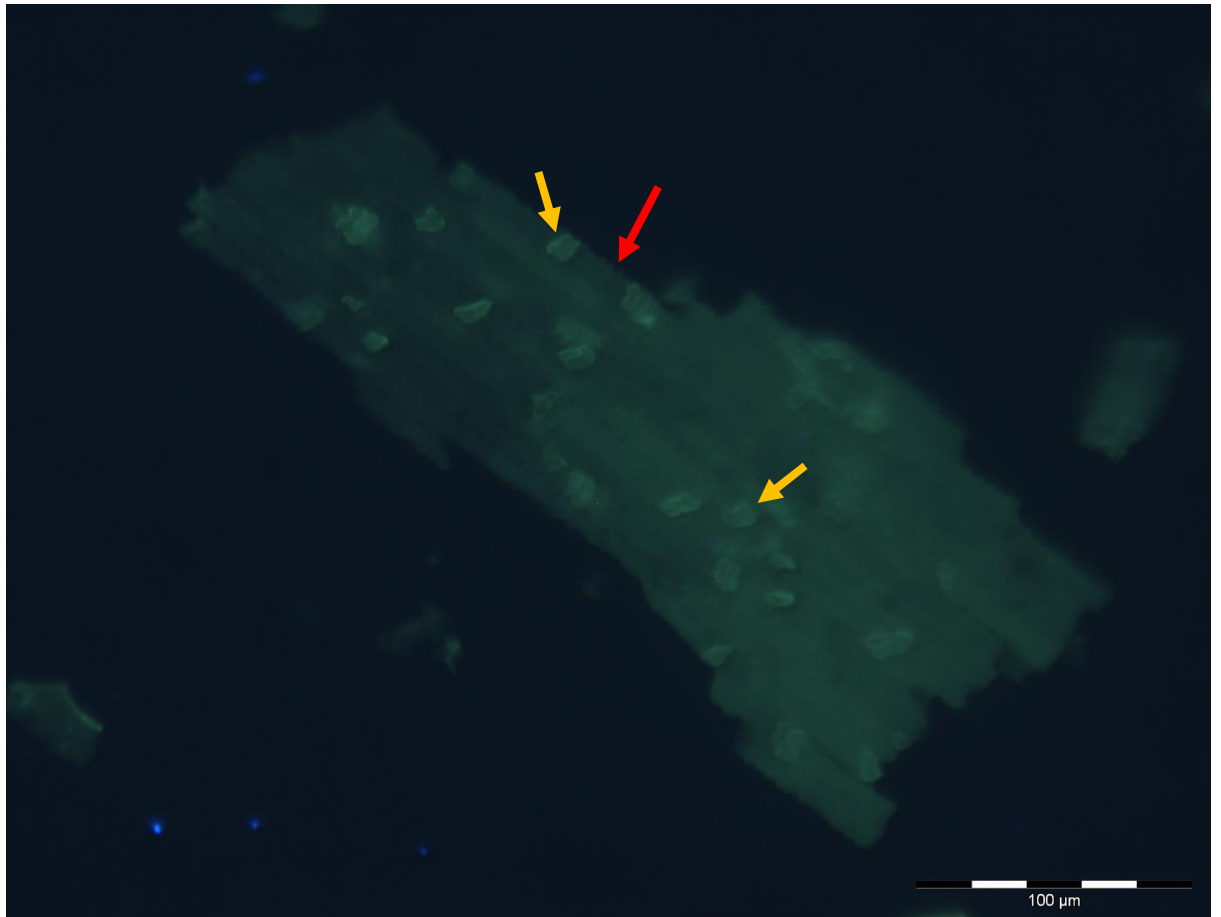


Figure 8.25 PDMPO stained silica from acid digested germinated rice seedlings at the fourth leaf stage. Arrows label areas of note, discussed in text.

A large silica structure, measuring over 300 μm in length from the leaf epidermis can be seen, showing the characteristic sinuate edges of the interlocking epidermal cells (Fig 8.25) (see red arrow). However, whilst these epidermal cells show the sinuate edges of epidermal cells, there are no signs of papilla across the surface of this structure, nor any depressions which would indicate their presence on the reverse of the structure. Numerous loose cells which appear to be silica cells, identified by their dumbbell-like shape, can be seen strewn across the surface of the epidermal structure (see gold arrows).

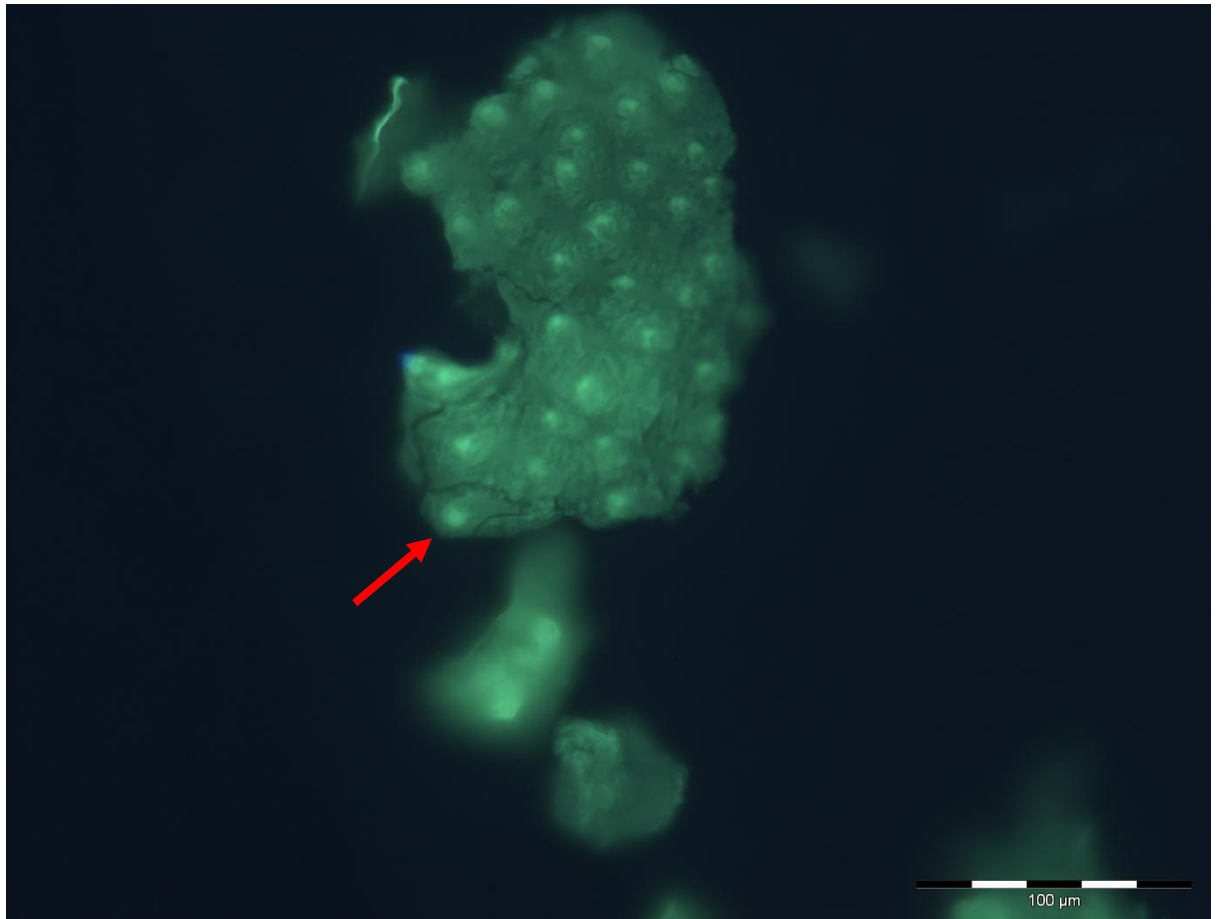


Figure 8.26 PDMPO stained silica from acid digested germinated rice seedlings at the fourth leaf stage. Arrows label areas of note, discussed in text.

Even in the fourth leaf stage of the rice seedling silica structures from the seed husk are still visible throughout the PDMPO stained sample (Fig 8.26). In this sample, a large section of silica is observable with a rough, textured appearance and punctate raised nodules covering its surface (see red arrow).

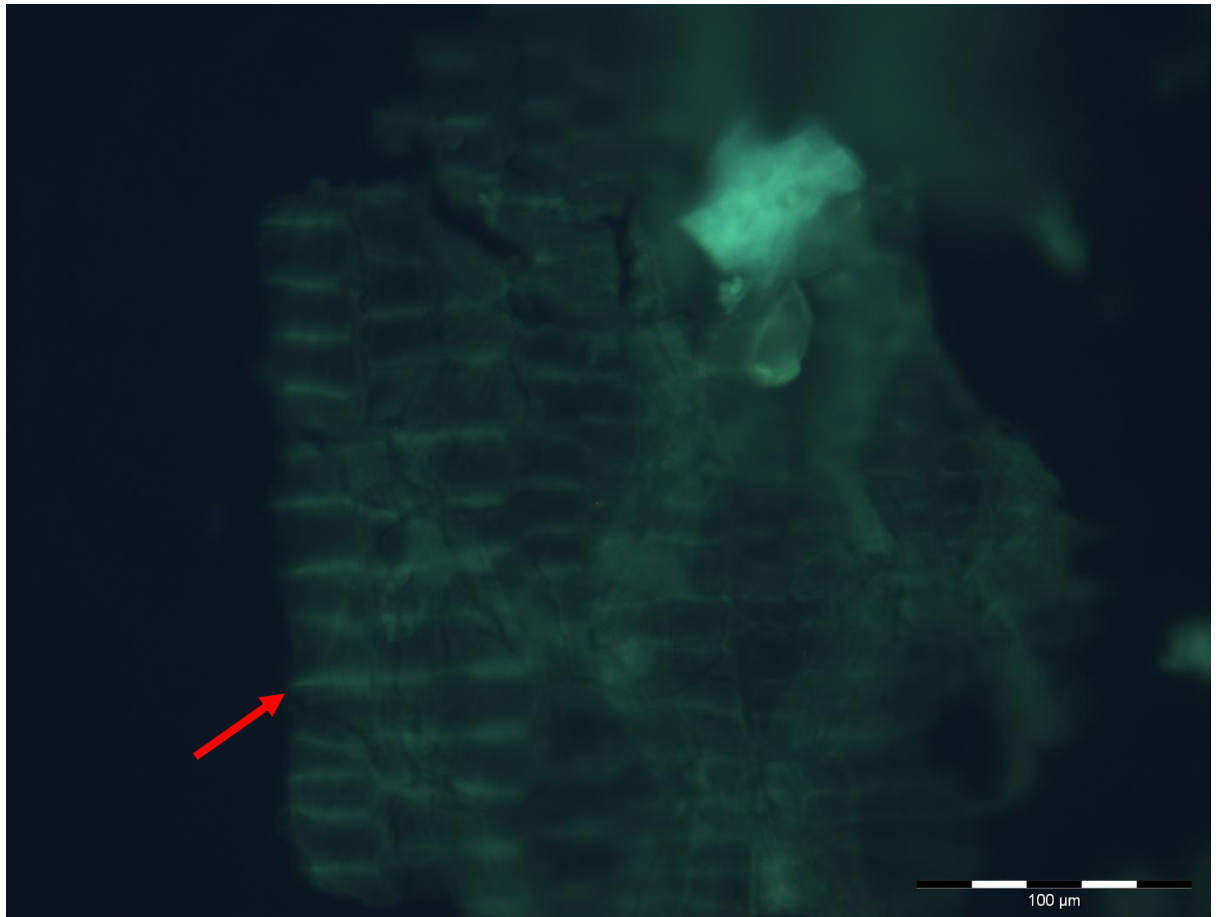


Figure 8.27 PDMPO stained silica from acid digested germinated rice seedlings at the fourth leaf stage. Arrows label areas of note, discussed in text.

Not all of the large silica structures are easily identifiable, with some samples sharing key characteristics with known structures but also lacking others (Fig 8.27). A large sheet of silica can be seen with transverse lines crossing its surface, indicating individual secondary epidermal cells which the silica sheet covered (see red arrow). It is not possible to determine this sample's orientation, whether the visible side is that which contacted the leaf tissue or not, due to the lack of either recessed or raised lines at the epidermal cells.

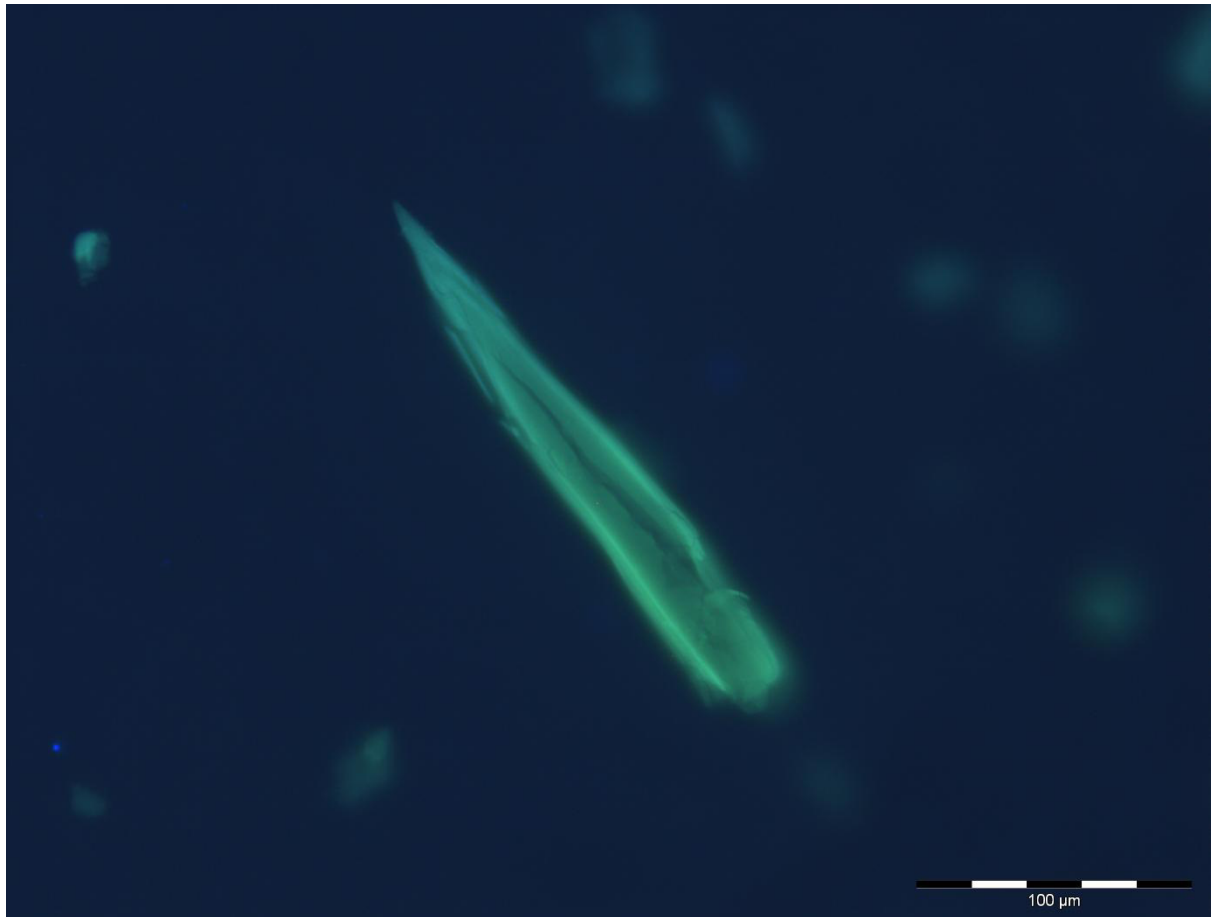


Figure 8.28 PDMPO stained silica from acid digested germinated rice seedlings at the fourth leaf stage. Arrows label areas of note, discussed in text.

A large silica shard can be seen, measuring over 200 μm in length (Fig 8.28). Whilst the shard shares the morphology of a trichome, it is far too large; trichomes average around 40-50 μm in length in one month old rice tissue. The silica structure is a shard which broke off from a much larger silica sheet from within the rice seed husk; similar structures have been observed throughout the earlier growth stages before the upper plant had developed, providing further evidence that this structure originated in the seed (Fig 8.5).

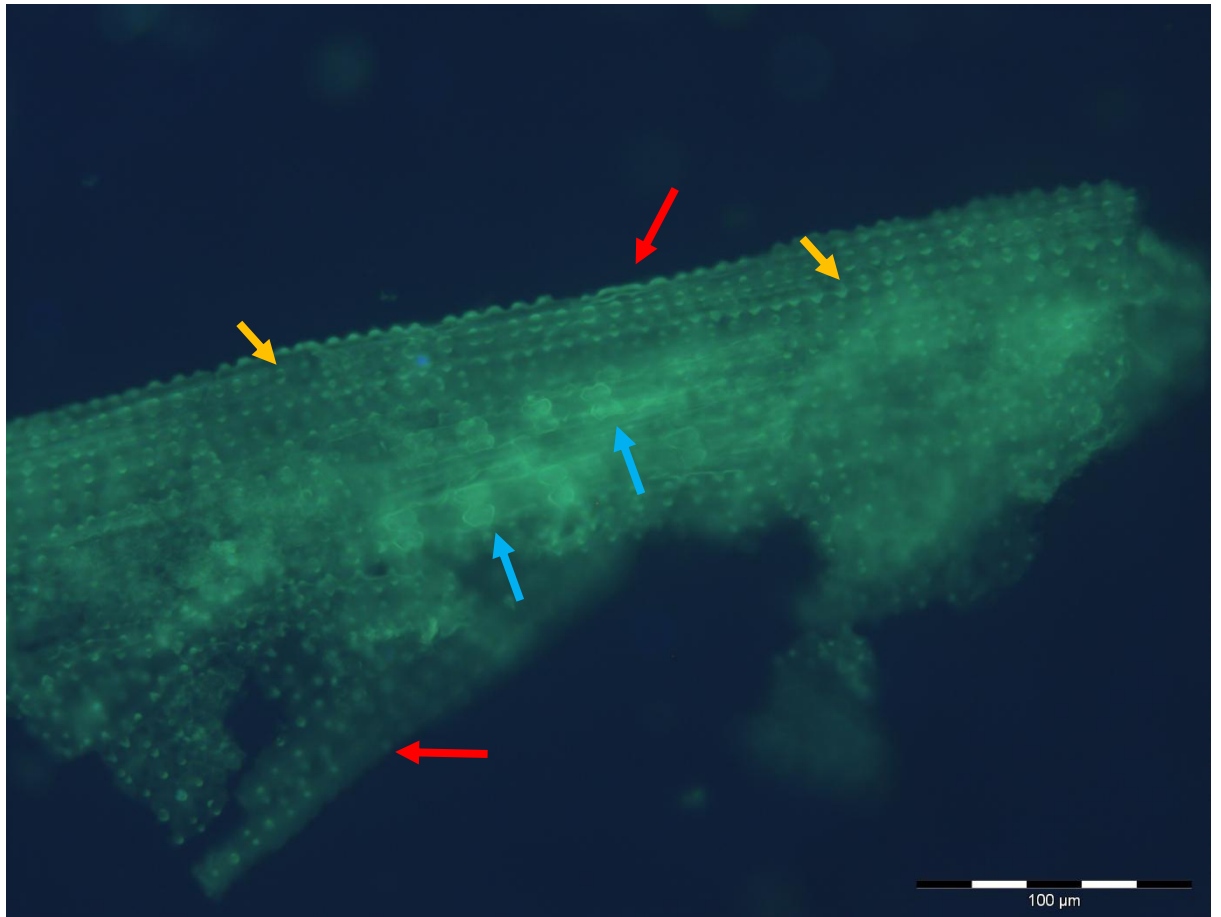


Figure 8.29 PDMPO stained silica from acid digested germinated rice seedlings at the fourth leaf stage. Arrows label areas of note, discussed in text.

Due to the PDMPO staining method visualising samples floating in a liquid, silica samples can overlap each other which obscures visibility of both samples; what appears to be a large silica structure from the epidermis is actually two similar structures stacked on top of each other (Fig 8.29) (see red arrows). Both silica structures originated from mature leaf epidermis, with papilla covering their surface, though the individual epidermal cell boundaries cannot be seen (see gold arrows). Two columns of silica cells can also be observed running across the upper silica structure, in a ladder-like formation; silica cells can be identified by their dumbbell shape (see blue arrows).

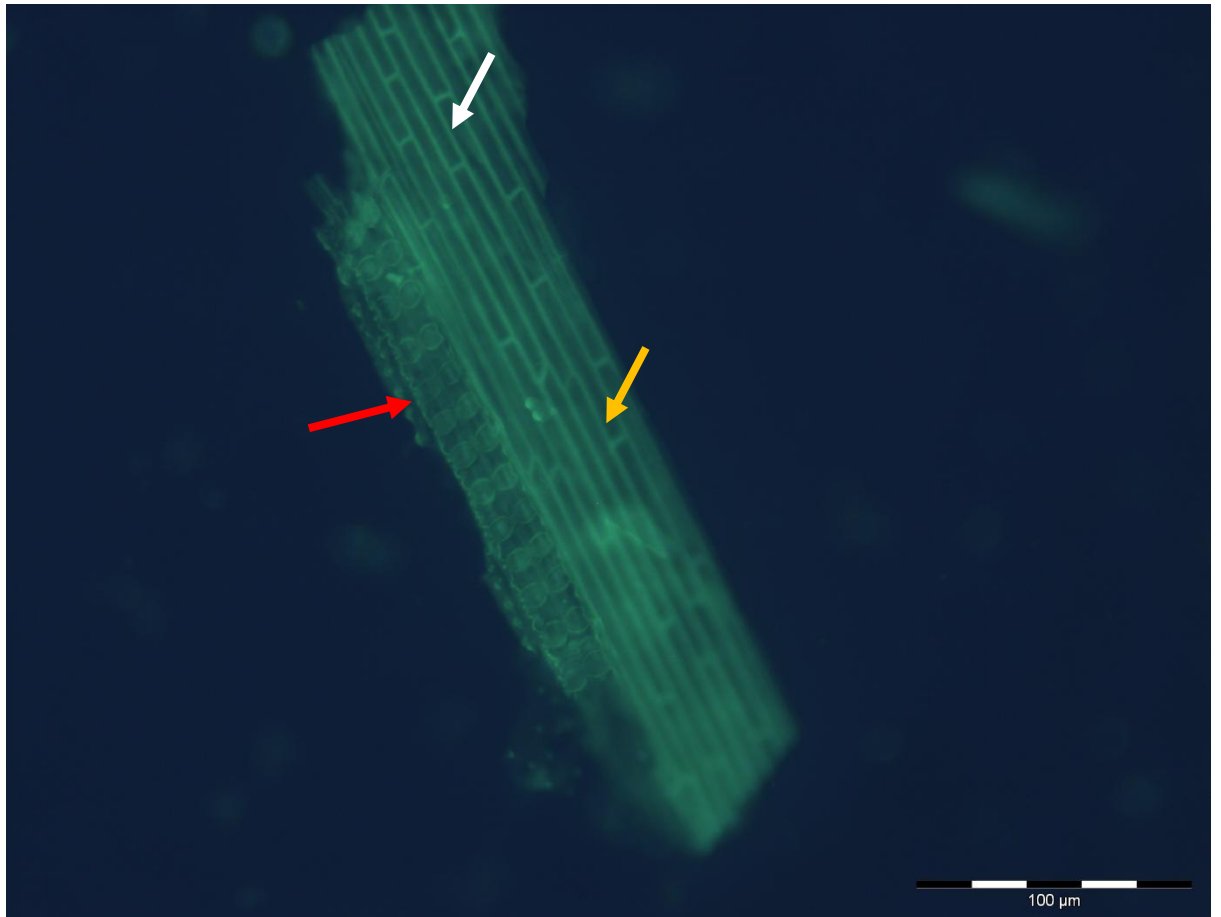


Figure 8.30 PDMPO stained silica from acid digested germinated rice seedlings at the fourth leaf stage. Arrows label areas of note, discussed in text.

The ladder-like columns of silica cells can be observed bordering both secondary epidermal cells (Fig 8.30) (see red arrow) as well as the normal, sinuate epidermal cells as seen previously (Fig 8.29). The secondary epidermal cells vary in length dramatically, with some cells as long as 120 μ m (see gold arrow) whilst nearby cells come in at a modest 50 μ m (see white arrow). The epidermal cells do not show signs of papilla along their upper surface.

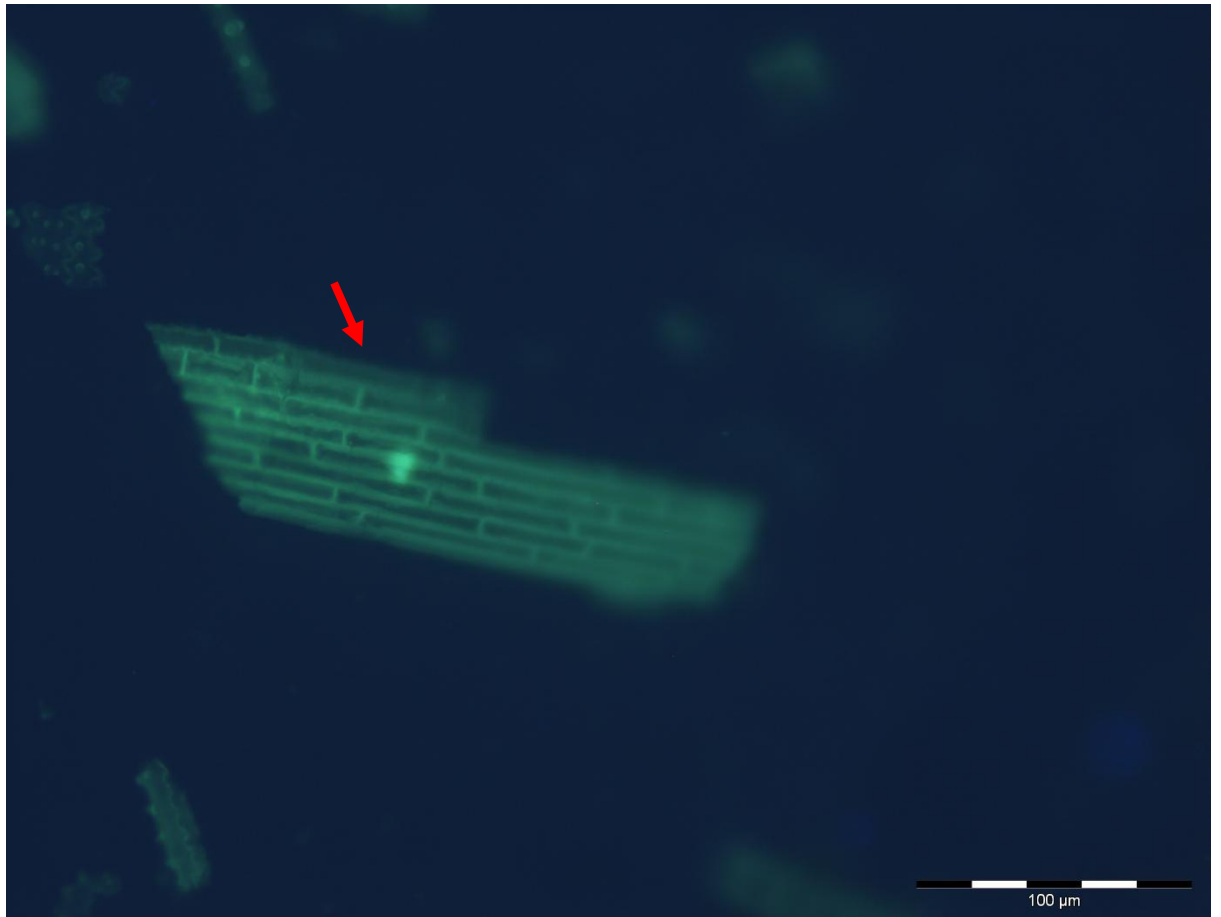


Figure 8.31 PDMPO stained silica from acid digested germinated rice seedlings at the fourth leaf stage. Arrows label areas of note, discussed in text.

No observable pattern can be seen which governs the length of individual secondary epidermal cells (Fig 8.31). Each cell is simply as long or short as it needs to be to fit into formation with the surrounding cells. The width of these cells is much more uniform, although there is still some variation; the majority of the cells in this sample are approximately 5 μm in width, but two wider columns of cells can be observed at the top of the sample, measuring around 10 μm (see red arrow).

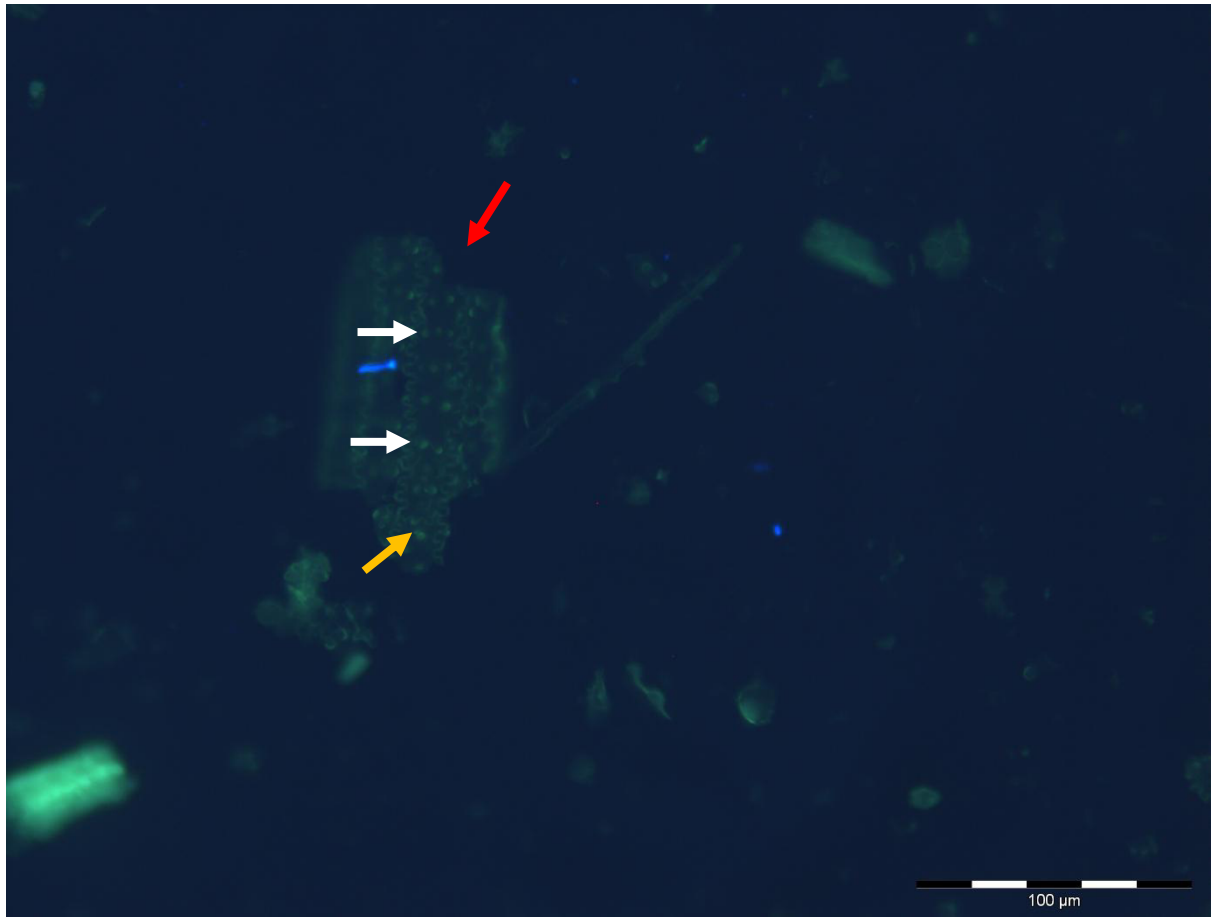


Figure 8.32 PDMPO stained silica from acid digested germinated rice seedlings at the fourth leaf stage. Arrows label areas of note, discussed in text.

A small piece of a larger epidermal silica structure was observed, showing the structure of an individual epidermal cell in great detail (Fig 8.32). The epidermal cell structure measures 100 μ m in length and 20 μ m in width, with a small section of the silica having broken away in the top right corner (see red arrow). The connection point between the epidermal cell and its neighbouring horizontal cell can be seen clearly (see gold arrow), along with its borders with both adjoining lateral neighbour cells. Papillas cover the surface of the epidermal cell, running up the length of the surface in groups of two or three clustered nodules (see white arrows). The epidermal cells sinuate edges are clearly visible, with the peaks and troughs of neighbouring cells interlocking with each other.

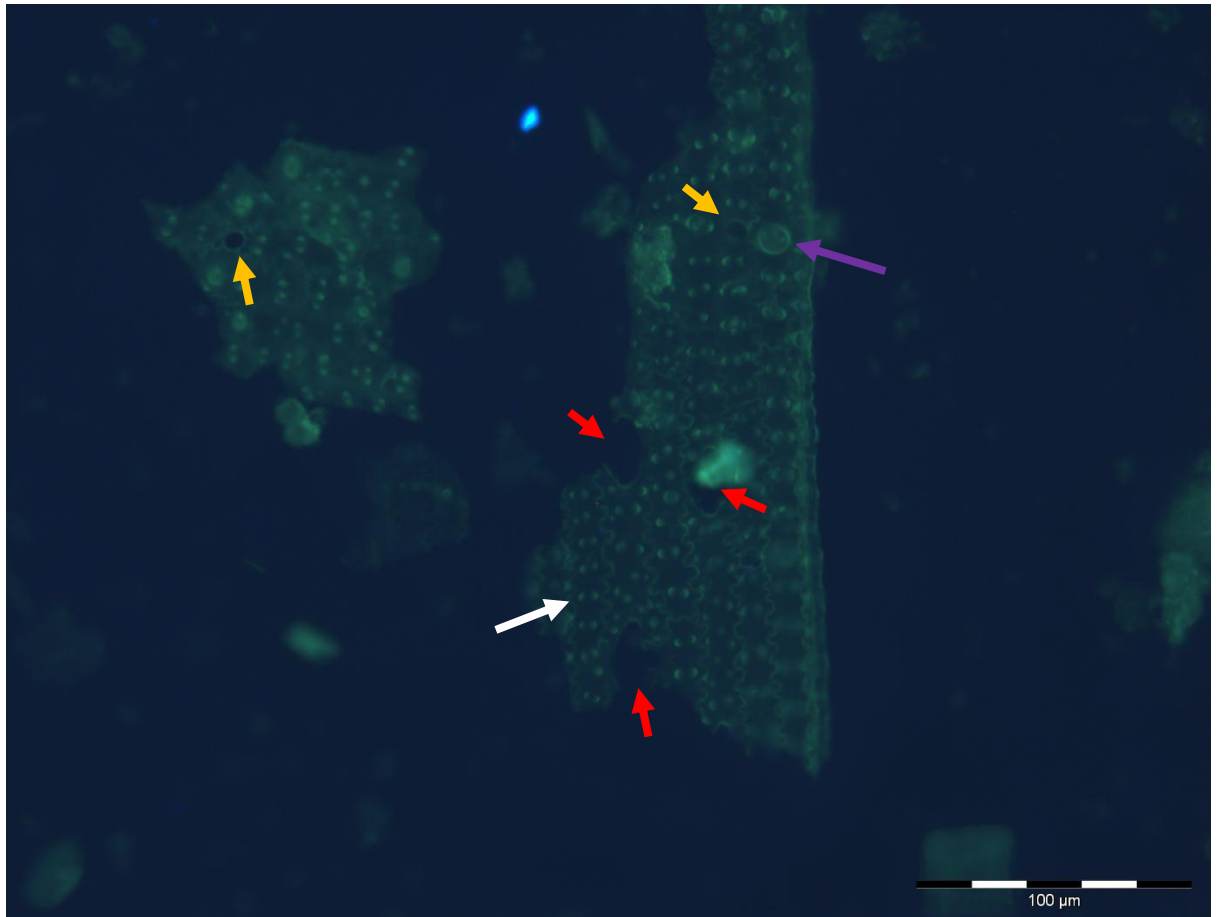


Figure 8.33 PDMPO stained silica from acid digested germinated rice seedlings at the fourth leaf stage. Arrows label areas of note, discussed in text.

Epidermal cells from the lower epidermis of the leaf are interspersed with stomata, which can be visualised in the silica structures which cover these surfaces (Fig 8.33). Whilst the guard cells of the stomata are not present, the stomatal aperture can be clearly seen at several points along a large epidermal silica structure (see red arrows). The edges of the neighbouring epidermal cells are clearly defined, ruling out the possibility that these holes are merely damaged sections. These stomatal openings are oval in shape and approximately 20 μm in length and 15 μm in width. In addition to these oval gaps, there are several circular holes visible at a number of points across the large silica structure and its smaller neighbour (see gold arrows). Epidermal cell boundaries are clearly defined, showing how the interlocking sinuate edges of each cell form the greater structure. Papillas cover the surfaces of the epidermal cells, running along their length in pairs (see white arrow). One large, bulbous nodule sits in the place of a papilla pairing on an epidermal cell (see purple arrow).

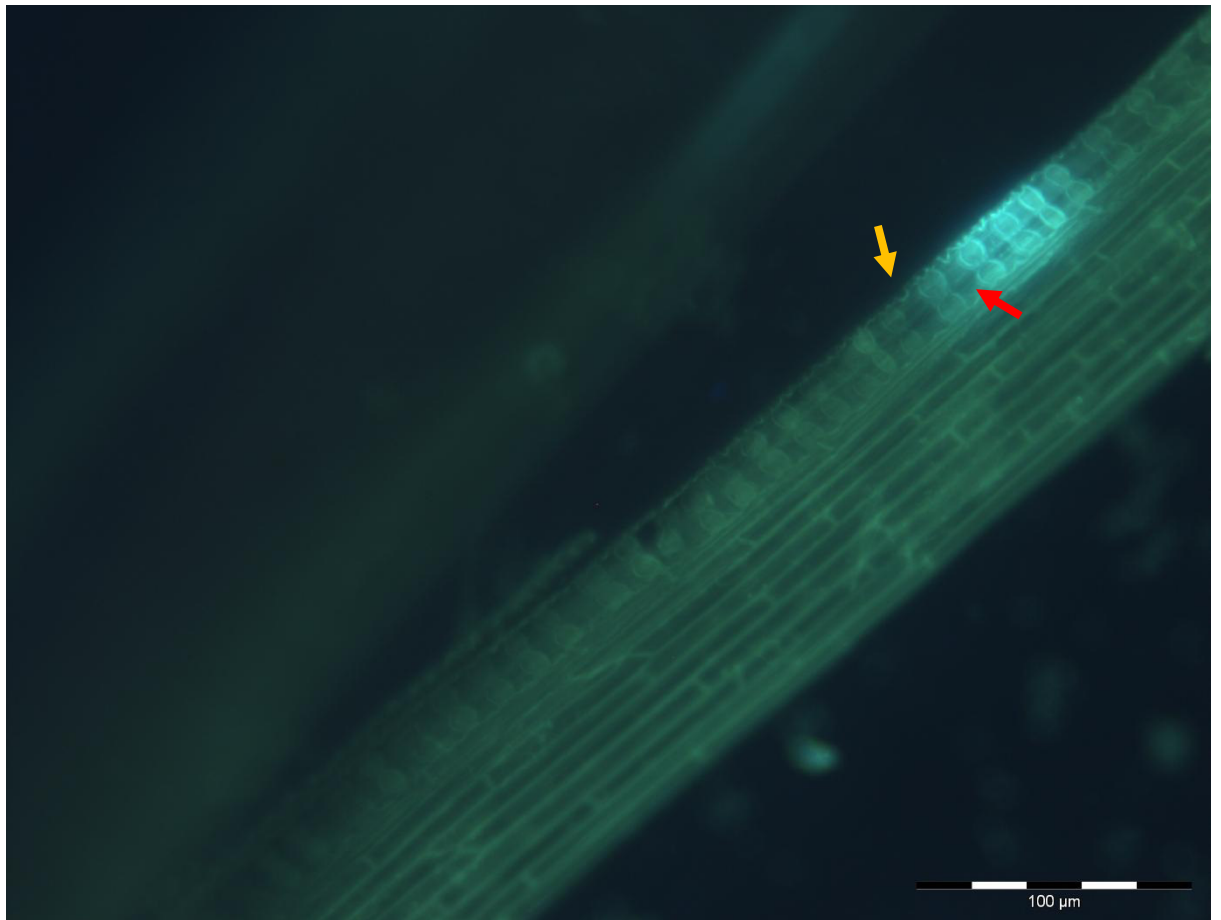


Figure 8.34 PDMPO stained silica from acid digested germinated rice seedlings at the fourth leaf stage. Arrows label areas of note, discussed in text.

Silica cells, arranged in ladder-like columns were primarily found to be neighbouring large areas of secondary epidermal cells (Fig 8.33). If each silica cell is considered to be a rung of a ladder, then the gaps between rungs are filled with phellum or cork cells (see red arrow). Whilst the secondary epidermal cells border one side of the silica structure, the opposing side of the cork and silica cells show wave-like edges, suggesting that the sinuate epidermal cells bordered this side (see gold arrow).

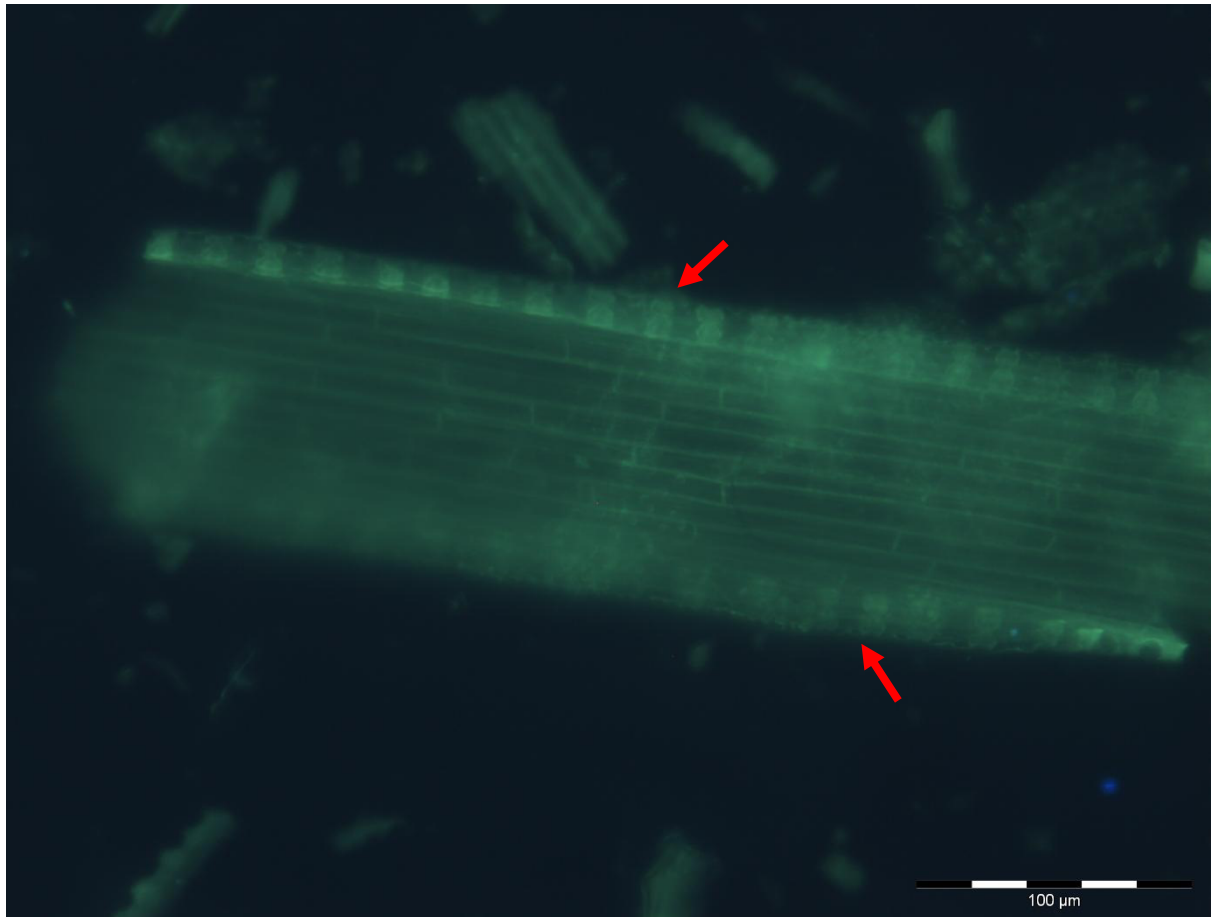


Figure 8.35 PDMPO stained silica from acid digested germinated rice seedlings at the fourth leaf stage. Arrows label areas of note, discussed in text.

Another area of secondary epidermal cells, this time flanked on both sides by a ladder-like structure of silica and cork cells (Fig 8.35). The section of secondary epidermal cells is ten cells wide, with the cells running parallel to the ladder structures on either side of them (see red arrows). Both external edges of the ladder-like structures show sinuate edges, suggesting that the primary, sinuate epidermal cells were located on either side of this silica structure (Fig 8.35).

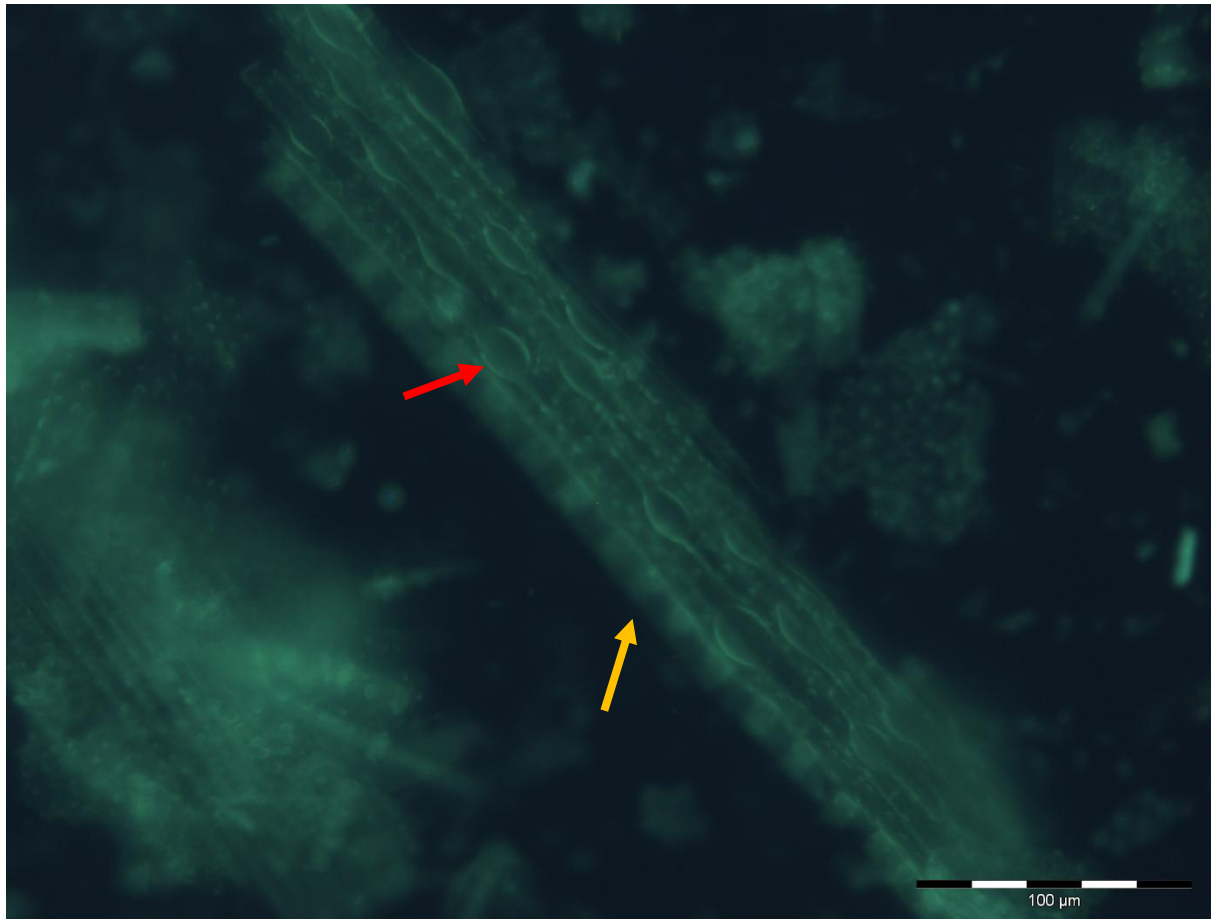


Figure 8.36 PDMPO stained silica from acid digested germinated rice seedlings at the fourth leaf stage. Arrows label areas of note, discussed in text.

In some cases, large bulbous nodules are interspersed between the papilla along the surface of epidermal cells; these structures are more widespread as the plant develops (Fig 8.36). The large nodules are raised significantly from the surface of the epidermal cell and extend across almost the whole width of the cell, sometimes even appearing to cause the cell to bulge out and become wider at their location (see red arrow). Though out of focus, a ladder-like column of silica and cork cells can be seen bordering this region of epidermal cells (see gold arrow).

8.3.6.1 Summary

At the fourth leaf stage, several new silica structures were observed in addition to those seen in previous samples. Silica cells, the dumbbell-shaped cells which run parallel to the vascular bundles along the surface of the leaf, were observed, both as loose cells (Fig 8.25) and in more complex, ladder-like structures (Fig 8.30, Fig 8.34, Fig 8.35 & Fig 8.36); these ladder-like structures were

primarily found running either side of areas of secondary epidermal cells. Though the larger nodules covering the surface in place of papilla were found in earlier sample groups, they were only as isolated occurrences, whereas at the fourth leaf stage a large silica structure was found showing numerous bulbous nodules on the surface of primary epidermal cells (Fig 8.36). In addition to these new structures, the familiar array of primary and secondary epidermal cells, stomata and seed husk silica structures were all common occurrences in the final group. Another unidentified silica structure covered in filamentous strands was found; this structure was only found in the two most developed growth stages of the plant (Fig 8.24).

8.4 Discussion

The silica digests of the un-germinated seeds showed, as would be expected, silica structures which mirrored the structure of the rice seed husk (Fig 8.1 & 8.2). The majority of this silica was in the form of small, broken fragments which are, on their own, difficult to identify. However, a larger piece of silica was found which showed more complex structural details; the silica structure showed raised nodules with a rough texture over its surface at regular intervals, whilst the main body of the structure was a smooth silica surface (Fig 8.1).

Silica is known to accumulate in rice seed husks at concentrations of 20-25%, concentrated primarily in the outer epidermis of the husk, though some is found at the lower epidermis near the rice kernel itself (Sharma et al., 1984). Whilst these structures were expected, the presence of a silica structure within both an un-germinated seed (Fig 8.3) and a germinated seed with root radical (Fig 8.7) appearing to show an imprint of leaf epidermal tissue was a highly unexpected result. These silica structures show the same sinuate pattern as seen in mature epidermal cells from the leaf, though they are smaller in size measuring only 5-10 μm across depending on whether the measurement was taken from the peak or trough of the situations, which were themselves more extreme in variation than those of normal epidermal cells. These developing epidermal cell structures were only found in the groups which preceded the formation of the

shoot apical meristem, after which point traditional epidermal cell structures were found in abundance as the shoot and leaves began to develop.

The earliest stage of rice leaf development occurs after germination, when the shoot apical meristem emerges from the seed, followed by the emergence of the primary leaf or coleoptile from the stem (Moldenhauer & Slaten, 2001). This early region of the seedling is known to develop not by cell division but rather cell elongation, which is to say that the individual cells stretch out to elongate the structure as a whole during this time of rapid growth (Attridge, 1991). If this early stage of cells is already present within the seedling, ready to emerge and stretch as the seed germinates, then it is entirely plausible that this is the cellular structure from which the silica samples showing epidermal-like cells originated; the discrepancies with morphology between the cells as a result of them having not undergone the phase of stretch growth upon germination. It has been previously shown that several foliage leaves are present in mature rice embryos within the seed, with early vegetative stages being incorporated into embryos before dormancy takes place (Itoh et al., 2005). Our results have shown the novel result that silicification of these tissues during seed development occurs during these early vegetative stages.

Whilst the novel silica structures from the coleoptile were only seen in the first two groups, the regular silica structures from the rice seed husk were seen throughout all growth stages: un-germinated seeds (Fig 8.1 & Fig 8.2), germinated seeds with radical (Fig 8.4 & Fig 8.5), germinated seeds with radical and shoot apical meristem (Fig 8.10 & Fig 8.11), second leaf stage (Fig 8.15 & Fig 8.17), third leaf stage (Fig 8.20) and finally the fourth leaf stage (Fig 8.24, Fig 8.26 & Fig 8.28). The ubiquity in silica structures from the rice seed husk shows the silica stored within the husk is not reutilised for the silicification of the newly developing rice seedling, at least not through the conversion of the silica back into silicic acid for reuse.

Upon the formation of the shoot apical meristem, there is a great deal more variation in the number of silica structures observed. Epidermal cells from the surface of the leaf can be observed

in great numbers, the silica structures which covered them showing a great mosaic of interlocking sinuate cells, covered with papilla (Fig 8.8 & Fig 8.9). Silicified secondary epidermal cells can also be observed at this early stage, lacking the sinuations and papilla of the primary cells (Fig 8.12).

The silicification of the leaf epidermal tissue is rapid, with cell surfaces being silicified seemingly as they develop. Due to the lack of comparable studies performed in rice, it is difficult to analyse these results in isolation, however, similar studies into the deposition of silica in developing seedlings have been undertaken. A study into the silicification of wheat found that the earliest silica deposition was in the roots, but that was once all the endodermal points of silicification in the root have been silicified, then almost all silicic acid was transported to the shoot for deposition there (Tubb, 1995). More importantly, it was noted that silicification of the root tissue occurred within the first 24 hours of seedling exposure to silicic acid, though with 24 hours being the first measuring point in their experiment, silicification may have occurred even quicker than that.

Accumulating research from several papers, one review suggested that silica deposition in grasses only occurs at the silica cells during cell expansion, whilst the epidermal cells did not silicify until the leaf was mature (Motomura et al., 2006). The results shown here defy that conclusion, with leaf epidermal cells showing signs of silicification not only during the first stages of leaf development (see section 8.3.3) but possibly even before that with the evidence of silicified epidermal cells in seedlings pre-shoot apical meristem (see sections 8.3.1 & 8.3.2). On the other side of their statement that silica cells are silicified earlier in development than epidermal cells, our data was again in conflict with theirs; silica cells were not detected until the fourth leaf stage, whereupon they were found in abundance (Fig 8.25, Fig 8.29, Fig 8.30, Fig 8.34 & Fig 8.35).

In both cases the discrepancy between the results found in previous studies and our own can be attributed to the different plant species studied. None of the previous studies into silicification through seedling development were performed using rice as a model plant. Comparing previous

works in other species of plants leads to an inevitable but predictable conclusion; different plant species have varying processes of silicification and comparing between species research is of limited use.

In all growth stages after the formation of the shoot apical meristem, both primary and secondary epidermal cell structures were observed in the silica digests, however other structures associated with the leaf epidermis were not found until later stages of development. Trichomes, the spine-like cells which protrude from the leaf epidermis, were not seen until the third leaf stage and even then this was the only example of a silicified trichome that was observed (Fig 8.19). Searching for any sparsely distributed structure through PDMPO imaging always involves an element of luck; however the absence of trichomes in earlier samples suggests that these structures are not silicified in earlier stages of development. Trichome development has been shown to be basipetal in other species such as *Arabidopsis*, meaning development starts at the tip of the spine and develops towards the base (Evert, 2006). It is possible that silicification of the trichome may not begin until it has developed to its full size, explaining why no smaller, developing trichomes were observed.

Stomatal openings were visible in the silica structures as soon as leaf epidermal cells were visible, with the development of the shoot apical meristem (Fig 8.8). Whilst the opening is identifiable, the guard cells which cover the opening were not visible. Stomatal openings without their guard cells were also found in the third leaf stage (Fig 8.19) and fourth leaf stage (Fig 8.33). The lack of silicified guard cells leads to two possible conclusions; either guard cells are not silicified or that the guard cells are silicified but have become detached from the main silica structure during the acid digestion process. It has been previously shown through the use of transmission electron microscopy that guard cells in rice stomata accumulate silica in their cell walls (Ueno & Agarie, 2005). Therefore the logical conclusion is that the silicified guard cells became separated from the

silica structure or perhaps that they have not yet become silicified in these early developmental stages.

In the fourth leaf stage, several structures were observed which had not been seen previously: silica cells and large groupings of bulbous nodules across epidermal cells. Silica cells were found loose from other structures in one sample; although they were lying across the surface of a large epidermal structure they did not appear to be part of the structure itself (Fig 8.25). All other silica cell localisations showed them in ladder-like formations running intermittently with cork cells (Fig 8.30, Fig 8.34, Fig 8.35 & Fig 8.36). This ladder-like formation occurs at the epidermis above vascular bundles, providing structural support to the leaf by reducing torsion stress (Yamanaka et al., 2009). These silica cell supports run across the surface of the leaf following the veins, which contain the vascular bundles. However, at larger veins there are two ladder structures running parallel with an area of cells running between them. Silica cells are reported to be amongst the earliest cells to undergo silicification (Motomura et al., 2006); it may be that the increased mass of leaf tissue available for digestion in further developed rice plants led to the increased likelihood of observing these structures in later samples. As a further note, the observation of numerous large, intact silica cell/cork cell structures lends weight to the hypothesis proposed by Yamanaka that these structures provide structural support.

The ladder-like silica cell structures were commonly found running parallel to areas of secondary epidermal cells (Fig 8.30, Fig 8.34 & Fig 8.35). These secondary epidermal cells are similar in size to the more common primary epidermal cells, with the same general rectangular shape as well, though they lacked the sinuations and papilla. Recent work studying the morphological development of epidermal cells in rice leaves showed that these featureless secondary cells are in fact an early stage of development for the primary epidermal cells (Luo et al., 2012). Epidermal cells begin as featureless, rectangular cells before undergoing several morphological changes as they develop, becoming sinuate and covered with papilla (Fig 8.37 A-F). In this same image

sequence, the bulbous nodules seen along the surface of the epidermal cells in silica structures (Fig 8.36) can also be observed (Fig 8.37 D & E). These bulbous nodules appear as the epidermal cells are beginning to form their sinuate structure and papilla are appearing on their surface, before disappearing again in the epidermal cell's final stage.

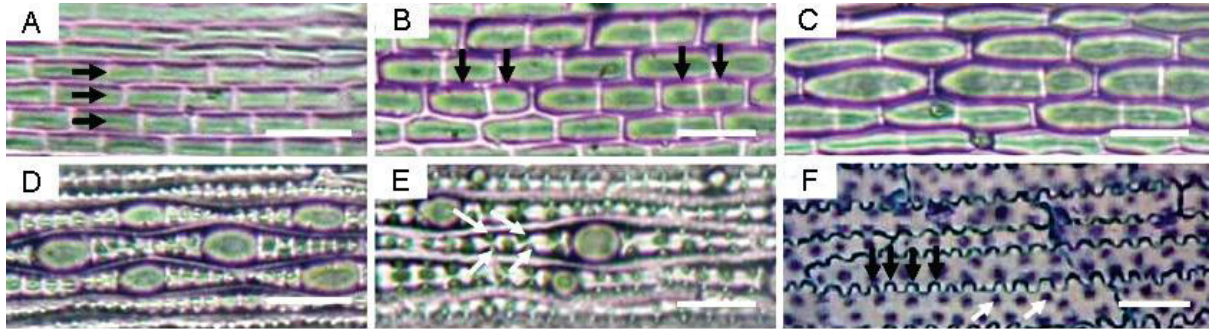


Figure 8.37 – Light microscopy image of developing rice leaf epidermal cells, showing the various stages of development from formation (A) to maturity (F) (Luo et al., 2012).

What has been labelled here as secondary epidermal cells are then in fact one and the same with the primary cells, but at an earlier stage in their development and as a result we can determine that silicified structures showing secondary epidermal cells are newly developing tissue.

Though smaller silica shards are often unrecognisable, it is usually possible to identify the larger pieces of silica which come from the acid digest. However, a large silica structure with what appear to be filamentous strands of silica covering its surface was observed in two growth stages: the third and fourth leaf stages (Fig 8.20 & Fig 8.24). No comparable structure within the rice plant itself could be identified either through our own knowledge or in the literature and whilst it is possibly a structure from the seed husk, it is perplexing that it was only observed in the two most advanced stages of the rice seedling.

Epidermal leaf tissue in rice seedlings has been shown to be silicified almost immediately after formation, with silicified epidermal cells and stomata visible in digests of the earliest shoot formation. What's more, shoot precursor cells show signs of silicification even before the seed has germinated. As the seedling develops, more advanced silica formations such as trichomes and silica cell support structures become visible in the digests. Epidermal cells are not only silicified

early, but before they have even fully developed. That these cells can be silicified and still undergo their complete development seems staggering; how could a cell with a silicified outer layer and cell wall undergo morphological changes that epidermal cells have been shown to (Fig 8.36)?

We can present several hypothesis on how this feat is achieved, though they are mere postulation at this time. In order to develop and alter their morphology whilst encased in silica, the epidermal cells of rice leaves could employ one of three proposed methods:

- **Dynamic conversion of silica into silicic acid** – It is possible that rice can alter the silica structures at its leaf epidermis, converting the silica back into silicic acid by an unknown mechanism to accommodate for cell division, elongation and morphological changes.
- **‘Hulking out’** – Given the brittle nature of the silica found at the leaf epidermis, it is possible that as a cell grows or divides it breaks free from its outer layer of silica. The silicification process would then begin anew, filling in the cracked areas of silica.
- **Silica, but not silica** – Almost all methods of observing silica in plant tissue are destructive and result in the alteration of organic conditions within the plant. It has been shown that within the xylem, rice can maintain a super-saturated concentration of silicic acid but that once removed from its environment, the solution quickly forms silica (Mitani et al., 2005). It is possible that the ‘silica’ at the leaf epidermis is maintained as silicic acid, or in another form, during cell development and only silicifies after cell development and division is completed, or if the closed environment is breached by invasive experimental methods.

Silicification has been shown to begin in leaf tissue before it has even emerged from the seed. Silica is present in the seeds both at the rice husk, but also in the rice plant embryo itself. From germination and the formation of the shoot apical meristem, typical silica structures from the leaf are seen in digests including epidermal cells and stomata. As the seedling ages new structures emerge such as trichomes and silica cells. Cells which were still developing were shown to be silicified, with the earliest leaf cells from the coleoptile and, later, epidermal cells which had not

developed their papilla or sinuate shape. These silicified structures of cells which had not fully developed led to the formation of several hypothesis on how the plant copes with the burden of silicified structures with regards to growth.

9. Conclusions

Various imaging methods were used to understand data on silica deposition in rice. Micro-PIXE and LEXRF were used to visualise silicon and aluminium deposition in cross-sections of intact rice leaf and root tissue, whilst fluorescence microscopy and SEM analysis of acid digested silica allowed for more detailed viewing of the silica structures themselves.

9.1 Silicon and Aluminium Interactions

Micro-PIXE revealed silicon deposition at the upper and lower epidermis of rice leaves grown in the presence of silicon, whilst also confirming its absence in plants grown in silicon's absence (see Chapter 3). Silicon was heavily concentrated in the silica cells which run across the surface of the vascular veins in leaves. The epidermal layer of silicon and the heavy silicification of silica cells are well documented in rice, which served as confirmation that Micro-PIXE and LEXRF are useful techniques in detecting silicon in plant tissue (Ma et al., 2001; Ma & Yamaji, 2008; Yamanaka et al., 2009).

Using Micro-PIXE, aluminium was primarily detected at the rhizodermis of roots, and this aluminium layer was only detected in plants grown in the presence of aluminium (both the aluminium + and silicon/aluminium + groups). Micro-PIXE did not reveal any reliable evidence for aluminium detection in the leaf of the rice plants, suggesting that rice's aluminium tolerance is based on its ability to block aluminium entry into the root, rather than through the sequestration of aluminium into the leaf silica structures. Previous research agrees with the conclusion that aluminium is not taken up into the plant and stored, with studies into rice and wheat showing that aluminium resistance is achieved by silicon and aluminium interactions in solution forming Al-Si complexes, rather than in the plant itself (Ma et al., 1997; Ma et al., 1998). However, this does not explain the build-up of aluminium at the rhizodermis, which is not co-localised with silicon (see section 3.3.1.7). A study into the effects of toxic effects of aluminium in soybeans found that the presence of silicon caused the precipitation of hydroxyaluminosilicates, which in turn led to a

reduction in available phytotoxic aluminium in the growth solution (Baylis et al, 1994). It is possible that this co-localisation of silicon and aluminium at the silica cells is as a result of the uptake or formation of hydroxyaluminosilicates.

Conclusions are further complicated by the detection of silicon and aluminium co-localisation in LEXRF imaging at the silica cells in rice (see section 3.3.3). However, given that the concentration of aluminium found in the LEXRF imaging was low, peaking at 0.4mg/g, it is unlikely that these co-localisations of silicon and aluminium play a significant role in the amelioration of aluminium toxicity. Aluminium was detected at the silica cells in the same concentrations for plants grown in the presence and absence of added aluminium. LEXRF is the more accurate of the imaging methods used so it is unlikely that these readings were in error, especially given their consistent occurrence at specific locations. It is more likely that low background levels of aluminium present in the growth medium were taken up and deposited at the silica cells. Despite this, we have presented the first evidence of silicon-aluminium co-localisation in the leaves of rice (see section 3.3.3).

PDMPO staining of silica structures from the leaves of rice plants grown in the presence of both silicon and aluminium revealed no differences in silica morphology between those grown with silicon and aluminium versus those grown with silicon but without aluminium (see section 7.3.3). Given the complete lack of aluminium detection in the Micro-PIXE, and only minor aluminium detection in LEXRF imaging of the leaves of rice plants, this is not surprising. Aluminium was prevented from entering the rice plant, with significant aluminium build-up at the root rhizodermis but almost nothing detected beyond that or in the upper plant.

9.2 Silicification of Xylem

Amongst the most surprising results yielded by this research project was the discovery of silicified xylem vessels in acid digested rice tissue. PDMPO analysis of silica samples first revealed the presence of xylem-like silica structures (see section 7.3.1.5). Given the function of xylem vessels, it

seemed unlikely that they could function under such extreme silicification, even with their known role in transporting silicic acid at super-saturated levels through the plant (Mitana et al., 2005). It was hypothesised that these structures were not present in the living plant tissue but were in fact inadvertently created during the sample preparation and subsequent acid digestion. Silicic acid is transported through the xylem at super-saturated concentrations of up to 18mM in rice xylem, and this super-saturated xylem sap doesn't disappear once the plant has been harvested. It was thought that during the period where harvested and cut rice tissue was dried to a constant weight that the silicic acid in the xylem sap would polymerise to form silica.

To test this theory an experiment was devised where some rice plants would be dried to a constant weight before acid digestion, whilst others would be digested immediately after harvesting. Both sample groups were then viewed under SEM to analyse the silica structures found. Our hypothesis here was that if the xylem structures were only found in the dried sample group then they were formed as a result of the drying procedure and did not occur naturally in living rice plants. However, to our surprise silicified xylem vessels were observed in both the dried and non-dried sample groups (see section 5.3).

Given this result, we cannot rule out the possibility of xylem vessels being silicified under normal conditions in rice leaves, although there are still several explanations as to why these structures might appear in acid digests but not actually exist in planta. Whilst the drying procedure would certainly result in the polymerisation of silicic acid in the xylem, the acid digestion procedure itself takes place inside a microwave at 180°C. High temperatures have been shown to induce the polymerisation of silicic acid – this fact has even been exploited to map the xylem vessels of spruce trees by filling the xylem with silicic acid and then heating it to create a silica cast of the internal structure of spruce xylem (Persson et al., 2004).

Evidence on whether xylem tissues are silicified or not is inconclusive at this time; although silicified xylem structures are found in rice tissue, it seems unlikely that they would be able to

function under such conditions. Whilst the drying procedure used in the acid digest method has been ruled out as a source of the structures, the acid digest itself could still be the cause of their formation. The lack of silicon detection at the xylem in micro-PIXE and LEXRF supports the theory that xylem vessels are not silicified under normal plant conditions or that the sample preparation procedures involved in these techniques remove the silica before it is imaged.

9.3 The Role of Callose in Silicification

Following up from the pioneering work performed on horsetail (Law & Exley, 2011), our research into callose deposition in rice provided further evidence of the link between callose and silica deposition.

Aniline blue and immunofluorescence staining were used to identify locations of callose deposition in rice leaf tissue (see section 4.3). Callose deposition was commonly detected at the borders of the silica cells, the most heavily silicified cellular structures in rice leaf tissue, using both staining methods. Additionally, callose was detected at the epidermal cell walls, papilla, trichomes and stomata of rice leaves. When the callose staining images are cross-referenced with the PDMPO staining of silica structures found in rice leaves, striking similarities can be observed between the images, as shown below (Fig 9.1, Fig 9.2, Fig 9.3 & Fig 9.4).

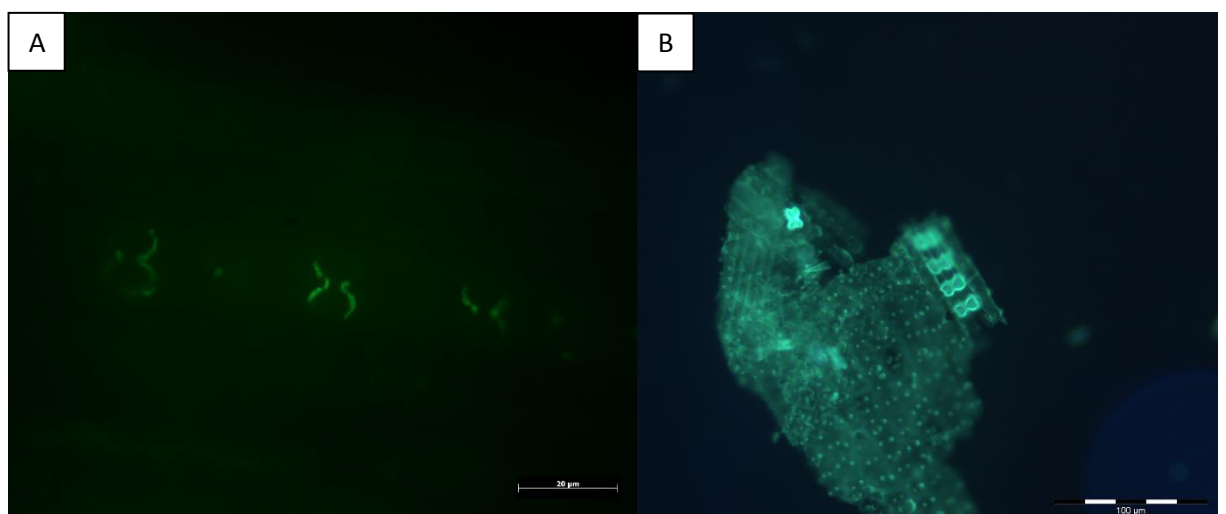


Figure 9.1 Comparison between immunofluorescence staining for callose at the silica cells in rice leaf tissue (A) and PDMPO stained silica cells obtained from acid digestion of rice leaf tissue (B).

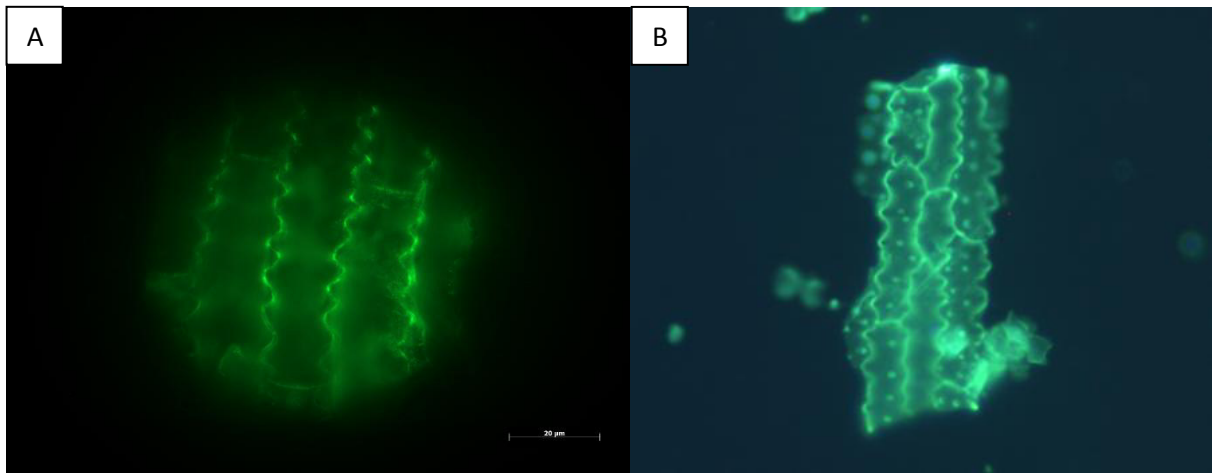


Figure 9.2 Comparison between immunofluorescence staining for callose at the epidermal cells in rice leaf tissue (A) and PDMPO stained epidermal cells silica structures obtained from acid digestion of rice leaf tissue (B).

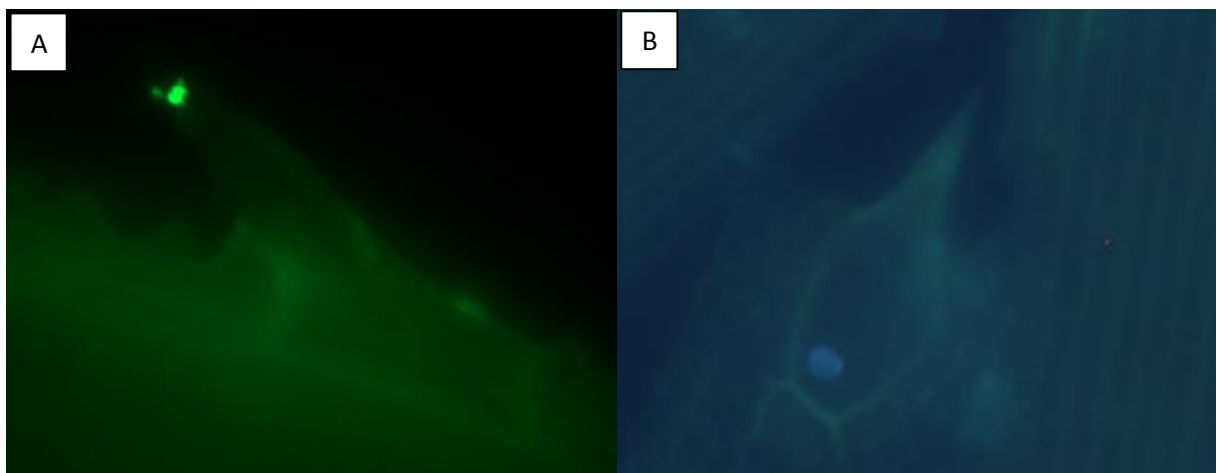


Figure 9.3 Comparison between immunofluorescence staining for callose at the trichome in rice leaf tissue (A) and PDMPO stained trichome silica structures obtained from acid digestion of rice leaf tissue (B).

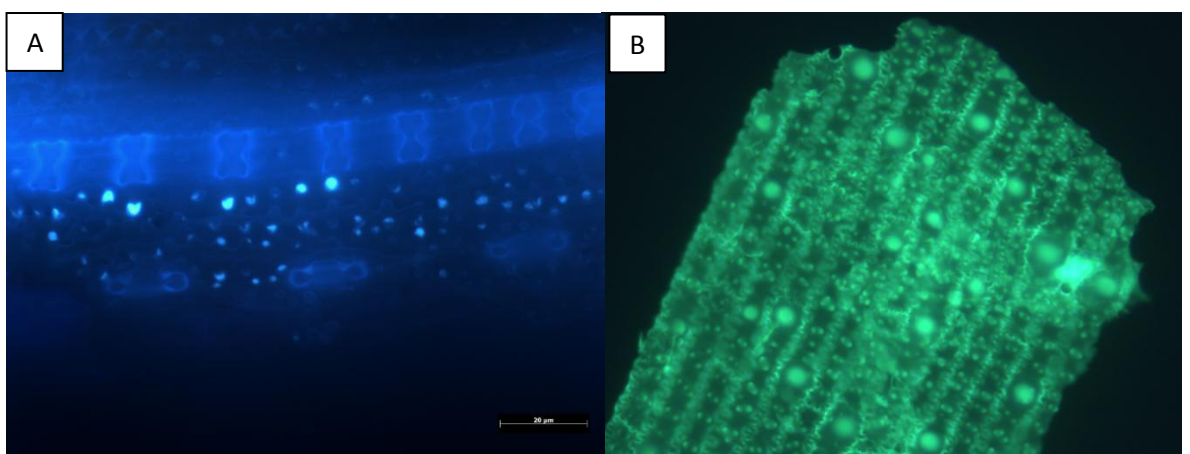


Figure 9.4 Comparison between aniline blue staining for callose at the papilla in rice leaf tissue (A) and PDMPO stained papilla silica structures obtained from acid digestion of rice leaf tissue (B).

Almost all areas of known silica deposition in rice leaves were shown to be areas of significant callose deposition: at the silica cells (Fig 9.1), at the leaf epidermis (Fig 9.2), at the trichomes (Fig 9.3) and at the various papilla and nodules which cover the leaf epidermis (Fig 9.4). One notable exception was the bulliform cells, which were not identified under callose staining. This is due to the positioning of the bulliform cells at the pivot point of curves in the leaf, where they are deeply embedded into the leaf tissue with only a small section of their surface exposed. Bulliform cells may also show callose deposition at their location, however they were not found during the aniline blue or immunofluorescence staining.

This strong co-localisation between callose and sites of silicification is further evidence of the theory that callose, and indeed other hemicelluloses, might act as a template for silica deposition. The idea that hemicelluloses could play a role in templating for silica was first suggested after a study into horsetails (Fry et al., 2009). This work was followed up on with a further analysis of horsetail using PDMPO staining to image silica from acid digests, where it was found that sites of silica deposition at the stomata matched known sites of callose deposition (Law & Exley, 2011). Our data not only supports this previous work, but also builds upon it by showing that the relationship between callose and silica deposition is not restricted to horsetail, but has now also been shown in rice.

Further work should focus its efforts on the possible interactions between callose and silicic acid, following on from the co-localisation studies. Callose production has been inhibited successfully in *Asplenium nidus* through the use of (1) 2-deoxy-d-glucose (2-DDG) or tunicamycin (Apostolakos et al., 2009). Analysing the effect that callose inhibition has on the silicification process in known biosilicifiers such as rice or horsetail could be a vital step in unlocking the secrets of biosilicification.

Some preliminary work has been performed using two mutant forms of *Arabidopsis*, one deficient in callose production whilst the other over-expresses callose. The callose over-expressing mutant

shows higher levels of silicification than the wild-type, whilst the callose deficient mutant shows reduced silicification. This work is in its infancy but it is already showing promising results (Fig 9.5).

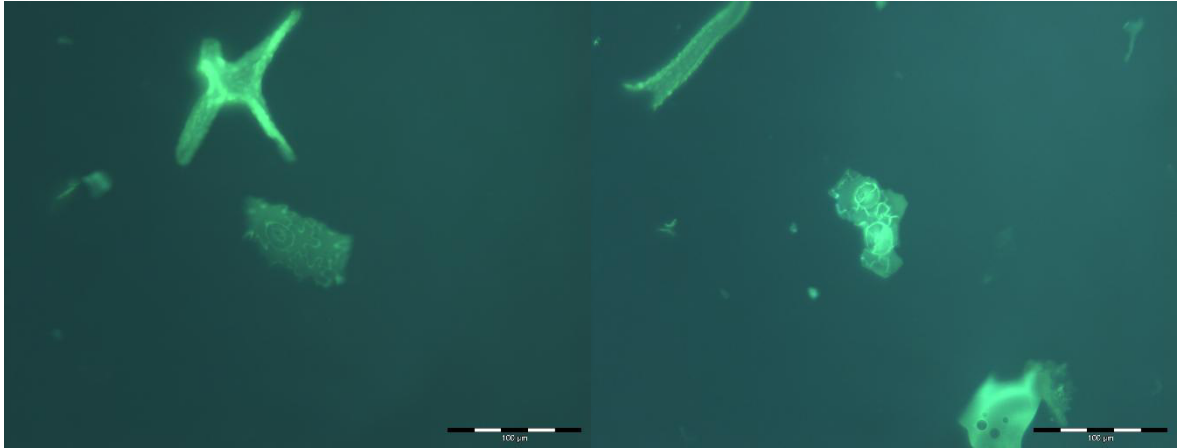


Fig 9.5 Two images of PDMPPO stained silica structures obtained for the acid digestion of Arabidopsis mutant which over-expresses callose.

9.4 Active or Passive Transport

The question of whether silicic acid uptake is an active or passive process has been the subject of significant research. Not all plants are silicon accumulators, and those that are accumulate silicon at different rates. Three methods of transport were proposed: active, passive and rejective (Takahasi et al., 1990). Due to the limitations of the current study rejective transport is of little concern, however active and passive transport are of great interest.

The discovery of super-saturated concentrations of silicic acid within the xylem of rice and wheat has led researchers to conclude that, in these plants at least, silicic acid uptake must be an active process (Mitani et al., 2005; Casey et al., 2003). However, rather than looking at the silicic acid levels in the plant, we took the opposite approach and monitored the silicic acid levels in a plant's growth solution over time. If a rice plant was taking silicic acid up actively against a concentration gradient then the level of silicic acid in the solution would be expected to drop. Our data show that in the ten replicates, only a single plant growth solution had dropped in silicic acid concentration, whilst the other nine growth solutions had either maintained their starting

concentration or increased their silicic acid concentration, suggesting that silicic acid is taken up passively rather than actively (see section 6.3.4).

Based on these findings, a hypothesis has been developed to explain how passive uptake of silicic acid could be responsible for the accumulation of a super-saturated solution of silicic acid over time. Silicic acid is a behavioural analogue of water and will, for the most part, follow water along its path through the transpiration stream, however it is a significantly larger molecule. As a result, not all channels through which water can flow will allow silicic acid. If 100% of the water channels allow silicic acid into the xylem but only 10% allow it to leave then silicic acid will accumulate in the xylem. Water transport is not driven by diffusion, but rather by hydrostatic pressure. Silicic acid is pulled into the xylem faster than it can diffuse out, causing it to accumulate beyond the concentration of the external solution. Eventually an equilibrium will be reached where the diffusion rate out of the xylem matches the rate at which silicic acid is pulled into the xylem.

9.5 Silicification of Developing and Motile Tissue

PDMPO analysis of silica structures from mature plants showed that bulliform cells are completely silicified (see section 7.3.1.3). Bulliform cells are motor cells that either accumulate or expel potassium to alter their water potential and turgidity, which in turn causes these cells to swell or shrink accordingly (Mauseth, 2011). Through the management of their internal water storage, bulliform cells can cause the leaf to bend and flex, curling it inwards to conserve water in drought conditions. The required mobility of these cells poses the question, how could they function whilst completely silicified?

Further to this, PDMPO analysis of silica structures throughout the early development of rice seedlings showed that the silicification of rice tissue is immediate, with the proto-leaves found inside the seed even showing signs of silicification (see sections 8.3). Throughout the early stages of growth and the formation of the shoot apical meristem formation, silica structures from the

epidermal cells were formed despite previous research suggesting that, in other species at least, the epidermal cells did not silicify during the leaf expansion stages (Motomura et al., 2006).

A secondary variant of epidermal cell was also found to be silicified during the development of rice seedlings, which lacked the papilla and sinuate shape of the primary epidermal cells (see section 8.3). Through cross-referencing the silica digest images with research into cellular formation in rice leaves, it was determined that these secondary epidermal cells are in fact primary epidermal cells at an earlier stage of development (Luo et al., 2012).

The discovery that immature cells which have not completed their development are silicified posed a similar issue to the silicification of cells which must alter their morphology to function; how can these cells be silicified and still complete their developmental cycles? A silica layer covering the surface of epidermal cells (as well as being incorporated into the cell walls themselves) is no small obstacle to overcome for a cell attempting to expand or alter its morphology. Three theories based on these observations have been put forward to suggest how developing cells might accomplish this, though they all apply to silicified bulliform cells too:

- **Dynamic conversion of silica into silicic acid** – It is possible that rice can alter the silica structures at its leaf epidermis, converting the silica back into silicic acid via an unknown mechanism to accommodate for cell division, elongation and morphological changes.
- **Breaking out** – Given the brittle nature of the silica found at the leaf epidermis, it is possible that as a cell grows or divides it breaks free from its outer layer of silica. The silicification process would then begin anew.
- **Silica, but not silica** – Almost all methods of observing silica in plant tissue are destructive and result in the alteration of organic conditions within the plant. It has been shown that within the xylem rice can maintain a super-saturated concentration of silicic acid, but that once removed from its environment the solution quickly forms silica (Mitani et al., 2005). It is possible that the 'silica' at the leaf epidermis is maintained as silicic acid, or in another

form, during cell development and only silicifies after cell development and division is completed, or if the closed environment is breached by invasive experimental methods.

Of the three possibilities, the theory that silicified cells are not in fact silicified, but rather covered with a more malleable layer of concentrated silicic acid is the most intriguing. It is known that rice can maintain a super-saturated concentration of silicic acid in solution within the xylem, and that this solution will begin to polymerise quickly once the closed environment of the living plant is broken (Mitani et al., 2005). It is possible that this super-saturated silicic acid is not immediately polymerised once it reaches the epidermis, but is maintained as either a silicic acid layer, or silicon in some other form, beneath the cuticle, either permanently or until cellular development has ceased in that region.

Every method used to image and identify silica within plant tissues requires that the tissue be disrupted in some way, either sectioned or destroyed outright, and these processes themselves could result in the formation of silica in areas that are otherwise not silicified, but are exposed to silicon in high concentrations. Whilst certain areas which do not require motility to function (such as the silica cells and epidermal layer of silica) are likely silicified upon their development ceasing, areas like the bulliform cells could maintain this malleable layer of silicon indefinitely.

Investigation into the functional capabilities of bulliform cells in silicified rice plants should be the focus of further work, as deciphering whether these cells do in fact still function under conditions of silicification will be vital in understanding the state in which silicon is stored in plants.

9.6 Final Word

The common consensus in regards to biosilicification is that certain plants accumulate silicon through the active uptake of silicic acid from the soil. From there, it is transported up through the xylem to the end of the transpiration stream, then it is unceremoniously dumped at the leaf epidermis where it polymerises into silica. The current research lends to quite the opposite conclusion, that silicon is taken up passively along with water into the xylem and transported to

sites of silicification, whereupon compounds such as callose provide a template for silica deposition at specific sites such as the silica cells, epidermal cells, papilla, trichomes and stomata. It is further suggested that silica detected in plant tissue could be stored in another form in planta to allow for cellular development and motility.

10. Reference List

- Agarie, S., Agata, W., Uchida, H., Kubota, F. & Kaufman, P.B. (1996). Function of silica bodies in the epidermal system of rice (*Oryza sativa* L.): testing the window hypothesis. *Journal of Experimental Botany*. 47(298): 655-660
- Agarie, S., Hanaoka, N., Ueno, O., Miyazaki, A., Kubota, F., Agata, W. & Kaufman, P. (1998). Effects of Silicon on Tolerance to Water Deficit and Heat Stress in Rice Plants (*Oryza sativa* L.), Monitored by Electrolyte Leakage. *Plant Production Science*. 1(2): 96-103
- Al-Maliki, F. (2012). Detection of Random Laser Action from Silica Xerogel Matrices Containing Rhodamine 610 Dye and Titanium Dioxide Nanoparticles. *Advances in Materials Physics and Chemistry*. 2(3): 110-115.
- American Phytopathological Society (2015). Microbe Genomics. [Online]. Available at: <http://www.apsnet.org/publications/apsnetfeatures/Pages/MicrobeGenomics.aspx> [Accessed: 21th June 2014].
- Apostolakos P, Livanos P, Nikolakopoulou TL, Galatis B. (2009). The role of callose in guard-cell wall differentiation and stomatal pore formation in the fern *Asplenium nidus*. *Annals of Botany*. 104(7): 1373-1387
- Arroyave, C., Tolrà, R., Thuy, T., Barceló, J., Poschenrieder, C. (2013) Differential aluminum resistance in *Brachiaria* species. *Environmental and Experimental Botany*. 89: 11–18
- Attridge, T.H. (1991). *Light and Plant Responses: A Study of Plant Photophysiology and the Natural Environment*. Cambridge: Cambridge University Press. Pg 65.
- Atwell, B.J., Kriedemann, P.E. & Turnbull, C.G.N. (1999). *Plants in Action: Adaptation in Nature, Performance in Cultivation*. China: Macmillan Publishers. Pp 161.
- Baylis, A.D., Gragopoulou, C., Davidson, K.J. & Birchall, J.D. (1994). Effects of silicon on the toxicity of aluminium to soybean. *Communications in Soil Science and Plant Analysis*. 25(5-6): 537-546.
- Bélanger, R.R., Benhamou, N. & Menzies, J.G. (2003). Cytological evidence of an active role of silicon in wheat resistance to powdery mildew (*Blumeria graminis* f. sp tritici). *Phytopathology*. 93: 402-412.
- Blackman, E. (1968). The pattern and sequence of opaline silica deposition in rye (*Secale cereal* L.) *Ann. Bot.* 32: 207-218.
- Blackman, E. (1969). Observations on the development of the silica cells of the leaf sheath of wheat (*Triticum aestivum*). *Canadian Journal of Botany*. 47: 827-838.
- Britez, R.M., Watanabe, T., Jansen, S., Reissmann, C. & Osaki, M. (2002). The relationship between aluminium and silicon accumulation in leaves of *Famea marginata*. *New Phytologist*. 156: 437-444.
- Callow, J.A. (2000). *Plant Trichomes: Incorporating advances in plant pathology: Plant Trichomes v. 31 (Advances in Botanical Research)*. London: Academic Press.
- Casey, W. H., Kinrade, S. D., Knight, C. T. G., Rains, D. W. & Epstein, E. (2004). Aqueous silicate complexes in wheat, *Triticum aestivum* L.. *Plant, Cell & Environment*. 27: 51–54.

- Chang, Y., Yamamoto, Y. & Matsumoto, H. (1999). Enhancement of callose production by a combination of aluminum and iron in suspension-cultured tobacco (*Nicotiana tabacum*) cells. *Soil Science & Plant Nutrition*. 45(2): 337-347.
- Chen, C. & Lewin, J. (1969). Silicon as a nutrient element for *Equisetum arvense*. *Canadian Journal of Botany*. 47: 125-131.
- Chen, X. Y. & Kim, J. Y. (2009). Callose synthesis in higher plants. *Plant Signaling & Behavior*. 4(6): 489-492.
- Cherif, M., Asselin, A. and Bélanger, R.R. (1994). Defence response induced by soluble silicon in cucumber roots infected by *Pythium* spp. *Phytopathology*. 84(3): 236-242.
- Chérif, M., Benhamou, N., Menzies, J.G., Bélanger, R.R. (1992). Silicon induced resistance in cucumber plants against *Pythium ultimum*. *Physiol Mol Plant Pathol*. 41: 411–425
- Currie, H. A. & Perry, C. C. (2007). Silicon in plants: biological, biochemical and chemical studies. *Annals of Botany*. 100: 1383-1389.
- Datnoff, L.E., Snyder, G.H. & Korndörfer, G.H. (2001). *Silicon in Agriculture, Volume 8 (Studies in Plant Science)*. 1st Edition, Amsterdam: Elsevier.
- Dickison, W.C. (2000) *Integrative Plant Anatomy*. 1st edition. Academic Press.
- Delhaize, E., Craig, S., Beaton, C. D., Bennet, R. J., Jagdish, V. C. & Randall, P. J. (1993). Aluminum Tolerance in Wheat (*Triticum aestivum* L.) (I. Uptake and Distribution of Aluminum in Root Apices). *Plant Physiol*. 1993 Nov; 103(3): 685–693.
- Epstein, E. (1994). The anomaly of silicon in plant biology. *Proceedings of the National Academy of Science*. 91: 11– 17.
- Epstein, E. (2001) Silicon in plants: Facts vs. concepts. In: Datnoff, L.E., Snyder, G.H. & Korndörfer, G.H. *Silicon in Agriculture, Volume 8 (Studies in Plant Science)*. 1st Edition, Amsterdam: Elsevier. Pp 1-15.
- Epstein, E. (2009). Silicon: its manifold roles in plants. *Annals of Applied Biology*. 155: 155-160.
- Eticha, D., Thé, C., Welcker, C., Narro, L., Staß, A. & Horst, W. (2004). Aluminium-induced callose formation in root apices: inheritance and selection trait for adaptation of tropical maize to acid soils. *Field Crop Research*. 93: 252-263.
- Evert, R.F. (2006). *Esau's Plant Anatomy: Meristems, Cells, and Tissues of the Plant Body: Their Structure, Function and Development*. 3rd Edition. Wiley-Blackwell. Pg 235.
- Exley, C. (1998). Silicon in life: a bioinorganic solution to bioorganic essentiality. *J Inorg Biochem*. 69: 139-144.
- Exley, C. (2009). Silicon in life: whither biological silicification? *Prog Mol Subcell Biol*. 47: 173-84.
- Exley, C. (2009b). Darwin, natural selection and the biological essentiality of aluminium and silicon. *Trends in Biochemical Sciences*. 34(12): 589-593.
- Fawe, A., Abou-zaid, M., Menzies, J.G. & Bélanger, R.R. (1998). Silicon-mediated accumulation of flavonoid phytoalexins in cucumber. *Phytopathology*. 88: 396-401.

- Fry, S. C., Nesselrode, B. H. W. A., Miller, J. G. & Mewburn, B.R. (2008) Mixed-linkage (1→3,1→4)-β-D-glucan is a major hemicellulose of Equisetum (horsetail) cell walls. *New Phytologist*. 179: 104-115.
- Guillon, J.M. (2004) Phylogeny of Horsetails (*Equisetum*) based on the Chloroplast rps4 Gene and Adjacent Noncoding Sequences. *Systematic Botany*. 29(2): 251-259.
- Hodson, M. J. & Evans, D. E. (1995). Aluminium/silicon interactions in higher plants. *Journal of Experimental Botany*. 46(283): 161-171.
- Holzhueter, G., Narayanan, K. & Gerber, T. (2003). Structure of silica in *Equisetum arvense*. *Anal Bioanal Chem*. 376: 512–517.
- Huang, J.W., Grunes, D.L. & Kochian, L.V. (1992). Aluminum effects on the kinetics of calcium uptake into cells of the wheat root apex. *Planta*. 188(3): 414-421.
- Hunt, J.W., Dean, A.P., Webster, R.E., Johnson, G.N. & Ennos, A.R. (2008). A novel mechanism by which silica defends grasses against herbivory. *Annals of Botany*. 102: 653-656.
- Itoh, J., Nonomura, K., Ikeda, K., Yamaki, S., Inukai, Y., Yamagishi, H., Kitano, H. & Nagato, Y. (2005). Rice plant development: from zygote to spikelet. *Plant Cell Physiol*. 46(1): 23-47.
- Kaufman, P.B., Dayanandan, P.B., Franklin, C.I. & Takeoka, Y. (1985). Structure and Function of Silica Bodies in the Epidermal System of Grass Shoots. *Ann Bot*. 55(4): 487-507.
- Kaulich, B., Gianoncelli, A., Beran, A., Eichert, D., Kreft, I., Pongrac, P., Regvar, M., Vogel-Mikus, K. & Kiskinova, M. (2009). Low-energy X-ray fluorescence microscopy opening new opportunities for bio-related research. *J. R. Soc. Interface*. 6: S641-S647.
- Lanning, F.C. (1963). Silicon in Rice. *Plant Constituents*. Vol. 11, No. 5, Sept-Oct. 1963
- Law, C. & Exley, C. (2011). New insight into silica deposition in horsetail (*Equisetum arvense*). *BMC Plant Biology*. 11: 112.
- Leng, X., Feng, Y., Li, X. & Sun, J. (2015). *Skeletonema cf. costatum* biogenic silica production rate determined by PDMPO method. *Advances in Environmental Science and Energy Planning*. 1:255-260.
- Lui, K., Kozono, D., Kato, Y., Agre, P., Hazama, A. & Yasui, M. (2005). Conversion of aquaporin 6 from an anion channel to a water-selective channel by a single amino acid substitution. *PNAS*. 102(6): 2192-2197.
- Luo, L., Zhou, W. Q., Liu, P., Li, C. X. & Hou, S. W. (2012). The development of stomata and other epidermal cells on the rice leaves. *Biologia Plantarum* 56(3): 521-527.
- Ma J. F. & Yamaji, N. (2008). Functions and transport of silicon in plants. *Cell Mol Life Sci*. 65(19): 3049-3057.
- Ma, J. F. (1988). Study on physiological role of silicon in rice plants. Master Thesis, Kyoto University.
- Ma, J. F. (1990). Studies on beneficial effects of silicon on rice plants. Ph. D. thesis, Kyoto University.

- Ma, J. F., Tamai, K., Yamaji, N., Mitani, N., Konishi, S., Katsuhara, M., Ishiguro, M., Murata, Y. & Yano, M. (2006) A silicon transporter in rice. *Nature*. 440: 688-691.
- Ma, J. F., Yamaji, N., Mitani, N., Tamai, K., Konishi, S., Fujiwara, T., Katsuhara, M. & Yano, M. (2007). An efflux transporter of silicon in rice. *Nature*. 448: 209-212.
- Ma, J.F. & Takahashi, E. (2002). *Soil, Fertilizer, and Plant Silicon Research in Japan*. 1st Edition, Amsterdam: Elsevier.
- Ma, J.F. (2004). Role of silicon in enhancing the resistance of plants to biotic and abiotic stresses. *Soil Science and Plant Nutrition*. 50 (1): 11-18
- Ma, J.F., Goto, S., Tamai, K. & Ichii, M. (2001b). Role of root hairs and lateral roots in silicon uptake by rice. *Plant Physiology*. 127: 1773-1780.
- Ma, J.F., Miyake, Y. & Takahashi, E. (2001) Silicon as a beneficial element for crop plants. In: Datnoff, L. E, Snyder, G. H. & Korndorfer, G. H. eds. *Silicon in agriculture*. Amsterdam: Elsevier Science, pp 17-40
- Ma, J.F., Sasaki, S. & Matsumoto, H. (1997). Al-induced inhibition of root elongation in corn, *Zea mays* L. is overcome by Si addition. *Plant Soil*. 188: 171-176
- Ma, J.F., Yamaji, N., Mitani, N., Xu, X., Su, Y., McGrath, S.P. & Zhao, F. (2008). Transporters of arsenite in rice and their role in arsenic accumulation in rice grain. *PNAS*. 105: 9931-9935.
- Matoh, T., Murata, S. & Takahashi, E. (1991). Effect of silicate application on photosynthesis of rice plants. *Jpn. J. Soil Sci. Plant Nutr.* 32: 248-251
- Matsumoto, H. (2000). Cell biology of aluminum toxicity and tolerance in higher plants. *Int Rev Cytol*. 200, 1-46.
- Meng, Y.L., Lui, Z. & Rosen, B.P. (2004). As(III) and Sb(III) uptake by GlpF and efflux by ArsB in *Escherichia coli*. *Journal of Biological Chemistry*. 279: 18334-18341.
- Mesjasz-Przybyłowicz, J. & Przybyłowicz, W. (2002). Micro-PIXE in plant sciences: Present status and perspectives. *Nuclear Instruments and Methods in Physics Research B*. 189: 470-481.
- Mitani, N., Ma, J. F. & Iwashita, T. (2005). Identification of the silicon form in xylem sap of rice (*Oryza sativa*). *Plant Cell Physiology*. 46(2): 279-283.
- Moldenhauer, K. & Slaton, N., (2001). Rice growth and development. In: Slaton, N.A. (Ed.), *Rice Production Handbook*. Misc. Publ. 192. Coop. Ext. Service, University of Arkansas, Little Rock, pp. 7-14
- Motomura, H., Fujii, T. & Suzuki, M. (2006). Silica Deposition in Abaxial Epidermis before the Opening of Leaf Blades of *Pleiblastus chino* (Poaceae, Bambusoideae). *Annals of Botany*, 97 (4): 13-19
- Myburg, A. A., Lev-Yadun, S., and Sederoff, R.R. (2013). Xylem Structure and Function. In: *eLS*. Chichester: John Wiley & Sons Ltd.
- Nguyen, M. X., Moon, S. & Jung, K. H. (2013) Genome-wide expression analysis of rice aquaporin genes and development of a functional gene network mediated by aquaporin expression in roots. *Planta*. 238(4): 669-81.

- Ning, D., Song, A., Fan, F., Li, Z. & Liang, Y. (2014). Effects of Slag-Based Silicon Fertilizer on Rice Growth and Brown-Spot Resistance. *PLoS One*. 9 (7) e102681
- Okuda, A. & Takahashi, E. (1961). Studies on the physiological role of silicon in crop plant. Part 3 Effect of Various amount of silicon supply on the growth of rice plant and its nutrient uptake. *J. Sci. Soil and Manure*. 32: 533-537.
- Orlić, I. (1999). Analytical Chemistry of Aerosols: Science and Technology edited by Kvetoslav R. Spurny. Chapter 13 – The analysis of individual aerosol particles using the nuclear microscope. Pp 278.
- Ortega, R., Devès, G. & Carmona, A. (2009). Bio-metals imaging and speciation in cells using proton and synchrotron radiation X-ray microspectroscopy. *Journal of the Royal Society Interface*, 6 (Suppl 5): S649–S658.
- Passioura, J. B. (2010). Plant–Water Relations. In: *eLS*. Chichester: John Wiley & Sons Ltd.
- Pendle, A. & Benitez-Alfonso, Y. (2015). Immunofluorescence Detection of Callose Deposition around Plasmodesmata Sites. *Methods in Molecular Biology*. 1217: 95-104.
- Perry, C.C. & Fraser, M.A. (1991). Silica deposition and ultrastructure in the cell wall of *Equisetum arvense*: the importance of cell wall structures and flow control in biosilification. *Phil. Trans. R. Soc.* 334: 149-157
- Persson, P. V., Fogden, A., Hafrén, J., Daniel, G. & Iversen, T. (2004). Silica-cast replicas for morphology studies on spruce and birch xylem. *IAWA Journal*. 25(2): 155-164.
- Rafi, M.M. & Epstein, E. (1999) Silicon absorption by wheat (*Triticum aestivum* L.) *Plant and Soil*, 211: 223–230.
- Rahman, T., Kawamura, K., Koyama, H. & Hara, T. (1998). Varietal differences in the growth of rice plants in the response to aluminium and silicon. *Soil Sci. Plant Nutr.* 44: 423-431.
- Ramirez, A. M., Stoop, G., Menzel, T. R., Gols, R., Bouwmeester, H. J., Dicke, M. & Jongsma, M. A. (2012). Bidirectional secretions from glandular trichomes of pyrethrum enable immunization of seedlings. *Plant Cell*. 24(10): 4252-4265.
- Raven, J. A. (2001). Silicon transport at the cell and tissue level. In: Datnoff, L. E., Snyder, G. H. & Korndorfer, G. H. eds. *Silicon in agriculture*. Amsterdam: Elsevier Science, 41–55.
- Rodrigues, F.A., Benhamou, N., Datnoff, L.E., Jones, J.B. & Bélanger, R.R. (2003). Ultrastructural and cytochemical aspects of silicon-mediated rice blast resistance. *Phytopathology*. 93: 535-546.
- Rost, F.W.D. (1995). Fluorescence Microscopy: Volume 2. *Cambridge University Press*. Pg 373.
- Rost, T. L. (1997). Dermal Tissue System. [Online]. Available from: <http://www-plb.ucdavis.edu/labs/rost/rice/leaves/dermal.html> [Accessed 13th January 2014].
- Roy, A.K., Sharma, A. & Talukder, G. (1988). Some aspects of aluminum toxicity in plants. *The Botanical Review*. 54(2): 145-178.
- Sangster A.G. (1977) Characteristics of silica deposition in *Digitaria sanguinalis* (L.) Scop. (crabgrass). *Annals of Botany*, 41: 341–350.
- Savant, N.K., Snyder, G.H. & Datnoff, L.E. (1997). Silicon management and sustainable rice production. *Advances in Agronomy*. 58: 151-199.

- Schneider, T., Strasser, O., Gierth, M., Scheloske, S. & Povh, B. (2002). Micro-PIXE investigations of apoplastic iron in freeze-dried root cross-sections of soil grown barley. *Nuclear Instruments and Methods in Physics Research B*. 189: 487–493.
- Sharma, N.K., Williams, W.S. & Zanguil, A. (1984). Formation and Structure of Silicon Carbide Whiskers from Rice Hulls. *Journal of the American Ceramic Society*. 67, 715-720.
- Shimizu, K., Del Amo, Y., Brzezinski, M. A., Stucky, G. D. & Morse, D. E. (2001). A novel fluorescent silica tracer for biological silicification studies. *Chem Biol*. 2001, 8: 1051-1060.
- Simpson, T.L. & Volcani, B.E. (1981). *Silicon and Siliceous Structures in Biological Systems*. New York: Springer-Verlag.
- Singh, V. P., Tripathi, D. K., Kumar, D., Chauhan, D. K. (2011). Influence of exogenous silicon addition on aluminium tolerance in rice seedlings. *Biol Trace Elem Res*. 144(1-3): 1260-1274.
- Sommer, M., Kaczorek, D., Kuzyakov, Y. & Breuer, J. (2006). Silicon pools and fluxes in soils and landscapes – a review. *Journal of Plant Nutrition and Soil Science*. 169: 310-329.
- Street-Perrott, F.A. & Barker, P. A. (2008). Biogenic silica: a neglected component of the coupled global continental biogeochemical cycles of carbon and silicon. *Earth Surface Processes and Landforms*. 33(9): 1436-1457.
- Takahashi, E., Ma, J. F. & Miyake, Y. (1990). The possibility of silicon as an essential element for higher plants. *Comments Agricultural and Food Chemistry*. 2: 99-122.
- Tamai, K. & Ma, J. F. (2003). Characterization of silicon uptake by rice roots. *New Phytol*. 158: 431-436.
- Tian, D., Tooker, J., Peiffer, M., Chung, S.H. & Felton, G.W. (2012). Role of trichomes in defense against herbivores: comparison of herbivore response to woolly and hairless trichome mutants in tomato (*Solanum lycopersicum*). *Planta*.; 236(4): 1053-66.
- Tolrà, R., Vogel-Mikuš, K., Hajiboland, R., Kump, P., Pongrac, P., Kaulich, B., Gianoncelli, A., Babin, V., Barceló, J., Regvar, M. & Poschenrieder, C. (2010). Localization of aluminium in tea (*Camellia sinensis*) leaves using low energy X-ray fluorescence spectro-microscopy. *J Plant Res*. 124(1): 165-172.
- Tubb, H. J. (1995). Anatomical, developmental and physiological aspects of silica in wheat. Ph. D. Thesis. Oxford Brookes University.
- Ueno, O. & Agarie, S. (2005). Silica Deposition in Cell Walls of the Stomatal Apparatus of Rice Leaves. *Plant Prod Sci*. 8(1): 71-73.
- Valencia College (2015). Phloem Lab. [Online]. Available at: http://faculty.valenciacollege.edu/tklenk/ePlantPhys2008/labs/phloem%20lab/Phloem%20labwpi_cs_files/image015.jpg. [Accessed 11th April 2014].
- Vancells, J.C. (2014). Direct vs indirect immunofluorescence. [Online] Available from: <http://www.abcam.com/secondary-antibodies/direct-vs-indirect-immunofluorescence> [Accessed: 4th July 2014].
- Vogel-Mikuš, K., Pongrac, P., Pelicon, P., Vavpetič, P., Povh, B., Bothe, H., Regvar, M., 2009. Micro-PIXE analysis for localisation and quantification of elements in roots of mycorrhizal metal-tolerant plants, In: Varma, A., Kharkwal, A.C. *Soil Biology*, 18, Springer, Heidelberg, pp. 227-242.

- Vogel-Mikuš, K., Simcic, J., Pelicon, P., Budnar, M., Kump, P., Necemer, M., Mesjasz-Przybyłowicz, J., Przybyłowicz, W.J. & Regvar, M. (2008). Comparison of essential and non-essential element distribution in leaves of the Cd/Zn hyperaccumulator *Thlaspi praecox* as revealed by micro-PIXE. *Plant, Cell and Environment*. 31: 1484–1496.
- War, A.R., Paulraj, M.G., Ahmad, T., Buhroo, A.A., Hussain, B., Ignacimuthu, S., & Sharma, H.C. (2012). Mechanisms of plant defense against insect herbivores. *Plant Signaling & Behavior*, 7(10): 1306-1320.
- Wissemeier, A. H., Klotz, F. & Horst, W.J. (1987). Aluminium Induced Callose Synthesis in Roots of Soybean (*Glycine max* L.). *Journal of Plant Physiology*. 129(5): 487-492.
- Yamaji, N. & Ma, J. F. (2009). A transporter at the node responsible for intervascular transfer of silicon in rice. *The Plant Cell*. 21: 2878-2883.
- Yamaji, N., Mitani, N. & Ma, J.F. (2008). A transporter regulating silicon distribution in rice shoots. *The Plant Cell*. 20: 1381-1389.
- Yamanaka, S., Takeda, H., Komatsubara, S., Ito, F., Usami, H., Togawa, E. & Yoshino, K. (2009). Structures and physiological functions of silica bodies in the epidermis of rice plants. *Applied Physics Letters*. 95: 123703.
- Yoshida, S. (1965). Chemical aspects of the role of silicon in physiology of the rice plant. *Bull. Natl Inst. Agric. Sci. B*. 15: 1-58.
- Yost, C. L. & Blinnikov, M. S. (2011). Locally diagnostic phytoliths of wild rice (*Zizania palustris* L.) from Minnesota, USA: comparison to other wetland grasses and usefulness for archaeobotany and paleoecological reconstructions. *Journal of Archaeological Science*. 38: 1977-1991.
- Zelinová, V., Halušková, L., Huttová, J., Illéš, P., Mistrík, I., Valentovičová, K. & Tamás, L. (2011). Short-term aluminium-induced changes in barley root tips. *Protoplasma*. 248: 523-530.
- Znanchor, P. & Nedoma, J. (2008). Application of the PDMPO technique in studying silica deposition in natural populations of *Fragilaria crotonensis* (*Bacillariophyceae*) at different depths in a eutrophic reservoir. *J Phycol* 44: 518-525.